# FINAL STUDY REPORT (MAY THROUGH NOVEMBER 1966)

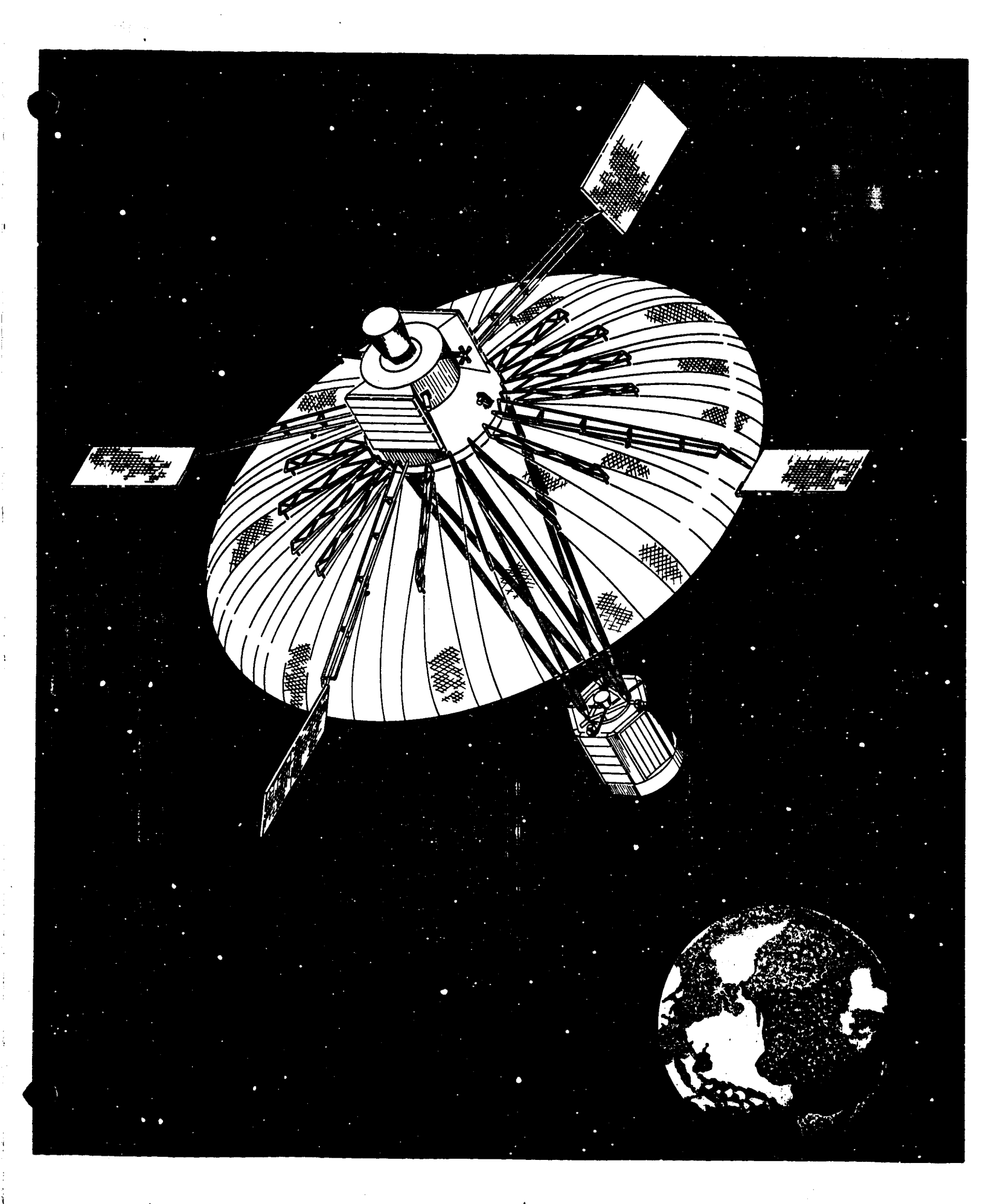
**VOLUME I** 

BOOK 1

AN ADVANCED STUDY OF AN APPLICATION TECHNOLOGY SATELLITE (ATS-4) MISSION

NATIONAL AERONAUTICS AND SPACE ADMINISTRATION GODDARD SPACE FLIGHT CENTER GREENBELT, MARYLAND

a	N 67 - 2460 <b>1</b>	
FORM 60	(ACCESSION NUMBER)	(THRU)
FACILITY	(PAGES)  (PAGES)  (NASS CR OR TMX OR AD NUMBER)	(CATEGORY)



# PRECEDING PAGE BLANK NOT FILMED.

### TABLE OF CONTENTS

### VOLUME I BOOK 1

Section																	Page
1	INTF	RODUCT	ION		• •	• •	•		•	•	٥	•	•	•		•	1-1
2	PRO	JECT O	BJECTIVES	s	• •		•		•			•	•	•	•	•	2-1
3	PRO	JECT F	EASIBILIT	Y	• •	• •	•		•	۰			a		'n		3-1
4	EXP	ERIMEN	T DESCRI	PTION A	AND J	USTI	FICA	ATIO	n.	•	•	•	•	•	•	•	4-1
	4.1		al														4-1
	4.2	Parabo	oli <mark>c Ant</mark> enna	a Exper	iment	• •	۰		•	•	0	•	•	u	•	•	4-3
		4.2.1	Mechanica	ıl		• •	•			•	٠	•	•	٥	o	•	4-3
			Electrical														4-4
	4.3	Orienta	ation Contr	ol Expe	riment	t	•			۰				٥	٥	a	1-11
	4.4		d Array Exp														1-5
	4.5		rometer Ex														4-6
	4.6	Second	lary Experi	ments	• •	o •	•	• •	•	۰	0	۰	,	۰	۰	9	4-7
5	SPAC	CECRAF	FT DESCRI	PTION	• •	• •	•	•	o o	U	•	٥	a	٥	3	ü	5-1
	5.1		action														5.1-1
	5.2		ional Conce														5.2 - 1
		5,2,1	Mission R	equirem	ents a	and C	onst	rain	ts.	•	•	٥	a	,	9	•	5.2-1
			Launch Ve														5.2-2
		5.2.3	Mission P	rofile	o •	• •				•	•	٥	۰		,	J	5.2-3
		5.2.4	Payload C	apabilit	у .	• 0				•	•	0	o	•	a	<b>&gt;</b>	5.2-5
	5.3	System	Summary	۰ .	• •	• •	•		•	•	•	•		۰	۰	•	5.3 - 1
		5.3.1	Configurat	tion Des	cripti	on .	۰	٥ .		•	•	۰			•	•	5.3 - 1
		5.3.2	Subsystem	Summa	ıry .	• •	•			٥		٠	۰	Q	٠	•	5.3 - 9
			5.3.2.1	Power	Subs	ysten	١.			•	٥	•	۰	۰	•		5.3-10
			5.3.2.2	Guida	n <mark>c</mark> e an	d Cor	ntro	Sub	sys	tem			٥	۰	J	3	5.3-13
			5.3.2.3	TT &C	Subsy	stem	۱.			•	0	۰	۰	٥	۰	•	5.3-15
			5.3.2.4	Exper	iment	s Sub	syst	em.		٠	•		۰	۰	٥	3	5.3-15
			5.3.2.5	Thern													
			5.3.2.6	Modul													5.3-17
		5.3.3	System Pe														5.3-18
			5.3.3.1	Parab	olic A	ntenn	a E	xper	ime	nt	2	,	•	,	9	3	
			5.3.3.2	Orien													
			5.3.3.3	Pnase													5.3-21
			5.3.3.4	Comm													5.3-2
			5.3.3.5	Power													
			5.3.3.6	Space													

Section					Page
				owth Capability	5.3-29
	<b>5. 4</b>	Parab	oli <mark>c Anten</mark> na		5.4-1
		5.4.1	Selection of	of Antenna Concept	5.4-1
		5.4.2	Description	n of Selected Design	5.4-2
			5.4.2.1	Reflector and Feed	5.4-2
			5.4.2.2	Packaging	5.4-7
			5.4.2.3	Deployment	5.4-11
				erformance	5.4-12
		5.4.4	Reflector 1	Design	5.4-15
			5.4.4.1	Method of Construction	5.4 - 15
			5.4.4.2	Material Selection	5.4 - 23
			5.4.4.3	Structural Considerations	5.4-28
			5.4.4.4	Stowage and Deployment Behavior	5.4-30
			5.4.4.5	Performance in 1-g Environment	5.4-31
			5.4.4.6	Spacecraft Interface	5.4-31
		5.4.5	Deploymen	t Mechanism Design	5.4-33
		5.4.6	Feed Desig	m	5.4-34
		5.4.7	Thermal D	esign	5.4-36
	5.5	Guidan	ce and Cont	rol	5.5-1
		5.5.1	Summary.		5.5-1
		5.5.2	Functional	Description	5.5-9
			5.5.2.1	Station Acquisition Modes	5.5-9
			5.5.2.2	Orientation	5.5-25
			5.5.2.3	Orientation Control Operational Modes	5.5-34
			5.5.2.4	Station Capture and Station Change	5.5-42
			5.5.2.5	Restabilization	5.5-45
		5.5.3	Component	Description	5.5-45
			5.5.3.1	Spinup Motors	5.5-48
			5.5.3.2	Coning Control Accelerometer	5.5-48
			5.5.3.3	Precession Control Sun Sensor	5.5-49
			5.5.3.4	Precession Control Rf POLANG Measurement .	5.5-49
			5.5.3.5	Station Acquisition Sensor Signal Processor	5.5-51
			5.5.3.6	Station Acquisition and Despin Mass	
				Expulsion Subsystem	5.5-51
			5.5.3.7	Three Axis Gyro Package	5.5-58
			5.5.3.8	Orientation Control Sun Sensors	5.5-60
			5.5.3.9	Earth Sensor	5.5-64
			5.5.3.10	Polaris Star Sensor	5.5-68
			5.5.3.11	Orientation Control Sensor Signal Processor.	5.5-70
			5.5.3.12	Flywheel and Jet Controller	5.5-70
			5.5.3.13	Mechanical Flywheel	5.5-70
		-	5.5.3.14	Orientation Control and Stationkeeping Mass	
				Expulsion Subsystem	5.5-73

Section															Page
		5.5.4	Command,	Telemetry,	and Pr	rogra	mme	er In	ter	fac	e.		•	•	5.5-7
			5.5.4.1	Commands			•	• •						٠	5.5-7
			5.5.4.2	Telemetry										,	5.5-7
			5.5.4.3	Programme	er .	• •	•							•	5.5-8
		5.5.5	Mounting a	nd Field of V	View In	terfa	ce		•	۰			,		5.5-8
	5.6	Experi	iment Equip	ment	۰ .		۰				•		,		5.6-1
		5.6.1	General .				•	• •				٠			5, 6-1
		5.6.2	Parabolic .	Antenna			•		•	•		٠			5.6-2
			5.6.2.1	General .	• •						•	•		•	5.6-2
			5.6.2.2	Electronics	and R	F Eq						٠	a	•	5.6-4
			5.6.2.3	Geometric											5.6-1
		5.6.3	Orientation	Control Sys	tem.			• •	٠		٠		•		5.6-1
		5.6.4	Interferom	eter Experir	nent.		•		٠			•	•		5.6-1
			5.6.4.1	Introduction	n		•		•	•		•	•	•	5.6-1
			5.6.4.2	Basis of Sy	-										5.6-16
			5.6.4.3	Interferome	eter Fu	ndam	enta	ls.		•		•			5.6-17
			5.6.4.4	Detailed Int											5.6-21
			5.6.4.5	Weight and	Power	Esti	mate	s .		_	•			•	5.6-26
			5.6.4.6	Thermal E	fects				•		•		•	•	5.6-27
		5.6.5	Phase-Stee	red Array A	ntenna							•	۰	. •	5.6-25
	5.7	Telem	etry, Track	ing and Com	mand				•	•	•	•	۰	•	5.7-1
		5.7.1	System Red	quirements					۰	۰	٠	•	•	3	5.7-1
		5.7.2	Reference	Design Sumn	narv			• •	۰	۰	0	٥	•	•	
		5 <b>.7.3</b>	Command S	Subsystem O	neratio	n .		• •	۰	•	۰	٥	٠	٥	5.7-1
			5.7.3.1	Star Tracke	er Mem	orv		•	•	•	۰	•	٥	٠	5.7-5
		5.7.4			• •										5.7-11 5.7-12
			5.7.4.1	Telemetry								•	•	٠	0. (-12
					• . •										10
		5.7.5	Tracking S	ubsystem Op	eration		•	•	•	٠	•	٠	,	. a	
		5.7.6	TT &C Ante	nnas	01 40101	•	•	•	۰	•	•	٠			
			5, 7, 6, 1	Antenna Co	verage	•	• (		٥	۰	•	٠	•	٥	5.7-16
			5.7.6.2	Antenna De				• •	•	٠	•	•	9	J	5.7-16
		5.7.7		culations.						•	۰	• .	•	٠	5.7-18
		5.7.8		ation of Redu					٥	0	۰	٠	٥	•	5.7-22
				ight and Size				٠	۰	۰	•	•	٠	•	5.7-27
	5.8										٠			•	5.7-27
	0.0	5.8.1		• • • •										٠	5.8-1
		0.0.1	5.8.1.1	nts					•		3	٠	٠	u	5.8-1
			U. O. 1. 1	Launch Loa				•							_
			E 0 1 0	Sun-orienta						•	•	٠	٠	٥	5.8-1
			5.8.1.2	Orbit Load											
		5 0 0	Carla on4	Sun-orienta	uon.	• •	<b>0</b> 0	•	•	s	ه	•	a	•	5.8-3
		5.8.4	subsystem	Description	• •			•	q	0	٠	۰	٠	o	5.8-6

5.9       Spacecraft Design       5.9-1         5.9.1       Introduction       5.9-1         5.9.2       Launch Phase and Orbital Constraints       5.9-2         5.9.2.1       Launch Vehicle Constraints       5.9-2         5.9.2.2       Coast Apogee Firing and Orbital Injection       5.9-10         Constraints       5.9-20         5.9.3       Orbital Constraints       5.9-20         5.9.3       Spacecraft Structural Design       5.9-20         5.9.3.1       Earth Viewing Equipment Module       5.9-21         5.9.3.2       Feed Support Truss       5.9-29         5.9.3.3       Aft Equipment Module       5.9-34         5.9.3.4       Solar Array Panels and Support Trusses       5.9-36         5.9.3.5       Spacecraft Adapter       5.9-36         5.9.3.6       Structure Weight Summary       5.9-38         5.9.4       Solar Panel Stowage and Deployment       5.9-38         5.9.4.1       Solar Panel Stowage and Deployment       5.9-34         5.9.4.2       Combined Purpose Antenna Deployment       5.9-34         5.9.4.2       Combined Purpose Antenna Deployment       5.9-44         5.9.5.1       Introduction       5.9-48         5.9.5.2       Launch Configuration Beha	Section						Page
5. 8. 2.3 General Operational Characteristics 5. 8-10 5. 8. 2.4 Solar Array Capability 5. 8-11 5. 8. 2.5 Battery Capability 5. 8-20 5. 8. 2.6 Subsystem Efficiency and Margins 5. 8-21 5. 8. 2.7 Operational Flexibility 5. 8-21 5. 8. 2.8 Growth Capability 5. 8-22 5. 8. 3 Component Descriptions 5. 8-22 5. 8. 3 Component Descriptions 5. 8-22 5. 8. 3.1 Solar Array 5. 8-22 5. 8. 3.2 Batteries 5. 8-22 5. 8. 3.3 Voltage Limiter 5. 8-30 5. 8. 3.4 Battery Charge Regulator 5. 8-31 5. 8. 3.5 PWM Regulator 5. 8-31 5. 8. 3.6 Inverter 5. 8-32 5. 8. 3.7 Power Control Unit 5. 8-32 5. 8. 3.8 Summary of Component Characteristics 5. 8-32 5. 8. 3.8 Summary of Component Characteristics 5. 8-32 5. 9 Spacecraft Design 5. 9-1 5. 9. 1 Introduction 5. 9-2 5. 9. 2.1 Launch Phase and Orbital Constraints 5. 9-2 5. 9. 2.2 Coast Apogee Firing and Orbital Injection Constraints 5. 9-2 5. 9. 3.3 Orbital Constraints 5. 9-2 5. 9. 3.3 Spacecraft Structural Design 5. 9-21 5. 9. 3.1 Earth Viewing Equipment Module 5. 9-24 5. 9. 3.2 Feed Support Truss 5. 9-20 5. 9. 3.3 Aft Equipment Module 5. 9-24 5. 9. 3.4 Solar Array Panels and Support Trusses 5. 9-29 5. 9. 3.5 Spacecraft Adapter 5. 9-36 5. 9. 3.6 Structure Weight Summary 5. 9-38 5. 9. 4.2 Combined Purpose Antenna Deployment 5. 9-38 5. 9. 4.2 Combined Purpose Antenna Deployment 5. 9-34 5. 9. 4.2 Combined Purpose Antenna Deployment 5. 9-34 5. 9. 5. 9. 5. 1 Introduction 5. 9-48 5. 9. 5. 5. 1 Introduction 5. 9-48 5. 9. 5. 1 Launch Configuration Behavior 5. 9-48 5. 9. 5. 1 Launch Configuration Behavior 5. 9-48 5. 9. 5. 1 Launch Configuration Behavior 5. 9-53 5. 9-53 Effect of Structural Damping on Cone Angle 5. 9-53				5.8.2.1	Subsystem Selection	• •	5.8-6
5.8.2.4       Solar Array Capability       5.8-11         5.8.2.6       Subsystem Efficiency and Margins       5.8-20         5.8.2.7       Operational Flexibility       5.8-21         5.8.2.8       Growth Capability       5.8-22         5.8.3.1       Solar Array       5.8-22         5.8.3.2       Batteries       5.8-29         5.8.3.3       Voltage Limiter       5.8-30         5.8.3.4       Battery Charge Regulator       5.8-31         5.8.3.5       PWM Regulator       5.8-31         5.8.3.6       Inverter       5.8-32         5.8.3.7       Power Control Unit       5.8-32         5.8.3.8       Summary of Component Characteristics       5.8-32         5.9.1       Introduction       5.9-1         5.9.1       Introduction       5.9-1         5.9.2.1       Launch Phase and Orbital Constraints       5.9-2         5.9.2.2       Coast Apogee Firing and Orbital Injection       5.9-2         5.9.3.3       Orbital Constraints       5.9-20         5.9.3.3       Feed Support Truss       5.9-20         5.9.3.3       Feed Support Truss       5.9-29         5.9.3.4       Solar Array Panels and Support Trusses       5.9-36         5				5.8.2.2	Subsystem Block Diagram		5.8-8
5.8.2.5       Battery Capability.       5.8-20         5.8.2.6       Subsystem Efficiency and Margins       5.8-21         5.8.2.7       Operational Flexibility       5.8-21         5.8.2.8       Growth Capability       5.8-22         5.8.3.1       Solar Array       5.8-22         5.8.3.2       Batteries       5.8-29         5.8.3.3       Voltage Limiter       5.8-30         5.8.3.4       Battery Charge Regulator       5.8-31         5.8.3.5       PWM Regulator       5.8-31         5.8.3.6       Inverter       5.8-32         5.8.3.7       Power Control Unit       5.8-32         5.8.3.8       Summary of Component Characteristics       5.8-32         5.9.1       Introduction       5.9-1         5.9.2       Launch Phase and Orbital Constraints       5.9-2         5.9.2.1       Launch Vehicle Constraints       5.9-2         5.9.2.2       Coast Apogee Firing and Orbital Injection       5.9-2         5.9.2.3       Orbital Constraints       5.9-20         5.9.3.3       Spacecraft Structural Design       5.9-20         5.9.3.4       Solar Array Panels and Support Trusses       5.9-24         5.9.3.5       Spacecraft Adapter       5.9-36				5.8.2.3	General Operational Characteristics	• a	5.8-10
5.8.2.6 Subsystem Efficiency and Margins 5.8-21 5.8.2.7 Operational Flexibility 5.8-21 5.8.2.8 Growth Capability 5.8-22 5.8.3 Component Descriptions 5.8-22 5.8.3.1 Solar Array 5.8-22 5.8.3.2 Batteries 5.8-29 5.8.3.3 Voltage Limiter 5.8-30 5.8.3.4 Battery Charge Regulator 5.8-31 5.8.3.5 PWM Regulator 5.8-31 5.8.3.6 Inverter 5.8-32 5.8.3.7 Power Control Unit 5.8-32 5.8.3.8 Summary of Component Characteristics 5.8-32 5.9.3 Spacecraft Design 5.9-1 5.9.1 Introduction 5.9-2 5.9.2.1 Launch Phase and Orbital Constraints 5.9-2 5.9.2.2 Coast Apogee Firing and Orbital Injection Constraints 5.9-2 5.9.3 Spacecraft Structural Design 5.9-21 5.9.3.1 Earth Viewing Equipment Module 5.9-34 5.9.3.2 Feed Support Truss 5.9-24 5.9.3.3 Fred Support Truss 5.9-24 5.9.3.4 Solar Array Panels and Support Trusses 5.9-36 5.9.3.5 Spacecraft Adapter 5.9-37 5.9.3.6 Structure Weight Summary 5.9-38 5.9.4 Separation and Deployment 5.9-38 5.9.4.1 Solar Panel Stowage and Deployment 5.9-38 5.9.4.2 Combined Purpose Antenna Deployment 5.9-34 5.9.4.3 Spacecraft/Booster Separation System 5.9-48 5.9.5.1 Introduction 5.9-48 5.9.5.1 Introduction 5.9-48 5.9.5.2 Launch Configuration Behavior 5.9-48 5.9.5.3 Effect of Structural Damping on Cone Angle 5.9-58				5.8.2.4	Solar Array Capability		5.8-11
5.8.2.7 Operational Flexibility				5.8.2.5	Battery Capability		5.8-20
5.8.2.8 Growth Capability.  5.8.22  5.8.3.1 Component Descriptions.  5.8.22  5.8.3.1 Solar Array.  5.8.22  5.8.3.2 Batteries.  5.8.29  5.8.3.3 Voltage Limiter  5.8.30  5.8.3.4 Battery Charge Regulator  5.8.31  5.8.3.5 PWM Regulator.  5.8.31  5.8.3.6 Inverter  5.8.32  5.8.3.7 Power Control Unit  5.8.32  5.8.3.8 Summary of Component Characteristics  5.8-32  5.9 Spacecraft Design  5.9.1 Introduction.  5.9-2  5.9.2.1 Launch Phase and Orbital Constraints  5.9-2  5.9.2.2 Coast Apogee Firing and Orbital Injection  Constraints  5.9-20  5.9.3.3 Spacecraft Structural Design  5.9.3.1 Earth Viewing Equipment Module.  5.9.3.2 Feed Support Truss  5.9-24  5.9.3.3 Aft Equipment Module  5.9.3.4 Solar Array Panels and Support Trusses  5.9.36 Structure Weight Summary  5.9.37  5.9.3.6 Structure Weight Summary  5.9.38  5.9.4.1 Solar Panel Stowage and Deployment  5.9.4.2 Combined Purpose Antenna Deployment  5.9.4.3 Spacecraft/Booster Separation System  5.9.4.5  5.9.5.1 Introduction  5.9-48  5.9.5.2 Launch Configuration Behavior  5.9-5.3  5.9-5.3 Effect of Structural Damping on Cone Angle  5.9.5.3 Effect of Structural Damping on Cone Angle				5.8.2.6	Subsystem Efficiency and Margins		5.8-21
5.8.3 Component Descriptions				5.8.2.7	Operational Flexibility	• •	5.8-21
5.8.3.1 Solar Array				5.8.2.8	Growth Capability		5.8-22
5.8.3.2 Batteries			5.8.3	Component	Descriptions	• •	5.8-22
5.8.3.2 Batteries				5.8.3.1	Solar Array		5.8-22
5.8.3.4       Battery Charge Regulator       5.8-31         5.8.3.5       PWM Regulator       5.8-31         5.8.3.6       Inverter       3.8-32         5.8.3.7       Power Control Unit       5.8-32         5.8.3.8       Summary of Component Characteristics       5.8-32         5.9       Spacecraft Design       5.9-1         5.9.1       Introduction       5.9-1         5.9.2       Launch Phase and Orbital Constraints       5.9-2         5.9.2.1       Launch Vehicle Constraints       5.9-2         5.9.2.2       Coast Apogee Firing and Orbital Injection       5.9-2         Constraints       5.9-20         5.9.3       Orbital Constraints       5.9-20         5.9.3       Spacecraft Structural Design       5.9-20         5.9.3       Spacecraft Structural Design       5.9-21         5.9.3.1       Earth Viewing Equipment Module       5.9-24         5.9.3.2       Feed Support Truss       5.9-29         5.9.3.3       Aft Equipment Module       5.9-36         5.9.3.4       Solar Array Panels and Support Trusses       5.9-36         5.9.3.5       Spacecraft Adapter       5.9-36         5.9.4.1       Solar Panel Stowage and Deployment       5.9-38				5.8.3.2			
5.8.3.5 PWM Regulator				5.8.3.3	Voltage Limiter	• (	5.8-30
5.8.3.5 PWM Regulator				5.8.3.4	Battery Charge Regulator		5.8-31
5.8.3.6 Inverter				5.8.3.5			
5.8.3.7 Power Control Unit				5.8.3.6			
5.8.3.8 Summary of Component Characteristics 5.8-32  5.9 Spacecraft Design				5.8.3.7	Power Control Unit	• (	
5.9       Spacecraft Design       5.9-1         5.9.1       Introduction       5.9-1         5.9.2       Launch Phase and Orbital Constraints       5.9-2         5.9.2.1       Launch Vehicle Constraints       5.9-2         5.9.2.2       Coast Apogee Firing and Orbital Injection       5.9-10         Constraints       5.9-20         5.9.3       Orbital Constraints       5.9-20         5.9.3       Spacecraft Structural Design       5.9-20         5.9.3.1       Earth Viewing Equipment Module       5.9-21         5.9.3.2       Feed Support Truss       5.9-29         5.9.3.3       Aft Equipment Module       5.9-34         5.9.3.4       Solar Array Panels and Support Trusses       5.9-36         5.9.3.5       Spacecraft Adapter       5.9-36         5.9.3.6       Structure Weight Summary       5.9-38         5.9.4       Solar Panel Stowage and Deployment       5.9-38         5.9.4.1       Solar Panel Stowage and Deployment       5.9-34         5.9.4.2       Combined Purpose Antenna Deployment       5.9-34         5.9.4.2       Combined Purpose Antenna Deployment       5.9-44         5.9.5.1       Introduction       5.9-48         5.9.5.2       Launch Configuration Beha				5.8.3.8	Summary of Component Characteristics .	• (	
5.9.2       Launch Phase and Orbital Constraints       5.9-2         5.9.2.1       Launch Vehicle Constraints       5.9-2         5.9.2.2       Coast Apogee Firing and Orbital Injection       5.9-10         5.9.2.3       Orbital Constraints       5.9-20         5.9.3       Spacecraft Structural Design       5.9-21         5.9.3.1       Earth Viewing Equipment Module       5.9-24         5.9.3.2       Feed Support Truss       5.9-29         5.9.3.3       Aft Equipment Module       5.9-34         5.9.3.4       Solar Array Panels and Support Trusses       5.9-36         5.9.3.5       Spacecraft Adapter       5.9-36         5.9.3.6       Structure Weight Summary       5.9-38         5.9.4.1       Solar Panel Stowage and Deployment       5.9-38         5.9.4.1       Solar Panel Stowage and Deployment       5.9-38         5.9.4.2       Combined Purpose Antenna Deployment       5.9-48         5.9.4.3       Spacecraft/ Booster Separation System       5.9-44         5.9.5.1       Introduction       5.9-48         5.9.5.2       Launch Configuration Behavior       5.9-48         5.9.5.3       Effect of Structural Damping on Cone Angle       5.9-53		5.9	Spaced	raft Design		• •	
5.9.2       Launch Phase and Orbital Constraints       5.9-2         5.9.2.1       Launch Vehicle Constraints       5.9-2         5.9.2.2       Coast Apogee Firing and Orbital Injection       5.9-10         5.9.2.3       Orbital Constraints       5.9-20         5.9.3       Spacecraft Structural Design       5.9-21         5.9.3.1       Earth Viewing Equipment Module       5.9-24         5.9.3.2       Feed Support Truss       5.9-29         5.9.3.3       Aft Equipment Module       5.9-34         5.9.3.4       Solar Array Panels and Support Trusses       5.9-36         5.9.3.5       Spacecraft Adapter       5.9-36         5.9.3.6       Structure Weight Summary       5.9-38         5.9.4.1       Solar Panel Stowage and Deployment       5.9-38         5.9.4.2       Combined Purpose Antenna Deployment       5.9-38         5.9.4.3       Spacecraft/ Booster Separation System       5.9-48         5.9.5.1       Introduction       5.9-48         5.9.5.2       Launch Configuration Behavior       5.9-48         5.9.5.3       Effect of Structural Damping on Cone Angle       5.9-53			5.9.1	Introduction	n		5,9-1
5.9.2.1 Launch Vehicle Constraints			5.9.2	Launch Pha	ase and Orbital Constraints		
5.9.2.2 Coast Apogee Firing and Orbital Injection Constraints							
Constraints				5.9.2.2			
5.9.2.3       Orbital Constraints       5.9-20         5.9.3       Spacecraft Structural Design       5.9-21         5.9.3.1       Earth Viewing Equipment Module       5.9-24         5.9.3.2       Feed Support Truss       5.9-29         5.9.3.3       Aft Equipment Module       5.9-34         5.9.3.4       Solar Array Panels and Support Trusses       5.9-36         5.9.3.5       Spacecraft Adapter       5.9-37         5.9.3.6       Structure Weight Summary       5.9-38         5.9.4       Separation and Deployment       5.9-38         5.9.4.1       Solar Panel Stowage and Deployment       5.9-38         5.9.4.2       Combined Purpose Antenna Deployment       5.9-44         5.9.4.3       Spacecraft/Booster Separation System       5.9-48         5.9.5.1       Introduction       5.9-48         5.9.5.2       Launch Configuration Behavior       5.9-48         5.9.5.3       Effect of Structural Damping on Cone Angle       5.9-53							5.9-10
5.9.3       Spacecraft Structural Design				5.9.2.3	Orbital Constraints		
5.9.3.1 Earth Viewing Equipment Module			5,9,3	Spacecraft			
5.9.3.2 Feed Support Truss					_		
5.9.3.3 Aft Equipment Module				5.9.3.2	<del>-</del>		
5.9.3.4 Solar Array Panels and Support Trusses				5.9.3.3	<del></del>		
5.9.3.5 Spacecraft Adapter				5.9.3.4			
5.9.3.6 Structure Weight Summary				5.9.3.5			
5.9.4 Separation and Deployment				5.9.3.6	-		
5.9.4.1 Solar Panel Stowage and Deployment			5.9.4	Separation	•		• 5.9 <b>-</b> 38
5.9.4.2 Combined Purpose Antenna Deployment					·		
5.9.4.3 Spacecraft/Booster Separation System				5.9.4.2	Combined Purpose Antenna Deployment .		
5.9.5       Structural Dynamic Considerations       5.9-48         5.9.5.1       Introduction       5.9-48         5.9.5.2       Launch Configuration Behavior       5.9-48         5.9.5.3       Effect of Structural Damping on Cone Angle       5.9-53				5.9.4.3		•	
5.9.5.1 Introduction			5.9.5	Structural			
5.9.5.2 Launch Configuration Behavior					-	•	
5.9.5.3 Effect of Structural Damping on Cone Angle 5.9-53							
1 mg						•	
				5.9.5.4	Orbital Configuration Behavior		5.9-5

Section									Page
	5.9.6	Thermal (	Control				_		5.9-58
		5.9.6.1	Summary of Selected Configuration						5.9-58
		5.9.6.2	Equipment Mounting	•	•	٠	•	•	5.0.50
			Company M. C	•	•	•	•	•	5.9-59
		5.9.6.3	Semipassive Temperature Control	•	•	•	•	•	5.9-59
		5.9.6.4	Passive Temperature Control		•	•		•	5.9-61
		5.9.6.5	Configuration Thermal Analysis.		•	•	•		5.9-62

### TABLE OF CONTENTS

### VOLUME I BOOK 2

Section						Page
6	SPA	CECRA	FT TRADEC	OFF AND ANALYSIS	•	6.1-1
	6.1	Introd	uction	• • • • • • • • • • • • • • • • • • • •		6.1-1
	6.2	Config	guration Sele	ection		6. 2-1
		6.2.1	Approach	to Configuration Selection	•	6. 2-1
		6.2.2	Launch Ve	hicle Considerations		6. 2-5
			6.2.2.1	Atlas/Agena-D Launch Vehicle	•	6.2-9
			6.2.2.2	TITAN III-C Launch Vehicle	•	6.2-10
			6.2.2.3	SLV3C/Centaur Launch Vehicle		6. 2-11
		6.2.3	Early Cone	ceptual Designs	•	6. 2-22
			6.2.3.1	First Stage Designs	•	6. 2-23
			6.2.3.2	Major Tradeoffs	•	6. 2-27
			6.2.3.3	Second Stage Designs	•	
		6.2.4		e Designs	•	6, 2-35
		6.2.5	Deployed (	Configuration	•	6. 2-41
			6.2.5.1	Structural Considerations	•	6. 2-48
			6.2.5.2	Equipment Module Deployment	3	6. 2-52
		6.2.6		Fixed Feed Configuration	•	6, 2-56
			6.2.6.1	Alternate Solar Panel Stowage Arrangement .	•	6, 2-66
			6.2.6.2	Aft Equipment Module Design	,	6, 2-68
			6.2.6.3	Apogee Motor Packaging Provisions.		6. 2-73
	6.3	Parabo	oloid Antenn	a		6, 2-73
				or Selected Reflector Concept	•	6.3-1
			6.3.1.1	Antenna Requirements	٠	6, 3-1
			6.3.1.2	Survey of Potential Reflector Concepts	٠	6.3-1
		6.3.2		dies of Selected Concept	۰	6.3-1
			6.3.2.1	Paraboloid Reflector Configuration	•	6.3-26
			6.3.2.2	Thermal Considerations	•	6.3-26
		6.3.3		alysis of Selected Configuration	•	6. 3-50
			6.3.3.1	Dogian Chitania	•	6.3-65
			6.3.3.2	Structural Analysis	٠	6. 3-65
			6.3.3.3		•	6.3-67
			6.3.3.4	Deployment Analysis	•	6.3-8
		6.3.4		Dynamic Analysis	•	6.3-99
		0.0.1	6.3.4.1	istortion Analysis	•	6.3-104
			6.3.4.2	Introduction	•	6. 3-104
			6.3.4.3	Thermal Analysis	•	6.3-104
		635		Structural Deformation	•	6.3-105
		0.0.0	REFERENCE TO TE	mance Analysis	٥	6.3-132
			6.3.5.1	Introduction.		6 3-132

Section					Page
			6.3.5.2	Feed Configuration Studies	• 6.3-136
			6.3.5.3	Selected Feed Configuration	• 6.3-144
			6.3.5.4	Monopulse	
			6.3.5.5	Beam Steering	• 6.3-147
			6.3.5.6	RF Loss Budget Cassegrain vs Prime Focus.	
			6.3.5.7	Additional Strut Loss	
			6.3.5.8	Thermal Distortion Loss	
			6.3.5.9	RF Loss Budget-Final	
			6.3 5.10	References for Section 6	
	C 4	Cuidas		1	
	6.4		Summary.	rol	
					6.4-1
		6.4.2	Tradeon A	nalysis	6.4-4
			6.4.2.1	Spacecraft Configuration Considerations	6.4-4
			6.4.2.2	Earth Sensor/Star Trackers	6.4-6
			6.4.2.3	Three Axis Control/Spin Stabilization During	
				Station Acquisition Sequence	6.4-8
			6.4.2.4	Polaris Star Sensor/Gyrocompassing	6.4-9
			6.4.2.5	Momentum Storage Devices	6.4-11
			6.4.2.6	On-Off/Proportional Flywheel Control	6.4-15
			6.4.2.7	Spacecraft Orientation During Vernier	
			<i>c</i> 4 9 0	Thrusting	6.4-16
		•	6.4.2.8	Yaw/Roll Axis Stabilization to the Sun	6.4-17
			6.4.2.9	Orientation Control/Stationkeeping Mass	
			0.40.40	Expulsion Subsystem.	6.4-18
			6.4.2.10	Accelerometer/Gryo for Coning Control	6.4 - 31
			6.4.2.11	Sattion Acquisition and Despin Mass	
			6.4.2.12	Expulsion Subsystem	6 <b>.</b> 4 <b>-</b> 34
		612	Design Ana	Spinup Motor	
		0.4.0	6.4.3.1		6 <b>.</b> 4 <b>-</b> 46
				Transfer Orbit Disturbance Torques	6.4-47
			6.4.3.2	On-Station Disturbance Torques	6.4 - 52
			6.4.3.3	Control Static and Dynamic Performance	
				Analysis	6.4-68
			6.4.3.4	Earth Pointing Error Analysis	6.4-113
	6.5	TT &C	Subsystem T	Tradeoffs and Analysis	6.5-1
				Band Communication Link	6, 5-1
		6.5.2	Tracking A	nalysis	6.5-3
		6.5.3	Antenna Co	nfiguration Tradeoff	6. 5-7
		6.5.4	Analysis of	Memory Requirements	
	6.6	Power			6.5-11
		6.6.1		Convironment Requirements	6. 6-1
			6.6.1.1	Trapped Radiation	6.6-1
			6.6.1.2	Colon Const. D. D. M.	6. 6-1
			6.6.1.3	Primary Galactic Cosmic Rays	6 <b>.</b> 6-2
			. 4 . 4 . 4 . 6 . 4	y Caractic Cosmic Rays	0 0 1

<u>Section</u>				Page
	6.6.2	Energy Sou	rce Selection	6. 6-5
	6.6.3	Array Conf	iguration Selection	6.6-6
		6.6.3.1	Array Location on Vehicle	6.6-6
		6.6.3.2	Array Configuration Studies	6.6-19
		6.6.3.3	Comparison of Four-Panel Configuration with	
			Two-Panel Configuration	6.6-30
	6.6.4	Array Desi		6.6-33
		6.6.4.1	Array Sizing and Performance	6, 6-33
		6.6.4.2	Solar Cell Selection	6. 6-33
		6.6.4.3	Solar Cell Characteristics	6.6-35
		6.6.4.4	Solar Cell Loss Analysis	6.6-35
		6.6.4.5	Solar Cell Radiation Degradation Analysis	6.6-38
		6.6.4.6	Cover Thickness Selection	6.6-40
		6.6.4.7	Launch Array Power Analysis	6, 6-42
	6.6.5	Batteries.	Lauren Array Fower Analysis.	6. 6-43
	0.0.0	6. 6. 5. 1	Requirements	
			•	6. 6-43
		6. 6. 5. 2	Selection of Battery Type	6, 6-43
		6, 6, 5, 3	Method of Sizing	6.6-44
		6. 6. 5. 4	Effect of Two Paddles Versus Four Paddles	6. 6-45
		6. 6. 5. 5	Effect of Load Timing on Batteries	6. 6-45
		6. 6. 5. 6	Battery Description	6.6-47
		6. 6. 5. 7	Battery Performance Summary	6. 6-47
	6.6.6		system Analysis	6. 6-50
		6.6.6.1	Power Distribution Selection (DC versus AC)	6.6-50
		6.6.6.2	Power Conditioning Equipment Selection	6.6-52
		6.6.6.3	Selected Power Subsystem Performance	6.6-61
	6. 6. 7	References		6. 0-66
6.7	Spaced	eraft Design		6. 7-1
	6.7.1	Structural	Analysis	6, 7-1
		6.7.1.1	Critical Loading	6. 7-2
		6.7.1.2	Preliminary Design Philosophy	6.7-3
		6.7.1.3	Methods of Analysis	6 <b>. 7-</b> 3
		6.7.1.4	Selected Configuration Design Rationale	
			and Tradeoffs	6. 7-5
	6.7.2	Separation	and Deployment	6. 7-48
		6.7.2.1	Design Criteria	6.7-48
		6.7.2.2	Deployment Mechanism Selection.	6. 7-48
		6.7.2.3	Spacecraft/Booster Separation System	6. 7 <b>-</b> 55
	6.7.3			6. 7-58
	0.1.3	6.7.3.1	Dynamics	6. 7-58
			Design Criteria	6. 7-59
		6.7.3.2	Dynamic Environment	
		6.7.3.3	Methods of Analysis	6. 7-61
		6.7.3.4	Configuration Selection Support Studies	6. 7-67

Section												Page
		6.7.4	Electronic	ackaging	•		٠	•	•	•	•	6 <b>. 7-</b> 88
			6.7.4.1	Design Criteria								6. 7-88
			6.7.4.2	Selected Configurations	۰	۰	٠	•	•		•	6. 7-89
			6.7.4.3	Alternate Approaches	•	۰	۰		۰		•	6.7-91
			6.7.4.4	Areas for Further Study	٥	•	۰	•	•	۰		6. 7-96
	6.8	Apoge	e Motor Sele	tion							۰	6, 8-1
										۰	•	6.8-1
		6.8.2		or Requirements								6.8-2
		6.8.3	Apogee Mo	or Selection - SLV-3A/Agen	a D			۰		۰		6.8-3
		6.8.4	Apogee Mo	or Selection - SLV-3C/Centa	aur	۰	۰					6.8-5
			6.8.4.1	Final Apogee Motor Selection							-	
				the SLV-3C/Centaur								6, 8-11
			6.8.4.2	Recommended Apogee Motor								
				Centaur Configuration								6 <b>,</b> 8 <b>-1</b> 3
			6.8.4.3	Surveyor Motor Developmen								6, 8-13

### TABLE OF CONTENTS

### VOLUME I

### воок з

ction		P
7 FL	IGHT DYNAMICS	7
7.1	Introduction	7
7.2	Reference Design Sequence of Events - Summary	7
	7.2.1 Launch Trajectory - General	7
	7.2.2 Booster/Launch Phase	7
	7.2.3 Initial/Acquisition Phase	7
7.3	Operating Longitude Evaluation	7
	Ascent Trajectory Selection	7
	7.4.1 Trajectory Influencing Parameters	7
	7.4.2 Launch Vehicle Constraints	7
	7.4.3 Trajectory Selection	7
7.5	Initial Acquisition Phase Analyses	7
	7.5.1 Spin-Up Motors	7
	7.5.2 Transfer Trajectory Analysis	7
	7.5.2.1 Plane Change Velocity Requirements	7
	7.5.2.2 Apogee Motor Payload Analysis	•
	7.5.2.3 Reference Design Orbit Characteristics	,
	7.5.3 Vernier Velocity Requirements	,
	7.5.3.1 Reference Design Vernier Velocity Requirements.	,
	7.5.3.2 Preliminary Velocity Requirements Analysis	7
	7.5.3.3 Injection Bias Analysis	,
	7.5.3.4 Despin	,
7.6	Initial Stabilization and Deployment	•
7.7	Synchronous Orbit Stationkeeping Requirements	'
	7.7.1 Dynamics	•
	7.7.1.1 Nominal Orbit	•
	7.7.1.2 Perturbations	•
	7.7.2 Velocity Requirements	1
	7.7.2.1 East-West	
	7.7.2.2 North-South	
	7.7.3 Tracking for Orbit Determination	
7.8	Operational System	
. • •	7.8.1 Launch and Parking Orbit	
	7.8.1.1 Atlas Flight Phase	
	7.8.1.2 Centaur Separation	
	7.8.1.3 Launch-to-Injection Operations	
	7.8.1.4 Perigee Burn	

Section				Page
			Transfer Orbit	7-71
			Vernier Maneuvers	7-73
		7.8.4	Despin, Deployment, and Initial Stabilization	7-74
			Final Station Acquisition	7-76
		7.8.6	Operational Systems Contingency Planning	7-76
8	EXF	ERIME	ENT OPERATIONAL PHASE SEQUENCE	8.1-1
	8.1	Genera	al	8.1-1
	8.2	Experi	iment Axes Reference	8, 2-1
	8.3	Parab	olic Antenna	8.3-1
		8.3.1	General Discussion	8. 3-1
		8.3.2	Technical Background of Measurements	8.3-2
			8.3.2.1 Introduction	8. 3-2
			8.3.2.2 Direction and Gain	8.3-2
		8.3.3	Selection of Parameters	8.3-7
			8.3.3.1 General	8.3-7
			8.3.3.2 In-Space Measurements	8.3-8
			8.3.3.3 Ground Testing	8.3-9
		8.3.4	In-Space Measurement Techniques	8.3-11
			8.3.4.1 Gain	8.3-11
			8.3.4.2 Antenna Geometry Measurements	8.3-12
			8.3.4.3 Boresight	8.3-13
		8.3.5	Experiments	8.3-19
			8.3.5.1 Listing of Experiments	8.3-19
			8.3.5.2 Basic Electrical Measurements	8, 3-25
			8.3.5.3 Basic Geometric Measurements	8, 3-33
			8.3.5.4 Supporting Electrical Measurements	8.3-37
		8.3.6	Derivation of Equipment Requirements	8.3-40
			8.3.6.1 Electrical Measurements Experiments Equipment.	8.3-40
			8.3.6.2 Geometric Measurement Experiment Equipment .	8.3-54
			8.3.6.3 Summary of Required Equipment	8.3-55
	8.4	Orient	tation Control System	8.4-1
		8.4.1	General Discussion	8.4-1
			Listing of Experiments	8.4-3
			Basic Experiments	8.4-5
			8.4.3.1 General	8.4-5
			8.4.3.2 Pointing Performance	8.4-5
			8.4.3.3 Tracking Performance	8.4-8
		8.4.4	Equipment Requirements	8.4-10
	8.5	Interfe	erometer	8.5-1
		8.5.1	General	8.5-1
			Listing of Experiments	8.5-2

Section			Page
		8.5.3 Basic Experiments	8.5-4
		8.5.3.1 General	8.5-4
		8.5.3.2 Experiment I-1 - Verification of Operation	8.5-5
		8.5.3.3 Experiments I-2 and I-3 - Internal Parameter	
		Measurements	8.5-7
		8.5.3.4 Experiment I-4 - Angle Error Measurement -	
		Medium Accuracy	8.5-10
		8.5.3.5 Experiment I-5 - Angle Error Measurement -	
		High Accuracy	8.5-12
		8.5.3.6 Experiment I-6 - Field of View	8.5 - 14
		8.5.3.7 Experiment I-8 - Angle Difference Measurement .	8.5-16
		8.5.3.8 Experiment I-11 - Spacecraft Pointing	8.5-18
		8.5.3.9 Experiment I-13 - System Life Verification	8.5-19
		8.5.3.10 Experiment I-18 - Thermal Cycle Monitoring	8.5-21
		8.5.4 Derivation of Equipment Requirements	8.5-23
	0 6	Phase-Steered Array Antenna	8.6-1
	8.0	8.6.1 General	8.6-1
		8.6.2 Technical Background of Measurements	8.6-1
		8.6.2.1 General	8.6-1
		8.6.2.2 Component Similarity	8.6-2
		8.6.2.3 Impedance Match	8.6-2
		8.6.2.4 Physical Geometry	8.6-3
		8.6.2.5 Radiation Characteristics	8.6-3
		8.6.3 Parameter Selection	8.6-4
		8.6.3.1 General	8.6-4
		8.6.3.2 Internal Parameters	8.6-5
		8.6.3.3 Gain	8.6-5
			8, 6-5
		8.6.3.4 Beam Pointing Direction	8.6-6
		8.6.4 Experiments	8.6-6
		8.6.4.1 List of Experiments	8.6-11
		8.6.4.2 Basic Electrical Measurements	8. 6-20
		8.6.5 Derivation of Equipment Requirements	8.7-1
	8.7	Supplementary Experiments	8.7-1
		8.7.1 General	8.7-1
		8.7.2 Prime Experiment Augmentation	8. 7-1
		8.7.2.1 Parabolic Antenna Geometric Instrumentation	
		8.7.2.2 Parabolic Antenna Ultra-Wide Band	8. 7-2
		Communications	8. 7-2
		8.7.2.3 Parabolic Antenna Side Lobe Measurement	
		8.7.2.4 Polarization Measurements from the Parabolic	8.7-2
		Antenna	8.7-3
		8.7.2.5 Monopulse Installation	V/6 F 4/

Section			Page
		8.7.2.6 Phase-Steered Array Monitoring	8.7-5
		8.7.2.7 Interferometer Yaw Axis Stabilization	8.7-5
		8.7.2.8 Synthetic Angle Generation	8.7-6
		8.7.2.9 Interferometer Transmit Mode	8.7-8
		8.7.3 Prime Experiment Applications	8.7-9
		8.7.3.1 High Data Rate Meteorological Sensor	8.7-9
		8.7.3.2 FM and TV Direct Broadcast	8. 7-13
		8.7.3.3 Navigation and Air and Ship Traffic Control	8. 7-21
		8.7.3.4 Communications with Low-Orbit Spacecraft	8. 7-22
		8.7.3.5 Multiple Access Communications Satellite	8. 7-2
		8.7.4 Passenger Experiments	8.7-20
		8.7.4.1 Millimeter Communications and Transmission	8. 7-2
		8.7.4.2 Laser Communications and Transmission	8.7-28
		8.7.4.3 Earth Radiation Measurements	8.7-28
	8 8	Operational System for Experiments	8.8-1
	0.0	8.8.1 General	8.8-1
		8.8.2 Experiment Operational System Requirements	8.8-2
		8. 8. 2. 1 Operational Flow	8.8-2
		8. 8. 2. 2 ATS-4 Ground Station Operational and Experi-	
		mental Capability Requirements	8.8-5
		8.8.3 Experiment Control	8.8-13
		8.8.4 Data Acquisition, Processing and Display	8.8-2
		8.8.5 Contingency Planning	8.8-2
		8.8.6 Reporting	8.8-2
9	SUP	PPORT OPERATIONS	9-1
	9.1	Introduction	9-1
		Summary	9-1
		Equipment Requirements	9-1
		Mechanical Support Equipment (MSE)	9-1
		9.4.1 Scope	9-1
		9.4.2 Study Approach	9-5
		9.4.3 Mechanical Support Concepts	9-5
		9.4.3.1 Vehicle Assembly and Handling	9-5
		9.4.3.2 Alignment Equipment and Deployed Antenna	
		Measurements	9-7
		9.4.3.3 Mass Properties, Spin Balance and Apogee	
		Thrust Vector Alignment	9-7
		9.4.3.4 Deployment	9-9
		9.4.3.5 Pneumatic and Fuel Servicing and Leak Testing.	9-10
		9.4.3.6 Vibration	9-10

ction																			]
			9.4.3.7	Struc	etura!	l Stati	с Те	st						•	_		_		
			9.4.3.8														•	•	
			9.4.3.9	_										·	•	•	•	•	
			9.4.3.10								•	•	•	•	•	•	•	•	
			9.4.3.11	Ther	mal-	Vacuu	m T	ests	١.	•	•	•	•	•	•	•	•	•	
			9.4.3.12															•	
			9.4.3.13	3 Tran	sport	ation	and	Shin	nir	10		•	•	•	•	•	•	•	
		9.4.4	Equipme	nt and	Con	nplexi	v Ar	onra	iss	-6 1]	•	•	•	•	•	•	•	•	
	9.5	Electr	ical Supp	ort Eq	uipm	ent (E	SE)	,		<b></b>	•	•	•	•	•	•	•	•	
		9.5.1	Scope.		•					•	•	•	•	•		•	•	•	٠
		9.5.2	Approach	h			•				•	•	•	•		•	•	•	
			9.5.2.1	Gene	ral .							•	•	•	•	•	•	•	
			9.5.2.2	Fail S	Safe.									•	•	•	•	•	
			9.5.2.3	Huma	ın Fa	ctors												•	
			9.5.2.4													•	•	•	
			9.5.2.5													•	•	•	
			9.5.2.6	Parts	١												•	•	
			9.5.2.7	Use o	f Te	lemeti	v Su	ıbsv	ste	ms	fo	r '	Tes	tin	σ.		•		
		9.5.3	Electrica	al Supp	ort (	Conce	ots					_			ъ.	•	•		
			9.5.3.1	Gener	ral .												•		
			9.5.3.2	Subsy	stem	Test	s.										•		
			9.5.3.3	Earth	Viev	ving E	quir	mei	nt I	Mod	dul	e 7	'es	ts		•	•	•	
			9.5.3.4	Aft E	quipr	nent N	Iodu	le T	'es	ting	ŗ				•		•		
			9.5.3.5	Syste	m Te	ests .			•		•				•		•	•	
			9.5.3.6	Therr	nal V	/acuur	n Te	sts								•	•		
			9.5.3.7	RF.													•		
			9.5.3.8	Pad					•										
		9.5.4	Equipme	nt List	t.				•										
9	9.6	Test F	acilities				•												
			Test Fac																
			Test Fac																
			9.6.2.1	Vibra	tion,	Deplo	oyed										•		
			9.6.2.2	Large	Ante	enna F	RF T	esti	ng						_	_			
9	9.7	Launch	Facilitie	es .											•		•		
		9.7.1	Mechanic	al Sup	port	Opera	ition	s .							•			•	
		9.7.2	Existing	Launc	h Fac	cilitie	s.		,										
9	8.6	Orbital	Support									_						•	
9	9.9	Softwar	e						,					•	•	•	•	•	

Appendix A.	Parabolic Reflector Feed Selection Charts	A-1
Appendix B.	Launch Window Restriction Due to Precession Control Sun Sensors	В-1
Appendix C.	Transfer Orbit Disturbance Torque Analysis	C-1
Appendix D.	On-Station Disturbance Torque Analysis	D-1
Appendix E.	Mathematical Model for Orientation Control Servo Analysis	E-1
Appendix F.	Stability Investigation and Pointing Error Analysis of the Three-Axis Star Tracker System	F-1
Appendix G.	Solar Array Computer Program	G-1
Appendix H.	Radiation Effects on Silicon Solar Cells	H-1
Appendix I.	Basic Design Data for Subsystem Comparison	I-1
Appendix J.	Coupling of Structural Flexibility with a Control System Feedback Loop .	<b>J</b> -1
Appendix K.	Coning Control	K-1
Appendix L.	Elements of Monopulse	L-1
Appendix M.	Plume Calculations for Walter Kidde Two-Pound Thrust Nozzle and for a Resistance Jet Ammonia Nozzle	M-i

### TABLE OF CONTENTS

# VOLUME II

#### PRELIMINARY PROGRAM PLAN

Section																Page
1	INT	RODUCT	non				•		•	•			•		•	1-1
2	PRO	JECT S	CHEDULE				•			•						2-1
	2.1	Introd	uction .								_					2-1
	2.2	Phase	d Project	Planning .									•	•	•	2-1
	2.3			e						•	·	•	•	•	•	2-12
	2.4			Utilization								•		•	•	2-14
	2.5			s						•	•	•	•	•		2-15
3	ENG			LOPMENT.				• •		•	•			•	•	3-1
	3.1	Introd	uation													
	3. 2			oblem Area		• •	•	• •	•	•	•	٠	•	•	•	3-1
	J. 2														•	3-1
		2 2 2	Spaggara	c Antenna D .ft Structure	everop	ment	•	• •						•	•	3-2
		J. 4. 4										•		•	•	3-3
			3.2.2.1 $3.2.2.2$	Ascent En								•			•	3-3
		2 2 2		Orbital Er Environme					•	•	•	•	٠	•	•	.5-4
		0.2.0	3. 2. 3. 1												•	3-4
			3. 2. 3. 1									•				3-5 3 - 5
		3 2 4		Aft Equipm al Power and	nent Mo d Dieta	oaute ibutio	• •	• •	•	•	•	•	•	•	•	3-5
		J. 4. T	3. 2. 4. 1	Batteries											•	3-6
			3. 2. 4. 1	Power Pro											•	3-6
		3 2 5		Sensing and					•							3-7 3-7
		0.2.0	3. 2. 5. 1	IR Sensor									-		-	
			3. 2. 5. 1	Ground St					•		•	•	•	٠	•	3-7
			0, 2, 0, 2	Interface		Orien	itatio	n Co								3-8
			3. 2. 5. 3	Attitude C	ontrol	Durin	g Init	tial	•	•	•	•	•	•	•	
				Acquis												3-9
			3.2.5.4	Long Life								•	•	•	•	3-10
			3.2.5.5	Orientatio				• •	•	•	•	•	•	•	•	
				Operati												3-10
		3.2.6	Telemetr	ry Tracking					•	•		•	•	•	•	3-10
		3.2.7	Propulsio						•	•	•	•	•	•	•	3-10
			3.2.7.1	Vernier P				•	•	•	•	•	•	•	•	5-11
			3.2.7.2	Stationkee				•	•	•	•	•	•	•	•	3-11
		3.2.8		nal Experim				•	•	•	•	•	•	•	•	3-12
			3. 2. 8. 1	Parabolic				ent	•	•	•	•	•	•	•	3-12
			3. 2. 8. 2	Phased Ste						•	•	•	•	•	•	3-15
			3. 2. 8. 3	Interferon					U111	•	•	•	•	•	•	3-16
			3. 2. 8. 4	Orientatio					•	•	•	•	•	•	•	3-18
			_				-L-C+11			•	•	•	•	•	•	0 10

Section		Pa	ıge
		3.2.9 Ground Station Operation and Data Analysis	20
		3. 2. 9. 1 Determination of Experiment Down Link	
		Equipment and Functions to be Provided at	
		Each ATS-4 Station	-20
		3. 2. 9. 2 Data Acquisition, Logistics, Merging,	
		Storage	-2(
		3. 2. 9. 3 Attitude Determination During Transfer Orbit,	
		Apogee Burn and Achievement of	
		Synchronous Orbit	-21
		3.2.9.4 Determination of Spacecraft and Experiment	
		Axes Orientation During Flight	-21
		3.2.10 Ground Handling, Test and Checkout Equipment	-22
	3.3	Davelonment Annacch	-22
			-23
		00000-1- / - 1	-23
		0 0 0 Th	ر. ز.2.
		0 0 4 0-1- 4	-24 -24
		0 0 5 04	 -24
			-25
		0 0 7 Th. 44 = t	5 25
			,
4	INTE	GRATED TEST	. 1
			•
	4.1	Principal Features	. }
	4.2	Component Test	
	4.3	Constant March	1
		4 9 1 Tm II and a Constant Constant	1
		4.3.2 Field Tests	. 11
		4 0 0 Therestone 4 m 4 m 1	-11
		4.3.3.1 Engineering Development Spacecraft 4-	-11
		4.3.3.2 Structural Dynamic Model	-12
		4 0 0 0 4 1111 1 0 1 1 2 - 1	-13
		4 0 0 4 - 1 11 1 1	-13
		4005 77744 3535	-13
		4 0 0 0 01 27 12	· 1:}
		4 0 0 5 77 74 1	13
		4 0 0 0 7/11/1 77 1	-14
	4.4	α	- 14
5	MAN	GEMENT AND SUPPORT ASPECTS	1
	5. 1	Project Control	- 1

5.1.1 Uniform Project Control       5-2         5.1.2 Schedule Integration       5-4         5.1.3 Project Visibility       5-4         5.1.4 Interface Control       5-5         5.1.5 Approach       5-6         5.2 Configuration Management       5-7         5.2.1 Introduction       5-7         5.2.2 Guidelines       5-8         5.2.2.1 Configuration Identification       5-5         5.2.2.2 Configuration Control       5-9         5.2.3 Requirements       5-10         5.2.4 Approach       5-10         5.2.5 Implementation       5-11         5.3.1 Introduction       5-12         5.3.2 Approach       5-13         5.3.3 Requirements       5-13         5.3.4 Critical Areas       5-13         5.3.4.1 Data Identification       5-13         5.3.4.2 Acquisition, Storage and Retrieval       5-14         5.3.4.3 Timely and Accurate Input/Output       5-15         5.4 Manufacturing/Facilities       5-16         5.4.2.1 In-Process Handling       5-16         5.4.2.2 Alignment of Critical Subsystems and Components       5-16         5.4.2.3 Solar Array Fabrication       5-20         5.5.1 Make or Buy       5-20         5.5.2 Source Selec	Section		Page
5.1.2 Schedule Integration       5-4         5.1.3 Project Visibility       5-4         5.1.4 Interface Control       5-5         5.1.5 Approach       5-6         5.2 Configuration Management       5-7         5.2.1 Introduction       5-7         5.2.2 Guidelines       5-8         5.2.2.1 Configuration Identification       5-9         5.2.2.2 Configuration Control       5-9         5.2.2.3 Requirements       5-10         5.2.4 Approach       5-10         5.2.5 Implementation       5-11         5.3 Introduction       5-12         5.3.1 Introduction       5-13         5.3.2 Approach       5-13         5.3.3 Requirements       5-13         5.3.4 Critical Areas       5-14         5.3.4 Timely and Accurate Input/Output       5-13         5.3.4.2 Acquisition, Storage and Retrieval       5-14         5.3.4.3 Timely and Accurate Input/Output       5-15         5.4 Manufacturing       5-16         5.4.2.1 In-Process Handling       5-16         5.4.2.2 Alignment of Critical Subsystems and Components       5-16         5.4.2.3 Solar Array Fabrication       5-20         5.5.1 Make or Buy       5-20         5.5.2 Source Selection			
5.1.2 Schedule Integration       5-4         5.1.3 Project Visibility       5-4         5.1.4 Interface Control       5-5         5.1.5 Approach       5-6         5.2 Configuration Management       5-7         5.2.1 Introduction       5-7         5.2.2 Guidelines       5-8         5.2.2.1 Configuration Identification       5-9         5.2.2.2 Configuration Control       5-9         5.2.2.3 Requirements       5-10         5.2.4 Approach       5-10         5.2.5 Implementation       5-11         5.3 Introduction       5-12         5.3.1 Introduction       5-13         5.3.2 Approach       5-13         5.3.3 Requirements       5-13         5.3.4 Critical Areas       5-14         5.3.4 Timely and Accurate Input/Output       5-13         5.3.4.2 Acquisition, Storage and Retrieval       5-14         5.3.4.3 Timely and Accurate Input/Output       5-15         5.4 Manufacturing       5-16         5.4.2.1 In-Process Handling       5-16         5.4.2.2 Alignment of Critical Subsystems and Components       5-16         5.4.2.3 Solar Array Fabrication       5-20         5.5.1 Make or Buy       5-20         5.5.2 Source Selection		5.1.1 Uniform Project Control	5-2
5.1.4 Interface Control       5-5         5.1,5 Approach       5-6         5.2 Configuration Management       5-7         5.2.1 Introduction       5-7         5.2.2 Guidelines       5-8         5.2.2.1 Configuration Identification       5-5         5.2.2.2 Configuration Accounting       5-9         5.2.2.3 Requirements       5-10         5.2.4 Approach       5-10         5.2.5 Implementation       5-11         5.3 Data Management       5-12         5.3.1 Introduction       5-12         5.3.2 Approach       5-13         5.3.3 Requirements       5-13         5.3.4 Ortical Areas       5-13         5.3.4 Critical Areas       5-14         5.3.4.2 Acquisition, Storage and Retrieval       5-14         5.3.4.3 Timely and Accurate Input/Output       5-15         5.3.5 Implementation       5-16         5.4.1 Introduction       5-16         5.4.2.1 In-Process Handling       5-16         5.4.2.2 Alignment of Critical Subsystems and Components       5-16         5.4.3 Facilities       5-20         5.5.1 Make or Buy       5-20         5.5.2 Source Selection       5-24         5.5.3 Subcontractor Management and Control       5-2		5.1.2 Schedule Integration	5-4
5.1,5 Approach       5-6         5.2 Configuration Management       5-7         5.2.1 Introduction       5-7         5.2.2 Guidelines       5-8         5.2, 2.1 Configuration Identification       5-9         5.2, 2.2 Configuration Control       5-9         5.2, 2.3 Requirements       5-10         5.2.4 Approach       5-10         5.2.5 Implementation       5-11         5.3 Data Management       5-12         5.3.1 Introduction       5-13         5.3.2 Approach       5-13         5.3.3 Requirements       5-13         5.3.4 Critical Areas       5-14         5.3.4.1 Data Identification       5-14         5.3.4.2 Acquisition, Storage and Retrieval       5-14         5.3.4.3 Timely and Accurate Input/Output       5-15         5.4 Manufacturing/Facilities       5-16         5.4.2.1 In-Process Handling       5-16         5.4.2.2 Alignment of Critical Subsystems and		5.1.3 Project Visibility	5-4
5.2       Configuration Management       5-7         5.2.1       Introduction       5-7         5.2.2       Guidelines       5-8         5.2.2.1       Configuration Identification       5-5         5.2.2.2       Configuration Accounting       5-9         5.2.2.3       Requirements       5-10         5.2.4       Approach       5-10         5.2.5       Implementation       5-11         5.3       Data Management       5-12         5.3.1       Introduction       5-12         5.3.2       Approach       5-13         5.3.3       Requirements       5-13         5.3.4       Critical Areas       5-13         5.3.4       Critical Areas       5-14         5.3.4.1       Data Identification       5-14         5.3.4.2       Acquisition, Storage and Retrieval       5-14         5.3.4.2       Acquisition, Storage and Retrieval       5-15         5.3.5       Implementation       5-15         5.4.1       Introduction       5-15         5.4.2       Manufacturing/Facilities       5-16         5.4.2.1       In-Process Handling       5-17         5.4.2.3       Solar Array Fabrication		5.1.4 Interface Control	5-5
5.2.1 Introduction       5-7         5.2.2 Guidelines       5-8         5.2.2.1 Configuration Identification       5-5         5.2.2.2 Configuration Control       5-9         5.2.2.3 Requirements       5-9         5.2.4 Approach       5-10         5.2.5 Implementation       5-11         5.3 Data Management       5-12         5.3.1 Introduction       5-12         5.3.2 Approach       5-13         5.3.3 Requirements       5-13         5.3.4 Critical Areas       5-14         5.3.4.1 Data Identification       5-14         5.3.4.2 Acquisition, Storage and Retrieval       5-14         5.3.5 Implementation       5-15         5.3.5 Implementation       5-15         5.4.2 Manufacturing/Facilities       5-16         5.4.2.1 In-Process Handling       5-16         5.4.2.2 Alignment of Critical Subsystems and       Components         5.4.2.3 Solar Array Fabrication       5-20         5.5.1 Make or Buy       5-20         5.5.2 Source Selection       5-24         5.5.3 Subcontractor Management and Control       5-26         5.6 Product Assurance       5-26		5.1.5 Approach	5-6
5.2. 2 Guidelines       5-8         5.2. 2. 1 Configuration Identification       5-5         5.2. 2. 2 Configuration Control       5-9         5.2. 3 Requirements       5-10         5.2. 4 Approach       5-10         5.2. 5 Implementation       5-11         5.3 Data Management       5-12         5.3. 1 Introduction       5-12         5.3. 2 Approach       5-13         5.3. 3 Requirements       5-13         5.3. 4 Critical Areas       5-14         5.3. 4. 1 Data Identification       5-14         5.3. 4. 2 Acquisition, Storage and Retrieval       5-14         5.3. 4. 3 Timely and Accurate Input/Output       5-15         5. 4. Manufacturing/Facilities       5-16         5. 4. 2 Manufacturing       5-16         5. 4. 2. 1 In-Process Handling       5-16         5. 4. 2. 2 Alignment of Critical Subsystems and Components       5-16         5. 4. 2. 3 Solar Array Fabrication       5-20         5. 5. 1 Make or Buy       5-20         5. 5. 1 Make or Buy       5-24         5. 5. 3 Subcontractor Management and Control       5-26         5. 6 Product Assurance       5-26	5.2	Configuration Management	5-7
5. 2, 2, 1       Configuration Identification       5-5         5. 2, 2, 2       Configuration Control       5-9         5. 2, 2, 3       Configuration Accounting       5-9         5. 2. 3       Requirements       5-10         5. 2. 4       Approach       5-10         5. 2. 5       Implementation       5-11         5. 3       Data Management       5-12         5. 3. 1       Introduction       5-12         5. 3. 2       Approach       5-13         5. 3. 3       Requirements       5-13         5. 3. 4       Critical Areas       5-14         5. 3. 4       Critical Areas       5-14         5. 3. 4. 1       Data Identification       5-14         5. 3. 4. 2       Acquisition, Storage and Retrieval       5-14         5. 3. 5       Implementation       5-15         5. 4       Manufacturing/Facilities       5-16         5. 4. 1       Introduction       5-16         5. 4. 2. 1       In-Process Handling       5-16         5. 4. 2. 1       In-Process Handling       5-17         5. 4. 2. 3       Solar Array Fabrication       5-20         5. 5       Procurement       5-20         5. 5. 1<		5.2.1 Introduction	5-7
5. 2. 2. 2       Configuration Control       5-9         5. 2. 2. 3       Configuration Accounting       5-9         5. 2. 3       Requirements       5-10         5. 2. 4       Approach       5-10         5. 2. 5       Implementation       5-11         5. 3       Data Management       5-12         5. 3. 1       Introduction       5-12         5. 3. 2       Approach       5-13         5. 3. 2       Approach       5-13         5. 3. 3       Requirements       5-13         5. 3. 4       Critical Areas       5-14         5. 3. 4. 1       Data Identification       5-14         5. 3. 4. 2       Acquisition, Storage and Retrieval       5-14         5. 3. 4. 3       Timely and Accurate Input/Output       5-15         5. 4       Manufacturing/Facilities       5-16         5. 4. 1       Introduction       5-16         5. 4. 2       Manufacturing       5-16         5. 4. 2. 1       In-Process Handling       5-16         5. 4. 2. 2       Alignment of Critical Subsystems and       Components       5-18         5. 4. 2. 3       Solar Array Fabrication       5-20         5. 5. 1       Make or Buy       5-2		5.2.2 Guidelines	5-8
5.2.2.2 Configuration Control       5-9         5.2.2.3 Configuration Accounting       5-9         5.2.4 Requirements       5-10         5.2.5 Implementation       5-11         5.3 Data Management       5-12         5.3.1 Introduction       5-12         5.3.2 Approach       5-13         5.3.3 Requirements       5-13         5.3.4 Critical Areas       5-14         5.3.4.1 Data Identification       5-14         5.3.4.2 Acquisition, Storage and Retrieval       5-14         5.3.4.3 Timely and Accurate Input/Output       5-15         5.4 Manufacturing/Facilities       5-16         5.4.1 Introduction       5-16         5.4.2 Manufacturing       5-16         5.4.2.1 In-Process Handling       5-17         5.4.2.2 Alignment of Critical Subsystems and       Components       5-18         5.4.2.3 Solar Array Fabrication       5-20         5.5.1 Make or Buy       5-24         5.5.2 Source Selection       5-24         5.5.3 Subcontractor Management and Control       5-26         5.6 Product Assurance       5-26		5.2.2.1 Configuration Identification	5-5
5.2.2.3 Configuration Accounting       5-9         5.2.3 Requirements       5-10         5.2.4 Approach       5-10         5.2.5 Implementation       5-11         5.3 Data Management       5-12         5.3.1 Introduction       5-12         5.3.2 Approach       5-13         5.3.3 Requirements       5-13         5.3.4 Critical Areas       5-14         5.3.4.1 Data Identification       5-14         5.3.4.2 Acquisition, Storage and Retrieval       5-14         5.3.4.3 Timely and Accurate Input/Output       5-15         5.4 Manufacturing/Facilities       5-16         5.4.1 Introduction       5-16         5.4.2 Manufacturing       5-16         5.4.2.1 In-Process Handling       5-16         5.4.2.2 Alignment of Critical Subsystems and		<del>-</del>	5-9
5. 2.4 Approach		<del>-</del>	5-9
5.2.5 Implementation		· ·	5-10
5.3 Data Management. 5-12 5.3.1 Introduction 5-12 5.3.2 Approach 5-13 5.3.3 Requirements 5-13 5.3.4 Critical Areas 5-14 5.3.4.1 Data Identification 5-14 5.3.4.2 Acquisition, Storage and Retrieval 5-14 5.3.4.3 Timely and Accurate Input/Output 5-15 5.3.5 Implementation 5-15 5.4 Manufacturing/Facilities 5-16 5.4.1 Introduction 5-16 5.4.2 Manufacturing 5-16 5.4.2.1 In-Process Handling 5-16 5.4.2.2 Alignment of Critical Subsystems and Components 5-18 5.4.3 Facilities 5-20 5.4.3 Facilities 5-20 5.5.1 Make or Buy 5-24 5.5.2 Source Selection 5-24 5.5.3 Subcontractor Management and Control 5-26 5.6 Product Assurance 5-26		5.2.4 Approach	5-10
5.3       Data Management       5-12         5.3.1       Introduction       5-12         5.3.2       Approach       5-13         5.3.3       Requirements       5-13         5.3.4       Critical Areas       5-14         5.3.4.1       Data Identification       5-14         5.3.4.2       Acquisition, Storage and Retrieval       5-14         5.3.4.3       Timely and Accurate Input/Output       5-15         5.3.5       Implementation       5-15         5.4       Manufacturing/Facilities       5-16         5.4.1       Introduction       5-16         5.4.2       Manufacturing       5-16         5.4.2.1       In-Process Handling       5-17         5.4.2.2       Alignment of Critical Subsystems and       Components       5-18         5.4.2.3       Solar Array Fabrication       5-20         5.5.1       Make or Buy       5-20         5.5.2       Source Selection       5-24         5.5.3       Subcontractor Management and Control       5-26         5.6       Product Assurance       5-26		• •	5-11
5. 3. 2 Approach	5.3	•	5-12
5.3.3 Requirements 5.3.4 Critical Areas 5-14 5.3.4 Critical Areas 5-14 5.3.4.1 Data Identification 5-14 5.3.4.2 Acquisition, Storage and Retrieval 5-15 5.3.5 Implementation 5-15 5.4 Manufacturing/Facilities 5-16 5.4.1 Introduction 5-16 5.4.2 Manufacturing 5-16 5.4.2 Manufacturing 5-16 5.4.2 Manufacturing 5-16 5.4.2.1 In-Process Handling 5-17 5.4.2.2 Alignment of Critical Subsystems and Components 5-18 5.4.2.3 Solar Array Fabrication 5-20 5.4.3 Facilities 5-20 5.5.1 Make or Buy 5-24 5.5.2 Source Selection 5-24 5.5.3 Subcontractor Management and Control 5-26 5.6 Product Assurance 5-26		5.3.1 Introduction	5-12
5.3.3 Requirements       5-43         5.3.4 Critical Areas       5-14         5.3.4.1 Data Identification       5-14         5.3.4.2 Acquisition, Storage and Retrieval       5-14         5.3.4.3 Timely and Accurate Input/Output       5-15         5.3.5 Implementation       5-15         5.4 Manufacturing/Facilities       5-16         5.4.1 Introduction       5-16         5.4.2 Manufacturing       5-16         5.4.2.1 In-Process Handling       5-17         5.4.2.2 Alignment of Critical Subsystems and       Components         Components       5-20         5.4.3 Facilities       5-20         5.5.1 Make or Buy       5-24         5.5.2 Source Selection       5-24         5.5.3 Subcontractor Management and Control       5-26         5.6 Product Assurance       5-26		5.3.2 Approach	5-13
5.3.4.1 Data Identification		• •	5-13
5. 3. 4. 2 Acquisition, Storage and Retrieval			5-14
5. 3. 4. 3 Timely and Accurate Input/Output		5.3.4.1 Data Identification	5 - 14
5. 3. 4. 3 Timely and Accurate Input/Output 5-15 5. 3. 5 Implementation 5-15 5. 4 Manufacturing/Facilities 5-16 5. 4. 1 Introduction 5-16 5. 4. 2 Manufacturing 5-16 5. 4. 2. 1 In-Process Handling 5-17 5. 4. 2. 2 Alignment of Critical Subsystems and Components 5-18 5. 4. 2. 3 Solar Array Fabrication 5-20 5. 4. 3 Facilities 5-20 5. 5 Procurement 5-20 5. 5 Procurement 5-20 5. 5 Source Selection 5-24 5. 5. 3 Subcontractor Management and Control 5-26 5. 6 Product Assurance 5-26			5-14
5. 3. 5 Implementation       5-15         5. 4 Manufacturing/Facilities       5-16         5. 4. 1 Introduction       5-16         5. 4. 2 Manufacturing       5-16         5. 4. 2. 1 In-Process Handling       5-17         5. 4. 2. 2 Alignment of Critical Subsystems and       Components         Components       5-18         5. 4. 2. 3 Solar Array Fabrication       5-20         5. 4. 3 Facilities       5-20         5. 5. 1 Make or Buy       5-24         5. 5. 2 Source Selection       5-24         5. 5. 3 Subcontractor Management and Control       5-26         5. 6 Product Assurance       5-26			5-15
5.4       Manufacturing/Facilities       5-16         5.4.1       Introduction       5-16         5.4.2       Manufacturing       5-16         5.4.2.1       In-Process Handling       5-17         5.4.2.2       Alignment of Critical Subsystems and         Components       5-18         5.4.2.3       Solar Array Fabrication       5-20         5.4.3       Facilities       5-20         5.5       Procurement       5-20         5.5.1       Make or Buy       5-24         5.5.2       Source Selection       5-24         5.5.3       Subcontractor Management and Control       5-26         5.6       Product Assurance       5-26		· · · · · · · · · · · · · · · · · · ·	5-15
5. 4.1 Introduction       5-16         5. 4.2 Manufacturing       5-16         5. 4. 2.1 In-Process Handling       5-17         5. 4. 2.2 Alignment of Critical Subsystems and       5-18         Components       5-20         5. 4. 2. 3 Solar Array Fabrication       5-20         5. 4. 3 Facilities       5-20         5. 5 Procurement       5-20         5. 5. 1 Make or Buy       5-24         5. 5. 2 Source Selection       5-24         5. 5. 3 Subcontractor Management and Control       5-26         5. 6 Product Assurance       5-26	5.4	·	5-16
5. 4. 2       Manufacturing        5-16         5. 4. 2. 1       In-Process Handling        5-17         5. 4. 2. 2       Alignment of Critical Subsystems and           Components            5. 4. 2. 3       Solar Array Fabrication           5. 4. 3       Facilities            5. 5       Procurement             5. 5. 1       Make or Buy              5. 5. 2       Source Selection		8	5-16
5. 4. 2. 1       In-Process Handling			5-16
5. 4. 2. 2 Alignment of Critical Subsystems and Components		<b>8</b>	
Components       5-18         5.4.2.3       Solar Array Fabrication       5-20         5.4.3       Facilities       5-20         5.5       Procurement       5-20         5.5.1       Make or Buy       5-24         5.5.2       Source Selection       5-24         5.5.3       Subcontractor Management and Control       5-26         5.6       Product Assurance       5-26			
5.4.2.3 Solar Array Fabrication       5-20         5.4.3 Facilities       5-20         5.5 Procurement       5-20         5.5.1 Make or Buy       5-24         5.5.2 Source Selection       5-24         5.5.3 Subcontractor Management and Control       5-26         5.6 Product Assurance       5-26			o-18
5. 4. 3 Facilities       5-20         5. 5 Procurement       5-20         5. 5. 1 Make or Buy       5-24         5. 5. 2 Source Selection       5-24         5. 5. 3 Subcontractor Management and Control       5-26         5. 6 Product Assurance       5-26		1	5-20
5.5 Procurement		· ·	
5.5.1 Make or Buy	5.5		
5.5.2 Source Selection	<b>3.</b> 3		
5.5.3 Subcontractor Management and Control			
5.6 Product Assurance			
	5.6		
	0.0		
5.6.2 Problems			
5. 6. 3 Approaches to Problem Solutions			

Section	Pag	ţе
	5.6.3.1 Long Life System Requirements	27
	5.6.3.2 Handling of Equipment	
	5.6.3.3 Traceability	29
	5.6.3.4 Subcontractor and Associate Contractor	
		30
5.7		31
		31
	3, 1, 1, 1 and 1 a	31
	5.7.1.2 Special Attention to the Long-Life Problem 5-	32
	01111 110611111 210111111111111111111111	32
	of the Contractor, Cabronier restaurant to the contract of the	33
5.8	Safety	35
	5.8.1 Introduction	35
	order in particular to the transfer of the tra	36
	5. 5. 5 Maioty 1 mm requirements	36
	of of 1 Hisbootatou Pariety 1 10B1am Reduit of the 1	37
	of the fraction of the first of	38
5.9	Parts Program	39
	5.9.1 Introduction	59
	5.9.2 Parts Policy	39
	5.9.3 Selection and Approval	40
	5.9.3.1 Approved Lists	4()
	5.9.3.2 Standardization of Parts, Materials, and	
	Processes	40
	5. 9. 3. 3 Qualification	41
	5.9.3.4 Nonstandard Parts Approval	41
	5. 9. 3. 5 Use of Approved Lists	42
	5.9.3.6 Parts and Materials Application Review 5-	43
	5.9.4 Parts Screening	-43
	5.9.4.1 Test Program	43
	5. 9. 4. 2 Typical Screening	14
	5.9.5 Specifications 5	-44
	5. 9. 5. 1 Standards	-44
	5. 9. 5. 2 New Drawings	-45
	5.9.5.3 Document Approval	-45
	5.9.6 Product Engineering Standards	-45
	5. 9. 6. 1 Design Standards 5	-45
	5. 9. 6. 2 Process Standards	-46
	5.9.7 Failure Reporting and Analysis	46
		17
	·	-47
		-47
		17

Section																					Page
6	COST		• • •	•		• .	•		•	•			•	•	•			•		•	6-1
	6.1	Cost E	Breakdow	n .			•														6-1
	6.2	Expen	diture Ra	te .					_					•	•	•	•	•	•	•	6-5
	6.3	Phasir	ng Alterna	ative	S		•	•	•	•	•	•	•	•	•	•	•	•	•	•	0-5
		6 9 1	Dane M	41-	<b>.</b>	٠, ٠	• •	•	•	•	•	•	•	•	•	•	•	•	•	•	6-5
		0.3.1	Four-M	ontn	Bre	akp	oint	٠	•	•	•	•	•	•	•	•					6-6
		6.3.2	Six-Mon	th B	real	kpoi:	nt .														6-6
		6.3.3	Eight-M	onth	Bre	eakn	oint									•	-	•	•	•	0 0
		634	Twolvo	Mont	-L				•	•	•	•	•	•	•	•	•	•	•	•	りーり
		0.0.7	Twelve-	MI OIL	ın E	srea.	kpoin	It	•	•	•	•	•	•	•	•		•			6-7
		6.3.5	Summar	У.			_	_			_										1. 6

#### LIST OF ILLUSTRATIONS

Figure		Page
5.2-1	ATS-4 Mission Sequence	5.2-4
5.3-1	Selected Configuration (Orbital View)	5.3 - 2
5.3-2	ATS-4 Selected Configuration, Inboard Profile and Orbital	
	Configuration	5.3-5
5.3-3	ATS-4 System Block Diagram	5.3-11
5.3-4	ATS-4 Payload Growth	5.3 <b>-3</b> 0
5.4-1	Petaline Rigid Reflector Configuration	5.4 <b>-3</b>
5.4-2	Deployment Drive Mechanism	5.4 - 5
5.4-3	Feed Configuration	5.4 - 7
5.4-4	Stowed Configuration	5.4 - 9
5.4-5	Reflector, Typical Sector	5.4-16
5.4-6	Panel Structure Composite	5.4-17
5.4-7	Deviation from True Contour	5.4-18
5.4-8	Configuration of Expanded Metal for RF Reflecting Material	5.4-19
5.4-9	Deployment Trusses	5.4-21
5.4-10	Interface Ring	5, 4-25
5.4-11	Three-Foot Diameter Demonstration Model	5, 4-32
5.4-12	Composite Feed on Earth Viewing Equipment Module	
5.4-13	Influence of Open Area on Antenna Design	
5.4-14	ATS-4 Parabolic Antenna Temperature Distribution	
5.4-15	Antenna Isotherms 39-90	
5.5-1	ATS-4 Guidance and Control Subsystem Block Diagram	
5.5-2	Spacecraft Configuration Station Acquisition	
5.5-3	Coning and Precession Control	
5.5-4	Principle of Orientation Measurement	
5.5-5	Sun Sensor	
5.5-6	Rhumb Line Precession	
5.5-7	ATS-4 Reference Design: Antenna Half-Beam Angle During	
0.0 .	Transfer Orbit	5.5-22
5.5-8	Impulse Requirement versus Spin Rate	
5.5-9	Sun Acquisition	
5.5-10	ATS-4 Configuration-Orientation Control	
5.5-11	On-Station Orientation Control	
5.5-12	Integrated Stationkeeping-Wheel Unloading Mass Expulsion	
0.0-12	System Control Logic	5, 5-39
5.5-13	Thrust and Impulse Required for East-West Station Change	
5.5-14	Spin Sun Sensor Output	
5.5-15	Polarized RF Antenna.	
5.5-16	Pulse Lengths for Various RPM's and 9's	
5.5-17		
	Effect on I <sub>sp</sub> for Various Pulse Widths for Hydrazine	
5.5-18	Radial Impulse Efficiency.	
5.5 - 19	Station Acquisition System Schematic	5.5-56

Figure		Page
5.5-20	RAPS Rate Mode Total Uncertainty Limits	5.5-59
5.5-21	Miniature Rate Integrating Gyro	
5.5-22	Director, Cone Angle Sun Sensor, Coarse Eye Assembly	5.5-62
5.5-23	Control Axes Coarse Sun Sensor Set Relative Response	0.00
	Characteristic	5.5-62
5.5-24	Single Eye Output versus Angle Characteristic	5.5-63
5.5-25	Acquisition Scan Pattern	5.5-65
5.5-26	Possible Tracking Scan Patterns	5.5-65
5.5-27	OAO Flywheel Cross Section	5.5-71
5.5-28	General Electric Resistance Jet System	5.5-74
5.5-29	Liquid Ammonia, Zero-g Storage Tank Schematic	5.5-75
5.5-30	Polaris Sensor View Angles	5.5-83
5.5-31	Pitch and Roll Sun Sensors Fields of View	5.5-84
5.5-32	Station Acquisition and Yaw Sun Sensor Fields of View	5.5-64 5.5-85
5.6-1	Large Parabolic Antenna Experiment Subsystem	5.6-7
5.6-2	Typical Receiver	5.6-9
5.6-3	Typical Transmitter	5.6-9
5.6-4	Relation of Incident Signal to Interferometer Antennas	5.6-17
5.6-5	Phase Comparison System	5.6-19
5.6-6	Phase Diagram for $\Sigma$ - $\Delta$ System	5.6-19
5.6-7	$\Sigma$ - $\Delta$ System	5.6-19
5.6-8	Pilot Tone Concept	5.6-21
5.6-9	Antenna Location on Cannister	5.6-22
5.6-10	ATS-4 Interferometer System, Block Diagram	5.6-23
5.6-11	System Block Diagram	5.6-30
5.7-1	TT&C Subsystem Block Diagram Reference Design	5.7-6
5.7-2	Goddard R&R S-Band Transponder	5.7-7
5.7-3	Command Decoder, Functional Block Diagram	5.7-8
5.7-4	Relay Logic	5.7-10
5.7-5	Typical Main Frame	5.7-10
5.7-6	ATS-4 Reference Design: Antenna Half-Beam Angle During	0.1-14
	Transfer Orbit	5.7-17
5.7-7	Half-Beam Angle Definition	5.7-17
5.7-8	ATS-4 Reference Design: Antenna Half-Beam Angle During	0.1-11
	Vernier Maneuvers While in Synchronous Orbit	5.7-18
5.7-9	Antenna Coverage	5.7-19
5.7-10	Antenna Switching Reference Configuration	5.7-19
5. 7-11	Antenna Design	5. 7-20 5. 7-21
5.7-12	TT&C Block Diagram, Redundant Configuration	5. 7-21 5. 7-29
5.7-13	Antenna Switching, Redundant Configuration	7 - 01
	The state of the s	0.1-31

Figure		Page
5.8-1	Load Power Requirements During Launch Transfer Orbit	<b>5.</b> 8−2
5.8-2	Load Power Requirements During Near-Synchronous Orbit	
	Vernier Maneuvers	5.8-2
5.8-3	ATS-4 Reference Design Load Requirements	5.8 - 4
5.8 - 4	Power Subsystem, Block Diagram	5.8-9
5.8-5	Solar Array Power	5.8-12
5.8-6	Daily Average Array Power versus Time in Orbit (For Equinox and	
	Summer Solstice Orbits)	5.8-13
5.8-7	End-of-Life Array Power for Equinox Orbits	5.8-14
5.8-8	End-of-Life Array Power for Summer Solstice Orbit	5.8-15
5.8-9	Solar Array Power Capability of Loads for Equinox Orbits	5.8-16
5.8-10	Solar Array Power Capability of Loads for Summer Solstice Orbits .	5.8 - 16
5.8-11	Solar Array V-I Curves	5.8-17
5.8-12	Solar Array Output During Stowed Launch Spin Mode	5.8-19
5.8-13	Solar Array Power Capability at Loads During Stowed Launch	<b>5</b> 6 00
E 0 14	Spin Mode	5.8-20
5.8-14	Y-Axis Panels Area Growth Capability	5.8-22
5.8-15	ATS-4 Solar Cell Arrangements	5.8-25
5.9-1	Inboard Profile and Orbital Configuration	5, 9-3
5.9-2	Static and Dynamic Envelope	5.9 - 7
5.9-3	Launch Availability versus Limit Bending Moment	5, 9-10
5.9-4	Nozzle Locations and Plume Details	5.9-11
5.9-5	Delta Motor (TE-364-3)	5.9-14
5.9-6	Maximum Expected Outside Surface Temperature versus	
F 0 F	Time for TE-M-364-4-3	5.9-15
5.9-7	TE-M-364-3 Altitude Thrust and Chamber Pressure versus Time	5.9-17
5.9-8	G-Loading Versus Time During Apogee Burn	5.9-17
5.9-9	Thrust and Chamber Pressure versus Time, Motor B	5.9-19
5.9-10	Relation of Major Structural Elements of Selected Configuration	5.9-25
5.9-11	Truss Tube End Design Concept	5, 9-31
5.9-12	Solar Panel Latching	5.9-41
5.9-13	Separation Nut Operation	5, 9-47
5.9-14	Response of Upper Mass (Mass 1) versus First Mode Shape	<b>5.9-</b> 50
5.9-15	Typical Shutter Assembly	5.9-59
5.9-16	Typical Shutter System Characteristics	5.9-60
5.9 - 17	Earth Viewing Equipment Module	5.9-64
5.9-18	EVM Panel Temperature Distribution ( <sup>O</sup> R) Based on Continuous	
	Experiment Operation	5.9 - 66
5.9-19	EVM Panel 4 Transient Thermal Performance	5.9-67
5.9-20	Alt Equipment Module Overall Component Installation	5.9-68
5.9-21	AFT Equipment Module	5,9-69
5.9 - 22	AEM Panel Temperature Distribution (OR)	5.9-74
5.9-23	Truss Nodal Designation	5,9-73

Figure		Page
5.9-24	Transient Strut Temperature Profile ( ${}^{\circ}$ R), $\alpha/\epsilon = 1$	5.9-75
5.9-25	Transient Strut Temperature Profile (OR), $\alpha/\epsilon = 1$	5.9-76
5.9-26	Transient Strut Temperature Profile ( ${}^{O}$ R), $\alpha/\epsilon = 2$	5.9 - 76
5.9-27	Transient Strut Temperature Profile ( ${}^{O}R$ ), $\alpha/\epsilon = 2$	5.9-77
5.9-28	Transient Strut Temperature Profile (OR), $\alpha/\epsilon = 3$	5.9-77
5.9-29	Transient Strut Temperature Profile ( ${}^{\circ}$ R), $\alpha/\epsilon = 3$	5.9-78
5.9-30	Maximum Solar Flux Distribution During Equinox	<b>5.9-</b> 80
5.9-31	Maximum Solar Flux Distribution During Summer Solstice	5.9-81
5. 9-32	Maximum Solar Flux Distribution for Inclined Paddles	5, 9-82
5.9-33	Average Solar Paddle Temperature for the Antenna-Mounted	
	Four-Paddle Spacecraft	5 <b>. 9-</b> 83
5.9-34	Absorbed Free Molecule Heat Flux for Parking Orbit of	
	80 Nautical Miles	5.9-85
5.9-35	Absorbed Free Molecule Heat Flux for Parking Orbit of	
	90 Nautical Miles	5.9-85
5.9-36	Absorbed Free Molecule Heat Flux for Parking Orbit of	
	100 Nautical Miles	5.9-85
6.2-1	Basic Spacecraft Arrangements Used in Configuration Tradeoff	
0.2.1	Studies	6.2-3
6.2-2	Candidate Launch Vehicles and Early Conceptual Approaches.	6, 2-7
6.2-3	Launch Availability versus Limit Bending Moment	6,2-15
6.2-3	Launch Availability versus Engine Deflection	6.2-10
6.2-4	Static and Dynamic Envelope	6.2-17
6.2-6	First Stage Design, Split Module Concept	6,2-28
6.2-7	First Stage Design, Single Module Concept.	6.2-25
6.2-8	First Stage Design, Deployed Phased Array Concept	6.2-29
6.2-9	Star Tracker System for Orientation Control, View Angles	
6.2-10	Polaris Tracker System for Orientation Control, View Angles	
6.2-11	Second Stage Design, Phased Array Concept	
6.2-12	Second Stage Design, Deployed Feed Concept	6, 2-38
6.2-13	Third Stage Design, Tandem Concept	6.2-43
6.2-14	Third Stage Design, Deployed Phased Array Concept	6.2-4
6.2-15	Deployed Configuration	
6.2-16	Structural Load Paths	
6.2 - 17	Electrically Powered Deployment System	
6.2-18	Mechanically Powered Deployment System	
6.2-19	Alternate Fixed Feed Design, Extended Surveyor Apogee Motor	
6.2-20	Alternate Fixed Feed Design, Antares I Apogee Motor	
6.3-1	Wire-Grid Structure	
6.3-2	Wire-Grid Structural Member	
6.3-3	Tolerance Limitation of Mesh Attachment Method	
6.3-4	Solar Collector Orbital Sequence	

Figure		Page
6.3-5	Chemically Rigidized Reflector (Two-Foot Model)	6.3-9
6.3 - 6	Mirror-Supported by Rigid Foam (44.5-Foot Model)	6.3-9
6.3-7	Cross Section of Rigidized Solar Concentrator	6.3-10
6.3-8	Solar Concentrator (Initial and Final Fabrication Phases)	6.3-1
6.3-9	Stretched-Screen Reflector Surface Contour Accuracy	6.3-12
6.3-10	Thermal Deflection Comparison	6.3-13
6.3-11	Design with Cables Behind Reflector Surface	6.3-14
6.3-12	Swirlabola Antenna	6.3-14
6.3-13	Deployment of a Petal Antenna	6.3-15
6.3-14	Aluminum-Sandwich Frame Member	6.3-18
6.3-15	Typical Sector of Petal Lattice Pattern	
6.3-16	Ultimate Tensile Strength versus Temperature for Aluminum and	6, 3-27
6.3-17	Titanium	
6.3-18	Yield Strength versus Temperature for Aluminum and Titanium Modulus of Elasticity versus Temperature for Aluminum and Titanium	6, 3-32
6.3-19		6.3-33
0.0-15	Coefficient of Thermal Expansion versus Temperature for Aluminum	
6.3-20	and Titanium	6.3 - 33
0.0-20	Possible Configuration of Expanded Metal for RF Reflecting Material	
6.3-21		6.3-35
6.3-22	Reverse Folding Pattern, Triangular Petals Folded Outward	6.3-41
6.3-23	Deployment Scheme  Reverse Folding Detterm Triangular Details Division in the Publishing Details of the Publishing Details	6.3 - 45
6.3-24	Reverse Folding Pattern, Triangular Petals Folded Radially Outward.	6.3 - 51
6.3-25	Reverse Folding Pattern, Triangular Petals Folded Towards Center.	6.3-51
6.3-26	Causes of Thermal Deflections	6.3 <b>-5</b> 2
6.3-20		6.3-54
6.3-28	Internal Geometry Effects - Antenna Blockage	6.3-54
6.3-29	Two-Node Thermal Model	
6.3-30	One-Dimensional Heat Transfer	6.3-59
6.3-31	Analytical Model	6.3 - 59
6.3-32	Average Antenna Temperature	6.3-60
6.3-33	Temperature Differentials Through the Thickness	6.3 - 61
6.3-34	Temperature Differentials Tip-to-Tip	6.3-62
6.3-35	Isotherms for Solid and Open And	6.3-63
6.3-36	Isotherms for Solid and Open Antenna at 90-Degree Orbital Position .	6.3 - 64
6.3-37	Folded Reflector Load Distribution and Geometry.	6.3-69
6.3-38	Radial Petal Member, Typical Section	6.3 - 70
	Approximate Loading of a Beam	6.3 - 75
6.3-39	Computer Loads Printout, Stress Analysis and Margin of	
e o an	Safety Calculation	6.3-77
6.3-40	Computer Loads Printout, Stress Analysis, and Margin of Safety	
	for One of Six Members Common to Truss Point 89	6.3 - 79

Figure		Page
6.3-41	Computer Loads Printout, Stress Analysis, and Margin of Safety	
	for One of Six Members Common to Truss Point 89	6.3-80
6.3-42	Computer Loads Printout, Stress Analysis, and Margin of Safety	
	for One of Six Members Common to Truss Point 89	6.3-81
6.3-43	Computer Loads Printout, Stress Analysis, and Margin of Safety	
	for One of Six Members Common to Truss Point 89	6.3-82
6.3 - 44	Computer Loads Printout, Stress Analysis, and Margin of Safety	
	for One of Six Members Common to Truss Point 89	6.3-83
6.3-45	Computer Loads Printout, Stress Analysis, and Margin of Safety	
	for One of Six Members Common to Truss Point 89	6.3-84
6.3-46	Member Loads at Joint 89	6.3-85
6.3-47	Model Used for Face Sheet - Core Thermal Compatibility Analysis	6.3-85
6.3-48	Truss Members	6.3-92
6.3 - 49	Two-Node Diameter Mode of Vibration	6.3-100
6.3-50	45-Degree Sector of Antenna Representing Overhanging Beam on Two	
	Supports	6.3-100
6.3 - 51	Antenna Isotherms 39-90	6.3-106
6.3-52	Antenna Isotherms 39-0	6.3-106
6.3 - 53	Antenna Isotherms 39-45	6.3-106
6.3 - 54	Antenna Isotherms 39-135	6.3-106
6.3-55	Antenna Isotherms 39-180	6.3-106
6.3 - 56	Deformed Shape at Below Ambient Temperatures (Free Hub,	
	No Deployment Trusses)	6.3-111
6.3 - 57	Deformed Shape at Below Ambient Temperature (Fixed Hub,	
	No Deployment Trusses)	6.3-111
6.3 - 58	Structural Simulation for Digital Computer Program	6.3-114
6.3 - 59	Computer-Drawn Schematic (or a Structural Antenna Simulation)	6.3-115
6.3-60	Contour Deflection for Fixed Hub	6.3-118
6.3-61	Contour Deflection for Free Hub	6.3-118
6.3-62	Antenna Deflections Due to Temperature Gradients, Displacements	
	of Radial Members $\theta = 180$ Degrees	6.3-119
6.3-63	Antenna Deflections Due to Temperature Gradients, Displacements	
	of Radial Members $\theta = 160$ Degrees	6.3-119
6.3-64	Antenna Deflections Due to Temperature Gradients, Displacements	
	of Radial Members $\theta = 140$ Degrees	6.3-120
6.3-65	Antenna Deflections Due to Temperature Gradients, Displacements	
	of Radial Members $\theta = 120$ Degrees	6.3-120
6.3 - 66	Antenna Deflections Due to Temperature Gradients, Displacements	
	of Radial Members θ 100 Degrees	6.3-121
6.3-67	Case 39-90. Deviation Plot (Symmetrical about Centerline)	6.3-122
6.3-68	Truss Geometry and Nomenclature used for Feed Distortion Analysis.	6.3-130
6.3-69	0.3 f D Geometry	6.3-132
6.3 - 70	0.4 f/D Geometry	6.3-133

Figure		Page
6.3-71	0.5 f/D Geometry	6.3-133
6.3 - 72	Cassegrain Antenna Nomenclature	6.3-135
6.3-73	Subreflector Blocking Gain Loss	6.3-136
6.3 - 74	Subreflector Included Angle versus 2f/d for 30-Foot Diameter	
	Parabola	6.3-136
6.3-75	Horn Aperture and Length versus Secondary Focus H, $F/D = 0.3$	6.3-137
6.3-76	Horn Aperture and Length versus Secondary Focus H, $F/D = 0.4$	6.3-137
6.3-77	Horn Aperture and Length versus Secondary Focus H, $F/D = 0.5$	6.3-138
6.3-78	Syncom SHF Feed Patterns	6.3-148
6.3-79	Feed Configuration	6.3-148
6.3-80	Gain Degradation versus Scan Angle	6.3-149
6.3-81	Gain Performance for Scanning Scheme	6.3-150
6.3-82	Loci of Best Azimuth Focus for Various Elevation Angles $\theta$	6.3-151
6.3-83	Comparison of Point Source and Line Source E-Plane Patterns,	0.0 101
	15-Degree Steering	6.3-151
6.3-84	Coma Coefficient versus Scan Angle	6.3-153
6.3-85	Subreflector Grid Sizes	6.3-158
6.3-86	Strut Model Configuration	6.3-159
6.3-87	Three-V Strut Model Configuration	6.3-159
6.3-88	Four-Strut Model	6.3-160
6.3-89	Three V Struts on 2-Foot Diameter Circle	6.3-160
6.3-90	Three V Struts on 54-Inch Diameter Feed Circle	6.3-161
6.3-91	450-Foot Test Range, From Source	6.3-161
6.3-92	Measured Patterns	6.3-163
6.3-93	Case 39-90, Deviation Plot (Symmetrical About Centerline)	6.3-171
6.4-1	Star Tracker Field of View Requirements	6.4-7
6.4-2	Antenna Half-Beam Angle During Vernier Maneuvers During	<b>3.</b> L 1
J. 1 2	Synchronous Orbit	6.4-17
6.4-3	Data for GE Resistance Jet	
6.4-4	Resistance Jet Stationkeeping/Orientation Control Subsystem (GE)	
6.4-5	Propellant Weight versus Total Impuse at 1800°F (GE System)	
6.4-6	Total System Weight versus Total Impulse (GE System)	6.4-23
6.4-7	Mollier Chart of Properties of Ammonia	6.4-25
6.4-8	AVCO Resistance Jet Subsystem	6.4-27
6.4-9	Propellant Weight versus Total Impulse (I <sub>sp</sub> = 150 sec),	
0 4 10	AVCO System	6.4-28
6.4-10	Total System Weight versus Total Impulse (AVCO System)	6.4-28
6.4-11	GE Resistance Jet and AVCO Resistance Jet Operating Temperatures.	6.4-30
6.4-12	Coning Control Sensor Location	6,4-33
6.4-13	Regulated and Blowdown Monopropellant System	6.4-37
6.4 - 14	Bipropellant System Schematic	6.4 - 40
6.4 - 15	Total Impulse for Various Spin Rates and Ir/r	6.4 - 43

Figure		Page
6.4-16	Candidate Spinup Motors	6.4-45
6.4-17	ATS-4 Spacecraft Configuration	6.4 - 48
6.4-18	X <sub>B</sub> and Y <sub>B</sub> Components of Aerodynamic Torque	6.4 - 50
6.4-19	$X_B$ and $Y_B$ Components of Magnetic Torque	6.4 - 51
6.4-20	$X_B$ and $Y_B$ Components of Gravity Gradient Torque	6.4 - 53
6.4-21	Assumed Configuration for Disturbance Torques	6.4 - 56
6.4-22	Disturbance Torque Profile (Yaw Axis Pointed to Local Vertical)	6.4 - 57
6.4-23	Disturbance Torque Profile (Yaw Axis Pointed to 0° Pitch, 8.7° Roll).	6.4-58
6.4-24	Disturbance Torque Profile (Yaw Axis Pointed to Rosman Station)	6.4-59
6.4-25	Disturbance Torque Profile (Yaw Axis Pointed to Mojave Station)	6.4-60
6.4-26	Flywheel Momentum Profile (Yaw Axis Pointed to Local Vertical)	6.4 - 62
6.4-27	Flywheel Momentum Profile (Yaw Axis Pointed to 0° Pitch, 8.7° Roll).	6.4 - 63
6.4-28	Flywheel Momentum Profile, Autumnal Equinox, (Yaw Axis	
	Pointed to Rosman Station)	6.4-65
6.4-29	Flywheel Momentum Profile (Yaw Axis Pointed to Mojave Station)	6.4-67
6.4-30	Locus of Spin Axis After Booster Separation	6.4 - 71
6.4-31	Coning Damper	6.4 - 72
6.4-32	Thruster Efficiency versus Pulse Width	6.4 - 77
6.4-33	Apogee Motor Burn	6.4-81
6.4-34	Initial Stabilization Pitch Axis	6.4 - 84
6.4-35	Sun Stabilization System, Block Diagram	6.4-85
6.4-36	Gyroscopic Torques	
6.4-37	Attitude and Sun Sensor Geometry	6.4 - 87
6.4-38	Phase Plane Diagram	6.4-90
6.4-39	Earth Stabilization Roll Axis, El	
6.4-40	Earth Stabilization Pitch Axis, E2	
6.4-41	Earth Stabilization Roll Axis, E3	6.4-93
6.4-42	Earth Stabilization Pitch Axis, E4	6.4 - 93
6.4-43	Earth and Star Stabilization System	
6.4-44	Nonlinear Flywheel	6.4 - 95
6.4-45	Velocity-Momentum Transfer Function for Rigid Vehicles with	
	Flexible Appendages	6.4 - 95
6.4-46	Attitude Geometry	6.4 - 97
6.4-47	Earth Scanner Geometry	6.4-98
6.4-48	Flywheel Unloading Jet Controller	6.4 - 99
6.4-49	Signal Processing Null	6.4-100
6.4-50	Open Loop Frequency Response	6.4-100
6.4-51	Sun Sensor Geometry for Star Stabilization	6.4-10
6.4-52	Primary Pointing System, Block Diagram	6.4-10
6.4-53	Roll Axis Pointing, P2	6.4-10
6.4-54	Pitch Axis Pointing, P5	
6.4-55	Yaw Axis Pointing, P8	

Figure		Page
6.4-56	Roll Axis Pointing, P1	6.4-106
6.4-57	Pitch Axis Pointing, P4	6.4-106
6.4 - 58	Yaw Axis Pointing, P7	6.4-106
6.4 - 59	Roll Axis Pointing, P3	6.4-107
6.4-60	Pitch Axis Pointing, P6	6.4-107
6.4-61	Roll Axis Slew, S1	6.4-108
6.4 - 62	Roll Axis Slew, S2	6.4-108
6.4-63	Roll Axis Slew, S3	6.4-108
6.4-64	Pitch Axis Slew, S4	6.4-108
6.4-65	Roll/Pitch Axis Slew, Yaw Axis, S5	6.4-109
6.4-66	Gravity Gradient Rod, Roll Axis Slew, S6	6.4-109
6.4 - 67	Roll Axis Track, T6	6.4-111
6.4-68	Roll Axis Track, T1	6.4-111
6.4-69	Roll Axis Track, T2	6.4-111
6.4-70	Roll Axis Track, T3	6.4-112
6.4-71	Pitch Axis Track, T4	6.4-112
6.4 - 72	Roll Axis Track, T5	6.4-112
6.5-1	Results of Tracking Analysis	6.5-4
6.5 - 2	Minimum $\Delta t$ for Memory	6.5-11
6.5-3	Maximum $\Delta t$ for Memory	6.5-13
6.6-1	Trapped Electron Environment	6.6-2
6.6 - 2	Solar Flare Environment	6.6-3
6.6 - 3	Segment of 30-Foot Diameter Petal Antenna Reflector	6.6-11
6.6-4	Segment of 30-Foot Diameter Petal Antenna Reflector	6.6-11
6.6-5	Sun Shadow Distribution	6.6-13
6.6-6	Bypass Diode Functional Arrangement	
6.6-7	Comparison of V-I Curves for a Partially Shaded Array Series	
	String, With and Without Bypass Diodes	6.6-15
6.6-8	Illustration of Effects of a Number of Elements Shaded on	
	Degradation of an Array Series String Operating at String	
	Peak Power Voltage	6.6-16
6.6-9	Illustration of Effects of a Number of Elements Shaded on	
•	Degradation of an Array Series String When Operating	
	Voltage is Off Peak Power Point of Array	6.6-16
6.6-10	Array Located in Shadow of Antenna Reflector Structure	6.6-18
6.6-11	Dependence of Solar Cell Output on Angle of Incidence	6.6-22
6.6-12	Orbital Variations of Geometry Factor $K_G/\cos \psi$	6.6-25
6.6-13	Comparison of Four-Panel and Two-Panel Solar Array Power	
	Capability at Loads	6.6-32
6.6-14	Efficiencies of 1-Ohm Centimeter and 10-Ohm Centimeter Cells	J, J DE
	Subjected to Radiation Degradation	6.6-34
6.6-15	Solar Cell Degradation After Two Years	6.6-38
~		5.5 50

Figure		Page
6.6-16	One Ohm-Centimeter Solar Cell Degradation versus Orbit Time	6.6-39
6.6-17	Maximum Power Degradation versus Orbit Time	6.6-40
6.6-18	Ten Ohm-Centimeter Solar Cell Degradation versus Orbit Time	6.6-41
6.6 - 19	Solar Cell Cover Thickness Optimization	6.6-42
6.6-20	Power Distribution Comparison	6.6-51
6.6 - 21	Power System Block Diagram, Series Regulator	6.6-53
6.6-22	Power System Block Diagram, Series Regulator with Voltage Limiter.	6.6-54
6.6-23	Power System Block Diagram, Shunt Regulator	6.6-54
6.6-24	Load Sharing Problems	6.6-55
6.7 - 1	Coordinate and Normalized Sign Conventions	6.7-5
6.7-2	Primary Structure Model	6.7-6
6.7-3	Results of Feed Support Truss Tradeoff Study	6.7-8
6.7-4	Geometry of the Aft Structure	6.7-10
6.7-5	Tape Drive Deployment System	6.7-50
6.7-6	Solar Panel Latching and Deployment Design	6.7-53
6.7-7	Coordinate Convention and Locations, Deployed Configuration	6.7-58
6.7-8	Coordinate Convention and Locations, Selected Configuration	6.7-59
6.7-9	Coordinate Conventions and Locations, Antenna-Mounted Solar	0.1-92
	Array Configuration	6.7-70
6.7-10	Response Coordinate Locations, Selected Configuration	6.7-76
6.7-11	Launch Response Coordinate Locations, Deployed Configuration	6.7-77
6.7-12	Typical Electronic Panel, Alternate Approach	6.7-93
6.7-13	Voyager Standard Panel	6.7-98
6.8-1	Antares I (X254AI)	6.8-8
6.8-2	Antares II (X259A2)	6.8-9
6.8-3	Delta Motor (TE-364-3)	6.8-9
6.8-4	Extended Surveyor Motor	6.8-10
7.2-1	ATS-4 Reference Design Ascent Trajectory Ground Trace	7-4
7.2-2	Perigee Burn Description and Orientations	7-5
7.2-3	Apogee Burn-Circularizing and Plane Change Maneuver	7-6
7.4-1	Variation of Injection Longitude with Launch Azimuth, Perigee	
	Burn Crossing, Apogee Burn Opportunity	7-12
7.4-2	Effect of Launch Azimuth on: (1) Apogee Longitude at Injection, ι <sub>I</sub> , (2) Additional Apogee Inclination Change, Δi, (3) Corresponding	
	Apogee Velocity Penalty, $\Delta V$	7-12
7.5-1	Perigee Velocity Impulse versus Inclination Change at Perigee	7-19
7.5-2	Apogee Velocity Impulse versus Inclination Change at Apogee	7-19
7.5-3	Variation of Total Velocity Impulse (from 100 nm Circular	7-13
	Parking Orbit to Synchronous (Ircular Equatorial Orbit)	
	versus Inclination Change at Perigee	7 10
7.5-4	Variation of Perigee Burn Thrust Direction with Inclination	7-19
• • • • •	Change at Perigee	7-19

Figure		Page
7.5-5	Variation of Apogee Burn Thrust Direction with Inclination	
<b>5 5</b> 0	Change at Apogee	7-21
7.5-6	Variation of Required Transfer Orbit Payload with Apogee Burn	
7.5-7	Velocity Impulse	7-21
1.0-1	Payload Loss, and Inclination Change, of Transfer Orbit as Function of Excess Perigee Velocity	
7.5-8	Payload Determination (Non-Optimum Apogee Motors)	7-22
7.5~9	Determination of Payload Capabilities for Modified Surveyor and	7-23
	Antares I Apogee Motors as a Function of Maximum Centaur	
	P/L Capability	7-24
7.5-10	Variation of Useful Payload into Synchronous Orbit with Maximum	1-24
	Centaur Capability	7-26
7.5-11	Growth Capability as a Function of Maximum Centaur Capability	1-20
	and Various Retro Motors	7-26
7.5 - 12	Description of Orbit Injection Error Sources and Vernier Engine	
	Thrust Directions	7-28
7.5-13	Variation of Vernier Velocity Requirements with Apogee Burn	
	Orientation Error	7-38
7.5-14	Variation of Total Payload Weight Cost with Launch Azimuth (or	
	Injection Longitude) and Orientation Errors at Apogee Burn	7-43
7.5-15	Variation of Total Payload Weight Cost with Apogee Motor	
	Orientation Errors	7-43
7.7-1	Variation of Maximum Longitude Excursion with Synchronous	
779	Orbit Inclination	7-59
7.7-2	Variation in Maximum Longitude Excursion with Eccentricity or	
7.7-3	Apogee-Perigee Distance	7-60
1.1-3	Variation of Individual Velocity Impulse Magnitude with Time	
7.7-4	Duration Between Thrusting	7-62
7.7-5	ΔV Required to Zero Out Inclination (Impulse Applied at	7-62
0	Nodal Crossing)	7 64
7.7-6	Thrust Inefficiency versus Error in Longitude of Nodal Crossing	7-64
7.7-7	Determination of Uncertainty in Nodal Location	7-64 7-67
7.8-1	ATS Ground Station Activity During Vernier Maneuvers.	7-75
	The same account of the same state of the same s	1-15
8.3-1	Spillover Efficiency and Illumination Efficiency	8.3-4
8.3-2	Composite Patterns Measured on 30-Foot Paraboloid at 1700,	0.0-4
	1820 and 1900 MHz	8.3-5
8.3 - 3	Sidelobe Level Versus Edge Illumination	8.3-7
8.3-4	Large Aperture Antenna Equal Power Contours at 8.0 GHz Frequency.	8.3-1
8.3-5	Large Aperture Antenna Main Lobe Patterns	8.3-1
8.3-6	Graphic Representation of RF Boresight Measurement Technique	8.3-1
8.3 - 7	Curve Fitting Angle Data	8.3-1

ıge
3-18
3-27
3-27
3-34
3-53
3-53
7-7
7-8
7-9
8-3
8-26
3
26
29
3- 3- 7- 7- 8- 8- 3

### LIST OF TABLES

Tables		Page
4.1-1	Value of ATS-4 Experiments to Operational Missions	4-2
5, 2-1	Launch Vehicle Capability	5.2-6
5. 3-1	Parabolic Antenna Performance	5.3-19
5.3-2	Orientation Control System Three-Sigma Error Budget	5.3-20
5.3-3	Orientation Control Subsystem Performance Summary	5.3-21
5.3-4	Performance Requirements Summary - Phase-Steered Array Antenna .	5.3-22
5.3-5	Interferometer Performance Summary	5.3-23
5.3-6	Interferometer Error Budget	5.3-23
5.3-7	Command and Telemetry Subsystem Capability	5.3-24
5.3-8	Power Subsystem Capability	5.3-26
5.3-9	Detail Weight Summary of Selected Design	5.3-27
5.3-10	Inertia and Center-of-Mass Summary	5.3-28
5. 4-1	Parabolic Antenna Experiment Loss Budget	5.4-13
5. 4-2	Comparison of Feed System Requirements	5.4-35
5.5-1	Error Budget	5.5-7
5.5-2	Weight and Power Summary for Initial Acquisition and Orientation	
0.0 =	Control Subsystems	5.5-8
5.5-3	Station Acquisition Impulse Requirements	5.5-10
5. 5-4	Mass Expulsion Subsystem Requirements for Orientation Control	0,0 10
J. J-4	and Stationkeeping	5.5-37
5. 5-5	Component Description	5.5-46
5, 5-6	Impulse Requirements for Station Acquisition and Despin Mass	0.0 10
	Expulsion Subsystem	5.5-52
5.5-7	Station Acquisition System Weight	5.5-58
5. 5-8	Resistance Jet System Weight	5.5-76
5.5-9	Command Requirements	5.5-78
5.5-10	ATS-4 Telemetry Requirements	5.5-79
5. 5-11	O/C Component Mounting, Alignment and Field of View Requirements .	5.5-86
5.6-1	Large Parabolic Antenna Experiment Equipment Characteristics	5.6-5
5.6-2	Geometric Instrumentation	5.6-12
5.6-3	Weight and Power Estimates for the Interferometer System	5.6-26
5.6-4	Major Characteristics of Phase-Steered Array Antenna System	5.6-31
5. 7-1	Telemetry Requirements	5.7 <b>-</b> 3
5.7-2	Significant Reference Configuration Parameters	5.7-5
5.7-3	Margin Calculations-Telemetry Data	5.7-23
5.7-4	Margin Calculations-Tracking	5.7-24
5.7-5	Margin Calcularions-Command Link	5.7-25
5.7-6	Summary of Component Power, Weight and Size	5.7-26
5.7-7	Summary of Design Status	5.7-32
5.8-1	Summary of Array Power and Energy Capability	5.8-12
5.8-2	Battery Depths of Discharge for New and Old Arrays	5.8-21
5.8-3	Summary of Power Conditioning Equipment Operating Efficiencies	5.8~33
5. 8-4	Summary of Power Subsystem Weights and Sizes	5.8-34
5.8-5	Summary of Power Conditioning Equipment Thermal Dissipations	3.0-3 <del>4</del> -,5-
5, 9-1	Atlas/Centaur Qualification Test Specifications	.s- 5.9-9

### LIST OF TABLES (Cont'd)

<u>Tables</u>		Page
5. 9-2	Payload Capability Using TE-364-3 Improved Delta Motor	5.9-16
5.9-3	Performance and Physical Data on the Improved Delta	
	Motor (TE-364-3)	5. <b>9-1</b> 8
5. 9-4	Performance Parameters for Optimum Motor Extended Surveyor	5.9-19
5.9-5	Summary of Spacecraft Design Constraints and Significance to	
	Selected Design	5.9-22
5.9-6	Major Structural Elements	5.9-27
5. 9-7	Structure Weight Summary	5.9-39
5. 9-8	Response Accelerations to Base Excitation	5.9-52
	Comparison of Analog Simulation Transfer Functions with Transfer	
	Functions used for Selected Configuration	<b>5.9-</b> 55
6. 2-1	Launch Vehicles Comparison	6.2-9
6, 2-2	Titan III C-Flight Loads Environment	6.2-12
6.2-3	Summary of Maximum Measured Flight Loads (Atlas/Centaur	
	Flight AC-2 to AC-6)	6.2-21
6. 2-4	Deployed Antenna Frequency Comparison	6.2-31
6.2-5	Performance of Deployed Configuration	6.2-52
6.2-6	Deployed Configuration Weight Summary	6.2-53
6.2-7	Deployment System Comparison	6.2-67
6.3-1	Comparison of Space Deployable Antennas	6.2-23
6. 3-2	ATS-4 Structural Parameters	6.3-29
6.3-3	Mechanical Properties of Aluminum and Titanium	6.3-34
6. 3-4	Effect of Temperature on the Tensile Strength of FM-1000	
	Adhesive Bonded Aluminum Honeycomb Panels	6.3-37
6.3-5	Effect of Temperature and Vacuum on the Tensile Strength	2.0.00
	of FM-1000 Adhesive Bonded Aluminum Honeycomb Panels	6.3-38
6.3-6	Estimate of Mass Properties	6.3-49
6. 3-7	Maximum Compression Load Launch Condition	6.3-68
6.3-8	Truss Member Loads	6.3-94
6.3-9	Directional Displacements for Structural Joints (1 of 6) thru (6 of 6)	6.3-123
6. 3-10	Feed Thermal Displacements	6.3-131
6. 3-11	Antenna Loss Budget No. 1	6.3-154
6. 3-12	Antenna Loss Budget No. 2	6.3-155
6.3-13	Antenna Loss Budget No. 3	6.3-156
6.3-14	Final Configuration Loss Budget	6.3-171
6.4-1	Body Rate and Acceleration Amplitude for Practical Sensor Locations.	6.4-35
6.4-2	Atlantic Research Corporation Spinup Motor Data	6.4 - 42
6.4-3	Atlantic Research Corporation Motor Data	6.4-44
6.4-4	Spacecraft Parameters Associated with On-Station Disturbance	
	Torque Computation	6.4 - 55
6.4-5	Sun Stabilization System Nomenclature	6.4 - 88
6.4-6	Sun Stabilization System Parameter Values	6.4 - 89

# LIST OF TABLES (Cont'd)

<u>Tables</u>		Page
6.4-7	Three-Sigma Error Budget Data	6.4-114
6.5-1	136 HMZ TLM (Carrier and Data).	6.5-2
6.5-2	Position and Velocity Error.	6.5-2 6.5-5
6.5-3	Antenna Configuration Tradeoff For Alternate Design Configuration	6.5-8
6.6-1	Yearly Integrated Intensities of Solar Cosmic Rays	
6.6-2	Abundancy of Cosmic Rays	6.6-4
6.6-3	Power Equation Factors for Various Array Configurations	6.6-5
	$P = K(A_T) (K_G) F_T F_S$	6.6-26
6.6-4	Array Area Requirements for Various Configuration (300 watt maximum array).	
6.6-5	Maximum Power Required from Battery-Watt Hours	6.6-29
6.6-6	Battery Sizing and Performance	6,6-44
6.6-7	Time and Power Required to Recharge Batteries (33 A-HRS).	6.6-46
6.6-8	Power Distribution Weight Comparison	6.6-49
6.6-9	Power Conditioning Equipment Weight Summary	6.6-52
6.6-10	Power Systems Comparison Summary	6.6-56
6. 7-1	Ultimate Launch Loads (g)	6.6-60
6. 7-2	Separation Device Tradeoff Chart.	6.7-2
6. 7-3	Sinusoidal Vibration Testing Specifications	6.7-56
6. 7-4	Sinusoidal Vibration Testing Specifications.  Transfer Functions for ATS-4 Configuration with Automa Management of the Au	6.7 - 59
<b>0.</b> 1	Transfer Functions for ATS-4 Configuration with Antenna-Mounted	
6. 7-5	Solar Arrays	6.7 - 72
0 0	Point One on Deployment Column	
6. 7-6	Antenna with $f/D = 0.4$ .	6.7-72
6. 7-7	Frequency Shift with f/D Variation	6.7-75
6. 7-8	Launch Accelerations for the Selected and Deployed Configuration	6.7-75
0. 1 0	Due to A1 g or RAD/sec <sup>2</sup> Input	
6. 7-9	Mass Distributions.	6.7-77
6. 7-10	Frequency Comparison Sologted and Donloved Food Confirmation	6.7-78
6. 7-11	Frequency Comparison Selected and Deployed Feed Configuration	6.7-81
6. 7-12	Control Transfer Functions.	6.7-82
6. 7-13	Transfer Functions for Gravity Gradient Rods	6.7 - 84
6. 8-1	Payload Capability Using TE-364-3 Delta Motor.	6.7-86
6.8-2	Apogee Motor Tradeoff Matrix.	6.8-3
6. 8-3	Physical and Performance Data of Str. Matter	6.8-4
6.8-4	Physical and Performance Data of Six Motors Considered  Data on Candidate Apogee Motors.	6.8-7
6.8-5	Apogee Motor Puff Chart.	6.8-7
0, 0-0	Apogee Motor Full Chart	6.8-12
7.2-1	Sequence of Events	7-3
<b>7.</b> 4-1	Perigee of Transfer Orbit at First Equatorial Crossing of	1-0
	Parking Orbit	7-11
<b>7.</b> 4 <b>-</b> 2	Perigee of Transfer Orbit at Second Equatorial Crossing of	1-11
	Parking Orbit	7_11

# LIST OF TABLES (Cont'd)

Tables		Page
7.5-1	Summary of Total Vernier Maneuver Impulse Requirements	7 <b>-27</b>
7.5-2	Vernier Weight Tradeoff Summary	7-42
7.5-3	Injection Bias Summary ( $\theta_{\rm c} = 1$ degree)	7-52
7. 7-1	In-Orbit Stationkeeping Velocity Requirements	7-66
7. 7-2	Orbit Determination Summary	7-69
8. 3-1	Individual Experiments - Parabolic Antenna	8.3-20
8.3-2	Required Signal Characteristics - Parabolic Antenna Measurements	8.3-42
8. 3-3	Gains and Beamwidths - Perfect 30-Foot Parabolic Antenna	8.3-43
8.3-4	System Performance Parabolic Antenna Transmission Measurements.	8.3-45
8. 3-5	System Performance Gain Standard Antenna Transmission Measurements	
8. 3-6	System Performance Parabolic Antenna Receiving Measurements	8.3-45
8. 3-7	Limiting Power and Bandwidth Requirements Parabolic Antenna	8.3-45
8. 3-8	On-Board Equipment Characteristics Parabolic Antenna	8.3-48
	16	0 0 40
8. 3-9	Experiment Equipment Summary	8.3-49
8.4-1	Individual Experiments - Orientation Control System	8.3-55
8.5-1	Individual Experiments - Interferometer	8.4-3
8.5-2	Interferometer Telemetry Monitoring Signals.	8.5-2
8.6-1	Individual Experiments - Phased Array Antenna	8.5-6
8.6-2	System Performance Steered Phase Array Antenna-Transmission	8.6-6
	and Reception Measurements (RF Bandwidth: 30 MHz)	8.6-21
8. 7-1	System Performance High Data Rate Meteorological Sensors - Satellite to Surface (10 GHz; TV Data Rates)	
8. 7-2	Weight and Power Requirements of Sensors and Optics.	8.7-11
8. 7-3	Transmission Link Characteristics Audio FM Broadcast to Home	8.7-13
8. 7-4	TV Receiving Sets	8.7-15
8. 7-5	User Accessibility Versus Field Strength	8.7-17
8. 7-6	Field Strength Versus On-Board Radiated Power.	8.7-17
8. 7-7	Limited Area Audience Experiment	8.7-18
8. 7-8	TV Broadcast Configurations Link Calculations	8.7-19
8. 8-1	System Performance MOL Relay - MOL to Satellite - TV Bandwidths.	8.7-24
8. 8-2	Experiment and Ground Station Capability Tradeoffs Required and Recommended Transmitting/Receiving Frequencies	8,8-6
8. 8-3	for Ground Stations .  ATS-4 Operational Ground Station Configuration Matrix Assuming	8.8-8
	Additional ATS-4 Antenna at Rosman	8.8-10
8. 8-4	ATS-4 Operational Ground Station Configuration Matrix Assuming	
	One Antenna Per Station with Interchangeable Feeds	8.8-13
8. 8-5	Operational Integration of Experimental Tasks, Facilities and	
	Schedule.	8.8-15

# LIST OF TABLES (Cont'd)

Tables			Page
8. 8-6	Experiment Combinations	•	8.8-18
8. 8-7	Contingency Matrix	•	8.8-2
9. 2-1	Ground Support Summary Matrix	•	9-2
9,4-1	Equipment List (MSE)	•	9-15
9, 5-1	Equipment List (ESE)	•	9-21
9.8-1	Ground Station Equipment Requirements Summary	•	9-30
9.9-1	ATS-4 Computer Program Requirements	•	9-33

# SECTION 1 INTRODUCTION

This report is submitted in compliance with Contract NASW-1410 dated 12 May 1966, "An Advanced Study of an Application Technology Satellite (ATS-4) Mission." The study was directed toward establishing the feasibility of meeting the mission objectives which centered upon the development and demonstration of a large aperture, deployable satellite antenna and the precision spacecraft stabilization techniques required for accurate orientation of a parabolic antenna, a phased array and an interferometer. The mission is accomplished from a synchronous equatorial orbit.

A feasible spacecraft configuration is defined and an analysis of the performance capabilities is presented. A preliminary program plan for spacecraft development including identification of and approaches to the solution of engineering development problems and an estimate of the program schedule and development costs is included.

The experiments basic to the mission are dependent upon the orientation and control system for successful demonstration. The conceptual design and analysis for the control system experiment and the interferometer were generated by the General Electric Company. Goodyear Aerospace Corporation was given a subcontract to study the feasibility of the parabolic antenna design and experiment. The data generated by Goodyear was compared with and supplemented by independent analyses conducted by General Electric. The antenna shown in the conceptual design of the ATS-4 spacecraft is basically a Goodyear concept. However, the spacecraft interface with the antenna is such as to accommodate any parabolic reflector which meets the interface requirements specified in NASA Performance and Test Specifications Large Aperture Antenna - ATS-4-GSFC S-733-Pc. The phased array information was supplied by NASA/GSFC.

The inclusion of the Goodyear antenna in the baseline design should be construed only as an indication of one feasible antenna design. It is not considered appropriate for General Electric to recommend a specific contractor for the flight antenna development until further

independent development of candidate antenna concepts is completed. However, a petal type antenna is required to meet the efficiency requirement at 10 GHz and a simple erection system with inherent self-locking of the petals is desirable. The Goodyear antenna meets all these requirements.

This report is divided into two volumes. Volume I contains a summary of the study program and the technical discussions. Volume II contains a Preliminary Program Plan. For convenience, Volume I is divided into three books. Book 1 (Sections 1 through 5) contains the general mission discussions and a comprehensive summary of the design of the baseline spacecraft. Book 2 (Section 6) contains the detailed discussion and tradeoff analyses for the spacecraft. Book 3 (Sections 7 through 9 and Appendices) contains the launch phase sequence, experiment selection and operational sequence, the ground equipment and ground station considerations, and the technical appendices.

#### SECTION 2

#### PROJECT OBJECTIVES

The objective of the NASA Application Technology Satellite Program is to provide the opportunity to research, develop and flight test techniques and technologies that are common to a variety of future satellite applications. It is through this type of program that the National Aeronautics and Space Agency is able to assure that proven techniques and technological alternatives are available to users for optimum design of truly cost-effective operational systems.

The prime ATS-4 project objectives are the development and demonstration of a large aperture, deployable, satellite antenna and precision spacecraft stabilization techniques commensurate with beam width requirements necessary for accurate orientation of large aperture antennas, high resolution meteorological sensors and TV cameras.

Though the ATS-4 mission study was directed to meet these objectives via a satellite in synchronous equatorial orbit with all prime experiments directed at the earth, the technological and engineering data gained and the majority of the hardware to be developed was required to be applicable for use in deep space without restriction on the direction of pointing.

While deployment of large flexible structures in space has been demonstrated on other programs, the maintenance of precise contours as required for X-Band has not been a requirement. Likewise, precise stabilization of these structures has not been attempted and fundamental dynamic behavior data has not been collected.

OAO has been designed with the potential for precise pointing capability by virtue of a system utilizing star trackers which is adequate for astronomy and space navigation. However, the requirement for precise pointing to and tracking of any earth station or man-made target in space requires the development and demonstration of new sensors, components, and techniques.

The combination of prime experiments on ATS-4 (30-foot parabolic antenna, orientation control, interferometer, and phased array) provides a broad base for advancing scientific knowledge and engineering proficiency in the fields of communications, satellite control, and navigation. The technical data derived from these experiments will be of inestimable value in contributing to the support of future operational satellites using large aperture antennas and interferometer techniques. In addition, the ATS-4 spacecraft can be used as a test bed to prove out equipment and demonstrate special features of future operational satellites.

High-data-rate communications is characteristic of the many advanced application systems that will be necessary in the 1970's if the national goals in space exploration and utilization are to be achieved. As an example, the inadequacy and the limitations of present communications systems was lucidly demonstrated during the 1965 Mariner probe to Mars where data rates of 8-1/3 bps resulted in transmission times of many hours to transmit a single frame of TV information. For planetary missions, the desired transmission rates are on the order of  $10^5$  to  $10^6$  bps. These rates will be adequate to handle high-resolution TV requirements and a variety of scientific and engineering nonimaging sensors.

The high cost of lunar and planetary probes makes it imperative that means of achieving high data rates be developed in order to obtain maximum cost effectiveness of satellite systems. A major factor in obtaining high data rates for interplanetary links is utilization of high-gain antennas in space. The 30-foot X-Band parabolic antenna experiment will demonstrate feasibility, determine attainable performance and cost, and provide design data applicable to the solution of problems that could be encountered in developing multifrequency, high-date-rate operational systems.

Synchronous satellites, such as ATS-4, are ideally located for use as test beds for high-data-rate communications relay and tracking systems, AM, FM and TV broadcast relays, synoptic meteorological systems, radio-astronomical systems, and multiple-access communications satellites.

Communications relay and tracking systems, particularly systems which are capable of satellite-to-satellite transfer of information, could be used as direct satellite links to the Manned Space Center without using the ground link network. Such a system would reduce

considerably the number of ground stations required, provide continuous high-data-rate communications between a manned spacecraft and the Manned Space Center, and provide continuous high-accuracy tracking (range, range rate and angle data). This type of system, by using frequencies in which the atmosphere is virtually opaque, would result in nearly complete immunity to intercept or jamming by surface installations.

A synchronous satellite functioning as a multiple-access communications satellite could provide direct communications from a small surface installation to any desired point. This application would be valuable in supporting tactical over-the-horizon air operations, in supporting small rapidly-moving tactical ground operations, and in post-strike communications.

A synchronous satellite would be in an ideal position to function as a test bed for meteorological sensors, observing over one-quarter of the earth's surface. Analysis of the data resulting from such observations would permit meteorologists to determine the relative value of the various parameters observed in predicting weather. Improvement of weather forecasting based on synoptic data obtained by satellite would permit highly reliable five-day forecasts. President Johnson stated (in 1963 while Chairman of the National Aeronautics and Space Council) that if weather could be predicted accurately only five days in advance, the following cost savings would be possible:

- \$2 1/2 billion a year in agriculture
- \$45 million in the lumber industry
- \$100 million in surface transportation
- \$75 million in retail marketing
- \$3 billion in water resources management

These savings are for the United States alone. Worldwide benefits would be many times as great. Improved forecasts would be of great value to the military in their operations, such as air strikes, refueling, amphibious operations, etc. which are dependent on good weather, could be planned more efficiently and with an increased probability of success.

The discussion of use experiments in Section 8.7 includes margin calculations which show that it is feasible to demonstrate large portions of these advanced operational systems with relatively minor additions to the ATS-4 spacecraft payload. As an example, the spacecraft has been designed to accommodate large variations in electrical load and concentrated heat loads. Thus, a 50-watt transmitter could be accommodated easily without change to the satellite. With such a transmitter, FM voice broadcasting at 0.8 GHz could be received on a uhf channel of a home TV receiver. Depending on the success of transmitter developments, a minimum of four to eight hours of broadcast service could be provided during any 24-hour period. This would be more than adequate for demonstration purposes.

#### SECTION 3

#### PROJECT FEASIBILITY

The overall ATS-4 project objectives can be achieved within the time frame associated with a 1971-1970 launch. A 41-month program from start of Phase C to flight is considered feasible. There are no program critical items requiring specific research and development. Some program elements such as the parabolic reflector and its feeds and the orientation control system will require a longer development cycle (about 4 months longer) than the rest of the program elements and must be started before Phase C. All program elements pose engineering challenges which will require great care in design.

It is quite feasible to design, develop, and manufacture a deployable 30-foot parabolic reflector that will maintain in orbit the surface accuracies required to achieve a 50 percent efficient antenna system for frequencies of 0.8 to 8.0 GHz. A 30-foot aperture is not large enough to act as an efficient reflector at 0.1 GHz. The fact that the base line antenna system does not reach the 50 percent efficiency goal at this frequency is due to the choice of antenna size, not surface contour accuracy, and is in no way a reflection on the feasibility of building a larger reflector to meet this requirement.

This study has similarly shown that a combined reflector and feed system can be designed to meet the 50 percent efficiency system requirements (the same exception at 0.1 GHz applies here).

The orientation control system recommended can meet the  $\pm 0.1$  degree pointing requirements, can exceed the tracking requirement of  $\pm 0.5$  degree while tracking at 10 milliradians/minute, and can exceed the horizon-to-horizon slew rate.

The interferometer system recommended also meets all the required performance characteristics to operate as both an open loop attitude sensor and as a closed loop orientation control sensor with an accuracy of better than ±0.02 degree.

The phased array information was supplied by the NASA/GSFC cognizant Technical Officer. This equipment also appears to be feasible.

A satellite incorporating all four of these prime experiments can be designed within the weight (4000 pounds) and volume (Surveyor shroud with 15-foot cylindrical extension) restrictions for launch into a synchronous equatorial orbit using the Atlas (SLV-3C)/Centaur launch vehicle and the available Improved Delta 3rd stage used as an apogee motor. Compromises required of individual experiments to integrate them into one satellite system can be reduced to a level such that all performance goals are met except for the parabolic antenna system efficiency. The blockage and reflectance losses contributed by the phased array and the larger strut assembly required because of the severe lateral load environment specification imposed for this study, caused the antenna efficiency to range from approximately 43 percent to 49 percent. Sections 5 and 6 of this report discuss this point in detail.

The two-year life requirement for all satellite systems also appears to be attainable. Inherently short lived components such as tape recorders are not required. After initial deployment of the antenna the satellite configuration remains fixed. The number of solenoid, switch, and relay actuations are well within the present state of the art.

It is feasible to plan and execute an in-space test program that will determine the level of performance of the prime experiments and which will demonstrate the use of this equipment. It is also feasible to add additional equipment to obtain technological and engineering data and to demonstrate specific elements which will be required for future operational missions.

The development of a modified Surveyor motor would make it possible to use the full capabilities of the Centaur vehicle for putting payloads into synchronous orbit. This could make it possible to add up to 400 pounds of additional payload in orbit. The modification is considered quite feasible by the motor manufacturer and would require a minimum of engineering and test firings.

Ground and orbital support equipment and software requirements are all well within the state of the art. Some equipment is nonstandard but can be designed and built well within the required time period.

#### SECTION 4

#### EXPERIMENT DESCRIPTION AND JUSTIFICATION

#### 4.1 GENERAL

The four prime experiments specified for the ATS-4 program are:

- 1. Deployment, pointing and utilization of a large parabolic antenna for radio communications
- 2. Active precision spacecraft stabilization with possible augmentation by passive means
- 3. Deployment, pointing and utilization of a high-gain, multibeam, electronically steered array
- 4. Demonstration of a precision radio interferometer as a sensor for spacecraft attitude and/or antenna pointing reference.

A general discussion leading to the justification of these experiments is included in Section 2, Project Objectives. Table 4.1-1 indicates how and where each experiment would contribute to the future operational missions. In this matrix, demonstration should be interpreted to mean either complete demonstration or demonstration of selected elements. Engineering data is data immediately applicable for use in design and scientific data is data which could be used to advance the state of the art.

The parabolic antenna, being a large flexible structure, also provides the opportunity to develop engineering data on structural behavior, particularly damping coefficients in space. This secondary experiment, with its associated research and development to provide the required instrumentation, is worthy of serious consideration. A detailed discussion of the experiments and derivation of the measurement program is presented in Section 8. A brief summary follows.

LEGEND: D - Demonstration
E - Engineering Data
S - Scientific Data

## 4.2 PARABOLIC ANTENNA EXPERIMENT

This experiment is defined in the study work statement as follows:

"The large parabolic antenna experiment shall have a minimum aperture diameter of 30 feet with an objective of achieving the largest feasible aperture and shall be capable of both transmit and receive operation at frequencies up to 10 GHz. Specifically, the antenna feed system shall be capable of transmitting at 100, 800, 2300, and 7300 MHz and shall also be capable of receiving at 1700, 2100, and 8000 MHz. It is not necessary that either transmission or reception be simultaneous on all of the above frequencies. Bandwidth capability of the system at the specified frequencies shall be 10 percent. System antenna efficiency shall be at least 50 percent."

The measurements program for this experiment falls into two principal categories: mechanical parameter measurements and electrical parameter measurements.

#### 4.2.1 MECHANICAL

Demonstration of deployment and surface contour characteristics is required. Deployment will be monitored by make or break electrical sensors mounted on the antenna deployment booms and selected petal sections. In addition, strain gauges mounted on the links between the antenna and deployment booms will be monitored and the results correlated with ground tests to determine that abnormal forces were not present during deployment. Due to the nature of the antenna construction, confirmation that all booms are in place and locked and that no abnormal forces are present or occurred during deployment is sufficient to verify the integrity of the deployed antenna.

Surface contour characteristics will be measured with strain gauges and temperature sensors. Here contour deviations of 0.25 inch rms or greater will be required before detectable rf performance degradation will occur. Contour characteristics due to thermal environment will be thoroughly measured.

Optical measurement techniques will be used to measure feed movement relative to the parabola apex. Here movements of 0.15 inch or greater are of interest.

#### 4.2.2 ELECTRICAL

Gain, boresight, pattern, and bandwidth capability must be measured.

Absolute gain measurements for both the transmit and the receive modes will be made using standard gain antennas on the spacecraft as prime references. Gain data will also result from boresight and pattern measurements. Ten-watt transmitters are considered adequate for all tests.

Patterns and boresight measurements will be made by scanning the antenna beam across a ground station and the boresight and patterns determined through statistical analysis of the ground measurements. Boresight measurements to  $\pm$  0.03 degree accuracy are expected at the 8 GHz frequency.

General rf performance will be determined by transmitting and receiving test signals such as video, PCM, and special waveforms. Video signals constitute one of the most sensitive diagnostic tools for determining system amplitude and phase behavior.

Once the system characteristics have been determined, specific mission demonstrations can then be finalized and inserted into the overall test schedule.

#### 4.3 ORIENTATION CONTROL EXPERIMENT

This experiment is defined in the study work statement as follows:

"The orientation control system shall be capable of directing the main beam of the parabolic antenna to any point on the visible earth's surface to an accuracy consistent with the antenna beamwidth for the frequencies of interest (when used at 10 GHz, the orientation control system must be capable of a pointing accuracy of 0.1 degree). The time required to change the direction of the main beam from a terminal on one horizon to a terminal on the opposite horizon and stabilize within the required accuracy (i.e., plus or minus 0.1 degree) for a worst case maneuver will be no longer than 30 minutes. At a rate of 10 milliradians per minute, it shall be capable of tracking in response to ground commands with a pointing error

not exceeding 0.5 degree. The orientation control system shall demonstrate the specified performance during stationkeeping operations."

The measurements program for this experiment consists of exercising the system in its various modes recording internal parameters and antenna ground patterns.

The accuracy with which the orientation control system can maintain its direction will be measured by attempting to hold a given point for a prolonged period and measuring the error continuously with the interferometer, the earth tracking sensors, and the parabolic antenna (at 8 GHz). The distribution of error signals will directly verify the accuracy of the system in this mode.

To verify tracking capability both rate and the error between commanded angle and actual angle must be measured. Angles will be measured as above. The rate gyros will be used for monitoring rates. This experiment can be accomplished by commanding swings across a fixed ground station. Horizon-to-horizon slewing is merely a special case of tracking and data would be collected in exactly the same manner.

#### 4.4 PHASED ARRAY EXPERIMENT

This experiment is defined in the work statement as follows:

"The phased-steered array experiment shall be capable of simultaneous transmit and receive, multibeam operation in the 7-8 GHz frequency band. Phase-steering of this array may be accomplished either by means of a phasing network and discrete command or by means of pilot signals from the surface stations or some equivalent capability.

The array shall be capable of providing four beams (two for transmitting, and two for receiving) each with a minimum gain, including antenna network losses, of 30 dB with an objective goal of 45 dB. Each beam shall be pointed with an accuracy consistent with the beamwidth at 7 and 8 GHz."

The measurements program for this experiment is similar to the electrical measurements on the parabolic antenna in that gain and boresight must be determined. The program is more complex because four independent beams are involved and must be checked individually and in various combinations. Also, because the array is retrodirective, mobile and/or multiple ground station operation is required to obtain pattern and gain measurements. Again, the standard gain horns would be used in calibration for gain measurements. It is expected that accuracies of  $\pm$  0.5 degree will be sufficient for operational evaluation of array beam pointing. For this experiment heavy reliance on prior ground testing will be necessary.

One procedure for obtaining a primary lobe pattern analysis would be to have a ground station and an aircraft alternately cause the beams to be pointed at them. The aircraft flies across the beam (approximately 2500 miles). Signal strength changes at both the aircraft and ground station are measured during each switch. A fairly detailed measurement of main lobe structure of all four beams can thus be obtained.

Use experiments as indicated in Table 4.1-1 can then be exercised.

#### 4.5 INTERFEROMETER EXPERIMENT

This experiment is defined in the study work statement as follows:

"An interferometer system configuration, geometry and electrical/mechanical design will be selected so as to fully demonstrate the capabilities and limitations of an onboard interferometer, as a spacecraft attitude determination device. The interferometer antenna system will operate in a frequency range consistent with the attainment of the maximum resolution and accuracy performance characteristics required for the spacecraft orientation control system."

The measurements program for this experiment requires that boresight and angle measurement accuracy be determined and then to use the interferometer as a sensor in the orientation control loop.

The major problem will be to verify that any interferometer null shifts with time are small in comparison with the other experiments on board from which pointing data can be obtained. The interferometer is potentially the most accurate sensor on board the spacecraft and thus the usual requirement for measuring with more accurate instruments will not be possible and statistical analysis and correlation will be required.

Null shift can also be indirectly determined during angle measurement experiments. By measuring the angles subtended by a number of ground stations whose locations are accurately known, the angle measurement accuracy can be determined. In addition to the Rosman and Mojave ground stations, beacons spaced from 5 to 250 miles from these stations would be required.

The expected accuracy of the interferometer system is better than  $\pm$  0.02 degree. When substituted for the earth tracker in the orientation control loop it will therefore be possible to determine the relative benefits of using the interferometer as an orientation sensor. The attitude of the vehicle should be held more accurately and could simplify further testing of the parabolic antenna, phased array, and earth tracker.

The accuracy of the interferometer is not sufficient to use it directly as a navigation sensor. However, it would be very useful for tracking low orbiting satellites and even airplanes to allow the parabolic antenna main lobe to point directly at these vehicles. The technological information obtained would be directly applicable to building interferometers with longer baselines and consequently more accurate sensors.

#### 4.6 SECONDARY EXPERIMENTS

Since the consideration of secondary experiments was specifically excluded in the study work statement, no specific effort was directed in this area. The secondary experiments suggested in Section 8 came about as a result of studying the prime experiments. Some of these experiments will require additional equipment on board the spacecraft and some will require preliminary design effort to establish compatible spacecraft interfaces.

# A summary of suggested experiments is listed below:

- a. Detailed analysis of the dynamic behavior of the parabolic antenna structure for very small excursion; i.e.,  $\pm$  0.00035 inch.
- b. Monopulse experiments using the parabolic antenna to compare with interferometer for accuracy and versatility.
- c. Use of the interferometer as a yaw axis sensor.
- d. Synthetic angle generation for calibration of the interferometer from the ground.
- e. Detailed measurement of parabolic antenna side lobe structure.
- f. Polarization measurements using the parabolic antenna.
- g. Use of the interferometer in a transmit mode, measuring spacecraft altitude from the ground.
- h. Demonstration of ultra-wide band communications.
- i. High-data-rate meteorological sensors added to experiment complement.
- j. Demonstrate FM and TV broadcast.
- k. Use precise pointing capability to investigate millimeter wave communications problems.

#### SECTION 5

#### SPACECRAFT DESCRIPTION

#### 5.1 INTRODUCTION

The major objectives of the ATS-4 study, conducted by General Electric, were the definition and conceptual design of a feasible spacecraft system within the requirements framework established by NASA, and the identification of critical development areas which could be used as the basis for future NASA planning. The contract schedule presented definitive mission, experiment and operational requirements, including the identification of the four primary engineering experiments; parabolic antenna, orientation control, phased array and radio interferometer. Many additional experiments in support of other NASA programs are potential candidates for the ATS-4 mission; however, their consideration was not included as an element of this study. With the exception of the phased array, these prime experiments, and the instrumentation and equipment required for their space evaluation, were conceptually designed and evaluated during the study. The phased array conceptual design in development under NASA Contract NAS5-10101 was identified by the NASA/GSFC Technical Officer for use in the study.

Each of the prime experiments dictated unique spacecraft design requirements and necessitate basic tradeoffs between operational performance and design and deployment complexity. Some of the salient considerations are presented in the following summary.

- a. Parabolic Antenna Industry-wide surveys of antenna techniques revealed that only a rigid petal concept would approach the high efficiency contract requirements at high frequencies. The stowage size of a rigid petal antenna, the in-orbit lack of structural rigidity and the low rf blockage performance requirement significantly influenced the location and packaging of spacecraft equipment.
- b. Orientation Control A three-axis star tracker approach provides the best sensor accuracy for this application, but the field-of-view requirements are incompatible with protruding appendages such as the parabolic antenna. The orientation control subsystem establishes structural dynamic modal frequency requirements to eliminate control instability which would result from significant servo-elastic coupling. Lastly, separation of the spacecraft center of mass and center of pressure has a major effect on mass expulsion and momentum wheel capacity requirements, and must be minimized.

- c. Phased Array The large surface area (approximately 10 square feet) for antenna elements and the unobstructed field of view requirements of the phased array conflict with the minimum rf blockage requirements of the parabolic antenna. Additionally, the extremely high heat dissipation (approximately 400 watts) characterized by phased array operation is the most significant spacecraft thermal design constraint.
- d. Interferometer Interferometer accuracy, compatible with orientation control sensor requirements, can be obtained at X-Band frequencies without deployment. However, the essential elimination of antenna phase distortion necessitates careful packaging. Also, antenna separation distances and wave guide lengths must be preserved to maintain attitude accuracy. This further complicates packaging and thermal control due to the presence of the phased array.

The recommended spacecraft configuration represents the potential for maximum experiment performance without sacrificing deployment simplicity. Additionally, the spacecraft has been designed to the capability of an existing apogee motor (Improved Delta's new third stage), which will permit space evaluation of the prime experiments without apogee motor development. The selected configuration meets all of the contract requirements with the exception of parabolic antenna system performance and this varies from a maximum of 49 percent at 2.1 GHz to 38.5 percent at 100 MHz. It is a firm conviction, however, that this performance is the best that can be obtained under the conditions specified in the study requirements.

System and subsystem tradeoff decisions which evolved the configuration were based on performance, cost effectiveness (where possible) and gross reliability considerations. Indepth reliability analyses, including the identification of failure modes and effects and the apportionment of subsystem reliability goals were not included, but will be a part of future ATS-4 study efforts.

This section of the report presents the selected spacecraft configuration and a discussion of performance, growth and subsystem design. The selection rationale and in-depth design analysis are presented in Section 6.

#### 5.2 OPERATIONAL CONCEPT

The conceptual spacecraft design, presented in this section of the report, was selected after evaluating many design approaches against the specific mission requirements identified in the contract. Each launch vehicle, fairing and apogee motor combination presented unique design constraints in the form of packaging size, mating interface, payload capability, operational sequence, etc. The selection of each of these major elements is presented in detail in later sections of this report, but a summary is presented in this subsection in order to establish a proper reference for reviewing the selected design approach.

#### 5. 2. 1 MISSION REQUIREMENTS AND CONSTRAINTS

The ATS-4 mission, experiment and operational requirements as specified in the contract schedule, and as further identified by the NASA/GSFC Program Manager and Technical Officer, are presented in the following summary.

## a. Orbital Requirements

- Two-year mission life
- 1969 to 1970 launch period
- Synchronous equatorial orbit
- East-West stationkeeping 2 years
- North-South stationkeeping 1 year
- Repositioning capability 100 feet per second

#### b. Launch Vehicles and Fairings

- Atlas (SLV-3A)/Agena D standard Agena Clam Shell (SACS) Fairing minimum extension
- Atlas (SLV-3C)/Centaur standard Surveyor Fairing with a maximum cylindrical extension of 15 feet
- Titan IIIC (5 segment 120-inch VTC "O" stage) Titan Fairings available in the 1969-1970 time period

#### c. Parabolic Antenna Experiment

- Minimum aperture diameter of 30 feet
- System antenna efficiency at least 50%
- Operation at frequencies up to 10 GHz, specifically

Transmit	Receive	
100 MHz	1700 MHz	
800  MHz	2100 MHz	
2300 MHz	8000 MHz	
7300 MHz		

Bandwidth capability 10%

# d. Orientation Control Experiment

- Direct main beam of parabolic antenna to any point on the surface of the earth
- Pointing accuracy consistent with antenna beamwidth (e.g., 10 GHz,
   + 0.1 degree)
- Slew horizon to horizon and stabilize to within ± 0.1 degree in 30 minutes, maximum
- Track, by ground command, to within 0.5 degree at a rate of 10 milliradians per minute
- Demonstrate the above performance during stationkeeping

# e. Phase-Steered Array Experiment

- Simultaneous transmit and receive in the 7 to 8 GHz frequency band
- Four beams (2 transmit, 2 receive) with minimum system gain of 30 dB with goal of 45 dB
- Beam pointing accuracy consistent with beamwidth
- Conceptual design as being developed on NASA Contract NAS5-10101

## f. Interferometer Experiment

- Attitude determination experimental use
- Frequency range consistent with accuracy requirements of orientation control system

# g. Experiment Instrumentation

Determine and specify instrumentation required to evaluate the performance of the prime experiments

# 5. 2. 2 LAUNCH VEHICLE AND APOGEE MOTOR SELECTION

The Atlas (SLV-3C)/Centaur augmented with a solid apogee stage, is recommended for this attaining from the standpoint of performance - matched to mission requirements, cost effectiveness, and potential mission growth. The Atlas (SLV-3C)/Agena D launch vehicle with the SAGS fairing appears to be incompatible with the launch geometry of antenna concepts capable of meeting the specified mission requirements. Even if mission requirements were relaxed the Atlas/Agena D would offer marginal performance with no capability for additional experiments. The Titan IIIC has ample payload capability but was rejected on a cost effectiveness basis. It was assumed that Centaur structural modifications and Surveyor

fairing extensions will be developed for future NASA programs, independent of ATS-4, and that many of these programs will require the development of a standard, optimized apogee stage. These developments will optimize the SLV-3C/Centaur for synchronous missions. On this basis, the direct cost to the ATS-4 program would be significantly less with the use of the Atlas/Centaur launch vehicle than with the Titan IIIC.

For the reference design the Surveyor retro motor which is being modified for Improved Delta applications was selected on the basis of its assured availability with minimal nonrecurring cost. Further development of this motor will increase ATS-4 mission capability.

#### 5. 2. 3 MISSION PROFILE

The selected launch trajectory and sequence of events, for the reference design, are illustrated in Figure 5.2-1. The following describes each of the numbered sequences:

- 1. Launch from ETR, 90 degree launch azimuth,
- 2. Centaur first burn and coast
- 3. First equatorial crossing perigee of the transfer ellipse. A partial plane change is included in the second Centaur burn. The capability of the selected apogee motor is less than that required to inject the maximum Centaur payload; therefore, the excess Centaur capability is used to partially reduce the inclination.
- 4. After perigee burn the Centaur is reoriented to provide proper spacecraft apogee-burn attitude
- 5. Spacecraft separation and spin-up, spin stabilization being employed throughout the transfer orbit
- 6. First apogee possible attitude corrections commanded from Toowoomba, Australia
- 7. First perigee 100 nm, atmospheric drag at low altitude induces momentum vector precession
- 8. Second apogee 53 degrees W longitude spacecraft spin vector is precessed to correct attitude errors. Apogee burn is initiated to circularize and plane change the orbit

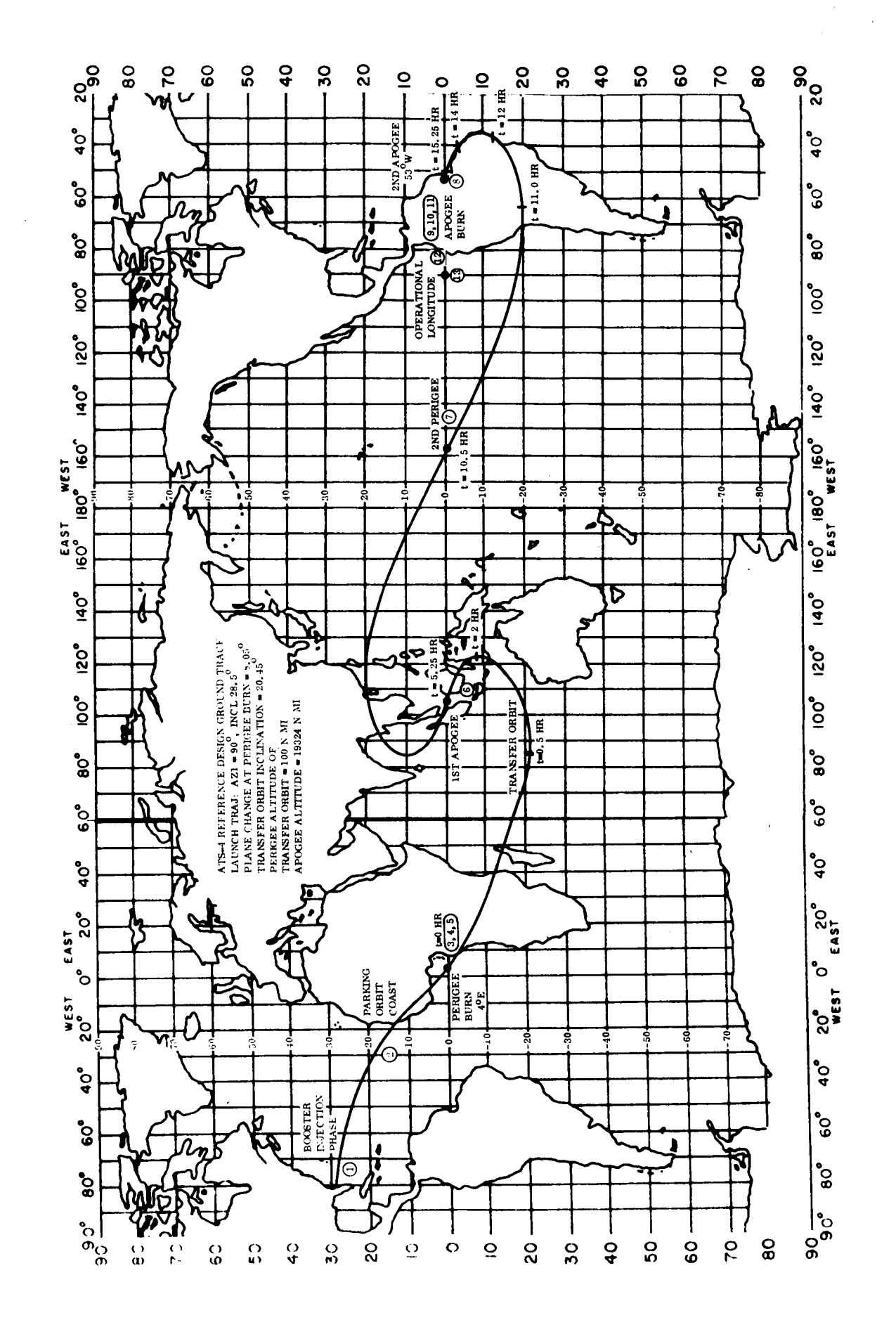


Figure 5. 2-1. ATS-4 Mission Sequence

- 9. Two day period of vernier thrusting using radial and axial hydrazine jets. The apogee-burn orientation of the spacecraft is maintained throughout this period. Injection errors are reduced to provide a 1-degree per day drift toward the West
- 10. Spacecraft despin, sun acquisition and antenna and solar array deployment
- 11. Initial stabilization sun acquisition, earth acquisition and Polaris acquisition (the yaw star reference)
- 12. Spacecraft drift rate continually reduced with stationkeeping thrusters spacecraft checkout. Thirty- to fifty-day period
- 13. Nominally established operational longitude 90 degree West.

# 5.2.4 PAYLOAD CAPABILITY

The synchronous orbit payload capability of the selected launch vehicle and apogee motor is presented in Table 5.2-1. The tabulation is based on a SLV-3C/Centaur maximum payload capability into the transfer ellipse of 4000 pound from a 28.5 degree inclined 100 mm park orbit, including the standard Surveyor fairing and its associated support equipment. A 15-foot cylindrical extension to the Surveyor fairing and its associated payload weight penalty have been officially established for the ATS-4 study. A significant weight penalty is attributed to the Centaur plane-change maneuver but results in an optimized synchronous altitude payload capability for the apogee motor selected. The payload/Centaur adapter weight estimate is based on a detailed design study, the results of which are presented later in this section. The resulting maximum spacecraft weight (including apogee motor fuel) after separation from the Centaur is 3,211 pounds. Approximately 6 pounds of fuel are expended in the spacecraft spin-up and coning control maneuvers prior to apogee burn. Apogee motor fuel weight, which is expended at second apogee of the transfer ellipse, is 1440 pounds. This results in a maximum spacecraft weight, after apogee burn, of 1771 pounds including 139 pounds of apogee motor weight which stays with the spacecraft throughout the mission.

Table 5.2-1. Launch Vehicle Capability

Atlas (SLV-3C)/Centaur Capability	4000.0 lb
Weight Penalties 15-foot Surveyor fairing ext. 75.0 lb 8.05 degree plane-change at perigee 578 lb	653.0 lb
Launch Weight Capability	3347.0 lb
Payload/Centaur Adapter	136. 0 lb
Separation Payload	3211.0 lb
Mass expulsion for spin-up and coning control	6.0 lb
Payload Weight for Apogee Burn	3205.0 lb
Apogee motor fuel weight (Improved Delta motor)	1440. 0 lb
Payload into Synchronous Orbit (Includes 139 lb of apogee motor dry weight)	1765.0 lb

## 5.3 SYSTEM SUMMARY

# 5.3.1 CONFIGURATION DESCRIPTION

The selected spacecraft configuration, illustrated in Figure 5.3-1, features a direct feed, 30-foot diameter aperture parabolic antenna (f/D = 0.4), with a six-member feed support truss connecting two thermally controlled spacecraft modules which house the spacecraft equipment, experiments, and apogee motor. Four non-sun-oriented solar array panels, with cells mounted on both sides, are deployed beyond the antenna for maximum efficiency. The parabolic antenna reflector is formed from sixty honeycomb petals (40 triangular and 20 trapezoidal) hinged together and pinned to a 86-inch diameter hub. Eighty percent of the petal material is removed for weight reduction and thermal see-through considerations. The rf surface is provided by a fine mesh bonded to the petals. The petals, manufactured to a true paraboloidal surface, are strained flat for stowage in the launch configuration. Deployment and rate control against strain energy release are provided by 20 back-deployment truss members which are activated from the aft (upper) equipment module. Throughout deployment, petal and hub structural continuity is maintained through rotating hinge joints.

Four of the antenna back-deployment trusses are extended and strengthened to provide support for the solar panels. The roll axis solar panels are in the pitch-roll plane and the pitch panels are at ± 30 degrees to the yaw axis. The deployed four-panel approach was selected because it minimized power profile variations and battery weight and offered better packaging and growth capability in comparison to a two-panel array (deployed along the pitch axis). Either approach is superior to moving the panels in closer to the equipment module (antenna shadows severely degrade array performance), or mounting panels on the antenna which would reduce antenna dynamic frequencies and force local structural increases which would upset deployment force symmetry. Sun-oriented arrays are not considered necessary for the basic mission power requirements.

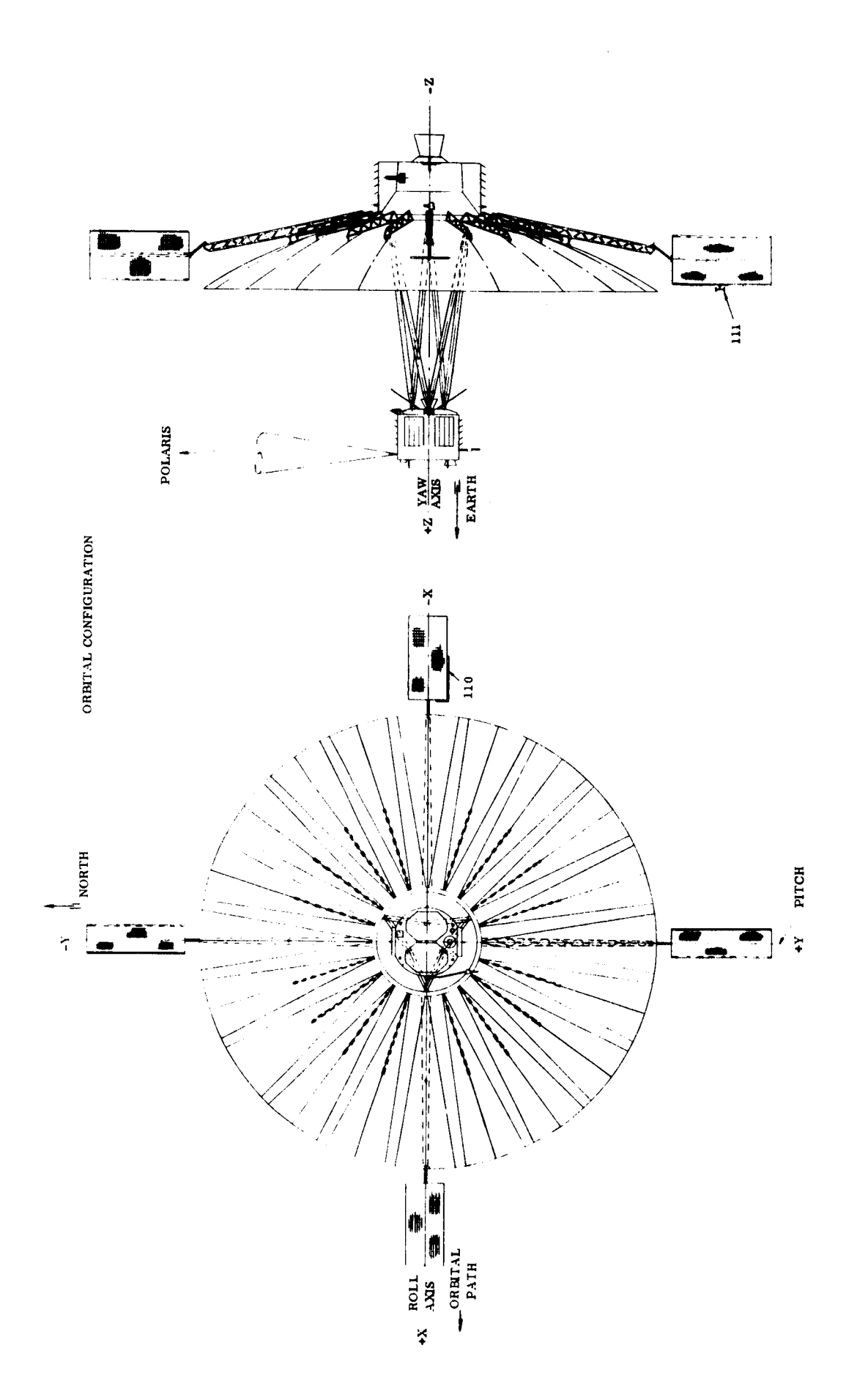
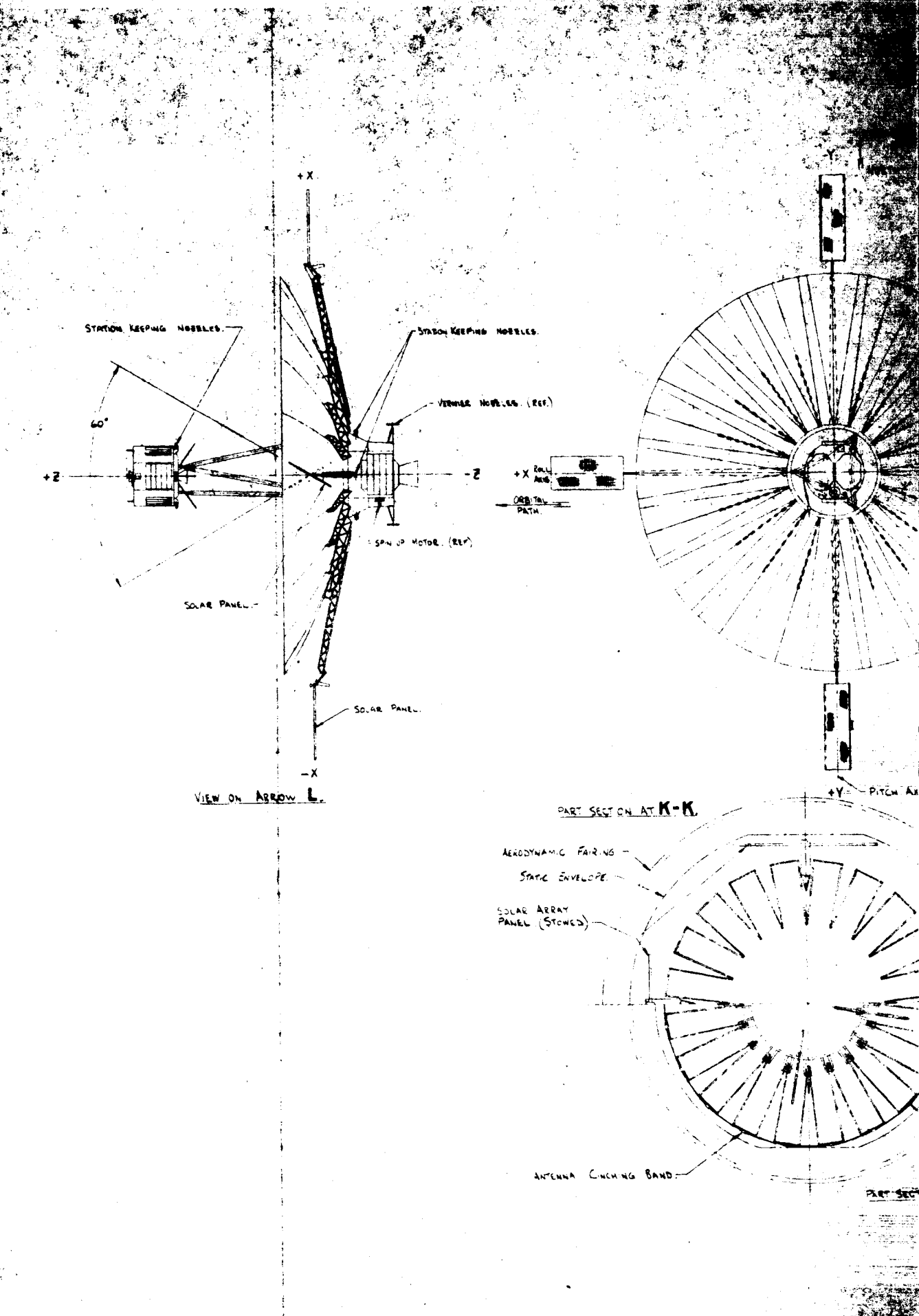


Figure 5.3-1. Selected Configuration (Orbital View)

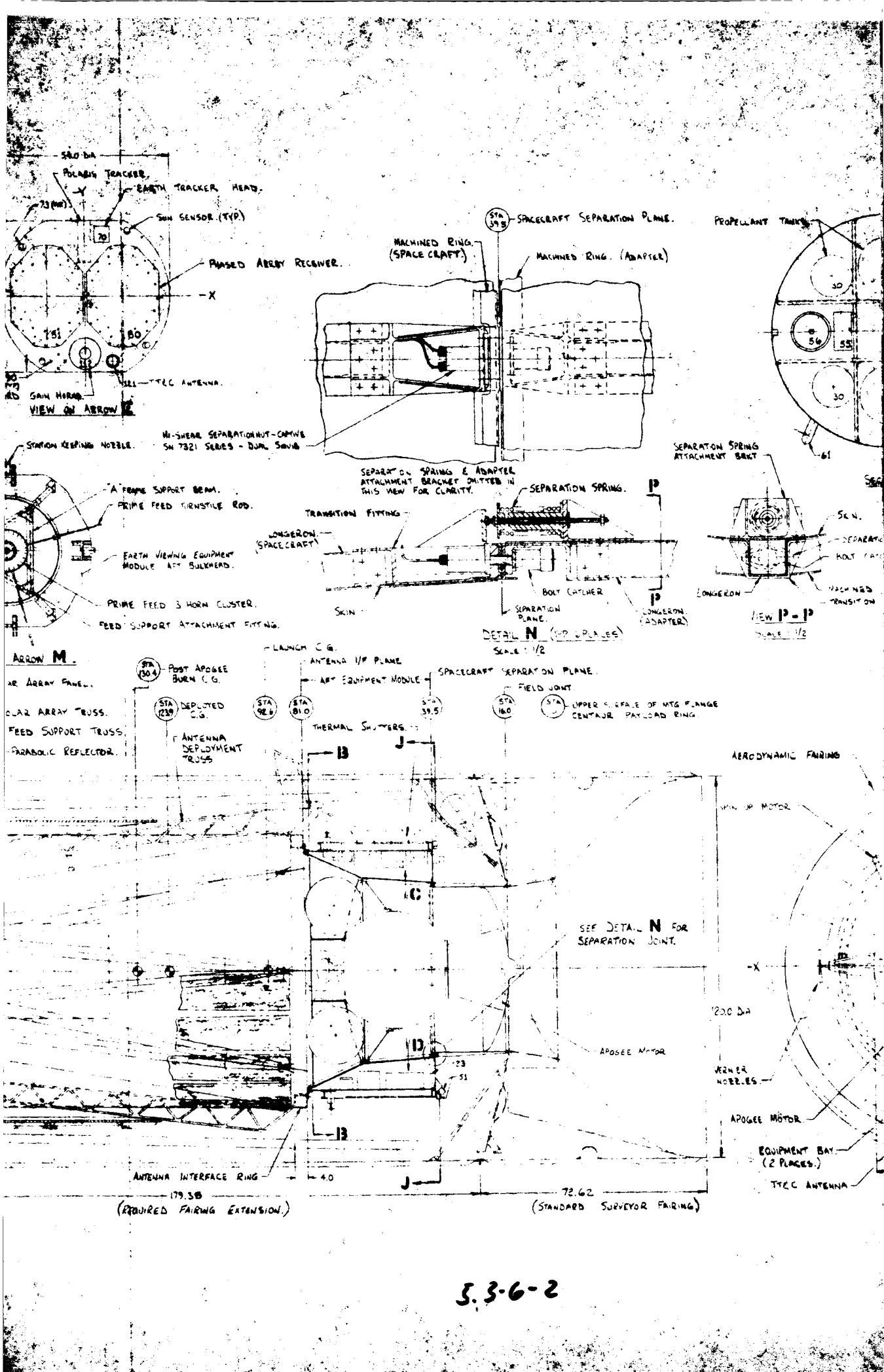
Figure 5.3-2 presents the selected configuration in the launch and orbital modes with cutaway views illustrating packaging and structural details. In the launch configuration, the folded antenna petals form a cylinder around the feed support tubes, emphasizing the matched geometry that results from an f/D of 0.4 and a 86-inch hub diameter. The solar panels are hinged back and snubbed to the deployment truss. Cinch-up is accomplished by a single circumferential band, located at the periphery of the open end of the antenna. This band snubs the antenna into a stowage bracket ring which is attached to the upper face of the earth viewing equipment module. A single deployment command is used to separate the cinch-up band and activate the back deployment motor. The back deployment trusses provide rate control for the strain energy induced deployment and insure the completed deployment of each antenna sector. Linkage, driven by deployment truss rotation about the hub, releases the solar array panels. In this way the solar array deployment is ganged to antenna deployment and does not require a separate command function. Solar array shear loads, while stowed, are transmitted to the earth pointing equipment module through clevis support pads.

The compatibility of the launch configuration with the static clearance envelope of the extended Surveyor fairing is illustrated in Figure 5.3-2. No part of the spacecraft violates the static or dynamic clearance envelopes determined for the ATS-4 program. The 15-foot cylindrical extension to the Surveyor fairing would be added between the present Surveyor cylindrical section, which mates to the Centaur, and the tapered nose fairing. The spacecraft launch vehicle adapter is similar to the Surveyor design and mates with the Centaur at the Centaur/Surveyor mating flange located at Centaur Station 172.45 (identified as spacecraft station zero). This mating station has been recommended for the ATS-4 program, but will require redesign to accommodate the higher payload weights and cg locations. The upper section of the adapter mates with the bottom surface of the aft equipment module. Adapter/spacecraft separation is provided by six dual squibbed explosive nuts. The adapter remains with the Centaur after separation.



5.3-5

MAX STATIC ENVELOPE :
(AT DIAMETER.) MIN STATIC ENVELOPE --(AT FLATS.) SECTION H-H - 120 -SMITIC ENVELOPE. AERODYNAMIC FAIRING (STANDARD SURVEYOR FAIRING.) 5.3-6-1



" NUT (SMCECRAFT) HER. (ADAPTER.) - ANTENNA INTERFACE RING

VIEW J-J

Figure 5.3-2. ATS-4 Selected Configuration, Inboard Profile and Orbital Configuration

5.3-6-3 5.3-5/6

The aft equipment module is built around a structural shell which transmits spacecraft loads directly to the adapter and provides a mounting surface for the concentrated mass of the apogee motor. Apogee motor attachment is provided by a machined girth ring which is furnished with the motor and is being developed for the Improved Delta application. A sixpoint attachment is used between the motor and the shell to facilitate alignment of the thrust vector with the spacecraft center of mass. Thirty sheets of aluminized mylar provide thermal isolation between the apogee motor, which remains with the spacecraft throughout the mission, and the payload. Thermal conduction is limited by the six-point attachment previously mentioned. Vernier propulsion and stationkeeping propellant tanks and equipment. and the orientation control momentum wheels, are packaged in a network of shear beams above the apogee motor. One sector of this area is maintained clear of equipment for two-arm access to facilitate arming and fusing of the apogee motor. Electronic components and batteries are housed in two separate equipment bays, designed as cupolas or dormers, mounted on the spacecraft pitch axis and provided with louvered heat rejection surfaces. The externally mounted equipment bays are not a part of the primary structural path but are hinged at the top to provide accessibility for repair and replacement of components without requiring removal of the bays, thermal control equipment or functioning components.

The earth viewing equipment module houses the phased array, interferometer, orientation control sensors, high frequency transmitters and receivers for the parabolic antenna and supporting telemetry and command equipment. The bottom section of this module is detachable and provides a mating surface for antennas and equipment requiring earth viewing. The phase array antennas occupy most of the available area (approximately 10 square feet) but all of the equipment has an undisturbed field of view. Particular emphasis was placed on mounting the interferometer antennas to prevent phase distortions. The Polaris sensor (yaw reference) is also mounted on this surface but views North along the negative pitch axis. This permits a clear field of view past the deployed antenna and solar array, but a short sun shield will still be required. Mounting the phased array, interferometer and attitude sensors on the same physical surface will eliminate many of the mechanical boresight problems and will simplify the operational correlation of experimental data.

The earth viewing equipment module has six independent payload bays. Five of the bays are provided with thermal louvers for controlled heat rejection. Component accessibility is available either on an individual panel basis, or by removing the bottom section of the module for ready access to all bays. Six heat rejecting surfaces were determined to be necessary because of the number of high heat dissipating components, particularly the phased array TWT's and electronics. The top surface of this module is used for mounting the prime feed horns and dipoles for the parabolic antenna, providing a short feed distance to the high frequency transmitters and receivers.

Telemetry, tracking and command (TT&C) antenna coverage is provided by two flush cavity antennas mounted on the end surfaces of the two equipment modules and a combined-purpose externally mounted antenna. The externally mounted antenna is used for telemetry, tracking and polarization angle measurements. Polarization measurements are used in conjunction with solar aspect sensors to determine spacecraft attitude during the spinning mode of operation. Prior to deployment, this antenna is mounted on the side of the earth viewing equipment module, parallel to the spin axis, and extends beyond the module to eliminate pattern interferences. The antenna is rigidly mounted in this position for accurate polarization measurement. During deployment the antenna latching device is automatically released (ganged to solar array deployment) and the antenna springs back out of the field-of-view of the equipment mounted on the face of the module. The combined antenna is not used after deployment, operational and reorientation command and telemetry coverage being provided by the flush mounted antennas on the end of the spacecraft.

Standard gain antennas are provided for the evaluation of the parabolic antenna experiment and possibly for phased array evaluation. The X-Band and S-Band standard gain antennas are coaxially mounted horns located on the bottom surface of the earth viewing equipment module. The 800 MHz standard gain antenna is mounted on the edge of the positive pitch axis solar array panel. The positive roll axis solar panel is driven at 100 MHz for standard gain measurements. Diagnostic telemetry and command capability is required during experiment operation which precludes the use of the standard gain antennas for TT&C purposes.

Two solid rockets are located on the periphery of the aft equipment module for spacecraft spin-up after separation. One-pound hydrazine vernier thrusters are also located on the aft equipment module and used for cancelling out injection errors, coning and precession control, and spacecraft despin. These thrusters are used in conjunction with a ten-pound thrust hydrazine nozzle which is mounted radially on the roll axis solar array support truss, aligned with the spacecraft center of mass (after apogee burn). Spacecraft momentum wheel unloading, stationkeeping and repositioning are accomplished with resistance jets located on both of the equipment modules. In all cases, nozzles were located to eliminate plume impingement on the spacecraft.

The six-member diagonal support truss forms the structural link between the equipment modules and accurately locates the prime feed at the focus of the parabolic antenna. The truss design is of critical importance because of the high structural loadings induced by the no-notch vibration design criteria specified by NASA. Beryllium tubes, 3-1/4 inches in diameter, with bonded stainless steel end fittings have been selected to minimize rf blockage and phase distortion and to enable a minimum weight design capable of meeting the column buckling and stiffness requirements. Beryllium tubes of this diameter are state-of-art and readily available from manufacturers. The high thermal conductivity and specific heat of beryllium will aide in reducing the solar heating induced prime feed misalignments. The support tubes can also be used as conduits for the interconnecting (between modules) fuel lines, electrical harness and coax cabling.

#### 5.3.2 SUBSYSTEM SUMMARY

The configuration description presented in the previous subsection indicated the split equipment module approach that best meets the operational requirements of the ATS-4 mission. As much of the spacecraft equipment as possible was located in the aft module to minimize structural load penalties. However, the earth viewing equipment module contains the prime experiment electronics, sensors and support equipment found necessary to meet earth viewing requirements or to minimize the complexity of the intermodule harness. The payload division is best illustrated in the system block diagram, presented in Figure 5.3-3, in which the subsystem components have been arranged to emphasize the interface between the struct-

ural assemblies. The left side of the diagram represents the earth viewing module and the right side represents the aft equipment module. The parabolic reflector, solar arrays, and interconnections are illustrated in the feed support region between the equipment modules. Furthermore, the TT&C and standard gain antennas are mounted to simulate their relative locations on the spacecraft.

A brief summary of each of the operational subsystems is presented in the following paragraphs.

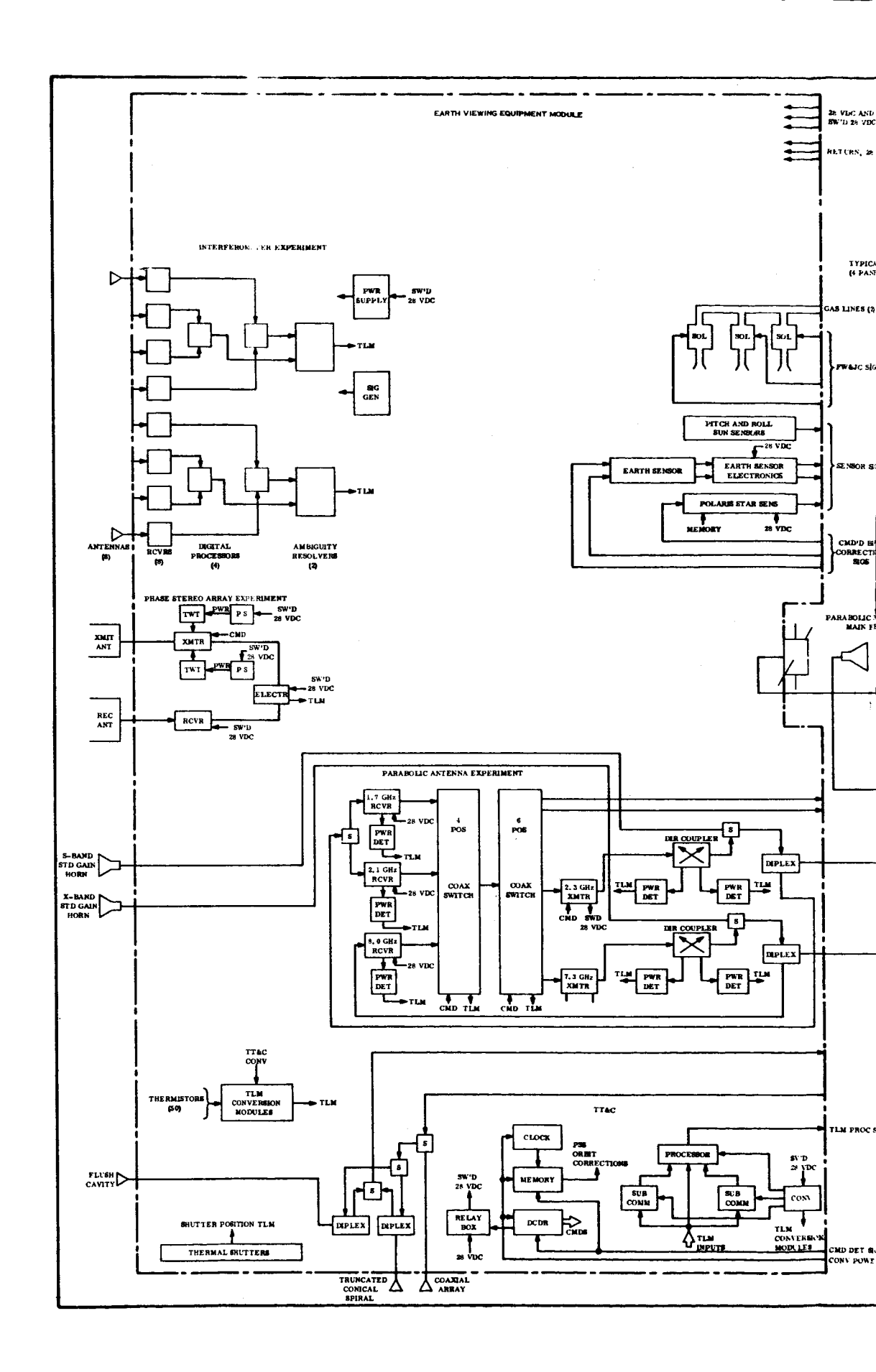
### 5.3.2.1 Power Subsystem

The power subsystem consists of a four-panel solar array, three nickel cadmium battery modules, three battery charge regulators, a voltage limiter, a pulse width modulated (PWM) regulator, a dc-ac 400-Hz inverter, and a power control unit. Primary power is derived from the solar cells with batteries supplying power to supplement the array during peak loads and for umbra conditions. These energy sources are connected to the PWM switching type regulator which provides a regulated 28 volt dc bus for the loads. The dc-ac 400-Hz inverter, operating off the 28-volt bus is provided for some of the power to the orientation control subsystem. The voltage limiter, a shunt regulator across part of the array, limits the array voltage supplied to the PWM regulator and to the battery charge regulator to a maximum of 43 volts. The battery discharge voltage established the lower limit of voltage supplied to the PWM regulator at 30.4 volts.

Wiring from each solar panel will include power leads from the full array and partial array, power return, regulated power for TLM sensors, and voltage and thermal sensor signals.

These lines will be dressed along the solar array deployment struts.

The 28-vdc power requirements of the equipment in the earth viewing module are supplied by the power subsystem. Maximum bus current will be approximately 16 amperes during phased array operation. Good wiring practice for space applications dictates:



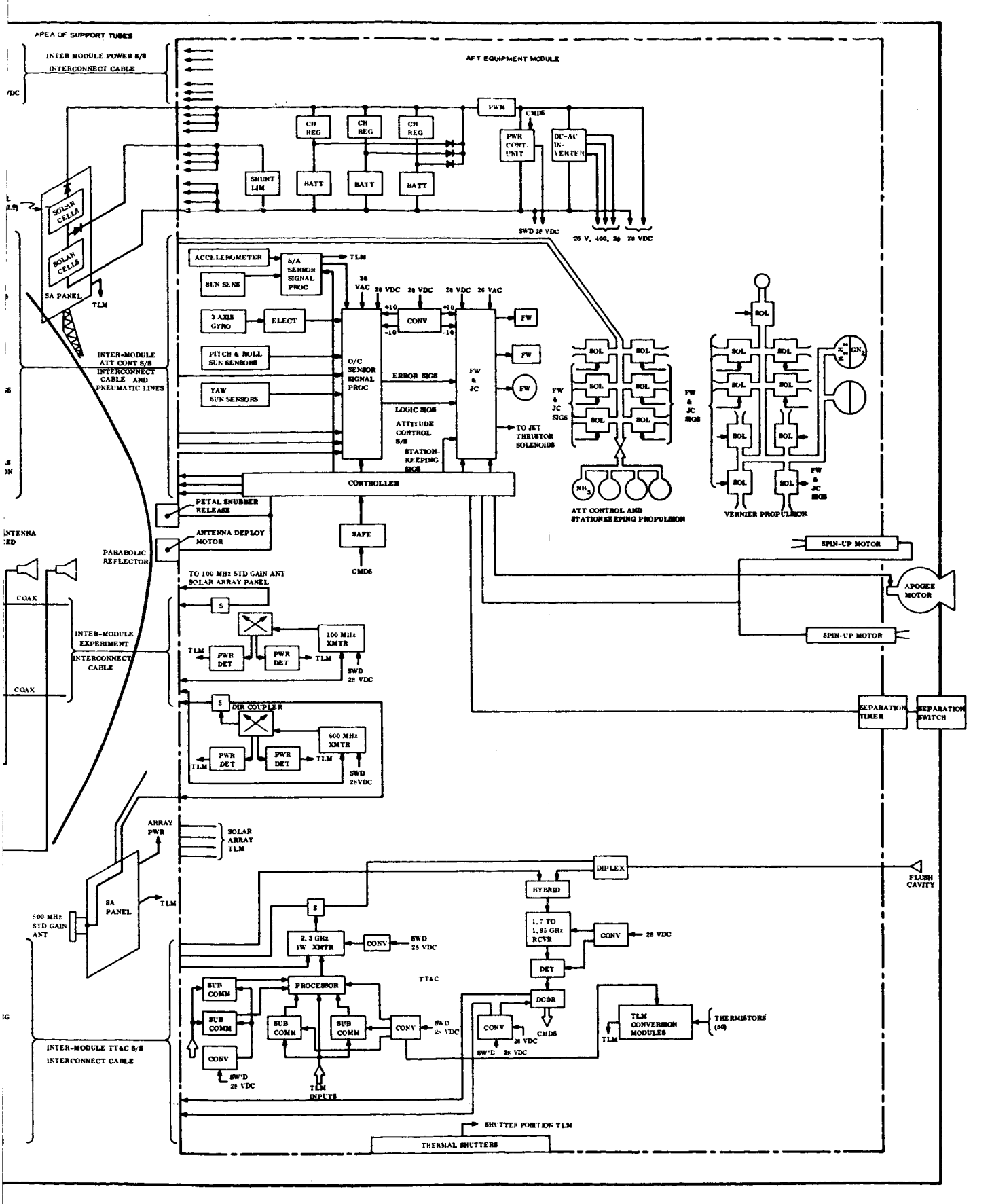


Figure 5.3-3. ATS-4 System Block Diagram



- a. No greater than 0.5-volt drop between power source and load
- b. No smaller than No. 22 wire size
- c. No one wire should carry more than 20 percent of the bundle capacity

Use of seven No. 20 AWG wires, each carrying 2.25 amperes, meets the good wiring practice for maximum current ratings. With estimated wire length of 20 feet and a nominal wire resistance of 9.7 ohms per 1000 feet, total line voltage drop will be 0.43 volt.

## 5. 3. 2. 2 Guidance and Control Subsystems

The guidance and control subsystem performs an unusual number of functions in that it is required to provide control not only in orbit, but also throughout the injection into orbit phase. The functions performed are briefly:

- a. Spinup
- b. Coning control
- c. Precession control
- d. Removal of orbit injection errors
- e. Despin
- f. Sun stabilization
- g. Earth stabilization (2 axes)
- h. Star stabilization (1 axis)
- i. Earth pointing to 0.10
- j. Pointing reorientation to any location on the visible earth's surface
- k. Tracking in response to ground commands
- 1. Stationkeeping
- m. Repositioning in longitude

An active system design has been selected for performing all functions in an integrated manner. Two solid propellant motors are used for spinup. The station acquisition sensor signal processor processes the angular accelerometer signal to actuate appropriate thrusters for coning control. Spin axis precession is controlled by thrusters which are actuated by ground command based on rf polarization angle measurements (made on the ground) and telemetered sun sensor signals. Injection errors are removed by thrusters actuated by ground command based on ground tracking data. Despin is performed by thrusters which fire automatically (after command initiation) in response to the signals from a three-axis rate gyro package. A single monopropellant hydrazine mass expulsion subsystem performs the thrusting required for coning control, precession control, vernier thrusting and despin. This mass expulsion subsystem is not required to operate after despin.

The orientation control sensor signal processor processes pitch and roll sun sensor and gyro signals to provide an error signal to the flywheel and jet controller to actuate the orientation control thrustors for alignment of the yaw axis to the sun. The earth sensor provides the control signals for earth stabilization. The yaw sun sensors provide control signals to actuate the yaw orientation control thrusters to align the negative pitch axis to the celestial north pole in order to acquire Polaris in the star sensor field of view. The star sensor provides the signal for controlling the yaw flywheel. The orientation control mass expulsion subsystem (resistance jets) provides all the control torques necessary for stabilization and flywheel unloading as well as the thrust for stationkeeping using a total of only nine thrusters.

Although the aft equipment module was designated for all housekeeping subsystems in order to minimize the size of the earth viewing module and reduce the rf field interference with the parabolic reflector, tradeoff analysis dictated that certain components of the housekeeping subsystems be located in the earth viewing module. The earth sensors and Polaris tracker require an unobstructed field of view. Three mass propulsion thrusters were placed on the earth viewing module to establish a total thruster configuration that brackets the spacecraft's center of mass.

Interconnections between components of the orientation control subsystem comprise: two pneumatic lines for the three thrusters; wiring to supply signals to the thruster solenoids; heater power to the thrusters; bias signals to the earth tracker and Polaris star sensor, for station change and slewing; and sun sensor, earth tracker and Polaris star sensor signals to the sensor signal processor.

# 5.3.2.3 TT&C Subsystem

The telemetry subsystem samples the diagnostic, operational and experimental monitors throughout the vehicle and transmits this information to the ground station. The telemetry subsystem is a real time PCM/PSK/PM system operating at S-Band. Data can be collected from up to 628 points and transmitted at data rates of 500 bps or 8 kbps. The PCM data bi-phase modules a 1.024 MHz subcarrier which then phase modulates the carrier.

The command subsystem provides for ground control of the payload and all vehicle subsystems. Commands are transmitted to the vehicle by frequency shift-keying subcarriers which are phase modulated onto the carrier. The command system is capable of executing up to 390 commands.

The tracking subsystem consists of a modified Goddard Range and Range Rate transponder.

Telemetry processing and command decoding equipment have been provided in both the earth pointing and the aft equipment modules. This packaging technique avoids the large bundle of wires that would otherwise be required for transporting the individual telemetry and command signals across the equipment modules interface.

# 5.3.2.4 Experiments Subsystems

To demonstrate the capability of a satellite to deploy, point and use large aperture antennas and other devices requiring precision pointing toward the earth's surface, a list of experiments has been prepared involving the use of a 30-foot parabolic reflector, an interferometer, a phase-steered array and the orientation control subsystem.

Four transmitters and three receivers, with associated switches, detectors, and reference antennas will support the parabolic antenna experiments. The inclusion of a four-position switch allows for switching of any receiver output to a six-position switch that in turn allows for switching to any transmitter, thus providing the flexibility of configuring the equipment for the listed experiments.

The radio interferometer is an X-Band, two speed system, with a nominal angular measurement accuracy of about 0.015 degrees and a field of view large enough to cover the visible earth disc. Its antennas will be 10 dBX-Band horns with the four fine measurement horns spaced about 44 wavelengths apart, and the four coarse horns at about 2 wavelengths. It will be designed to operate either open or closed loop; i.e., either to measure the angular direction of a beacon or to serve as the pointing sensor in the orientation control loop.

The phase-steered array is specified and requires little additional on-board equipment for evaluation. It is a four-beam, two-channel re-directive array, operating in the 7-8 GHz region, having two independent antennas of approximately 30 dB gain each.

Essentially no additional experiment equipment will be required for the orientation control experiment. Evaluation will be made by checking the performance of the orientation control system using the radio interferometer as a pointing sensor against the performance with the earth trackers.

# 5.3.2.5 Thermal Subsystem

The temperature control system for ATS-4 is an optimum combination of semi-passive and passive concepts utilizing shutters, coatings, insulation, heaters and the thermal mass of equipment and structure. All but one of the equipment mounting panels is equipped with an array of shutters. Passive areas are covered with super insulation. Exposed structure will be coated to minimize heat leaks. Space rated coatings or finishes will be applied to the parabolic antenna and the support truss between the equipment modules. Heaters will be used in the earth viewing module to maintain minimum temperature during extended off cycles.

### 5.3.2.6 Module Interface

The interface between the two equipment modules involves all subsystems.

#### Electrical interconnections include:

- a. Regulated 28-vdc power and power return lines
- b. Orientation control signals to thruster valve solenoids and heaters
- c. Bias correction signals to the earth trackers and Polaris star sensor
- d. Sun sensors, earth tracker and Polaris star sensor signals to the sensor signal processor
- e. Coaxial lines from the 100-MHz and 800-MHz transmitters to the parabolic antenna main feed
- f. Antenna experiment receiver output signals to the 100-MHz and 800-MHz transmitters
- g. Processed telemetry signals to the TLM transmitter
- h. Command detector signals to command decoder
- i. Converter dc power to the command clock, memory and decoder
- j. Command signals to the receiver
- k. TLM and tracking transmitter output to antenna.

In addition to the electrical interface, two pneumatic lines are required to the three thrusters in the earth viewing module.

#### 5.3.3 SYSTEM PERFORMANCE

The measure of the selected spacecraft configuration is the comparison of its design performance to the study requirements and to the performance of alternate design approaches. Tabulations of error budgets, mass and balance, CG locations and power capability aid in the evaluation and are presented in this subsection. Where applicable, performance requirement values from Section 5.2 are also included.

The spacecraft comparison must also be based on the subjective evaluation of the design approach, its feasibility, simplicity of deployment, growth capacity and potential development problem areas. Sections 5 through 9 of this report provide the information for this evaluation.

# 5.3.3.1 Parabolic Antenna Experiment

The loss budget for the parabolic antenna experiment, presented in Table 5.3-1, indicates that the desired efficiency of at least 50 percent is not realized with this design. Nevertheless, the antenna performance is extremely good except at the 100 MHz frequency where the reflector is small in comparison to the wavelength and excessive spillover and illumination losses occur.

A major contribution to the loss budget is the rf blockage and support truss reflection losses. These can be reduced in magnitude by decreasing the diameter of the earth viewing equipment module and/or by moving the support truss farther out, radially, from the boresight axis of the antenna. However, the former conflicts with the packaging requirements of the phased array and interferometer and the latter introduces undesired deployment complexity.

Under orbital conditions, solar heating will induce mechanical distortions in the reflector which will result in degraded rf performance. The reflector has been designed to minimize this effect. The thermal distortion losses indicated in Table 5.3-1 represent the rf degradation resulting from the worst case (edge on) solar illumination of the reflector.

Table 5.3-1. Parabolic Antenna Performance

Gain Loss in dB

	Loss			Freq	uency in (	Hz		
	Factors	0.1	0.8	1.7	2.1	2.3	7.3	8.0
1	Illumination and Spillover	2.32	1.38	1.92	1.38	1.50	1.40	1.40
2	Rf Blockage and Reflection	1.40	1.40	1.41	1.42	1.42	1.58	1.63
3	Thermal Distortion	0.00	0.00	0.01	0.02	0.02	0.17	0.30
4	Miscellaneous*	0.42	0.35	0.31	0.29	0.31	0.36	0.37
	Total Loss (dB)	4.14	3,13	3.65	3.11	3,25	3.51	3.70
	System Efficiency	38.5%	48.5%	43.1%	49%	47.5%	44.5%	42.7%

Includes: Wire mesh reflector loss, feed phase error, cross polarized loss, feed attenuation, transmission line loss, and VSWR reflection loss.

### 5.3.3.2 Orientation Control Experiment

The error budget presented in Table 5.3-2 illustrates the ability of the attitude control system to meet the stringent requirement of pointing, to within 0.1 degree, to any part of the visible earth. By the 3 nature of the error sources, the pointing will almost always be more accurate than the RSS accuracy shown in the table. During the normal operation of the parabolic antenna experiment, yaw axis accuracy is important only in the cross coupling it induces to the pitch and roll axes. However, high yaw accuracy is required for interferometer experiment operation and in the case of parabolic antenna boresight errors measurements. Many future ATS-4 experiments will probably also require high yaw accuracy.

The orientation control system performance is summarized in Table 5.3-3, for the conditions of pointing, slew, tracking and the initial stabilization maneuver. All contract requirements for these conditions are met.

The servo-elastic coupling of the spacecraft structure and the orientation control subsystem was minimized to the extent that it does not have a significant effect on system performance, even with structural dampling as low as 0.1 percent of critical (equivalent to material hysteresis). This decoupling was designed into the system by the early specification of structural frequency objectives.

Table 5.3-2. Orientation Control System Three Sigma Error Budget

_	Error Allocation	1
Error Source	Pitch-Roll	Yaw
Basic Sensor Error	0.05	0.02
Commanded Angle Resolution	0.02	0.003
Star Tracker Gimbal Offset	**	0.03
Earth Horizon Anomalies	0.004	
Sensor Control Axis Misalign.		
<ol> <li>Prior to Launch</li> <li>Due to Launch Effects</li> <li>Orbit Environment</li> </ol>	0.02 (incl. cal.) 0.01 0.01	0.003 0.01 0.01
Sensor Output Noise	0.02	0.03
Control Electronics Error	0.01	0.01
Momentum Storage Offset	0.03	0.05
Timing Error ST Gimbal Comm.	0.005	0.005
Spacecraft Angular Pos. Uncert.	0.03	
Spacecraft Drift	0.02	
Target Location Uncertainty	0.0003	. 0.0003
Yaw Cross Coupling Error	0.01	
Earth Sensor Readout	0.01	
3 <sup>σ</sup> Accuracy Per Axis	0.08	0.07
3 <sup>o</sup> Absolute Pointing Accuracy*	0.09	

<sup>\*</sup>Reference Section 6.4.3.4 for derivation

Table 5.3-3. Orientation Control Subsystem Performance Summary

Maneuver	Requirement	Performance
Earth Pointing	0.1 degree accuracy to any point on visible earth	0.09 degree, 3 <sup>o</sup>
Slew Maneuver	Slew from horizon to horizon and stabilize to ±0.1 degree in 30 minutes	Maximum of 25 minutes
Tracking	Track rate = 10 millirad/sec Max angular error = 0.5 degree	Angle error < 0.5 degree if wheels are initially at less than 40% max speed; therefore may require wheel unload at
Initial Stabilization:		initiation of maneuver
Sun Stabilization		Start from 180 degree error point, 1 to 2 hour stabilization time
Earth Stabilization		From 5 degree pitch, 25 degree roll and 0.02 de/sec in all axes = stabilize in 27 minutes max.
Star Stabilization		Stabilize to sum in 1 to 2 hours for acquiring Polaris in star sensor field of view

# 5.3.3.3 Phased Array and Interferometer

The phase-steered array will be similar to that developed under NASA/GSFC Contract NAS 5-10101. Table 5.3-4 illustrates the predicted performance characteristics of this equipment.

Table 5.3-4. Performance Requirements Summary - Phase-Steered Array Antenna

Parameter	Required	Achieved
Frequency	7-8 GHz	8 GHz
Multibeam Operation	4 beams, 2 each transmit and receive	4 beams, 2 each transmit and receive, full 2-channel operation
Gain	Minimum 30 dB on each beam	30 dB on each beam
Steering	Command or pilot signals	Pilot signals
Pointing Accuracy	Consistent with beamwidth	Within approximately 0.1 beamwidth

The interferometer was required to fully demonstrate its capability and limitation as an attitude determination device.

It was required that the interferometer should be designed to be sufficiently accurate to monitor the other precision systems on board; i.e., the orientation control system and the parabolic antenna at its highest frequency. It was also decided that the interferometer should be able to respond to an appropriate beacon anywhere on the visible earth disc. Its frequency was placed with the objective of obtaining the desired performance characteristics without requiring deployment.

The interferometer characteristics are given in Table 5.3-5 and the error budget is presented in Table 5.3-6.

Table 5.3-5. Interferometer Performance Summary

Parameter	Required	Achieved
Angle Measurement	Consistent with attitude control system require- ments	0.015 degree; 10error, which can be compared to the orientation control experiment earth tracker accuracy of 0.05 degree, 30
Field of View	Objective; visible earth disc (17.5 degrees)	≥ 23 degrees
Frequency	Consistent with accuracy and structural require- ments. Objective at non- interference with antenna experiments	10 GHz, providing antenna spacing of approximately 40 λ within 4-feet diameter. No antenna experiments above about 8.1 GHz.

Table 5.3-6. Interferometer Error Budget

Source	Error, Electrical Degrees, 10
Receiver Noise	0.080
Quantizing Error	0.088
Oscillator Noise	0.745
Video Processing	0.250
Microwave Components	9.000
Geometric Distortions	0.290
Geometric Error, One Plane Geometric Error, Two Planes	2.17 (0.0048) = 0.0104 degree 0.015 degree, 1 <sup>o</sup>

# 5.3.3.4 Command and Telemetry Subsystem

The capability of the Command and Telemetry subsystem is summarized in Table 5.3-7. An S-Band system has been selected with the capability of decoding 390 commands, and with a total telemetry input capability of 628 channels. The subsystem has been designed to meet the full operational system requirements with adequate margin; no one subsystem or operational requirement has been responsible for dictating the overall design.

Table 5.3-7. Command and Telemetry Subsystem Capability

Command	·
Frequency	1700-1850 MHz
Modulation	FSK/PM
Bit Rate	100 bps
Bit Rate Error	10 <sup>-5</sup>
Number Command Outputs:	
Available	390 commands
Required	320 commands
Telemetry	
Frequency and Power	2200-2300 MHz at 1 watt
Modulation	PCM/PSK/PM
Data Rate	500 bps (spin mode), 8 kbps (in-orbit)
Bits per word	7
Number TLM Inputs:	
Available	628 channels
Required	551 channels

## 5. 3. 3. 5 Power Subsystem Capability

A solar array battery system has been selected for this application. Its design performance is summarized in Table 5.3-8. The solar array has been sized for approximately 300 watts at the end of life after 22 percent degradation. Average power during solstice is less than this but the satellite does not go through the earth's umbra during solstice periods, which effectively increases array capability. Additionally, 103 pounds of batteries have been provided to supplement the solar array during periods of experiment peak power demands and also to supply power to the entire load when the spacecraft is in the earth's shadow, a maximum of 1.2 hours. Battery sizing assumed no recharge time between an umbra condition followed by the experiment's peak power load requirement. Therefore, complete experiment operational flexibility can be accommodated by the power subsystem.

The power equipment designed for the operational mission will also supply complete spacecraft needs during the initial acquisition phase of the mission.

### 5.3.3.6 Spacecraft Weight and Balance

A complete weight summary of the selected spacecraft configuration is presented in Table 5.3-9. In the following subsections of this report, each spacecraft subsystem is discussed in detail and a firm basis is established for the weight estimates. A growth allowance of 160.1 pounds has been added to the in-orbit design weight summary of 1533.7 pounds, to account for design growth and selected subsystem redundancy. Each of the items, in Table 5.3-9, marked with an asterisk (\*) are identical to the values identified in the Launch Vehicle Capability Summary presented in Table 5.2-1.

Table 5.3-10 presents the mass moments of inertia and cg locations for the selected configuration, for the in-orbit conditions and throughout the initial acquisition phases of the mission. Center of mass locations along the yaw axis (Zcg) are measured from spacecraft station zero (Centaur/payload mating plane) as illustrated in Figure 5.3-2. Two sets of values are presented in Table 5.3-10, representing the final design values and the design-freeze values used in the subsystem analysis. Traditionally, the detail analysis and sizing of structural members occurs after component definition. Therefore, the final design values of weights and inertias are not available in time for early subsystem analyses. Table 5.3-10 indicates off-axis cg locations; these would be balanced out during the detail design.

Table 5, 3-8. Power Subsystem Capability

		A Property Arresty	Avg. Energy	Average Array Power	Average Array Power Available to Load (Watts)
1. Array Capability		Solstice - Equinox (watts)	(watt-hr per Day)	Array Alone	Array and Battery
Start of Life	3	350 392	8400-9400	297-333	245-275
End of Life		272 304	6520-7250	231-258	190-212
2. Load Requirements	nts	watt-hr			
Base Load and Heaters Stationkeeping Experiments and Tracking Telemetry and Command	leaters d Tracking Command	2607 408 959 217 4191			
3. Battery Capability -	ity -	From Battery (watt-hr)	At Load (watt-hr)	Battery Charge Characteristics Time (Typical) Efficien	haracteristics Efficiency
(Total Energy Available from Battery = 1030 watt-hr)	/ailable 1030 watt-hr)				
30% Depth of Discharge 50% Depth of Discharge	scharge scharge	30 <b>9</b> 515	270	7.3 hr 9.0 hr	72% 68%

# Table 5.3-9. Detail Weight Summary of Selected Design

(109, 3)

(221.6)

4.5 4.5 5.0 9.0 10.0 15.0 24.4 31.6 40.0

35.0 10.0 7.0 4.0 2.0 2.0 4.0 1.0

Weight (lib)

Orientation Control - (Sensors, Mechanisms)		
Earth Sensors	10.7	
3-Axis Gyro Package	7.5	
Gyro Electronics	8. 0	
Sun Sensors (12)	2.7	
Polaris Star Sensor	12.0	
Sensor Signal Processor	15.3	
Momentum Device and Jet Controller	19. 2	
Momentum Device - Pitch	11, 3	
- Roll	11.3	
- Yaw	11, 3	
Initial Acquisition - (Sensors, Spin System)		(15. 5)
	2. 1	
Sun Sensors (2)	3. 2	
Electronics	7, 4	
Spinup Motors (2) (4.2 lb of fuel)	2.8	
Accelerometer	2.0	
Vernier Propulsion System		(35, 7)
Propellant Tank (2)	10,0	
Fill Valves (2)	0. 5	
Pressure Transducers (10)	5. 0	
N'C Explosive Valve	0.7	
Thrusters (Incl. Solenoids):		
1 lb level (8)	12.0	
	2. 0	
10 lb level (1)	4.5	
Gascous Nitrogen Temperature Transducers (2)	1.0	
•		
Stationkeeping (rientation Propulsion		(127.1)
Propellant Tanks (4)	7, 6	
Tank Wicking and Hardware	2. 4	
Explosive Valves (10)	3, 8	
Filter	2. 4	
Regulator, Pressure Transducer, Relief	1.8	
Solenoid Valves (18)	3.6	
Nozzles (9)	11,3	
Pressure Transducers (4) and Temperature Sensor		
Tank Skin (4)	1.8	
Ammonia Propella t	92. 4	
TT&C		(61.3)
Antenna (3)	2. 5	
Diplexer (3)	1.5	
RF Switches (4)	0.8	
Receiver	2. 0	
Command Detector	1.0	
Command Decoder	8.0	
Relay Box	5, 0	
Memory and Clock	6.0	
Sub-Commutator (6)	9. 0	
TLM Processor (Commutator) (2)	8.0	
	2.5	
TLM/TRK Transmitter	2. 5 3. 0	
TLM/TRK Transmitter Receiver Converter		
TLM/TRK Transmitter	3. 0	

SUBSYSTEM

Orientation Control - (Sensors, Mechanisms)

Experiments

Experiments

Receiver (1700 MHz)
Receiver (2100 MHz)
Receiver (8000 MHz)
Transmitter (800 MHz)
Transmitter (800 MHz)
Transmitter (800 MHz)
Transmitter (2300 MHz)
Transmitter (7300 MHz)
Transmitter
Electronics
- TWT (2)
Interferometer
(Incl. Antenna, Electronics, Power Divider)
Switches (5)
Electrical Switch Package
Ant. Multiplexer (2)
Std. Gain Antenna (800 MHz)
Std. Gain Antenna (800 MHz)
Std. Gain Antenna (8-Band)
Std. Gain Antenna (8-Band)
Reflector (nstrumemation

STIBS	YSTE	и

Power	Weight (1b)	(199.0)
Batteries (3)	103.0	
Battery Charge Regulator (3) Foltage Limiter Control	2. 0 3, 0	
oltage Resistor Assembly	4. 0	
Regulator	12. 0	
Oc/ac inverter	5. 0	
Power Control Unit Solar Array Panels (Exclusive of Honeycomb)	4.0 66.0	
Parabolic Antenna	66.0	(187.7)
reflector:		
Panel Frame	43.1	
Screen	10.7	
Panel Hinges	9.5	
Thermal Attachments	1.5 1.6	
Deployment Mechanism:	•••	
Hinges/Pins	8.8	
Actuators	45.1	
Tube	0.8	
Universals	3.0 11.8	
Trusses Motor	3,1	
Interface Mounting Ring	30.0	
Prime Feed Horn	10.0	
Launch Storage Provisions	8.7	
Apogee Motor - Dry Weight		(139.0)
Harness and Tubing		(72, 3)
Adapter Hardware - Spacecraft Mounted		(4.0)
Thermal Control		(64.7
Earth Viewing Equipment Shutters (5)	18.5 3.5	
Earth Viewing Equipment insulation and Paint (1) Earth Viewing Equipment Thermal Panels	3.5 3.5	
Aft Equipment Module Shutters (2)	12.2	
Aft Equipment Module Insulation and Paint	13.0	
Aft Equipment Module Thermal Panels	14.0	
(1) Portion Chargeable to Thermal Control of Space Items Excluding Phased Array	<b>78-</b>	
Structure		(296.5
Earth Viewing Equipment Module Structure	40.7	
Feed Support Trusses and Fittings (6 Adjustable	51.0	
6 Monoball only) Solar Array Trusses (4)	31.0	
Aft Equipment Module - Primary	73.0	
Aft Equipment Module - Primary Aft Equipment Module - Secondary	37.0	
Aft Equipment Bay Thermal Panel Support	17.0 37.5	
Solar Array Panels (Honeycomb/Supports Only) Solar Panel Latching and Deployment	9.3	
DESIGN WEIGHT	1533.7	
GROWTH ALLOWANCE	160.1	
ORBITAL WEIGHT	1693.8	
(Weight after vernier maneuvers and venting of remaining vernier propellant)		•
Vernier Propellant (Hydrazine)	71,2	
SYNCHRONOUS ORBIT WEIGHT	*1765.0	
Apogee Motor Fuel	1440.0	
PAYLOAD WEIGHT FOR APOGEE BURN	*3205.0	
Spinup and Coning Control	6.0	
Mass Expulsion:		
Spinup Propellant 4.2 lb		
Hydrazine 1.8 lb		
SEPARATION WEIGHT	*3211.0	
SEPARATION WEIGHT		
Spacecraft Adapter	136,0 *3347,0	

<sup>\*</sup>See Table 5, 2-1,

Table 5.3-10. Inertia and Center-of-Mass Summary

	Final Design Values	Design Freeze Values Used in Analysis	Units
Orbital Weight (Deployed)	1693.8	1695.0	<u>lb</u>
Xcg (Roll Axis)	0,50	0.2	in.
Zcg (Yaw Axis)	124.05	123.9	in.
Yeg (Pitch Axis)	0.40	-1.0	in.
Iox (Mass Moments of Inertia)	3799.81	3621.9	slug-
Ioz (Mass Moments of Inertia)	1653.42	1609.5	slug-
loy (Mass Moments of Inertia)	3212.63	3065.7	s lug-
Synchronous Orbit Weight (Folded)	1765.0	<u>1766. 0</u>	<u>lb</u>
Xcg (Roll Axis)	0 <b>. 4</b> 8	0.2	in.
Zcg (Yaw Axis)	130, 51	130.4	in.
Yeg (Pitch Axis)	0.39	-0.9	in.
Iox (Mass Moments of Inertia)	2974, 45	2799.7	slug-
Ioz (Mass Moments of Inertia)	349.29	308.0	slug-
Ioy (Mass Moments of Inertia)	2863.89	2719.0	slug-
2/3 Burn (Folded)	2245.0	2246.0	lb
Xcg (Roll Axis)	0.38	0, 2	in.
_ · · · · · · · · · · · · · · · · · · ·	113, 55	113.7	in.
Zeg (Yaw Axis)	0,30	-0.7	in.
Yeg (Pitch Axis)		3322.9	slug-
Iox (Mass Moments of Inertia)	3511.12	1	slug-
loz (Mass Moments of Inertia)	370.70	329.7	slug-
Ioy (Mass Moments of Inertia)	3400, 56	3241.3	_
1/3 Burn (Folded)	2725.0	2726.0	<u>lb</u>
Xcg (Roll Axis)	0.31	0.1	in.
Zcg (Yaw Axis)	102.56	102,8	in.
Yeg (Pitch Axis)	0.25	-0.6	in.
Iox (Mass Moments of Inertia)	3860.40	3662.0	slug-
Ioz (Mass Moments of Inertia)	385.85	344.8	slug-
loy (Mass Moments of Inertia)	3749.85	3581.1	slug-
Payload Weight for Apogee Burn (FOLDE	3205.0	3206.0	<u>lb</u>
Xcg (Roll Axis)	0, 26	0.1	in.
Zeg (Yaw Axis)	94, 85	95.2	in.
• •	94.85 0.21	-0.5	in.
Yeg (Pitch Axis)	4101.60	3896.4	slug-
Iox (Mass Moments of Inertia)		1	slug-
Ioz (Mass Moments of Inertia)	392, 82 3001 06	351.8 3815.4	slug-
Ioy (Mass Moments of Inertia)	3991.06 3211.0		
Separation Weight (Folded)		3212.0	lb in
Xcg (Roll Axis)	0, 26	0.1	in.
Zeg (Yaw Axis)	94.81	95.2	in.
Yeg (Pitch Axis)	0.21	-0.5	in.
Iox (Mass Moments of Inertia)	41 03. 24	3897.2	s lug-
Ioz (Mass Moments of Inertia)	394.38	351.8	slug-
Ioy (Mass Moments of Inertia)	3992.50	3816.2	slug
Launch Weight (Folded)	3347.0	3327.0	<u>16</u>
Xcg (Roll Axis)	0.25	0.1	in.
Zcg (Yaw Axis)	91.77	92.6	in.
Ycg (Pitch Axis)	0.20	-0.5	in.
Iox (Mass Moments of Inertia)	4275.53	4039.0	slug
loz (Mass Moments of Inertia)	416.40	364.8	slug
loy (Mass Moments of Inertia)	4164,79	3958.0	alug

#### 5. 3. 4 SYSTEM GROWTH CAPABILITY

The selected spacecraft configuration has been optimized for an existing apogee motor such that the four primary experiments, identified by NASA, and their associated instrumentation and electronics can be placed into synchronous orbit and evaluated with launch equipment existing or in development. The 160 pound of spacecraft growth capability, identified in the previous subsection, must be allocated to design growth and selected subsystem redundancy. The transmitting and receiving equipment, provided for the parabolic antenna evaluation, and the phased array can be used to perform selected operational experiments, but the additional ATS-4 experimental capability needed to support many of the future NASA programs is identified in the following growth items:

- The selected configuration was designed to a no-notch environmental specification. A more realistic and detailed identification of a launch vehicle environmental design criteria will result in an approximate 60 pound reduction in structural weight. For example, the upper equipment module was designed to lateral loading of 16 g. A notched specification would reduce this to approximately 4 g.
- The SLV-3C/Centaur capability of inserting a 4000 pound payload into the transfer ellipse was established for this study. Independent estimates are available from government and contractor sources which place this capability at 4200 to 4400 pound.
- The selected configuration was optimized to the capability of an existing apogee motor. An optimized launch vehicle capability would be realized through apogee motor development.

Growth items 1 and 2 are readily available and should be added to the 160 pounds previously mentioned to provide approximately 280 pounds for design growth, redundance and selected additional experiments. Item 3 is of significant importance to the ATS-4 program. Figure 5.3-4 illustrates the spacecraft growth capability as a function of apogee motor development and SLV-3C/Centaur payload capability into the transfer orbit, under standard conditions. The extended Improved Delta motor is illustrative of an optimized motor in that cylindrical casing extensions were assumed to match the full capability of the SLV-3C/Centaur. The Antares I motor is available with no development, but has a poor packaging geometry (see Section 6.8). It is apparent from this figure that apogee motor development is the key to future ATS-4 experimental growth with a maximum realizable growth capability of approximately 400 pound.

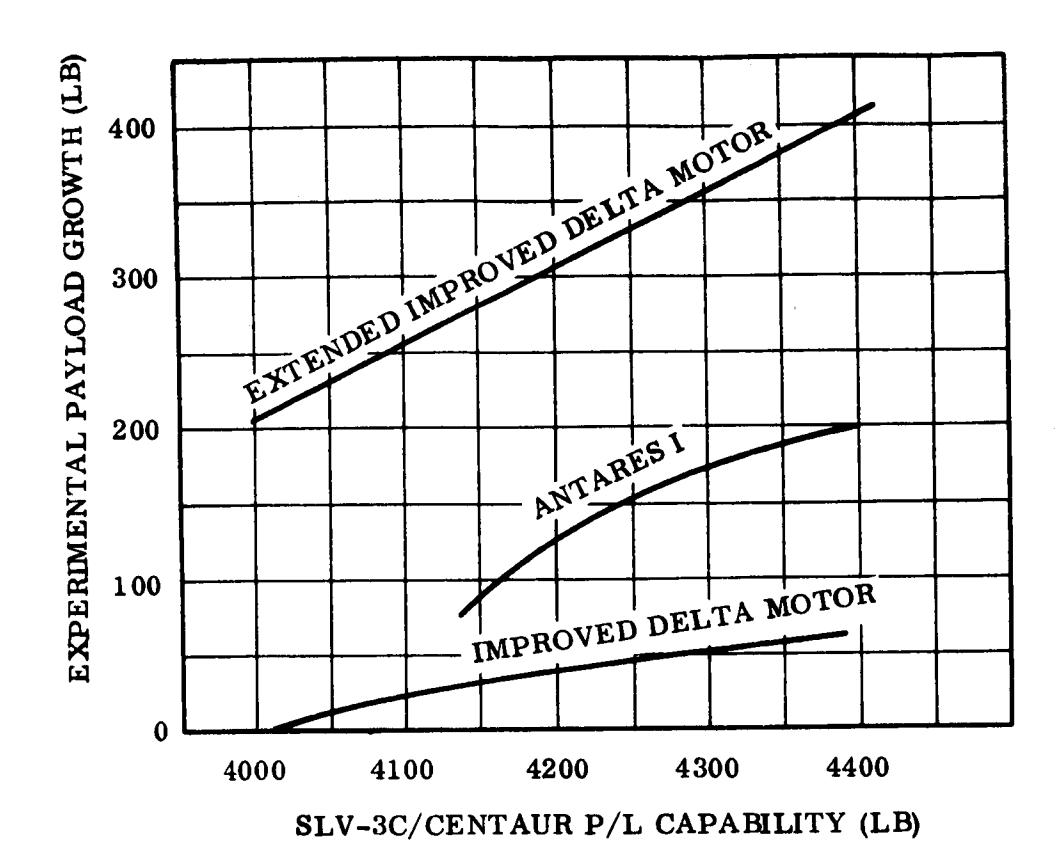


Figure 5.3-4. ATS-4 Payload Growth

Not all of the potential growth capability is available for experiments; structure, power, orientation control, and telemetry subsystems would also share in the growth. However, only the structure and power percentage of the total growth is significant.

- Structure. Both of the spacecraft equipment modules can accommodate additional a. experiments and can be lengthened for additional volume and heat dissipation capability without requiring additional fairing extensions. The aft equipment module payload compartments can be lengthened, in conjunction with the lowering of the separation interface, or additional compartments can be added. This section of the spacecraft is designed for dynamic stiffness and only about 5 percent of the growth added in this area would be in structure. The earth viewing equipment module support structure has been designed for strength, additional payload will increase spacecraft bending loads and approximately 15 percent of the growth added to this module would have to be in structure. A major tradeoff in considering ATS-4 growth capability is the potential degradation of the performance of the prime experiments. Premium earth viewing area available for mounting sensors is extremely limited without increasing parabolic antenna rf blockage or causing phased array or interferometer phase distortion. Additional ATS-4 experiments, which require earth sensing, can be added at the expense of additional rf blockage or they can be deployed out past the parabolic antenna, or look through it. A possible solution is to tradeoff the experimental worth of the phased array in comparison to other earth viewing experiments. The phased array occupies approximately ten square feet of prime surface area, weighs 100 pounds, utilizes about 700 watt-hours of battery power per hour of operation, and accounts for most of the severe thermal design problems of the earth pointing equipment module.
- b. Power. Power subsystem growth requirements cannot be determined prior to the establishment of an operational plan. High power level experiments can be operated on a reduced duty cycle using batteries without requiring significant solar array growth. The solar array capability of the selected configuration is extremely flexible. The array has been designed for end of life degradation. Approximately 22 percent additional capacity is available early in life, which could be used to accommodate a variety of operational experiments on a shared duty cycle with the prime experiments. A 10-percent increase in capability can be obtained by adding an additional 10 mils of cover glass. A 64 percent area increase can be accommodated without panel folding. Additional requirements could be accommodated with hinged panels or sun oriented paddles could be incorporated for an increased capability. As paddle weights increase, support truss stiffness would also have to be increased for the same frequency requirements.

### 5.4 PARABOLIC ANTENNA

#### 5. 4. 1. SELECTION OF ANTENNA CONCEPT

The antenna configuration selected to satisfy the ATS-4 mission and system requirements consists of a 30-foot diameter paraboloid reflector, with an f/D of 0.4, and a composite feed made up of three concentric circular horns and a turnstile.

The reflector diameter selected is the minimum permitted for this experiment. Larger diameters have the potential of increased gains; however, they also have many detrimental characteristics that tend to overbalance the advantages. For example; larger diameters result in higher gain. but lower efficiencies and induce higher weights and lower natural frequencies, require finer pointing capability due to the narrower beam, and are much more complex to package and deploy.

The rigid Petaline reflector concept was selected after a study of alternate concepts that included: wire-grid surfaces inflation deployed and thermally deployed; chemically rigidized textile or film surfaces heat-activated and gas-catalyst-activated; and mechanically deployed rigid surfaces of umbrella, Swirlabola, and Petaline configurations. The selected configuration has major advantages over the others in that it has the minimum assembly tolerances, minimum thermal distortions, maximum stiffness, minimum requirement for special handling and test equipment, and maximum design and cost credibility due to the current extent of analysis and development.

Cassegrain and prime focus feed configurations were considered during the study for a range of reflector f/D ratios of from 0.3 to 0.5. Analysis of relative losses effectively eliminated the Cassegrain configuration. The choice of prime focus feed then eliminated the higher reflector f/D ratios due to undesirable structural dimensions and packaging problems. The lower f/D ratios resulted in undesirably small feed horn apertures. A value of f/D = 0.4 was therefore selected for the preferred configuration since it provided a feasible arrangement of acceptable dimensions. The feed configuration selected consists of three coaxial conical horns plus a turnstile consisting of four quarter-wave rods.

## 5.4.2 DESCRIPTION OF SELECTED DESIGN

## 5.4.2.1 Reflector and Feed

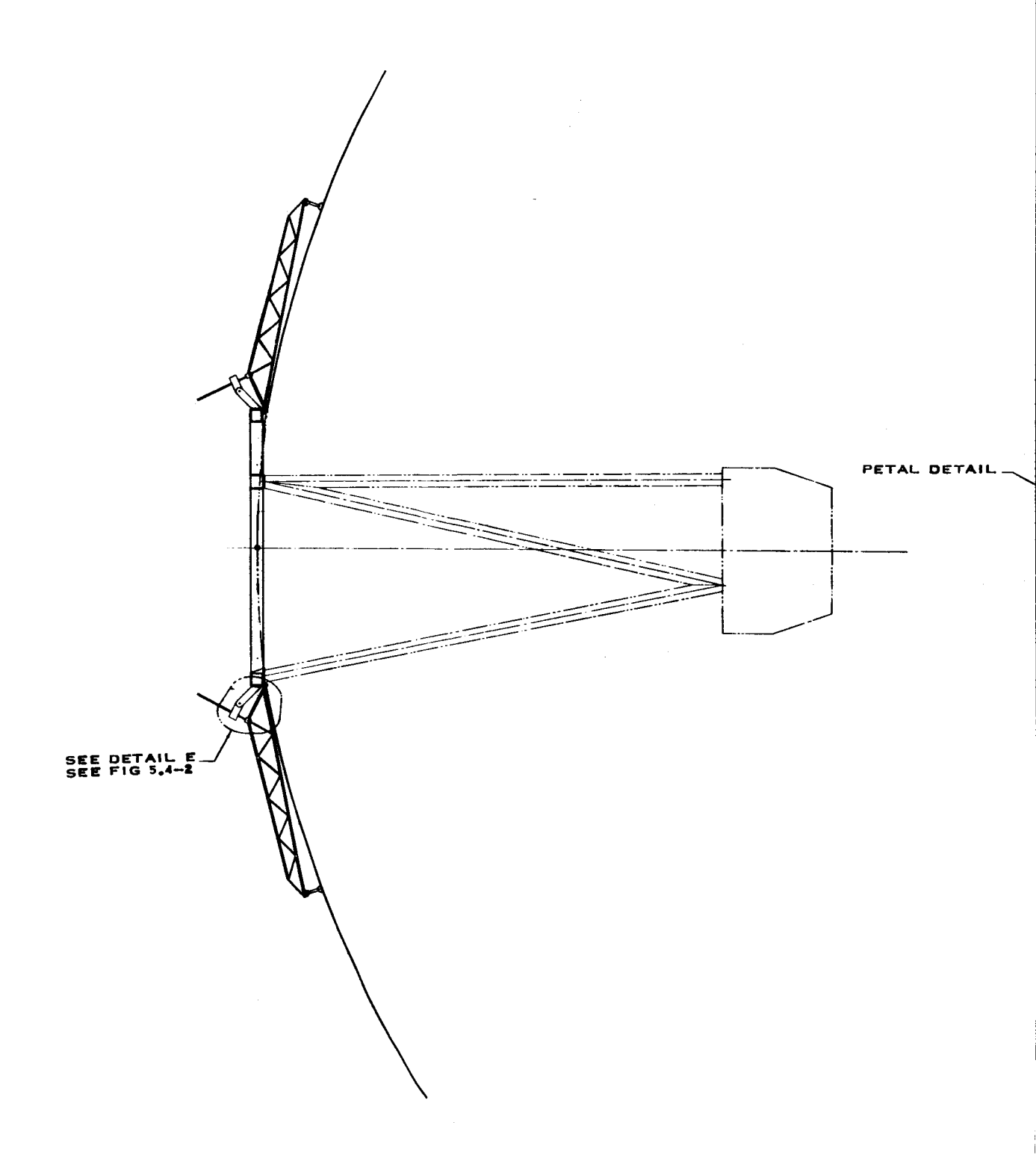
On the basis of conceptual studies, the Petaline rigid reflector configuration was selected for the ATS-4 antenna experiment (Figure 5.4-1).

The paraboloid surface is an assembly of 20 typical petal sector subassemblies. Each sector subassembly consists of two triangular petals and one trapezoidal petal. The shape of each petal is a true, double-curved radial segment of a paraboloid of revolution. The petals are connected by hinges, uniformly spaced along the petal edges. These hinge lines are curved in the deployed paraboloid. The composite structure of petals and hinges approaches the equivalent of a one-peice paraboloid. A detailed description of this construction is given in Section 5.4.4.

The paraboloid is deployed, and supported, by 20 deployment trusses. Four of these are of a special construction in order to also support and deploy the solar arrays. The remaining 16 are single-plane trusses of welded titanium tubing. These trusses are mounted to the back (convex) side of the reflector in order to eliminate rf blockage. A single link from the outboard end of the truss attaches to the petal sector at the intersection of the two triangular petals. This link accommodates geometry changes due to thermal expansion and deployment. The inboard end of the truss attaches to the interface hub ring through a hinge and through the drive mechanism shown in Figure 5.4-2.

The interface hub ring is a built-up titanium structure of rectangular cross section, with reinforcing bulkheads in the regions of the deployment drive mechanism, petal hinge, and the truss hinge attachments. This ring bolts to the Aft Equipment Module of the basic spacecraft.

The antenna feed, which is fixed to the Earth Viewing Module, consists of three concentric circular horns and a turnstile (see Figure 5.4-3). A detailed description of the feed and its performance is contained in Section 5.4.6.



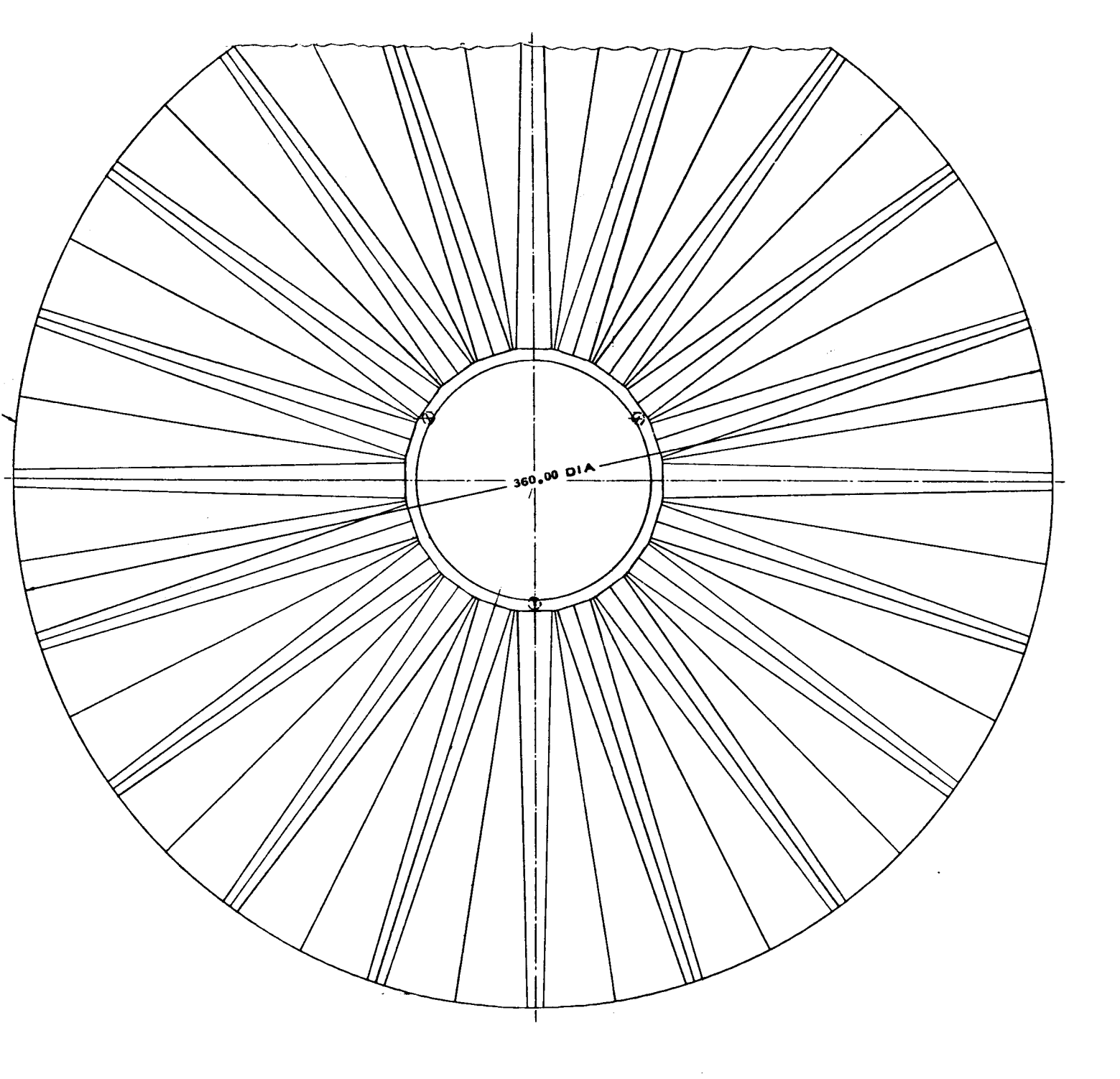
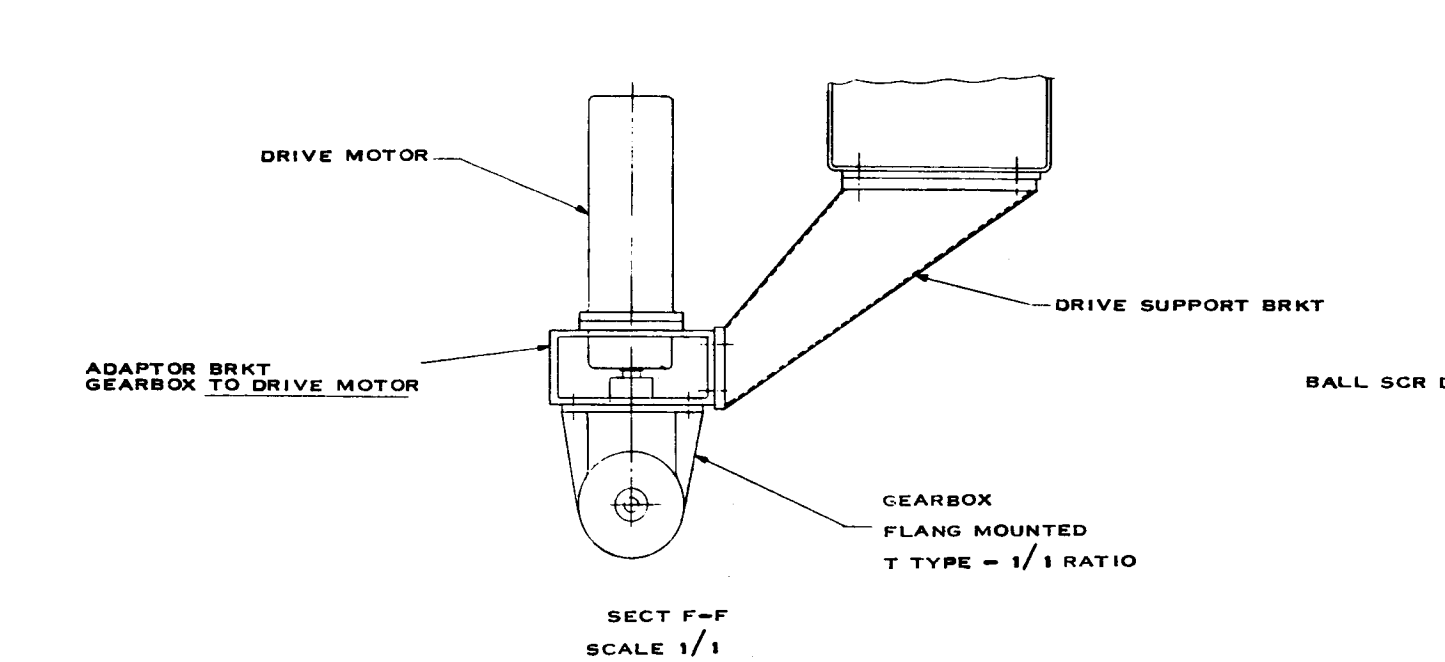
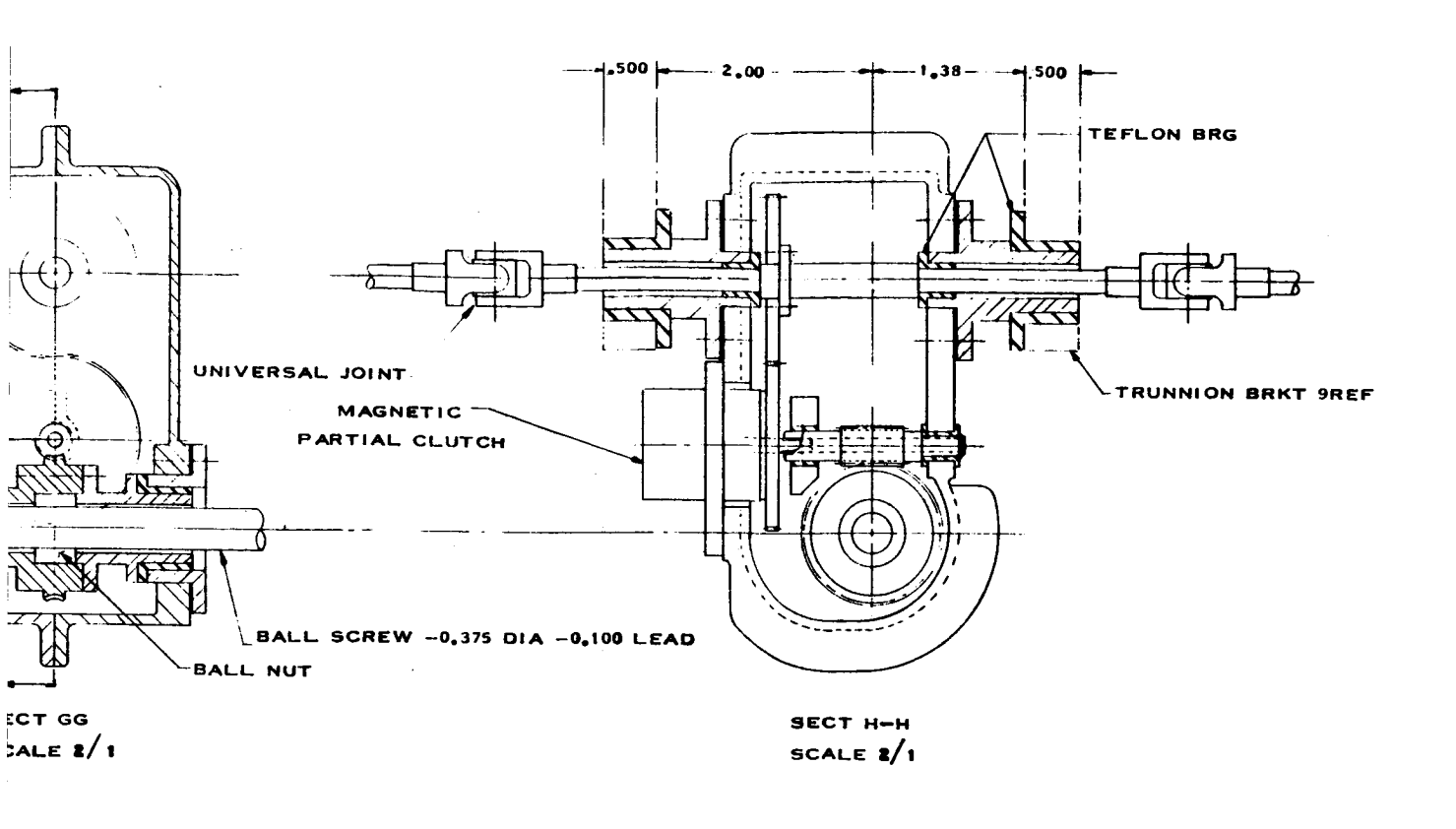


Figure 5.4-1. Petaline Rigid Reflector Configuration





SECT D-D (FIG 5.4-4)
SCALE 1/10



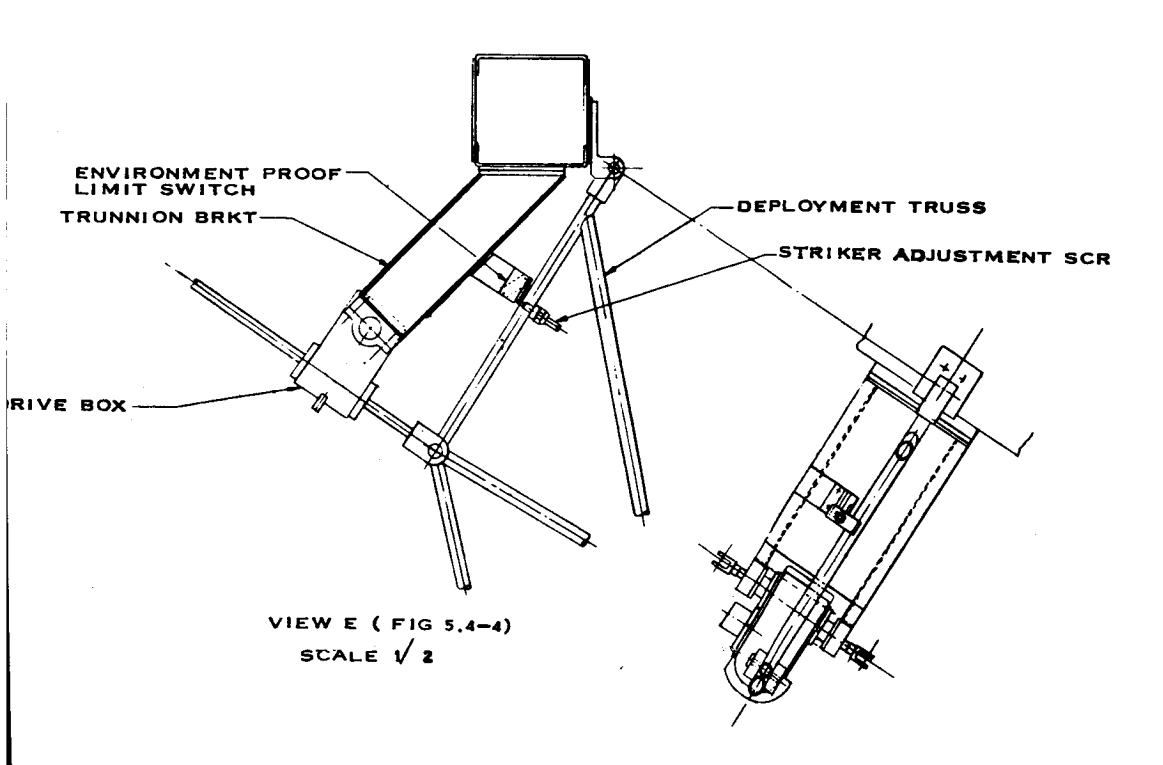


Figure 5.4-2. Deployment Drive Mechanism

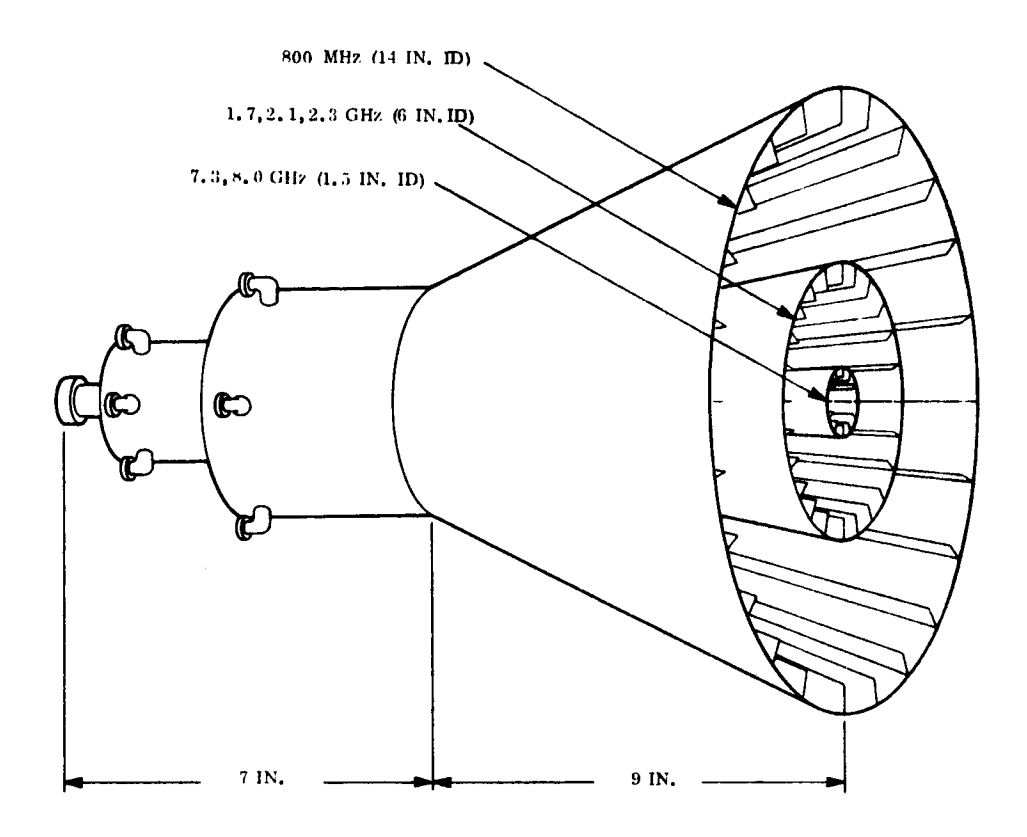
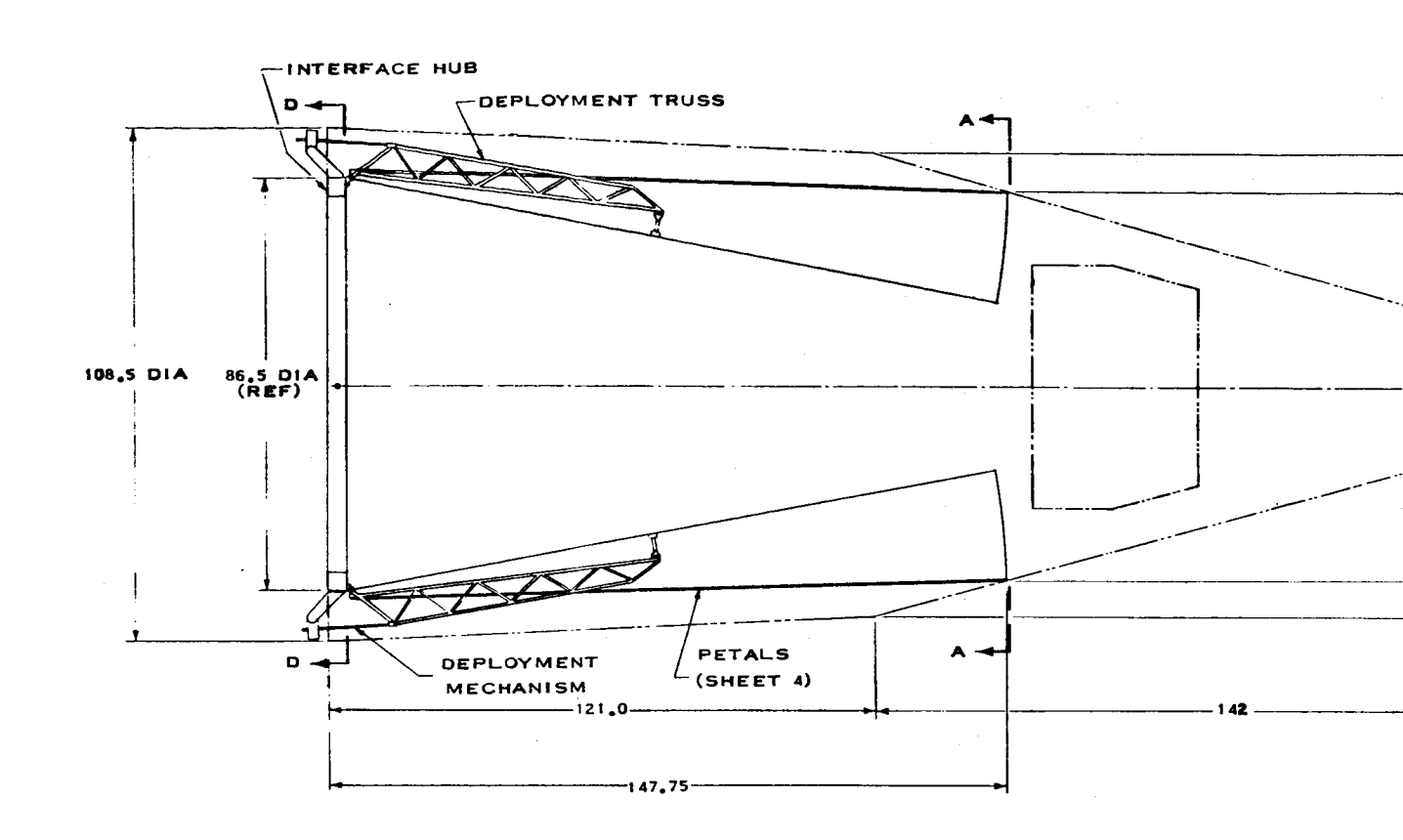


Figure 5.4-3. Feed Configuration

## 5.4.2.2 Packaging

Packaging of the curved-hinge reflector is accomplished by designing the petals with a flexural stiffness that will permit the petals to be flattened without inducing a high percentage of the allowable yield stress of the petal material. Thus, the paraboloid is essentially transformed into a cylinder and the curved hinge lines become straight-line elements of the cylinder. This design permits an accordion-like folding of the reflector structure. The strain energies imposed upon the petal structure, due to flattening of the petals, are a small percentage of the allowable yield stress of the material composite, so that creep phenomena is not a problem; therefore, at deployment, the petals return to the zero strain condition to which they were initially fabricated and assembled. Hinged connections between a central hub and the petals allow the reflector to package into a cylindrical envelope of a height approximately equal to the length of the petals.

The antenna can be stowed within the volume restraint(see Figure 5.4-4) which provides adequate static and dynamic clearance with the protective shroud. To survive the launch



TURNBUCK

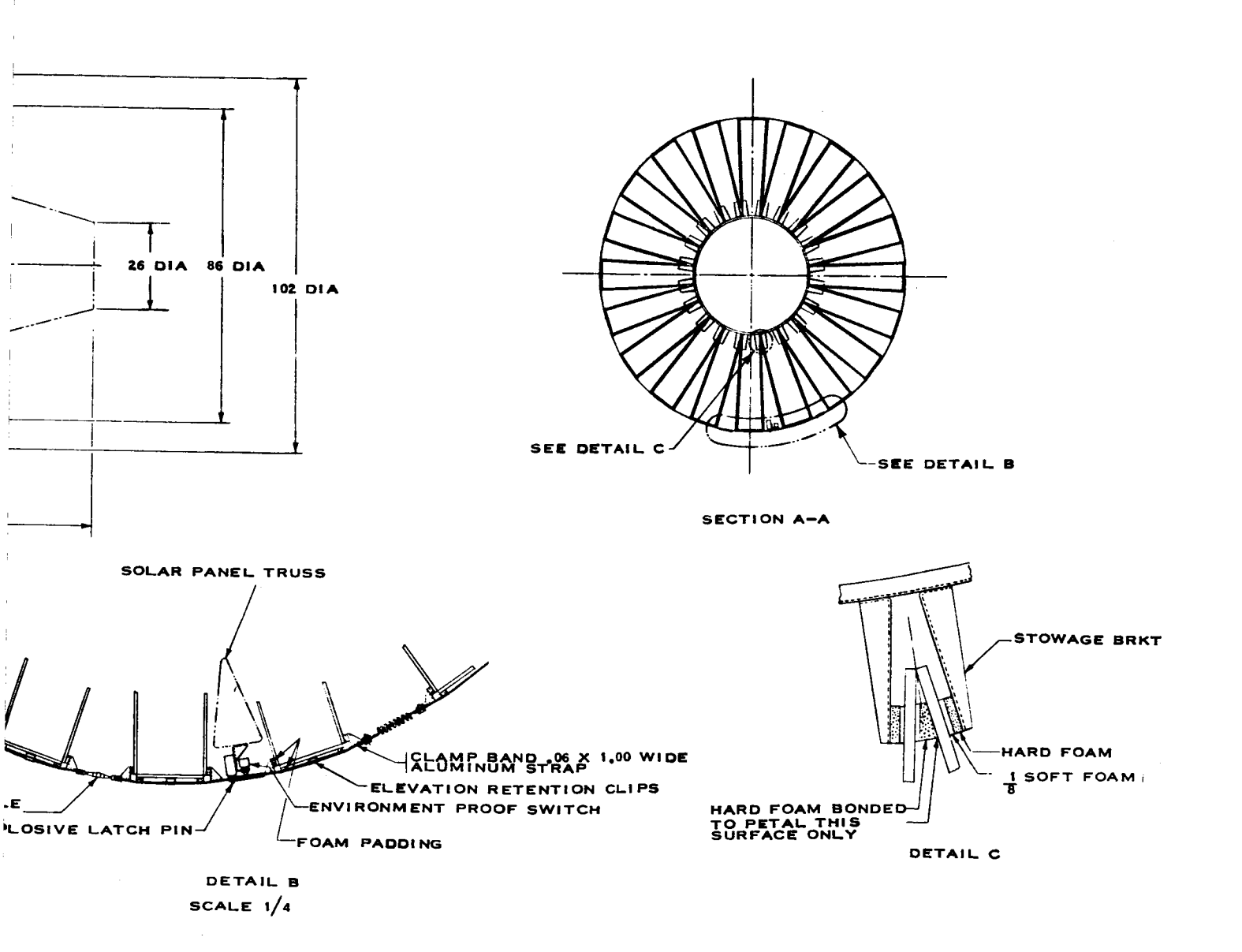


Figure 5.4-4. Stowed Configuration



environment, the folded petals are banded together and supported to form an integrated structure. The banding is done at the top of the petals as shown in Section A-A of Figure 5.4-4. The inner edges of the triangular panel are supported by the Earth Viewing Equipment Module through a fiberglass channel and stowage brackets on the antenna stowage support ring, as shown by Detail C of Figure 5.4-4. The petal surface is protected by pads of hard polyurethane foam with soft foam adjacent to the petal surface. A peripheral band clamp as shown by Detail B of Figure 5.4-4 snugs the accordion-folded petals into the stowage brackets of the inner ring and, in effect, packages the petals into an integrated cylindrical tube. Clips are provided on the petals for positioning the inner ring and the band for lateral retention during launch.

Detail B of Figure 5.4-4 shows the mounting of the explosive latch pin puller, the switch that senses ejection, and the turnbuckle for tightening the band.

# 5.4.2.3 Deployment

The deployment trusses actuate the petal sectors from the back of the reflector to minimize the rf degradation inherent in employing a metal mechanism in front of the reflective surface. The system consists of 20 ball screw actuators that pull a series of 20 trusses in outward radial arcs to move the petals from the cylindrical packaged state to the deployed parabolic form. The petal sectors are hinged at the ends of the trapezoidal panel bases to a box beam torus hub that also serves as the reflector interface.

The folding of the reflector petals from the fabricated, deployed, contoured condition induces strain energy in the flattening of the petal hinge line. The release of this stored energy must be closely controlled during the deployment cycle. The time (two minutes) allocated for this cycle will provide a slow excursion of the petals.

The outer attachment of each truss is made to the midpoint of the hinge line of the triangular panels of each sector. The attachment is made by single member links connecting the outboard end of the trusses to accommodate the change in hinge-line length from the petal folded condition to the deployed contour. The link also provides freedom for radial thermal expansion.

The drive mechanism is discussed in detail in Section 5.4.5.

#### 5. 4. 3 ANTENNA PERFORMANCE

Antenna performance is dependent upon preserving the detailed geometry of the structure, including feed, within certain limits. In addition to losses incurred by exceeding such tolerances, there are those losses inherent in the design as constrained by various factors. All of these variable and fixed losses are presented in Table 5.4-1, the loss budget for the antenna, which sums up the total used to arrive at an efficiency figure. This efficiency compares the antenna performance with that of an ideal uniformly illuminated aperture of the same dimensions. This ideal cannot be realized for parabolic antennas, even if there were no such losses other than those due to the illumination characteristics which involves spillover in the case of all practical feeds. An efficiency of 65 percent, based upon the illumination, is commonly accepted as good design practice in the case of simple feed horns. Detailed control of feed and aperture may raise this efficiency to 80 percent or better over a limited range of frequencies. This control is not feasible for the ATS-4 requirement; a 65 percent value, corresponding to 1.9 dB loss, may be taken as a practical ideal. The first two items in the loss budget, illumination efficiency and spillover efficiency, are the component losses to be considered in this context. The only significant departure from 1.9 dB occurs at 100 MHz, which is to be expected since the antenna is only about three wavelengths in diameter at this frequency. The other loss items are unavoidable due to various design constraints and/or environmental factors; the overall antenna performance as stated is therefore a realistic analysis of what may be expected from a good design if all factors are considered.

The strut reflection loss is shown as an estimated figure. Section 6.3.5 gives the detailed information upon which this estimate was based. Briefly, a measurement program was performed on a scale model at one frequency to determine the losses caused by feed support struts lying close to the feed. The corresponding value was found to be one dB for the configuration closely resembling the final selection. This value includes strut blockage loss, for which

Table 5.4-1. Parabolic Antenna Experiment Loss Budget

			FREQ	FREQUENCY (GHz)	Hz)		
ITEM	0.1	8.0	1.7	2.1	2.3	7.3	8.0
Illumination	1.20	0.72	0.22	08.0	1, 10	0.58	06.0
Spillover Efficiency	1, 12	99*0	1.70	0.58	0.40	0.82	0.50
Equipment Module Blockage	0.40	0.40	0.40	0.40	0.40	0.40	0.40
Strut Blockage	0.24	0.24	0.24	0.24	0.24	0.24	0.24
Strut Reflection Loss	0.76	92.0	92.0	0.76	0,76	0.76	0.76
Reflection Tolerance Loss	00.00	00.0	0.01	0.02	0.02	0.18	0.23
Loss Through Wire Mesh Reflector	00.00	00.00	00.0	00.00	00.00	0.03	0.04
Feed Phase Error Loss	0.05	0.01	0.04	0.04	0.04	0.04	0.04
Cross Polarized Loss	0.01	0.01	0.01	0.01	0.01	0.01	0.01
Feed Attenuation Loss (Including Circuitry)	0.20	0.20	0.20	0.20	0.20	0.20	0.20
Transmission Line Loss	0,01	0.03	0.01	0.01	0.01	0.05	0.05
VSWR Reflection Loss	0.15	0.10	0.05	0.03	0.05	0.03	0.03
Thermal Distortion Loss	0.00	00.0	0.01	0.02	0.02	0.17	0.30
TOTALS (dB LOSS)	4.14	3.13	3,65	3.11	3.25	3,51	3.70
EFFICIENCY (%)	38.5	48.5	43.1	49.0	47.5	44.5	42.7

a separate calculation was made and found to be 0.24 dB. The value of 0.76 dB was thus used for the strut reflection loss and applied as an estimate for all frequencies, based upon the single frequency measurement. The exact number undoubtedly will vary with frequency to an extent which is probably small. The struts tend to break up the primary pattern into a number of lobes, the number of which will increase with frequency. Thus, the total illumination over the reflector may not vary greatly; i.e., the narrowness of the higher frequency lobes will be compensated by their greater number. On the basis of the available information, the struct reflection loss estimate is intended to represent an available modifier order valide nor optimistic.

The reflector efficiency is degraded by distortions such as those produced by thermal effects. Contributions from the various parts of the reflector thus affected will not add up in phase, and the net result is a decrease in gain. The significance of the distortions lies in their magnitude as expressed in wavelengths, a common rule of thumb being that the rms error over the entire reflector should not exceed 1/16 wavelength. Thus, the highest frequencies are affected to the greatest extent. At 8000 MHz the highest operational ATS-4 frequency, the wavelength is 1.47 inches. The worst case deviations have been calculated to be 0.25 inch, in comparison, but these occur in a limited region near the edge of the reflector. Here the illumination is least, hence producing less error.

The analysis upon which the rf loss computation is based assumes that the errors are randomly distributed. This assumption is not entirely correct since the affected regions show local correlation to a certain extent. The fact that the worst deviations occur near the edge is of course another indication of nonrandomness, but tends to minimize the effects of correlation considering the integrated errors over the entire aperture. The worst case calculated value is 0.2 dB at 8000 MHz, to which is conservatively added another 0.1 dB to account for distortion of the feed itself. Calculations show that movement of the feed, due to thermal distortion, will not produce an error exceeding this amount.

The requirement for beam steering has been suggested as a valuable feature although not specifically requested as a contract item. It is feasible to move the horn cluster 12 inches laterally on the Earth Viewing Equipment Module, which would produce a steering of four degrees for all horn frequencies. This steering is not recommended for all of the frequencies, however, since the degradation in gain becomes severe at the upper end of the band. A feed tilt of seven beamwidths, for example, will decrease the existing efficiency by another 50 percent. Using this as a criterion, the frequency of 2.4 GHz may be steered, but the frequencies of 7.3 and 8.0 GHz may not, without incurring excessive losses.

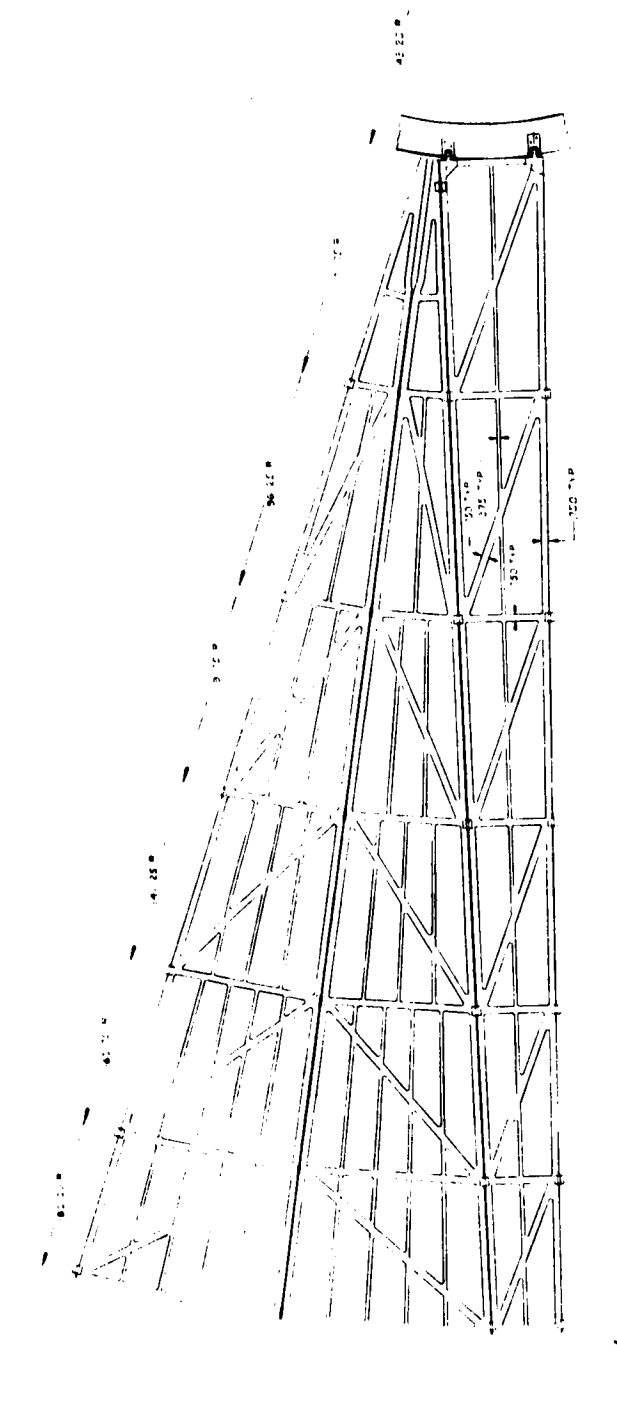
The use of monopulse tracking has also been suggested as desirable. Its implementation requires two extra receiver channels in the onboard equipment; this in conjunction with the attitude stabilization system would permit the antenna to orient itself to an earth-originated signal. In the present configuration such an operation is feasible only at the top of the frequency band, and would be realized by the use of two waveguide modes in the inner horn instead of one. The additional TM<sub>01</sub> mode produces a pattern with a null on boresight, which yields the required difference signal. The pointing information is derived by referencing it against the original TE<sub>11</sub> mode in the horn, which corresponds to the sum channel. Such a system is used in the Telstar ground equipment, and requires circularly polarized signals for proper operation.

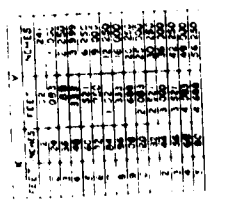
### 5.4.4 REFLECTOR DESIGN

#### 5. 4. 4. 1 Method of Construction

As mentioned previously, the deployed reflector surface is divided into 20 typical sectors, consisting of one trapezoidal petal and two triangular petals to comprise a total of 60 individual components (see Figure 5.4-1).

A typical sector (Figure 5.4-5) is formed of honeycomb sandwich, which is comprised of 0.0025-inch-thick titanium face sheets and a core of 0.125-inch cell honeycomb of 0.0007-inch thick aluminum. The composite thickness of the sandwich is 0.300 inch. The sandwich (Figure 5.4-6) is bonded together with FM-1000 adhesive.





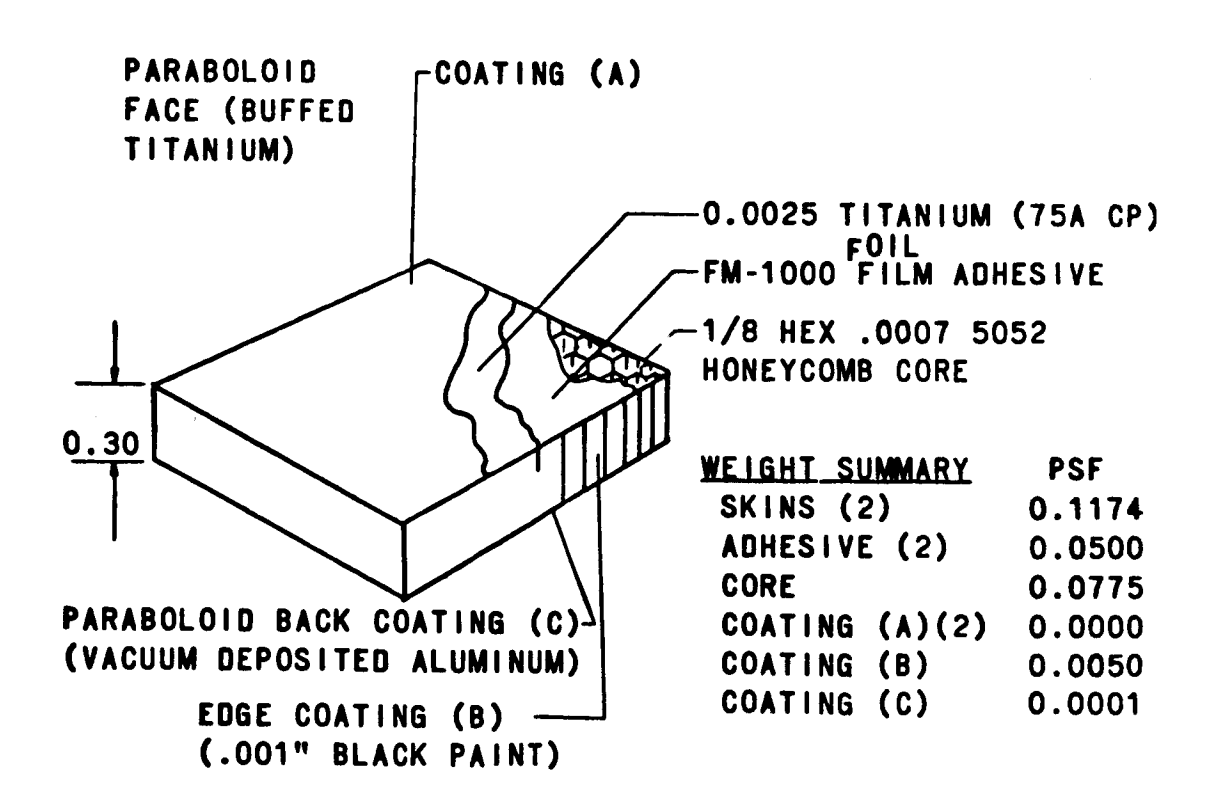


Figure 5-4.6. Panel Structure Composite

The parabolic shell is cut out 80 percent to minimize weight and thermal distortions. The cutouts reduce the reflector to 60 radial legs (which contain the hinges) and seven circumferential concentric rings which intersect the legs at the hinge points. The result is that each petal sector subassembly contains 16 trapezoidal and two triangular bays. A diagonal member is added to each of the trapezoidal bays for truss stability. Finally, additional radial members are provided to reduce the deviation of the final surface from a true paraboloid.

The major radial legs, the circumferential rings, and the diagonal members are 0.75 inch in width. The secondary radial members are 0.375 inch wide. The hinges are close tolerance and are designed to accommodate radial thermal expansion. A total of 400 petal interconnecting hinges are required. The described petal sector configuration is shown in Figure 5.4-5.

The sandwich lattice network of the reflector petal surface will be fabricated to a tolerance of  $\pm 0.032$  inch to the theoretical contour. To this must be added a deviation from true contour caused by the facet effect of the reflective screen material stretched across the openings cut in the structural contour. The maximum unsupported separation ( $\ell$ ) between contoured members has been limited to 4.875 inches in the panel cutout pattern. The deviation from true contour is derived from the formula  $\Delta E = \frac{\ell^2}{16\,\mathrm{f}}, \text{ where } \ell \text{ is the } \ell$ 

maximum open span between contour members and f is the parabolic focal length (see Figure 5.4-7).

$$\Delta E = \frac{\ell^2}{16f} = 0.010 \text{ in.}$$

where

 $\ell = 4.875$  in. maximum

f = 144.00 in.

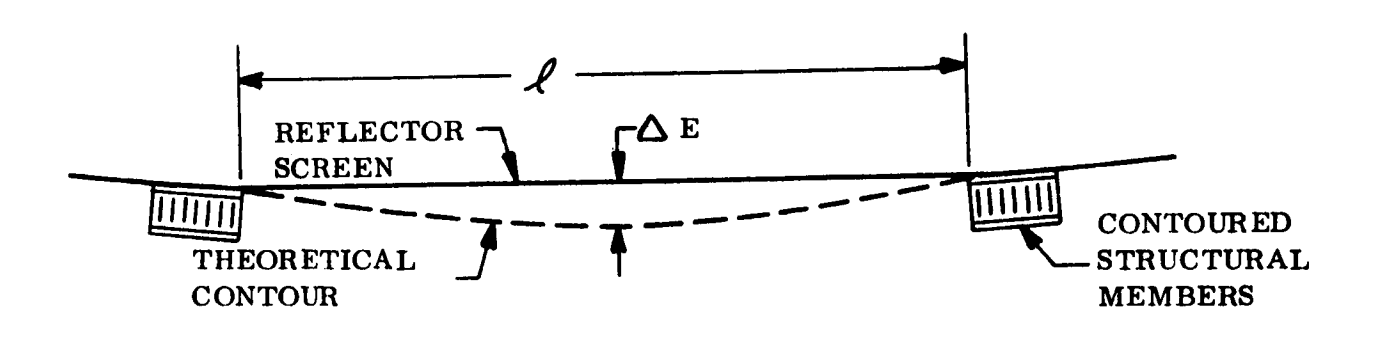


Figure 5.4-7. Deviation From True Contour

The hinge connection of the reflector to the central hub is made with hinge fittings attached to the corners of the trapezoidal petals (Figure 5.4-5). The rotating components and hinge

pins of these fittings are lined with Teflon bushings and separated with Teflon washers between moving adjacent metal parts. To distribute the concentrated loads from these hub hinges, the honeycomb face sheets of the trapezoidal petals have 0.0075-inch doublers applied from the hinge end out to the first petal hinge.

A radar reflective screen, made by expanding 0.003-inch-thick titanium foil with approximately 0.1-inch strand separations, is epoxy-bonded to the petal members to form the paraboloidal contour by spanning the open areas. The screen weighs 0.0065 psf and presents a frontal blockage of four percent. The screen will be bonded to the petal framework by applying the adhesive to the mesh and laying it on the petal surface. This procedure is used to minimize the extent to which the screen and adhesive will compromise the optical properties of the petal surface to which it is bonded. From the screen configuration shown in Figure 5.4-8, it is seen that the open area diameter is about 33 times the diameter of the mesh. If it is assumed that the adhesive will cover five times the mesh diameter, the remaining unaffected area will still be 85 percent of the original area. Thus, the effects of the

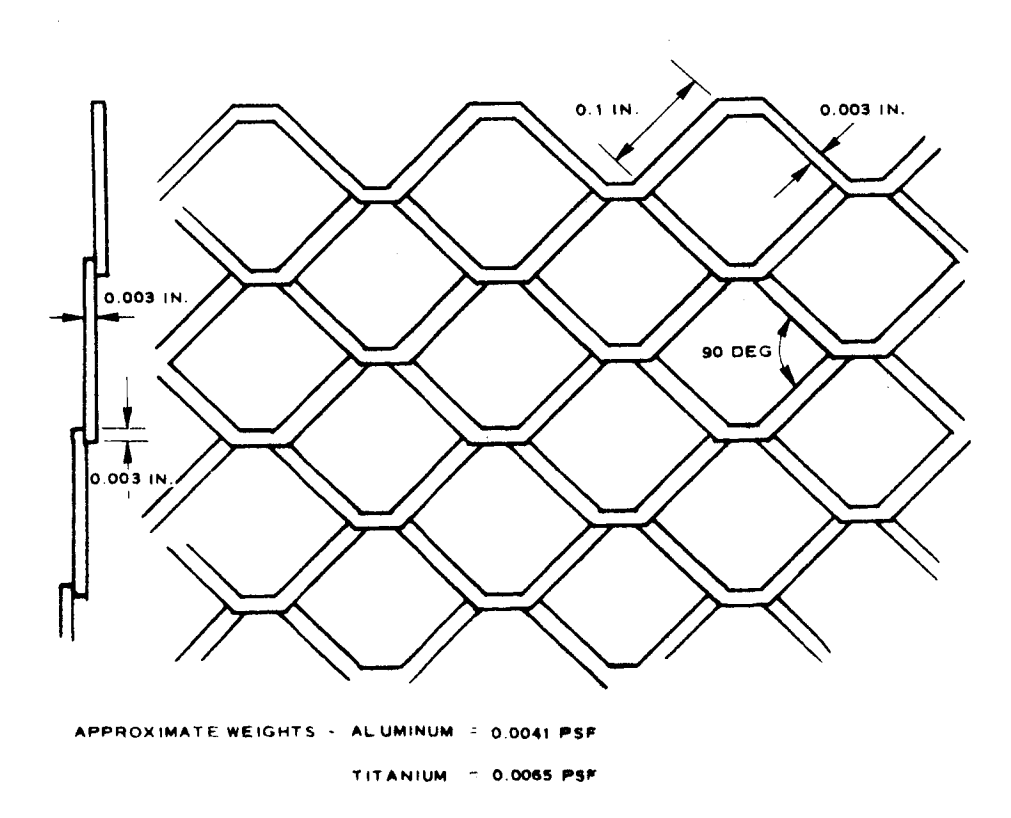


Figure 5.4-8. Configuration of Expanded Metal for RF Reflecting Material

mesh on the optical properties of this surface are not expected to be significant. Further development and testing will be required to establish manufacturing techniques and to evaluate the optical effects.

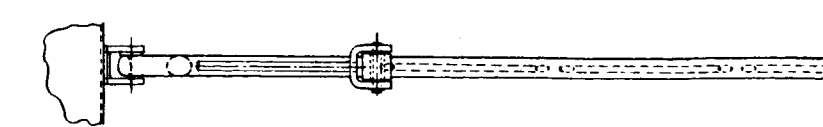
The recommended configuration for the deployment truss is considered to be a feasible approach to the reliable deployment of the paraboloid reflector (and the solar arrays) while at the same time offering the best overall structural load paths for adequate restraint during the launch phase.

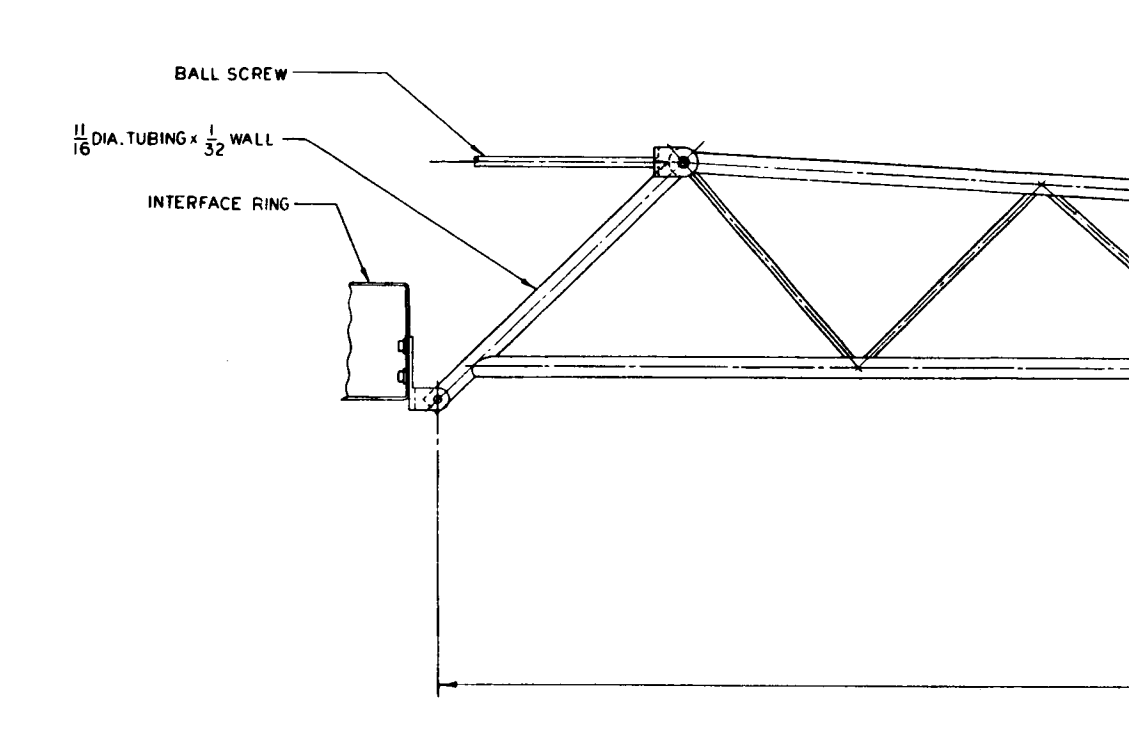
When stowed, the reflector is packaged in a cylindrical form circumferentially restrained at the upper end by an external "cinching" band and the antenna stowage support ring. The lower end is assembled to the hub interface ring. The deployment trusses provide additional restraint to the folded reflector near its center of mass.

The deployment trusses (Figure 5.4-9) are stowed parallel to and partially within the cylindrical envelope of the stowed reflector. The deployment trusses provide uniform and controlled motion of the reflector during deployment, as discussed in Section 5.4.5. Each of the 16 deployment trusses, as shown in Figure 5.4-9, is a single-plane truss of welded titanium tubing. The main chords are 0.6875-inch OD x 0.032-inch wall tubing, and the shear bracing is 0.25-inch OD x 0.032-inch wall tubing.

The attachment to the reflector is effected by a link that picks up the joint between the triangular petals. The link connection is shown in Detail J and Section K-K of Figure 5.4-9. The link provides compensation for the change in length of the petal hinge when going from the packaged cylindrical shape to the deployed paraboloidal configuration, and accommodates reflector geometry changes due to thermal expansion or contraction.

The trusses are tied to the spacecraft through a hinge attached to the hub interface ring and by the ball screw actuator rod. Teflon bushings and washers are used to separate metal parts that must experience relative motion.





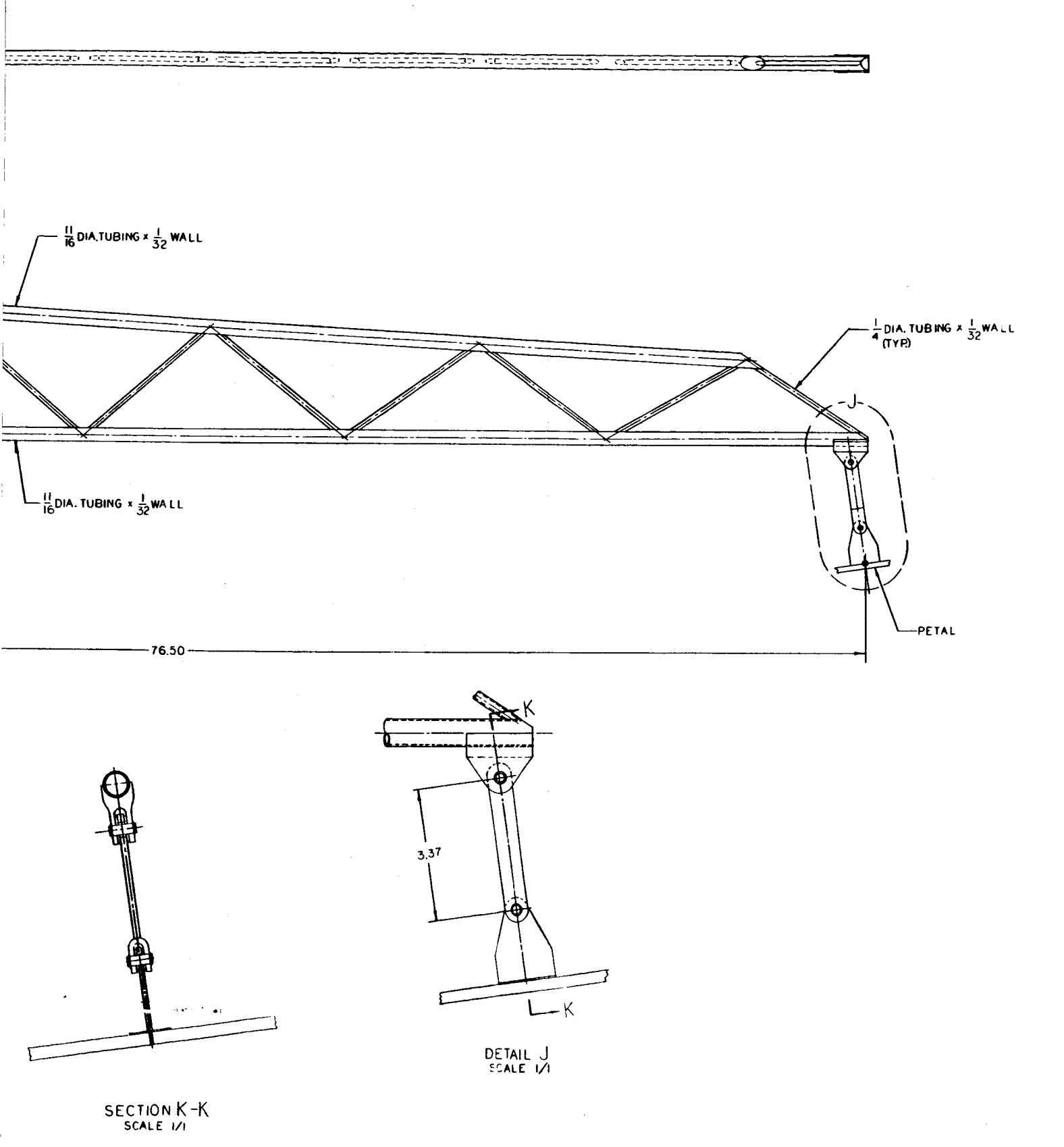


Figure 5.4-9. Deployment Trusses

The interface hub ring shown in Figure 5.4-10 is a torus of box-beam construction. The ring is fabricated by rolling the outer and inner channels of 0.040-inch-thick titanium stock and riveting 0.040-inch-thick titanium skins to the top and the bottom to form the box cross section. Bulkheads of 0.040-inch-thick stock are placed adjacent to the area of petal hinges, truss hinges, actuator mounting brackets and the drive motor brackets (see Section L-L of Figure 5.4-10). Local pads will be riveted to the box beam to mount these components and will be machined to the thickness shown in Sections M-M and N-N of Figure 5.4-10.

# 5.4.4.2 Material Selection

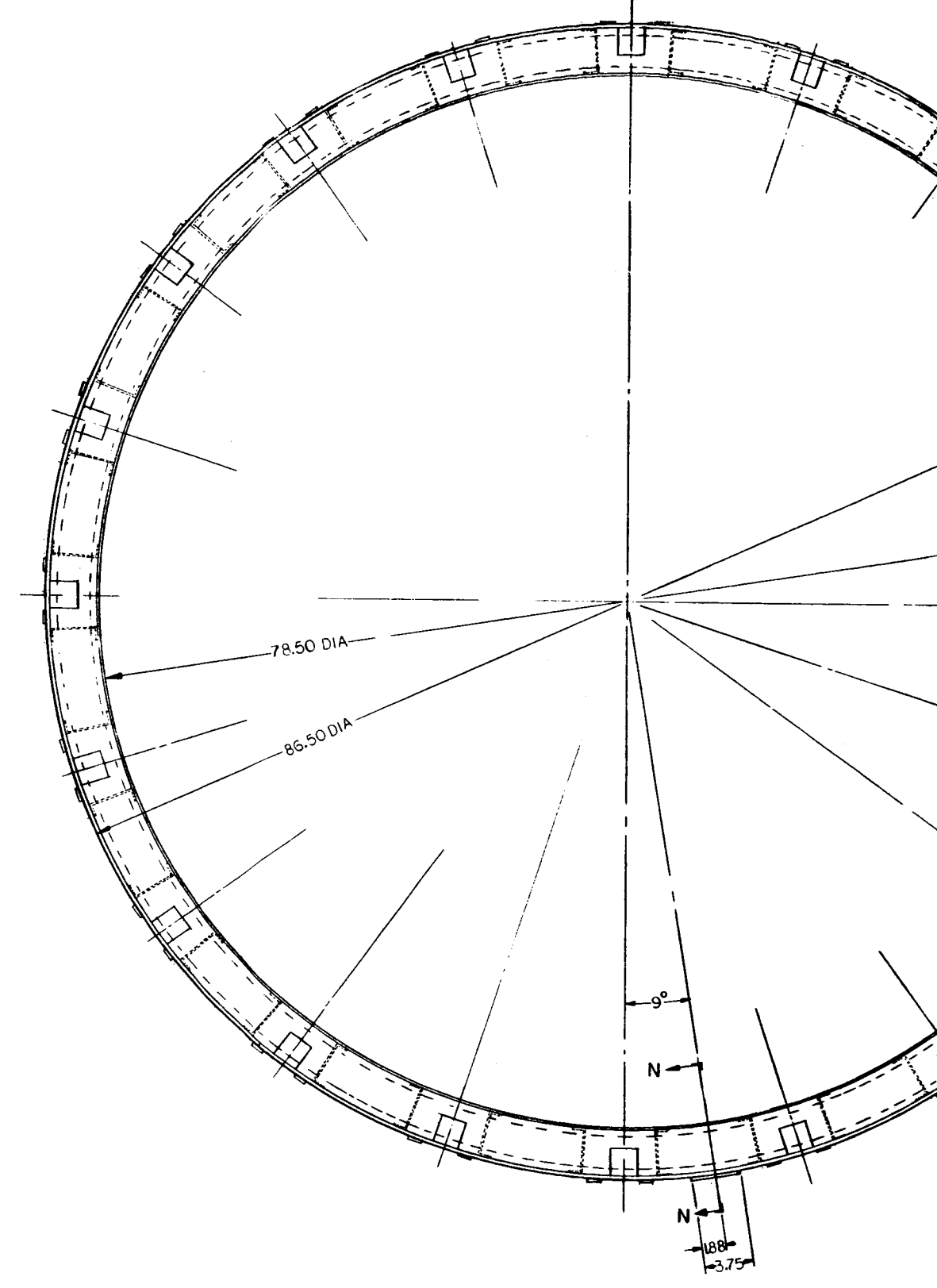
Titanium was chosen as the material for the petal honeycomb face sheets and the reflective screen; aluminum was selected for the petal honeycomb core. The honeycomb is bonded with FM-1000 adhesive.

Aluminum was considered for the face sheets but was eliminated because of its higher thermal coefficient of expansion and lower elastic modulus. Because the difference in thermal conductivity is not expected to significantly affect the paraboloid temperature distributions, the lower thermal expansion coefficient of the titanium will reduce thermal distortions and, consequently, the rf losses attributed thereto. The higher modulus of elasticity provides the stiffness necessary to ensure an adequately high reflector fundamental frequency and compatibility with the attitude control system.

Aluminum was chosen for the core material because of its lower density and compatibility with the design. Thermal stresses due to differential thermal expansion between the titanium faces and the bond, and between the bond and the aluminum core, are shown to be acceptible by conservative calculations (see Section 6.3).

Titanium was also chosen for the reflective screen because of its thermal compatibility with the titanium face sheets to which it is bonded.

FM-1000 adhesive was chosen as the bonding material based on its compatibility with the ATS-4 space environment. The Space Materials Handbook prepared for the Air Force



PLAN VIEW OF INTERFACE RING SCALE 1/4

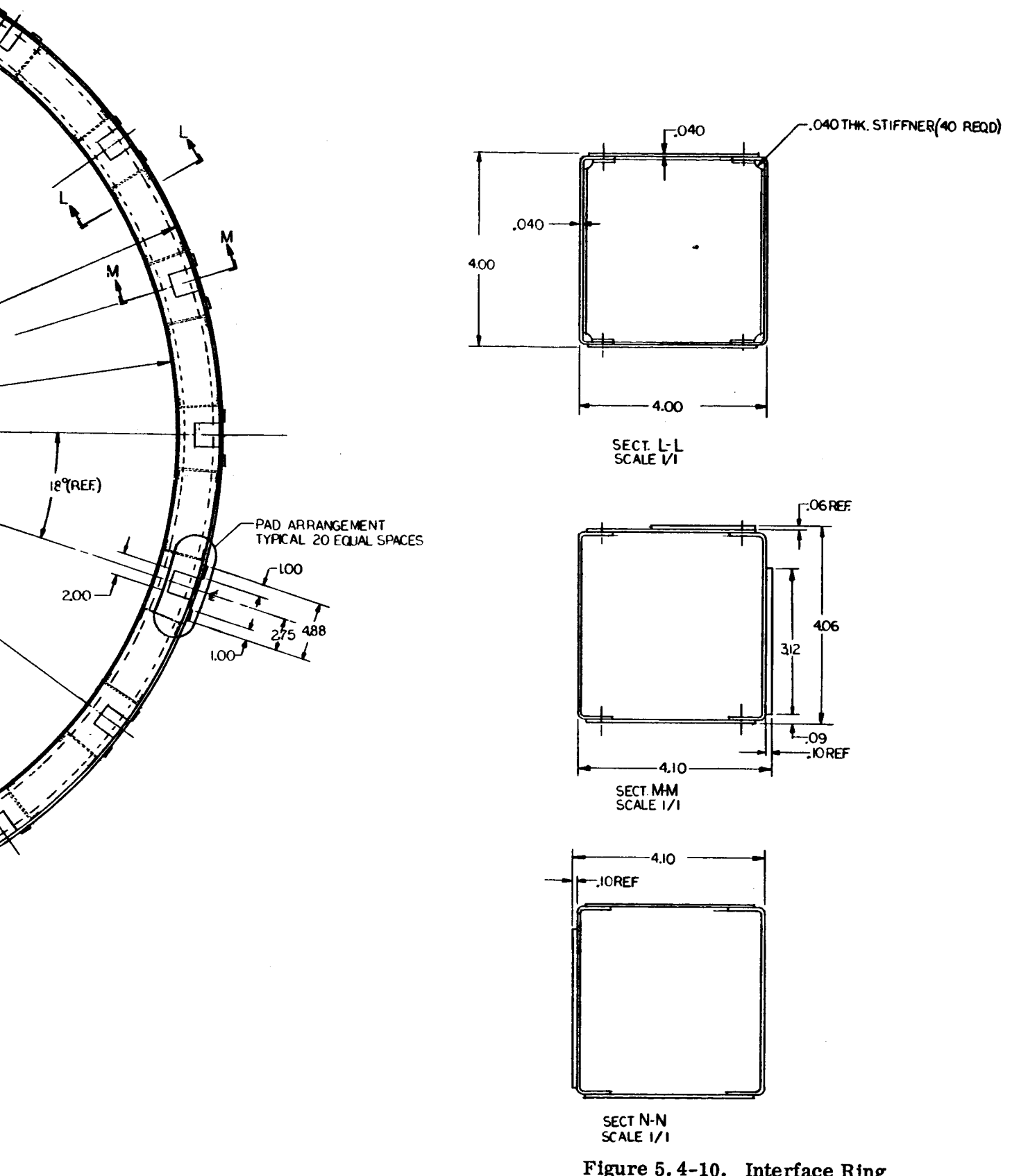


Figure 5.4-10. Interface Ring

Materials Laboratory (Wright-Patterson AFB) recommends this material for spacecraft bonding applications for space environments. Thermal control surface preparations for the reflector consist of:

a. Vapor-deposited aluminum on back (convex) face

$$(\alpha = 0.12, \epsilon = 0.04)$$

b. Buffed titanium on the front face

$$(\alpha = 0.45, \epsilon = 0.15)$$

c. Black paint on the edges of the petal members

$$(\alpha = \epsilon = 0.8)$$

The use of the optical properties shown produces tolerable thermal distortions and rf losses.

The vapor-deposited aluminum will be protected from oxidation in the earth environment by a 1000-3000 Å protective coating of Si0. This coating thickness will not significantly affect the optical properties of the aluminum. The aluminum is stable in the space thermal/vacuum/radiation environment, so that the optical properties noted may be considered to exist throughout the 2-year mission life.

Buffed titanium is also stable in space; the only potential deterioration is caused by erosion due to micrometeorites. Initial oxidation of the buffed titanium is considered in the measured optical properties given. Subsequent oxidation in the earth environment is slow enough to be considered not to have a detrimental effect on these properties. Should detailed thermal analysis indicate the need, vapor-deposited aluminum may also be applied to the front face of the reflector.

The black paint used on the edges of the petal members can be one of several space proven types. Space exposure for two years will not have any significant detrimental effects on its thermal performance.

The 16 basic and four solar panel deployment trusses and links are constructed of Ti 75A which is a commercially pure, weldable, alpha structure titanium. Titanium was selected over aluminum because of its lower thermal expansion coefficient and its compatibility with the reflector and hub.

The hub ring is also constructed of titanium for thermal compatibility. In this case, annealed Ti-6 A1-4V alpha-beta structure titanium is specified. This alloy is also weldable.

# 5.4.4.3 Structural Considerations

The reflector structure must survive the prelaunch environments (handling, transportation, etc.) and the ascent into orbit phase, and be capable of deployment and satisfactory performance when in orbit. During this study, analysis has indicated adequate capability of the reflector configuration presented to perform the ATS-4 mission.

The design objective of ground support equipment is to protect the antenna from prelaunch environments that might otherwise influence the final configuration and reflector design.

Therefore, the initial design of the reflector will be based on ascent and orbit considerations, and the effects of the prelaunch environments will be considered in establishing ground support equipment requirements. Consequently, the effect of these environments will be minimized.

In the stowed configuration, the reflector structure must survive all combinations of packaging steady-state acceleration, vibration, shock, acoustic, spin, and thermal loads without failure, excessive deformations, or compromise of its capability to deploy and function in orbit. The stowed reflector must also survive vibration test levels, which, in general, produce the critical accelerations of the structure. The resulting load levels are considered to be ultimate and include the effects of input amplification due to resonance.

The critical design conditions used for this study were:

a. Vibration test (acting separately)

- 1. Longitudinal response 30g (ult.)
- 2. Lateral response 13.65g (ult.)
- b. Spin 71 rpm

During launch, the reflector is attached at 40 points (hinges) to the hub interface ring. The reflector loads due to longitudinal vibration and steady state conditions are reacted at these hinges. These concentrated loads are carried by the trapezoidal petals above up to the first petal hinges. These column loads are combined with the lateral loads, due to straightening the petals for stowage, to give the critical beam-column condition. To withstand these loads, the basic reflector honeycomb therefore has doublers added in the areas of high loading to prevent column buckling and face sheet instability (intercell buckling).

The petal loads due to centrifugal forces from spin-up do not exceed those for the lateral vibration test condition and therefore are not critical for the petals. Similarly, the securing band loads due to spin-up are less critical than those from the lateral vibration test. The securing band is therefore designed to withstand the antenna loading from the test.

The hub interface ring redistributes the petal loads to the Aft Equipment Module. It is therefore critical for the vibration test conditions. It also is designed to have sufficient stiffness to prevent any strong dynamic coupling between the antenna and the spacecraft during these tests.

The principal structural loads in orbit occur due to deployment, thermal gradients, and control system impulses.

During deployment, the maximum load occurs near the end of the actuator stroke and is the force required to snap-through the petals. These loads are critical for the deployment mechanism, the deployment trusses, and the petals. The deployment trusses (Figure 5.4-9) are designed for stability under the snap-through load ( $\approx 3.0$  lb, ult.) and have ample margin. The deployment actuator is a purchased item and is designed to react deployment loads throughout the 18-inch stroke. The snap-through loading does not produce critical loads on the petals.

Thermal gradients occur in the deployed configuration due to uneven solar heating of the reflector. These gradients cause distortions which must be considered in the rf performance of the antenna. Gradients also produce thermal stresses of some significance in the hoop members of the reflector. Every effort is employed in the reflector design to minimize thermal gradients: the paraboloid is 80 percent cutout; the honeycomb face sheets are constructed of titanium; the surface optical properties are controlled with coatings; and the truss attachment permits free thermal displacements of the truss. This results in maximum distortion of +0.25 inch, highly localized, which has a minimum effect on rf performance.

Dynamic response of the reflector to orbital impulses does not produce any significant stresses. Although structural damping in this condition is essentially only that due to material hysteresis in the order of 1 percent of critical or less, the impulsive loads are not of such magnitude as to cause significant responses in the reflector. Another important requirement here is that the reflector fundamental frequency does not cause any strong coupling with the control system. The calculated fundamental frequency of greater than 2 cps meets this criterion.

# 5. 4. 4. 4 Stowage and Deployment Behavior

The reflector in the stowed condition has strain energy stored due to the straightening of the curved petal hingelines. The petals are restrained, at the outer end, by a peripheral band clamp which snugs them into brackets on the inner ring. The critical loads acting on the stowed reflector, as discussed in Section 5. 4. 4. 3, occur during launch into orbit, as represented by the vibration test environment, and during spin-up. During vibration test, the stowed reflector will see its critical loadings at the spacecraft fundamental frequencies of approximately 50 cps longitudinal and 11 cps lateral. The design objective will be to avoid dynamic coupling of the reflector and the basic spacecraft to avoid excessive displacements and loads. The stowed reflector installation will be designed, therefore, to provide adequate frequency separation. Lateral loads during spin-up are found to be less critical than those that occur in the lateral vibration test.

When the band clamp is released, the petal stored energy tends to deploy the reflector. Deployment velocity is controlled by the deployment trusses and actuators and all petals deploy in unison. As mentioned before the critical condition for the deployment trusses occurs near the end of the actuator stroke when the petals snap-through to take their deployed curvature. Figure 5.4-11 shows the deployment sequence.

# 5. 4. 4. 5 Performance in 1-g Environment

An analysis of the deployed reflector was performed to determine the loads and displacements that occur due to applying +1g parallel to the reflector axis to one pair of opposite quadrants and -1g to the other pair. This analysis represents the fundamental (first inextensional) mode of vibration for the reflector. With the exception of certain local areas of discontinuity (truss link attachment points) the maximum stresses calculated are well below allowable yield and intercell buckling allowable stresses.

From this analysis, it is concluded that the deployed reflector, supported at the hub, can support its own weight in the critical symmetrical (axis vertical, concave down) and unsymmetrical (axis horizontal) loading positions without experiencing excessive stresses or instability.

With proper design consideration for the areas of locally high stresses, the design will permit accelerations as high as 1.5g without yielding, instability, or failure of any element. This capability permits fullscale testing of the deployed antenna without imposing excessive fixture requirements.

# 5. 4. 4. 6 Spacecraft Interface

The stowed reflector is entirely supported by its interface hub ring and by the upper stowage bracket ring. The mechanical interfaces are, therefore, the attachments of these rings to the AEM and EVM structures, respectively.

The interface hub ring mates with the spacecraft through a bolted connection to the upper ring of the Aft Equipment Module. Differential thermal expansion will be a consideration of the

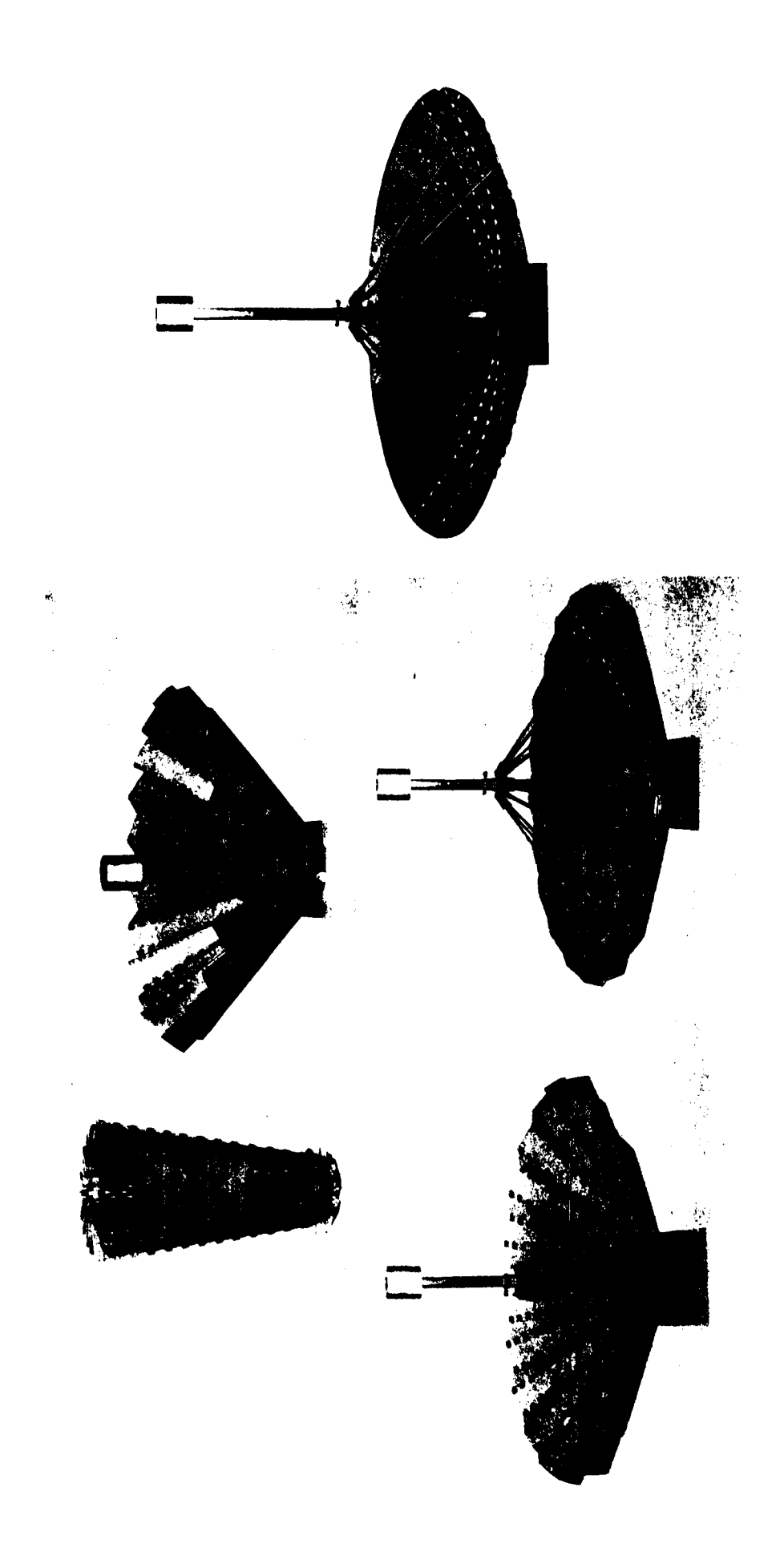


Figure 5. 4-11. Three-Foot Diameter Demonstration Model

final design of this joint. The upper stowage bracket ring is tied to the Earth Viewing Module through a bolted connection to a special support ring which is attached to the EVM lower support beams.

With a split upper stowage bracket ring, the reflector can be assembled to the otherwise completely assembled spacecraft by partially extending the petals, lowering it over the EVM, attaching the interface hub to the AEM, and then snugging the petals to the support brackets with the clamp band.

#### 5.4.5 DEPLOYMENT MECHANISM DESIGN

All the trusses must move in unison throughout the 2-minute deployment cycle. To ensure unison movement, a series of 20 ball screw actuators powered by interconnecting torque tubes and universal joints are used (see Section DD of Figure 5.4-2). The power source for the entire system is a single dc motor driving the torque system through a right angle gear box. To accommodate any differential thermal expansion affecting the system between the actuators, the torque tubes are joined to the universal joints with splines.

Theoretically, all trusses should arrive at the deployed position at the same time. But, due to possible windup and backlash in the torqued members, certain actuators may complete their travel slightly before others. To provide torque-carrying capability throughout the drive loop, without causing one screw to bind and stall the drive motor before all actuators have completed their travel, a magnetic particle clutch is coupled between the torque tube inputs and the worm gear drive for the ball screw. During actuation of the ball screw, the clutch is energized and capable of transmitting torque through the gear train. At the end of travel, a limit switch deactivates the clutch, halting torque transmission to the ball screw. A self-locking worm that drives the ball screw will hold the screw in position but permit torque transmission through the gear box to the next actuator.

The limit switches for each actuator are normally closed until the actuator reaches its end of travel and the switch is opened. When the last of any of the 20 switches is opened, the power to the motor is cut.

Except for the worm gear combination, all metal components of the deployment mechanism will be fabricated of commercially pure titanium. The worm gear combination will be the conventional steel gear with a bronze worm.

The titanium components are tentatively sized as follows. For the trunnion brackets, the sheet metal channels will be 0.040-inch-thick and the mounting plate, after machining, will be approximately 0.080-inch-thick. The interconnecting torque tubes will be 0.25-inch OD x 0.028-inch wall tubes to which the spline and fittings will be welded. The gear case will be cast with an average wall thickness of 0.090 inch. The ball screw will have a 0.375-inch pitch diameter with a 0.100-inch lead of solid metal.

### 5.4.6 FEED DESIGN

The composite feed for the large parabolic antenna consists of three concentric circular horns and a turnstile as shown in Figure 5. 4-12. The phase center of the horns is located

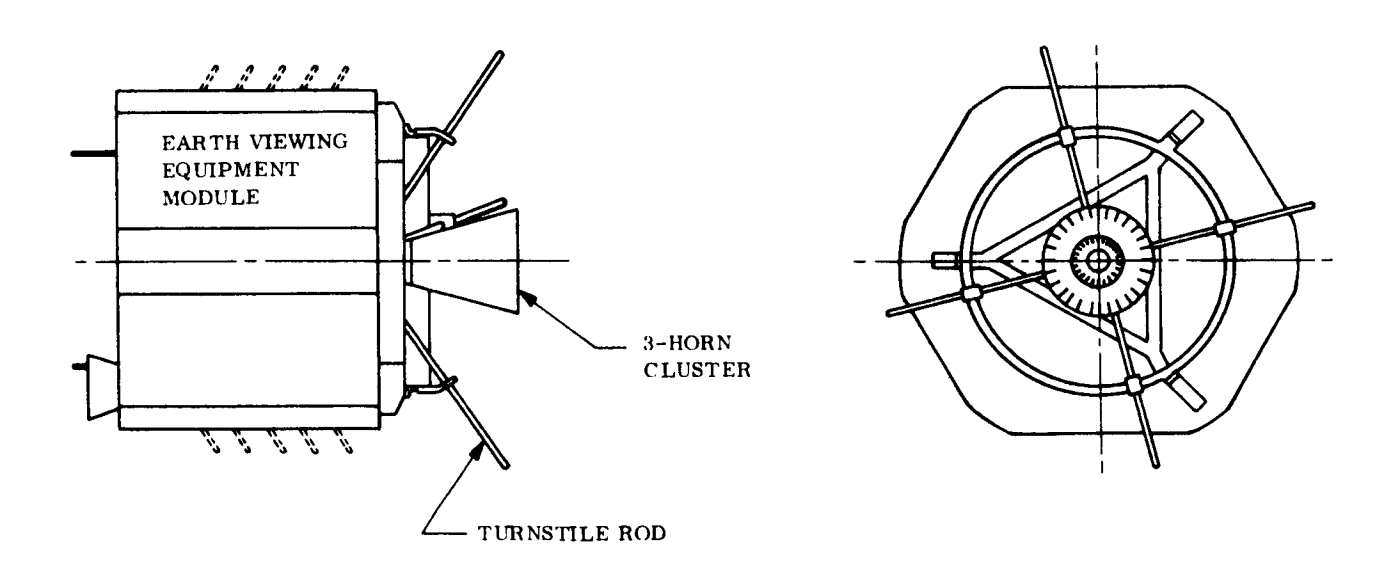


Figure 5.4-12. Composite Feed on Earth Viewing Equipment Module

approximately four inches behind the aperture plane, and the horn cluster is mounted on the equipment module so that this point is at the focus of the reflector parabola. The turnstile, for the 100 MHz operation, consists of four quarter wave rods projecting from the Earth Viewing Equipment Module at 90-degree intervals around the horns. The rods are inclined 30 with respect to the mounting surface to realize satisfactory radiating performance. Circular polarization is achieved by means of quadrature phasing in the feed cable system within the module.

The flared portion of the concentric horn cluster is 9 inches long; the inside diameter of the largest horn, for the 800 MHz operation, is 14 inches. The second horn has an inner diameter of 6 inches; this is used for 1.7, 2.1 and 2.3 GHz. The innermost horn has an inner diameter of 1.5 inches and is used for 7.3 and 8.0 GHz. Circular polarization is produced in the connecting wave guide for this horn whereas the other two each have four equally spaced probes to which appropriately phased lines are attached.

The concentric-horn approach was selected, on the basis of the feed trade-off studies, as being the best solution for the wide range of frequencies which are involved. Each horn, over its own range, can be optimized for beamwidth and VSWR. The phase centers of all lie close to one point which is then placed at the focus of the parabola. Such a design technique was used in the Syncom ground antenna system with success. In that application only two horns were used, one of which had a reduced bandwidth in comparison to the corresponding requirement on ATS-4. The extent of extrapolation of this technique is shown in the following table. On the basis of the Syncom experience, it is believed that the proposed design extension is feasible.

Table 5.4-2. Comparison of Feed System Requirements

SYNCOM		ATS-4		
Frequency Band - GHz	% Bandwidth	Frequency Band - GHz	% Bandwidth	
		0.8		
1.7 - 1.9	12.0	1.7 - 2.3	35.0	
7.1 - 7.8	10.0	7.3 - 8.0	10.0	

The phase center of the innermost horn should be aligned to within 0.1 inch of the focus to keep the defocusing loss under 0.1 dB. Calculations show that the displacement due to thermal distortion of the feed support rods will not exceed this figure. The tolerances on the lower frequency horns are relaxed in proportion to the wavelength. It is important in the feed design that the various phase centers lie within these tolerances.

The transmission lines into the feed horn cluster are very short, since the horn connectors are inside the Earth Viewing Equipment Module.

#### 5.4.7 THERMAL DESIGN

The thermal design of the parabolic antenna was achieved by a thermal-mechanical evaluation of structural, weight, and rf requirements. Basic dimensions and curvature were defined by rf requirements. A solid surface was not necessary nor desirable from a weight standpoint; therefore, an open structure was evaluated. The structural strength was constrained by ground handling and launch loads since the only significant loads imposed in orbit are those caused by thermal distortion. Parametric studies of various ratios of open area to total area resulted in the selection of 80 percent as a near optimum design thermally which could be accommodated structurally based on ground and launch loads. The 80 percent open area design has no special quality other than the fact that the percentage increase in area is decreasing rapidly at that point (see Figure 5.4-13). Using 80 percent provided adequate margin in structural strength and the effect of a greater open area was difficult to detect thermally because the differences would be within the inherent inaccuracies of the analytical techniques.

Parametric studies were performed to evaluate the influence of coatings on thermal distortion. As a result of these studies and the calculations of distortion, the coatings selected were buffed titanium for the inside (concave) surface ( $\alpha=0.45$ ,  $\epsilon=0.15$ ) and vapor-deposited aluminum for the outside (convex) surface ( $\alpha=0.12$ ,  $\epsilon=0.04$ ). These coatings have excellent degradation characteristics and long time exposure to the space environment will cause no significant change in optical properties. Flight data for several space vehicles support the reliability of vapor-deposited aluminum. And, since the buffer titanium is not really

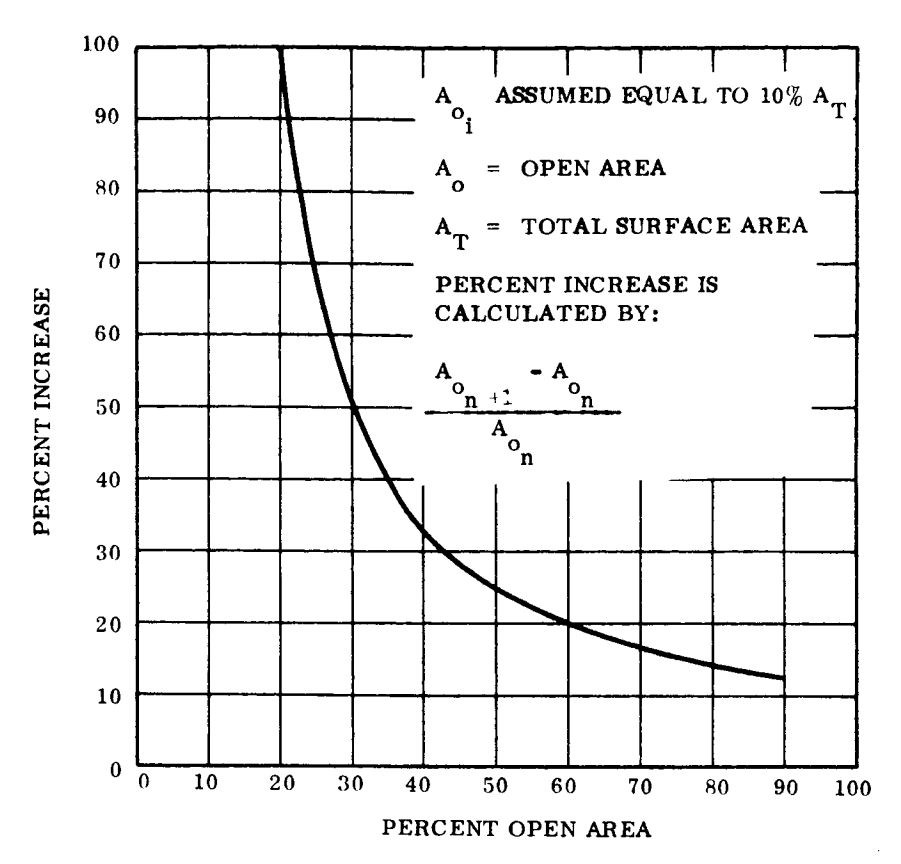


Figure 5.4-13. Influence of Open Area on Antenna Design

a coating but a mechanical surface finish, any degradation will be the result of micrometeorite erosion rather than a change in the molecular structure of the material.

A slight improvement in the temperature patterns was noted by the inclusion of a high  $\alpha$  and  $\epsilon$  coating (black) on the edges of honeycomb. This improvement is caused by the fact that as the angle between the antenna surface and the sun increases, the projected area of the surface decreases but the projected area of the edges of the cutouts increases. And conversely, by providing a high  $\alpha$  on the edges, more heat will be absorbed at the larger angles compensating for the decreased amount of energy absorbed on the antenna surface. In addition, the high  $\epsilon$  will provide greater cooling of the surfaces at small angles relative to the sun. Since a "black" coating will be used, no degradation is expected.

The least severe thermal gradients were found to occur for the case where the front and back of the antenna were coated with vapor-deposited aluminum ( $\alpha = 0.12$ ,  $\epsilon = 0.04$ ) and the

edges of the structural members were coated with black paint ( $\alpha = \epsilon = 0.8$ ) (see Figure 5.4-14). However, this case was not analyzed structurally because it was completed subsequent to the structural analysis. The temperature distribution used for the structural analysis and subsequent rf analysis (Figure 5.4-15) was obtained for the case where the front of the antenna was coated with polished titanium ( $\alpha = 0.45$ ,  $\epsilon = 0.15$ ), the back of the antenna was coated with vapor-deposited aluminum ( $\alpha = 0.12$ ,  $\epsilon = 0.04$ ), and the edges of the structural members were coated with black paint ( $\alpha = \epsilon = 0.8$ ). The thermal gradients for this case were more severe than for the case where the front and back of the antenna were coated with the same material. However, the distortions were structurally acceptable and they did not disturb the rf pattern significantly. The thermal analysis of the reflector is presented in detail in Section 6.3.4.

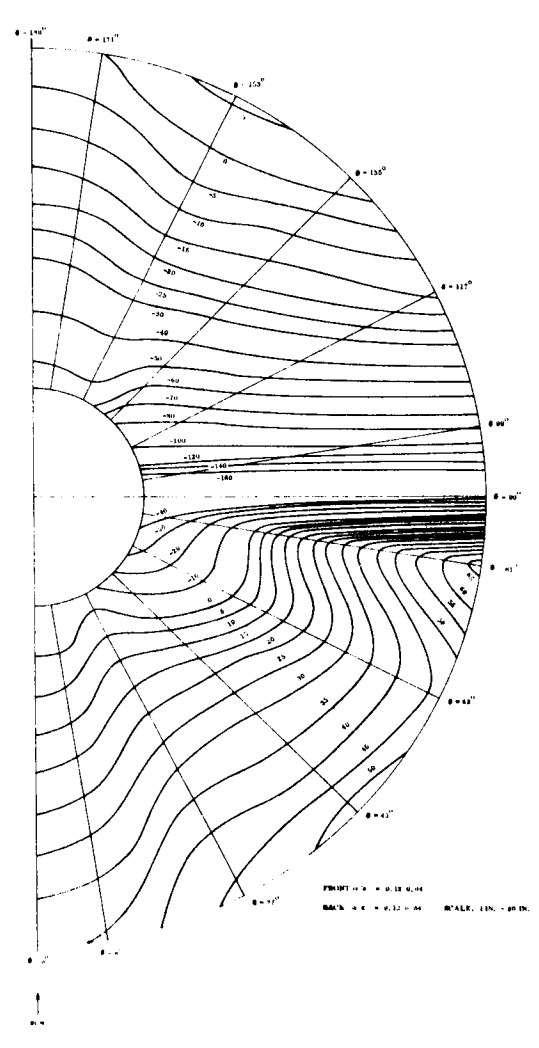


Figure 5, 4-14. Parabolic Antenna Temperature Distribution

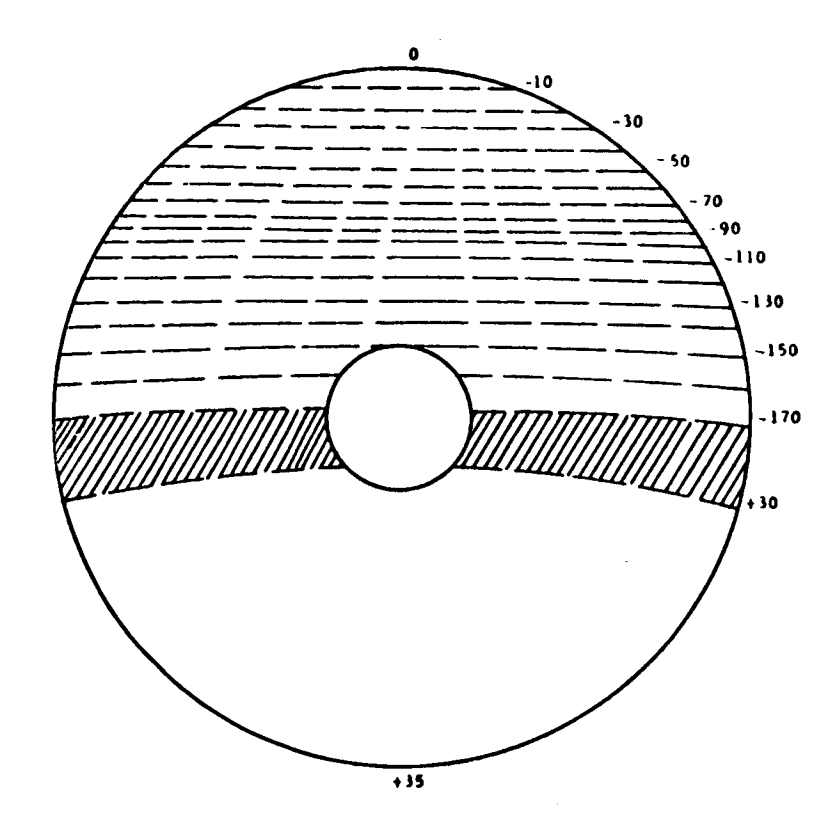


Figure 5.4-15. Antenna Isotherms 39-90

### 5. 5 GUIDANCE AND CONTROL

#### 5.5.1 **SUMMARY**

The orientation control requirements are specified as follows.

- a. Direct the main beam of the parabolic antenna to any point on the visible earth's surface with a pointing accuracy of 0.1 degree.
- b. Reorient the pointing direction from any point on the visible earth's surface to any other point, and stabilize at the new position to within the 0.1 degree accuracy within 30 minutes, for a worst case reorientation of 17.4 degrees.
- c. Track in response to ground commands with a pointing error not exceeding 0.5 degree for tracking rates up to 10 milliradians per minute.
- d. Meet the specified performance during stationkeeping.

In addition to these requirements the guidance and control system is required to perform the following functions.

- a. Spinup to provide spin stabilization during station acquisition.
- b. Control the coning induced by spinup, apogee motor burn and vernier thrusting and maintain coning control in the presence of structural damping with an unstable inertia ratio of approximately 10.
- c. Provide attitude control of the angular momentum vector during spin stabilization so as to have the proper spacecraft attitude for apogee motor burn and vernier thrusting.
- d. Provide vernier thrusting to remove injection errors and to establish conditions suitable for station capture by the stationkeeping subsystem.
- e. Despin the spacecraft after vernier thrusting.

An active system design has been selected as the baseline for performing all functions in an integrated manner. Spin stabilization with active coning and precession control is used during the station acquisition phase (booster separation to completion of vernier thrusting).

Spin stabilization was selected primarily because of the tradeoff between providing coning and precession control versus providing a three-axis orientation control subsystem. Active coning control is required because the spacecraft is spin stabilized about an axis other than the maximum moment of inertia axis which results in coning due to structural damping. Two solid propellant motors are used for spinup. The station acquisition sensor signal processor processes the output of an angular accelerometer to actuate appropriate thrusters. Spin axis precession is controlled by thrusters which are fired by ground command based on rf polarization angle measurements made on the ground and telemetered sun sensor signals from the spacecraft. Injection errors are removed by thrusters which are fired by ground command based on ground tracking data. Despin is performed by thrusters which fire automatically in response to the signals from a three-axis rate gyro package. A single monopropellant hydrazine mass expulsion subsystem performs the thrusting required for coning control, precession control, vernier thrusting and despin. This mass expulsion subsystem is not required to operate after despin, which is significant for reliability considerations.

earth sensor for control about two axes was selected with the third axis being controlled with a star sensor. (Initially it appeared that earth sensors would not provide the required accuracy.) Because of the limited field of view of the earth sensor, it is first necessary to provide a reference attitude from which to transfer to earth sensor control. This reference attitude is provided by establishing control to the sun. The orientation control sensor signal processor processes pitch and roll sun sensor and gyro signals to provide an error signal to the flywheel and jet controller to actuate the orientation control thrusters so as to align the yaw axis to the sun. Earth stabilization is then initiated when the space-craft is at the appropriate location in orbit. The earth sensor provides the control signals to drive the flywheels for earth stabilization to provide pitch and roll axis control to the earth. In order to provide an attitude about the yaw axis suitable for star acquisition, control about the yaw axis is first established with respect to the sun. The yaw sun sensors provide control signals to actuate the yaw orientation control thrusters to align the negative pitch axis to the celestial north pole in order to acquire Polaris in the star

sensor field of view. The star sensor provides the signal for controlling the yaw flywheel. The orientation control mass expulsion subsystem (resistance jets) provides all the control torques necessary for stabilization and flywheel unloading as well as the thrust for station-keeping using a total of only nine thrusters. Proportional flywheel control was selected over other modes of control such as limit cycle control with thrusters and on-off control of flywheels in order to meet the accuracy requirements and to avoid exciting the structure by repeated pulsating torques.

The location on earth to which the spacecraft is pointed and the tracking are controlled by ground command.

The block diagram for the guidance and control subsystem is shown in Figure 5.5-1. The sequence of events and the sensors and thrusters used for each phase of the guidance and control sequence are described below.

- a. Launch from ETR into a 28.5-degree inclined, 100 nm parking orbit.
- b. Yaw 31.3 degrees counterclockwise to obtain an orientation compatible with the 8.05-degree plane change at perigee burn.
- c. Initiate the second burn of Centaur at the first equatorial crossing. This results in a 20.45-degree inclined transfer orbit.
- d. Yaw 163.5 degrees cw to establish the desired apogee motor burn attitude.
- e. Separate from the booster. (A tip-off rate of up to 2 degrees/sec has been assumed with pitch error of 0.7 degree and yaw error of 1 degree.)

Items a. through e. are controlled by the booster.

- f. Spinup to 71 rpm in 1 to 2 seconds using two 300 lb (average) solid propellant motors.
- g. Reduce the coning to less than 0.5 degree using the accelerometer and 1 lb thrusters.
- h. Maintain coning to less than 1 degree in the presence of structural damping.

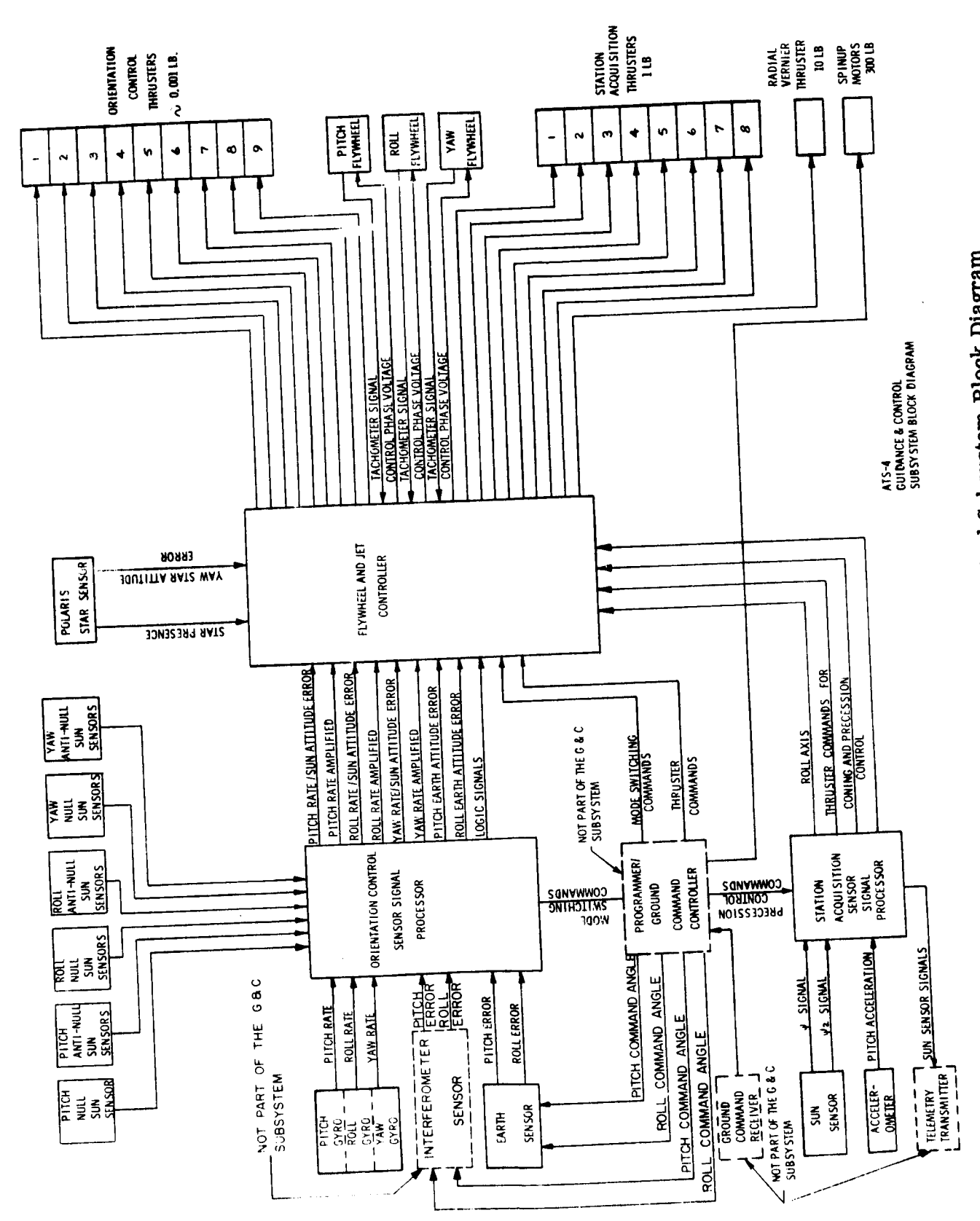


Figure 5.5-1. ATS-4 Guidance and Control Subsystem Block Diagram

- i. Determine in the proximity of first and second apogee the spin axis precession errors on the ground from rf polarization angle measurements and telemetered sun sensor signals. (The errors are those accruing during separation and spinup plus those due to disturbance torques.)
- j. Precess to the desired apogee motor burn attitude in accordance with ground commands and in conjunction with coning control using the 1 lb thrusters.
- k. Execute apogee motor burn at second apogee.
- 1. Reduce coning to less than 0.5 degree.
- m. Ground track the spacecraft to determine injection errors and orbit parameters.
- n. Determine the spacecraft attitude from rf polarization angle measurements and telemetered sun sensor signals and precess to reacquire the apogee motor burn attitude.
- o. Ground command  $\Delta V$  for the 1 lb and 10 lb vernier thrusters to remove injection errors and to establish a westward drift rate of 1 deg/day (equivalent to a  $\Delta V$  of 10 fps).
- p. Maintain coning and precession control during the vernier thrusting phase of approximately 2 days.
- q. Despin to less than 0.10 deg/sec using the three-axis gyro package and 1 lb thrusters.
- r. Vent the coning control/precision control/vernier adjust/despin mass expulsion subsystem while maintaining rate control with the gyros and 1 lb thrusters.
- s. Stabilize the negative yaw axis to the sun using roll and pitch sun sensors and gyros to control the orientation control thrusters. (Requires up to 2 hours for worst case initial conditions.)
- t. Deploy the parabolic antenna before 11:00 a.m. The attitude will be suitable for rf command and telemetry communication in the proximity of noon. (Deployment requires several minutes.)
- u. At approximately 11:30 a.m. activate the earth sensor and perform earth stabilization using the earth sensor and pitch and roll flywheels. (Requires approximately 20 minutes for worst case initial conditions.) The orientation control thrusters are used for flywheel unloading as required.

- At approximately 4:00 p.m. initiate yaw stabilization to the sun to align the negative pitch axis to the celestial North Poleusing yaw sun sensors (properly aligned for the time of year) and yaw gyro controlling the orientation control thrusters. (Requires up to 2 hours for worst case initial conditions.)
- w. Prior to 8:00 p.m. acquire Polaris and transfer yaw control to the Polaris star sensor and yaw flywheel. The orientation control thrusters are used for flywheel unloading as required.
- x. Program commands for offset pointing.
- y. Reorientation and tracking maneuvers are ground commanded by programming bias commands to the earth sensor and Polaris star sensor.
- z. Perform station capture at 90° W. longitude, stationkeeping and station change.

This guidance and control subsystem design meets all the requirements stated above. The 0.1° accuracy requirement is feasible as shown on Table 5.5-1; however, mechanical and electrical misalignment of the antenna and rf distortion are not included. Analog computer studies have shown that the error accrued during flywheel loading is within the 0.03 degree for pitch and roll and the 0.05 degree in yaw shown in Table 5.5-1 with the preferred configuration including sensor noise and disturbance torques up to 10 times the expected maximum torque. An integrated attitude control/stationkeeping mass expulsion subsystem is employed. With this approach the flywheels will maintain control during stationkeeping thus maintaining the 0.1 degree pointing accuracy while stationkeeping. Actually, the flywheels will be unloaded in the initial portion of the stationkeeping thrusting period, with subsequent unloading as required during stationkeeping. The spacecraft can be recriented from horizon to horizon in 23 minutes for 40 percent initial wheel speed, which is well within the 30 minute requirement. The spacecraft will track a ground commanded rate input of 10 milliradian per minute with 0.28 degree maximum error for 40 percent initial wheel speed, which is well within the 0.5 degree requirement. All the analog computer studies which included sun stabilization, earth stabilization, pointing, reorientation and tracking were made with structural dynamics using a damping factor of 0.001. Satisfactory control dynamic performance was achieved by minir izing the bandwidth of the control subsystem so as to provide more than an order of magnitude difference between the natural frequencies of the structure and the bandwidth of the control loop. The

control loop bandwidth for the selected design is 0.2 rad/sec compared with the lowest natural frequency of the preferred structure of 12.3 rad/sec (5.5 rad/sec was used in the control system analog computer study).

Table 5.5-1. Error Budget

ERROR SOURCE	ERROR ALLOCATION		
	Pitch - Roll	Yaw	
Basic Sensor Error	0.05	0.02	
Command Angle Resolution	0.02	0.003	
Star Tracker Gimbal Offset		0.03	
Earth Horizon Anomalies	0.004		
Sensor Control Axis Misalignment			
<ol> <li>Prior to Launch</li> <li>Due to Launch Effects</li> <li>Orbit Environment</li> </ol>	0.02 (incl. cal.) 0.01 0.01	0.003 0.01 0.01	
Sensor Output Noise	0.02	0.03	
Control Electronics Error	0.01	0.01	
Momentum Storage Offset	0.03	0.05	
Timing Error of Comm.	0.005	0.005	
Spacecraft Angular Pos. Uncert.	0.03		
Spacecraft Drift	0.02		
Target Location Uncertainty	0.0003	0.0003	
Yaw Cross Coupling Error	0.01		
Earth Sensor Readout	0.01		
3 <sub>♂</sub> Accuracy Per Axis	0.08	0.07	
3σ Absolute Pointing Accuracy (ref. Sect. 6.4.3.4)	0.09		

Table 5.5-2 presents a list of the components forming the guidance and control subsystem and the weight and power required for each along with total weight and average power for the subsystem. The total weight of the guidance and control subsystem excluding electrical harnessing is 364.8 pounds. The power required during pointing; that is, after stabilization to the earth and star is 82.8 watts average.

5.5-7

Table 5.5-2. Weight and Power Summary for Station Acquisition and Orientation Control Subsystems

Component	No. Required	Weight per System (lb)	Average Power (watts)
Sensors			1 5 7
Station Acq. Sun Sensors	1 Set	2.1	
Station Acq. Accelerometer	1	2.8	10.6
and Elect.	_		
O/C 3 Axis Gyros and Elect.	1	15.5	30.0
O/C P & R Sun Sensors	2 Sets	1.8	
O/C Y Sun Sensors	1 Set	0.9 12.0	8.0
O/C Polaris Star Sensor O/C Earth Sensor	1	10.7	7.0
O/C Earth Sensor	1	10.7	1.0
Control Electronics			
Station Acquisition Sensor	1	3.2	8.0
Signal Processor			
O/C Sensor Signal Processor	1	15.3	30.0
O/C Flywheel and Jet Controller	1	19.2	15.0
Actuation System			
Spinup Motor (4.2 lb of Fuel)	2	11.6	
Coning and Precession Control	1		
and Vernier Adjust and Despin			
1. Fuel - Prior to Apogee		1.8	
- After Apogee Burn		71.2	
2. Tankage and Hardware		35.7	
O/C Mass Expulsion and Stakpg.	1		12.8
1. Fuel		92.4	
2. Tankage and Hardware		34.7	
Flywheels	3 (1 per axis)	33.9	10
Totals		364.8	82.8 (during pointing)

### 5. 5. 2 FUNCTIONAL DESCRIPTION

A functional description of the preferred design for the guidance and control subsystem is presented in this section. The description is divided according to the five basic guidance and control modes; namely, station acquisition, orientation control stabilization, orientation control operational modes, station capture and station change, and restabilization. So as to identify the various control modes the description of the guidance and control subsystem is presented as a discussion of the following control modes.

# a. Station Acquisition Modes

- 1. Separation and Spinup
- 2. Transfer Orbit
- 3. Apogee Motor Burn
- 4. Vernier Thrusting

#### b. Orientation Control Stabilization Modes

- 1. Despin
- 2. Sun Stabilization
- 3. Deployment
- 4. Earth Stabilization
- 5. Star Stabilization

# c. Orientation Control Operational Modes

- 1. Pointing
- 2. Reorientation
- 3. Tracking
- 4. Flywheel Unloading and Stationkeeping
- 5. Interferometer Control
- d. Station Capture and Station Change Modes
- e. Restabilization Modes

# 5. 5. 2.1 Station Acquisition Modes

This phase commences at separation of the ATS-4 spacecraft from the Centaur launch vehicle, and consists of the following functions:

- a. A pair of spin motors is fired which spins up the spacecraft about its axis of symmetry (the  ${\bf Z}_5$  axis).
- b. During the transfer orbit (duration 15.75 hr) an active onboard coning damper consisting of an angular accelerometer, switching logic and two thrusters controls coning of the spin axis.
- c. Prior to apogee burn, the spacecraft spin axis is precessed to a specified attitude. Attitude information is derived from an onboard sun sensor and from measurement at the ground station of the polarization vector of a radio signal transmitted from the spacecraft. Vehicle attitude is computed on the ground and attitude correction is made by ground command of two onboard thrusters (the same thrusters as are used for the coning damper).
- d. After apogee burn the spacecraft spin axis precession error and coning is removed prior to vernier propulsion. During vernier propulsion (duration of approximately 2 days) the precession control is used as required to correct the spin axis attitude.

The spacecraft configuration during station acquisition is shown in Figure 5.5-2. A block diagram of the coning and precession control system is shown in Figure 5.5-3. A summary of impulse requirement (including spin-down) is given in Table 5.5-3. (The impulse and fuel weight requirements are given in detail in Section 5.5.3.6.)

Table 5.5-3. Station Acquisition Impulse Requirements

Function	Impulse (lb-sec)	
Coning Control	245	
Precession Control	264	
Axial $\Delta$ V <sub>a</sub>	5439	
Radial A V <sub>r</sub>	8159	
$\Delta V$ to initiate maneuver to 90 deg W.	723	
Despin from 71.7 rpm.	617	
Total	15447	

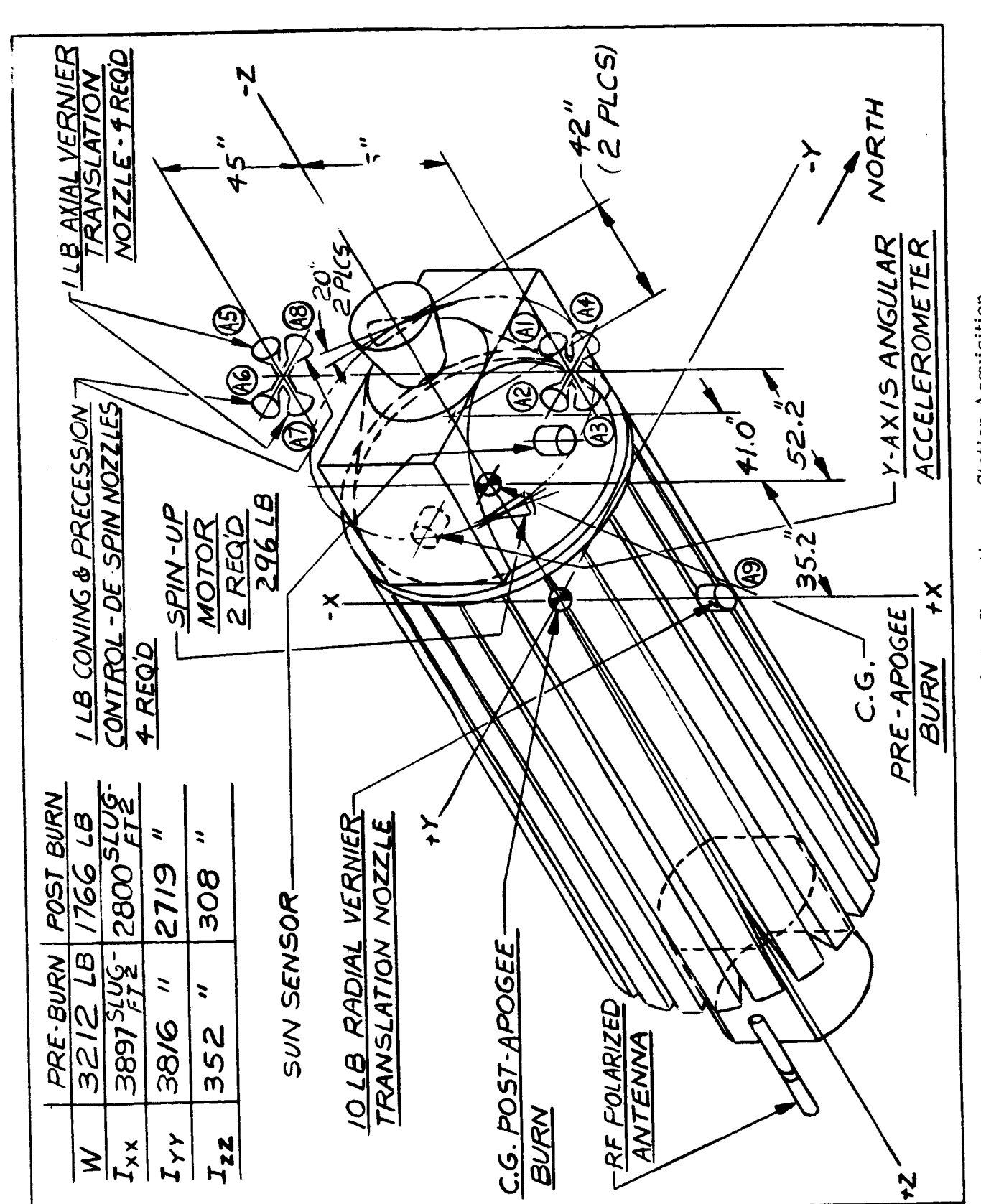


Figure 5.5-2. Spacecraft Configuration -- Station Acquisition

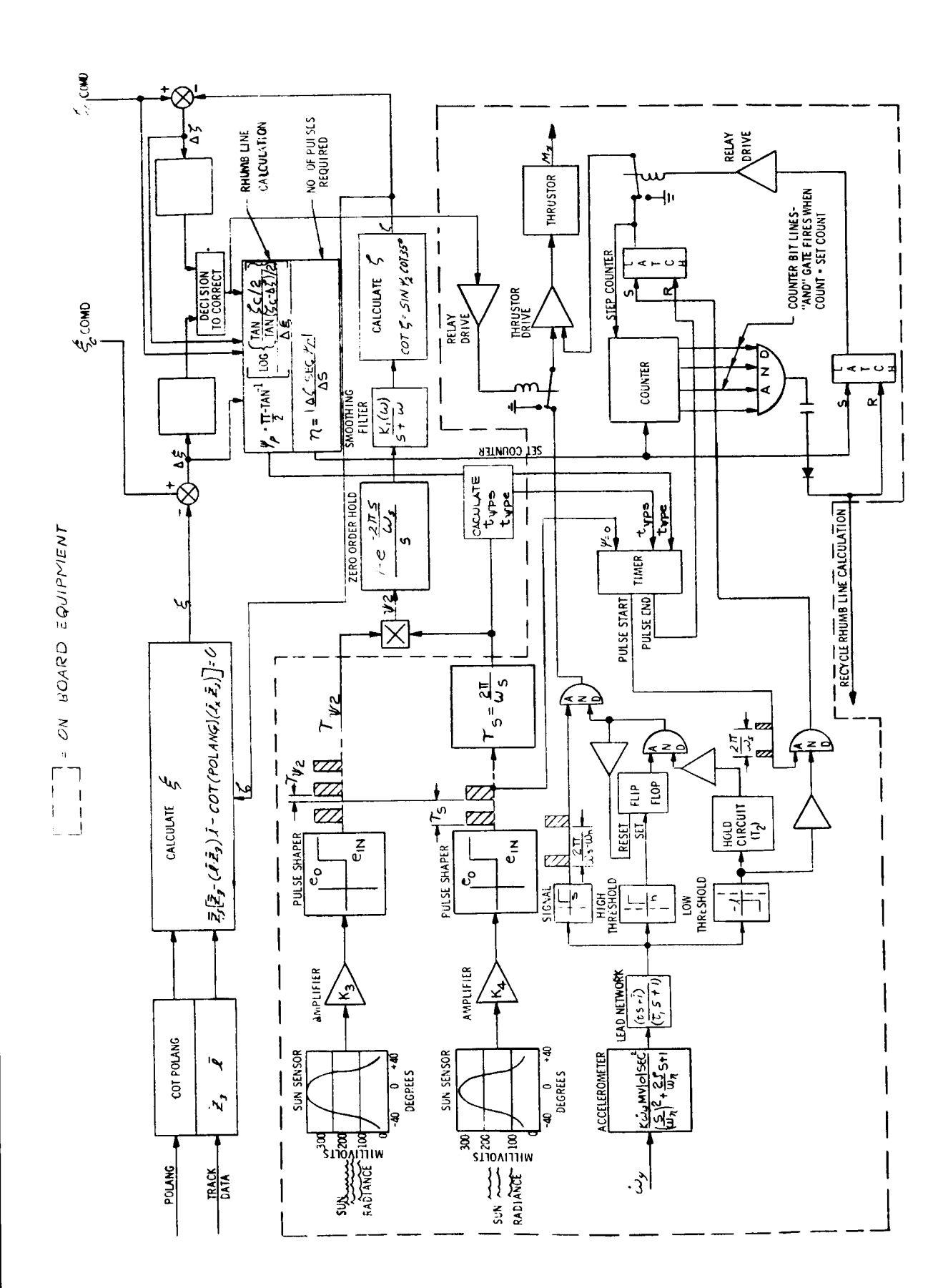


Figure 5.5-3. Coning and Precessing Control

# 5.5.2.1.1 Separation and Spinup

The attitude of the ATS-4 spacecraft at Centaur separation will be within  $\frac{1}{2}$  0.7 degree in pitch and  $\frac{1}{2}$  1.0 degree in yaw (Centaur coordinates) of the specified attitude, and tip-off angular rates of  $\frac{1}{2}$  deg/sec may exist about all body axes. A 2-second delay is allowed for the spacecraft to clear the Centaur before the spin motors are fired.

The spin motors consist of a matched pair of spin rockets with a nominal burn time of 1 sec. The total impulse (L) required per rocket to produce a spin rate of  $W_S$  radian/sec is given by

$$L = \frac{I_z W_s}{2r_s}$$

where  $I_z$  is the spin axis moment of inertia and  $r_s$  is the moment arm. For the selected configuration  $I_z = 352 \text{ slug ft}^2$ ,  $r_s = 3.29 \text{ ft}$ , and the desired spin rate is in the range of 7.32 to 8.37 radian/sec (70-80 rpm, refer to Section 5.5.2.1.3). Thus the required spin motor size is in the range 392-448 lb-sec. An available spin motor has been selected which gives 402 lb-sec total impulse, which will produce a spin rate of 7.51 radian/sec (71.7 rpm). This value has been used as the design spin rate.

Coning of the spacecraft spin axis after spinup is caused by the tip-off rates about the body x and y axes and by disturbance moments M<sub>X</sub> and M<sub>y</sub> during spinup caused by spin motor misalignment, thrust mismatch and thruster burn time variation. Precession error of the angular momentum vector after spinup is due to initial error at spacecraft separation, motion during the interval between separation and spin motor ignition, and precession during spinup. An analysis of these effects is given in Section 6.4.3.3.1. For the design spin rate of 71.7 rpm, the precession angle is 9.4 degrees and the cone half-angle is 7.5 degrees.

#### 5.5.2.1.2 Transfer Orbit

After spinup, coning of the spacecraft spin axis is reduced by an onboard coning damper.

Operation of the damper commences automatically when the coning amplitude exceeds

1 degree (cone half-angle) and continues until the amplitude falls below 0.5 degree. The mode of operation is as follows: (Refer to Figure 5.5-3).

The output from an angular accelerometer, which senses angular acceleration about the body y-axis, is fed through a lead network (which compensates for thruster time lag) to three threshold switches in parallel. The threshold settings correspond to coning amplitude of

- a. 0.25 degree (signal switch)
- b. 0.5 degree (low threshold switch)
- c. 1.0 degree (high threshold switch)

Suppose that the coning amplitude exceeds 1 degree. All threshold switches give an output pulse train with a repetition rate of  $(W_s - W_n)/2\pi$  pps, where  $W_n$  is the coning frequency. The signal switch pulses occur when the angular acceleration about the body y-axis is positive. The flip-flop is set to 1 by the high threshold switch, and the hold circuit maintains the low threshold switch output at the 1-level. Thus the first AND-gate output is 1 and the signal pulse train passes through the second AND-gate causing positive torque pulses to be applied about the x-axis (thrusters A4 and A8, Figure 5.5-2) and reducing the coning amplitude (see Section 6.4.3.3.1 for system equations of motion with pulsed torques). When the coning amplitude falls below 1 degree, the flip-flop remains set and the first AND-gate remains at 1 until the coning amplitude falls below 0.5 degree at which time the hold circuit no longer gives an output and the first AND-gate output drops to 0. This inhibits further torque pulses, and also resets the flip-flop to 0. Coning control does not start again until the high threshold (1 degree) is exceeded. The use of three thresholds as described above is considered necessary because the coning motion of a spinning vehicle causes cyclic exchange of angular momentum between the x and y body axes, and requires pulsed torques for active damping. If the use of a single threshold is contemplated, the difficulty arises that, as the coning amplitude approaches the threshold, the pulse on-time becomes small, and the thruster efficiency drops off sharply, so that the reduction in cone amplitude per pulse becomes infinitesimal. Thus, the coning amplitude approaches the

threshold asymptotically, and fuel consumption continues over a long period. The rate at which coning is removed is given by

$$dc/dt = -T/4I_zW_3$$

(Reference Section 6.4.3.3.1). For the selected configuration dc/dt = -0.047 deg/sec before apogee burn and dc/dt = -0.093 deg/sec after apogee burn. The duty cycle of the thrusters is about 50 percent, and the impulse required per degree of coning is 23.5 lb-sec/deg, and 11.9 lb-sec/deg respectively prior to and after apogee motor burn.

Disturbance torques due to aerodynamic, gravity gradient, solar pressure and the Earth's magnetic field forces during the 15.75-hour transfer orbit are discussed in Section 6.4.3.1. The precession caused by these torques, together with that occurring during separation and spinup, is summarized below.

Source	Pitch (Deg)	Yaw (Deg)
Separation and Spinup	6.65	6.65
Aerodynamic	2.4	0
Gravity Gradient	0.04	0.03
Magnetic Field	0.003	0.005
Solar Pressure	0.03	0
RSS/Axis	7.25	6.65
RSS/Total	9.8	Deg

(Note that Pitch and Yaw column headings refer to motion out of, and in, an inertially fixed plane which is horizontal at apogee.)

Prior to apogee burn, the attitude of the spacecraft spin axis is measured and precession errors are corrected. The principle of the orientation measurement is shown in Figure 5.5-4.

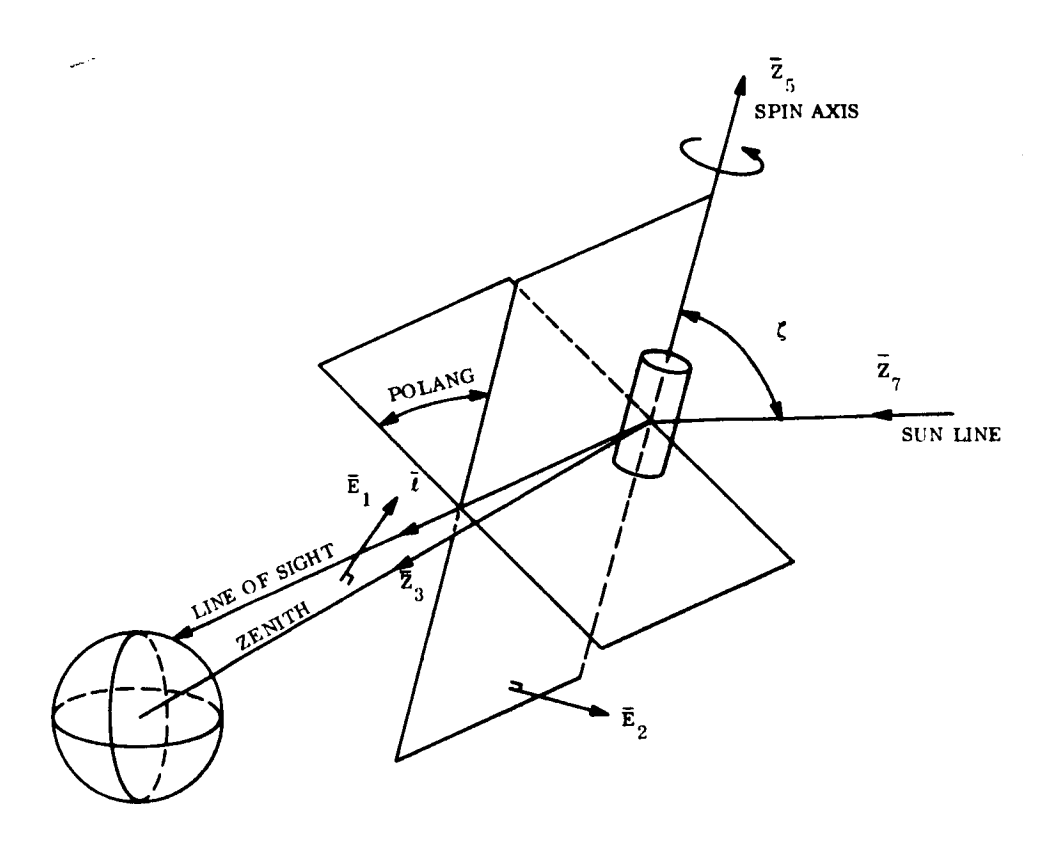


Figure 5.5-4. Principle of Orientation Measurement

An on-board sun sensor determines the angle  $\zeta$  between the spacecraft spin axis and the sun line. Measurement at the ground station of the direction of the polarization vector of an rf signal from the spacecraft permits the rotation of the spacecraft spin axis about the line of sight to be determined (POLANG). Thus, the sun sensor locates the spin axis on a cone, and the polarization measurement locates the spin axis in a plane. A two-fold ambiguity in spin axis attitude is present; however, if  $\zeta$  is large (> 60 degrees) the two attitudes are almost opposite, and the ambiguity is removed, since precession errors will not exceed 90 degrees. The principle of the sun sensor is shown in Figure 5.5-5. Two slit-type sensors are used; the  $\psi$ -sensor (field of view lies in the body x-z plane), and the  $\psi_2$ -sensor (field of view is rotated by 35 degrees about the x-axis out of the x-z plane). As the spacecraft spins, the  $\psi$  and  $\psi_2$  sensors give pulse outputs when the sun line intercepts their respective fields of view. The time difference between the signals,  $\tau_{\psi_2}$ , can be reduced to a spin angle  $\psi_2$  by normalizing with respect to the spin rate. The angle between the spacecraft spin axis and the sun line is then given by

In the block diagram of Figure 5.5-3, sun sensor outputs are telemetered to the ground station where the spin rate is determined from the  $\psi$  sensor pulse repetition rate  $(1/\tau_s)$  and  $\psi_2$  and  $\zeta$  are calculated.  $\zeta$  is then compared with the command value  $\zeta_c$  and the error  $\Delta \zeta$  is obtained. The  $3\sigma$  error of this sensor is considered to be  $^{\pm}$  0.5 degree.

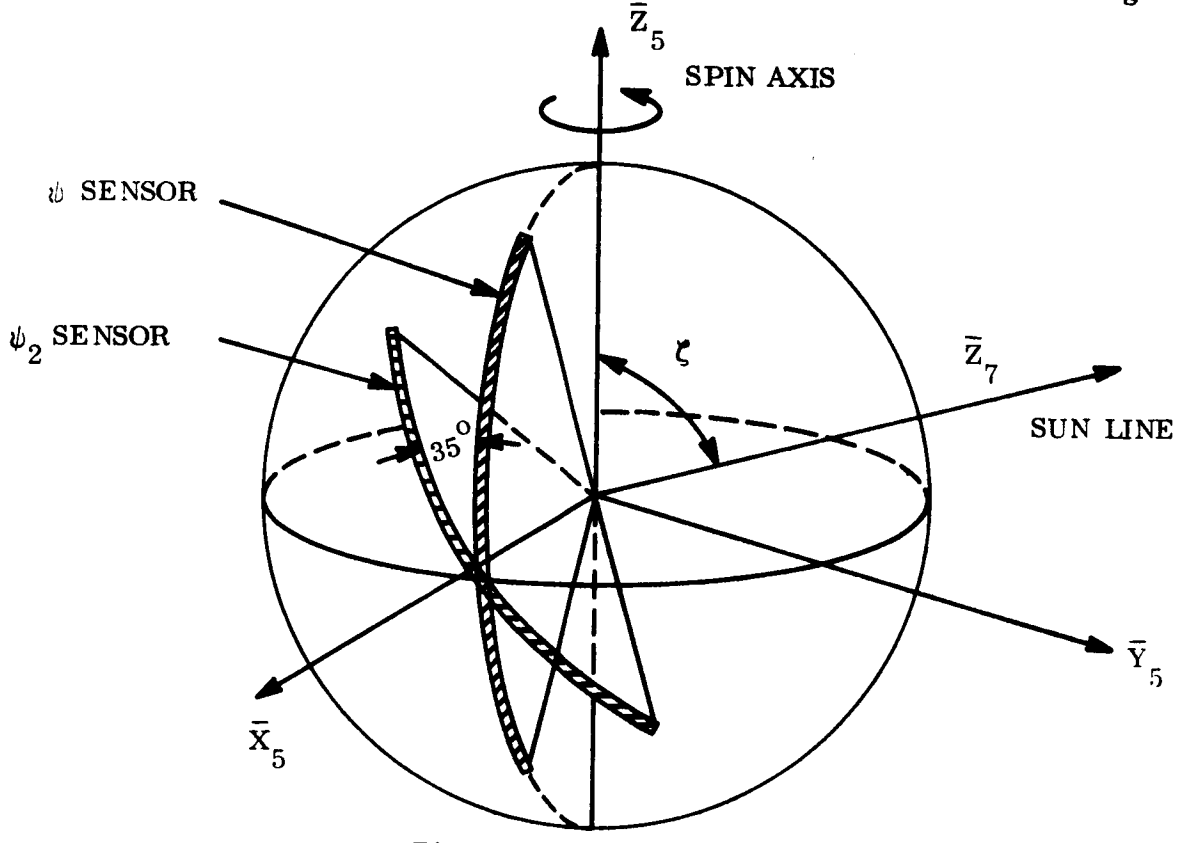


Figure 5.5-5. Sun Sensor

The polarization sensor consists of (1) an onboard polarized rf antenna, which gives a toroidal radiation pattern with the polarization vector parallel to the spin axis  $\overline{Z}_5$ , and (2), ground station equipment which measures the angle POLANG (Ref. Figure 5.5-4). The Euler angle  $\xi$  (Ref. Figure 5.5-6) is calculated from the relation

$$\overline{Z}_5 \cdot \left[\overline{Z}_3 - (\overline{\ell}, \overline{Z}_3)\overline{\ell} - \cot(POLANG)(\overline{\ell}_x \overline{Z}_3)\right] = 0$$

where  $\overline{Z}_5$  is the spacecraft spin axis attitude,  $\ell$  is the line of sight from the ground station, and  $\overline{Z}_3$  is the spacecraft zenith.  $\overline{Z}_5$  is determined with respect to the inertial  $(X_1 \ Y_1 \ Z_1)$  frame by the Euler angles  $(\xi, \zeta)$  and by the sun Right Ascension RA and declination  $\delta_s$ .  $\ell$  is determined by the ground station latitude  $\beta$  and longitude  $\lambda$ , time t, and the line of sight azimuth  $A_z$  and elevation  $\eta$ .  $\overline{Z}_3$  is determined by the spacecraft position coordinates  $u, \Omega, \nu$ . These quantities are required for the determination of  $\xi$  from POLANG.

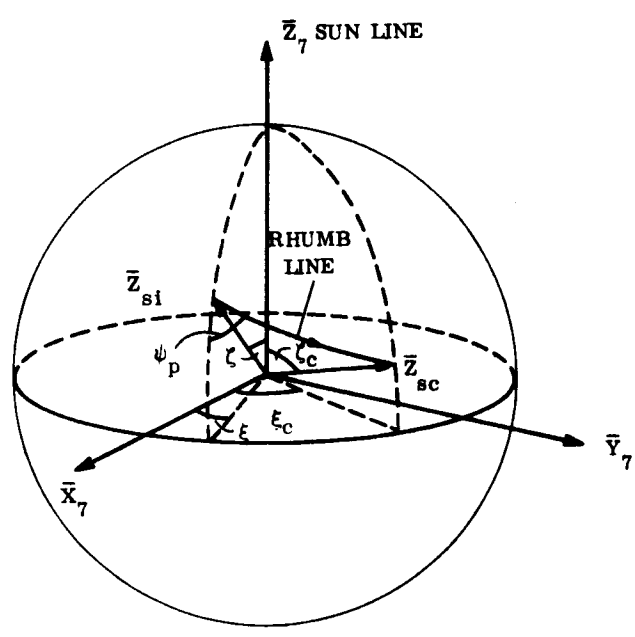
An appreciation of the error contributions in the determination of  $\xi$  from POLANG may be obtained by noting that the vector  $\overline{E}_1$  (Ref. Figure 5.5-4) is located in inertial space by the determination of spacecraft zenith and line of sight from the ground station. The vector  $\overline{E}_2$  is obtained by rotating  $\overline{E}_1$  about the line of sight by the angle POLANG. The 35 accuracy of determination of  $\overline{E}_2$  is stated to be  $\pm$  1° rotation about the line of sight (refer verbal information supplied by Mr. H. Gerwin of NASA/GSFC). The contribution of error in the sun sensor measurement to the rotation about the line of sight is zero when the sun line is along the line of sight (this is considered to be the optimum condition) and remains small providing that the angle between the sun line and the line of sight does not exceed about 30°.

The sun sensors and rf sensor information thus give the Euler angles  $\zeta$  and  $\xi$  of the spacecraft spin axis with respect to the sun-coordinate system  $(X_7, Y_7, Z_7)$ . The desired spin axis attitude is specified by the values  $(\xi_c, \zeta_c)$ . The simplest method of precessing the vehicle to  $(\xi_c, \zeta_c)$  is to apply about the  $X_5$  body axis a series of moment impulses whose timing is delayed by  $(\frac{\pi}{2} + \psi_p)/W_s$  with respect to the main sun sensor output signal  $(W_s$  is the spin rate). The angles  $\zeta$ ,  $\xi$  are analogous to latitude and longitude respectively in a frame in which the sun line is the analog of the North Pole; the impulse train at constant  $\psi_p$  causes the spin axis to describe a rhumb line (a line which makes a constant angle with the meridians). The equation of the rhumb line is given by

$$\cot \psi_{\mathbf{p}} = \frac{\log \left| \tan \left( \zeta_{\mathbf{c}}/2 \right) / \tan \left( \zeta/2 \right) \right|}{\left( \xi_{\mathbf{c}} - \xi \right)}$$

Rhumb line precession is illustrated in Figure 5.5-6. The angle through which the spin axis moves between  $(\xi, \zeta)$  and  $(\xi_c, \zeta_c)$  is given by

$$S_1 = \left| (\zeta_c - \zeta) \sec \psi_p \right|$$



 $ar{z}_{si}$  INITIAL POSITION OF SPIN AXIS  $ar{z}_{sc}$  COMMAND POSITION OF SPIN AXIS

Figure 5.5-6. Rhumb Line Precession

From the viewpoint of fuel consumption, the most economical way of precessing the space-craft is by a great circle route between  $(\xi, \zeta)$  and  $(\xi_c, \zeta_c)$ , for which the precession angle is given by

$$S_2 = \cos^{-1} \left[ \cos \zeta \cos \zeta_c + \sin \zeta \sin \zeta_c \cos (\xi_c - \xi) \right]$$

However, great circle precession would necessitate a variable timing angle  $\psi_p$ , and the advantage in fuel consumption is not considered to be sufficient to justify the increase in complexity associated with this method. Referring to the block diagram of Figure 5.5-3, the angles  $\zeta$  and  $\xi$  are calculated on the ground from the telemetered sun sensor signals

and the rf sensor intelligence, and the attitude errors  $\Delta \zeta$  and  $\Delta \xi$  are obtained. The rhumb line phase angle  $\psi_p$  is calculated and the number of impulses required to correct the attitude is obtained from the relation

$$n = S_1/\Delta s = \left|\Delta \zeta \sec \psi_p\right|/\Delta s$$

where  $\Delta s$  is the precession angle per impulse, given as a function of the design impulse width  $\psi_{_{\rm W}}$  and the precession moment M by

$$\Delta s = 2M \sin (\psi_W/2)/I_z W_s^2$$

From  $\psi_p$ ,  $\psi_w$ , and  $W_g$ , pulse start (t  $\psi_{pS}$ ) and pulse end (t  $\psi_{pe}$ ) time delays are calculated and are telemetered to an onboard timer, which generates pulse start and pulse end trains with phasing corresponding to  $\psi_p$ ; that is, when the pulse trains are applied to the thruster drive, the thruster impulses will be centered at  $\psi = \frac{\pi}{2} + \psi_p$  (the  $\psi$ -sun sensor signals occur at  $\psi = 0$ ). The start pulses are passed through an AND-gate to which the second input is the inverted signal from the low threshold of the coning control. Thus, if the coning amplitude exceeds 0.5 degree, the start pulses are inhibited when coning would be increased by the application of a thruster impulse. If the coning amplitude is less than 0.5 degree, the start pulses pass through the AND-gate at all times. From the AND-gate the start pulses set a latch which outputs to the thruster drive, and also gives a counter step signal. The end pulses reset the latch. The number of impulses is set into an onboard counter, and each time the latch is set the counter is stepped down. When the counter output is zero the latch output is switched off and a signal is telemetered to the ground.

For the selected configuration  $\psi_W$  = 75 degrees (Refer Section 6.4.3.3.1) and the precession angle per impulse  $\Delta s = 0.029$  degree prior to apogee burn and  $\Delta s = 0.057$  degree after apogee burn. The precession rates are 2.07 deg/min and 4.08 deg/min., and the impulse required is 12.1 lb-sec/deg and 6.2 lb-sec/deg. It is estimated that errors in the rhumb line precession will be primarily due to uncertainty in the thruster time lags. If the thrust impulse width varies by  $\Delta t_W$  and the center is displaced by  $\Delta t_d$  relative to the design values, the errors in  $\psi_p$  and  $s_1$  will be given by

$$\Delta \psi_{p} = W_{s} \Delta t_{d}$$

$$\Delta S_{1} = W_{s} \Delta t_{w} S_{1} / \psi_{p}.$$

The error in the final position due to  $\Delta\psi_p$  may be approximately determined by assuming great circle instead of rhumb line precession; the approximation is good providing that  $\zeta > 60$  degrees. The error due to  $\Delta S_1$  may be obtained by resolving  $\Delta S_1$  into  $\zeta$  and  $\xi$  components. The result is ( $\Delta\psi_p$ ,  $\Delta S_1$  small)

$$\Delta \zeta_{c} = \sin S_{1} \sin \zeta \sin \psi_{p} \Delta \psi_{p} / \sin \zeta_{c} + \cos \psi_{p} \Delta S_{1}$$

$$\Delta \xi_{c} = \sin S_{1} \cos \psi_{p} \Delta \psi_{p} / \sin \zeta_{c} \cos (\xi_{c} - \xi) + \sin \psi_{p} \Delta S_{1}$$

Typical values are 
$$\Delta t_d = 0.010$$
 sec,  $\Delta t_w = 0.020$  sec,  $W_s = 7.51$  rad/sec,  $\psi_w = 1.31$  radian  $(75^\circ)$ ,  $\zeta = 70^\circ$ ,  $\zeta_c = 80^\circ$ ,  $(\xi_c - \xi) = 15^\circ$ . Thus  $\psi_p = 54.8^\circ$ ,  $S_1 = 17.3^\circ$ ,  $\Delta \psi_p = 4.3^\circ$ ,  $\Delta S_1 = 2.0^\circ$ , and  $\Delta \zeta_c = 1.0^\circ + 1.2^\circ = 2.2^\circ$   $\Delta \xi_c = 0.8^\circ + 1.6^\circ = 2.4^\circ$ 

Thus the residual error after the open loop correction is about 3.3 degrees, or 19 percent of the initial  $S_1$ . After two and three open loop corrections, the error would be 0.63 degree and 0.12 degree due to  $\Delta \psi_p$  and  $\Delta S_1$ . The maximum fuel consumption would correspond to (1+0.19+0.04)  $S_1=1.23$   $S_1$ 

A plot of the rf sensor beamwidth required to ensure that the polarized signal is received by Rosman ground station during the period preceeding apogee burn is shown in Figure 5.5-7. This plot assumes zero precession error. To obtain the rf sensor beamwidth requirement, the precession error of the spacecraft spin axis should be added to the beamwidth shown in Figure 5.5-7.

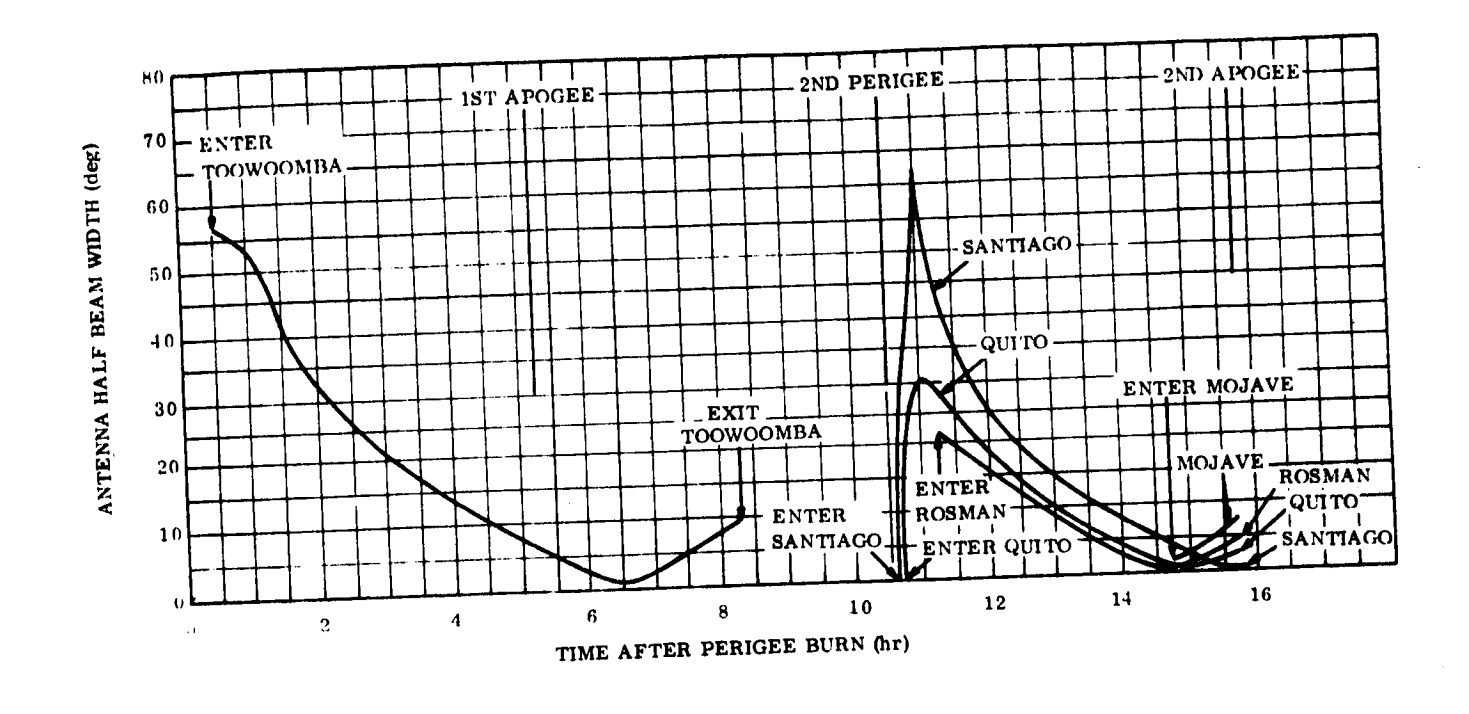


Figure 5.5.-7. ATS-4 Reference Design: Antenna Half-Beam Angle During Transfer Orbit

# 5.5.2.1.3 Apogee Motor Burn

Misalignment of the apogee motor thrust vector causes a migration of the spacecraft spin axis at motor ignition and a complex coning motion. A second migration of the spin axis occurs at burnout. The migration at ignition and the initial value of the cone angle are given to a good approximation by (Ref. Section 6.4.3.3.1)

$$\epsilon_a = F \ell_a \Delta_a / I_z W_s^2$$

where F is the motor thrust,  $\ell_a$  is the moment arm, and  $\Delta_a$  is the thrust misalignment. The migration at burnout is given by the above relation with appropriate values for  $\ell_a$ ,  $\Delta_a$  and  $I_z$ . Taking  $\Delta_a$  = 0.25 degree,  $\ell_a$  = 52.0 in. at ignition and 87.4 in at burnout, the migration at ignition and burnout is given by

ignition 
$$\epsilon_a = 30.8/W_s^2$$
 deg = 0.55 deg at 71.7 rpm

burnout 
$$\epsilon_a = 60.8/W_s^2 \text{ deg} = 1.08 \text{ deg at } 71.7 \text{ rpm}$$

The mean cone angle at ignition is 30.8/W<sub>s</sub> degrees. During motor burn, the increasing misalignment moment arm due to center of mass shift tends to increase the cone angle, and the motor jet damping and active coning damper reduce the cone angle. Digital computer solutions of the equations of motion without the coning damper show that the jet damping effect approximately counter balances the moment arm increase, as shown by the examples of Section 6.4.3.3.1. After burnout, the maximum value of the coning amplitude is given by

$$C_{a} = \tan^{-1} \frac{2F \ell_{a} \Delta_{a} I}{I_{z} (I - I_{z}) W_{s}^{2}}$$

Thus  $C_a = \tan^{-1} (2.32/W_s^2) = 2.36$  degrees for the design spin rate. Since the migration of the spin axis at apogee motor ignition is proportional to  $1/W_s^2$ , increasing the spacecraft spin rate will reduce the attitude error during apogee burn and hence the error in apogee motor velocity increment. However, it is necessary to operate a thruster in a pulsed mode to remove vernier velocity errors perpendicular to the spin axis after apogee burn, and the thruster effeciency decreases with decreasing on-time and hence with increasing spin rate. Thus an optimum spin rate may be determined which gives the minimum impulse requirement for vernier thrusting, coning and precession control, and spin down. A curve of impulse requirement as a function of spin rate is shown in Figure 5.5-8, from which the optimum spin rate is in the range 70-80 rmp. This is the basis for the design spin rate of 71.7 rpm (see Section 6.4.3.3.1 for a detailed discussion).

# 5.5.2.1.4 Vernier Thrusting

As noted above, the spacecraft spin axis may have an attitude error due to sun sensor and rf sensor errors and apogee burn migration of

$$(0.5^2 + 1.0^2 + 0.55^2 + 1.08^2)^{1/2} = 1.66 \text{ deg}$$

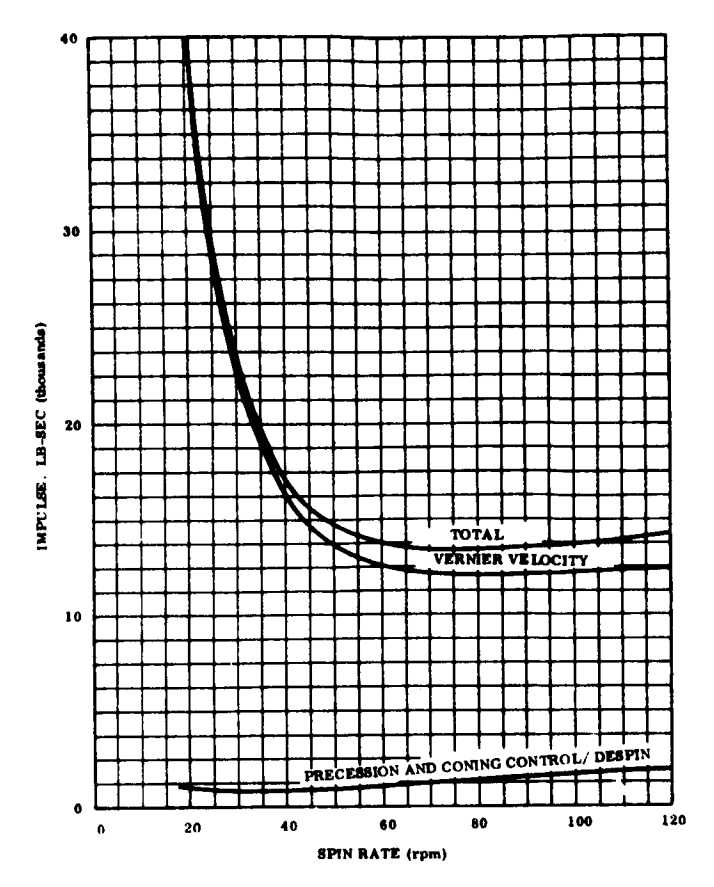


Figure 5.5-8. Impulse Requirement vs Spin Rate

and a coning amplitude of 2.36 degrees. Operation of the coning damper will reduce the coning amplitude to less than 0.5 degree shortly after apogee burn.

During the 2-day period after apogee burn, vernier thrusting will remove the radial velocity error (normal to the spacecraft spin axis)  $\Delta V_r = 123.0$  fps, and the axial velocity error (parallel to the spacecraft spin axis)  $\Delta V_a = 89.2$  fps (refer to Section 6.4.3.3.1 for derivation of  $\Delta V_r$  and  $\Delta V_a$ ). The vernier velocity correction will be made in two stages, each consisting of the following sequence of events.

- a. measure  $\Delta V_r$  and  $\Delta V_a$  by tracking
- b. measure spin axis attitude error
- c. correct spin axis attitude
- d. correct  $\Delta V_a$
- e. correct  $\Delta V_r$

 $\Delta V_a$  will be removed using 1-pound thrusters A3 and A7, or A1 and A5 (Ref. Figure 5.5-2) operating in the continuous mode.  $\Delta V_r$  will be removed using 10-pound thruster A9, operating in the pulsed mode (duration 175 m/sec) once per spin revolution. Thus, the time required to remove  $\Delta V_a/2 = 44.6$  fps will be

$$\frac{\text{m}\Delta V_a^{/2}}{2} = \frac{54.84 \times 44.6}{2} = 1223 \text{ sec} = 20.4 \text{ min}$$

and the time required to remove  $\Delta V_r/2 = 61.5$  fps may be obtained from the velocity increment per revolution which is F sin ( $\psi_w/2$ )  $\Delta t/m$  ( $\psi_w/2$ ) = 0.0301 fps. Thus the velocity increment per minute is 71.7 x 0.0301 = 2.16 fps/min, and the time to remove 61.5 fps is 28.5 min.

The principle of operation of the 10-pound radial thruster is similar to that of the precession control, except that the thruster is located to give a nominally zero moment about the spacecraft center of mass, so that the primary effect of thruster operation is spacecraft translation rather than precession. From the measurement of the direction of  $\Delta V_r$  by tracking, the correct spin phase angle  $\psi_p^{-1}$  for the radial thrusting will be determined. Due to the uncertainty in the c.m. location after apogee burn of  $\pm$  1.0 in., each radial thrusting period may produce a precession moment impulse of  $m(\Delta V_r/2)$  (1/12) = 281.1 lb-ft-sec, corresponding to a precession angle of 7 degree. Thus, an axial velocity equal to  $(\Delta V_a/2)$  sin (3.5 deg) = 3.75 fps may be produced during each radial thrusting period An allowance of 10 percent has been added to  $\Delta V_a$  and  $\Delta V_r$  to cover errors of this type.

# 5.5.2.2 Orientation Control Stabilization Modes

### 5.5.2.2.1 Despin

This mode of operation is initiated by ground command after completion of vernier thrusting just prior to sun stabilization. The purpose of this mode is to reduce space-craft rates to less than 0.1 deg/sec about the three control axes. The vernier orbit adjust and coning and precession thrusters (hydrazine system) are utilized to provide the

control torques in this mode. The thrusters are controlled by the outputs of three despin rate threshold detectors in the flywheel and jet controller (FWJC) that are actuated by the amplified and shaped 3-axis rate gyro package signals. (Ref. Figure 5.5-9)

Despin is initiated upon recept of the Despin Command from the ground. This command enables the yaw despin detector in the FWJC and activates the yaw gyro. The yaw thrusters (A2 and A8 Figure 5.5-2) produce a despin acceleration of -1.4 deg/sec<sup>2</sup>, reducing the spin rate to nominally zero in 5.1 minutes. Signal flow for this operation (Ref. Figure 5.5-9) is from the yaw rate gyro to the sensor signal processor (SSP) to the FWJC to the yaw despin thrusters. When the spin rate is reduced to less than 0.2 deg/sec, the SSP generates the null state of the Yaw High Rate Null (YHRN) logic signal. This signal is used to enable the pitch and roll despin detectors in the FWJC. At this time pitch and roll rates will also be reduced. Signal flow during the reduction of the pitch and roll rates is identical with the yaw sequence as described above. Reduction of these rates to 0.1 deg/sec is expected to take 1 to 2 seconds.

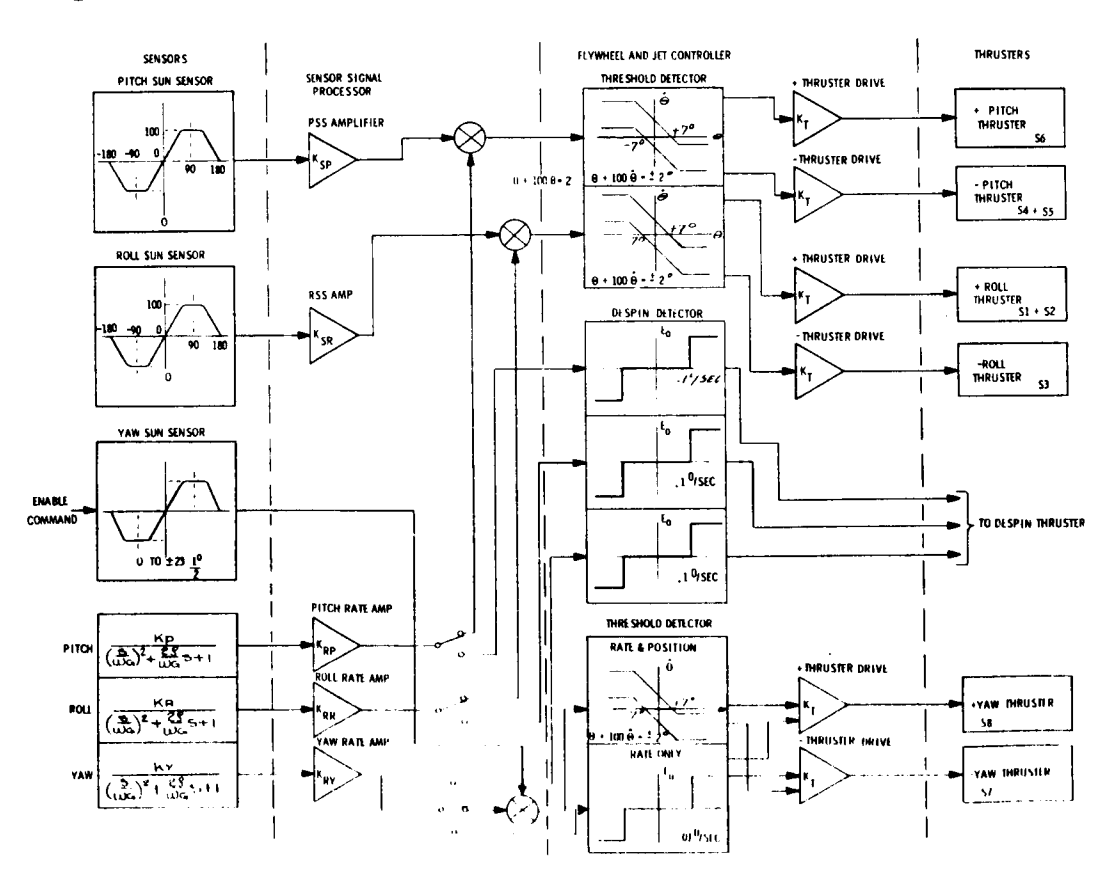


Figure 5.5-9. Sun Acquisition

The SSP generates Pitch, Roll and Yaw Despin Rate Null (PDRN, RDRN AND YDRN) logic signals, each in the null state when the respective rates are less than 0.1 deg/sec. When the PDRN, RDRN, and YDRN are all in the null state, a Despin Mode Complete (DMC) logic signal is generated in the SSP. This signal is used to initiate venting of the remaining hydrazine in the hydrazine system. Venting is to be done with hemispherical caps that nominally produce no net torque during the venting process. The despin detectors and thrusters remain enabled during this operation to react against any net torque produced by possible assymmetrical venting. When the venting process is essentially 100 percent complete, a Despin Venting Complete (DVC) logic signal is generated. This signal is utilized to initiate the stabilization of the yaw axis to the sun line.

### 5.5.2.2.2 Sun Stabilization

At the initiation of this mode of operation, the spacecraft may be at any arbitrary orientation. Thus in order to achieve orientation control, a sensor having spherical coverage is necessary. The radiation level produced by the sun is such that it is a readily detected and an unmistakenly identifiable body. No other reference can compare in brightness and therefore ease of detection. Thus, the sun is the best reference for initial orientation control. A simple arrangement of sun sensors around the spacecraft with a  $4\pi$  steradian field of view allows acquisition and stabilization to the sun line from any initial attitude. Approximately one hour prior to despin, the attitude stabilization thruster nozzle heaters (all except S9, Ref. Figure 5.5-10) are turned on in order to acquire the desired operating temperature of the thrusters. Upon receipt of the Despin Venting Complete logic signal, the pitch and roll sun sensor (SS) channels of the sensor signal processor (SSP) are activated, and the 3-axis gyro package outputs are switched to the proper channel to initate stabilization of the negative yaw axis to the sun. The pitch and roll sun sensors provide attitude error information with respect to the sunline, with the gyros sensing spacecraft angular rates. The sensor signal processor amplifies and combines the pitch and roll rate and attitude signals to provide an input to the FWJC. This input causes the jet threshold detectors to actuate the thrusters in accordance with specified switching lines so as to result in the pitch and roll axes stabilizing perpendicular to the sunline using thrusters S4, S5 and S6 for pitch control and thrusters S1, S2 and S3 for

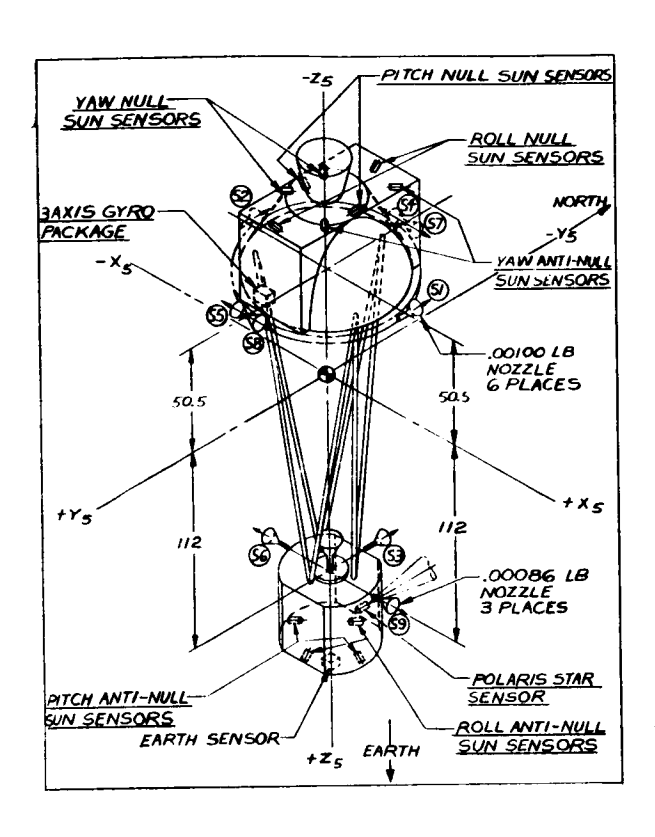


Figure 5.5-10. ATS-4 Configuration-Orientation Control

roll control. The SSP amplifies the yaw rate signal to provide an input to the yaw threshold detectors to reduce and thus maintain the yaw rate within the threshold detector deadband using thrusters S7 and S8.

Signal flow (Figure 5.5-9) for the pitch and roll channels if from the pitch (roll) sun sensor and gyro to the SSP to the FWJC to the appropriate positive or negative pitch (roll) thrusters. Signal flow is identical for the yaw channel but no sun sensors are used.

Initial stabilization to the sun is accomplished in one to two hours (Ref. Section 6.4.3.3.2) from any initial orientation. Orientation control of the pitch and roll axes results in pointing of the yaw axis to within  $\pm 2$  degrees of the sunline, with yaw rate controlled to 0.00 + 0.01 deg/sec.

The following thrusters are actuated to produce the appropriate positive or negative control moments for orientation stabilization: (see Figure 5.5-9 and 5.5-10)

# a. Yaw

- 1. Positive Moment S8
- 2. Negative Moment S7

### b. Roll

- 1. Positive Moment S1 plus S2
- 2. Negative Moment S3

### c. Pitch

- 1. Positive Moment S6
- 2. Negative Moment S4 plus S5

The SSP generates Pitch, Roll and Yaw Rate Null (PRN, RRN, YRN) and Pitch and Roll Sun Attitude Null (PSAN, RSAN) logic signals. The pitch (roll, yaw) rate null logic is in the null state when the pitch (roll, yaw) rate is less then 0.01 degree/second; the pitch (roll) attitude null logic is in the null state when the pitch (roll) SS error is less than 1.0 degrees. The SSP will process these signals to generate a Sun Stabilization Complete (SSC) logic signal which will be in the complete state when the PRN, RRN, YRN, PSAN, and RSAN are all in the null state. For prolonged operation in the sun pointing mode, it becomes necessary to be concerned about shadowing of the spacecraft by the earth. Depending upon the launch time, earth shadowing could occur on the first orbit prior to initiation of earth stabilization. When the spacecraft enters the earth's shadow, the sun sensors will provide no control information. Furthermore, the sun sensors will provide an erroneous signal as the earth's shadow is approached due to earth albedo. In order to curtail the possibility of large attitude and rate excursions due to the spurious errors expected while in earth's shadow, the thruster system will be disabled by ground command. After the thrusters are re-enabled by ground command, restabilization to the sun then occurs as required to return to the sun pointing mode. During the time that the jets are disabled (up to 80 minutes) the spacecraft could drift a maximum of 20 degrees about an arbitrary axis based on a maximum limit cycle rate of 0.004 deg/sec as discussed in Section 6.4.3.3.2.

# 5. 5. 2. 2. 3 Deployment

After sun stabilization vehicle orientation and rate will be favorable for communication with the ground around noon. That is, the vehicle orientation is well established, permitting telemetry and commands to be transmitted through antennas designed for this orientation. At this time the Deploy Parabolic Antenna command is transmitted from the ground to initiate deployment. Deployment is expected to be complete in several minutes. The orientation control system will remain active during the deployment. At the conclusion of this operation, vehicle angular rates are expected to be reduced due to the increase of inertia. At this time an Antenna Deployment Complete (ADC) logic signal is generated. The presence of the complete state of this signal is used to enable the earth stabilization logic.

# 5.5.2.2.4 Earth Stabilization

At noon the spacecraft orientation is such that a minimum transient occurs for transfer to an earth pointing orientation. Therefore, after deployment, approximately one-half hour before noon, earth stabilization is initiated. At this time, the positive yaw axis (along which the earth sensor looks) is oriented within 23.5 degrees of the local vertical, depending on the time of year (0 degrees at the equinoxes, 23.5 degrees at the solstices). To allow capture at any time of the year the earth sensor (ES) field of view therefore must be a minimum of about ± 20 degrees (15 degrees to the edge of the earth, plus 5 degrees to ensure capture). It is necessary that the earth sensor have this field of view in both pitch and roll since yaw attitude is not controlled at this time. Upon receipt of the Initiate Earth Stabilization command, and provided the conditions existing at the end of sun stabilization still exist (SSC is in the complete state) and the parabolic antenna is successfully deployed (ADC is in the complete state), the SSP generates an Enable Earth Stabilization (EES) logic signal. This signal is an input to the earth sensor and initiates the earth sensor search mode. Upon recognizing the radiance emitted by the earth the earth sensor switches from the search to acquired mode. The earth sensor then generates an Earth Acquired (EA) logic signal to indicate the change from the search to the acquired mode. With the EA logic signal in the acquired state and all the conditions necessary for initiation of earth stabilization still existing the SSP generates a Switch To Earth Sensor

(STES) logic signal. Upon receipt of this signal the pitch and roll gyros and threshold detectors are disabled, the mechanical flywheels enabled, and orientation control of the pitch and roll axes switched to the earth sensor (Figure 5.5-11). Rate information is derived by processing the earth sensor attitude error signals. The flywheels (FW) provide control torque in pitch and roll, with the pitch and roll thrusters providing torques for momentum unloading of the FW's. Flywheel unloading is inhibited until the earth stabilization transient is essentially completed. The yaw axis remains on rate control using the yaw gyro and thrusters. The SSP processes the ES signals to generate rate plus position information to be used as input signals to the FWJC which result in actuation of the FW's. The SSP also processes the yaw rate gyro signal to actuate a rate threshold detector in the FWJC to control rate about the yaw axis.

The SSP generates Pitch and Roll Earth Attitude Null (PEAN, REAN) logic signals. The earth attitude null signals are in the null state when the pitch (roll) error is less than 0.1 degree. The SSP also generates an Earth Stabilization Complete (ESC) logic signal that is in the complete state only when PEAN and REAN are in the null state. Orientation control of the pitch and roll axes to within  $\pm$  0.09 degree (3  $\sigma$  absolute) of the local vertical and a yaw rate controlled to within 0  $\pm$  0.01 deg/sec are expected at the conclusion of earth stabilization. Earth stabilization is expected to be complete in approximately 27 minutes (Ref. Section 6.4.3.3.3).

#### 5. 5. 2. 2. 5 Star Stabilization

During this mode yaw axis sun sensors and gyros provide control information to align the pitch exis normal to the orbit plane in order that the star sensor field of view intercepts Polaris. For an earth oriented spacecraft in equatorial orbit. Polaris is a near ideal reference. No nearby star is comparable in brightness, and its closeness to the north celestial pole permits tracking with a sensor having a relatively narrow field of view. Since the properly stabilized spacecraft rotates about a north-pointing axis at a nominal one revolution per day, Polaris appears to describe an approximate 0.9 degree radius circle over this period. To account for this apparent movement, star sensor or earth sensor command angles are programmed. The commands are programmed by an onboard clock which will be periodically updated from the ground. The appropriate command angle

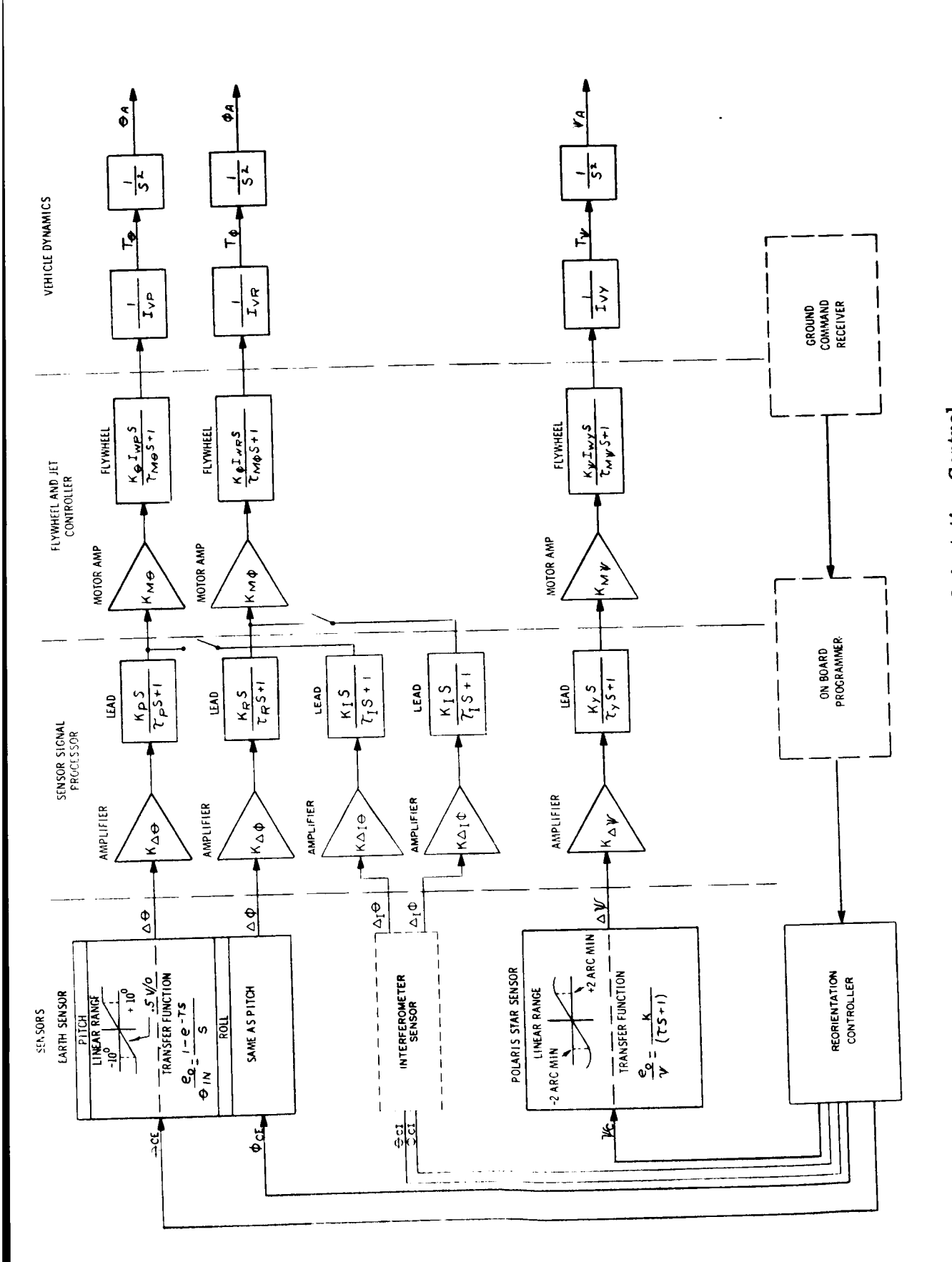


Figure 5.5-11. On-Station Orientation Control

programming is initiated prior to starting the star stabilization sequence. The star stabilization sequence consists of two subsequences; namely, yaw sun stabilization and star acquisition. The yaw sun sensor loop is enabled and yaw axis control is switched to this reference. The mounting configuration of the yaw sun sensor is such that the pitch axis is aligned normal to the orbit plane, causing the star sensor field of view to intercept the Polaris star, allowing star acquisition to occur and yaw control to be transferred to the star sensor. Yaw sun stabilization is initiated at approximately 4:00 p.m. Upon receipt of the Initiate Yaw Sun Stabilization (IYSS) command and provided the ESC logic is in the complete state, the SSP will generate an Enable Yaw Sun Stabilization (EYSS) logic signal. This signal will be an input to the yaw sun sensor channel of the SSP and the FWJC. The SSP processes the yaw sun sensor and gyro signals (Figure 5.5-9) to generate input signals to a threshold detector in the FWJC which results in actuation of the yaw thrusters in accordance with appropriate switching lines for aligning the negative roll axis to the sunline. Orientation control of the roll axis to within + 1 degree of the sunline is expected at the conclusion of yaw sun stabilization. The SSP will generate a Yaw Sun Attitude Null (YSAN) logic signal which will be in the null state when the yaw sun sensor error is less than + 1 degree, and a Yaw Rate Null (YRN) logic signal which will be in the null state when the yaw rate is less than 0.01 deg/sec. At this time the true roll axis lies nominally in the orbit plane and the pitch axis normal to the orbit plane. The Polaris Star Sensor (PSS) generates a Polaris Star Presence (PSP) logic signal which will be in presence state when Polaris is in the field of view of the sensor. When the PSP is in its presence state and YSAN and YRN are in their null states and ESC is in the complete state, the SSP will generate a Switch to PSS logic signal. This signal is an input to the FWJC enabling the yaw flywheel which provides control torques on PSS control. Rate information is derived by processing the PSS signal. The yaw thrusters are used to momentum unload the yaw flywheel. During this time the yaw sun sensor loop will continue to operate in support of the PSS loop in the event the PSS does not capture yaw control initially. Signal flow on PSS control (Figure 5.5-11) is from the PSS to the SSP to the FWJC to the FW which is momentum unloaded by the yaw thursters. The PSS will have a square 4 x 4 degree field of view with ground commanded electronic gimballing of ± 9 degrees about the spacecraft roll axis so as to maintain the star within the field of view during offset pointing,

and time programmed commands of the PSS or ES to account for the apparent 0.9 degree circular motion of the star. The FWJC will generate a Yaw Polaris Attitude Null (YPAN) logic signal which will be in the null state whenever the PSS error signal is less than 0.05 degree. The PSS will be mounted so as to have its optical axis along the negative pitch axis of the spacecraft. Orientation control of the yaw axis of ± 0.07 degree absolute with respect to the Polaris starline is expected. The SSP will generate a Star Stabilization Complete (SSC) logic signal which will be in the complete state when the following logic states exist: Earth Stabilization Complete is in the complete state, PSS star presence is in the presence state and the YPAN is in the null state. At this time the yaw gyro and sun sensor will be disabled automatically by the SSC logic signal.

# 5.5.2.3 Orientation Control Operational Modes

### 5. 5. 2. 3.1 Pointing

Pointing is merely a continuation of control existing at the end of star stabilization. In the absence of any further ground commands, the control system holds a local vertical orientation of the spacecraft. For prolonged operation in this mode, the expected orbital disturbance torques cause momentum loading of the flywheels. Disturbance torque and corresponding angular momentum profiles are shown in Section 6.4.3.2. In order to continuously maintain attitude control it is thus necessary to momentum unload the flywheels periodically with the mass expulsion system. The requirements for an operation of wheel unloading are discussed in detail in Section 5.5.2.3.4.

The orientation control errors resulting due to flywheel loading meet the 0.03 degree for pitch and roll and the 0.05 degree for yaw allowed in the error budget. These accuracies were met in the presence of sensor noise after filtering was added (Ref. Section 6.4.3.3.5).

### 5.5.2.3.2 Reorientation

Reorientation to any point on the visible earth's surface is to be performed upon receipt of the appropriate ptich and roll ground commands (Figure 5.5-11). The change in pointing direction is accomplished in a closed loop mode of operation. That is, step position

commands are sent to the earth sensor thus creating error signals to the pitch and roll flywheels that are nulled only when the desired orientation is achieved. Pointing to any location on the visible earth's surface is achieved without degradation of pointing accuracy (0.09 deg  $3_{\sigma}$ ).

The effect of structural dynamics on reorientation performance has been shown to be negligible by analog simulation studies for a structural damping factor of 0.001. Reorientation from horizon to horizon is accomplished in approximately 23 minutes in response to a 17.4-degree step command as shown in Section 6.4.3.3.6. Thus the requirement of reorienting from horizon to horizon and settling within 30 minutes is easily met. Satisfactory reorientations of this magnitude were demonstrated on the computer with the flywheels momentum loaded up to 40 percent of capacity prior to the initiation of the maneuver.

Presented in Section 6.4.3.2 are the disturbance torque and corresponding momentum profiles for offset pointing to Rosman, Mojave and a 8.7-degree roll offset. As with the local vertical orientation, any prolonged operation at a particular offset requires eventual unloading of the flywheels. The most severe offset conditions appears to be the 8.7-degree roll offset. An explanation of the flywheel unloading mechanism is presented in Section 5.5.2.3.4.

### 5.5.2.3.3 Tracking

The orientation control system is required to follow a rate of 10 milliradians per minute and hold a steady state error not exceeding 0.5 degree during this track. The ability of the system to meet these requirements is shown in Section 6.4.3.3.7. The maximum expected error is 0.15 degree, occurring at the beginning and end of the tracking maneuver. The error is reduced to approximately the steady state pointing error for 90 percent of the maneuver. Settling time after removal of the ramp command is in the order of 3 to 5 minutes.

Tracking requirements can be met with initiation of the ramp occurring at flywheel speeds up to 40 percent of rated as shown in Section 6.4.3.3.7. The maximum expected error, again occurring only at the beginning and end of the maneuver, is 0.28 degree, thus meeting the 0.5-degree requirement.

# 5. 5. 2. 3. 4 Flywheel Unloading and Stationkeeping

5. 5. 2. 3. 4.1 General. The mass expulsion subsystem is required to provide attitude control torques during initial stabilization, restabilization, and flywheel unloading and to provide the necessary impulse for initial station capture, E-W and N-S stationkeeping and E-W station change. A system utilizing the same thrusters to perform both orientation control and stationkeeping functions affords the following advantages:

- a. Minimum hardware weight since the number of thrusters, piping, wiring, etc., are minimized.
- b. Minimum fuel since stationkeeping and flywheel unloading can be accomplished simulatneously.
- c. Minimum integration with spacecraft configuration.
- d. Minimum cost.

The only penalty of this type system is the additional control logic necessary for the selection and actuation of the proper thrusters. This penalty, however is small in comparison to the savings afforded by this design approach.

5.5.2.3.4.2 <u>Impulse Requirements</u>. The impulse requirements for the two year mission life are presented in Table 5.5-4.

5.5.2.3.4.3 Thrust and Moment Levels. In order to limit deformation of the parabolic antenna to acceptable levels during stabilization, stationkeeping and flywheel unloading, it is necessary that the thrust and moment levels generated during these operations be less than 0.5 lb and 0.208 ft-lb (40 oz-in.), respectively. In addition certain minimum constraints are dictated by stationkeeping and orientation control requirements.

The minimum total thrust necessary for N-S stationkeeping is 0.002 lb, (results in approximately 4.2 hours of thrusting), for E-W stationkeeping 0.00092 lb, and for E-W station change 0.00252 lb (for example, to reposition 60 degrees to the West using the

Table 5.5-4. Mass Expulsion Requirements for Orientation Control and Stationkeeping Subsystem

		Impulse (lb-	sec)
		First Year (90°W)	Second Year (150°W)
	STATIONKEEPING		
1.	E-W Capture	529	
2.	E-W Stationkeeping		
	a. Triaxiality	125	280
	b. N-S Cross Coupling	124	
3.	N-S Stationkeeping	10950	
	ORIENTATION		
1.	Momentum Unloading		
	a. Pitch	*	*
	b. Roll	*	30.5
	c. Yaw	*	*
*	Total Impulse required is 61. respectively. All but half the		
2.	Initial Stabilization and Restabilization	143	143
E-1	V STATION CHANGE	5290	
то	TAL	17160	453.5
то	TAL FOR 2 YEARS	17615 li	b-sec

alloted  $\Delta V$  of 100 fps, results in a station change time of 24 days). The moments produced by the jets must be limited so as to be compatible with flywheel stall torque in order to avoid loss of control during momentum unloading. The thruster configuration is as shown in Figure 5.5-10. A total of nine thrusters are utilized (six 0.001 lb and three 0.00086 lb). Three thrusters produce a total thrust of 0.00286 lb in the E-W or N-S directions. The jet moment is 1.6 in.-oz in pitch and roll and 0.7 in.-oz in yaw compared with a flywheel

stall torque of 2 in.-oz. Thus, the thrust and moment levels are well within the limits imposed by antenna deformation, and also meet stationkeeping station change and unloading requirements.

5.5.2.3.4.4 <u>Stationkeeping - Wheel Unloading</u>. In order to perform stationkeeping and wheel unloading simultaneously, an integrated control logic scheme is required (See Figure 5.5-12). This logic enables the mass expulsion subsystem to perform station-keepting and flywheel unloading separately or simultaneously by selecting and actuating the proper thrusters. The logic operates on the following general principles:

- a. When it is necessary to stationkeep and flywheel speed exceeds 20 percent of full speed, system logic is arranged such that a torque is generated about the desired axis (also providing stationkeeping impulse) only until the particular flywheel is below 5 percent speed at which time the active thruster configuration is changed to provide only a translational force with thrusting continuing until the required stationkeeping impulse has been provided.
- b. When flywheel speed exceeds 75 percent of full speed, regardless of station-keeping requirements, the flywheels are unloaded to 5 percent. The unloading times are 3.0 minutes for the pitch and roll flywheels and 6.9 minutes for the yaw flywheel.

The logic diagram of Figure 5.5-12 is simply the implementation of these two concepts. The thrusters are used as follows:

- a. Thrusters S1, S2 and S3 are used for N-S stationkeeping and roll and yaw flywheel unloading.
- b. Thrusters S4, S5 and S6 are used for E-W stationkeeping, pitch flywheel unloading, and yaw flywheel unloading prior to station change since the impulse required will be toward the east (since the spacecraft is east of the stable point). After station change, thrusters S7, S8 and S9 perform the same functions as S4, S5 and S6 except that the impulse will be toward the west since the spacecraft will now be west of the stable point.

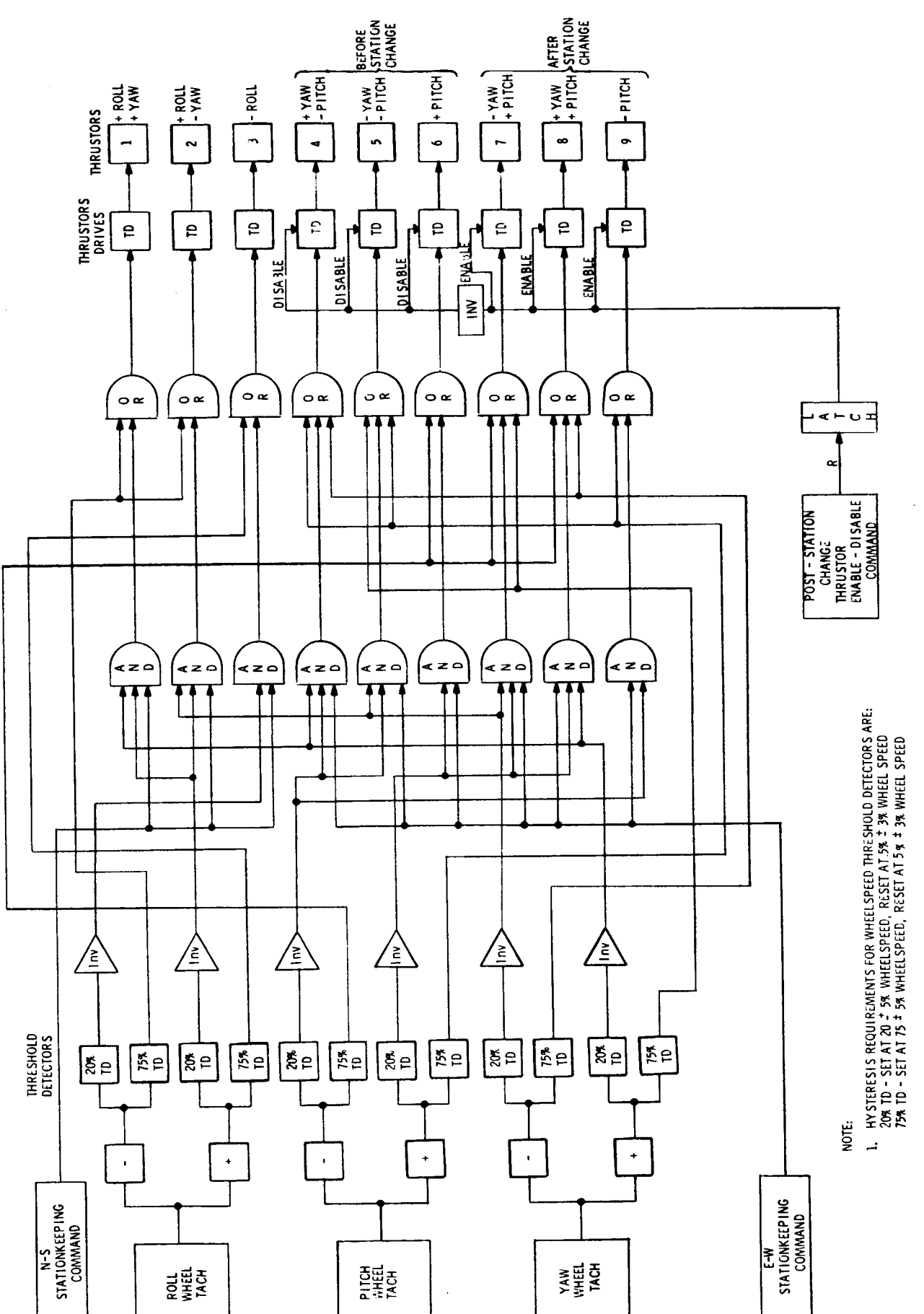


Figure 5.5-12. Integrated Stationkeeping-Wheel Unloading Mass Expulsion System Control Logic

From Section 6.4.3.2, the maximum momentum storage requirement for each of the wheels and the residual momentum after 24 hours are as follows:

	Momentum Storage ft-lb-sec	Daily Residual Momentum ft-lb-sec
Pitch	0.50	0.02
Roll	0.65	0.28
Yaw	1.38	0.10

For flywheel unloading at 75 percent of rated momentum, 1.5 ft-lb-sec of momentum will be stored in the flywheel prior to unloading. Based on the momentum storage requirements and the residual momentum, the flywheels will need to be unloaded every 50 days for pitch, every three days for roll and every day for yaw. For a typical pointing orientation, such as to the Rosman station, the momentum storage requirement and the residual momentum after 24 hours are as follows:

	Momentum Storage ft-lb-sec	Daily Residual  Momentum  ft-lb-sec
Pitch	0.48	0.02
Roll	0.45	0.06
Yaw	1.16	0.06

Thus for pointing to Rosman the flywheels will need to be unloaded every 51 days for pitch, every 17.5 days for roll and every 5.6 days for yaw.

In order to minimize thruster firing cycles the yaw flywheel would be unloaded by both the N-S and E-W stationkeeping jets. In order to add the required N-S stationkeeping velocity increment, the N-S thrusters must be fired at least once every two days. Firing at 2-day intervals requires approximately 5.8 hours of thrusting time which is beyond the 5-hour period considered efficient for N-S stationkeeping. For certain pointing attitudes

the yaw flywheel requires unloading daily. Thus the N-S stationkeeping thrusters will be fired either once a day for 2.93 hours or once every two days for 5.8 hours as required to meet stationkeeping and flywheel unloading requirements. The need for daily unloading of the yaw flywheel can readily be overcome by increasing the unloading speed to 85 percent. This would result in an insignificant decrease in pointing accuracy.

For the second year when there is no requirement for N-S stationkeeping the N-S thrusters would still be used for roll and yaw flywheel unloading with the yaw flywheel also being unloaded during E-W stationkeeping. For this case the heaters would not be required to preheat the N-S thrusters because the impulse expended is so small that the decrease in specific impulse to 100 seconds has little effect on total system weight. During the first year the N-S thrusters are fired at the appropriate node to accomplish N-S stationkeeping. During the second year the N-S thrusters will be fired automatically as required to unload the yaw and roll flywheels. In this situation flywheel unloading will occur such that 1.5 ft-lb-sec (75 percent speed) will be removed, thus flywheel unloading in roll and yaw will occur only every 5.3 days on roll and every 15 days in yaw for the worst case pointing attitude and every 25 days in roll and every 25 days in yaw for pointing to Rosman.

For flywheel unloading at 75 percent of rated momentum the pitch flywheel has a minimum excess momentum storage capability of 1.0 ft-lb-sec. Since the maximum pitch daily residual momentum is 0.02 ft-lb-sec, the pitch flywheel need be unloaded only once every 50 days. In order to maintain an E-W station location limit cycle within 0.03 degree, it is necessary to fire the E-W thrusters for 48 minutes every 24.5 days the first year and for 60 minutes every 18.2 days the second year (Ref. Section 7.7.2). Thus no additional thruster firings beyond those required for E-W stationkeeping are required for pitch flywheel unloading.

#### 5.5.2.3.5 Interferometer Control

Interferometer control would be initiated by ground command while in the pointing mode after observing by telemetry that the interferometer attitude errors were reasonable. Orientation control using the interferometer would involve the use of the interferometer output rather than the earth sensor output and appropriate gain and signal shaping net-

works in the SSP as shown in Figure 5.5-11 to acquire the desired accuracy and system dynamic performance. Command angle information would be supplied to the interferometer, as is done for the earth sensor, in order to maintain the desired pointing attitude and to perform maneuvers.

### 5.5.2.4 Station Capture and Station Change

### 5.5.2.4.1 Station Capture

At second apogee of the transfer orbit, the apogee motor is fired and ideally places the satellite in a synchronous, circular, equatorial orbit at 53 W. However, due to errors in the perigee burn and in the apogee burn, the ideal orbit is not attained. The actual orbit is determined by ground tracking, and the vernier propulsion system is used to remove injection errors. A residual velocity of 10 ft/sec between actual and synchronous orbit velocity will be introduced during vernier correction, causing a drift of the spacecraft toward the west (toward the desired 90 W longitude location). After the orientation control system has positioned the spacecraft to an earth pointing orientation, the orientation control thrusters will be used to gradually reudce the drift. Thrusters S4, S5 and S6 are used for this purpose. The total impulse required to perform this maneuver is 529 lb-sec.

### 5. 5. 2. 4. 2 E-W Station Change

At the end of the first year in orbit, the operating longitude of the spacecraft will be changed. A  $\Delta V$  of 100 fps has been allowed for this maneuver. For design purposes it has been assumed that the reposition maneuver will be from  $90^{\circ}W$  to  $150^{\circ}W$ , and that the maximum maneuver time is 30 days. The maneuver could be performed with no coast time or with essentially a 30-day coast time. The case of no coast time results in minimum required thrust level but maximum impulse. The case of a 30-day coast time results in a high thrust level and low impulse. The relationship that 10 fps of  $\Delta V$  results in a drift of 1 deg/day is used for evaluating thrust level versus impulse required.

The reposition angle is related to time as follows:

$$\theta = \frac{\Delta V}{10} \frac{t_a}{2} + \frac{\Delta V}{10} t_c + \frac{\Delta V}{10} \frac{t_d}{2}$$

where:

 $\theta$  = angle tranversed in degrees

 $\frac{\Delta V}{10}$  = drift rate in deg/day when  $\Delta V$  is the drift velocity at time  $t_a$  in fps.

t<sub>2</sub> = accelerating time in days

 $t_c = coast time in days$ 

t<sub>d</sub> = deceleration time in days

It is assumed that  $t_a = t_d$ ; thus  $t_c = 30$  days  $-2t_a$  and the relation for  $\theta$  becomes:

$$\theta = \frac{\Delta V}{10} t_a + \frac{\Delta V}{10} (30 - 2t_a)$$

$$= 30 \frac{\Delta V}{10} - \frac{\Delta V}{10} t_a$$

the  $\Delta V$  at time  $t_a$  is:

$$\Delta V = A_a t'_a$$
 where  $A_a = acceleration in ft/sec2
 $t'_a = accelerating time in sec$$ 

the thrust is equal to

$$F = mA_a = \frac{1700 \text{ lb}}{32.2 \text{ ft/sec}^2} A_a$$

The equation for  $\theta$  may be rewritten in terms of F as:

$$\theta = 3 \frac{32.2}{1700} F t' a - \frac{32.2}{17000} F t a t' a$$

where F is in pounds.

For  $\theta = 60 \deg$ 

$$F = \frac{60}{\frac{32.2}{1700} \begin{pmatrix} 3t' & -\frac{t_a t'}{10} \\ & & 10 \end{pmatrix}} = \frac{60 \times 1700}{32.2 \times t'} \begin{pmatrix} 3 - t_a \\ & 10 \end{pmatrix}$$

Tne impulse required is

$$I = F(2t_a)$$
 lb-sec

The thrust and impulse required are shown in Figure 5.5-13 as a function of the thrusting time for 20-and 30-day repositioning times.

Tne 100 fps impulse specified for repositioning is equal to

$$100 \frac{\text{ft}}{\text{sec}} \times \frac{1700 \text{ lb}}{32.2 \text{ ft/sec}^2} = 5290 \text{ lb-sec}$$

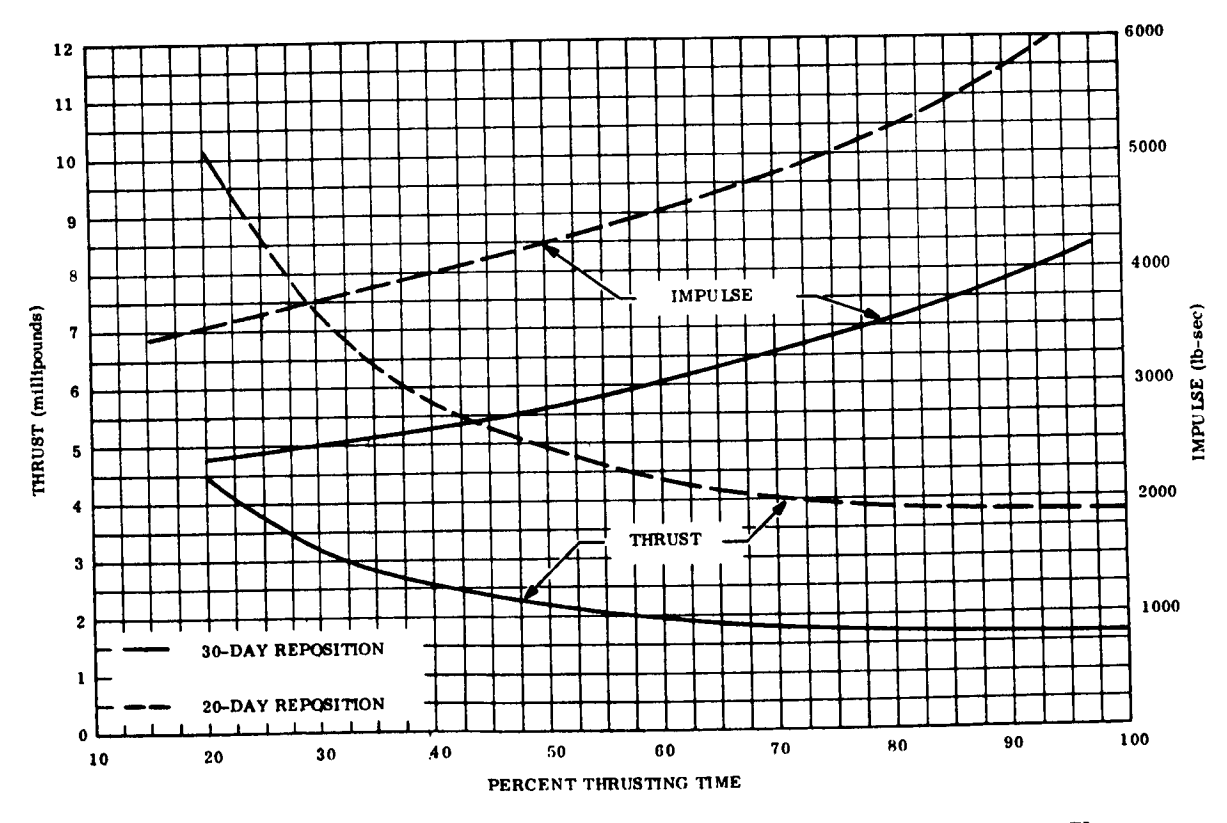


Figure 5.5-13. Thrust and Impulse Required for East-West Station Change

It appears that the 100 fps of  $\Delta V$  is more then sufficient for a 30-day resposition time, if the reposition maneuver is through 60 degrees. This repositioning could be accomplished in 20 days with the 100 fps using a thrust of 3.8 millipounds. However, the repositioning will take somewhere between 20 and 30 days for the chosen thrust level of 2.86 millipounds.

# 5.5.2.5 Restabilization

During the course of the two-year mission, the possibility of momentary loss of control exists. Depending on the nature of the failure and the length of time elapsing before correction of the fault is made, restabilization may require one or all of the control sequences. A serious malfunction thus would require, for restabilization, first stabilization to the sun, and then sequencing through earth capture and Polaris capture to again attain the final earth pointing orientation; a malfunction of less serious nature would possible require only star restabilization. The sequence of control modes necessary for restabilization is thus a function of the type and length of failure. The functional description of operation during restabilization is thus covered in the preceeding sections with the following exceptions:

- a. Performance during restabilization to the sun will be different since the parabolic antenna is now deployed thus changing the inertia about the control axes. This has been evaluated in the control analysis computer studies discussed in Section 6.4.3.3.8 and poses no problem.
- b. It is necessary to add an electrical bias to the yaw sun sensor channel of the SSP to reflect the difference in earth line/sun line at restabilization with respect to that which existed at launch in order to acquire Polaris.

### 5.5.3 COMPONENT DESCRIPTION

A description of the hardware associated with preferred design of the guidance and control subsystem is presented in the ensuing section. A description of each component is presented along with the development status, weight, power, size, and command and telemetry requirements. Table 5.5-5 is a guidance and control component list presenting a summary of weight, power, size and similarity with existing hardware on other programs. A detailed functional description of equipment operation is given in Section 5.5.2, and in block diagram form in Figures 5.5-3, 5.5-9, 5.5-11, and 5.5-12.

Table 5.5-5. Component Description

Component or Subsystem	Weight (1b)	Volume (x) in. : (y) in. : (z) in.	Power (watts)	Justification
Earth Sensor				Advanced Technology Division of American
a. Sensor Head	5.2	5 X 5 X 5		Standard - Apollo sensor with MOGO electronics
b. Electronics	2	5 x 5 x 4		
Total	10.7		7.0	
3-axis Gyro Package	2.7	3.5 x 5.5 x 8.5	15.0	CAO RAPS gyro
Gyro Electronics	8.0	2 x 7 x 10	15.0	OAC RAPS electronics less position mode equipment
12 Sun Sensors	2.7	1.55 x 1.5 dia	;	Similar to OAO coarse sun sensors
Polaris Star Sensor	12.0	4, 5, 13	8.0	Modified Canopus tracker
Sensor Signal Processor	15.3	12, 6, 5	30.0	Serves approximately same function as OAO SSP and TC; weight 30% of OAO unit by use of microelectronics
Flywheel and Jet Controller	19.2	10, 10, 5	15.0	Same function as OAO FWJC plus stationkeeping thruster logic; weight $40\%$ of OAO unit by use of microelectronics
Flywheels				
a. Pitch	11.3	5.5 x 11.8 dia		
b. Roll	11.3	5.5 x 11.8 dia	10	OAO fine flywheels
c. Yaw	11.3	5.5 x 11.8 dia		
Total	33.9			
Station Acquisition Sun Sensors	2.1	4 x 6 x 6	i i	Similar to sensor used on Syncom and Early Bird
Station Acquisition Accelerometer and Electronics	8	3 x 4 x 5	9.7	Hone, well type GG125

Table 5.5-5. Component Description (Cont'd)

Component or	Weight	Volume (x) in.;	Power	Justification
Subsystem	(1b)	(y) in.; (z) in.	(watts)	
Station Acquisition Sensor Signal Processor	3.2	1 x 7 x 10	3.0	
Spin-up Motor (2)	11.6	2. 9 dia x 14 each		Atlantic Research Corp. MARC 7E1 1.35-KS-300
Station Acquisition Mass Expulsion System				Blowdown hydrazine system
Fuel	73.0	,		Eight 1-lb thrusters
Tankage and Hardware	35.7			One 10-lb thruster
Total	108.7			
Orientation Control Mass Expulsion System				9 GE resistance jets (ammonia propellant).
Fuel	92. 4			Six 0.00100 lb thrusters
Tankage Thrusters	34.7		12.8	Three 0.00086 lb thrusters
Total	126.4			
Total Attitude Control Systems	364.8		82. 8 (during pointing)	pointing)

# 5.5.3.1 Spinup Motors

The spinup motor selected is the Marc 7E1 (1.35-KS-300) motor developed by the Atlantic Research Corporation. This motor is qualified and to date 296 of these motors have been manufactured and 23 have been fired. Salient characteristics are:

Isp	sec	190
Average Thrust	lbf	296
Burn Time	sec	1.002
Total Impulse	lb-sec	402.7
Propellant Weight	lb	2.13
Inert Weight	lb	3.67
Burnout Weight	lb	3.67
Total Weight	lb	5.80
Motor Length	inches	14.7
Motor Diameter	inches	2.9
Operating Limits	$^{\mathbf{o}}\mathbf{F}$	-40 to $+200$
Average Chamber Pressure During Burn	psi	1220

## 5.5.3.2 Coning Control Accelerometer

The accelerometer selected for the onboard coning control is the Honeywell Type GG125 miniature angular accelerometer whose characteristics are:

Pickoff Sensitivity	$0.1725 \text{ v/radian/sec}^2$
Threshold	$0.0003  \mathrm{rad/sec}^2$
Linear Acceleration Sensitivity	$0.001  \mathrm{rad/sec^2/g}$
Pickoff Excitation	10 ma, 5600 Hz
Heater Power (watts)	7.6 operating (28 v)
Weight	<ul><li>0.8 lb for accelerometer</li><li>2.0 lb for associated electronics</li></ul>
Size	2.0 in. x 1.9 in. dia

#### 5.5.3.3 Precession Control Sun Sensor

This device is of the type which has been used on other spin stabilized communication satellites such as Syncom and Early Pird. The two nearly planar (1-deg wide) fields of view form an X whose intersection lies on the  $X_5$  axis. One planar field of view element lies in the  $X_5$  - $\overline{Z}_5$  plane, and extends 42 deg on either side of the  $\overline{X}_5$  axis (total of 84 deg). The second sensor element is inclined 35 deg cw to the  $\overline{X}_5 - \overline{Z}_5$  plane, as seen from the coordinate origin, and extends 55 deg on either side of the  $\overline{X}_5$  axis (total of 110 deg). Sun-referenced orientation data is generated on the basis of the time separation and sequence of the two output pulses which are produced for each vehicle rotation about the  $\overline{Z}_5$  axis. (Clearly, only one pulse is produced when the sun line is in the vehicle  $\overline{X}_5 - \overline{Y}_5$  plane). The output of either

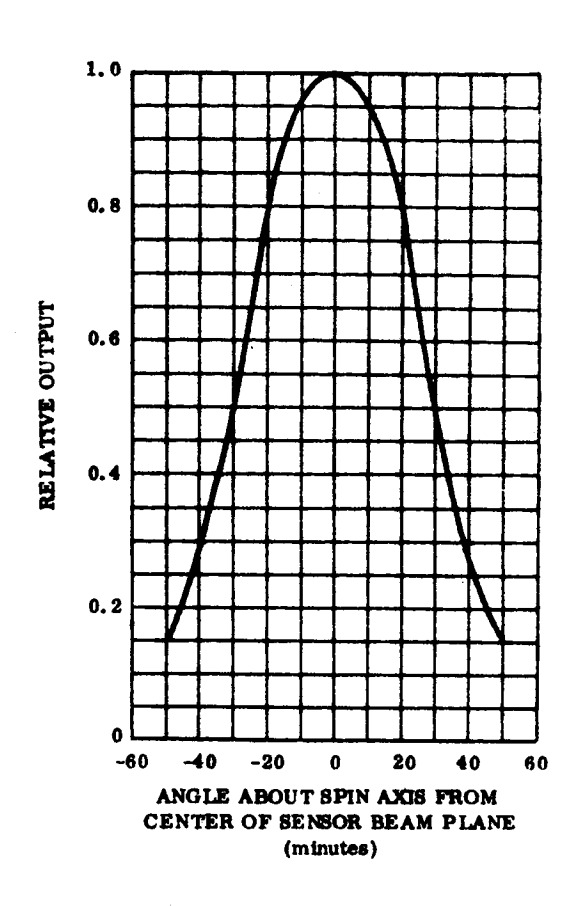


Figure 5.5-14. Spin Sun Sensor Output

sensor is shown in Figure 5.5-14. Each sun sensor consists of a double slit assembly which limits the field of view to the planar form described above, and a silicon photovoltaic element which gives an output as a cosine function of the incident radiation. The rise time of the photovoltaic element is very short (10 percent to 90 percent in 20  $\mu$  sec).

# 5.5.3.4 PRECESSION CONTROL RF POLANG MEASUREMENT

Onboard equipment for the rf POLANG measurement consists of an antenna with a toroidal radiation pattern shown in Figure 5.5-15. The polarization vector is parallel to the spacecraft spin axis. The beamwidth (-3 dB points) is  $\pm$  20 degrees. Since a 9.8-degree spin axis precession error may occur during transfer orbit, the effective antenna beamwidth is reduced to  $\pm$ 10.2 degrees. Thus, (ref. Figure 5.5-7) the rf polarized signal will be received by Rosman ground station for approximately 3 hours prior to apogee burn (12.75 to 15.75 hours after apogee burn).

The angle POLANG is related to the vector  $\overline{Z}_5$  (spin axis),  $\overline{l}$  (line of sight) and  $\overline{Z}_3$  (spacecraft zenith) by the relations (refer R.H. Greene, "Early Bird Placement in a Stationary Orbit; Launch and Control System Maneuvers". AIAA Paper 66-262):

$$\begin{vmatrix} \sin POLANG \end{vmatrix} = \begin{vmatrix} \overline{E}_1 \times \overline{E}_2 \end{vmatrix}$$
  
 $\cos POLANG = \overline{E}_1 \cdot \overline{E}_2$ 

where

$$\bar{E}_1 = \frac{\bar{Z}_3 \times \bar{\ell}}{|\bar{Z}_3 \times \bar{\ell}|}$$

$$\mathbf{E}_{2} = \left| \frac{\overline{\mathbf{Z}}_{5} \times \overline{\boldsymbol{\ell}}}{\overline{\mathbf{Z}}_{5} \times \overline{\boldsymbol{\ell}}} \right|$$

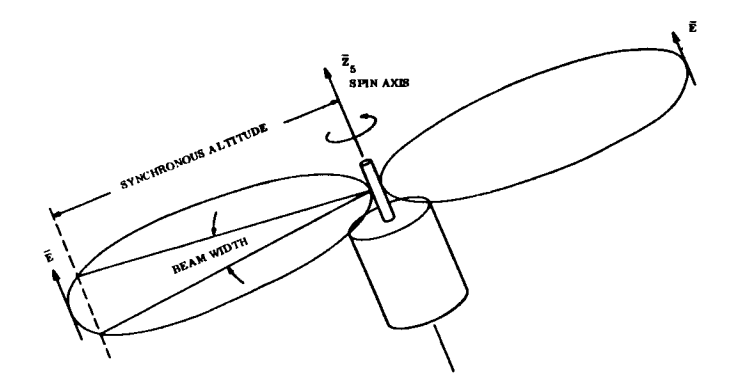


Figure 5.5-15. Polarized RF Antenna

Expressing  $\overline{Z}_3$ ,  $\overline{Z}_5$  and  $\overline{I}$  in terms of the inertial frame X, Y, Z, gives the following relations

$$\overline{Z}_{3} = (-\cos u \cos \Omega + \sin u \cos \nu \sin \Omega) \overline{X}_{1} + (\sin u \sin \nu) \overline{Y}_{1}$$

$$+ (-\cos u \sin \Omega - \sin u \cos \nu \cos \Omega) \overline{Z}_{1}$$

$$\overline{Z}_5 = (\sin\zeta\sin\xi\sin\mathrm{RA} - \sin\zeta\cos\xi\cos\delta_{\mathrm{S}}\cos\mathrm{RA} \\ + \cos\zeta\cos\delta\cos\mathrm{RA})\,\overline{X}_1 + (-\sin\zeta\cos\xi\cos\delta_{\mathrm{S}} - \cos\zeta\sin\delta_{\mathrm{S}})\,\overline{Y}_1 \\ + (-\sin\zeta\sin\xi\cos\mathrm{RA} - \sin\zeta\cos\xi\sin\delta_{\mathrm{S}}\sin\mathrm{RA} + \cos\zeta\cos\delta_{\mathrm{S}}\sin\mathrm{RA})\,\overline{Z}_1$$

$$\overline{X} = \cos \eta \sin Az \sin (\lambda + W_e^{t}) + \cos \eta \cos Az \sin \beta \cos (\lambda + W_e^{t})$$

$$- \sin \eta \cos \beta \cos (\lambda + W_e^{t}) \overline{X}_1 + (\cos \eta \cos Az \cos \beta + \sin \eta \sin \beta) \overline{Y}_1$$

$$+ (-\cos \eta \sin Az \cos (\lambda + W_e^{t}) + \cos \eta \cos Az \sin \beta \sin (\lambda + W_e^{t})$$

$$- \sin \eta \cos \beta \sin (\lambda + W_e^{t}) \overline{Z}_1$$

The above relations may be reduced to the equation

$$\cot POLANG = \frac{\overline{Z}_5 \cdot \left[\overline{Z}_3 - (\overline{\ell} \cdot \overline{Z}_3) \cdot \overline{\ell}\right]}{\overline{Z}_5 \cdot (\overline{\ell}_x \overline{Z}_3)}$$

from which

$$\overline{Z}_5 \bullet | \overline{Z}_3 - (\overline{\ell} \bullet \overline{Z}_3) \overline{\ell} - \cot (POLANG) (\overline{\ell} \times \overline{Z}_3) | = 0$$

It may be noted that, of the spacecraft orientation Euler angles ( $\zeta$ ,  $\xi$ ,  $\psi$ ) only  $\zeta$  and  $\xi$  appear in  $\overline{Z}_5$ . Since  $\zeta$  is determined by the sun sensor, then  $\xi$  can be determined from the measurement of POLANG.

Inputs required for the computation of  $\xi$  at the ground station are thus spacecraft position coordinates (u,  $\Omega$ ,  $\nu$ ) sun right ascension (RA) and declination ( $\delta_s$ ), sun sensor angle ( $\zeta$ ) ground station latitude ( $\beta$ ) and longitude ( $\lambda$ ), line of sight elevation ( $\eta$ ) and azimuth (Az), time, and POLANG.

#### 5.5.3.5 Station Acquisition Sensor Signal Processor

Onboard equipment includes coning control logic, sun sensor amplification and signal shaping circuits, precession control timing and pulse counting logic, and interface circuitry for providing signals to the thruster drive circuitry in the FWJC. The expected weight and average power of this equipment is 3.2 pounds and 3 watts.

## 5. 5. 3. 6 Station Acquisition and Despin Mass Expulsion Subsystem

It is required that the vernier system provide a total of 246 fps to a 1732-pound spacecraft. This  $\Delta V$  is distributed 139 fps in the radial direction (123 fps + 10 percent for vernier velocity error  $\pm 3.5$  fps to initate maneuver to  $90^{\circ}$ W) and 107 fps in the axial direction (89.2 fps  $\pm 10$  percent for vernier velocity error  $\pm 9$  fps to initiate maneuver to  $90^{\circ}$ W). A single 10-pound nominal thrust radial thruster and a total of eight 1-pound nominal thrust transverse and axial thrusters are required. The  $\Delta V$  figures include a 10 percent margin.

For precession control a total impulse capability of 264 lb-sec is specified, while coning control requires 254 lb-sec. Despin requirements total 617 lb-sec. A total included radial thrusting angle of 75 degrees per revolution was chosen after analysis of total impulse and time implications realized with larger and smaller angles (Ref. Figure 6, 4-49). Impulse requirements are summarized in Table 5, 5-6.

Table 5.5-6. Impulse Requirements for Station Acquisition and Despin
Mass Expulsion Subsystem

ITEM	Impulse (lb-sec)	Pulse Width (msec)	Specific Impulse (sec)	Fuel Weight (lb)
(a) <u>Before Apogee Burn</u> Coning control (7.5 <sup>0</sup> )	176	400	222	0.79
Precession Control (9.8°)	146	175	205	0.71
(b) <u>During Apogee Burn</u> Coning Control	40	400	222	0.18
(c) <u>After Apogee Burn</u> Coning Control (2.4 <sup>0</sup> )	29	400	222	0.13
Precession Control (15.6°)	118	175	205	0.58
Axial $\Delta V_{a}$ (89.2 fps + 10%)	5 <b>.</b> 439		222	24.5
Anial <b>A</b> . V <sub>a</sub> (9 fps) Initiate Maneuver to 90 <sup>0</sup> W	497		222	2.24
Radial $\triangle$ V $_{\mathbf{r}}$ (123 fps + 10%)	8159	175	217	37.6
Radial <b>Δ</b> V <sub>r</sub> (3.5 fps) Initiate Maneuver to 90 W	226	175	217	1.04
(d) <u>Despin</u>	617		222	2.73
TOTALS	15,447			70.55

5.5.3.6.1 Impulse Requirements

The precession and coning impulse requirements involve use of the 1-pound thrusters in a pulsed mode ( $W_s = 71.7 \text{ rpm}$ ) such that the pulse width is approximately 175 msec and 400 msec, respectively. Analysis of data provided by propulsion contractors indicates a most probable  $I_{sp}$  for a 1-pound thruster in steady state to be 222 seconds. Therefore, since a 175 msec pulse width will degrade  $I_{sp}$  below this performance level, an  $I_{sp}$  of 205 seconds was assumed for the precession control. An  $I_{sp}$  of 222 seconds was assumed for the coning control. The propellant weight for precession and coning is then

Precession 264/205 = 1.29 lb HydrazineConing 245/222 = 1.10 lb Hydrazine

For despin a specific impulse of 222 seconds was assumed for the two 1-pound thrusters firing in a steady-state mode to despin the spacecraft. Propellant weight required is

$$\frac{617}{222} = 2.73 \text{ lb Hydrazine}$$

For the axial adjustment in orbit, requiring 107 fps, a steady-state firing of two 1-pound thrust engines is used.  $\Delta V = 107 = g I_{sp} log \frac{W1}{W2}$ , where  $(W_1 - W_2)$  is the propellant weight. For a steady-state  $I_{sp}$  of 222 seconds, 26.7 lb of Hydrazine are required.

Total velocity in the radial direction is 139 fps. From Figure 5.5-16, for a thrusting angle of 75 degrees per revolution and a vehicle spin rate of 71.7 rpm, a nominal pulse width of 175 msec is required. From Figure 5.5-17 an I sp of 217 seconds is estimated for the 10-pound thruster. With reference to Figure 5.5-18 it is seen that a radial impulse efficiency of approximately 93 percent is realized at the thrusting angle of 75 degrees. Therefore, a total of 38.6 pounds of Hydrazine propellant are required. A total weight of 70.5 pounds of impulse propellant is required. Assuming tank expulsion efficiency of 97 percent, a total of 73 pounds of Hydrazine should be tanked.

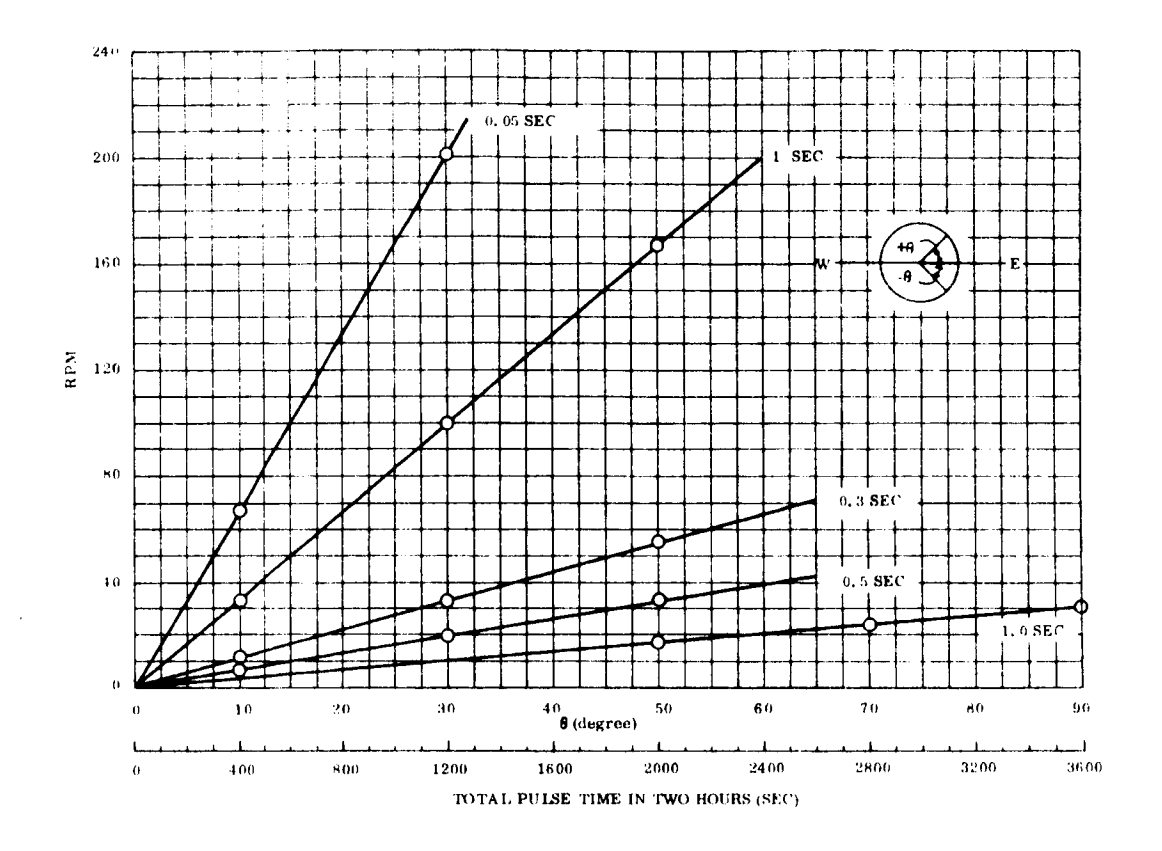


Figure 5.5-16. Pulse Lengths for Various RPM's and  $\theta$ 's

### 5.5.3.6.2 Thrust Level

The thrust level of the coning and precession control, and axial  $\Delta V_a$  thrusters, is determined by the following factors:

- a. Precession angle per impulse should not exceed 0.1 degree thrust level less than 2 lb.
- b. Time to precess through 10 degrees should not be excessive (i.e., 20 minutes) thrust level greater than 0.3 lb.
- c. Deceleration during despin should not be excessive (2 deg/sec) thrust level less than 1.4 lb. Despin time should not be excessive (i.e., 10 min.) thrust level greater than 0.4 lb.
- d. Equipment simplification if identical nozzles can be used for coning and precession control and for axial  $\Delta V_a$ . Removal of  $\Delta V_a/2 = 44.6$  fps should not take more than 30 min. Thrust level greater than 0.7 lb.

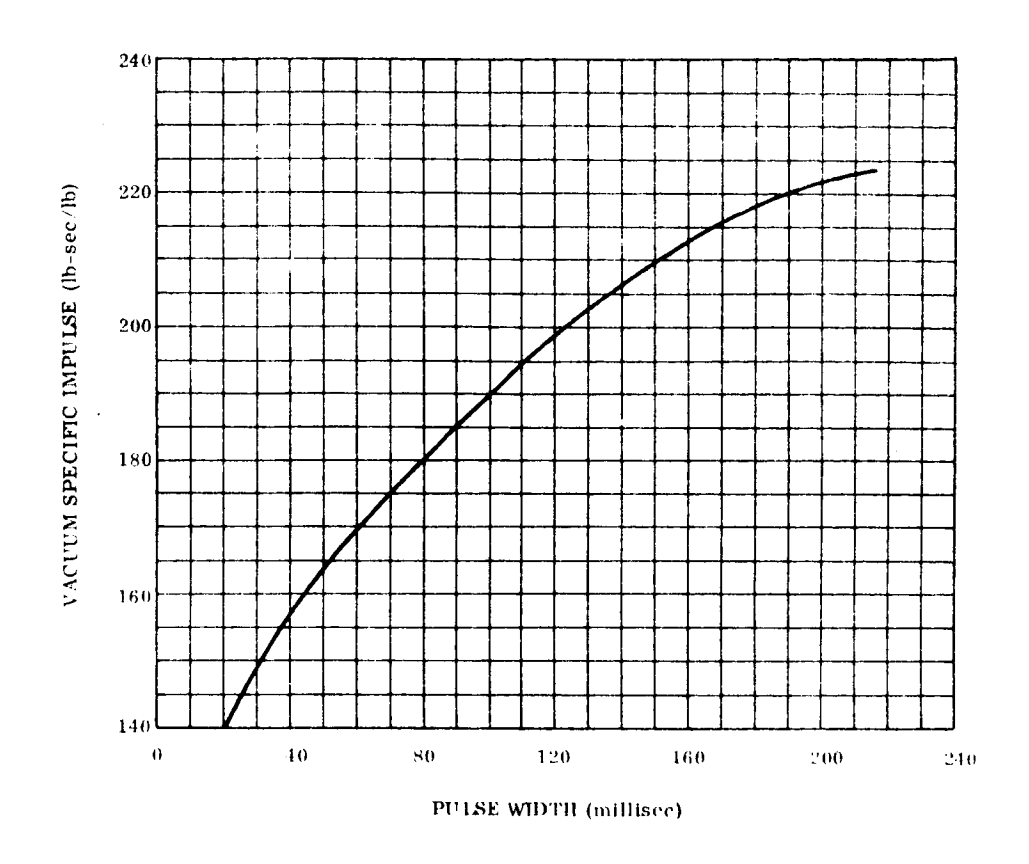


Figure 5.5-17. Effect on  $I_{\mbox{sp}}$  for Various Pulse Widths for Hydrazine

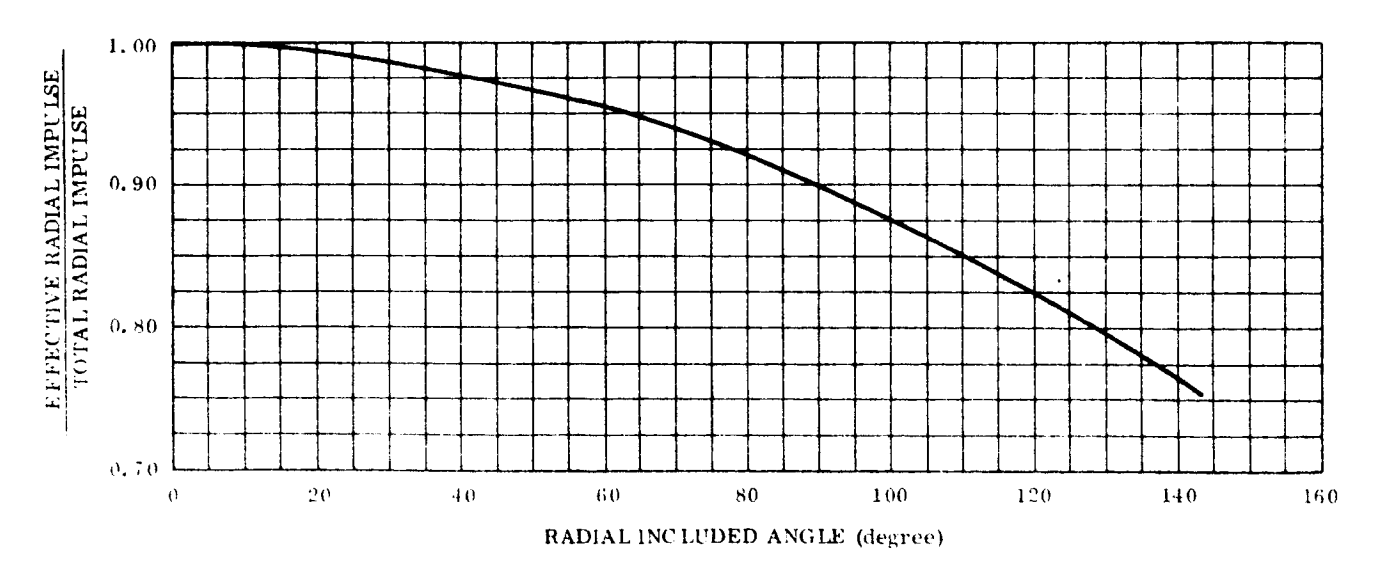


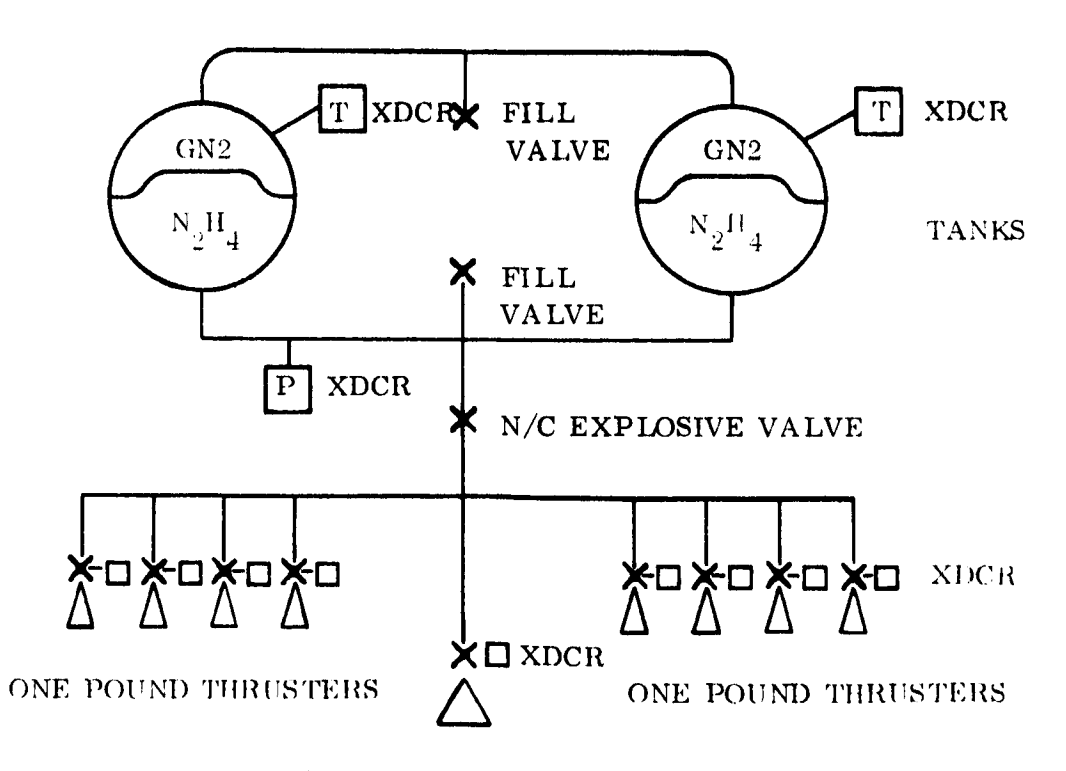
Figure 5.5-18. Radial Impulse Efficiency

On the basis of the above considerations, the thrust level of 1 lb was selected for the coning and precession control and axial  $\Delta V_a$  thrusters. Equipment simplification would be achieved if a 1-lb nozzle were used for the radial  $\Delta V_r$ ; however, removal of  $\Delta V_r/2=61.5$  fps in less than 30 minutes requires a thrust level of greater than 9.5 lb, and on this basis the 10-lb level was selected for the radial  $\Delta V_r$  thruster.

#### 5.5.3.6.3 System Design

Figure 5.5-19 is a schematic of the Hydrazine Monopropellant system. Pressure transducers, explosive valves, and fill valves are readily available as qualified hardware on other programs. Tanks shown are assumed to be 16-inch spheres, newly developed. Specific thruster models have not been chosen although existing hardware requiring minimum modification is available at Walter Kidde, Rocket Research and Hamilton Standard.

The pressurant is assumed to be gaseous nitrogen at an initial pressure of 350 psi. This requires approximately 4.5 pounds  $\mathrm{GN}_9$  between the two tanks.



TEN POUND THRUSTER

Figure 5.5-19. Station Acquisition System Schematic

For a tank to hold 73 pounds of Hydrazine expended in a blowdown mode of operation at an ullage ratio of 0.5 (nominal) the tank volume will be

73 lb x 
$$\frac{\text{ft}^3}{60 \text{ lb}}$$
 x  $\frac{1728 \text{ in.}^3}{\text{ft}^3}$  x 2 = 4210 in.

It is required for ease of spacecraft packaging and cg control that two tanks, each with a capacity of 2105 in. <sup>3</sup> be used. The ALPS generant tank (JPL) is approximately the correct size for use in ATS-4. However, it weighs 21 pounds due to a 1500 psi working pressure requirement. A Bell Aerosystems Apollo Program tank is available. This tank is 12.5 in. in diameter by 23.7 in. long and weighs 8.3 pounds. The development of a new tank may also be considered. For a volume of 2105 in. <sup>3</sup> in each tank, a spherical tank of about 16 inches in diameter is required. A working pressure of 350 psi decaying to 175 psi should be compatible with both thruster sizes. Burst pressure is therefore 770 psi. Assuming use of Titanium-6 Aluminum-4 Vanadium with an ultimate strength of 155,000 psi, a minimum wall thickness of 0.020 inch and a resultant tank weight of 3.1 lb (allowing 20 percent of basic shell weight for girth rings, bosses, and weld joints) results. The weight of the butyl rubber diaphragm and accompanying hardware is estimated at 1.9 pounds for a total tank weight of 5 pounds. A design and development effort based on the JPL-ALPS design and development program will be used in order to take maximum advantage of existing information.

5.5.3.6.4 System Weight

Table 5.5-7 summarizes the system weight.

Table 5.5-7. Station Acquisition System Weight

Component	Qty.	Weight	Total
	Per	per unit	Weight
	System	(lb)	(lb)
Propellant Tanks Fill Valves Pressure Transducers Explosive Valve Temperature Transducers One-Pound Thrusters Ten-Pound Thrusters Hydrazine Propellant Gaseous Nitrogen	2	5.0	10.0
	2	0.25	0.5
	10	0.5	5.0
	1	0.7	0.7
	2	0.5	1.0
	8	1.5 (typ)	12.0
	1	2.0 (typ)	2.0
	AR	73.0	73.0
	AR	4.5	4.5
TOTAL			108.7 lb

### 5.5.3.6.5 Command and Telemetry Requirements

The command requirements consist of an explosive valve signal and nine solenoid valve signals. Telemetry will be needed for ten pressure transducers and two temperature transducers.

#### 5.5.3.7 Three-Axis Gyro Package

The three-axis gyro package chosen for this system is the OAO RAPS package and associated control electronics except that the electronics associated with the attitude mode used on OAO will not be included. Presented below are the important parameters of this package:

Weight: 15.5 pounds

Power: 30 watts

Threshold:  $0.0002^{\circ}/\text{sec}$ Scale Factor:  $60 \text{ v/}^{\circ}/\text{sec}$ 

Total Uncertainty:  $\pm 0.18 \pm 3\%$  of point, volts (see Figure 5.5-20)

Gyro Spin Motor Excitation: 26 v, 3 ø, 400 Hz Gyro Signal Generator Excitation: 13 v, 1 ø, 800 Hz

Three Kearfott C70 2465 006 (Alpha Series) high accuracy miniature floated rate integrating gyros are used in this package, and provide an output voltage equal to the specified gradient in millivolts/second per milliradian/second of input angle change.

The voltage output is primarily an 800 Hz signal, but has some wheel perturbation superimposed on the output signal. The perturbations produced by the wheel are the source of loop noise which is amplified by the system electronics and filtered at the demodulator and torque amplifier modules to reduce the level to that permissible in the system.

In order to obtain increased spin motor life, the following features are incorporated into the gyro design:

- a. Bearing dimensions and finishes exceed ABEC 9 tolerances.
- b. Class AAA balls with a high degree of roundness and matching.
- c. The use of double-vacuum melted 52100 steel for balls and races.
- d. Special bearing cleaning technique.
- e. Extended run-in of spin motor with constant monitoring of motor performance to weed out potential early failures.
- f. Reduced preload to the lowest value consistent with satisfactory gyro performance. (The preload reduction will result in lower stress levels and thus increased life).

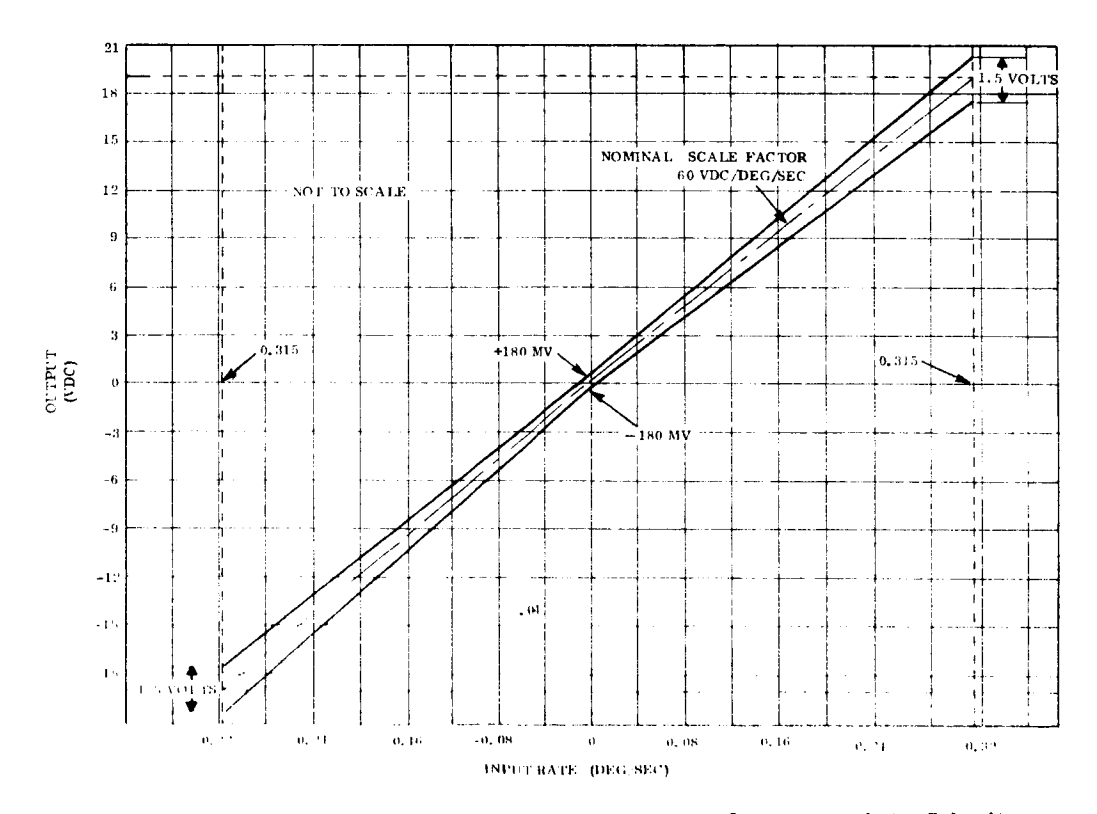


Figure 5.5-20. RAPS Rate Mode Total Uncertainty Limits

Also in order to reduce contamination, the following action has been taken:

- a. Better surface finish of piece parts has been incorporated to reduce contamination given off by parts and assemblies.
- b. Improved the compatibility of design to tooling and processing techniques used in producing contamination-free gyros.
- c. Tightened pivot jewel radial clearance to reduce the number of particles that could enter the gap.
- d. Increased the gap between the float assembly and stationary parts to reduce effects of contamination.

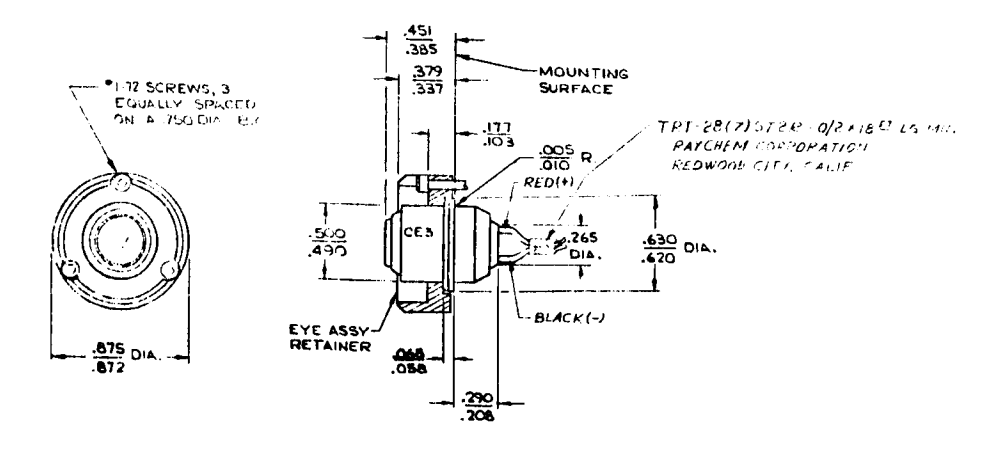
A detailed description of the gyro is given in Figure 5.5-21. This gyro is currently being flown on Nimbus vehicles and has accumulated approximately 5000 hours in test and in-orbit use.

## 5.5.3.8 Orientation Control Sun Sensors

Since the vehicle may have any orientation at the start of initial stabilization, the sun sensor subsystem must have a total field of view of  $4\pi$  steradians (one sphere). The system will consist of a group of individually mounted silicon detectors, such as the CE-3 Coarse Eyes manufactured by Ball Brothers and used on the OAO spacecraft. (Ref. Figure 5.5-22). The characteristic output of this device is shown in Figure 5.5-23. In general four eyes will be used in a set to generate a transfer function similar to that shown in Figure 5.5-23, for a single axis, the actual transfer functions depending upon the particular eye orientations and shading arrangements chosen.

Three sun sensor sets, pitch, roll and yaw, are required. The normal axes of the pitch and roll eyes will lie in the roll-yaw and pitch-yaw planes, respectively, and their combined null axis will coincide with the yaw axis. The normal axes of the yaw eyes lie in the pitch-roll plane, with the null parallel to the vehicle roll axis.

Figure 5.5-21. Miniature Rate Integrating Gyro



## NOTES:

- 1. DETAIL REQUIREMENTS FOR P-1 PER SVS 3220 AND FOR P-2 PER SVS 7439.
- 2. PART TO INCLUDE MANUFACTURER'S IDENTIFICATION.

Figure 5.5-22. Detector, Cone Angle Sun Sensor, Coarse Eye Assembly

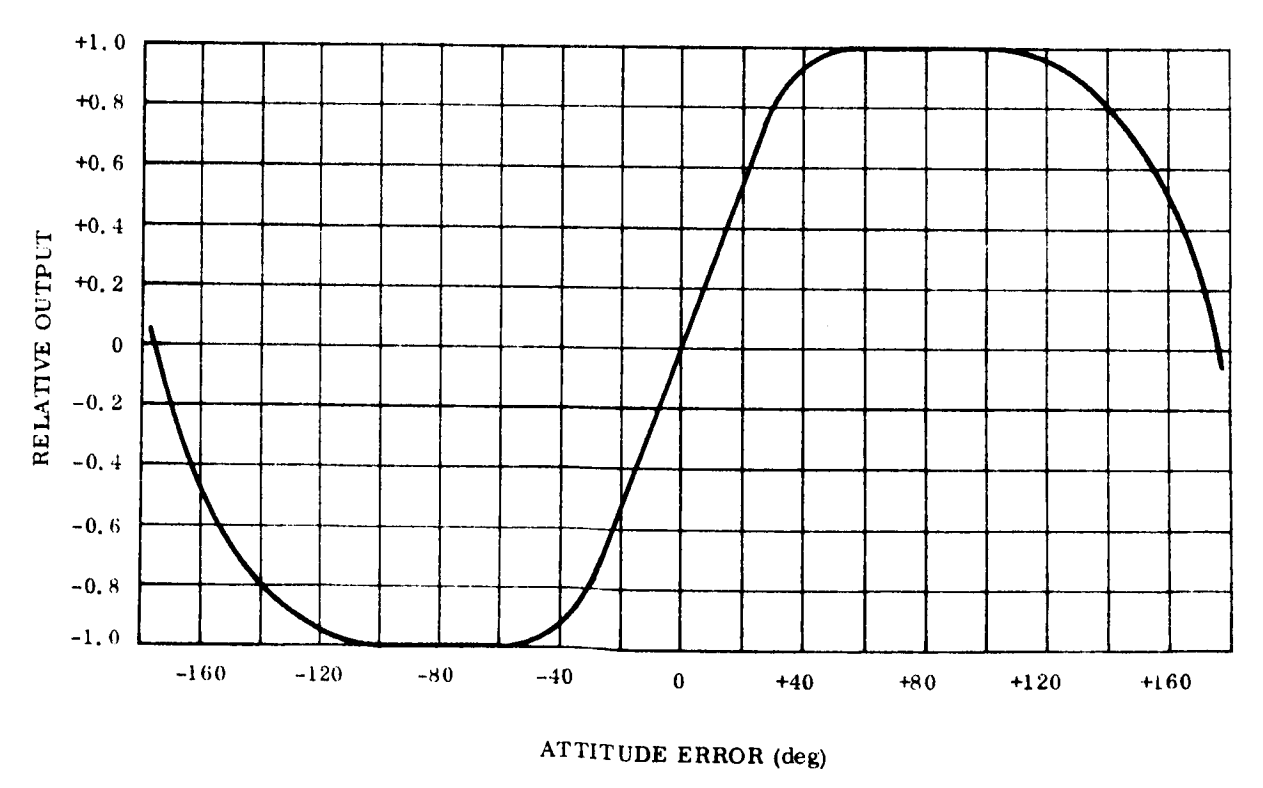


Figure 5.5-23. Control Axes Coarse Sun Sensor Set Relative Response Characteristic

As shown in Figure 5.5-24, each individual sensor or eye has a hemispherical field of view with the output varying nearly as the cosine of the offset from the normal axis. Maximum output is the order of 0.75 ma with solar illumination. The slope of the output from a pair of eyes connected in series opposing with normal axes at 90 degrees to one another is 24  $\mu$ a/degree, with a null stability of 0.5 degree. The anti-null produced at 180 degrees from the zero-degree null is unstable since a small output produces a control system response to increase the sensor output. While some difficulties have been experienced in operating these sensors at very low temperatures ( $\stackrel{\sim}{=}$  -100°F), it is anticipated that design improvements and adequate spacecraft thermal design will prevent such problems on ATS-4.

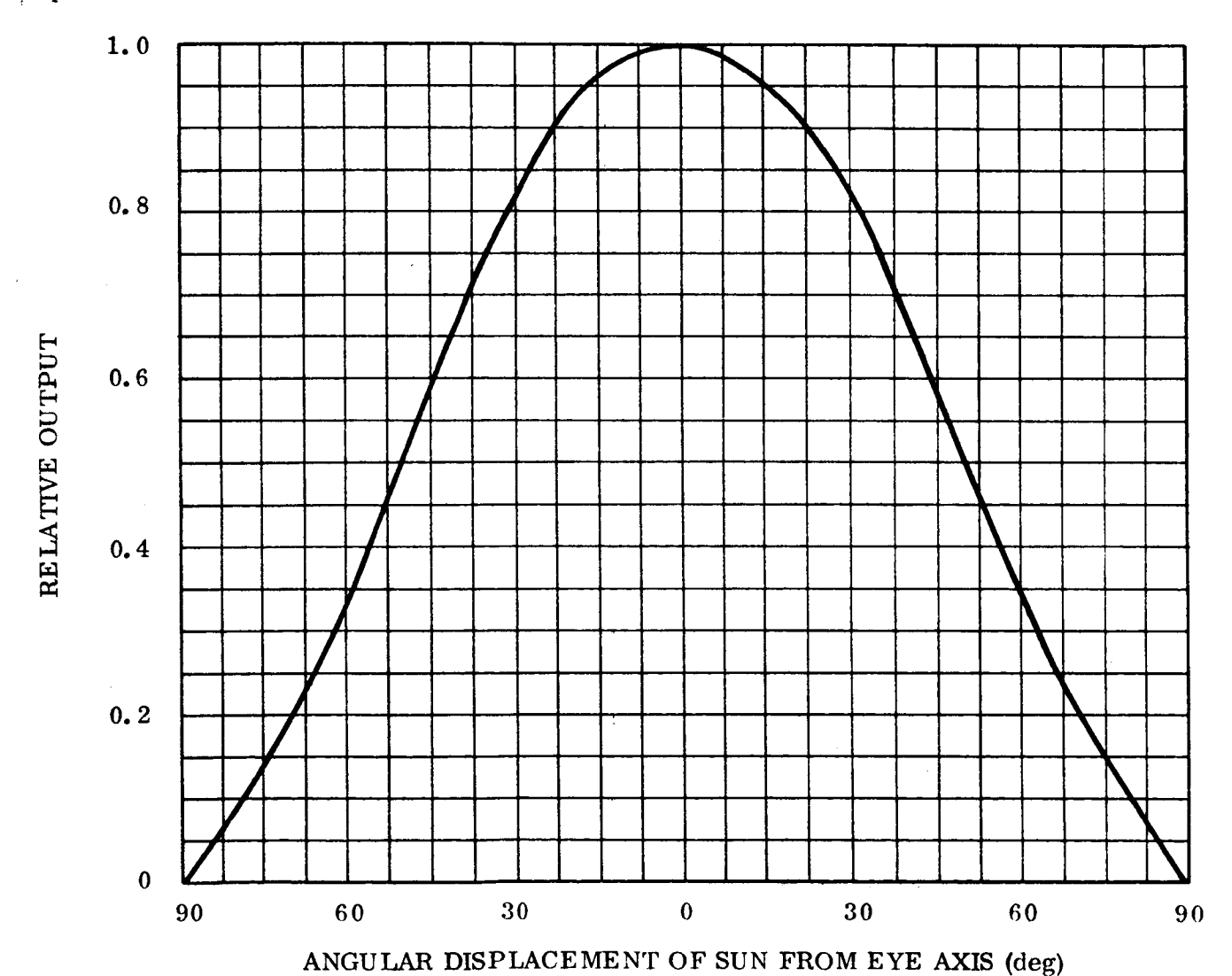


Figure 5.5-24. Single Eye Output vs Angle Characteristic

# 5.5.3.9 Earth Sensor

An advanced system now under development by the Advanced Technology Division, American Standard Corporation is proposed as the earth sensor for ATS-4. The basic concept of this sensor (being developed for the Apollo program) has been proven in breadboard form.

The Apollo sensor employs two servo-driven mirrors in a dual reflection system to provide a versatility in choice of scan pattern that is not easily achieved by any other means. Essentially the infrared energy received from a small (about 1 degree) conical field of view is reflected first off one mirror onto the second, then into the IR telescope/detector. With the angle of the first mirror controllable in one axis and that of the second mirror in the orthogonal axis, the view field can be pointed or scanned in any desired pattern within a rectangular or square total field determined by the angle limitations of the mirrors.

For the ATS-4 application, two scan patterns would be employed. During the earth acquisition phase of the mission, a rectilinear or raster scan will continually search for earth over a 40 by 40 degree total field (see Figure 5.5-25). Following acquisition the sensor will track the center of the earth disc.

The scan versatility provided by the independently controlled mirrors allows consideration of a number of ways to track the center of the earth. The major considerations in selecting a specific scan pattern are (a) accuracy, (b) solar rejection, (c) complexity of associated circuitry.

Depending on the time of year and time of day, from synchronous altitude the Sun can appear at any position in the near vicinity of earth; consequently, it is necessary to provide for a change in the normal scan pattern to eliminate the error the sun would produce. This will generally also require an appropriate change in the logic circuitry that converts detected signal into error signals useful to the control system.

More study is required in order to select an optimum concept; however, several possibilities are described below:

On-axis crossed line scan. In this concept a full-field scan across Earth is made first in one axis: then, with the mirror fixed at the earth center line as determined from the two edge crossings, the second mirror is scanned to determine the orthogonal axis center line. This procedure is continued with each mirror alternately scanning then remaining fixed while the second is scanned. The result is a crossed line scan pattern with the intersection of the pattern lines tracking the center of the earth even though the spacecraft is pointing off of the local vertical. This is illustrated in Figure 5.5-26.

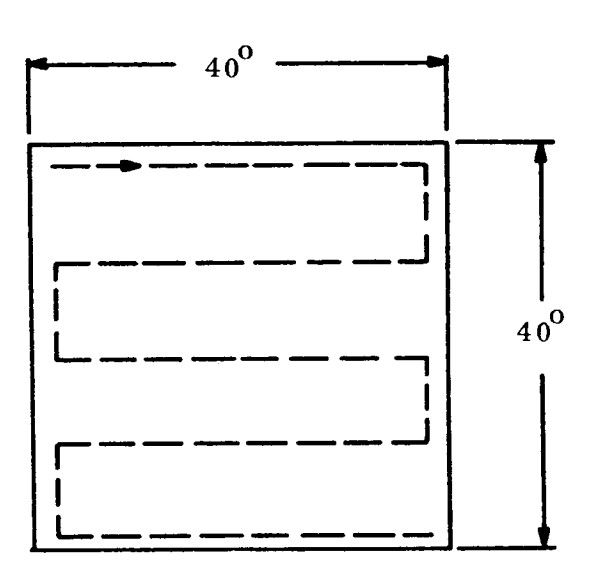
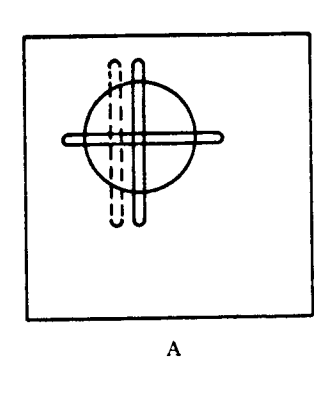
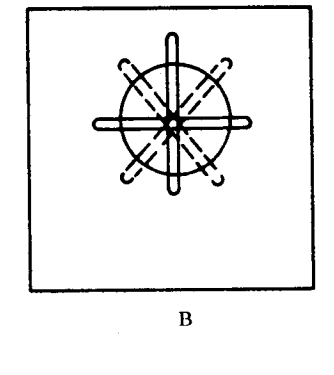
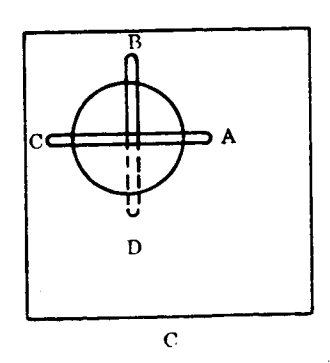


Figure 5.5-25. Acquisition Scan Pattern







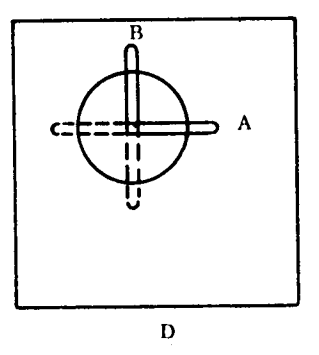


Figure 5.5-26. Possible Tracking Scan Patterns

In the event the sun appears in or near on the scan-line fields, that scan can be offset a few degrees to follow a parallel line (as indicated by the dotted line in Figure 5.5-26). At the same time the error generation logic must be changed to factor in the scan change.

The signal to offset the scan because of imminent problems from the sun can be triggered in several ways:

- 1. It could be commanded, based on a ground prediction that the sun will be in the field of one scan line.
- 2. The sun could be sensed by a separate sensor viewing through the two mirrors in parallel with the IR telescope. The instantaneous view field of this sun sensor would be wider than that of the earth detector for sun sensing prior to the sun's appearance in the scan field.
- 3. The high peak signal caused by the prime sensor from the sun in its view field could also provide the offset trigger.

All three choices above have disadvantages. The first adds a command requirement not otherwise needed. The second and third provide automatic offsetting, but there is no easy means of determining when it is safe to reset back to normal scan. In addition the third method - employing the prime detector to sense the sun - must inevitably suffer error during the transition phase when the sun is close or just entering the field of view, but not sufficiently in to provide the high level required for scan offset triggering.

b. Rotating cross-line scan. This concept is identical to that in a. above during normal scan. But when the sun is in or close to either line scan field, the pattern is rotated to a new position  $45^{\circ}$  from the original. This is shown in Figure 5.5-26. At the same time the scanned pattern is rotated, the logic is changed so that the output errors are still generated in the desired axes. This is a simple computation,  $Ex = K (E_A - E_B)$  and  $E_y = K (E_A + E_B)$ , and will analytically cause no reduction in accuracy.

There is no theoretical preference of scan axis angle, consequently no pressing need to return to the nonrotated pattern. This simplifies automating the switching. The system would be bistable. Upon sensing the sun in either mode, the sensor changes to the alternate and remains there until again the sun causes a change back.

While in theory this seems a good solution, mechanization of the  $45^{\circ}$  rotated scan is somewhat complex. For scans along the lines of rotation of the mirrors, one mirror remains fixed while the other moves. This is a relatively simple action. However, to scan at  $45^{\circ}$  requires the simultaneous and closely phase controlled

rotation of both mirrors. The practicality of this approach must be studied in greater detail. It should be noted that ATD has demonstrated angle scan capability with the breadboard version of this sensor.

c. Three-point tracking. The concepts described in a. and b. above derive two-axis error information by sensing four horizon crossings around the earth disc. But since only three points on a circle determine its center (or only two points if the radius is known, see d. below), the scan pattern could be as shown in Figure 5.5-26. The normal mirror action would be the same as described in concept a., except that in one axis the scan line is only half as long and cuts across the horizon at only one point.

In the event the sun appears in any scan field the pattern would rotate in 90° increments until the sun is on the unscanned side of earth. Since the four possible scan patterns are equally accurate, tracking can continue with the new pattern until the sun again causes a rotation.

As in the other concepts the error computation must change as the pattern is rotated. Typically the computation for the two axes is:

$$\mathbf{E}_{\mathbf{x}} = \mathbf{A} - \mathbf{C}$$

$$E_{V} = B - \frac{A + C}{2}$$

The calculation is independent of the radius of the earth disc as viewed by the sensor.

The major disadvantage to this concept is the requirement of four different tracking modes, compared with two in the other concepts.

d. Two-point tracking. Provided the radius of the earth image is known to the sensor logic, only two horizon crossings are required to determine the center. This can be implemented by an extrapolation of concept c. in which both scan lines cross at only one point on the horizon. This is shown in Figure 5.5-26. A mode switch to the alternate pattern shown dotted can now be triggered by the sun in or near the field of either scan line.

Again as the pattern is switched the logic must be changed appropriately, but only two equally valid modes are required. The error calculation for this concept is typically:

$$Ex = A - R$$

$$\mathbf{E}_{\mathbf{v}} = \mathbf{B} - \mathbf{R}$$

where R is a priori information in the logic.

While simplest of all the concepts to implement, this one is also the least accurate. The value of the earth radius preset into the logic would be an average for the slightly oblate image as viewed from the spacecraft (unless additional complexity were added to update the radius value depending on spacecraft positions). The very slight error thus incurred may still be significant relative to the accuracy requirement of the sensor.

Any one of the above four scan pattern concepts is capable of accomplishing the task required of the ATS-4 sensor, but without more detailed considerations of the specific design problems and tradeoffs it is not possible to make a choice at this time.

With any of the tracking concepts described it will be possible to generate error signals about any specific point within a solid angle encompassing at least the entire earth disc. This is accomplished by a digital position command directing the sensor logic to determine error signals for the position of the center of earth relative to the commanded position. Since the control system will act to decrease the error signal to zero, the spacecraft and antenna will be pointed to the commanded position.

## 5.5.3.10 Polaris Star Sensor

As a yaw control reference, it is proposed that the star Polaris be tracked. For an equatorial orbit, Polaris is a near-ideal yaw reference. There are no close neighbor stars of comparable intensity and Polaris is only 0.9 degree off the celestial pole.

The star tracker requirements are similar to those of a Canopus sensor as used on interplanetary spacecraft. Since only a single axis reference is required, the star is tracked in one axis and allowed to move, effectively, in the other axis. Compared to a Canopus tracker, however, the Polaris sensor must sense a considerably fainter source. Canopus is nearly three magnitudes brighter, and thus has more than twelve times the intensity of Polaris. This may pose a problem in attempting a simple modification of an available Canopus sensor, although the vendor of the Canopus sensors for the Mariner flights maintains that the Mariner sensor has adequate sensitivity and requires only resetting the acceptance gates to convert to a Polaris sensor. In any event there are existing star sensors

that can sense stars more than a magnitude fainter than Polaris, therefore no serious sensitivity problem is foreseen.

Since the Mariner Canopus sensor has undergone extensive study and development, and has performed successfully, it will be taken as a baseline design to be modified for the ATS-4 mission. (This is a feasible approach; however, additional study is warranted to tradeoff this concept against modification of other sensors or against a completely new design.) The Canopus sensor employs an image dissector tube for detection. By means of an internal aperture the detector tube, through the optics, views a narrow (4 by 0.86 degrees) slit field of view instantaneously. This slit field is then electronically caused to oscillate about a center position in a direction orthogonal to the long dimension. Logic circuitry can determine the field-of-view position at the time a star is detected and provide a position error signal output. Small effective star motions along the length of the slit field will have no effect.

The signal-to-noise ratio of a Canopus-type sensor is in part affected by the total solid angle instantaneous field of view. The larger this field, the more background light is detected. For this reason it will not be practical to provide adequate slit field length to permit full movement of the spacecraft in roll for off-axis pointing without longitudinal repositioning of the slit. However, longitudinal repositioning is already provided in the Canopus sensor in which the 11 degrees long slit field is electronically gimballed\* to cover the 32 degree total field required for Canopus tracking. For the Polaris sensor a 4 degree long instantaneous field is proposed, with provisions for electronic gimballing over a range of  $\pm 9$  degrees. The gimbal angle will be updated appropriately by command when the vehicle is to be pointed to a new position. The 4-degree long slit field will, however, allow the  $\pm 9$  degree apparent motion of Polaris around the celestial pole, due to its slight off-pole position, without gimbal repositioning. Some field is allowed in addition so that the number of digitally updated positions is limited to a practical value.

<sup>\*</sup> The term "gimbal" is used here to describe the effective result obtained. It is emphasized that no actual mechanical gimbaling is employed. The sensor is completely without moving parts.

Along the scanned axis the instantaneous field will be 0.86 degree and the scan ±2 degrees as in the Canopus sensor. Thus the detection circuitry and associated logic can be identical with that already developed.

## 5.5.3.11 Orientation Control Sensor Signal Processor (SSP)

The SSP performs the signal amplification and shaping of all sensor signals. It also generates most of the system logic and switching functions. The complexity of this item is comparable to the OAO pitch, roll and yaw SSP's and torque controller, but it is expected to have a weight approximately 30 percent of that of the OAO units by utilization of microelectronic circuitry. The expected weight and power of this unit are approximately 15.3 pounds and 30 watts respectively.

## 5.5.3.12 Flywheel and Jet Controller (FWJC)

The FWJC contains the threshold detectors used to generate appropriate switching lines for the pitch, roll, and yaw thrusters: thruster drive amplifiers, the control electronics for driving the flywheels and the logic necessary for implementation of the integrated orientation control/stationkeeping mass expulsion subsystem. This package is comparable in complexity to the OAO pitch, roll and yaw FWJC's, and is expected to weigh approximately 19.2 pounds (40 percent of the OAO unit's weight) by utilization of microelectronic circuitry. The expected power consumption is 15 watts.

#### 5.5.3.13 Mechanical Flywheel

The flywheel chosen for this system is the Bendix 2 ft-lb-sec momentum wheel which was developed and qualified on the OAO Program by General Electric. A cross-sectional view of this flywheel is shown in Figure 5.5-27.

The flywheel is essentially a servomotor with a large inertia rotor. The Bendix family of flywheels provides a number of important design features. The deep groove bearings are made from 440C stainless steel to an above-standard hardness of Rockwell C60 minimum. The bearings are mounted with spherical type self-aligning bushings. On this wheel a small finite preload is established and maintained through a special assembly at the top

Figure 5.5-27. OAO Flywheel Cross Section

bearing. A stationary shaft passing through the center of the flywheel serves as a stable reference for preload adjustment. Preload is not affected by changes in loading from expansions in the housing due to changes in temperature or external pressure because of a slip fit condition existing between two sleeves in the upper bearing assembly. This feature helps to maintain the proper preload at all conditions of test and flight and thereby improve long-life performance.

The bearings are lubricated with MIL-L-6085A oil, which has a relatively low vapor pressure and low starting torque capabilities. Lubricant retention is augmented by the use of a labyrinth bearing shield. Nylasint lubricant reservoirs are provided. Sacrificial evaporation of the lubricant maintains vapor pressure of the lubricant in the bearing chamber in the event the hermetic seal of the main housing fails.

The rotating element is machined from a single piece of stock to provide maximum stability of balance and bearing alignment. Small gaps between the housing and the wheel rim limit wheel vibration amplitudes during test and launch environments, thus preventing damage to the rotor bearings.

The wheel is pressurized to a small fraction of one atmosphere of helium. The gas contains 2 to 5 percent of oxygen to replenish surface oxides which may actually contribute to the lubrication of critical surfaces.

The functional specification and interface requirements are tabulated below:

•	Momentum at 900 rpm	2.06 ft-lb-sec (rated momentum)
•	Rotor Inertia	$0.0219 \pm 3\% \text{ slug-ft}^2$
•	Rated Speed	900 rpm minimum at rated voltage
•	Stall Torque	2.0 - 2.3 in. oz
•	Operating Temp Range	0°F to 160°F
•	Voltage Input	26 vac, 400 Hz (+5%, - 10%), 2 phase
•	Power Input	
	Stall	3.6 watts nominal
	Rated Speed	3.2 watts nominal
	Reversing Load	5.0 watts nominal
•	Time Constant	$213 \sec \pm 18\%$
•	Gain	0.015 ft-lb-sec/volt
•	Speed Indication	ac tachometer
•	Size	11-3/4 in. dia by $5-1/2$ in. high
•	Weight	11.3 lb

### 5.5.3.14 Orientation Control and Stationkeeping Mass Expulsion Subsystem

It is required to provide a total impulse of 1,058 lb-sec for E-W capture and stationkeeping, 5,290 lb-sec for E-W station change, 10,981 lb-sec for N-S stationkeeping and roll momentum unloading, and 286 lb-sec for initial stabilization and restabilization. The total impulse requirement is 17,615 lb-sec (Ref. Table 5.5-4). The selected thruster configuration shown in Figure 5.5-28 consists of nine nozzles, five single and two dual, which may be operated individually in various combinations to produce spacecraft translation and simultaneous momentum wheel unloading. The thrust levels are 0.00086 lb (3 nozzles) and 0.00100 lb (6 nozzles). Based on the impulse requirement, thrust levels and thrusting duration (periods of 1 to 3 hours for the majority of the impulse), an ammonia propellant resistance jet subsystem has been selected. At the design operating temperature of 2000 F, the fuel I sp is 240 sec; however, this temperature requires a 4-hour warmup period. To

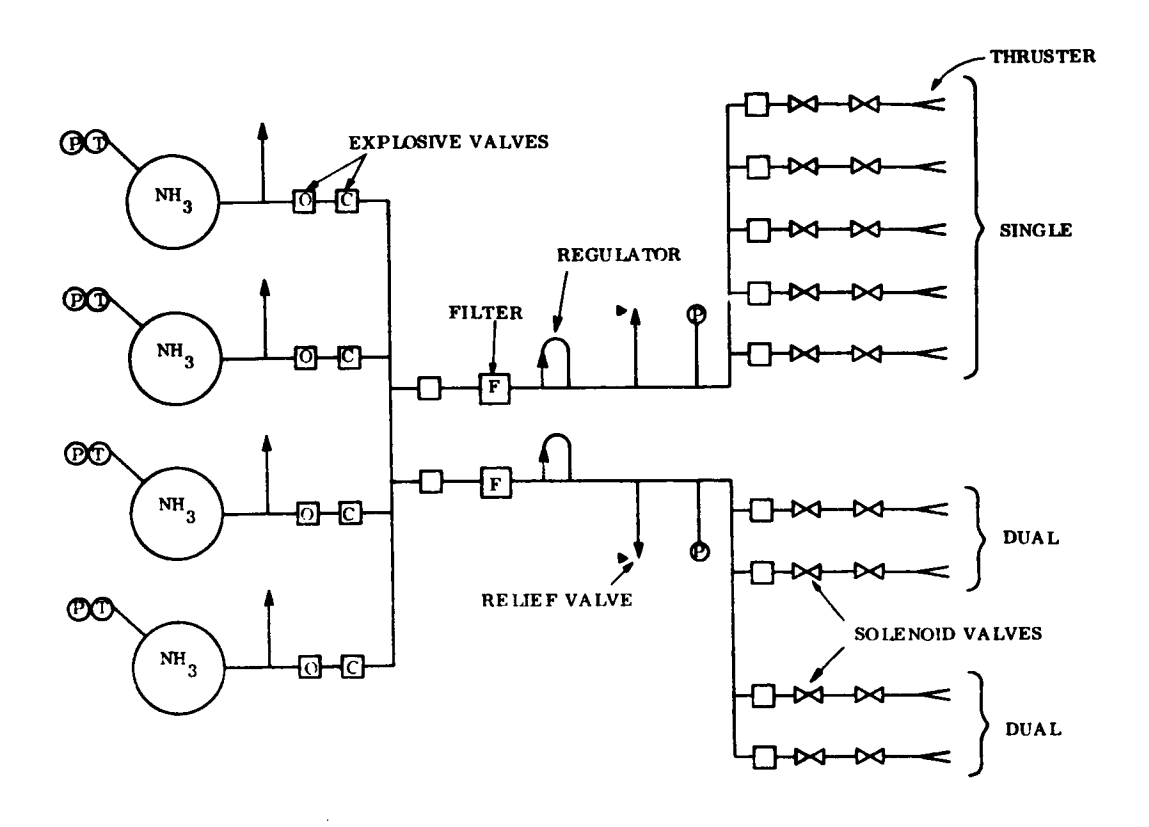


Figure 5.5-28. General Electric Resistance Jet System

reduce the system power requirement, a 1-hour warmup period will be allowed before thruster operation, at which time the operating temperature will be approximately  $1800^{\circ}$  F and the fuel I sp is 210 sec. The value of I = 210 sec has been used to determine the weight of fuel required, which is, allowing 10 percent for leakage and tank expulsion efficiency,  $\frac{17,615}{210} + 10\% = 92.4$  lb

To store the fuel, four aluminum tanks having a volume of 1167.5 cu in. each are required. The propellant tank design is shown in Figure 5.5-29. Tank design data are:

a. Diameter: 13.1 in.

b. Design Pressure: 300 psi

c. Proof Pressure: 310 psi

d. Burst Pressure: 660 psi

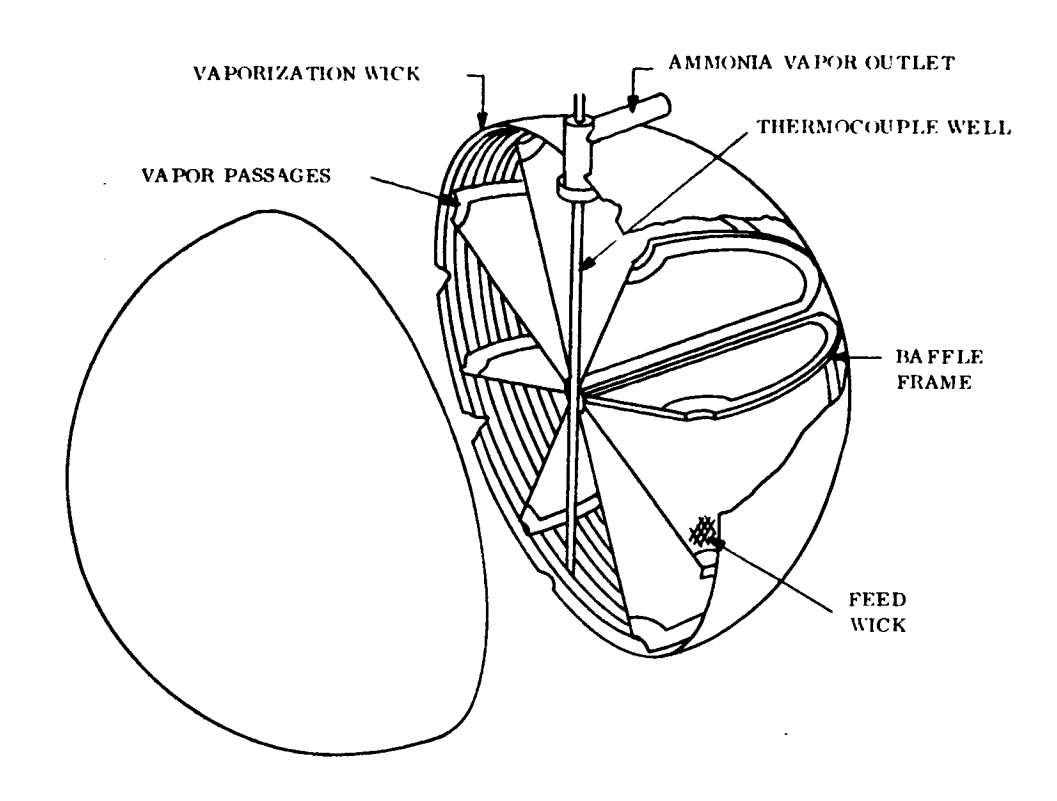


Figure 5.5-29. Liquid Ammonia, Zero-g Storage Tank, Schematic

Using these pressures a wall thickness of .0164 inches is needed. This is unrealistic on the basis of handling and manufacturing, therefore a wall thickness of 0.022 inch is selected.

# 5.5.3.14.1 System Weight

Table 5.5-8 is a complete listing of the hardware for the resistance jet system and the associated weights.

Table 5.5-8. Resistance Jet System Weight

Part	Weight (lb)
4 Propellant tank shells	7.6
10 Explosive valves (5 N/O, 5 N/C)	3.8
11 Filters	2.4
2 Regulators, 2 pressure transducers, 2 relief valves	1.8
18 Solenoid Valves (Carleton)	3.6
9 Thrusters:	
5 single	8.0
2 duals	3.3
Tank internal parts (wicking, etc.)	2.4
4 Pressure transducers	1.8
TOTAL	34.7

## 5.5.3.14.2 System Power

\$.5.3.14.2.1 N-S Thruster Requirements. A single thruster uses 25 watts and needs a warmup time of 1 hour to reach 90 percent of its operating temperature (1800°F). This results in a power requirement of 75 watts for 4 hours per day or 300 watt-hours per day for daily stationkeeping or 75 watts for 6.8 hours every 2 days for stationkeeping. During the second year when there will be no N-S stationkeeping the flywheel unloading requires that the thrusters be actuated for about 7 minutes every 15 days. Due to the short thrusting time needed for flywheel unloading, the thruster will be used without warmup time. This results in a specific impulse of about 100 seconds. The heater will only be turned on while thrusting to move the ammonia farther above the saturation line on the enthalpy-entropy curve. This is done so that when the ammonia expands in the nozzle, it will not become liquified or freeze.

5.5.3.14.2.2 E-W Thruster Requirements. A single thruster uses 25 watts and a dual thruster uses 30 watts. Warmup time for both is 1 hour for 90 percent of operating temperature (1800°F). One duty cycle being considered is to actuate the E-W thrusters only to unload the pitch flywheel when necessary (a small amount of E-W stationkeeping impulse would occur) and to perform the remaining E-W stationkeeping approximately every 20 days. The thrusters must be actuated for about 54 minutes for stationkeeping every 20 days.

This would be preceded by a 1-hour warmup period to take advantage of the higher specific impulse. This results in a power requirement of 0 for the first 19 days of a 20 day cycle and 85 watts for 1.9 hours on the twentieth day.

Summarizing, the total power required is 75 watts for 4 hours every day plus 85 watts for 1.9 hours on the twentieth day of each 20-day cycle. This results in a peak power of 160 watts and an average power of 12.8 watts.

## 5.5.3.14.3 Command and Telemetry

Telemetry is required for 13 pressure transducers and 11 temperature transducers. Command signals are required for 18 solenoid valves and 10 explosive valves.

# 5.5.4 COMMAND, TELEMETRY, AND PROGRAMMER INTERFACE

## 5.5.4.1 Commands

A total of approximately 86 commands will be required. These commands are described in Table 5.5-9. The commands listed fall into three general categories; (a) as backups to automatic sequencing normally performed by onboard logic, (b) those used to initiate control modes and to execute ground commanded maneuvers and (c) those used to effect corrective procedures necessary to return system operation to normal in the event of a malfunction.

#### 5.5.4.2 Telemetry

Adequate telemetry is necessary in order to accurately ascertain the important operating parameters of the orientation control system, and for diagnostic information in the event of a component or system malfunction. A total of approximately 145 signals are required to be telemetered and are described in Table 5.5-10.

Table 5.5-9. ATS-4 Command Requirements

Function 1	Time of Occurrence				Maximum Command Rate	Type of Command		
		Powered Flight	Coast/ Injection	Orbital		On Only	On/Off	Data (No. of Bits)
Enable Sun Stabilization	1			х			x	
Antenna Erect	1			х		х		
Enable Earth Stabilization	1			х			х	
PSS Commands	1			х			х	10
Earth Sensor Commands	2			x	One per minute		х	10
Enable Yaw Sun Stabilization	1			x			x	
Switch to ES Control	1			x			х	
Gyro Power	1			x			х	
Gyro Heater	1			x			х	
FW Enable	3			х			x	
Switch to PSS Control	1			х			х	
PSS Power	1			х			х	
Earth Sensor Search	1			х			х	
PSS Power	1		:	х	•		x	1
Earth Sensor Power	1			х			х	
Thruster Detec- tor Enable	6		х	х			х	
Auto Unload Disable	3			x			х	
FW Emergency Unload	3			x			x	
Auto 40% Unload	3			х			х	
Sun Sensor Enable	3			x			х	
E-W Station- keeping	1			x			х	
N-S Station- keeping	1			х			х	
Resistance Jet Prop. Shut-Off Valve	10			x			x	
Resistance Jet Solenoid Position		<u> </u>		x		1	x	
Resistance Jet Heater Control	7			х		<b>†</b>	x	
Vernier Solenoid Position	10		x	x			x	
Yaw Sun Sensor Bias	1			х			х	
	ONLY	REQUIRED	FOR INTE	RFACE WI	TH POSSIBLE EXPERI	MENTS		
Switch FW to IS	1			x			×	
Switch FW	1			x		1	х	

Table 5.5-10. ATS-4 Telemetry Requirements

Function	Number	Frequency	Powered Flight	of Occurrer Coast.' Injection	Orbital	Analog	Digital	Accuracy Requirements
			1.1611	Injection		<del> </del> -	ļ	<del> </del>
Piloh Rate Null	1				×	1	×	± 10% FS
Roll Rate		<del></del>	<del> </del>			<del> </del>	ļ	110/13
Null	<u> </u>	L			×	<u> </u>	x	
Yaw Rete Null	ı				×		×	
Pitch Sun	···	<del> </del>	<del> </del>	<del>                                     </del>		<del> </del>	<del> </del>	<del> +</del>
Att. Null	<u>1</u>		<u> </u>		×	ļ	x	
Roll Sun Att. Null	1		i		×	İ	×	
Yaw Sun		t	<del> </del>	<b></b>		<del> </del>	1	<del> </del>
Att. Null Antenna		ļ	ļ		×	ļ	×	
Erect	i		1		×		×	
Antenna Erect			1			<u> </u>	<b>†</b>	† <del></del>
Compl. Initiate Sun	1	<u> </u>	<del> </del>	<b>}</b> -	×	<b></b>	×	<del></del>
Stabilization	1		1		×		, x	
Sun Stabil.								
Complete Enable Earth	1		+	<del> </del>	- ×	<del> </del>	* ×	<del> </del>
Stabilization	1			İ	x		×	
Pitch Earth	1				×		×	
Att. Null Roll Earth	1	<del> </del>	+	<del> </del>	<del>  ^</del>	<del> </del>	<del>  ^</del>	+
Att. Null	1			1	х		x	
Earth Sensor Acquired search	1				x		×	
Earth Stabil.		<del> </del>	+	<del> </del>	<del>  ^-</del> -	<del> </del>	<del> </del>	<del>                                     </del>
Complete	1	ļ		ļ	×	<b></b>	×	1
Polaris Star Presence	1			[	×	l	×	
PSS Attitude		1	† — —	†		<del>                                     </del>		1
Null FW	. 1	<del> </del>	ļ	<del> </del>	×	<del> </del>	x	<del>  </del>
FW Direction	3	L		1	×	.1	x	1 1
FW Rpm	3				×	х		± 37- FS
Sun Attitude		†	1		1	<del>                                     </del>	1	<del> </del>
Error	3		1		×	×		
Rate Gyro				1	<b>†</b>		†	1
Signals Amplified	3	<del> </del>		<del> </del>	×	x	<del> </del>	<del></del>
Rate	3				x	х	<u> </u>	
Earth Sensor Attitude Error	2	1			x	×		
PNS Error		<del> </del> -		<del> </del>	+	+ <del>x</del>	+	<del> </del>
Earth Sensor		1			<b>†</b>	<del></del> -	<del> </del>	
Position Amp. Earth Sensor	3	+	<del>                                     </del>		×	- X	<del> </del>	- <del> </del>
Radiance Level	2				×	x		
PSS Servo Amp. Output				1	i .			
PSS Refer. Amp.	1	<del> </del>		1	x	×	<del> </del>	1
Output	1	ļ		4	x	x	<del> </del>	
PSS High Voltage Supply	1				×	x	}	í l
Shift Counter	<del> </del> -	+	<del></del>		1		1	1
Rits	10	ļ		<del></del>	×	x	<del> </del> -	±10% FS
Pull In Drop Out	9	+		+	X	X X	+	<del>+</del>
Control Flip		<b>†</b>				1		
Flops Thruster Solenoi	3	1 per		ļ	x	<del></del>	×	<del></del>
Position	9	3 sec	İ		×	i	x	±10%
Ammonia	1	1 per		1	T	T		
Resurvoir Pressure	1	10 min	×	x	×	×		±1/%
Animonia	6	1 per	<u> </u>	† · · · · ·	<del>†</del>	1	1	T
Reservoir Temp	ļ	10 min	x	x	x	×		±1 <sup>(0)</sup>
Thruster Pressure	7	1 per 10 min	×	x	×	x	1	±1%
Thruster	1	1 per	1	T	T			1
Temperature Pressure Tank	7	10 min		+	<u>x</u>	- x		+
Solenoid Pos.	2	10 min	x	×	×		×	±10°5
Hydrazine	T	1 per				1		T
Reservoir Temp.  Ilydrazine	2	10 min	<u>_</u> ×	×	×	×	+	+1'\\\\\\\\\\\\\\\\\\\\\\\\\\\\\\\\\\\\
Reservoir	1	10 min	x	×	×	x		±1"
Pressure Vernier Nozzle	<del> </del>	1 per		+	<del></del>	-+		<del></del>
Pressure	9	10 min		x	x	x	Ĺ	<u>+</u> 1',
Nuzzle Solenoid	<b>†</b>	1 per						
Position Vaw Sun	9	10 min	+	x	×		<del>*</del>	±10 <sup>1</sup> / <sub>1</sub>
Sensor Bias	1				x		x	103
FW Servo	†	1	1	T		T	1	
Amp, Output	+3	<del></del>			X			<u> </u>
		ONLY	REQUIRED F	OR INTERFA	CE WITH	POSSIBLE E	APERIMEN'	15
Switch FW	<b>.</b>					ļ	*	1
To IS Seitch FW	+	· · · · · · · · · · · · · · · · · · ·						<del></del>
to Monopulse	1.		1				1	
18 Peror 18 Nulls					*	*		
	ľ		1		1 ***		1	
Манариће	ı	1	1	1		1 .	4	1
Manopulse Execus Vanopulse	1.		Į.	1	``	1 '	1	

## 5.5.4.3 Programmer

#### 5.5.4.3.1 General

In order to meet pointing accuracy requirements, it is necessary to account for the apparent 0.9-degree radius circular motion of Polaris as the orbit is traversed. In order to accomplish this, either the Polaris star sensor or earth sensor command angles must be periodically updated. To keep the error introduced by this apparent motion to an acceptable level, the updatings must occur at intervals of no longer than 1 minute. Since it is not desirable nor feasible to require the continuous operation of a ground station for the generation of these commands, an onboard programmer will be provided for this purpose. The programmer operation would be synchronized periodically from the ground.

Since the command angle updating of the earth sensors is also required to account for actual station latitude and longitude this sensor was chosen to accept the programmer corrections. It will, however, still be necessary to provide command angle information to the Polaris star sensor in order to electronically gimbal the 4 x 4 degree field of view in conjunction with reorientation commands.

#### 5.5.4.3.2 Requirements

The programmer must provide the following bias command functions to the pitch and roll earth sensor channels:

Roll Command Function:  $(90 - \delta) \sin (W_e^t + \phi) \sin \phi_c$ Pitch Command Function:  $(90 - \delta) \sin (W_e^t + \phi) \cos \phi_c \sin \phi_c$ where  $\delta$  = declination of Polaris, 89.09 deg  $\phi_c \theta_c$  = Roll and Pitch command angles ranging from 0 to  $\pm$  8.7 deg

The resolution of the above command functions is required to be at least 0.02 deg.

#### 5. 5. 5 MOUNTING AND FIELD OF VIEW INTERFACE

The orientation control sensors and thrusters must be mounted and aligned with a high degree of accuracy so that alignment errors do not contribute significantly to total system inaccuracy. Sensor field of view requirements must be met in order to assure correct and continual operation of the orientation control system over the design range of spacecraft attitudes. This field of view requirement may be the result of the field over which the sensor should be able to view its stimulus. For instance, the sun sensors should have spherical field of view so as to provide control signals from any spacecraft orientation. Having objects protrude into the spherical field of view of the sun sensors causes blind spots. The consequence of these blind spots depends upon where they exist with respect to the null plane of the sensors. Other sensors which new to view their stimuli over only a portion of the celestial sphere may require an unobstructed field of view greater than that required to merely view the stimuli. For instance, the unobstructed field of view require for the Polaris Star Sensor to view Polaris is 1.8 x 19.2 degrees solid angle; however, the required unobstructed field of view is greater than this in order to avoid having reflected light enter the sensor optics. A sun shield will be required for the Polaris Star Sensor. The requirements of the sun shield become increasingly severe as the unobstructed field of view is decreased. The sensor fields of view for the selected spacecraft configuration are discussed below.

- a. <u>Earth Sensor</u>. The actual unobstructed field of view is considerably greater than the 20 x 20 degree solid angle required.
- degree rectangular field as shown on Figure 5.5-30. A solar panel presents the first obstruction in the sensor's field of view. This occurs at an angle of 30.5 degrees which is well outside the field of view required for viewing Polaris. The sun shield must be designed to avoid the effect of reflected sun light introduced at an angle of 20.9 degrees from the starline. Based on experience with the OAO star trackers, this is expected to pose no serious problem.
- c. Pitch and Roll Sun Sensors. The four pitch sun sensors can theoretically provide control signals to control the attitude about the pitch axis regardless of the roll attitude. The same can be said for the four roll sun sensors. However, the gain of the sun sensors decreases in accordance with the cosine of the angle between the sunline and the null plane of the sensors. For instance, when the roll axis is 60 degrees from being perpendicular to the sunline, the output of the pitch sun

sensors is reduced to 0.5 of the output when the roll axis is aligned perpendicus to the sunline. In addition, since both the pitch and the roll sun sensors each ideally spherical coverage, there will actually be no blind spots in control of the spacecraft unless the protrusions cause a blind spot for the pitch and roll sensor. simultaneously; provided that the blind spots do not occur in the null plane of the pitch or roll sensors. As shown on Figure 5.5-31 for the folded configuration, the sun sensors have unobstructed fields of view out to 64 degrees from the null plane for the pitch sensors and no obstructions for the roll sun sensors mounted on the aft equipment module. The fields of view for the sun sensors mounted on the earth viewing equipment module have fewer obstructions than those mounted on the primary equipment module. These obstructions in the sun sensor fields of view will have no consequence on sun stabilization of the pitch and roll axes for the folded configuration. For the deployed configuration, when these sun sensors are used for restabilization, the solar panels and antenna are a significant obstruction in the sensor fields of view which will cause blind spots even in the null plane. This will not, however, prevent stabilization to the sun. It may, depending upon spacecraft attitude and rates, require actuation of the thrusters by ground command to provide conditions conducive to capture.

- d. Yaw Sun Sensors. The four yaw sun sensors also theoretically provide a spherical field of view. However, the yaw axis is aligned to the earth when these sensors are used and, therefore, only a limited field of view is required. The initial obstruction in the yaw sun sensor field of view is the solar array. This is the same appears 17.7 degrees from the null plane as shown in Figure 5.5-42 and the reflected light will be attenuated from that received by the same sensor direction the sun and because the reflected light will be basically symmetrical as experienced by the sun sensor when the attitude about the yaw axis is controlled to the sun, the reflections are not expected to pose a serious problem. A sun reflection shield could be provided if necessary.
- e. <u>Station Acquisition Sun Sensor</u>. The actual unobstructed field of view is in excess of the required field of view as shown in Figure 5.5-32.

The mounting, alignment and field of view requirements of the various sensors and thrusters are presented in Table 5.5-11.

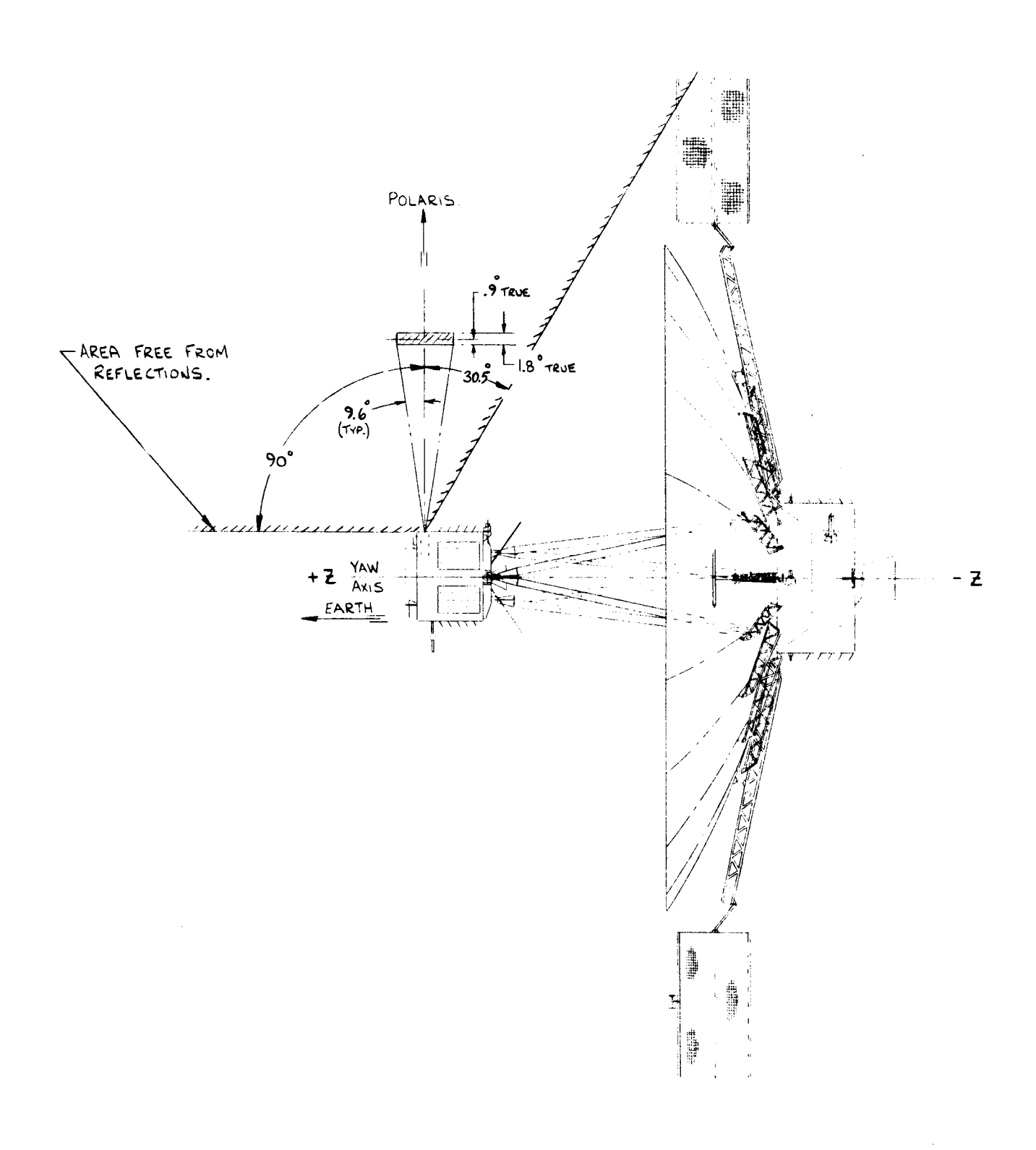


Figure 5.5-30. Polaris Sensor View Angles

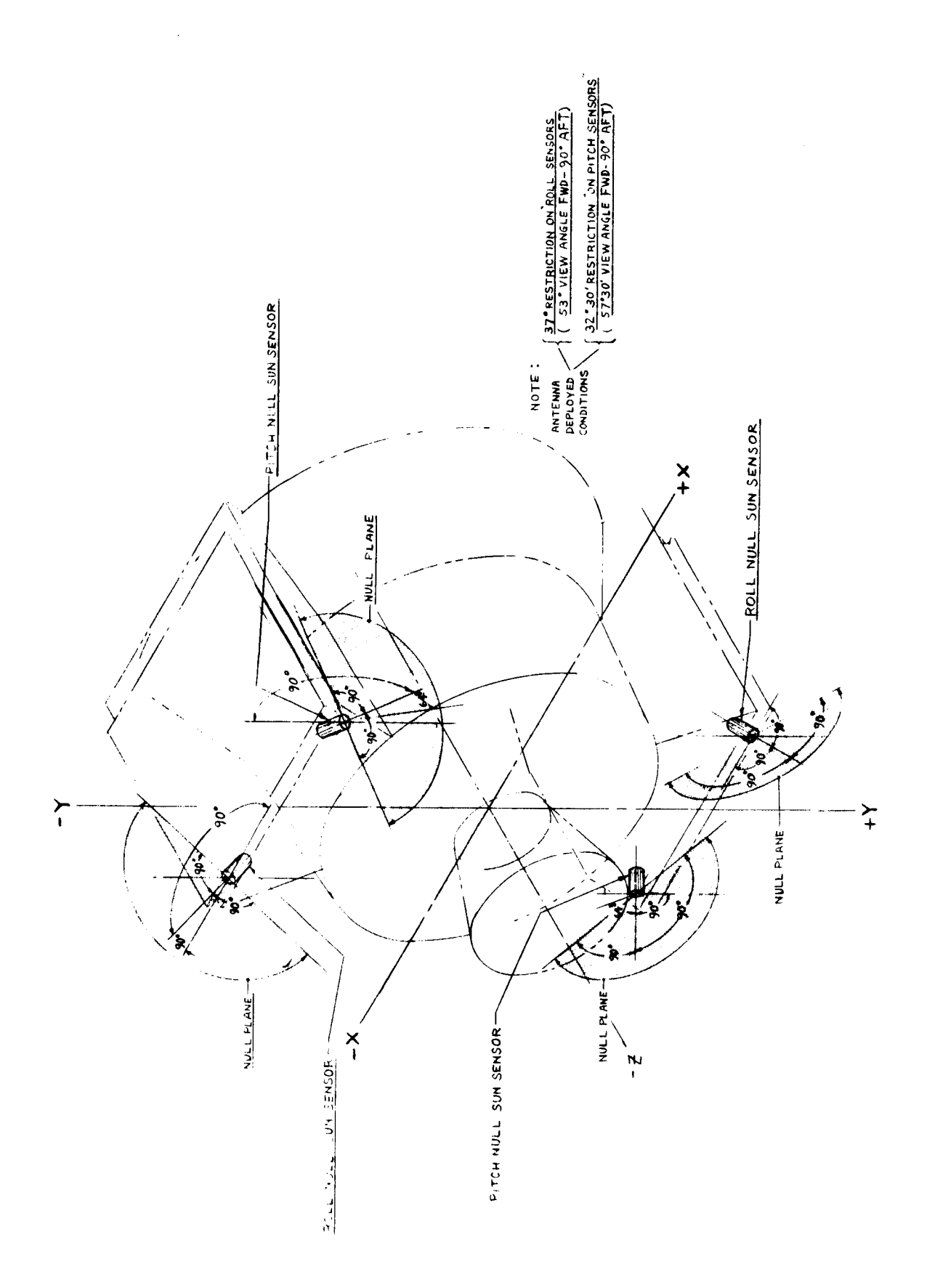


Figure 5.5-31. Pitch and Roll Sun Sensors Fields of View

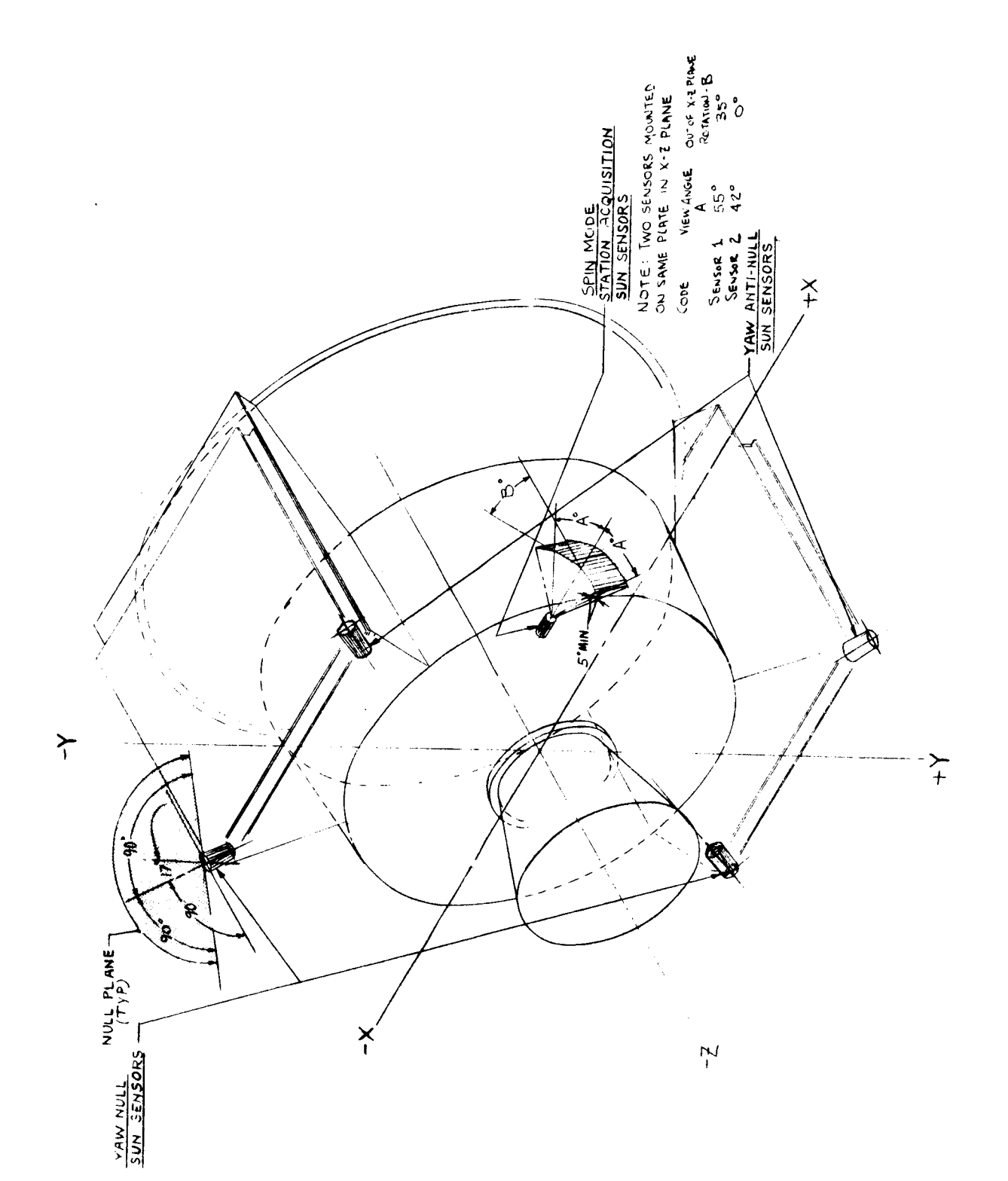


Figure 5.5-32. Station Acquisition and Yaw Sun Sensor Fields of View

# Table 5.5-11. O/C Component Mounting, Alignment and Field of View Requirements

FIELD OF VIEW REQUIREMENTS	Each set of four eyes must be distributed about the spacecraft such that it has, in sum, an essentially spherical fiteld of view prior to and after deployment. The location of the eyes shall be such that shading by and reflections from the various protuberances of the spacecraft are minimized.	Each set of four eyes must be distributed about the spacecraft such that it has, in sum, an escentially sherical field of view prior to and after deployment. The location of the eyes shall be such that shading by and reflections from the various protuberances of the spacecraft are minimized.	None	The location of the earth sensor shall be such that shading by and reflections from the various protuberances of the spacecraft do not occur within a ± 25° square of a line parallel to the spacecraft yaw axis and passing through the earth sensor pitch and roll null point.
ALIGNMENT REQUIREMENTS	The pitch (roll) eyes shall be aligned such that their normals make angles of 50 degrees with the negative yaw axis (null set) and 30° with the positive yaw axis (anti-null set) The pitch (roll) angles shall be measured in a plane parallel to the plane of the roll-yaw (pitch-yaw) control axes.  The pitch (roll) sun sensors shall be aligned such that the sensor null occurs within 2 arc minutes of the spacecraft yaw axis.	The yaw eyes shall be aligned such that their normals make angles of 50 degrees with the negative "roll" axis (mill set) and 30° with the positive "roll" axes. The angles shall be measured in a plane parallel to the plane of the pitch-roll control axes. The "roll" axis is defined by a positive yaw rotation of the roll axis through an angle measured in the pitch-roll control axis plane and equal to the angular difference in sunlineer the angular difference in sunlineer the time of launch. The yaw sun sensor shall be aligned such that the sensor null occurs within 2 arc minutes of the "roll" axis.	The gyros shall be aligned such that their input axes are perpendicular to their respective mounting fixture axes within 8 arc minutes. The pitch, yaw and roll mounting fixture axis shall be aligned to the spacecraft control axes within 7 arc minutes	The earth sensor shall be aligned such that the null plane of the pitch channel defines a plane parallel to the yaw-pitch plane, and the null plane of the roll channel defines a plane parallel to the yaw-roll plane of the mount. The mount shall be aligned such that the yaw-pitch plane and the yaw-roll plane of the mount are within 10 arc seconds of the respective spacecraft control axis planes.
MOUNTING	Two sets of eyes)  (one pitch, one roll)  mounted on each end of the spacecraft yaw axis, each eye mounted separat- ely.	One set of eyes mounted on each end of the space-craft roll axes, each eye mounted separately on the primary control compartment.	Mounted in the control compartment	The earth sensor shall be mounted in the control compartment on the positive end of the space-craft yaw axis.
COMPONENT NAME	Pitch and Roll Sun Sensors	Yaw Sun Sensor	3 Axis Gyro Package	Earth Sensor
METI	-	~	n	4

Table 5.5-11. O/C Component Mounting, Alignment and Field of View Requirements (Continued)

FIELD OF VIEW REQUIREMENTS	The location of the star sensor shall be such that shading by and reflections from the various spageraft protuberances do not occur within a 29 half cone angle of the optical axis of the sensor.	None		The sensgr field-of-view must be unobstructed for ±45 along the yaw axis and ±60 along an axis 35° from the yaw axis.	None
ALIGNMENT REQUIREMENTS	The star sensor shall be aligned such that the pitch, yaw and roll axes of the sensor are parallel to the pitch, yaw and roll axes of the spacecraft within 10 arc seconds.	Each unit shall be aligned such that its spin axis is parallel to its respective control axis within 10 arc minutes.	The roll (pitch, yaw) thrusters shall be aligned such that the thrust vector is within a 30 arc minute half come angle of a perpendicular to a plane which contains respectively the roll (pitch, yaw) axes. This tolerance must be reduced if the thrusters are displaced from the pitch-yaw (roll-yaw, roll-pitch) plane.	The sun sensor assembly shall be aligned such that the $\psi$ sensor has its wide field-of-view axis aligned along the yaw axis to within 0.3 .	The accelerometer shall be aligned such that its sensitive axis is perpendicular to the yaw axis within 6 arc minutes and perpendicular to the roll axis within 0.30
MOUNTING	Mounted on the negative end of the spacecraft pitch axis.	Three units mounted in the control compartment, one per axis.	These will be mounted on the extremities of the spacecraft structure so as to acquire a torque compatible with the flywheels. The thruster shall be mounted so as to provide acceptable plume clearance with the spacecraft structure and shall not be mounted on any deployable structure.	Mounted on the outside of the pri- mary control compartment	Mounted in the primary control compartment with the input axis parallel to the pitch axis
COMPONENT NAME	Polaris Star Sensor	Flywheels	Mass Expulsion Thrusters	Initial Acquisition Sun Sensor	Accelerometer
Mati	<b>⊬</b> ∩	9	L	œ	თ

# 5.6 EXPERIMENT EQUIPMENT

### 5.6.1 GENERAL

The experiment equipment (listed below) is that equipment which is used for one of the prime experiments.

Experiment Equipment Summary

Prime Experiment	Experiment Equipment	Weight (lb)	Power (watts)
Parabolic Antenna	Instrumentation to measure geometric configuration and dynamic behavior. RF equipment for measurements.	86.6	80
	Electronics - transmitters receivers, electronic switches, etc for measurements, standard gain antennas.		
Orientation Control System	Incorporated in orientation control system.	NA	NA
Interferometer	Interferometer antennas and electronics. Instrumentation to measure geometric distortion. Instrumentation to monitor dynamic behavior:	35	39.25*
Phase-Steered Array Antenna	Antenna elements and electronics. Internal monitoring equipment for measuring.	100	420

Because of the peculiar circumstances surrounding the development of the various prime experiment equipments, the depth and detail of discussion of this equipment in this section will not be uniform from one experiment to another. The parabolic antenna system, for

<sup>\*</sup>For planning purposes, it was assumed that the low-power circuitry will not be available, so that the power required rises to about 39.25 watts. This results in more conservative estimates of power requirements. In the discussion of the interferometer in this section, availability of low-power circuitry is assumed.

example, because of its complexity and importance, is considered separately as a major system (Section 5.4) and is described in considerable depth. The separate experiment equipment required, electronics, rf equipment, etc., while necessary and important, is not as critical as the antenna itself, and, therefore, exhaustive discussion is not required to prove that the experiment objectives can be met.

Somewhat the same situation exists with respect to the orientation control system. This system is discussed thoroughly, virtually in its entirety, in the section devoted to that purpose. It is necessary only to summarize in this section.

The phase-steered array is to be furnished, and its characteristics were specified. The technical characteristics are well described in the referenced technical reports, and are summarized here merely for convenience.

With the radio interferometer, somewhat more detail is required. The characteristics of the interferometer are intimately connected with successful and efficient performance of the prime experiments, and since the detailed discussion of the proposed equipment has been submitted in a separate publication, a comprehensive summary is provided here.

### 5.6.2 PARABOLIC ANTENNA

### 5.6.2.1 General

The parabolic antenna system is described in Section 5.4 of this report. The antenna is a 30-foot diameter paraboloid, petalline structure, designed to provide nearly full gain at frequencies up to 10 GHz. Evaluation of the parabolic antenna, and validation of the design, constitute the objectives of the parabolic antenna prime experiment; perhaps the most important and difficult of the four prime experiments. The measurements required to achieve these objectives are discussed in some detail in Section 8. The major requirements are:

- a. Monitor Deployment
  - Verify successful deployment
  - Analyze any significant malfunction
  - Verify that the dynamic behavior during and after deployment involves no significant anomalies
- b. Measure the geometric behavior of the antenna
  - Static configuration
    - . Thermal deformation
    - . Any anomalies in dynamic behavior which are severe enough to significantly affect the antenna performance
  - Basic electrical characteristics
    - . Gain
    - . Boresight
    - . Secondary radiation patterns
  - Antenna/feed system performance
    - . Distortion, as a function of bandwidth
    - . Tuning range
    - . Efficiency

The onboard equipment for the parabolic antenna experiment must be designed primarily to support the above the above measurements. This equipment will fall mainly into the following categories:

- a. <u>Electronics</u>. Transmitters, receivers, signal and data processing equipment, switches, and power level measuring equipment.
- b. RF Equipment. Directional couplers, diplexers, rf attenuators, etc. which are required for measurement rather than being part of the antenna system per se.

c. Geometric and Thermal Instrumentation. Such instruments as thermisters, strain gauges, and other devices for measuring temperatures, geometric characteristics and dynamic behavior.

# 5.6.2.2 Electronics and RF Equipment

a. <u>Subsystem</u>. The onboard communication subsystem required for the large parabolic antenna experiment is illustrated in Figure 5.6-1. The characteristics of the equipment are summarized in Table 5.6-1.

The large antenna consists of a 30-foot diameter parabolic reflector, three conical feed horns for L, S, and X-Band which are combined in coaxial configuration, and a turnstile feed for 100 MHz.

Each horn feed has two terminals, i.e., it can accept a receive or transmit channel. The subsystem employs three receivers and four transmitters capable of receiving and/or transmitting at the specified frequencies tunable over a 10 percent frequency range and at a minimum bandwidth of 8 to 30 MHz from vhf through X-Band, respectively. Any one of the receivers may either operate by itself with measurements of its output characteristics telemetered to ground, or may feed any one of the transmitters for transmission to ground (over a wider bandwidth). Any one of the transmitters may also operate separately or in combination with a receiver.

The connections between receivers and transmitters are accomplished by two command-controlled, multiposition coaxial switches. Each switch position will be telemetered for command verification.

To provide verification of a received signal, each receiver will be associated with a power detector that will pick up a signal from one of the front-end stages of the receiver.

To measure forward and reflected power in the transmit channels, a directional coupler in combination with two power detectors will be placed in the transmission line between transmitter and antenna feed. Also in series with the directional couplers will be commanded coaxial switches that will connect the transmitters either to the parabolic antenna feeds or to the standard gain antennas in order to measure antenna gain. One standard gain horn will handle L or S-Band frequencies and one will operate on X-Band frequencies. Two standard gain antennas will be utilized for 100 MHz and 800 MHz, respectively. The power detectors will be utilized to complement the gain measurements by measuring power flow either to the large antenna or to the standard gain antennas. The power detector outputs will be telemetered to ground and used in making link power budget checks, as well as backup gain measurements.

Table 5.6-1. Large Parabolic Antenna Experiment Equipment Characteristics

Component	Weight (lb)	Volume (Size-in.)	Power (watt)	Duty Cycle	Heat Dissi- pation (watt)	Temp. Range ( <sup>O</sup> C)
		*	<del> </del>			
		SUMM.	ARY T			
Receivers (3)	13.5	32.6 cu in.	12.06	Variable	12, 66	-10 ± ma
Transmitter				1		
100 MHz	5.0	32.38 cu in.	30	Variable	26	
Transmitter			} }			
800 MHz	9,0	24.16	30	Variable	20	
Transmitter				i		
2300 MHz	10.0	75.38	50	Variable	40	
Transmitter						
7300 MHz	15,0	123,38	70	Variable	60	
Switches	17.0	28.8	-	Variable	-	
Multiplexers (2)	1.0	48	-	Variable	-	
Standard Gain Antenna	9.0	NA.	-	Variable		
Reflector Instrumen-						
tation	4.1	NA.	-	Variable	-	
		RECEIVER (L,	S. X-BA	ND)		
			1	, , , , , , , , , , , , , , , , , , ,	Ì	
Limiter	0.2	0.75 dia. x 3	-	Variable	-	
TDA	0.2	4 cu in.	0.5	Variable	_	-35 - ±85
YIG Filter	0.5	1,2 cu in.	0.2	Variable		-20 - +80
Tuning Control	0.4	2 cu in.	0.5	Variable	- !	
Power Detector	0.5	2 cu in.	0.5	Variable	-	
Coupler Isolator	0.1	1.5 x 1 x 0.5	-	Variable		-55 - +125
Mixer/Preamp	$\frac{1.0}{0.2}$	2.5 x 1.2 x 1.2	-	Variable	-	-40 - +105
VTO		3 cu in.	0.05	Variable	-	-55 - +100
Tuning Control	0.5 0.5	5 cu in.	1.0	Variable	- 1	-50 - 470
Main IF Amp	0.3	2 cu in.	0.5	Variable		
Coupler :	0.1	3 cu in.	0.1	Variable	-	-55 - 4100
Limiter/		1,5 x 1 x 0.5	-	Variable		-55 - +125
Discriminant	0.1	3 cu in.	0.17	Variable	_	-55 - +100
Amplifier	0.1	1 cu in.		Variable		
Total ·	1.5	32.6 cu in.	0.5 4.02	variane	-	
	<u></u>	RANSMITTER DRIV	ER/P.A.	STAGES		
\$7 L.C						
Vhf Uhf	1.0	5 cu in.	25, 3	Variable	15, 3	-55 - +100
2300 MHz	2.9	5 cu in.	25, 3	Variable	15, 3	· 55 - +100
7300 MHz	3,9	48 cu in.	45.3	Variable	35.3	-55 ~ +100
TOOU MILE	8.9	96 cu in.	65, 3	Variable	55, 3	-55 - +100
	SWIT	CHING AND MULTH	LEXING	EQUIPMENT		
Position Coax (10)	10	257 cu in.	-	Variable	-	· 55 = +100
** Electrical						
Switch Package	7	30.75 cu in.	-	Variable		- <b>55</b> - +100
Multiplexers (2)	4				1	
	'1	48 cu m.	-	Variable	-	-55 = +100

Table 5.6-1. Large Parabolic Antenna Experiment Equipment Characteristics (Cont'd)

Component	Weight (lb)	Volume (Size-in.)	Power (watt)	Duty Cycle	Heat Dissi- pation (watt)	Temp. Range ( <sup>O</sup> C)
		STANDARD GA	AIN ANTE	NNAS		
		\$1.4 (\$\frac{1}{2}\$\)				
Standard Gain Dipole 100 MHz	2	NA (Excitation of solar paddle)	-	Variable	-	-55 - +100
Standard Gain Dipole 800 MHz	2	Length - 3 in.	-	Variable	-	-55 - +100
L. S-BD Standard Gain Horn and X-Band Standard		Coaxial; Length - 12 in. Aperture dia-				
Gain Horn	ā	meter - 9 in.	-	Variable	-	-55 <b>-</b> +100
	. (OIN A NG 3 1 1 1 1 1	oppy duties at 6 V	DAND, LO	W DOWND	em A C De	
IYPICA	I. TRANSMIT	TER (UHF, L,S, X-	BAND LO	W POWER	STACIFE	
Ferrite Switch	0.5	2.1 x 1.1 x 1	10 (for 50μ sec)	Variable	-	-20°C - ±80°C
Switch Control	0.5	2 cu in.	0.5	Variable	-	-200C - +80 <sup>0</sup> C
Fixed Frequency Power Source	1.0	5 cu in.	1.0	Variable	-	-20°C - +80°C
UP Converter	0.5	5 cu in.	1.0	Variable	_	-20°C - 180°C
VTO	0.5	5 cu in.	1.0	Variable	-	-20°C - +80°C
Tuning Control	0, 5	2 cu in.	0.5	Variable	_	-20°C - +80°C
YIG Filter	0.5	1.2 cu in.	0.2	Variable	-	-20°C - +80°C
Tuning Control	0.5	2 cu in.	0.5	Variable	-	-20°C - ±80°€
Coupler	0.1	$1.5 \times 1 \times 0.5$	-	Variable	***	-20°C - ⊤80°C
Bandpass Filter	0.5	$2.5 \times 1.7 \times 0.5$	-	Variable	-	-20°C - +80°C
Isolator	1,0	2,5 x 1,2 x 1,2	-	Variable		$-20^{\circ}C = +80^{\circ}C$
	<u>T7</u>	PICAL TRANSMITT	ER (VHF)	LOW POW	ER STAGES	
Ferrite Switch	0, 5	2.31 cu in.	10 (for			
tottic swiren	V/• +)	J. 07 CM III.	50 μsec)	Variable	_	-20°C - +80°C
Switch Control	0.4	1.8 cu in.	0.5	Variable	-	$-20^{\circ}\text{C} - 480^{\circ}$
Fixed Frequency Power Source	0.8	4.0 eu in.	1.0	Variable		-20 <sup>0</sup> C - +80 <sup>0</sup>
UP Converter	0.5	1.0 cu in.	1.0	Variable	_	-20°C - 480°
VTO	0.3	3 cu in.	1.0	Variable	_	-20°C - +80°
Tuning Control	0.3	1 cu in.	0.5	Variable	_	-20°C80°
Filter	0.2	1 cu in.	0.2	Variable		$-20^{\circ}C - +80^{\circ}$

Summary shows total weights. Individual breakouts are included in Summary.

** Ferrites (5)	- 2,5 lb
Power Det. (8)	4.0 16
Directional Coupler (5)	0.5,16
Total	7,016

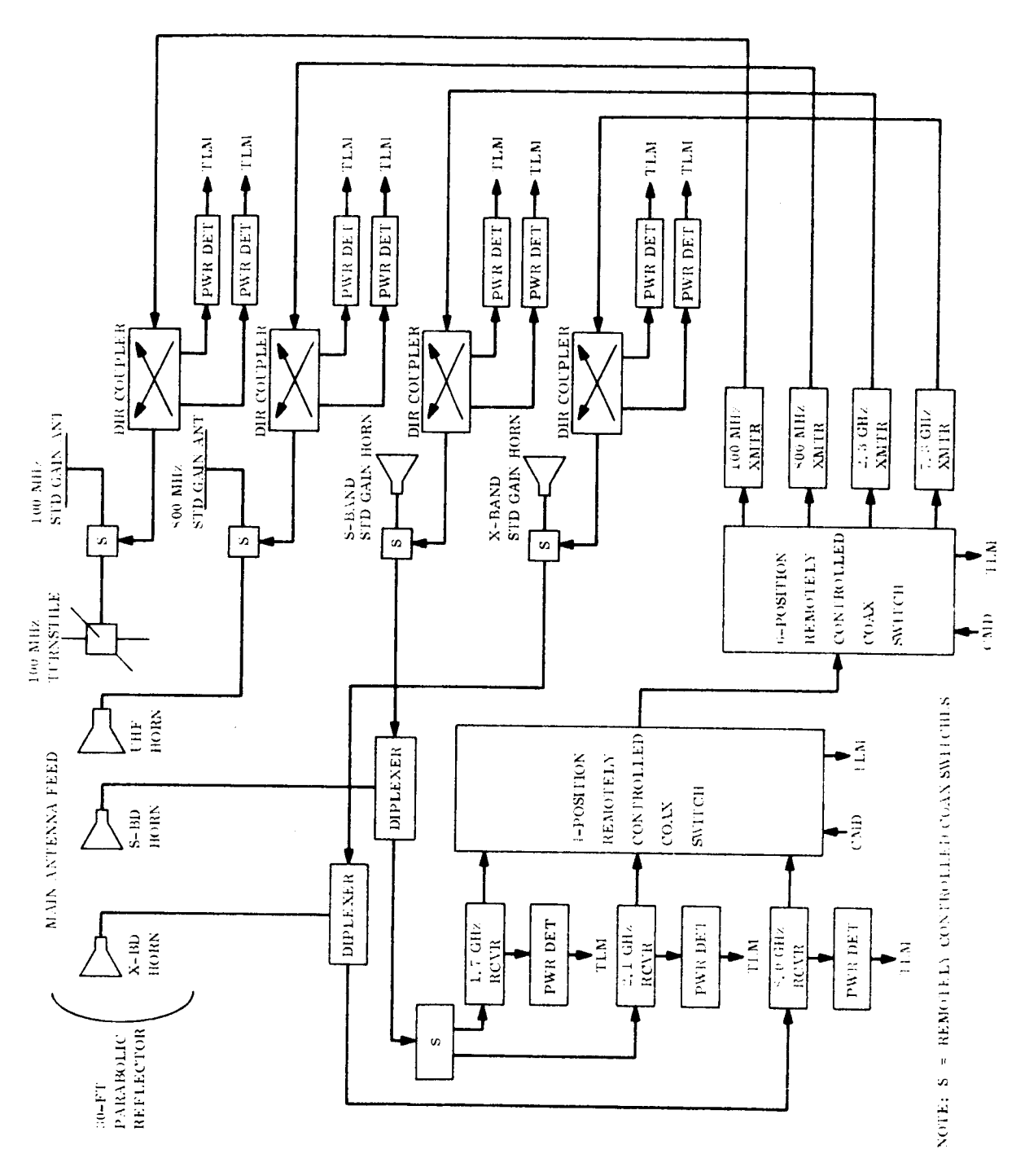


Figure 5.6-1. Large Parabolic Antenna Experiment

All switching functions required during the measurements will be initiated by command signals from ground. The TT&C subsystem operates independently of the experiment electronics subsystem for the large antenna experiment and is not shown in Figure 5.6-1. However, a transponder combination of the communication subsystem at S-Band may be used as a backup for ranging information using ATS range and range rate equipment.

All significant functions in the subsystem components will be telemetered as diagnostic data for evaluation on the ground.

- Receivers. All the receivers will consist of solid-state components throughb. out. Figure 5.6-2 illustrates in detail a typical receiver for L, S, or X-Band. The received signal from the horn feed is preamplified in a tunnel diode amplifier (TDA) after it has passed a diode limiter to prevent burnout of the TDA. Since the TDA is a wideband amplifier that covers the whole 10 percent tuning range, a tunable YIG filter acts as a preselector filter that is tuned by the tuning control unit. A preselected number of receive frequencies may be tuned by command. The signal is then down-converted to an intermediate frequency (IF) by a mixer-preamplifier associated with a voltagetuned oscillator, which in turn is tuned by a tuning control unit that is actuated by commands. The coax isolator prevents spurious frequencies from entering the YIG filter. The IF signal is further amplified in the IF amplifier whose output is either coupled out to the multiposition coax switch, to enter a transmitter, or coupled to a signal demodulator. The demodulator consists of a limiter and discriminator-amplifier. The demodulated signal is then telemetered to ground.
- Transmitters. The details of a typical transmitter are illustrated in Figure 5.6-3. The 100 MHz and 800 MHz transmitters will provide approximately 10 watts output; they will consist completely of solid-state circuits. Their circuitry, and especially the packaging, will deviate somewhat from the L, S, and X-Band transmitters; however, their building blocks will be essentially identical, with the exception of the power amplifier, containing a traveling wave tube (TWT) of approximately 10 watts output. The transmitter may operate in two modes. Either an IF signal from a receiver will be up-converted in frequency by a mixer and VTO, which is tuned by a remotely-controlled tuning control, or a fixed frequency from a local oscillator will substitute for the IF signal. The signal from the up-converter will then be filtered by an electronically controlled YIG filter, similar to the one used in the receiver, and will then be preamplified after passing through a coupler, and amplified to its proper power level in a power amplifier. The output signal of the power amplifier will pass a bandpass filter and isolator before it feeds the large antenna for transmission to ground. Provision will be made to couple a second signal with a different frequency to the preamplifier and power amplifier. This signal will come from a separate signal generator unit and may be designed to cover, for example, the S-Band range. It may be considered as an added feature. The signal generation unit will consist of a fixed-frequency power source,

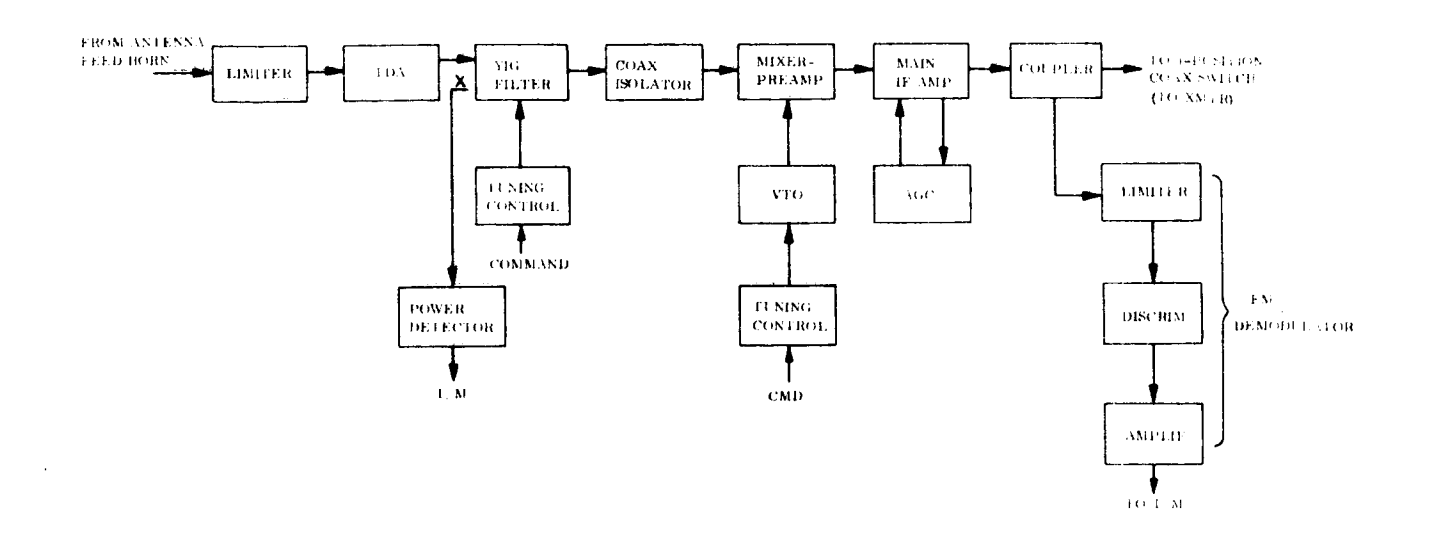


Figure 5.6-2. Typical Receiver

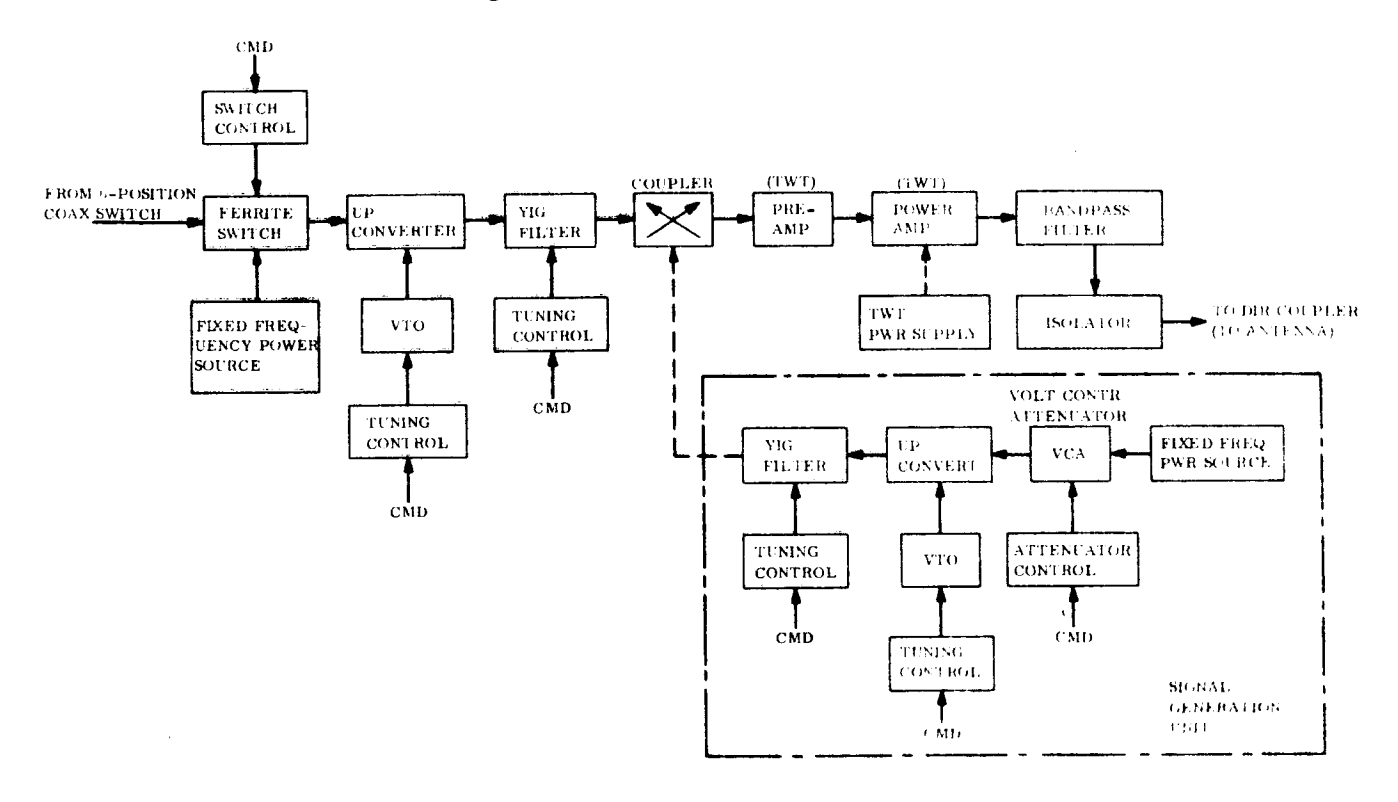


Figure 5.6-3. Typical Transmitter

a voltage-controlled attenuator, an up-coverter, a voltage-tuned oscillator (VTO), and a tuned YIG filter with tuning control. By passing two independent signals through the power amplifier, effects of intermodulation and phase shift may be studied. The two frequencies may be located at the extreme ends of the specified 10 percent tuning range. The power amplifiers, which contain TWT's, will require a separate power supply; all other components may be designed to draw their prime power from the regulated bus.

d. Standard Gain Antenna. The spacecraft carries four standard gain antennas as references against which the large antenna may be measured. Two of the antennas are conical horns similar to those used in the primary feed system; these are mounted on the face of the Earth Viewing Equipment Module. The complete coaxial set of three was not employed since the diameter of the 800 MHz horn is too large for convenient installation. The 800 MHz standard gain antenna is a sleeve dipole mounted on the edge of one of the pitch axis solar panels, and uses the panel as a reflector. The 100 MHz standard gain antenna is realized by shunt feeding the roll axis solar panel as an antenna.

In addition to the coaxial horn pair mounted on the face of the equipment module, there are four other antenna systems of varying complexity, namely:

- 1. Interferometer
- 2. Phased Array
- 3. TT&C Cavity

Although the layout of the various antennas was chosen to minimize mutual coupling effects insofar as possible, the freedom of location was too restricted to reduce all of these to completely negligible amounts. This means that pattern studies must be carried out when the spacecraft is built in order to assess these effects properly. Insofar as the standard gain horns are concerned, such effects are not harmful provided they are known, so that proper calibration of the patterns may be made.

The same condition holds true for the standard gain antennas which utilize the solar panels. Their patterns may be determined from scale model measurements of the entire spacecraft, with absolute calibration being made against standard laboratory horns.

Design details of the various standard gain antennas are given below.

1. Coaxial horn pair: covers 1700 to 8000 MHz

Aperture diameter: 9 in. Length: 12 in. Weight: 5 lb 2. Sleeve Dipole: 800 MHz

Length: 7 in.

Height of mounting support: 3 in.

Weight: 2 lb

3. Shunt feed for solar paddle: 100 MHz
Consists of 1/4 in. conductor, spaced 1 in. off edge of solar paddle.
Length approximately 40 inches, terminating in connector at end of paddle.

Weight: 2 lb

# 5.6.2.3 Geometric Instrumentation

The geometric monitoring instrumentation is listed in Table 5.6-2. This instrumentation is chosen to perform the following functions:

- 1. Verify deployment
- 2. Detect and identify any significant deployment malfunctions
- 3. Detect and identify any thermal or static distortions large enough to significantly affect the required performance of the antenna
- 4. Detect and measure any vibrations large enough to significantly affect the required performance of the antenna

Two subcommutators are provided for those measurements which must be made while the antenna is being deployed. The microswitches will close when significant discrete actions have been completed in the deployment process, e.g., deployment arms locked into their final positions, hinge lines in position. The strain gauges will record stress-induced displacements as deployment proceeds, and any abnormal stresses after deployment has been completed.

The thermistors will provide a continuous temperature map of the paraboloidal surface, a number of front-to-back temperature gradient measurements, and temperatures at a number of points along and about the structure, including the support struts, and the feed assembly. A number of thermistors will perform two functions by being placed beside strain gauges: contributing to the temperature field measurements and providing data for temperature compensation of the strain gauges.

Table 5.6-2. Geometric Instrumentation

Instrument	Purpose	Number Required	Weight Each (1b)	Weight Total (lb)	Power Each (watt)	Power Folal (watt)	Data Rate Each (bps)	Data Rate Total (bps)	Accuraes	Lecations	Consment
Microsofich	To verify final loca- tion of structural n embers after deployment	eg G	-	٠,	Negligible	Negligible	NA	NA	NA	Magnetic clutches. joint in de- ployment arms. hinge lines	Sampled once at de- ployment, then as required for trouble shooting, i but per sample per unit
Stain Cauge	To determine stresses in structural rembers during and after deployment	91	Negligible	, p. n5	20 e	1.52	0.1	ca @ 89 : 17 1:	10-20 L in in	Deployment arms, struts, artenna surface (one panel neavity instrumented, the others very lightly	During deployment At intermittent in- tervals after de- ployment
Them serve	To provide temperature field and data for temperature compensation of strain gauges	3.02	Negligible	<0,45	10.0	1.02	0.0544	<b>6</b> .5	3 5	the by each strain gauge, others on antenna surface, on feed structure, and one by each accelerometer	
Accelerometers	To measure vibration and damping wherever amplitudes exceed allowable thresholds	T.	0, 25	6)	0.1	0.8	24	224	6 x 10 - 4 g	At points of maxi- mum displacement on reflector	
Voltage Pickoff	To measure torque motor voltage during deployment	1	:	1	-	ŀ	I-	P-			
('ur <b>re</b> nt Pickoff	To measure torque motor current during deployment	-	ì	1	1	1	t-	1-			

The accelerometers are designed to measure significant vibrations. (It is anticipated that with rare exceptions, vibrations will be at or near the minimum detectable levels, but detection of any significant disturbances will be quite important.)

The thermistors will be designed for absolute accuracies of approximately  $5^{\circ}F$  absolute and  $2^{\circ}F$  or better relative (i.e., temperature changes) over a temperature range of from  $+100^{\circ}F$  to  $-200^{\circ}F$ . Interspersed will be a number of multielement installations designed to provide absolute accuracies of  $2^{\circ}F$  or better, as reference values from which the other thermistors can measure. Thermistors are very small resistors with a reverse temperature-resistance characteristic. They will be intimately bonded to the structure so that exact temperatures can be obtained. The thermistor will be in the 200-ohm range and will be installed in a simple circuit with voltage control by a zener diode which provides excellent long-term voltage stability. Each circuit will be calibrated so that close piece part tolerances will not be required and the close overall accuracy is still obtained.

The hinge lines will be monitored with at least one strain gauge and one thermistor each. In addition, microswitches will be placed in selected locations on the deployment structure joints and the magnetic clutches and strain gauges on the structural members which carry loads during deployment, and on the struts and other members whose normal loading will be important during experiment operations. One panel will be heavily instrumented with thermistors and strain gauges (at least 10 of each), the others lightly. This is a compromise between the desire to have complete information and the incorporation of an excessive number of instruments.

The strain gauges being considered are small wire or foil elements which will be bonded to the structure. Thus, any deflection of the structure will cause a corresponding elastic change in the sensing element. Most gauges would be installed in bridge circuits which will provide better accuracy and compensate for temperature variations. A thermistor will be mounted adjacent to the strain gauge installation as an additional check or compensation for temperature variations. These thermistors will be part of those used in obtaining the temperature map described above. Strain measurement accuracies of the order of  $10-20~\mu-in./in.$  can

be obtained, with good temperature calibrations. The miniature microswitches will be normally open and will close upon successful closure of the hinges.

Approximately eight accelerometers will be distributed about the reflector, to verify that vibration amplitudes are within tolerances and to obtain approximate measurements of frequencies and damping characteristics. These will be inertial-quality accelerometers with preamplifiers mounted to the accelerometer or very nearby. The two to three cubic inch accelerometer, which weighs approximately 4 ounces, will not adversely affect the response of the large structure. Some temperature insulation, such as a multilayer aluminized mylar blanket, might be required, but it appears at present that active temperature control (i.e., heaters) can be avoided. Temperature changes would affect long-term accuracy of the accelerometer, but short-term data will be within the accuracy required. A thermistor will be located on each accelerometer.

### 5.6.3 ORIENTATION CONTROL SYSTEM

The Orientation Control System is described in some detail in Section 5 of the present report. This description covers the Orientation Control System operation during the entire life of the satellite. However, this section will be concerned only with on-station operation, the period during which the Orientation Control prime experiment is to be performed.

The Orientation Control System is an active three-axis orientation control system which is designed to meet the requirements of the Orientation Control prime experiment. Three-axis orientation control is achieved on station using earth sensors (ATD Apollo Sensor with MOGO electronics) for pitch and roll axis control and a Polaris star sensor (probably a Canopus tracker) for yaw. Orientation control torques are provided by mechanical flywheels, unloaded by the integrated wheel unloading-stationkeeping mass expulsion system.

Slight additional equipment is required to permit substitution of other qualified pointing sensors (i.e., the radio interferometer) in the control loop in place of the earth sensors. This equipment is relatively simple; the major requirements are reliability of operation and careful design to ensure that impedances, bandwidths and other crucial signal and electrical parameters of the other sensors are suitable.

The equipment will consist mainly of shaping networks and attenuators to control the frequency and phase characteristics of the signals from the pointing sensors. (They can either make the sensor signal and impedance characteristics identical to those of the earth sensors, or they can introduce controlled differences.) The detailed designs will depend upon final sensor designs. Such equipment is passive, requiring no power. Weights are in the order of a few ounces.

### 5.6.4 INTERFEROMETER EXPERIMENT

# 5.6.4.1 Introduction

This section presents a description of a preliminary interferometer system designed to demonstrate the capabilities and limitations of an onboard interferometer used as a space-craft attitude determination device. The interferometer design provides for two basic operating modes.

- a. Interferometer used as an attitude sensor in the orientation control loop. It can be used as a reference to point the spacecraft axis at a given ground site, or at any known angle offset from a given ground site within the interferometer field of view.
- b. Used in an open loop manner, the interferometer output signals can be used to accurately measure the angle of arrival of a signal source with respect to the spacecraft axis.

To provide a bais for this preliminary interferometer design a set of requirements were generated, based on the objectives of the interferometer experiment; mainly, to demonstrate the capabilities and limitations of an onboard interferometer as a sensor for spacecraft attitude and/or large antenna pointing reference. The following basic requirements were used as a design goal:

Overall Accuracy

0.01-0.04 deg

Unambiguous FOV

23 deg

Maximum Weight

40 lb

Maximum Size

Contained within the diameter of the equipment module (4 ft)

Maximum Power (input)

50 watts

The system design described here has the capability of meeting or exceeding all of these specifications. Preliminary analysis indicates it will provide a pointing accuracy of 0.015 degree over the entire field of view (23 degrees). The interferometer can provide a pointing reference for the large antenna, which can be offset from the interferometer reference station by any angle within the 23 degree field of view.

### 5.6.4.2 Basis of System Selection

A study was conducted to select an interferometer system concept, generate a detailed system diagram, and analyze the performance of that system. This study is summarized in a final report\*. The major items discussed below were considered in the tradeoff study conducted to arrive at a system concept.

Selection of the system operating frequency (9.97 GHz) was based on the following considerations:

- a. System accuracy (with a maximum baseline length constrained to 4 feet)
- b. Ground transmitter power requirements
- c. Propagation effects (refraction, attenuation and polarization)
- d. Equipment component size, weight, and accuracy.

A two-speed system was chosen as the only practical way to provide an accuracy of 0.01 degree and still provide an unambiguous field of view of 23 degrees or more. The basic equipment configuration chosen was a straight IF (10 kHz) phase comparison system using a digital phase detector for improved linearity and accuracy. A pilot tone technique (described later) was employed to cancel receiver rf and IF phase changes. This approach was

<sup>\*&</sup>quot;ATS-4 Satellite Interferometer Design Study", R.A. Kyle, General Electric Co., TISR66ELS-89, August 1966.

taken rather than the  $\Sigma$ - $\Delta$  system approach because it allowed greater overall accuracy and eliminated the mechanical phase shifters and drives required in the  $\Sigma$ - $\Delta$  approach. A fairly complete error analysis of the system was performed on the study\* and is included in the final report.

# 5.6.4.3 Interferometer Fundamentals

An interferometer is, essentially, a phase-sensitive detector of an incoming radio wave. The interferometer antennas are usually spaced at least one wavelength apart. Thus, any radio wave incident upon the antennas from an angle will be received with a different phase on each antenna. The task for a precision interferometer system is then, to carefully preserve and measure the phase relationships of the signals in each antenna channel. The signal processing equipment that accomplishes this task must be both precise and durable, for a precision spacecraft interferometer.

Consider a pair of interferometer antennas separated by a distance of  $d_{\lambda}$  wavelengths, as shown in Figure 5.6-4. It may be assumed that both antennas receive a signal of the same amplitude, since they are essentially at the same point in the far field amplitude pattern of a remote source. However, the phase of the two signals will be different. This fact is

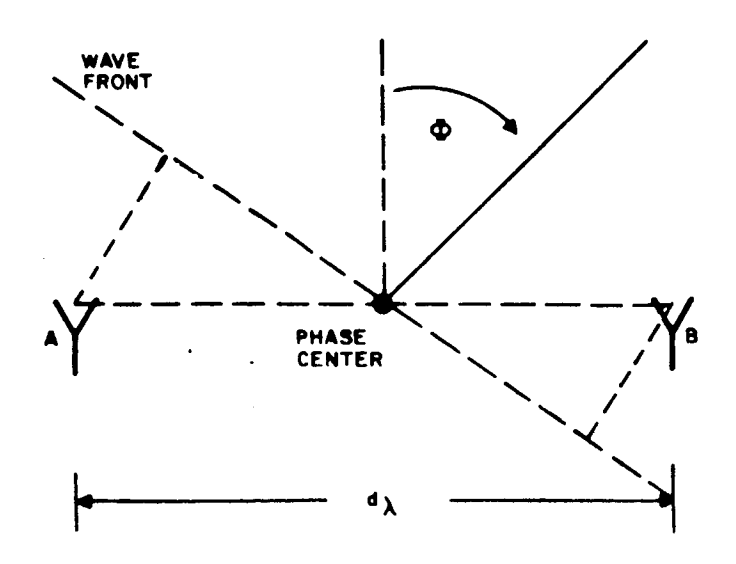


Figure 5.6-4. Relation of Incident Signal to Interferometer Antennas

apparent when the wavefront of a signal incident from an angle  $\emptyset$  is considered. To reach antenna A, the radio wave must travel an additional distance from antenna B. As Figure 5.6-4 shows, this additional distance is equal to  $d_{\lambda} \sin \emptyset$ . This is equivalent to an electrical phase difference of

$$\theta = 2\pi d_{\lambda} \sin \phi \text{ radians}$$
 (5.6-1)

By assuming a phase center between the two antennas, the phase may be divided between them so that the signal received on antenna A and B may be expressed as

$$A = C e^{-j\pi d} \lambda \sin \phi$$

$$A = \int_{-j\pi d} \sin \phi$$

$$B = C e$$

$$(5.6-2)$$

where C represents the equal signal amplitudes received by the two antennas.

Now a signal exists, on channel A and channel B, which is a function of the angle of incidence of an incoming radio wave. There are two basically different techniques used for the extraction of this single information. The most direct method is illustrated in Figure 5.6-5. In this method, the incoming signals are first reduced to an IF and amplified. The signals are then passed through a limiter to assure that both of them are still of the same amplitude. Next, the signals are fed to a phase detector that produces an output signal

$$v = K 3\pi d_{\lambda} \sin \phi$$

where K depends upon the characteristics of the phase detector.

The other basic method of extracting the phase involves converting the basic phase information on each channel to amplitude information, and detecting in an amplitude detector. The principle involved in this method is shown in the phasor diagram of Figure 5.6-6

( $\theta = 2\pi \ d_{\lambda} \sin \phi$ ). The two signals A and B, of equal and opposite phase displacements, are added and subtracted. The resulting sum signal  $\Sigma$  and difference signal  $\Delta$  are seen to be orthogonal, with the phase information essentially contained in  $\Delta$ .

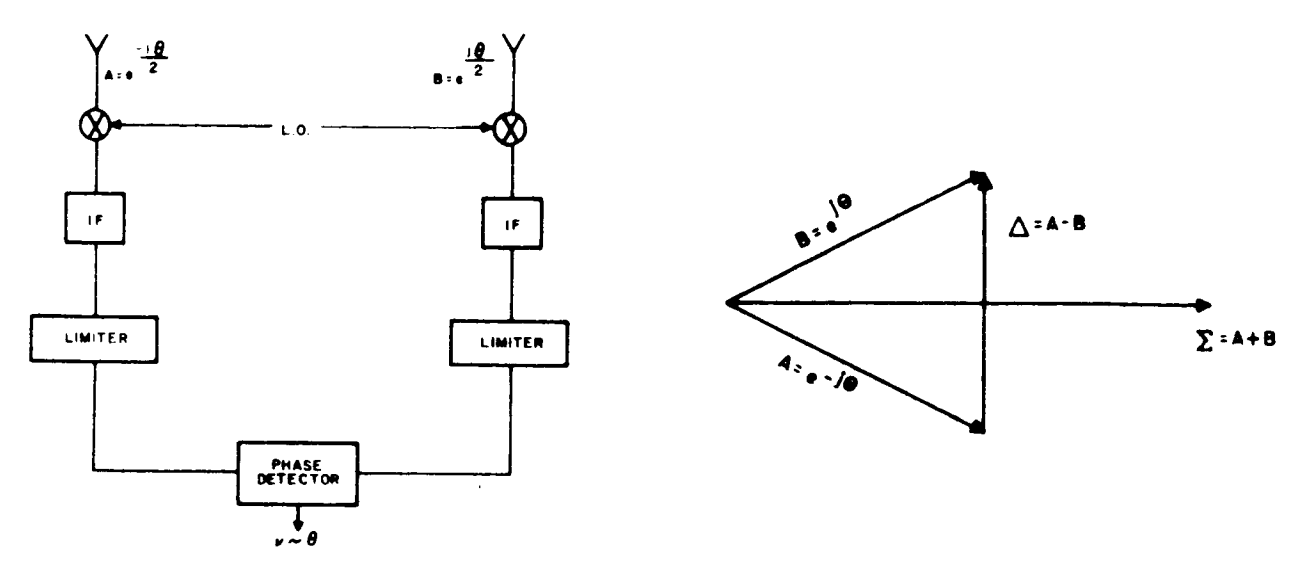


Figure 5.6-5. Phase Comparison System

Figure 5.6-6. Phasor Diagram for  $\Sigma$  and  $\Delta$  System

The implementation of this system is shown in Figure 5.6-7. The signals A and B are added and subtracted in a hybrid. The resulting  $\Sigma$  and  $\Delta$  signals are then reudced to an IF

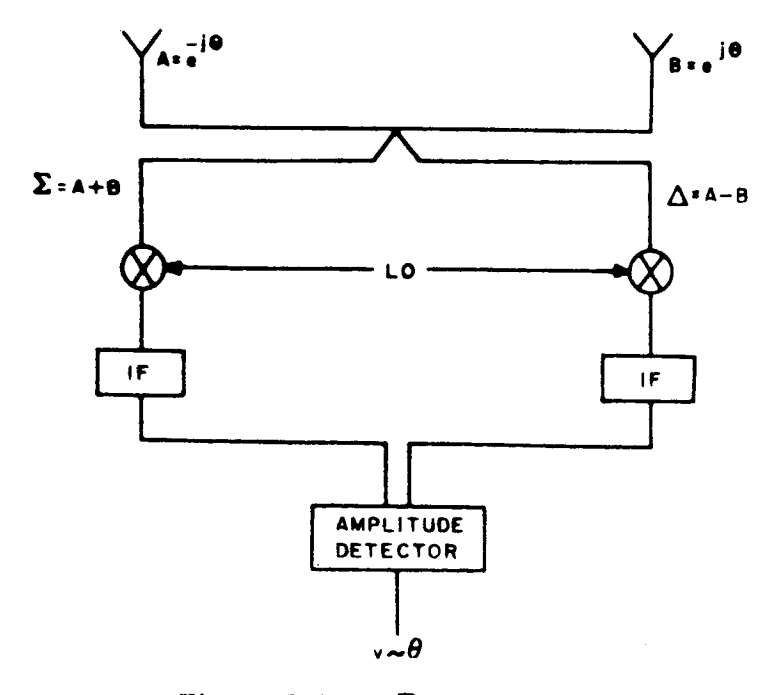


Figure 5.6-7.  $\Sigma$  and  $\Delta$  System

amplified, and detected in an amplitude detector. The output of the amplitude detector is

$$v = K' 2\pi d_{\lambda} \sin \phi \qquad (5.6-4)$$

where K' depends upon the characteristics of the amplitude detector. Note that this output voltage is essentially the same as that for a straight phase comparison system, as given in equation (4).

In a practical interferometer system, the accuracy of the angle measurement is degraded by the phase instabilities of the receiver components. In order to significantly reduce this problem, the pilot tone concept has been developed. By using the technique shown in Figure 5.6-4 the effect of phase instabilities in the mixer and IF stages of a receiver may be virtually eliminated.

The basic concept of the system is to add to the incoming signal, a pilot tone offset from the signal frequency by a small amount (e.g., 10 kHz). The signal-pilot tone combination pass through the mixer and IF. Since they are at nearly the same frequency, they experience very nearly the same phase shift in passing through these components. As both signals pass through the square-law detector, they mix together, and the output may be filtered at their difference frequency. At the different frequency between the incoming signal and pilot tone, all of the common phase shifts experienced through the receiver cancel. (The introduction and cancellation of phase errors is illustrated in Figure 5.6-8.) Thus, the output from the detector is very nearly the phase of the signal as received at the antennas, uncontaminated by the phase instabilities of the receiver.

In an actual system incorporating the pilot tone, the tone can be generated by a phase-locked loop at a frequency about 10 kHz from the signal frequency. In such a system it is important that the pilot tone transmission lines, leading up to the point of injection, be of equal length. (This is the same type of requirement as that of the equal line lengths required from antenna to receiver.) This is not necessarily a severe requirement, but if it is not met, an error will be introduced which will not be cancelled. The error will be equal to the difference in electrical length of the transmission lines and is represented by  $\theta_2' - \theta_1'$  in Figure 5.6-8.

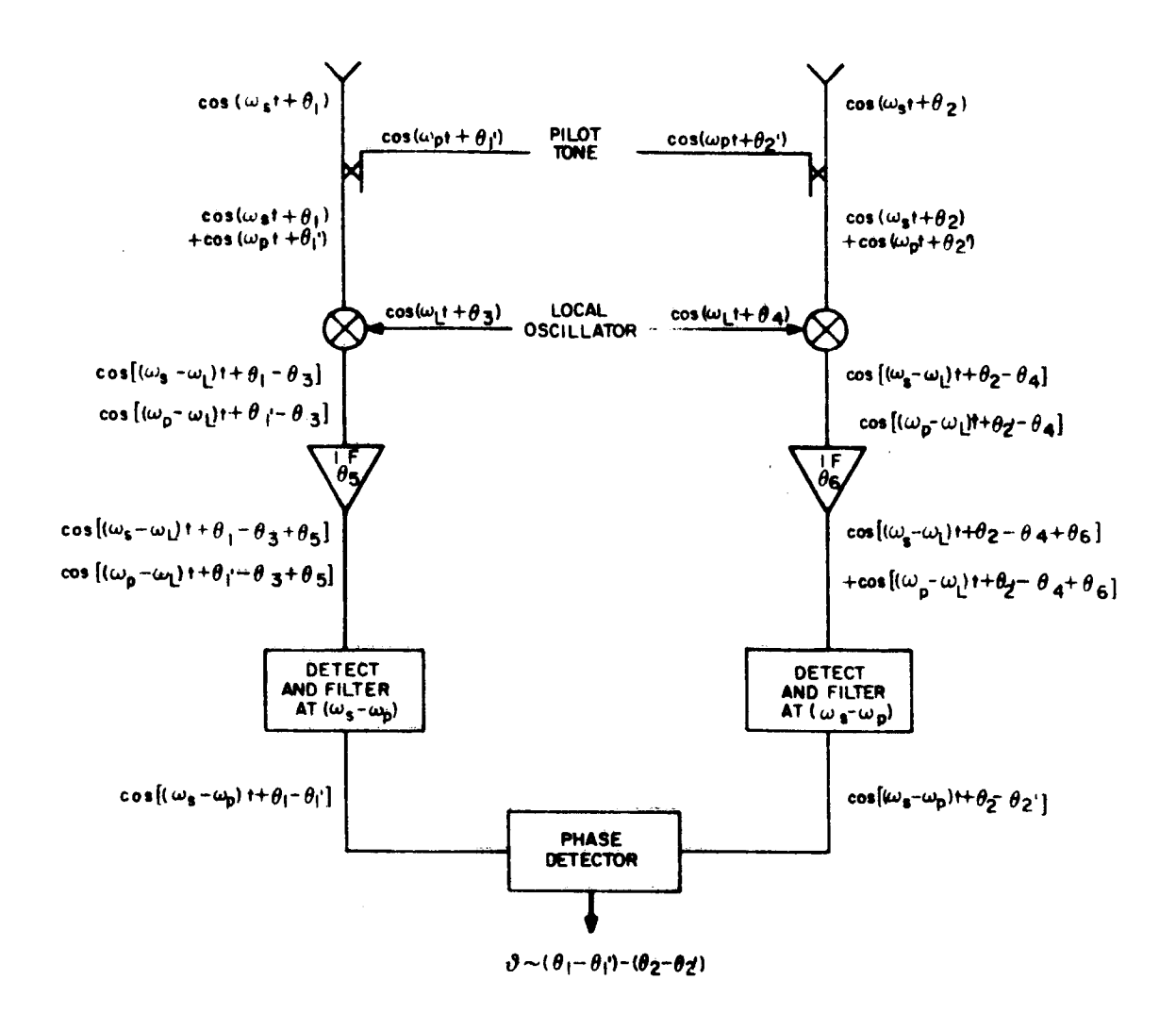


Figure 5.6-8. Pilot Tone Concept

# 5.6.4.4 Detailed Interferometer Design

The operating frequency and tentative location of the interferometer have been determined. Now, the antenna separations may be chosen, so as to provide high accuracy together with unambiguous operation over field of view desired. Since the fine system is limited to a 4-foot baseline, its separation will be  $39\lambda$  (46.2 in.) at 9.97 GHz. The separation necessary to provide unambiguous operation over a  $23^{\circ}$  sector is 2.3 $\lambda$  (2.7 in.). The earth subtends  $17.5^{\circ}$  at synchronous orbit heights. The coarse and fine systems have been designed to provide eight channels of information rather than the possible minimum of five channels. The redundant channels were added to increase the reliability of the system. One possible interferometer configuration, located on the subsatellite, is shown in Figure 5.6-9.

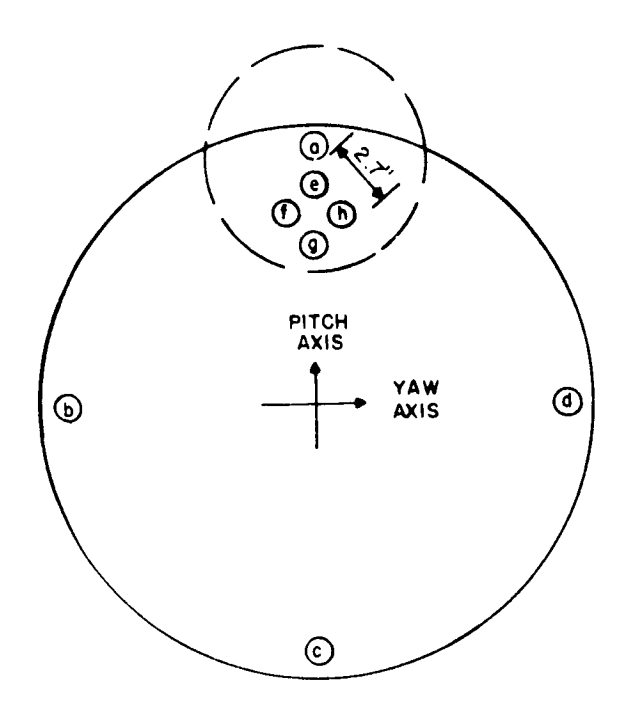
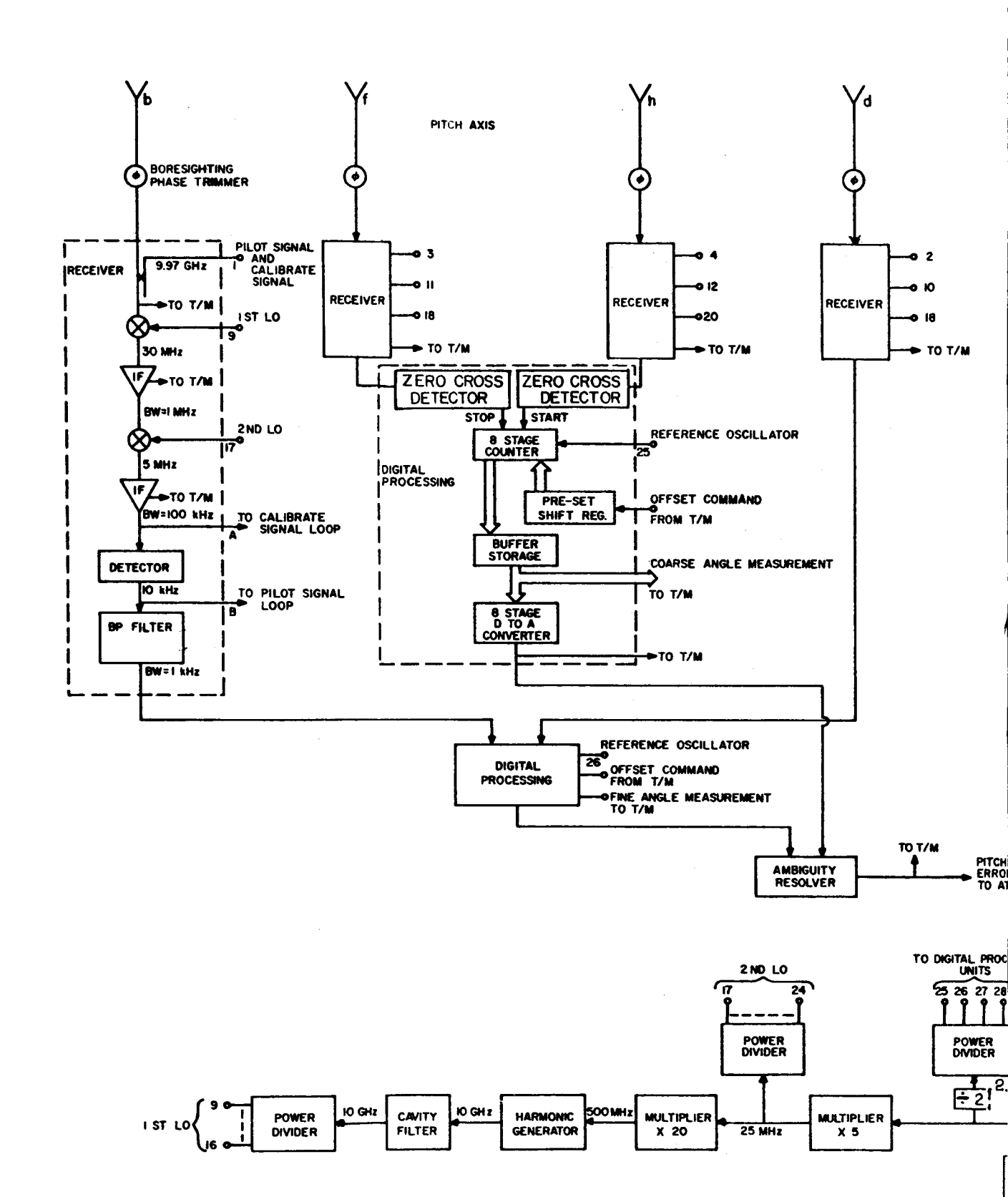
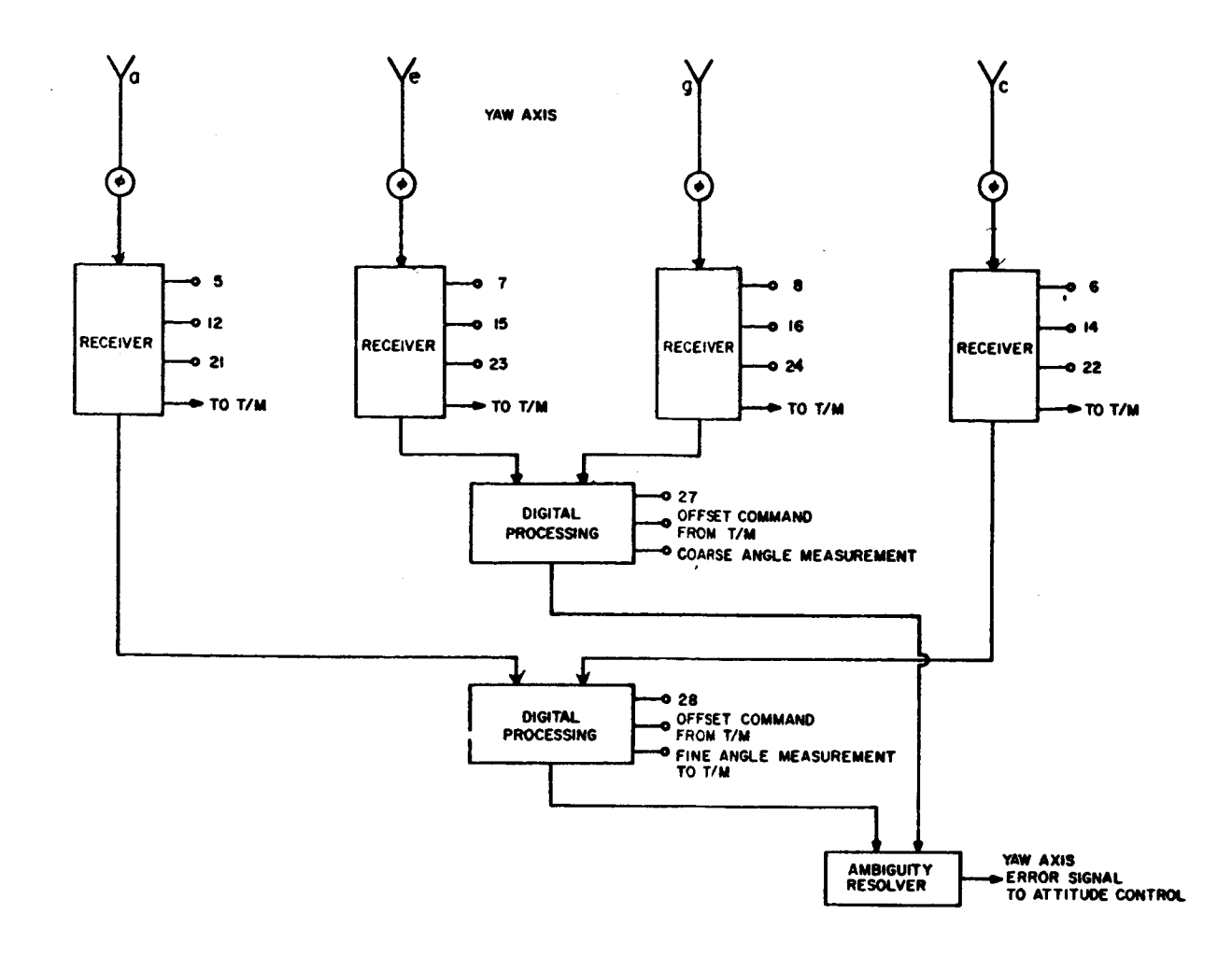


Figure 5.6-9. Antenna Location on Cannister

A detailed block of the system is shown in Figure 5.6-10. Preliminary weight and power estimates place the weight of the system at about 35 pounds and the maximum power consumption at about 9 watts. The system has a field of view of 23° and, based on the error analysis has a total angular accuracy of 0.013° for two-axis operation. A circularly polarized cw signal at 9.97 GHz is received on a standard 10 db horn antenna and added to a pilot tone separated in frequency by 10 kHz.

The signal and pilot tone are fed into a dual conversion receiver which empolys a 30-MHz first IF, a 5-MHz second IF, and a square law detector. The detector output is passed through a bandpass filter centered at 10 kHz. Since the pilot tone and signal frequency are separated by only 10 kHz, both should experience very nearly the same phase shift passing through the receiver. Thus, when they are detected at their difference frequency, the receiver phase errors will be very nearly cancelled.







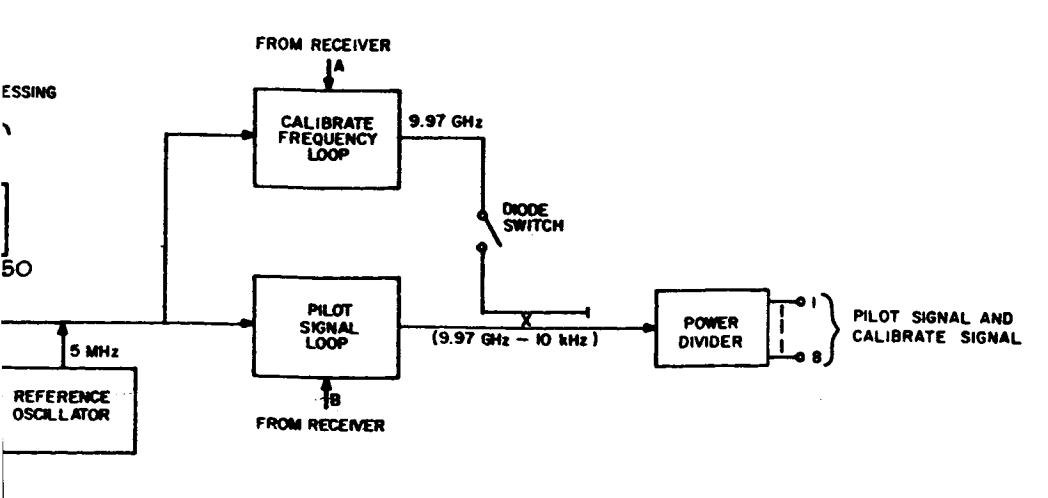


Figure 5.6-10. ATS-4 Interferometer System, Block Diagram

5.6.24

The 10-kHz signal from the filter is passed into a zero cross detector. This detector creates a series of trigger pulses, with every positive spike representing a positive-going zero crossing of the 10-kHz signal. The first positive spike from the right-hand interferometer channel (looking from the satellite toward the earth) turns the counter on and the first spike from the left-hand antenna turns it off. This arrangement produces a very linear precision phase measurement. In order to minimize the effect of the phase noise present in the system, 128 of these angle measurements are averaged for each angle measurement read into the telemetry system.

In order to provide an error signal suitable for use with the orientation control system, the digital angle measurement is passed into a digital-to-analog converter and then to an ambiguity resolver. The ambiguity resolver inputs are the coarse and fine error signals of one interferometer axis. Its output is the coarse system error signal until that signal has dropped below a predetermined level, which is well within the fine system ambiguity separation. The ambiguity resolver then inhibits the coarse error signal and its output becomes that of the fine system. Thus the interferometer will provide an error signal accurate to within the 0.013 degree error of the fine system.

Provision is also made for the addition of an offset to the error signal. This would enable the interferometer system to point the satellite antenna at any desired angle relative to the incoming signal. Thus, a large parabolic dish aboard the satellite, for example, may be pointed to any point on the Earth's surface by using another point (location of the transmitter) as a reference. This may be accomplished by introducing the negative of the desired angular offset as a command offset, to be added to the output of the appropriate counters. However, in order to provide a stable error signal for certain angular offsets, it is necessary to make provisions in the fine system to switch operation away from regions in the counter's operation occurring near the 360-degree points. This problem is unique to the fine systems. The angular offsets where this problem might occur will be known on the ground, and when it is desired to introduce these particular offsets, the negative 10-kHz zero crossing will be used for the stop pulse. This will produce a stable error signal. The angular offset produced in any case is of an accuracy comparable to that of the basic system.

# 5.6.4.5 Weight and Power Estimates

Weight and power estimates for the interferometer system are given in Table 5.6-3. All estimates do not include the effect of a power converter to match the power signals required to those available in the spacecraft. Such a converter could raise the weight estimate by about 5 pounds and the power by roughly 25 percent. It is seen that the weight of the basic interferometer system is 30.6 pounds with 8.8 watts of power being required.

There are two possibilities for reducing the weight of the interferometer which should be investigated further in a future study. One is the possibility of reducing the system to five or even three channels. This provides a reduction in system redundancy and/or accuracy as well as in weight. The other possibility is that of using stripline for the microwave portions of the system. This approach, also, may save weight at the expense of system accuracy and reliability.

Table 5.6-3. Weight and Power Estimates for the Interferometer System

	Basic Interferometer	Weight Each	Power Each	Total Weight	Total Power
No.	Item	(lb)	(watts)	(lb)	(watts)
8	Antennas	0.22	0	1.8	0
8	Phase Trimmers	0.22	0	1.8	0
8	Directional Couplers	0.13	0	1.1	0
15	Hybrid Junctions	0.19	0	2.9	0
8	Isolators	0.13	0	1.1	0
8	Balanced Mixers	0.32	0	2.6	0
20'	Waveguide Sections (alum.)	0.3	0	6.0	0
8	30 MHz IF Amplifier	0.25	0.05	2.0	0.4
8	5 MHz IF Amplifier	0.3	0.05	2.4	0.4
1	Pilot Tone Generator	1.6	0.40	1.6	0.4
1	Calibrate Signal Generator	1.5	0.1	1.5	0.1
1	Diode Switch	0.3	0.1	0.3	0.1
1	Reference Frequency Source	0.7	2.0	0.7	2.0
1	Frequency Multiplier for LO 1 and LO 2	1.0	3.0	1.0	3.0
1	Yaw Axis Digital Processing (13 modules, 3 cordwood modules)	1,9	1.2	1.9	1.2
1	Pitch Axis Digital Processing (13 modules, 3 cordwood modules)	1.9	1.2	1.9	1.2
	Totals			30.6 lb	8.8 w

### 5.6.4.6 Thermal Effects

Thermal expansions caused by temperature changes will induce deformations in the interferometer antenna structure. These will include deformations and misalignments of the horns themselves as well as changes in spatial relations, but only the latter will be large enough to affect interferometer performance.

Spatial displacement of the interferometer antennas can occur in any of the three dimensions, with the following effects:

- a. Along the line joining two antennas, changing the separation distance
- b. Along the line of the interferometer boresight; this will cause boresight error
- c. Perpendicular to both of the above; this will cause nonorthogonality of the axes.

Change of antenna separation, in a. above, can be either or both of two types; each will induce a different type of error. These are:

- (1) Antenna Separation Change. Wherein the distances between the antennas to the electronics remain equal. In this type of deformation, no boresight error is introduced; angle measurement error is introduced, and will increase with the angle. For small displacements, the resultant angle measurement error will be directly proportional to the error in separation. In order to keep this error to negligible values, the displacement must be of the order of 0.01λ.
- (2) Electrical Path Length Change. Wherein the electrical path lengths from the antennas to the electronics become unequal. This would introduce both a boresight and an angle measurement error. In order for this error to remain negligible, this deformation must also be on the order of  $0.01\lambda$ .

Of these displacements, b. and c. will be held to negligible values since the wave guides will be constructed of a low thermal expansion material and be housed in a thermally controlled environment. For example, with a 1-inch deep wave guide constructed of Invar and assumed unrestrained by structural support, the maximum gradient through the wave guide in order to maintain boxesight errors below 0.1% is calculated below.

$$\Delta T = \frac{2d \delta}{\propto L^2}$$
 where  $\delta = 0.01\lambda$ 

$$L = \text{waveguide length}$$

$$d = \text{waveguide depth}$$

$$\alpha = \frac{2(1.0) (0.01)1.18}{0.5(48)^2 (10)^{-6}}$$
 expansion for Invar = 0.5 x 10<sup>-6</sup> in./in./ F
(This (\alpha) is very conservative in the 30° to 120°F region)

This gradient across a 1-inch waveguide is much higher than can reasonably be expected. For a separation distance change (case 1), the temperature extremes of interest are peak comperatures away from initial calibration temperature. The EVM will be thermally controlled between the limits of  $+30^{\circ}$ F to  $+120^{\circ}$ F (ref. Section 5.9.6).

Taking the maximum  $\Delta$  T from  $70^{\circ}$ F

then 
$$\delta = \propto \Delta \text{ TL}$$
  
=0.5(10)<sup>-6</sup> (50) (48)  
=0.0012 in.

which is an order of magnitude less than the allowable deviation. For a reasonable thermal condition of one side of the EVM at 30°F and the opposite side at 120°F, the total difference of each half of an arm will be of like magnitude to the above.

The use of Invar for the waveguide material is an obvious solution to the thermal distortion problem; however, a lighter, less thermally stable material may be proven adequate when details of thermal environments and structural restraints are factored into the analysis, or it may be desirable to add local strip heaters for absolute thermal control.

### 5.6.5 PHASE-STEERED ARRAY ANTENNA

The phase-steered array antenna will resemble the redirective or self-phasing system developed by the Hughes Aircraft Company under NASA/GSFC contract No. NAS5-10101.

The redirective, or self-phasing antenna system automatically forms a high-gain beam on receive to receive a signal with a wide modulation band. A narrow-band cw pilot signal is used to provide an appropriately phased local oscillator for each element, with which the phase of the modulation is adjusted to be equal in all the elements. The modulation, at IF, from each channel (element) is summed, amplified, converted to rf, amplified at rf in a traveling-wave-tube amplifier, and then distributed to each transmitting element for retransmission.

A station that desires to receive information retransmitted by a spacecraft sends up a cw transmitting pilot signal in the up-link band. This pilot is received in the receiving antenna channels and down-converted along with the receiving modulation and receiving pilot which have been sent from an earth transmitting station. The transmitting pilot is then filtered off and sent to a transmitting channel. In the transmitting module, it is mixed with the information to obtain at each transmitting element the modulated rf with the appropriate phase necessary to return it in the direction from which the transmitting pilot came. If rf amplifiers are available at the frequencies involved, their inclusion at each antenna element in the transmitting antenna would considerably improve the efficiency and performance of the system.

Separate antennas are used for receiving and transmitting; these antennas are identical except that they are scaled by the ratio of the transmitting frequency to the transmitting pilot. This design serves to keep all up-link signals in the up-link band. If the transmitting pilot were allowed in the down-link band, the same antenna could be used for both transmitting and receiving. The major characteristics of the antenna are shown in Table 5.6-3. A block diagram of the system is shown in Figure 5.6-11.

In order to fit the phase-steered array into the area available in the earth viewing module, it was necessary to make a slight modification to the element distribution within the array. The aperture area was preserved during this transformation. A total of six elements was affected. Three elements were removed from each side and relocated at the top and bottom of the array. Identical modifications in scale were made in the transitting and receiving

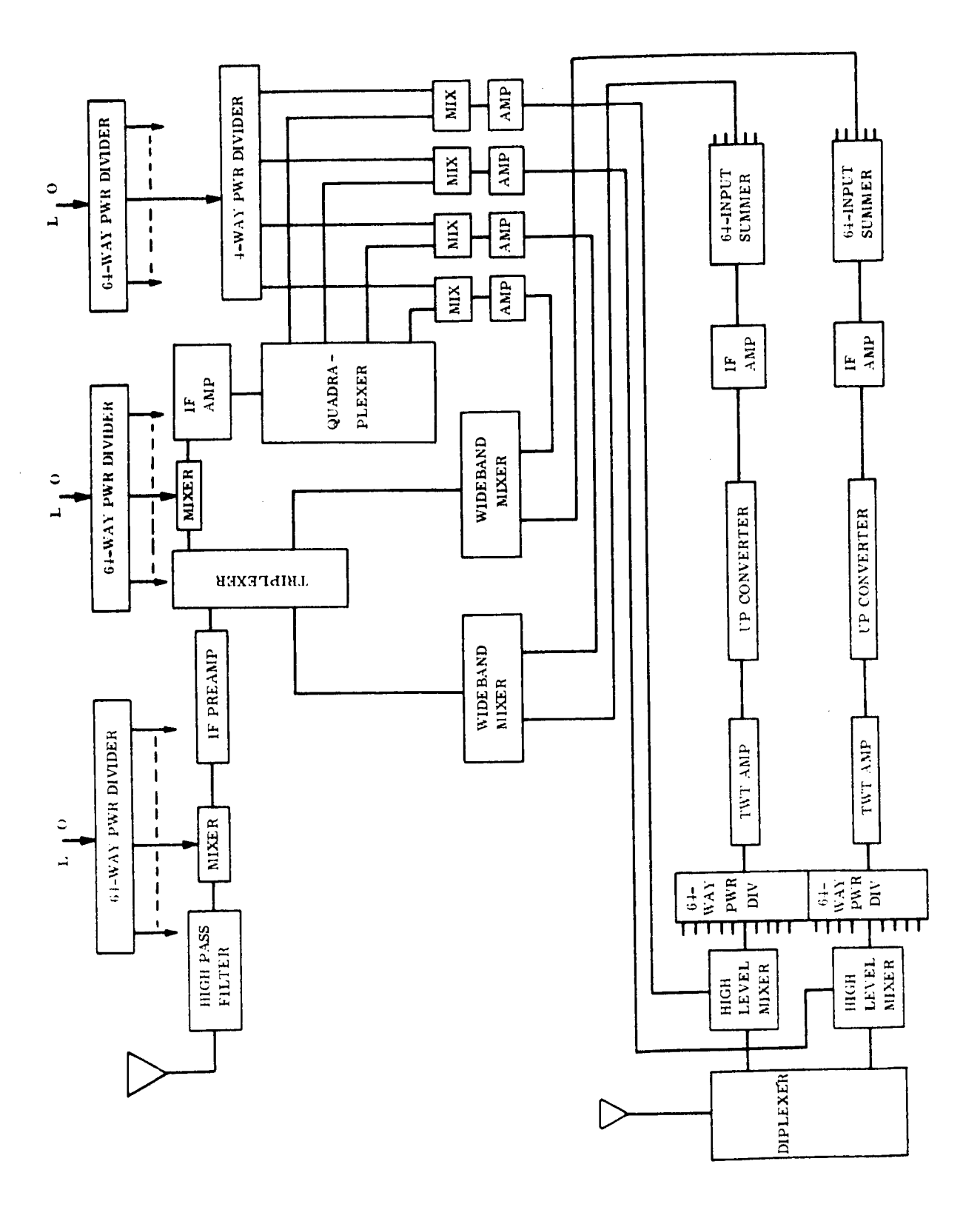


Figure 5.6-11. System Block Diagram

arrays. The gain is preserved, and a slight asymmetry in beam slope was the only result. This will have negligible effect on the system performance.

In order to simplify the thermal problem and provide a more efficient structural configuration, the major components of the phase-steered array were located as follows:

- a. Receiver and transmitter were placed on the forward face of the earth viewing module.
- b. The electronics were located on a thermally controlled surface within the module, as were the TWT's. The TWT's were located on panels separate from the electronics, in order to simplify the rejection of heat from the anodes.

Table 5.6-4. Major Characteristics of Phase-Steered Array Antenna System

Receiving Frequency	$8.00 \text{ GHz} \pm 0.175 \text{ GHz}$
Transmitting Frequency	$7.30~{\rm GHz} \pm 0.175~{\rm GHz}$
Total Bandwidth	Two 125 MHz information channels with a minimum guard band of 100 MHz
Polarization	Circular
Gain	$30~\mathrm{dB}$
Effective Radiated Power	+25 dBw
Total Weight	100 lb
Total Volume	7 ft <sup>3</sup>
Aperture, Receiving Antenna	30-inch diameter or equivalent
Aperture, Transmitting Antenna	30-inch diameter or equivalent
Prime Power Requirement	420 watts

# 5.7 TELEMETRY, TRACKING AND COMMAND

### 5.7.1 SYSTEM REQUIREMENTS

The TT&C subsystem is to provide the following capabilities in support of spacecraft operation:

- a. Telemetry and Command capability during all modes of operation
- b. Tracking accuracy 0.02°
- c. Attitude measurement during spin mode -10 accuracy
- d. Compatibility with ATS ground station where possible
- e. Command capability 320 outputs
- f. Continuous updating of star tracker gimbal angle
- g. Telemetry capability 600 inputs including operational, diagnostic, and experimental data

The hardware implementation required to realize these system requirements are discussed in the following paragraphs. A list of command and telemetry requirements for the system are given in Table 5.7-1.

### 5.7.2 REFERENCE DESIGN SUMMARY

An S-Band Telemetry, Tracking and Command subsystem has been selected for the reference design. Commands are transmitted to the vehicle as frequency-shift keyed subcarriers phase-modulated onto the carrier. Capability of decoding 390 commands has been implemented. Telemetry information is transmitted as PCM data which bi-phase-modulates a subcarrier which in turn phase modulates the transmitter. The telemetry subsystem has a total input capability of 620 channels. Telemetry data from the earth-viewing equipment module and aft equipment module is transmitted on a time-shared basis with the selection being made by ground command. Tracking is accomplished by utilizing a Goddard Range and Range Rate transponder. The selected antenna configuration provides 85 percent coverage during the spin mode and 100 percent coverage when earth stabilized. A minimum transmission margin is about 5 dB for all modes of operation.

Table 5.7-1. Telemetry and Command Requirements

			Telemetry Requirements	emente			
Measurement	No. of Points	Required Response	flubsystem	Measurement	No. of Points	Required Response	Subayatem
Transmitter/Receiver Pair	2	Slow	Payload	Shunt Limiter Dissipator Voltage	_	< 1 Hz	Power
Channel within Receiver	•	W)	Payload	Battery ON/OFF	8	< 1 Hg	Power
Channel within Transmitter	•	#O!#	Payload	Pitch Rate Null		A 1 Hg	340
RF Switch Positions	*0	#cl8	Payload	Holl Mate Null	-	A 1 Hg	040
Phase Array/Parabolic Antenna	-	Wale.	Payload	Yaw Rate Null		A 1 Hz	040
Receiver fignal Strength	<b>67</b>	<1 Hs	Payload	Pitch Bun Att, Null	-	A - Hg	040
Interferometer Elements On/Off	•	#low	Interferometer	Roll Sun Att.		× 1 %	0.00
Low Power Outputs	•	<1 Hs	Payload	Yaw Bun Att, Null		A 1 Hz	040
Low Voltage P. H. Voltages	*	<1 Hg	Phased Array	Antenna Erect	-	A 1 Hg	240
TWT Power Amp. Monitor	*	×1 ₩	Phased Array	Antenna Erect Complete	-	A 1 HR	040
L.O. Power Monitors	*	## **	Phaned Array	Initiate fun Stabilization	-	4 1 Hz	240
Attitude Read Cut	91	<10 Hg	Phased Array	Bun Stab, Complete		. Hg	040
Transmitter Forward Bower Meniter	4	¥	Payload	Enable Rarth Stab.	-	<del>.</del>	040
Transmitter Reflected Power Manitor	*	×	Payload	Pitch Rarth Att, Null	<b>-</b>	A 1 Kg	240
Antenna Deplayment	08	Moles.	Payload	Roll Earth Att. Null	-	A : #	240
Antena Biress	76	## t>	Payload	Earth Sensor Acquired	-	A	240
Antenna Temp, Dint,	108	#ale	Payload	Polaria star Prosent	-	* 1 Hg	040
Antenna Acceleremetera	og:	≠10 H#	Payland	Pag Att. Null	-	4 1 Ha	040
Jemanulated Heaelved Righel AGC Valtage	073 OB	× 10 Hs	Paylead Interferentes	FW Direction	<b>6</b> 7	* 1 HS	240
Phase Detestar Cutraut	D ==	, y	Intentanometer	FW RPM	<b>6</b> 73	A 1 Kg	040
Look Detector Outsut	- ,	. 5	Thtoulonomoton	Earth Stab, Complete		£ . ×	340
VOO Cantral Valtage		<10 Hs	Interferometer	Bun Att. Error	67	A 1 H	alec
	• •		The afternament of the	Rate Cyro Mgnals	<b>6</b> 2	£ .	290
Pilat Tene Level		2 10 Hz	interior une see	Amplified Rate	-	* : #	0.60
Int I's Outsut Level	* o	2 2	Interiornmeter	Sensor Attitude Error		# · v	040
and IF Cutnut Lave		## P P P		Par Hrror		£ .	040
And on Tunou Elemols	₽ ₹	EH 04.5	Interiorameter	Earth Bensor Position Amp		=	040
Thereby Street Stylens	# G	TH OOT >	Interferometer	Earth Sensor Radiance Level	-	= -	040
Figure County Montener	<b>.</b>	<b>=</b>	Interferameter	PAS Serve Amp Out		=======================================	0.00
Figure Counter Research	<b>a</b> r (	#de 008≥	interferemeter	PBB Ref. Amp Out	-	=	090
The and and Lice it would	mar (	< 10 HB	Interferemeter	PSS High Voltage Supply		£	290
tunk Presente		# T	Prepulaton	Roll Search Bian	_	=	240
	<b>(E)</b>	## **	Prepulsion	and Counter Dits	2	=	040
Temperature Menagara	90	< 1 Ha	Thermal	Arii In		= -	240
Receiver Bignal Birength	-	41 H	TTRE	Drop Out	•	= =	) U
Terremiter Mode Switch		# 1*	THEC	Control F/F	•	# · ·	040
Accept Neject Signal		# N	7740	Thruster Sciencid Position	=	=	040
Anwenne mytten Postaon A		= 7	7760	Reservoir Pressure	•	= -	90
Antenne Switch Posts on A	·	# :	1140	Pressure Tank Rolenoid Position	<b>S</b>	# :	290
Antenna awiren Posingn C			7760	Thruster Pressure	•	Y.	040
Antenna ewiten Pusision D	-	<1 Hs	TT&C	Spin Rate	78	× 1 Hr	a.e.

Battery Volume	· c	# T	Может	FW Servo Amp Out		===	90
Matters Change Course		:			_		
			Power	Station Aequisition, Sun Sensor	-	¥v	040
	<b></b> -	41 H	Power	704	· 77		
Battery Dishearge Current	<b></b>	€1 HI	Power	_			2
Array Bus Voltage		# T #	Power	*(178 discrete channels combined on 48 analog channels)	d on 43 a	nalog oha	nnela)
Array Bue Current		£ 7	Power			:	
Regulated Bus Voltage		=======================================	Power				
Regulated Bus Current	**	# T	Power				
Inverter Phase 1 Voltage	_	7	Power				
Inverter Phase & Voltage		7	Power				
			Command Requirements	7,000			
Command Function	$\vdash$	No. of Outwise	Pubayatem	Command Function	žđ	No. of Outputs	Bubavatam
Select Transmit/Receive Combination	_	e:	Payload	Batteries ON	H	_	Power
Receiver ON/OFF		63	Payload	Change Regulator No. 1, 2, 3, Normal Rate		63	Power
Transmitter ON/OFF		•	Payload	Charge Regulator No. 1, 2, 3, High Rate	18	67	Power
Antenna Selection	-	=	Payload	Enable Sun Stab. ON/OFF		~	290
Receiver Bandpass Selection		-	Payload	Antenna Erect			040
Transmitter LO Selection		•	Paylond	Enable Earth Stabilization ON/OFF		a,	080
Phase Array ON/OFF		œ	Phased Array	Enable Yaw Sun Stabilization ON/OFF		œ	240
Phase Array Filters		œ	Phased / "may	Switch to ET Control		<b>~</b>	040
TWT PS ON/OFF		•	Phased Arter	Gyro Power ON/OFF	_	a	000
Interferometer ON/OFF		CNI	Interferometer	Gyro Heater ON/OFF		N	040
Interferometer Antenna ON/OFF		91	Interferometer	FW Enable ON/OFF		œ	240
Polarisation Switch IN/OUT		•	Interferometer	Switch to PSS Control ON/OFF		N.	040
Asimuth Angle Offset		27	Interferometer	88P Power ON/OFF		N	040
Elevation Angle Office		81	Interferometer	Roll Search Bias ON/OFF		04	CAC
Receiver/Transmitter Mode		<b>~</b>	Interferometer	Earth Tracker Search ON/OFF		co.	0 <b>4</b> 0
Change in Averaging Time		œ	Interferometer	PBS Power ON/OFF		01	G&C
Transmitter ON			TT&C	Earth Tracker Power ON/OFF		CN .	0.00
Transmitter OFF			TT&C	Thrustor Detector Enable ON/OFF		12	200
TLM Processor No. 1 ON			TT&C	Auto Unload Disable ON/OFF		œ	0 <b>%</b> C
TLM Processor No. 2 ON			TT&C	FW Emergency Unload ON/OFF		œ	280
TLM Processor No. 1 OFF	-	-	TT&C	Auto 40% Unload ON/OFF		œ	240
TLM Processor No. 2 OFF		-	TT&C	Sun Sensor Enable ON/OFF		œ	240
Antenna Sub-Comm ON/OFF		<b>69</b>	TT&C	E-W Stationkeeping ON/OFF		ο <b>ι</b>	280
Receiver/Antenna B		-	TT&C	N-S Stationkeeping ON/OFF		co.	240
Receiver/Antenna D			TT&C	Resistojet Propellant Shut-Off Valve ON/OFF	E E	16	GAC
Transmit Antenna A		-	TT&C	Resistojet Solenoid Position		48	240
Transmit Antenna B			TT&C	Resistojet Heater Control		16	299
Transmit Antenna C		1	TT&C	Vernier Solenoid Position		28	242
Transmit Antenna D			TT&C	Yaw Sun Sensor Bias ON/OFF		21	299
Telemetry Mode ON		-	TT&C	Polaris SS Gimbal Angle Offset		15 bits	242
Tracking Mode ON		-	TT&C	Apogee Engine Firing Position		10 bits	299
Antenna Sub-Comm Speed-up ON/OFF		81	TT&C	Apogee Engine Firing Duration	· .	7 bits	280
Battery No. 1, 2, 3 OFF		က	Power	Apogee Engine, No. of Firings		10 bits	೦೩೦
	<u>-</u>			Total (Excluding data cmds) 320	<u>.</u>		

The significant parameters of the reference configuration are summarized in Table 5.7-2.

The TT&C subsystem uses all state-of-the-art components with the components being either a modification of a present design or a new design based on standard design techniques. The total subsystem weight is 73.3 pounds, including harnessing, and the power requirements are 18.4 watts continuous and 64.4 watts peak. A block diagram of the subsystem is shown in Figure 5.7-1.

Table 5.7-2. Significant Reference Configuration Parameters

Command Frequency	1700-1850 MHz
Modulation .	FSK/PM
Command Bit Rate	100 bps
Command Bit Error Rate	10 <sup>-5</sup>
No. of Outputs	390 implemented
No. of Telemetry Inputs	628
Bits Per Word	7
TLM Data Rate	500 bps or 8 kbps
Modulation	PCM/PSK/PM
Transmitting Frequency	2200-2300 MHz
Transmitter Power	1 Watt
Tracking	Goddard Range and Range Rate
Tracking Accuracy	0.02 <sup>0</sup>

#### 5.7.3 COMMAND SUBSYSTEM OPERATION

Command information will be transmitted to the vehicle as frequency-shift keyed (FSK) data phase-modulated onto the carrier. The command receiver will detect the carrier and provide the subcarriers to the command detector. Three subcarriers will be provided corresponding to a data 1, 0, and S. At the start of command transmission, a continuous stream of S pulses will be transmitted to turn on the decoding portion of the command subsystem. The command detector will demodulate the respective subcarrier and generate

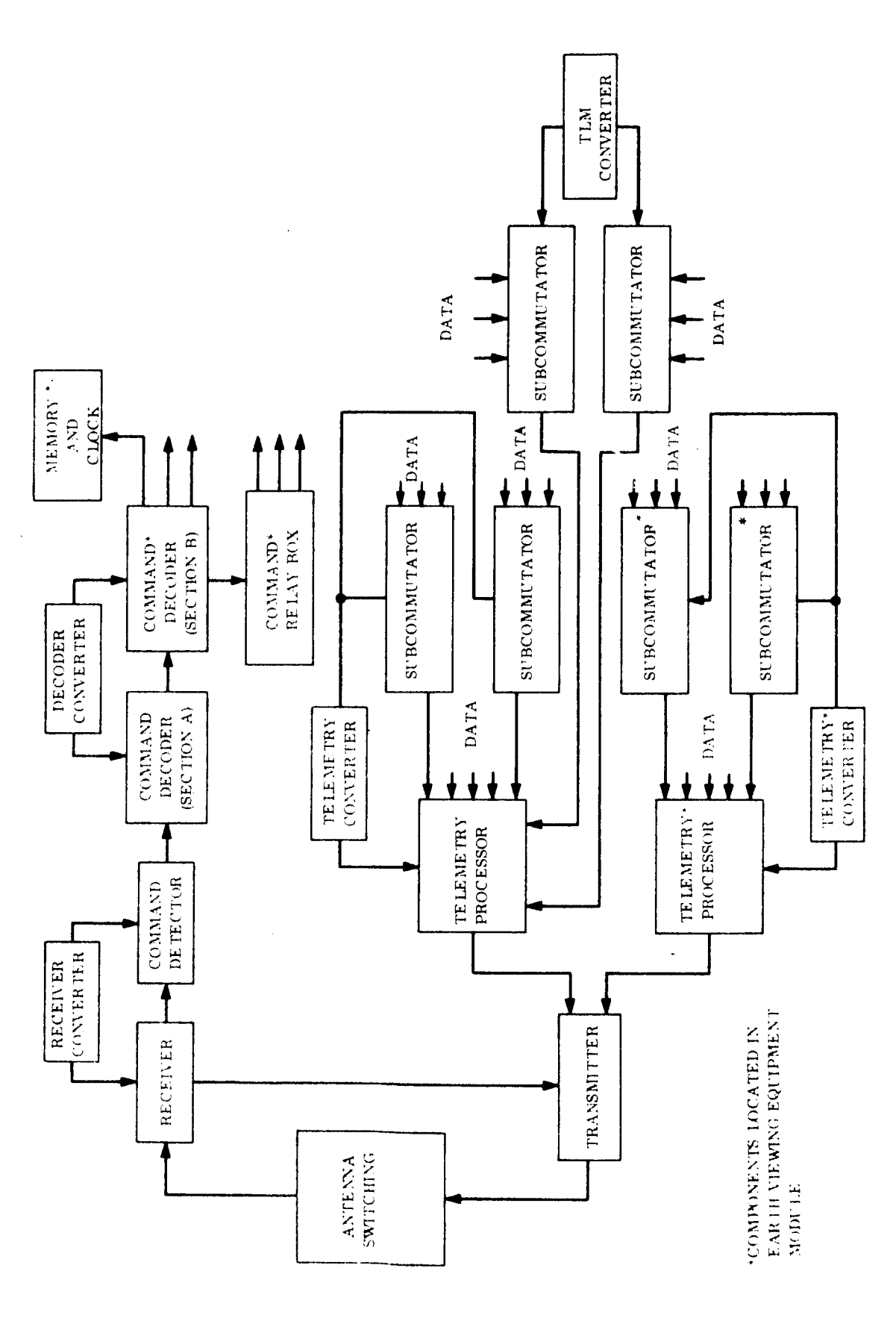


Figure 5, 7-1. TT&C Subsystem Block Diagram Reference Design

output pulses corresponding to the detected information, which is then provided to the command decoder. A squelch circuit in the command detector activates the decoder power supply when a signal above the preset threshold is received. The preamble of S-pulses is used to allow the decoder power supplies to attain the proper voltage levels before command information is transmitted. The receiver will be used for both tracking and command reception. A block diagram of the Goddard R and R transponder indicating the point where the command information is extracted is shown in Figure 5.7-2. The transmission of command and tracking data will be time-shared so as to minimize interference between the signals and minimize modifications required at the ground terminals. (Simultaneous operation would require additional equipment at the ground stations to mix the command and tracking data.)

The command decoder consists of two separate units; the main portion will be located in the aft equipment module, and the secondary portion located in the earth-viewing equipment module. These units shall be designated the A section and B section of the decoder, respectively. The A section contains the input logic, part of the control logic, and the

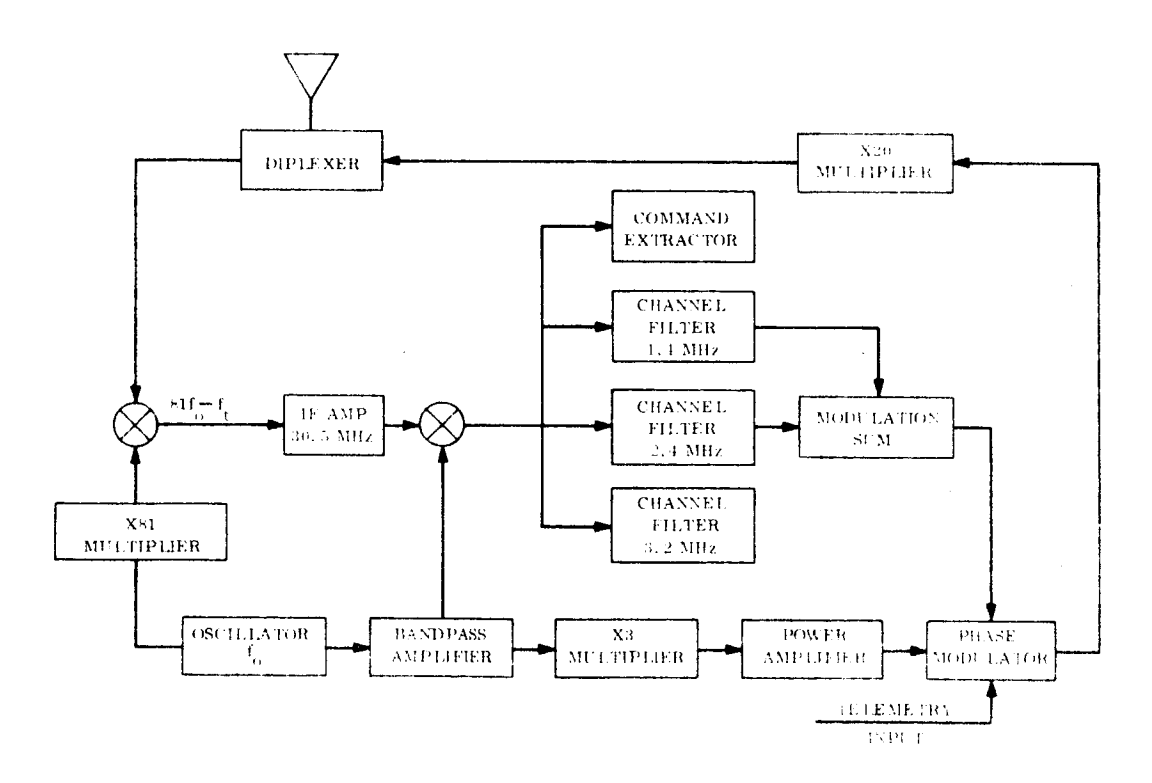


Figure 5.7-2. Goddard R&R S-Band Transponder

decoding matrixes required for commanding components in the aft equipment module. The B section contains control and decoding logic for commanding components in the earth-viewing equipment module and for interfacing with the Polaris star tracker and the memory. A functional block diagram of both sections of the command decoder is shown in Figure 5.7-3.

A command word consists of 26 bits: 5 bits for vehicle identification, 4 bits for word address, 15 function bits, 1 bit for parity, and 1 spare bit. When a command word is received the decoder checks the vehicle ID, the bit count, and parity in response to an S-pulse at the completion of the word. If the parity, bit count, and vehicle ID are correct, an execute signal is generated. This execute signal strobes the word address decoding matrix. If the word address indicates that the command is to be decoded in the A section, a strobe is applied to the decoding logic corresponding to the addressed word. The command corresponding to the states of the function bits is then executed. If the word address indicates that the command is to be decoded by the B section of the decoder, shift pulses will be generated to read the function bits and three of the address bits out of section A and into section B.

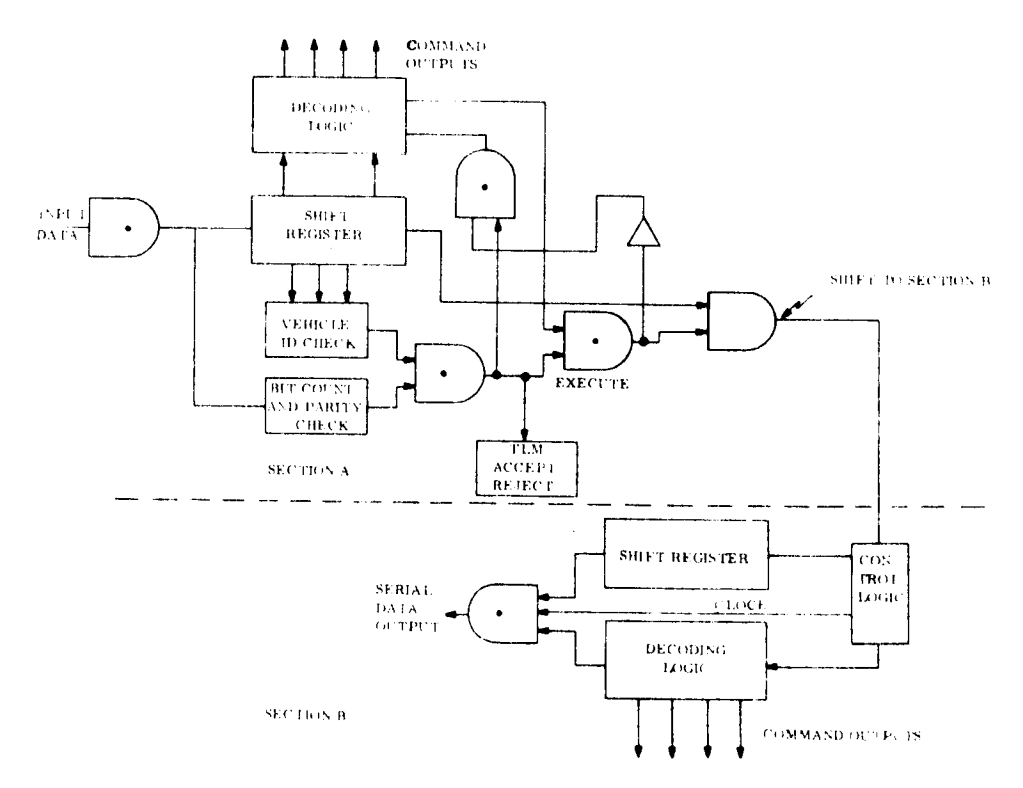


Figure 5.7-3. Command Decoder, Functional Block Diagram

Only one bit of the word address is used to determine if the A or B section is to be used. This bit would not have to be transmitted to the B section. At the completion of the transmission of the 18 bits to section B, an end-of-word pulse will be sent. The B section will then proceed to decode the address bits and to execute the command corresponding to the function bits.

When the execute signal is initiated in section A, an accept signal will be sent to the telemetry subsystem. In the absence of an execute signal, reject pulses will be sent to telemetry when S pulses are being received by the decoder.

Two decoding schemes will be implemented in the decoders. First, a large percentage of the decoding is to be performed on a per bit basis. That is, each bit represents a function When the bit is a one, the function is to be "enabled"; if the bit is a zero, the function is to be "disabled." Therefore, for each 15-bit command word implemented with this decoding, 15 ON/OFF commands can be provided.

The second decoding approach is implemented to decrease the number of command output drive circuits. It is used primarily in the experiment subsystem where a command is used to select one function out of a group of functions. As an example of the technique to be used consider the relay logic shown in Figure 5.7-4, which is to individually control eight ON/OFF relays. Eight latching relays are shown. If the first decoding approach was used to control these ralays, 16 output gates would be necessary. As shown in the figure, only eight output gates are required for this approach. (These gates, of course, require more drive capability than the 16-gate configuration.) This decoding logic will be implemented for those functions for which, if the control relay driver failed, total system failure would not occur. (One of the disadvantages of this approach is that if one relay fails, four functions will be affected.)

There are two components which require digital data from the command decoder. The star tracker requires 15 bits to define the offset angle (see Section 5.4). The orientation control subsystem also requires data to define the time of occurrence of vernier nozzle.

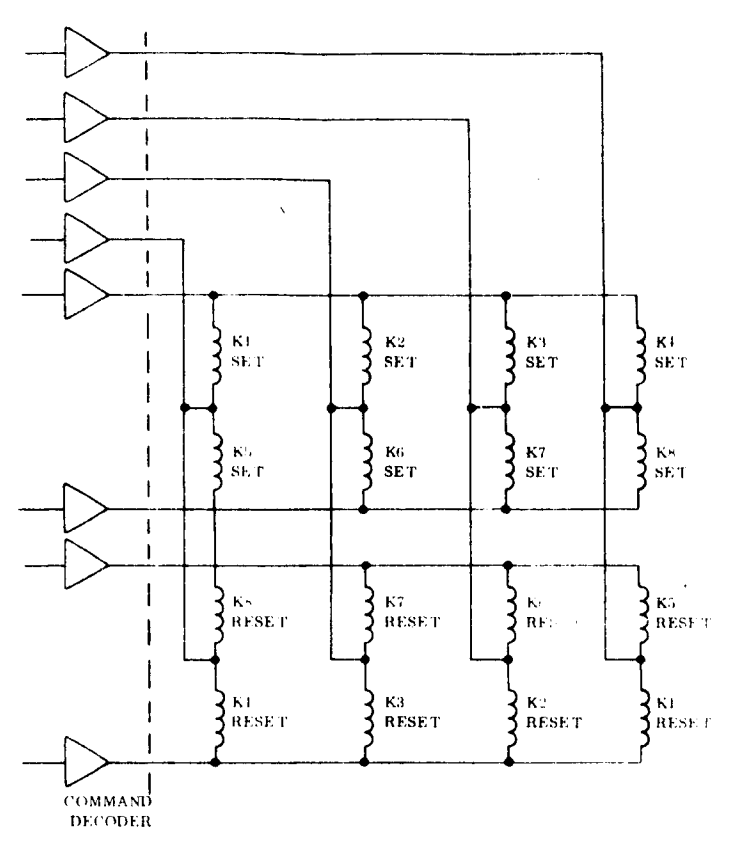


Figure 5. 7-4. Relay Logic

firing from the sun sensor reference point and the time duration of this firing. The time of radial nozzle firing from the reading of the sun sensor signal can vary from 0 to 800 milliseconds. It is desirable to have a timing resolution of 1 millisecond; therefore 10 bits are required for this function. It is also necessary to define the duration of the firing via the command system: this duration varies from 100 to 200 milliseconds with 1 millisecond resolution, requiring 7 data bits. The command subsystem must also provide data to define the number of firings which is to occur. This can vary from 1 to 1000 requiring 10 data bits. Two command addresses will be used to control the nozzle firing, one for the 10 bits defining the time of firing and 5 of the 7 bits defining the time duration, and the second for the 10 bits defining the number of firings and 2 bits to define the remainder of the time duration.

The remainder of the spacecraft requires ON/OFF or selection type of commands. There are 5 word addresses to decode these types of commands on the earth viewing-equipment module and 8 word addresses in the aft equipment module, providing a capability of 150 and 240 outputs, respectively.

### 5.7.3.1 Star Tracker Memory

The command system contains a memory which is used for updating the declination of Polaris as the vehicle orbits the earth. The following gimbal angle command is required for proper spacecraft orientation control.

Gimbal angle command =  $\theta_{\text{off}}$  + (90 deg -  $\delta$ ) sin ( $\omega_{\text{e}}$ t +  $\delta$ )

where  $\theta_{\text{off}}$  = offset pointing angle, -8.7 deg  $\leq$  9 off  $\leq$  +8.7 deg

 $\delta$  = declination of star (89.09° N)

 $\omega_{R}$  = rotational velocity of earth = 15 deg/hr

t = time in hours

 $\phi$  = phase angle  $0 \le \phi \le 180 \text{ deg}$ 

The use of this signal is described in detail in Section 5.4.

The command resolution of 20 arc-seconds is required. The  $\theta_{\rm off}$  will be established by the 15-bit command previously discussed, giving a resolution of 7 arc seconds. The sinusoidal function has a command resolution of approximately 13 arc-seconds. This sinusoidal function is generated by the memory. The period of the sinusoid is 24 hours. The memory contains a stored sine wave in the form of time increments. The contents of the memory are continuously compared to the reference clock. When the clock and a word in the memory agree an output pulse is generated to the star tracker incrementing the gimbal angle command by either plus one or minus one interval. The memory is presently sized for 250, 13-bit words. The clock resolution is 5 seconds. The selection of the parameters for this memory and a possible alternate approach is described in more detail in Section 6.6.4.

The initiation of the clock will be performed by ground command. There will be 12 points (2 hours apart) at which the clock can be started. This would mean that if the vehicle had lost its reference for some reason, then a maximum period of two hours is required before an accurate gimbal angle offset can be commanded.

## 5.7.4 TELEMETRY SUBSYSTEM

The telemetry subsystem samples the diagnostic, operational, and experimental monitors throughout the vehicle and transmits this information to the ground station. The telemetry subsystem is a PCM/PSK/PM system operating at a frequency in the 2200 to 2300 MHz range.

Data is transmitted at one of two possible data rates; 500 bps and 8 kbps. The low rate is used during the spin mode because of the low antenna gains. The desired data rate is selected by command. The PCM data bi-phase-modulates a 1.024 MHz subcarrier which phase-modulates the carrier.

The PCM format consists of a 128-word main frame with seven bits per word. A four-word frame sync is provided. Two telemetry processors and six subcommutators are implemented in the reference design. One telemetry processor and four subcommutators are located in the aft equipment module, and one telemetry processor and two subcommutators are located in the earth-viewing equipment module. The purpose of the separation is to minimize the cabling between the two equipment modules.

Only one of the telemetry processors will operate at a time, the selection being dependent on what experiments are being performed. Some data wires will still have to run between the equipment modules for the fore and aft monitoring which must occur "simultaneously."

During the spin mode, the telemetry subsystem will operate at a rate of 500 bps. The output of the telemetry transmitter will be switched between the "A," "B," and "C" antennas during this mode. The "A" antenna provides coverage for  $\pm 20$  degrees about the pitch-roll plane and is omnidirectional about the spin axis. The "B" antenna provides coverage in the positive yaw direction  $(\pm 70^{\circ})$  and the "C" antenna in the negative yaw direction  $(\pm 45^{\circ})$ . The selection of the proper antenna will be performed by ground command. During the stabilized mode, the telemetry subsystem can operate at either the 500-bps or 8-kbps rate, with the 8-kbps rate being preferred. The telemetry transmitter will operate with antenna "D" for this mode of operation. The "D" antenna is a high-gain antenna on the positive yaw axis.

While the parabolic reflector is unfolding, the telemetry subsystem will be commanded to the subcommutation "speed-up" mode. In this mode, the telemetry processor will only be sampling two channels, the two corresponding to the two subcommutators monitoring the large antenna. The sampling rates of these two subcommutators will be increased during this mode to provide the output data rate of 8kbps. Special synchronization words will be provided during this mode.

Each telemetry processor will have an input capability of 122 equivalent analog channels and each subcommutator will have a capability of 64 analog inputs. A typical main frame is shown in Figure 5.7-5. This provides a total capability of 378 equivalent analog channels for the aft equipment module and 250 equivalent analog channels for the earth-viewing equipment module.

The telemetry processor will be a design extension of the Gravity Gradient Test Satellite (GGTS) telemetry processor. The transmitter will be a modified version of the transmitting section of the Goddard Range and Range Rate transponder.

# 5.7.4.1 Telemetry Monitors Requiring Additional Circuitry

Only one source of data for diagnostic and operational telemetry requires a significant amount of additional circuitry to accomplish the measurement. This does not include telemetry associated with the experiments.

During the spin mode, it is necessary to determine the vehicle spin rate and spin vector attitude with the aid of sun sensors. Two sun sensors, with a view angle separation of about 35 degrees, are used as part of the attitude determination. It is necessary to determine the time difference of the intercept of the sun between the two sensors with a resolution of about 1 millisecond so that an attitude determination accuracy of 0.2 degrees can be achieved. This is accomplished by using a counter which is started by the interception of the sun by the "reference" sun sensor and stopped by the sun interception on the second sun sensor. A 1-kHz signal is gated into the counter during this period, providing the 1-millisecond timing resolution. The 1-kHz signal is obtained from the memory/clock.

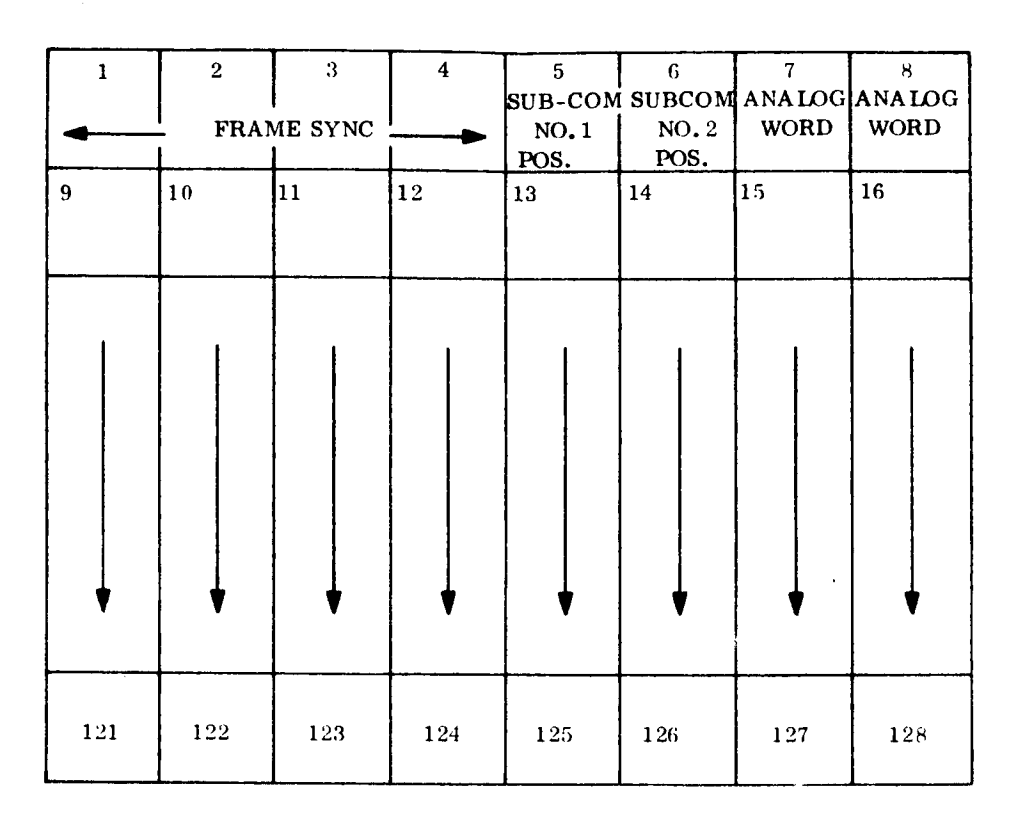


Figure 5.7-5. Typical Main Frame

It is also necessary to determine the spin rate by use of the sun sensor. This is implemented in a similar manner using the same 1-kHz clock, but starting and stopping the counter using the sun intercept signal from the reference sun sensor only. In this manner, a measurement is made every other revolution.

In order to be certain an erroneous telemetry signal does not occur due to the telemetry system sampling the counter while it is counting, an additional signal will be provided to telemetry (for each counter) to indicate that it is in a counting cycle. The first counter will be sampled at least twice per revolution, and the second counter at least once per revolution.

## 5.7.5 TRACKING SUBSYSTEM OPERATION

The Goddard Range and Range Rate System will be used to accurately track the spacecraft. A 2-channel, sequential mode of operation will be used with a highest major tone of 100 kHz. Tracking information will be time-shared with command and telemetry transmissions. The tracking transponder will consist of a section of the command receiver and the telemetry

transmitter. The extraction of the tracking information from the received signal is shown on a modified block diagram of the Goddard Range and Range Rate receiver (Figure 5.7-2).

When vehicle tracking is to take place, a command is transmitted to the vehicle to turn on the T&T transmitter and place it in the tracking mode. This essentially connects the tracking output of the receiver to the T&T transmitter. The ground station then proceeds to transmit the tracking data to the vehicle. If a command must now be sent or telemetry data is desired, the tracking will be terminated and the required commands transmitted to perform the desired functions.

During telemetry transmission, the ground station can still angle track; however, this does not provide the vehicle position accuracy required for the circulization of the orbit and stationkeeping.

During the vehicle spin mode only low-gain antennas are available. Preliminary calculations have indicated that the 1-watt transmitter will be sufficient for tracking during this period. The tracking subsystem was originally sized using the 10-watt transmitter in the experiment equipment. The higher power transmitter was chosen because poor antenna gains were expected furing this mode. However, the antenna gains proved to be higher than originally expected allowing the use of the 1-watt transmitter. The power profile during this mode assumes use of the 10-watt transmitter.

During the vehicle spin mode it is also necessary to determine vehicle attitude. This is accomplished by use of sun sensors and polarization angle measurements of the carrier transmitted via the "A" antenna. The telemetry/tracking carrier has tentatively been selected to be the reference signal for measuring the polarization angle, since utilization of this transmitter would not necessitate additional equipment. The transmission frequency is approximately 2300 MHz, and data on the Syncom polarization angle measurements in about the same frequency range (1820 MHz) indicates an accuracy of only 2 degrees. However, sufficient information on the present capabilities for measuring these angles is not available and the confidence level of the Syncom data was not certain. Therefore, a detail analysis and implementation of the measurement scheme could not be undertaken,

but it is believed that at least a ±1 degree accuracy can be attained. Results of a preliminary analysis indicates that it would be more desirable to transmit at X-band rather than S-band. S-band transmission has been utilized on the reference design until more information on the overall problem is attained. Additional discussion of polarization angle measurements is presented in Section 6.5.

#### 5.7.6 TT&C ANTENNAS

### 5.7.6.1 Antenna Coverage

It is desirable to have omnidirectional coverage for telemetry, tracking, and command in all modes of operation. However, due to mounting limitations, the size of the parabolic reflector and the type of coverage required, only 85 percent coverage has been realized during the spin mode and 100 percent during the stabilized mode.

There are three modes of operation in which the telemetry and command coverage constraints are different. The modes are: (a) transfer orbit/spin mode, (b) synchronous orbit/spin mode, and (c) synchronous orbit/stabilized mode.

During the transfer orbit the vehicle is spin stabilized. The time history of a required antenna half-beam angle to various ground stations, based on a minimum elevation angle of 5 degrees from the ground station is shown in Figure 5.7-6. The half-beam angle is as defined in Figure 5.7-7. The satellite is oriented 19.4 degrees to the equator during this mode. By using antenna "A" exclusively, sufficient data will be available to obtain a fix on the vehicle position. (Antenna "A" provides a 40° beamwidth, toroidial pattern about the spin axis.) Figure 5.7-6 indicates the amount of time telemetry data will be received

During the synchronous orbit/spin mode, the vehicle is still spinning with a orientation of the spin axis of 19.4 degrees to the orbital plane. Figure 5.7-8 shows the half-beam angle as seen from Rosman and Mojave during this mode of operation. The curves are cyclic with a period of approximately 24 hours. The telemetry coverage provided by each antenna during this mode of operation is shown in the illustration. No significant data is lost during the period when no coverage is obtained. During the synchronous orbit stabilized mode, only the high-gain antenna is used.

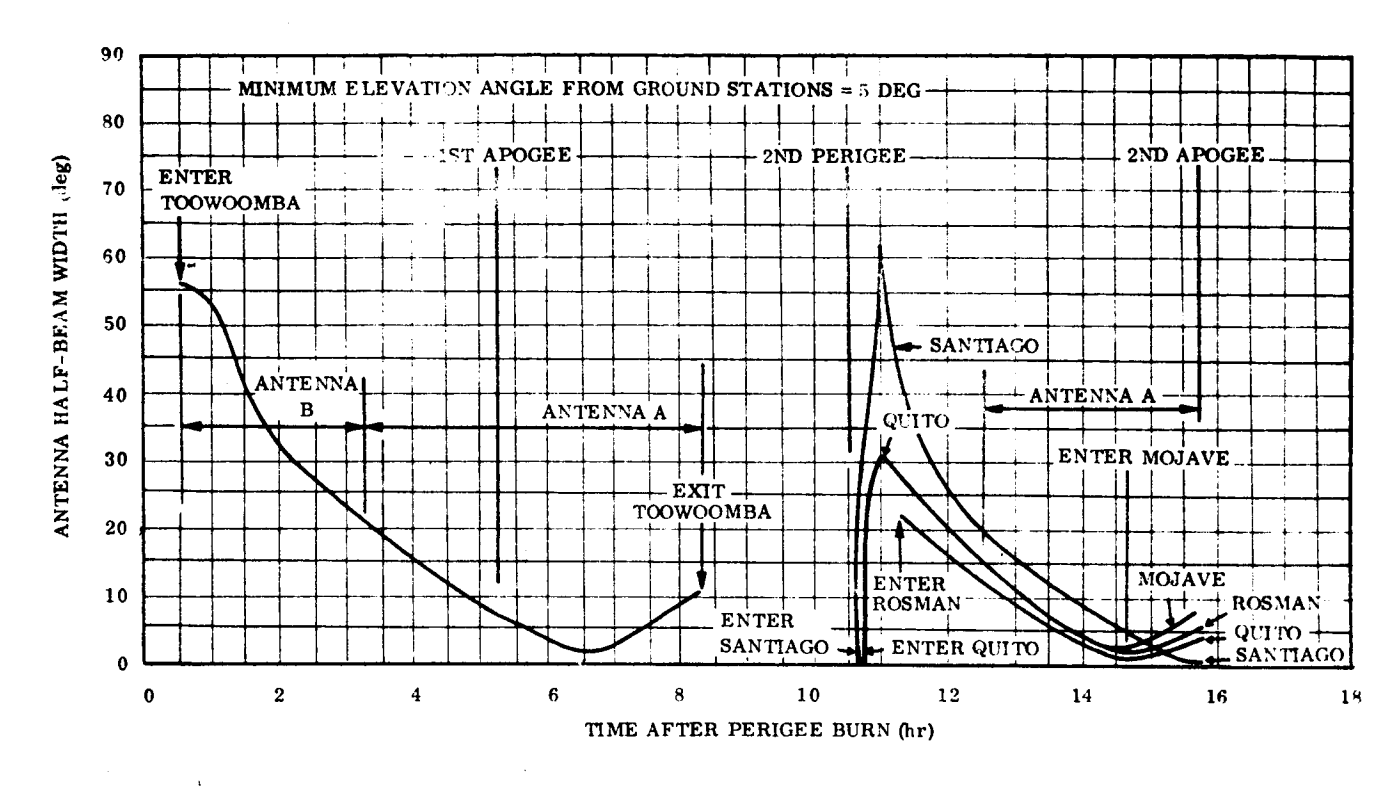


Figure 5.7-6. ATS-4 Reference Design: Antenna Half-Beam Angle During Transfer Orbit

The coverage provided by each antenna is summarized pictorially in Figure 5.7-9 and the switching requirements for the antenna is shown in Figure 5.7-10.

For command reception, two antennas are coupled together in order to provide a broad coverage. During the spin mode the input to the receiver will be obtained from antennas B and C. Due to combining of the antenna outputs, lobing patterns will be obtained in the pitch-roll plane (squinted in the negative yaw direction). During the earth-stabilized mode the inputs to the receiver will be obtained from antennas C

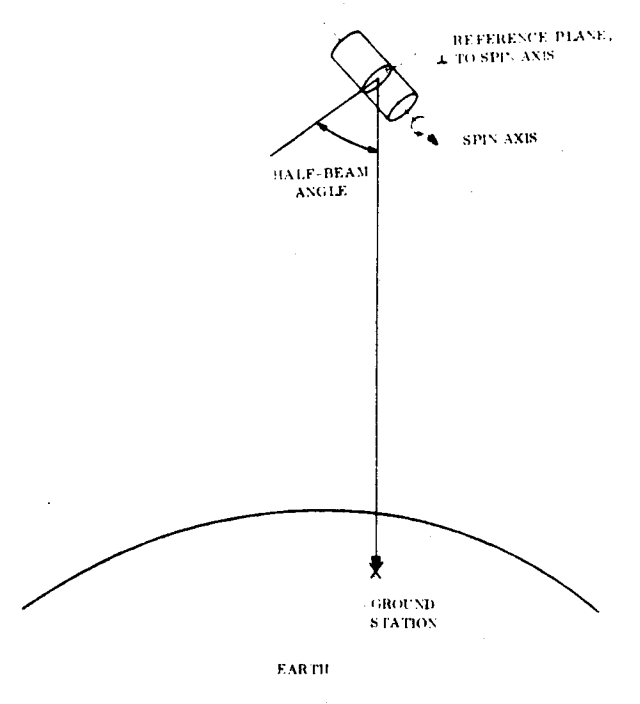


Figure 5.7-7. Half-Beam Angle Definition

and D. Switching from antenna B to antenna D will be accomplished by ground command and backed up by the unfolding of the parabolic reflectors. For this combination of antennas severe lobing will occur in the pitch-roll plane but this is of no significance as the vehicle is stabilized. The lobing patterns in the pitch-roll plane for both modes of operation are eliminated when the preferred redundant design (discussed in Section 5.6.8) is implemented.

### 5.7.6.2 Antenna Design

Three different types of antennas are required to provide the specified coverage for the TT&C subsystem.

A coaxial array is used for transmission of telemetry and tracking data and for the polarization measurements. A truncated conical spiral is used for transmission of telemetry and tracking data, and reception of command and tracking data. Two flush-mounted cavities are used for the transmission of telemetry and tracking data and for reception of tracking and command information.

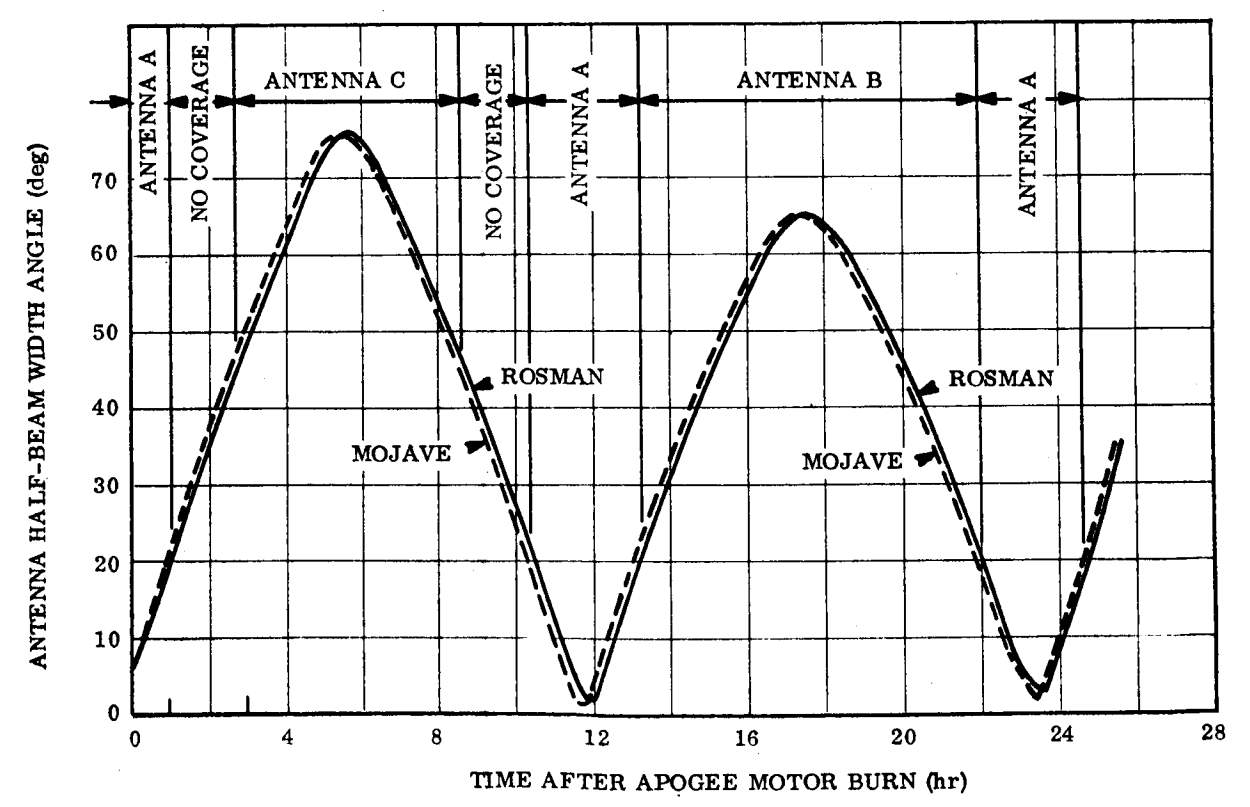


Figure 5.7-8. ATS-4 Reference Design: Antenna Half-Beam Angle During Vernier Maneuvers While in Synchronous Orbit

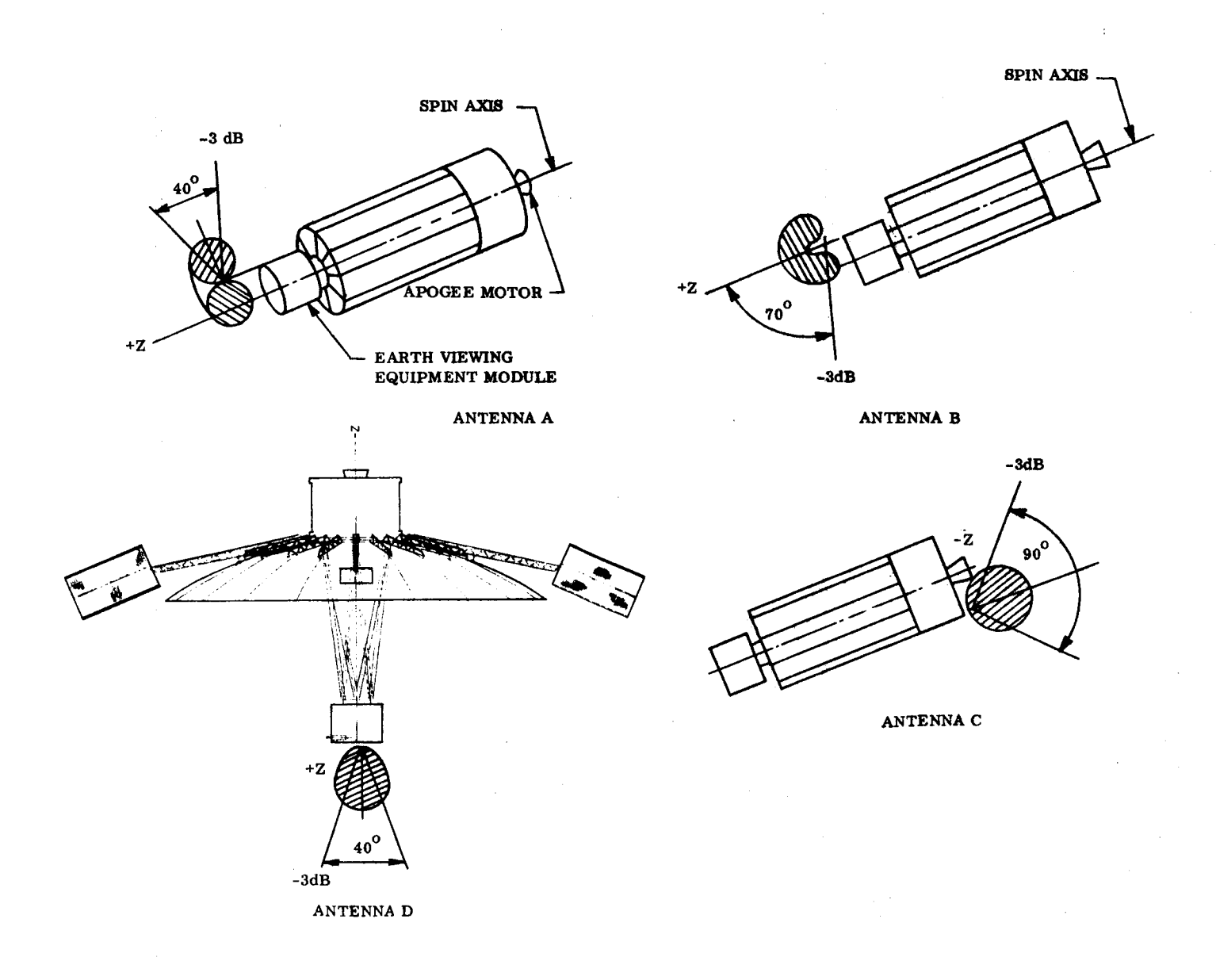


Figure 5.7-9. Antenna Coverage

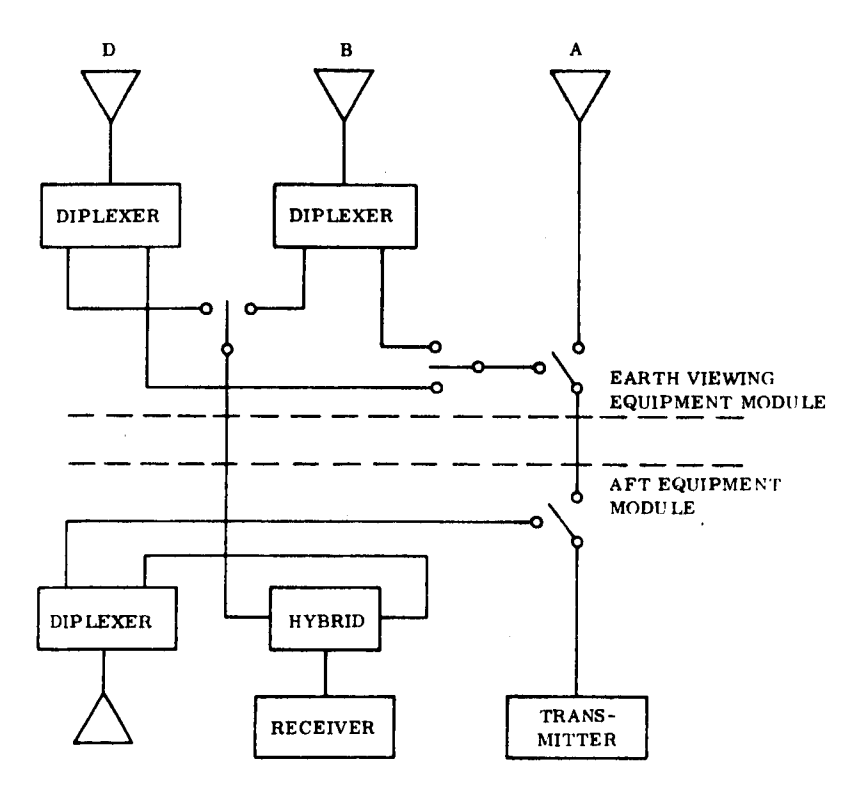


Figure 5.7-10. Antenna Switching Reference Configuration

One flush-mounted cavity (antenna D) is mounted on the face of the earth-viewing equipment module and the other (antenna C) on the aft equipment module with its axis in the negative yaw direction. Broad circular polarized patterns are obtained. The maximum gain referred to a circularly polarized isotropic antenna is 5 dB; +3 dB points are at  $\pm 30$  degrees and  $\pm 10$  dB points are approximately 140 degrees apart. The axial ratio at the  $\pm 10$  dB points is about 10 dB. The presence of the apogee motor will cause some interference patterns on the aft flushed-mounted cavity, but this is not expected to significantly affect the gain within the desired beamwidth. (The margin calculations for this antenna are based on  $\pm 3$  dB gain at  $\pm 45^{\circ}$ .)

The antenna consists of a 3-inch-diameter cavity 1.5 inches deep, containing a short helix feed encapsulated in polyurethane foam (see Figure 5.7-11). This is covered with a 1/2-inch-thick fiberglass disk. A mounting flange and TNC connector complete the assembly.

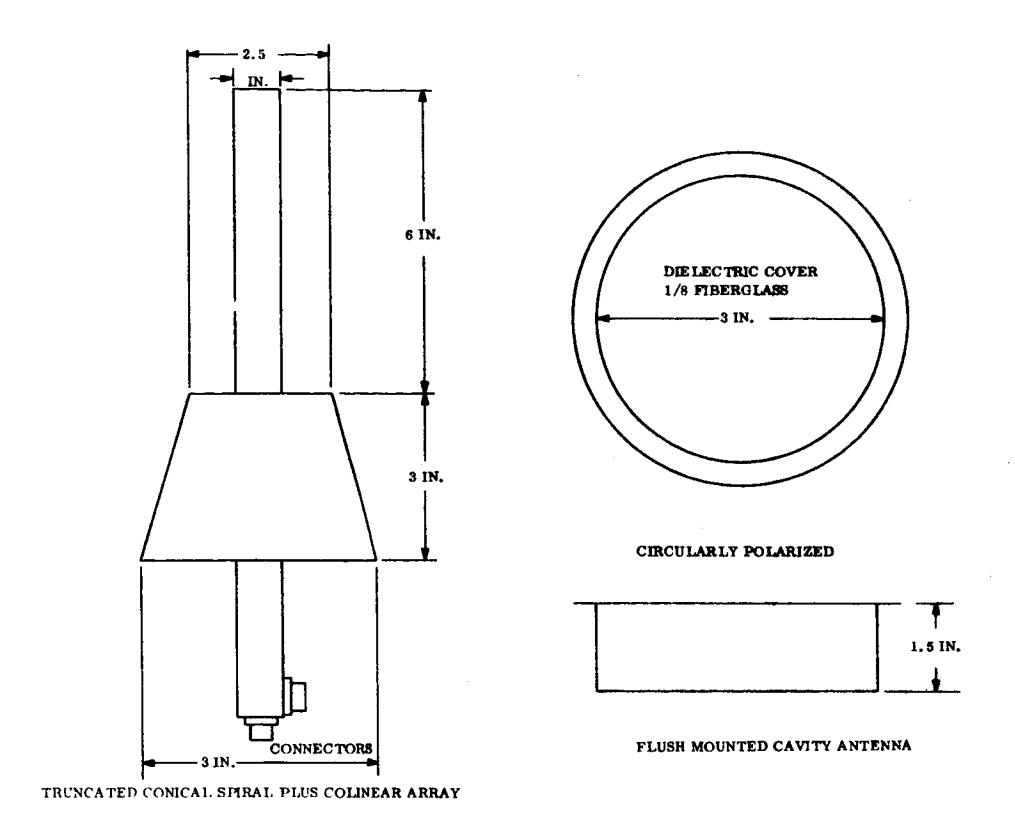


Figure 5. 7-11. Antenna Design

One truncated conical spiral, along with a colinear array, is required for coverage in the positive yaw direction during the spin mode. This antenna system is mounted on a rod extending from the earth-viewing equipment module. The rod allows the colinear array to be sufficiently separated from the equipment module so that significant blockage does not occur in the negative yaw direction. The colinear array is mounted coaxially on the truncated spiral (see Figure 5.7-11). When the parabolic reflector is unfolded, this antenna system is swung back, becoming parallel to the pitch-roll plane, so that it does not cause interference with the interferometer.

The gain of the truncated spiral within  $\pm 70$  degrees of the axis is -3 dB minimum. The 10-dB width is greater than 180 degrees and the axial ratio at 90 degrees is 6 dB. The conical spiral can be truncated since the extensive bandwidth capability of a full conical spiral is not required.

The colinear array (antenna A) resembles two dipole elements placed end to end, and is realized by the use of two circumferential slots in a dielectric filled coaxial line. The coaxial line. The colinear array is longitudinally polarized. The 3-dB width in the plane of polarization is 40 degrees, and the pattern is omnidirectional in the traverse plane.

The combined antenna assembly has an overall length of 9 inches and a maximum diameter (conical spiral base) of 3 inches.

#### 5.7.7 MARGIN CALCULATIONS

Margin calculations for the telemetry, tracking, and command links for the various modes of operation are given in Tables 5.7-3, 5.7-4 and 5.7-5. A deviation of 1.6 radians has been used for telemetry. This deviation has not been optimized. It may be possible to use a different index for the two telemetry rates so that a more optimum balance of margins can be achieved; however, the details of this have not been investigated.

The large variations in line loss are due to the long cable runs between the transmitter/
receiver and the antennas on the earth-viewing equipment module. The margin calculations
indicate that adequate margin in all modes of operations with the use of the 1-watt transmitter.

For the Goddard Range and Range Rate tracking system, a 2-channel, sequential mode of operation has been assumed with a highest major tone of 100 kHz. Receiver master bandwidth position No. 2 has been assumed in the calculations (Reference - Goddard Range and Range Rate (GRR-2) Design Evaluation Report - Contract No. NAS5-9731) for the stabilized mode and bandwidth position No. 4 for the spin mode. Based on the signal-to-noise ratios for each tone, as indicated in the margin calculation, an equivalent rms range error of approximately 8 meters, and an rms range rate error of better than 0.018 meters/sec can be expected.

Table 5.7-3. Margin Calculations - Telemetry Data

TEI	EME	TDV	DA1	ГΔ

TELEMETRY CARRIER

	Gain (dB)	Loss (dB)	Power (dBm)		Gein (dB)	Loss (dB)	Power (dBm)
Transmitter Power (1W)			30	Transmitter Power			30
Modulation Loss ( $\beta = 1.6$ )		1.87		Modulation Loss ( $\beta = 1.6$ )		6.85	
Line Loss				Line Loss			i
Antenna A		3.8	1	Antenna A	i	3.8	
Antenna B		3.8		Antenna B	!	3.8	
Antenna C	1	0.28	1	Antenna C	1	0.28	
Antenna D	1	3.4		Antenna D		3.4	
RF Swtiches				RF Switches			
		0.6		Antenna A	Ĭ	0.6	
Antenna A		0.9		Antenna B		0.0	
Antenna B Antenna C	1	0.3	1	Antenna C	ŀ	0.3	
Antenna C Antenna D	1	0.9		Antenna D	<b>[</b>	0.9	
Antenia D		0.5		Parison D		""	
Diplexer				Diplexer			
Antenna A			1	Antenna A	1		
Antenna B		0.4	1	Antenna B		0.4	
Antenna C		0.4		Antenna C	i	0.4	
Antenna D		0.4	;	Antenna D		0.4	
Vehicle Antenna Gain				Vehicle Antenna Gain			
Antenna A (± 20°)		3		Antenna A (± 20°)	1	3	
Antenna B (± 70°)		3	i	Antenna B (± 70°)	1	3	[
Antenna C (± 45°)		3		Antenna C (± 45°)	1	3	
Antenna D (± 30°)	3	_	]	Antenna D (± 30°)	3	1	İ
Space Losses (19,500 nm, 2300 MHz)		190.8		Space Loss (19,500 nm, MHz)		190.8	
		130.0			44.2		
Ground Antenna Gain (30 ft)	44.2			Ground Antenna Gain (30 ft)	44.2		
Power Available at Receiver				Power Available at Receiver	İ		
Antenna A	<b>\</b>		-125.97	Antenna A		1	-130.85
Antenna B			-126, 57	Antenna B		ļ	-131.55
Antenna C			-122.45	Antenna C		1	-127.43
Antenna D			-120.17	Antenna D		1	-125.15
Receiver Noise Density (Te = 400° K)		:	-127.6/Hz	Receiver Noise Power (Te = 400° K; 1 kHz bandwidth)			-142.6
,					İ	1	
Detection Noise Bandwidth	1			Threshold S/N	1	6	
500 bps		27		Required Power at Receiver	1		-136.6
8 kbps		39		Margin		ļ	
Detection Noise Power	1			Antenna A	5. 75	1	
500 bps			-145.6	Antenna B	5.05		
8 kbps			-133.6	Antenna C Antenna D	9. 17 11. 45	]	
Required S/N		8 <b>.6</b>		Agreema D	1 11,40	<u> </u>	
Required Power at Receiver							
•			-137				
500 bps			-125				
6 kbps							
Margin	1	Ì	1				
Antenna A	11,13						
Antenna B	10,43						
Antenna C	14, 55	[					
Antenna 1) - 500 bps	16, 83						
Antenna D - 8 kbps	4.83	ì	1				

Table 5.7-4. Margin Calculations - Tracking

SPIN MODE				STABILIZED MO			
	Gain (dB)	Loss (dB)	Power (dBm)		Gain (dB)	Loss (dB)	Power (dBm)
Transmitter Power (IW)	<del></del>		30	Transmitter Power (1W)			30
Modulation Loss	1			Modulation Loss			
		2.44		Currier		2.44	
Carrier Subcarrier	ļ	10.05		Subcarrier	ŀ	10. <b>05</b> 15. <b>6</b> 1	
Major Tone (2)		15.61		Major Tone (2)	į.	15.61 27.0	1
Minor Tone (5)		27.0		Minor Tone (5)	1	19. 52	
		19.8		Code		15.02	1
Line Losses			]	Line Losses	1	3.4	1
Antenna A		3.80				0.9	1
Antenna B Antenna C		0.28		RF Swiiches	1	0.9	İ
Antenna C				Diplexer		0.4	
RF Switches	}	ł					
Anterna A		0.60		Vehicle Antenna Gain	3		
Antonna B		0.90	ļ	Space Loss (19,500 nm, 2300 MHz)		190.8	ŀ
Antenna C		0.30	1	Space Loss (15, 500 mm, 2500 mmz)			
Diplexe:			<b>†</b>	Ground Antenna Gain (30 ft)	44.2		
Antonna A			1	Power Available at Passirer	1		
Antenna A Antenna B		0.40		Power Available at Receiver			-120.74
Antenna C		0.40	l	Carrier	!		-120.74
	1	1	i	Subcarrier	1		-128.33
Vehicle Antenna Gain	1		I	Major Tone (2) Minor Tone (5)	1		-145.3
Anteron A (± 20°)		3	I	Code			-138, 12
Antenna B (± 70°)		3	1				1
Antenna C (± 45°)	ŀ	3		Receiver Noise Density (460° K)			-172/H
Space Loss (19,500 nm, 2300 MHz)		190.8		Total Received Signal Power to Noise Pow	war Dansitu		
chart the first on unit once many	1			Total Received prights rower to Horse No.			1
Ground Antenna Gain (30 ft)	44.2	1	1		dBm/Hz		1
Power Available at Receiver	1			Carrier	51, 26		
Power Available at Receives	Antenna A	Antenna B	Antenna C	Subcarrier	43.65		
	(dBm/Hz)	(dBm/Hz)	(dBm/Hs)	Major Tone (2)	38.09		
Comment on	1	1 '		Minor Tone (5)	26.7		1
Carrier Subcarrier	- 126, 44 - 134, 05	-127.40 -134.75	-123.02 -130.63	Code	33.88		i
Major Tone (2)	-139,61	-149.00	-136, 19	Carrier Phase Lock Loop	(dB)	(d. <b>B)</b>	
Minor Tone (5)	-151.0	-151.70	-147.58			27.8	1
Code	-143.82	-144,52	-140, 40	Acquisition Bandwidth (600 Hz) Acquisition S/N	23.46	21.0	
		1	-172/Hz	Tracking Bandwidth (328 Hz)		25.16	1
Receiver Noise Density (Te - 460° K)		1	-1/2/nE	Tracking S/N	26. 1		
(16 · 400 · K)	i	ł				1	
Total Received Signal Power		1		Subcarrier Phase Lock Loop			1
to Noise Power Density			1	Acquisition Bandwidth (600 Hz)		27.8	Ì
Carrier	45.56	44.86	48.98	Acquisition S/N	15. 85	25. 16	
Subcarrier	37.95	37, 25	41.37	Tracking Bandwidth (328 Hz) Tracking S/ N	18. 49	-3.30	
Major Tone (2)	32.39	31.69	35. 81	I racking ov it	-05		
Minor Tone (5)	21.00	20.30	24.42	Major Ranging Tones			1
Cone	28. ln	27.48	31.60	Tracking Bandwidth (1 Hz)		0	1
Carrier Phase Lock Loop	(dB)	(dB)	(dB)	Tracking S/ N	38.09		1
Acquisition Bandwidth (60 Hz)	17.78	17.78	17. 78				
Acquisition S/N	27.78	27, 08	31.20	Minor Ranging Tones			1
Tracking Bandwidth (20 Hz)	13,00	13.00	13,00	Tracking Bandwidth (0.3 Hz)		-5.22	1
Tracking S/N	32.56	31.86	35.98	Tracking S/ N	31.92		
Subcarrier Phase Lock Loop			İ				1
Acquisition Bandwidth (60 Hz)	17.78	17. 78	17.78				
Acquisition S/ N	20.17	19.47	23.59				1
Tracking Bandwidth (20 Hz)	13. 00	13.00	13.00	1			
Tracking S/N	24.95	24.25	28.37				
Major Ranging Tones			1	4		1	
Tracking Bandwidth (0, 1 Hz)	-10.90	-10.00	10.55			1	1
Tracking Sandwidth (0, 1 Hz) Tracking S/N	-10.00 42.39	-10.00 41.69	-10.00 45.81			!	
			10.01				
Minor Ranging Tones							
Fracking Bundwidth (0. 1 Hz)	-10	-10.0	-10.00			1	1
Tracking S/ N	31	30.3	34.42	j .	ı	1	1

Table 5.7 - 5. Margin Calculations Command Link

	Gain (dB)	Loss (dB)	Power (dBm)
Transmitter Power (10 (kW)			70
Transmitter Antenna Gain	42		
Space Loss	•	188.6	
Minimum Vehicle Antenna Gain (Relative to CP)		20	
Line Losses		4	
Diplexer Loss		0.4	
RF Switch Loss	٠	0.4	
Power at Receiver			-101.4
Receiver Noise Density (10 dB NF)			-164/Hz
Baud Rate (1000 baud, 1 kHZ BW)		30	
Required S/N (10 <sup>-5</sup> baud error rate)		20.2	
Required Subcarrier Power			-113.8
Margin	12.4		

Table 5.7 - 6. Summary of Component, Power, Weight, and Size

Puty Cycle (\$)	  100 100 5  100 35 35 35 35 35 35 35 35 35 35 35 35
Total Power Dissipated (W)	8
Total Dissi	A             8   1.2   2.15   1.0
Total Input Power (W)	BI
Te Input J	64. 4 P
No. of Units Operating ® Same time	EI
No. Oper	<
28V Imput Power (each)	16 6.7 25 8.35 8.35
Vol. (each) (in. )	E I I I I I I I I I I I I I I I I I I I
Total Weight (lb)	BI 2 4 4 4 4 4 4 4 4 4 4 4 4 4 4 4 4 4 4
Total W	7 5 1 0 0 0 0 0 0 0 0 0 0 0 0 0 0 0 0 0 0
No. Req'd	色  よううゆことととしまるととと 4・一年
No.	<  4 W 4 L L L L L L L L L L L L L L L L L
Component Configuration	Atterna Atterna Atterna Atterna Atterna Atterna Atterna Atterna Atterna Command Decoder Command Decoder Relay Box Menory and Clock Sulformmutator TLM and Tracking Transmitter Mecaver Converter Decoder Converter TLM Converter TLM Converter Standard Cabling Conx Cabling TLM Processor

A - Non-Redundant Configuration
B - Preferred Configuration
\* - Power obtained from receiver converter
\*\* - Power obtained from decoder converter
\*\* - Fower obtained from TLM converter
\*\* - 5 W dissipated in sensors

### 5.7.8 IMPLEMENTATION OF REDUNDANCY

The reference design does not apply any redundancy to assure reliable system operation. However, the need for redundancy is obvious since a failure in a critical area could cause total mission failure. A preferred redundancy configuration has tentatively been established. This configuration is shown in Figure 5.7-12. Several changes have to be made to the basic reference design in order to implement the redundancy.

The use of two receivers eliminates the need for the hybrid, but this is replaced by an RF transfer switch. Each receiver will now be connected to a different antenna. This will eliminate the lobing encountered in the pitch-roll plane due to the use of the hybrid on the one-receiver configuration. The position of the transfer switch is to be controlled by a timer. The timer is reset each time the command system is interrogated. If no commands have been transmitted for some fixed period, the transfer switch will change position. The receivers and respective command detectors will operate continuously.

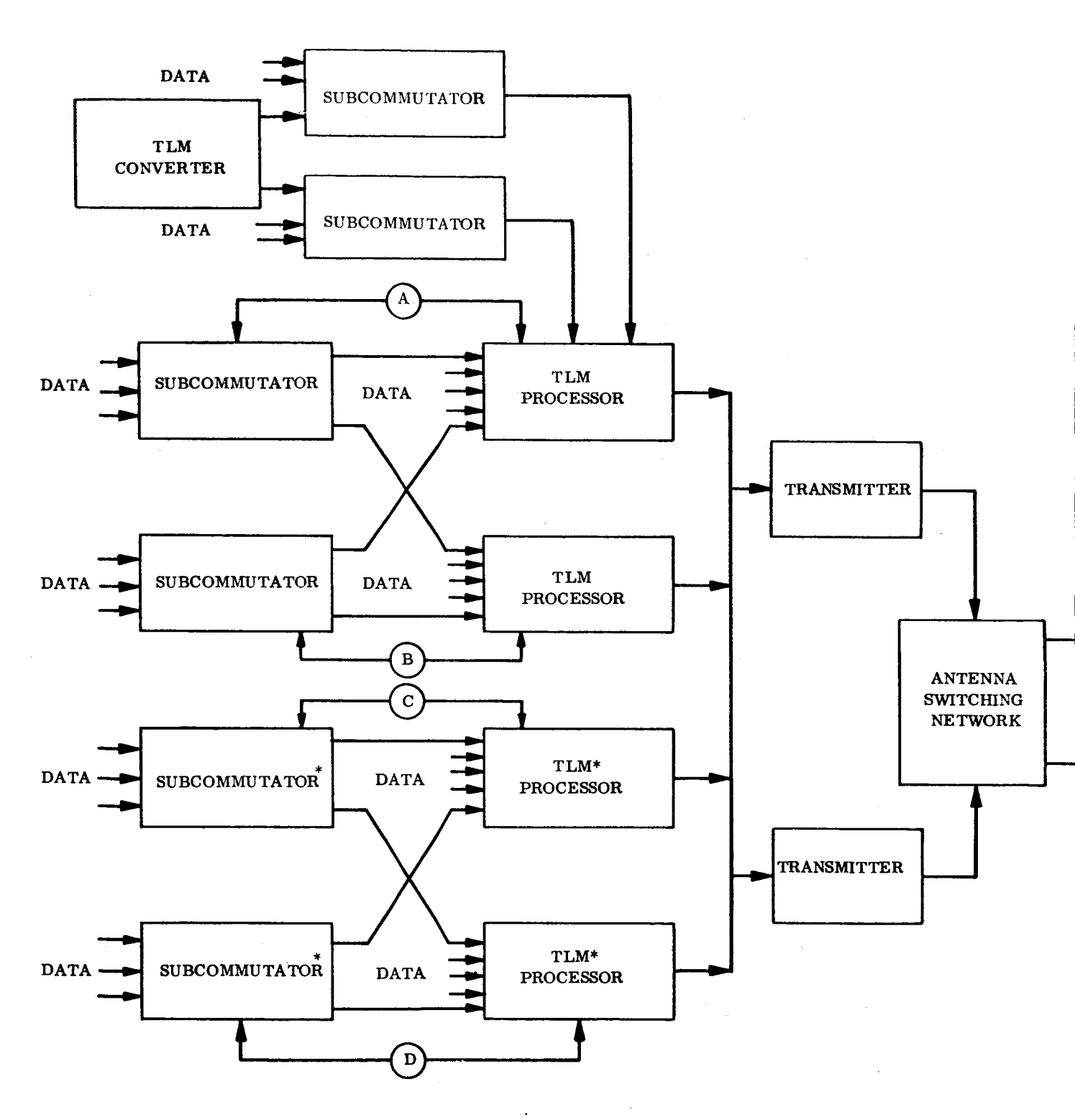
The spare bit in the command decoder will be used as a decoder identification bit. Commands transmitted to the vehicle via either of the receivers will be fed to both decoders. The decoder which is to process the command is controlled by the decoder identification bit. Only one decoder will be executing a command at a time.

For redundancy in the telemetry subsystem, block redundancy has been used for all components except the subcommutators.

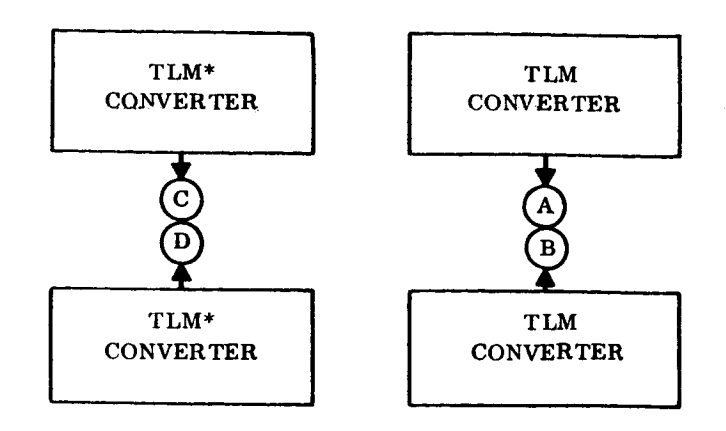
Changes in the antenna switching network are summarized in Figure 5.7-13. Power, weight, and size summary for the reference and redundant configuration is given in Section 5.7.9.

## 5.7.9 POWER, WEIGHT, AND SIZE SUMMARY

Table 5.7-6 summarizes the component power, weight, and size estimates of the reference design and the redundant design. The two sections of the command decoder have been considered as one unit for purposes of this chart. The decoder converters each have internal redundancy such that, if a section fails, at least one of the decoders will still be receiving



\*LOCATED IN EARTHVIEWING EQUIPMENT MODULE



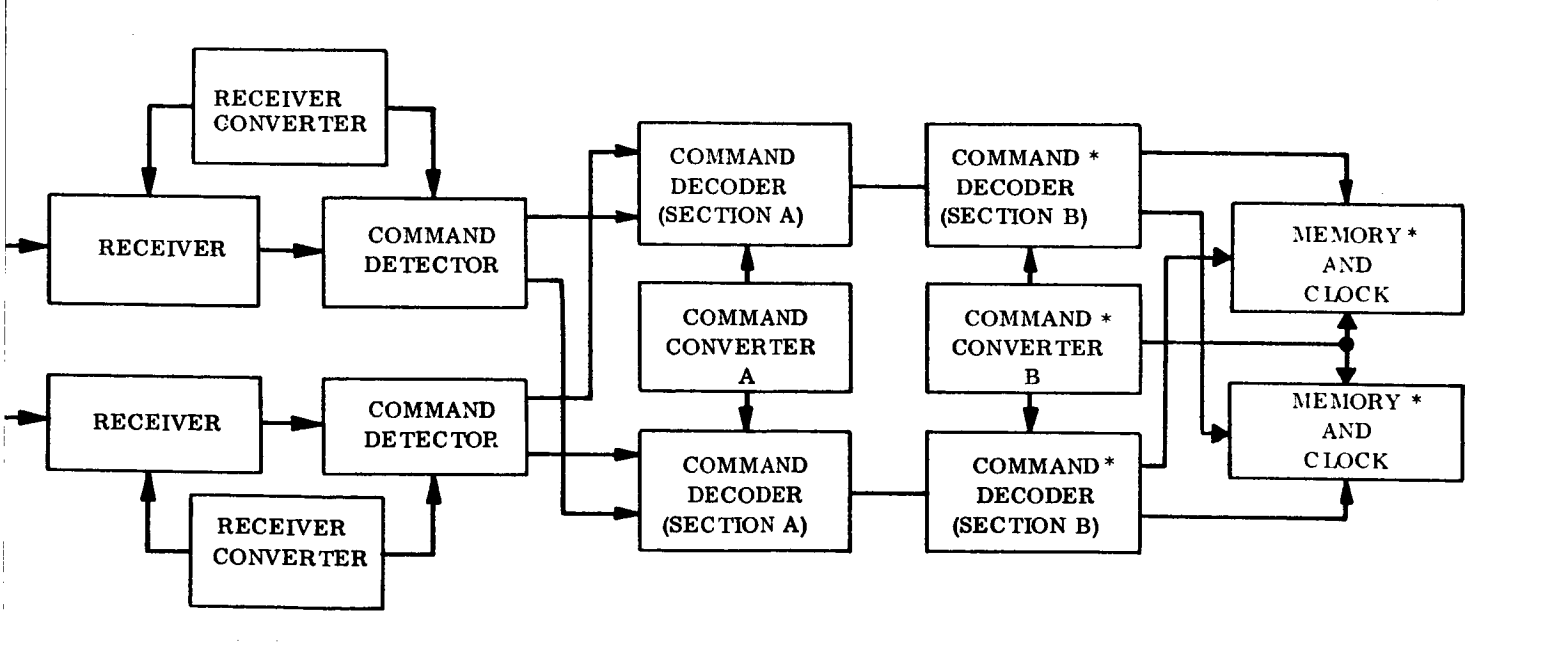


Figure 5.7-12. TT&C Block Diagram, Redundant Configuration



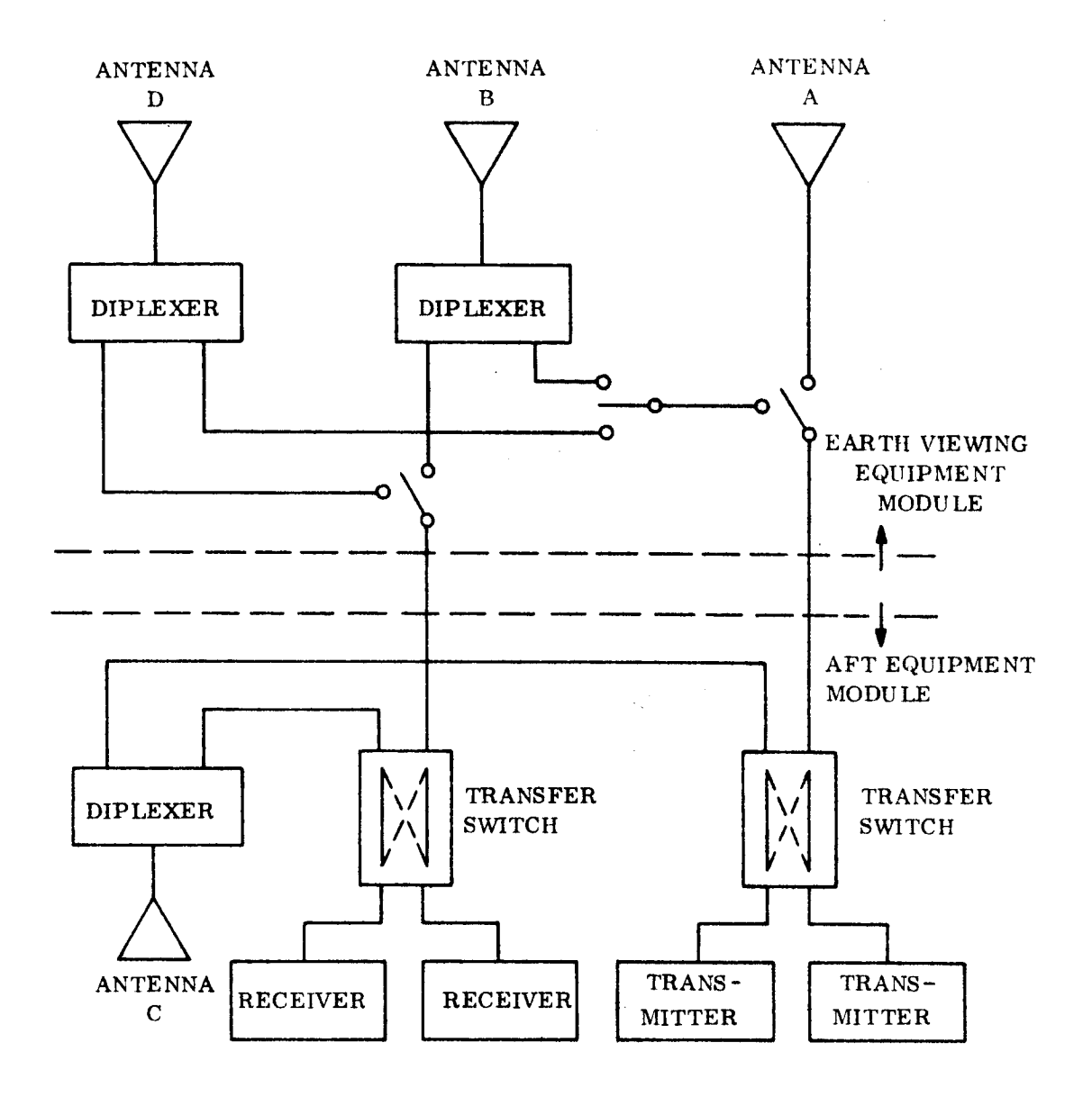


Figure 5.7-13. Antenna Switching, Redundant Configuration

power. The telemetry subcommutators have not been implemented redundantly in either mode since the failure of any subcommutator will not cause total mission failure. The duty cycles indicated in the diagram are based on a nominal 7-1/2 hour experiment per day, with a 5 percent duty cycle the remainder of the day. Table 5.7-7 summarizes the design status of the equipment.

Table 5.7-7. Summary of Design Status

Component	Design Status	Program	Comments
Receiver	Modified Motorola Transponder	Lunar Orbiter	
Command Detector	Modified TRW "SGLS" Signal Conditioner	AF Programs	
Command Decoder	New Design	-	Standard Design
Relay Box	New Design	_	<b>Approa</b> ch
Memory and Clock	New Design	_	<b>!!</b>
Subcommutator	New Design	_	**
Telemetry Processor	Modified GGTS TLM Processor	GGTS-GGII	
TLM and Tracking Transmitter	Modified Motorola Transponder	Lunar Orbiter	Standard Design Approach
Receiver Converter	New Design	-	**
Decoder Converter	New Design	-	''
TLM Converter	New Design	-	11

### 5.8 POWER

### 5.8.1 REQUIREMENTS

The power subsystem is required to supply electrical power to the spacecraft during two phases of launch and during orbital operation in a synchronous orbit. The subsystem must provide power for the orbital loads for a period of two years beginning in the time period 1969-1970. Power must be supplied for both the sunlit portions of the orbit and the umbra periods. The load requirements for the various mission phases are presented below.

## 5.8.1.1 Launch Load Profiles and Spacecraft Sun-Orientation

There are two phases of launch during which power is required for operation of the space-craft; for 15.75 hours during the transfer orbit and for about two days during the vernier maneuvers of the near-synchronous orbit. At the time these loads occur, the spacecraft is separated from the booster, is unshrouded in the stowed configuration of launch, and spinning at the rate of approximately 72 rpm. The orientation of the spacecraft spin axis to a normal to the equatorial plane may be as small as 65 degrees and the angle between the projection of the spin axis onto the ecliptic plane and the sun direction may be between 75 and 105 degrees. In addition, since launch may occur at any time of the year, the sun can be inclined plus or minus 23.5 degrees to the equatorial plane.

During the spin-stabilized orbit transfer phase, only telemetry, tracking, and polarization angle measurements power is required over and above the base load. In the near-synchronous phase, a few hours of thruster solenoid operating power is required. The following list contains the components and the power levels from which the load requirements of Figure 5.8-1 and 5.8-2 were generated.

Component	Power (Watts)	Duty Cycle
Orientation Control		
Signal Processor/Electronics	3	100%
Accelerometer	7.6	100%

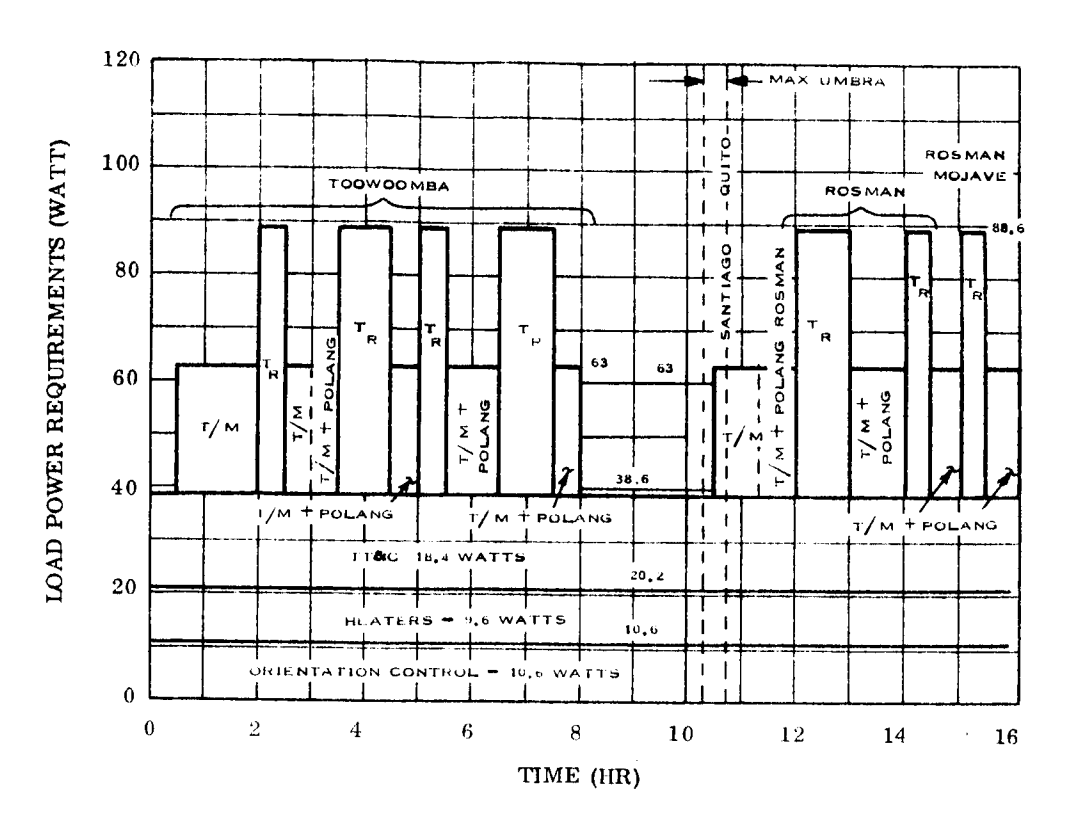


Figure 5.8-1. Load Power Requirements During Launch Transfer Orbit

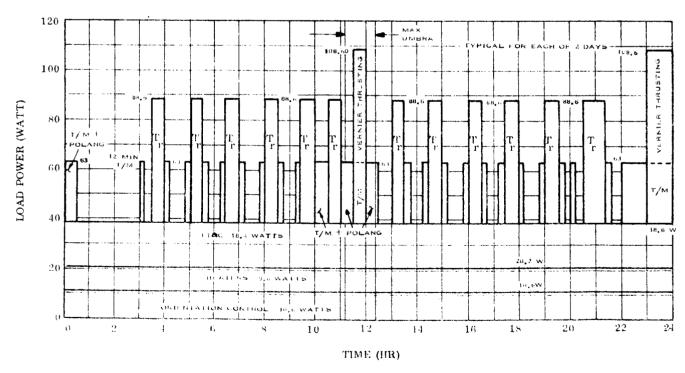


Figure 5, 8-2. Load Power Requirements During Near-Synchronous Orbit Vernier Maneuvers

Component	Power (Watts)	Duty Cycle
TT&C		
Receiver Converter	6.7	100%
Decoder Converter	11.7	100%
Tracking Transmitter	50	<b>25%</b> *
T/M Converter	8.35	) $60\%$ orbit-trans
T/M Transmitter	16	25% near-synch
Heaters	9.6	100%
Vernier Thrusting		(2. 5 hr
Solenoid Operator	45	10% maximum in synch orbit only)

<sup>\*</sup> Additional analyses have shown a good possibility of using the 16 watt tracking transmitter used in the in-orbit phase; however, the profile of Figures 5.8-1 and 5.8-2 will continue to show 50 watts.

#### 5.8.1.1.1 Transfer Orbit

The design load requirements for the transfer orbit phase of spacecraft operation, derived from the above table of component load requirements, are presented in Figure 5.8-1. All the loads in Figure 5.8-1 are in terms of the power required at 28 vdc. (Where necessary the power requirements for voltage conversion equipment have been included with the loads shown.) The period of maximum umbra which could occur during the equinox time of year is indicated in the illustration.

#### 5.8.1.1.2 Near-Synchronous Orbit

Similarly, the load requirements for the near-synchronous orbit phase of spacecraft operation are presented in Figure 5.8-2.

## 5.8.1.2 Orbit Load Profile and Spacecraft Sun-Orientation

The load requirements for the orbit phase of vehicle operation are presented in Figure 5.8-3. Except for 27 watts of the orientation control load requirements, which requires 400 Hz, 2-phase ac power, all the loads are in terms of the power required at 28 vdc. This reference design load profile is based on the following subsystem requirements:

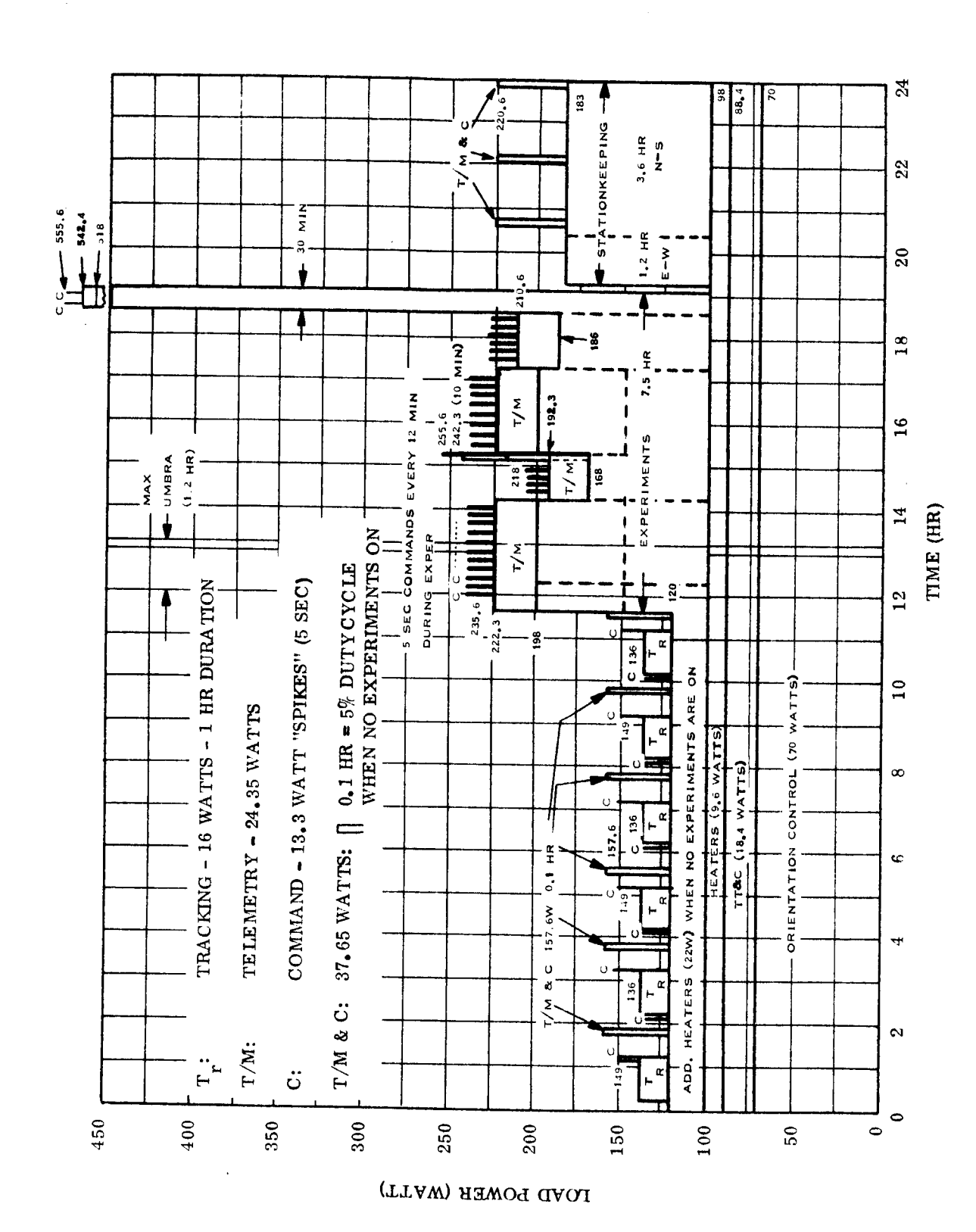


Figure 5.8-3. ATS-4 Reference Design Load Requirements

1. Orientation Control - (Either in orbit base loads, or initial stabilization)

	Earth Tracker	7	100% except Init. Stab.
	Star Sensor	, 8	100% except Int. Stab.
		30	100% except Init. Stab.
	Flywheel Motors	30 15	100% except Init. Stab.
	Flywheel and Jet Controller	30	100% except list. Stab.
	Sensor Signal Processor	30 15	Init. Stab. only
	3-Axis Gyro Package		· ·
	Gyro Electronics	15	Init. Stab. only
	Continuous	(70)	100% except Init. Stab.
	Initial Stabilization	60	Init. Stab. only
2.	Stationkeeping Thrusting:	85	20% ( $pprox 5$ hrs/day)
3.	Heaters:		
	Continuous	9.6	<b>100</b> %
	No experiment transmitters	22	<b>35</b> %
	or thrusters on.		·
4.	TT&C:		
	Receiver Converter	6.7	100%
	Decoder Converter	11.7	<b>100</b> %
	Tracking Transmitter	16	<b>25</b> %
	T/M Converter	8.35	30% + 5% when no exp. on,
	T/M Transmitter	16	30% - 100% during exps.
	Continuous	(18)	
		` '	

5. Experiments - The following list of experiments represents a typical ATS-4 measurement sequence and was derived for the purpose of sizing the power S/S. Additional experiment information is presented in Section 8. The experiment sequence is initiated 11.6 hours after the start of the ATS-4 day and terminates 7.5 hours later.

Time after start of experiments	M	Power Required
(Minutes)	Measurement	(Watts)
0000-0040	Parabolic Antenna Gain	50
0000-0040	Interferometer, Receive Mode	50
0040-0240	Parabolic Antenna Boresight	50
0040-0240	Interferometer, Reception Mode	50

Time after start of experiments (Minutes)	Measurement	Power Required (Watts)
0240-0340	Parabolic Antenna-Trans- reception	70
0330-0340	Interferometer, Receive Mode	50
0340-0540	Parabolic Antenna, Pattern	50
0340-0540	Interferometer, Receive Mode	50
0540-0700	Interferometer Exercises	88
0700-0730	Phased Array, 4-Beam	420

Summarizing the above data, the base load is 98 watts (70 watts orientation control, 18.4 watts TT&C, and 9.6 watts heaters). An additional 22 watts are required to provide heating when the experiment transmitters are not operating. For the typical ATS-4 day, six 1-hour tracking periods are shown. Telemetry data is normally required at a 5 percent duty cycle; during experiment operation however, continuous telemetry is required. Including heat-up time prior to thruster firing, approximately 4.8 hours of stationkeeping power at a level of 85 watts is required.

For design of the array and batteries, the time for occurrence of the umbra is as shown in Figure 5.8-3, whereas the peak load may occur at any time, including the umbra period.

During normal orbit operation, the spacecraft + Z-axis is directed toward the earth and lies in the equatorial orbit plane. The sunline therefore varies from lying in this plane for the equinox orbits to plus or minus 23.5 degrees inclination to the plane for the summer and winter solstice orbits, respectively.

#### 5.8.2 SUBSYSTEM DESCRIPTION

### 5.8.2.1 Subsystem Selection

#### 5.8.2.1.1 General

For the scheduled launch period of 1969-70, the orbit and mission life requirement of two years practically dictated the use of solar energy conversion using silicon solar cells as

the primary energy source, and the use of nickel-cadmium batteries for energy storage. The major tradeoff considerations in selection of the power subsystem are related to the selection of the optimum configuration for the array and the selection of the best power conditioning equipment to provide for the load requirements of the mission, with simplicity being a basic issue in all of the tradeoffs.

#### 5.8.2.1.2 Array

Considering the supporting role of the power subsystem relative to the primary mission objectives of the ATS-4 vehicle, a fixed array was chosen early in the design study for system simplicity and reliability over a sun-oriented array. The location, orientation, and number of array panels then became the major considerations.

As shown in detail in Section 6.6.3, the optimum location for the array panels considering minimum shadowing effects and minimum deployment complexity and weight, turned out to be at the periphery of the parabolic reflector. Although the parabolic reflector structure is over 75 percent porous to sunlight transmission, the shadowing effects on arrays deployed directly off the aft equipment module behind the reflector would reduce the array power output to practically zero without series element bypass diode protection in the array, and to about 50 percent with the use of bypass diodes for over 90 degrees of each orbit. The use of batteries to supplement array power during such long periods of severe reflector shadowing would involve a large weight penalty, as compared to the weight of structure required to deploy the panels to the periphery of the reflector structure where reflector shadow effects are minimized.

The number and orientations of the panels were selected to provide a relatively uniform array power output for all the orbital sun angles while accommodating minimum hinging and rotations for deployment from the stowed configuration of launch. Resultant symmetry of the deployed panel areas about the vehicle was also a basic consideration.

### 5.8.2.1.3 Power Conditioning Equipment

The power conditioning equipment comparison studies were directed toward providing a single regulated voltage to the loads. This single regulated voltage distribution system, which decentralizes any additional required voltage conversion equipment to the individual user loads, was selected over a centralized, multiple voltage distribution system for the flexibility it allows in accommodating individual load changes. For a vehicle designed to accommodate many experiments, with many different voltages and load distributions involved, flexibility of the power system was deemed essential for simplicity of integration between the loads and power system.

Both ac and de voltage distributions were compared. The selection of de voltage distribution was made due to a weight and efficiency advantage (see Section 6.6.6.1, Vol II).

After the selection of dc distribution, three methods of providing the dc voltage were compared. Of those compared, no strong advantages in weight or efficiency relative to the spacecraft weight and power capability were credible; therefore, a selection was made based primarily on simplicity of operation (see Section 6.6.6.2, Vol II).

## 5.8.2.2 Subsystem Block Diagram

A block diagram of the preferred power subsystem is presented in Figure 5.8-4 and consists of four solar array panels, three batteries, three battery charge regulators, a pulse width modulated (PWM) voltage regulator, a voltage limiter, a dc-ac inverter, and a power control unit. The function of the various components are as follows:

- a. Solar Array Serves as primary source of spacecraft power by photovoltaic conversion of solar radiation into electrical power.
- b. <u>Batteries</u> Supply power for umbra loads and for supplement to the array during peak loads of orbit day.
- c. <u>Battery Charge Regulators</u> The battery charge regulators control the rate of charge to the batteries to a safe level such that the batteries will not experience degradation due to excess charging.

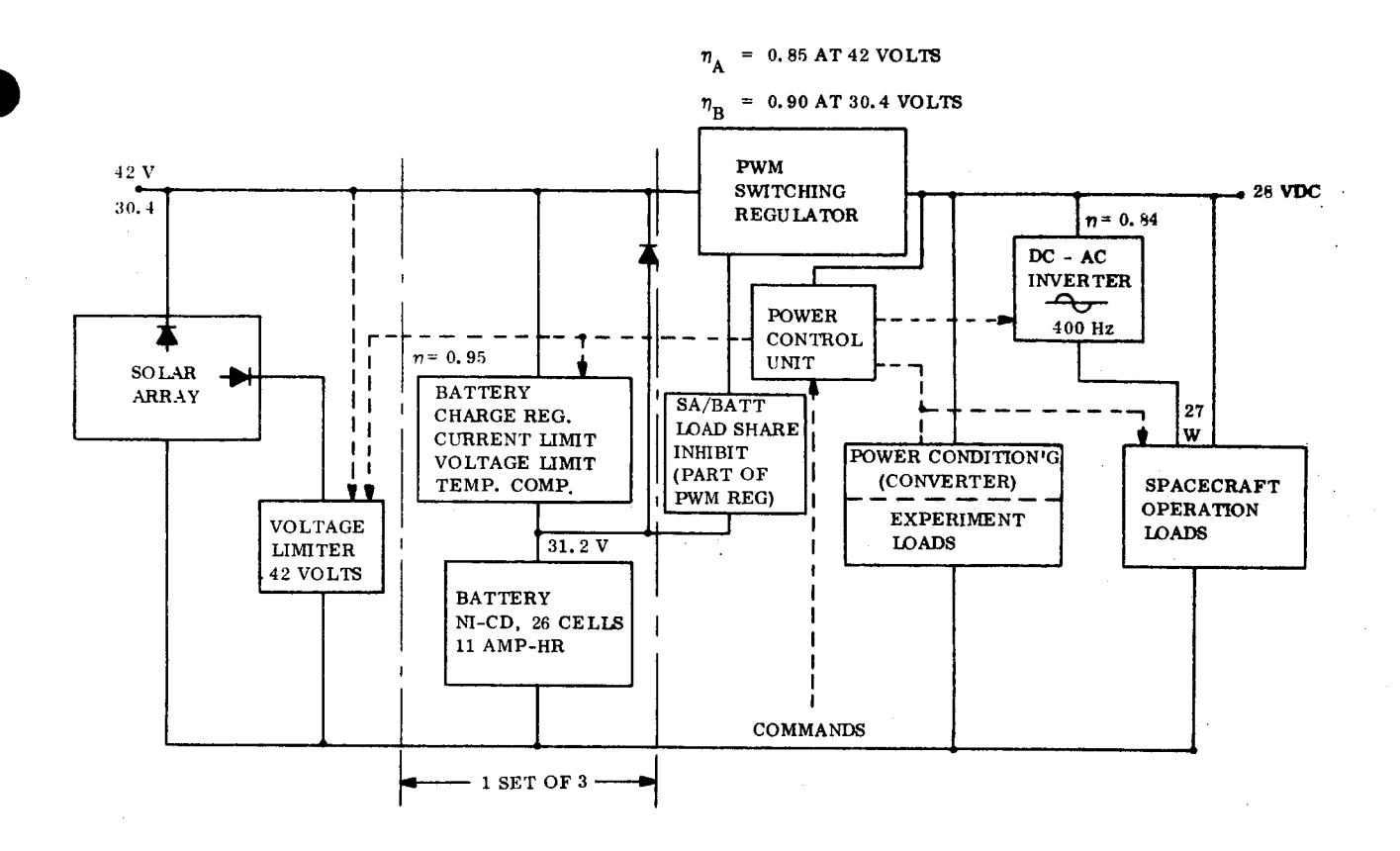


Figure 5.8-4. Power Subsystem, Block Diagram

- d. PWM Voltage Regulator The PWM voltage regulator converts the solar array and battery voltage variations to a regulated 28 ± 0.5 vdc. All spacecraft loads and experiment loads use the regulated dc voltage with the exception of 27 watts of Orientation Control power, for which a dc-ac inverter is provided. In addition, the PWM regulator provides a load-sharing inhibit function which releases the battery from sharing the load with the array when the array has capability to supply all the loads.
- e. <u>Voltage Limiter</u> The voltage limiter, set for 42 ± 1 volt, prevents the array voltage from rising above 43 volts during periods of excess power or during post-eclipse periods when the array is cold.
- f. <u>DC-AC Inverter</u> The dc-ac inverter provides 400 Hz, two-phase, sine wave power to the Orientation Control Subsystem for operation of guidance motors.
- g. Power Control Unit The Power Control Unit is the controllable junction between the power subsystem and user loads. It also houses monitoring devices.

### 5.8.2.3 General Operational Characteristics

As indicated on the block diagram of Figure 5.8-4, a regulated 28 vdc bus is provided from the primary and secondary energy source voltage variations of 42.0 to 30.4 volts (nominal range) through a PWM switching type regulator. The upper limit of 42.0 volts from the array is controlled by the voltage limiter, and the lower limit of source voltage is established from the battery discharge voltage.

The voltage limiter, battery/battery charge regulator, and loads are shunt loads on the solar array. The load has priority over all power. The sequence of operation for sunlight operation is as follows for various load conditions:

- a. Load demands are minimum and excess power is available:
  - 1. Battery is charged at maximum current limit.
  - 2. Voltage limiter is shunting excess power.
  - 3. PWM regulator input voltage is at 42 volts nominal.
- b. Load demands increase:
  - 1. Battery is charged at maximum current limit.
  - 2. Voltage limiter is off.
  - 3. PWM regulator input voltage is at 41 volts.
- c. Load demands increase again:
  - 1. Battery is charged at some current below maximum current limit.
  - 2. PWM regulator input voltage decreases from 41 toward 38 (the assumed partially charged battery voltage).
- d. Load demands increase again:
  - 1. Battery charge regulator is off.
  - 2. PWM regulator input voltage is at 38 volts.

- e. Load demand increases again:
  - 1. Battery discharges to share load with the array.
  - 2. PWM regulator input voltage is at 30.4 volts.
  - 3. Load/inhibit portion of PWM regulator is sensing currents and discharging capacitor at regular intervals to assure array is not load sharing with the battery when array has capability to supply all the load.
- f. Load demands decrease small amount:
  - 1. Battery and array load share.
  - 2. Array has capability to provide full load power without aid from the battery, but battery and array are locked in a load share mode until;
  - 3. Load/inhibit portion of PWM regulator automatically releases the battery from sharing load and all load is supplied by the array.

Load demand during eclipse is provided by battery only. During this condition:

- 1. Battery charge regulator is reverse biased.
- 2. Solar array and voltage limiter are diode isolated.
- 3. Load inhibit circuit is off.

Therefore, the selected system provides the 28 vdc regulated bus under all modes of operation.

### 5.8.2.4 Solar Array Capability

## 5. 8. 2. 4.1 Orbital Array Power Capability

Figure 5.8-5 shows the power available from the solar array at the design peak power point of 41 volts for both the equinox and summer solstice orbits. Array capability is shown for a new array and at the end of two years. In Table 5.8-1, a summary of the average power and the total energy capability represented by the curves of Figure 5.8-5 is presented. For comparison, the total energy required by the loads is also shown.

Table 5.8-1. Summary of Array Power and Energy Capability

	No	ew	2 year end-of-life			
	$*\psi = 0^{\mathbf{O}}$	$\psi = 23.5^{\circ}$	$\psi = 0^{\circ}$	$\psi = 23.5^{\circ}$		
Average Power, Watts	392	350	304	272		
Total Energy Per Orbit, Watt-hours	8950	8400	6930	6530		
Load Require- ments, Watt-hours		4191				

# \* $\psi$ = Sun-orbit Plane Inclination

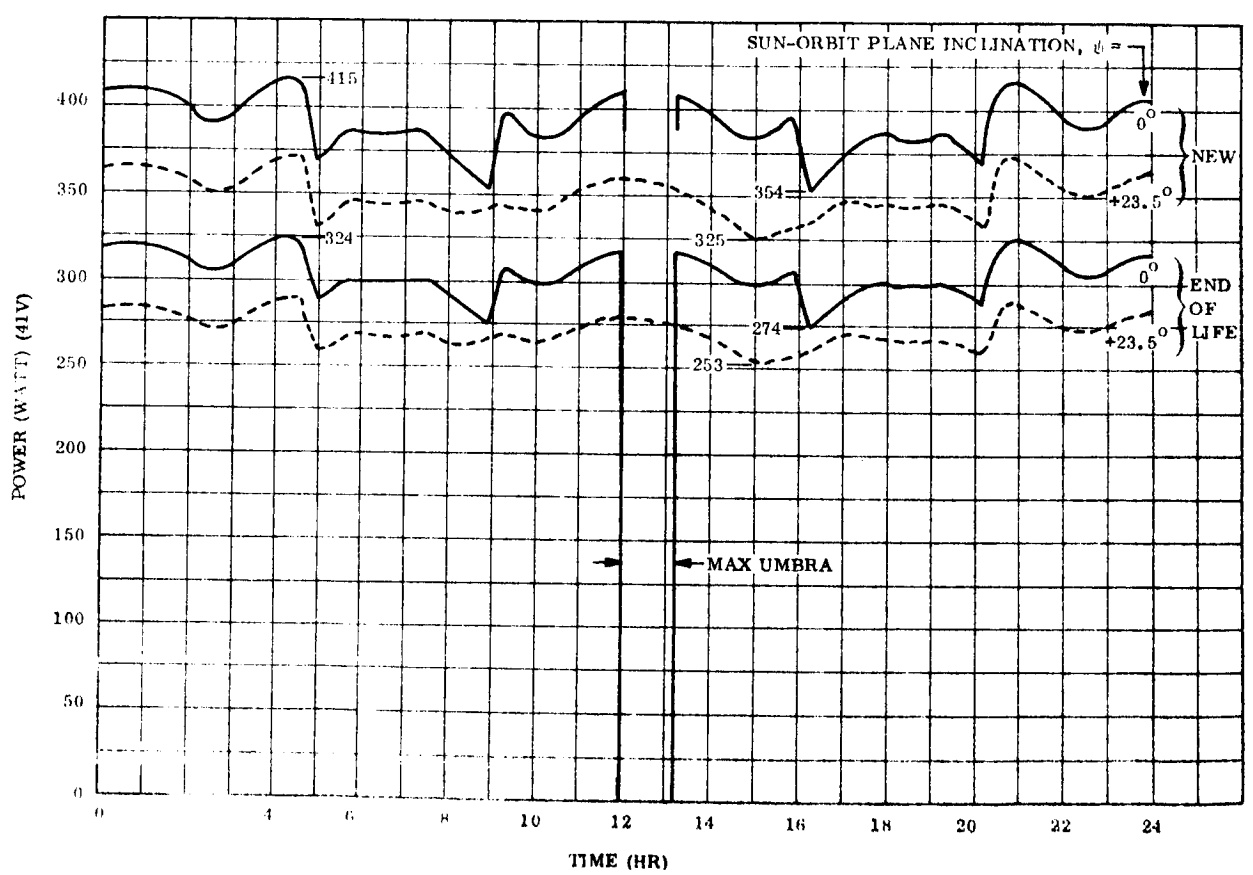


Figure 5.8-5. Solar Array Power

In Figure 5.8-6, the variation of the daily average array power for times between the new and end-of-life array capability is presented. The degradation shown is primarily radiation damage (20 percent at 2 years) with a three percent allowance for losses due to micrometeorites and random cell failures assumed linearly distributed with time.

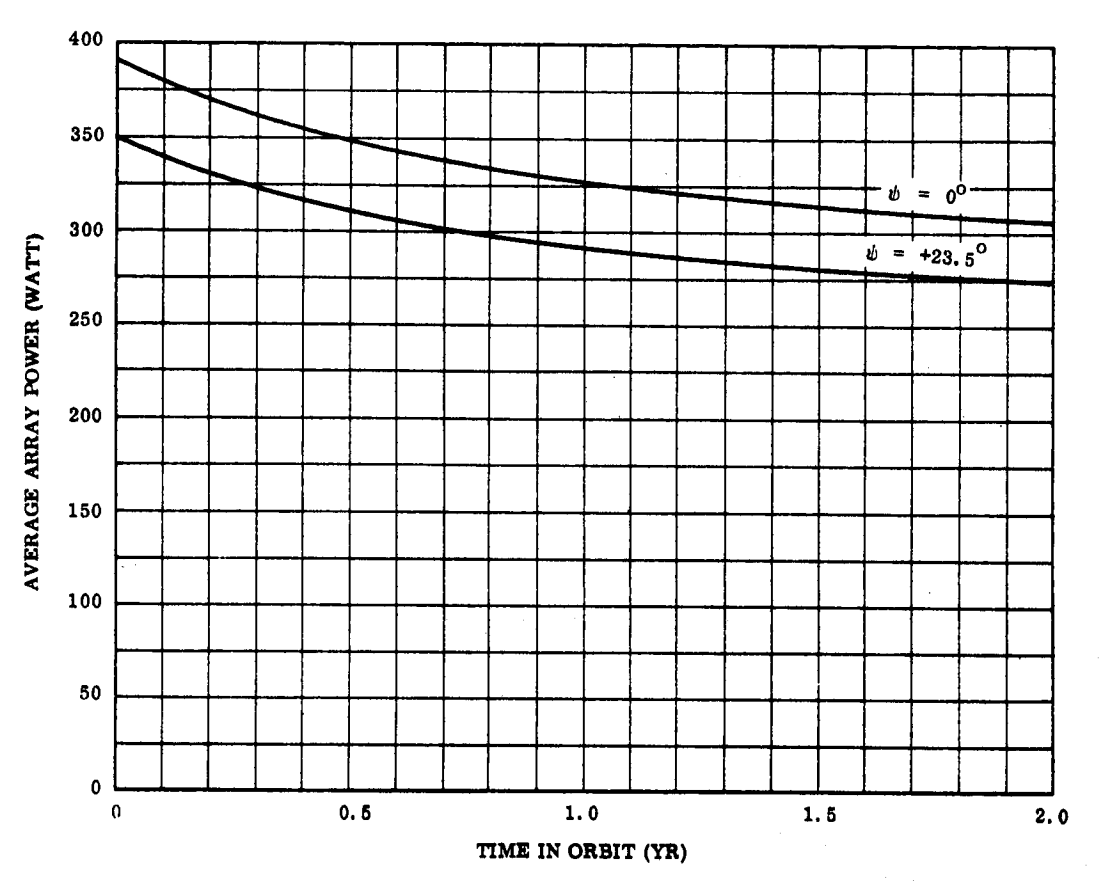


Figure 5.8-6. Daily Average Array Power vs Time in Orbit (For Equinox and Summer Solstice Orbits)

During each orbit, the solar array panels are subjected to various shadowing effects. There are three sources of shadows involved:

- a. Shadows on the X-axis panels due to the equipment modules, parabolic reflector, and feed support truss. (These shadows are most severe during the equipment orbits. During the solstice and near-solstice orbits, the earth-viewing equipment module does not shadow the X-axis panels and the shadowing of the panels begins at a lower angle of incidence due to the feed support truss.)
- b. Shadows on the Y-axis panels due to the center structural beams. (These shadows occur for both equinox and solstice and near-solstice orbits.)

c. Shadows on the Y-axis panels due to the parabolic reflector. (This shadowing condition exists only during the solstice and near-solstice orbits.)

Figure 5.8-7 shows the effects that these various shadowing conditions had in producing the resultant array power curve presented in Figure 5.8-5 for the equinox orbits. The total energy lost in an orbit due to the shadows is approximately 3.5 percent. Similar curves are presented in Figure 5.8-8 for the summer solstice orbit. The total energy lost in an orbit due to the shadows is 3.6 percent. Due to the asymmetry of the Y-axis solar panels with respect to the X-axis, it can be seen that the shadow losses due to the parabolic reflector shadowing the Y-axis panel are unsymmetrical with sun inclination angles to the spacecraft Z-axis during the orbit.

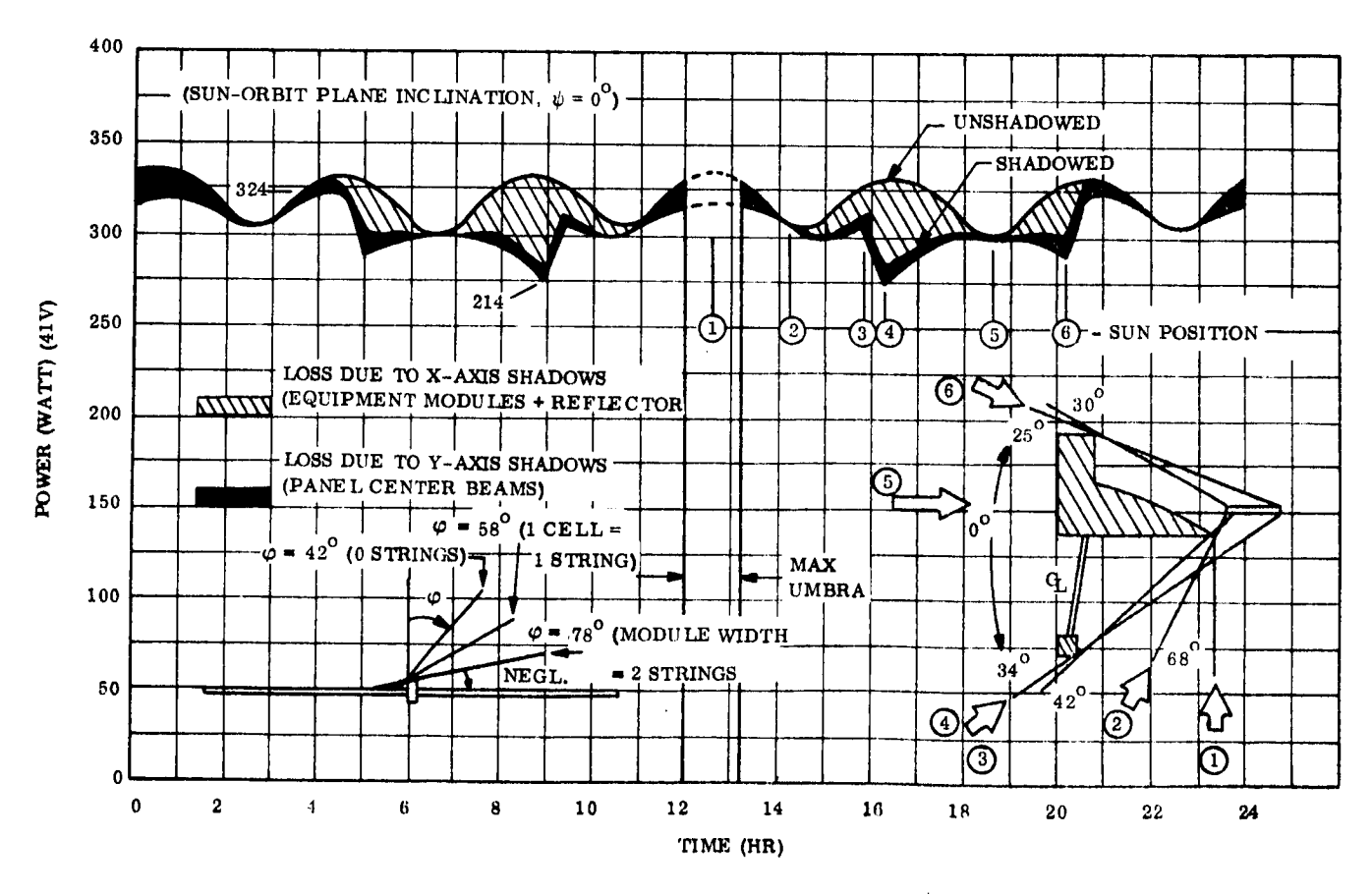


Figure 5.8-7. End-of-Life Array Power for Equinox Orbits

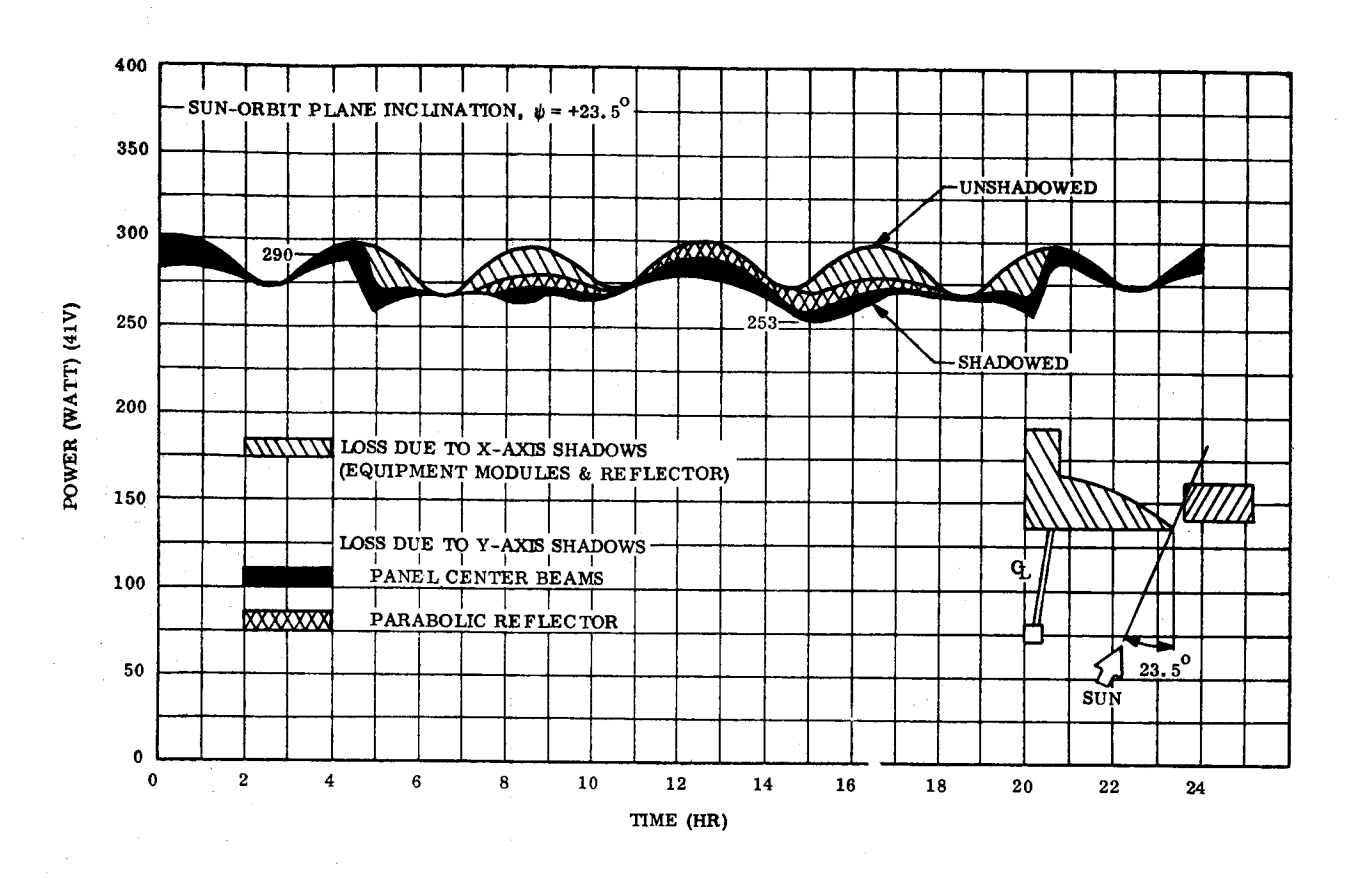


Figure 5.8-8. End-of-Life Array Power for Summer Solstice Orbit

In Figure 5.8-9, the end-of-life array capability at the loads (i.e., the 28 vdc regulated bus) is shown superposed on the load profile for the equinox orbit. The array power supplied to the bus is shown for both the case when the array alone is supplying power and when it is being supplemented by the battery. It can be seen from the figure that the array can supply the load power requirements without battery supplement except during the 1.2 hour umbra and during the 30 minute peak load of 555 watts. When battery supplemental power is required, the array supplies the power shown in the lower curve and all energy above this curve must be supplied by the battery. The total watt-hours of energy supplied to the loads by the battery for this orbit is 442 watt-hours.

Similar curves are presented in Figure 5.8-10 for the end-of-life summer solstice orbit. It can be seen that at this time, the array requires battery supplement for a second period of time lasting about two hours. The total watt-hours of energy supplied by the battery to the loads for this orbit is 266 watt-hours.

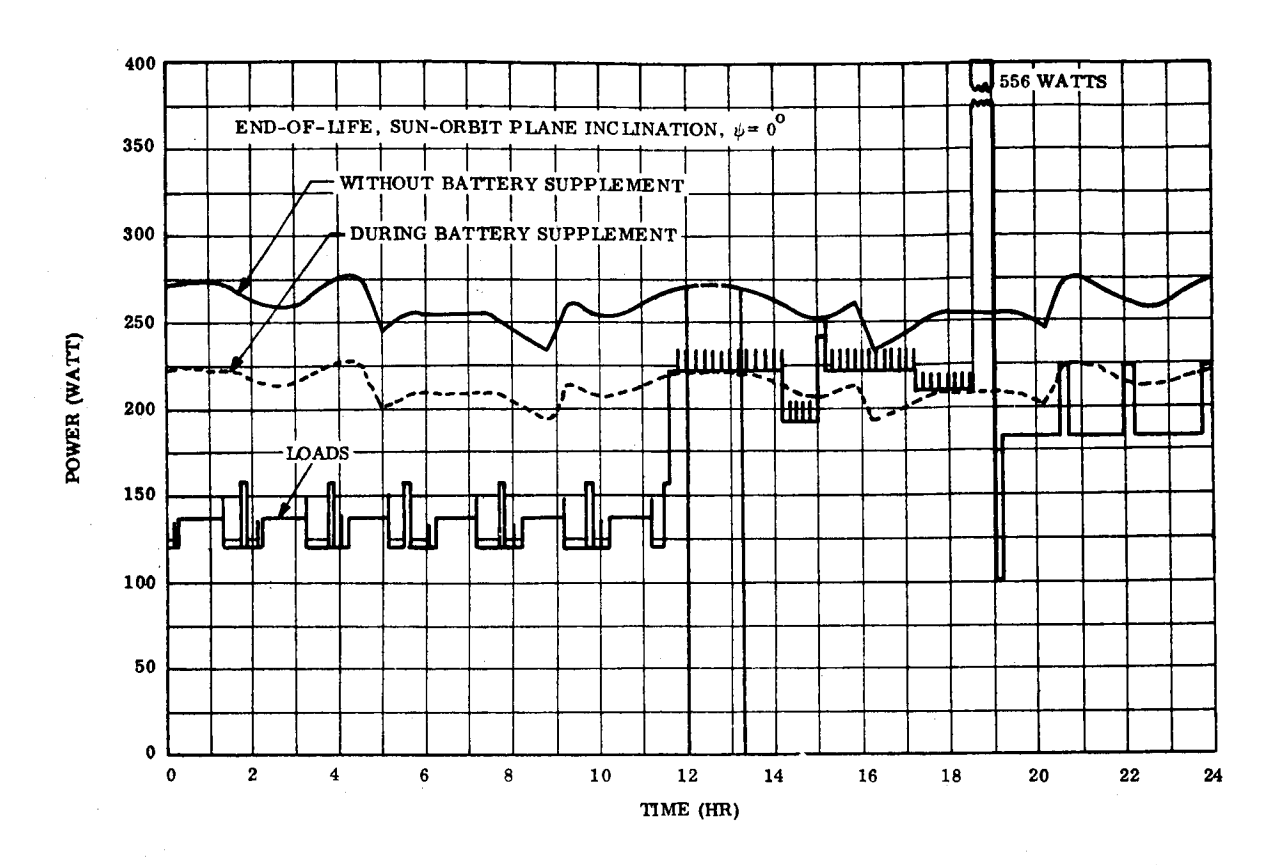


Figure 5.8-9. Solar Array Power Capability at Loads for Equinox Orbits

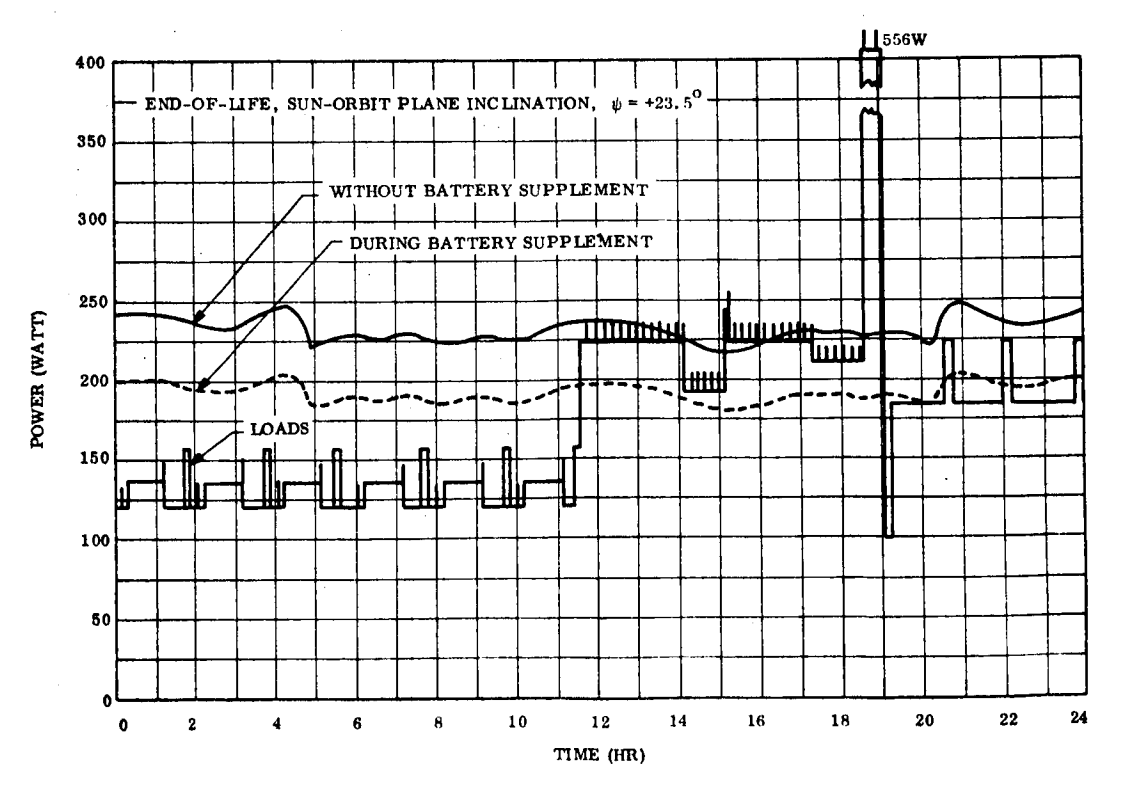


Figure 5.8-10. Solar Array Power Capability at Loads for Summer Solstice Orbit

In Figure 5.8-11, the maximum and minimum array V-I curves occurring throughout the life of the array are presented. The post-eclipse V-I curve establishes the voltage reducing requirement and thus array-tap point for the shunt voltage limiter.

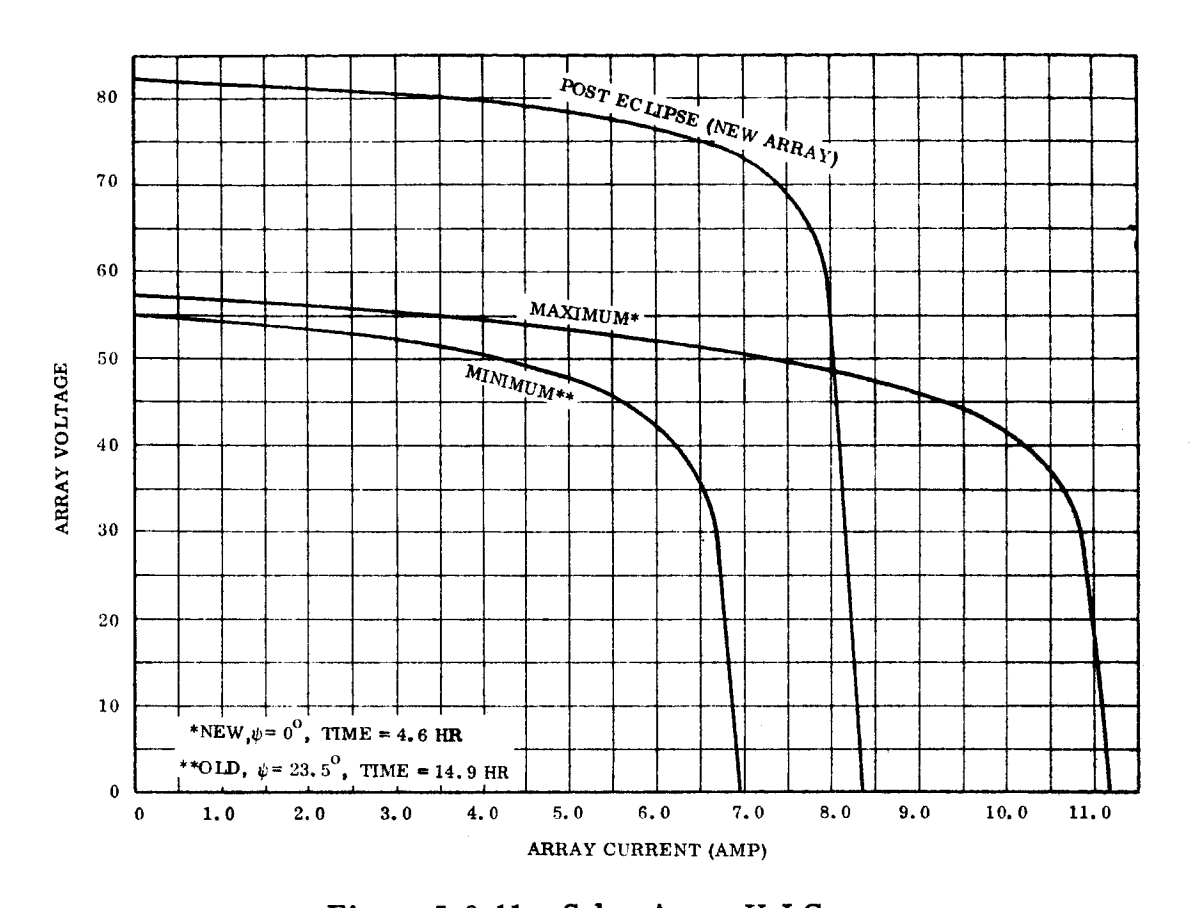


Figure 5.8-11. Solar Array V-I Curves

### 5.8.2.4.2 Basis For Array Performance

The above unshadowed performance of the array was calculated using the computer program described in detail in Appendix G. Modifications to these curves for shadow effects were determined by hand-calculations. The program calculates the array output based on the characteristics of a single solar cell, multiplying the voltages and currents by the number of cells in series and parallel, respectively, to obtain the voltage characteristics of the total array. The program takes into account the following parameters:

- a. Solar intensity
- b. Cell temperature

- c. Angle of solar incidence
- d. Basic cell characteristics
- e. Losses and uncertainties

The calculations were performed at five degree intervals for each of the two orbits considered. The values of the above parameters used to compute the array power outputs shown in Figures 5.8-5 through 5.8-8 and the V-I curves of Figure 5.8-11, are as listed below:

- a. <u>Cell temperatures</u> Obtained from temperatures presented in Section 5.9 for an equinox orbit. Appropriate corrections were made for the solstice orbit. (It can be seen that the temperatures range from a maximum of  $120^{\circ}$ F to a minimum of  $-150^{\circ}$ F when the panels are illuminated. The temperature goes to a minimum of  $-190^{\circ}$ F during the umbra).
- b. Basic cell characteristics Derived from V-I measurements made on a large group of solar cells under simulated air mass zero illumination over a range of temperatures (-200°F to +200°F). The general temperature-efficiency coefficient for these cells is 0.26 percent/°F (when referred to 85°F). Bare cell efficiency: 10.5% at air mass zero at mean earth-sun distance and cell temperature of 29°C.
- c. Solar intensity As shown in following data.
- d. Losses and uncertainties As shown in following data.

	Nev	v Array	Old Array (End of 2 years)		
	$\psi = 0^{\circ}$	$\psi = 23.5^{\circ}$	$\psi = 0^{\circ}$	$\psi = 23.5^{\circ}$	
Voltage Degradation Factor (due to radiation environment)	1.000	1.000	0.975	0.975	
Short Circuit Current Degradation Factors:					
Solar intensity	1.000	0.966	1.000	0.966	
Filter transmission loss	0.920	0.920	0,920	0.920	
Soldering process degradation	0.980	0.980	0.980	0.980	
Radiation damage	1.000	1,000	0.850	0.850	

·	New	Array	Old Array (End of 2 years)		
	$\psi = 0^{8}$	$\psi = 23.5^{\circ}$	$\psi = 0^{\circ}$	$\psi = 23.5^{\circ}$	
Micrometeorites and random cell failures	1,000	1,000	0.970	0.970	
Measurement uncertainty (0.96) Calculation uncertainty (0.95)	RMS= 0.936	0.936	0.936	0.936	
TOTAL	0.844	0.815	0.696	0.672	

The basis for the above factors is discussed in detail in Section 6.6.4.4. The computer program also accounts for the voltage drop of the blocking diodes associated with each series string, including the effects of blocking diode temperature (assumed to be the same as solar cell temperature).

## 5.8.2.4.3 Launch Array Power Capability

The power available from the solar array while illuminated in the stowed configuration of launch under the conditions specified in Section 5.8.1.1 is presented in Figure 5.8-12 for one revolution of the spacecraft.

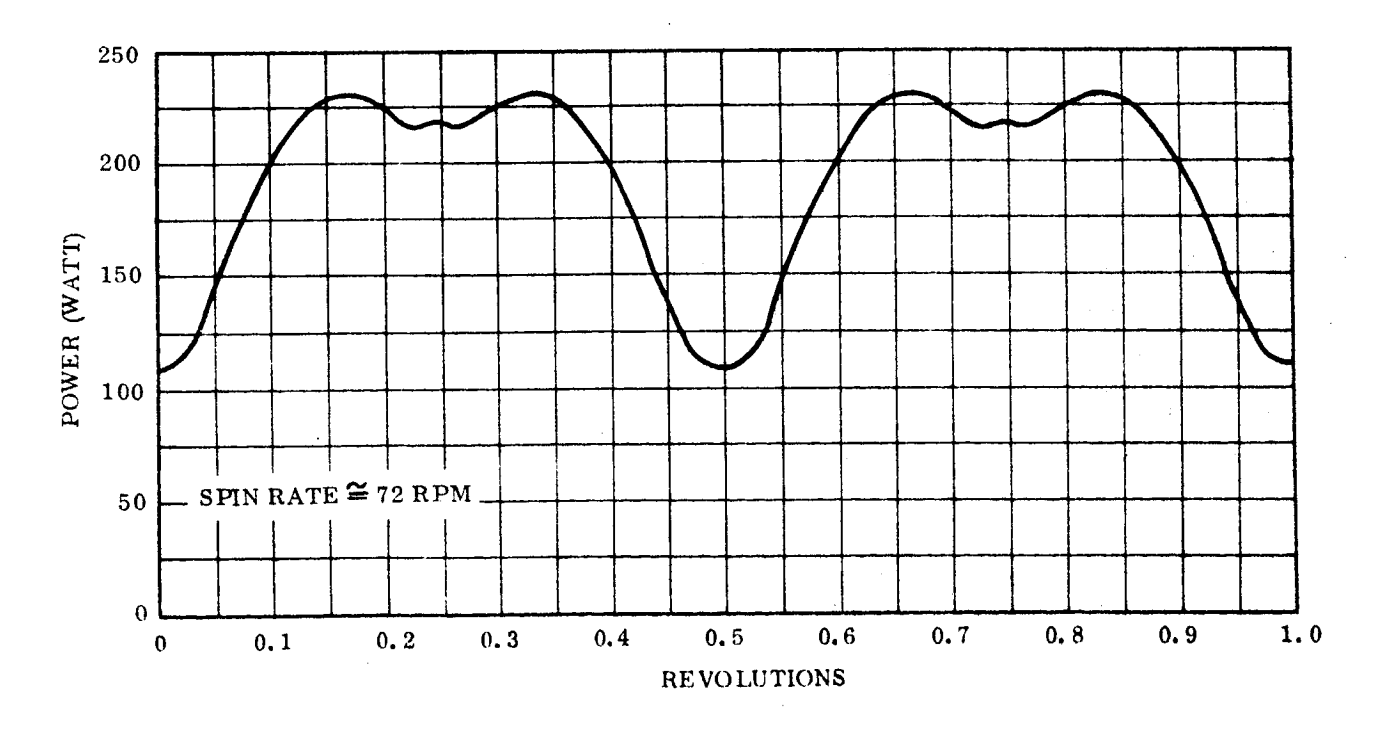


Figure 5.8-12. Solar Array Output During Stowed Launch Spin Mode

In Figure 5.8-13, the array bus capability at the loads is shown superposed on the maximum load requirement of 109 watts (reference Figure 5.8-2). It can be seen that battery supplement is required during a portion of each spacecraft revolution, but analysis shows that adequate power and time is available to recharge the battery during the other portions of the revolution, and that the net discharge of the battery is therefore zero.

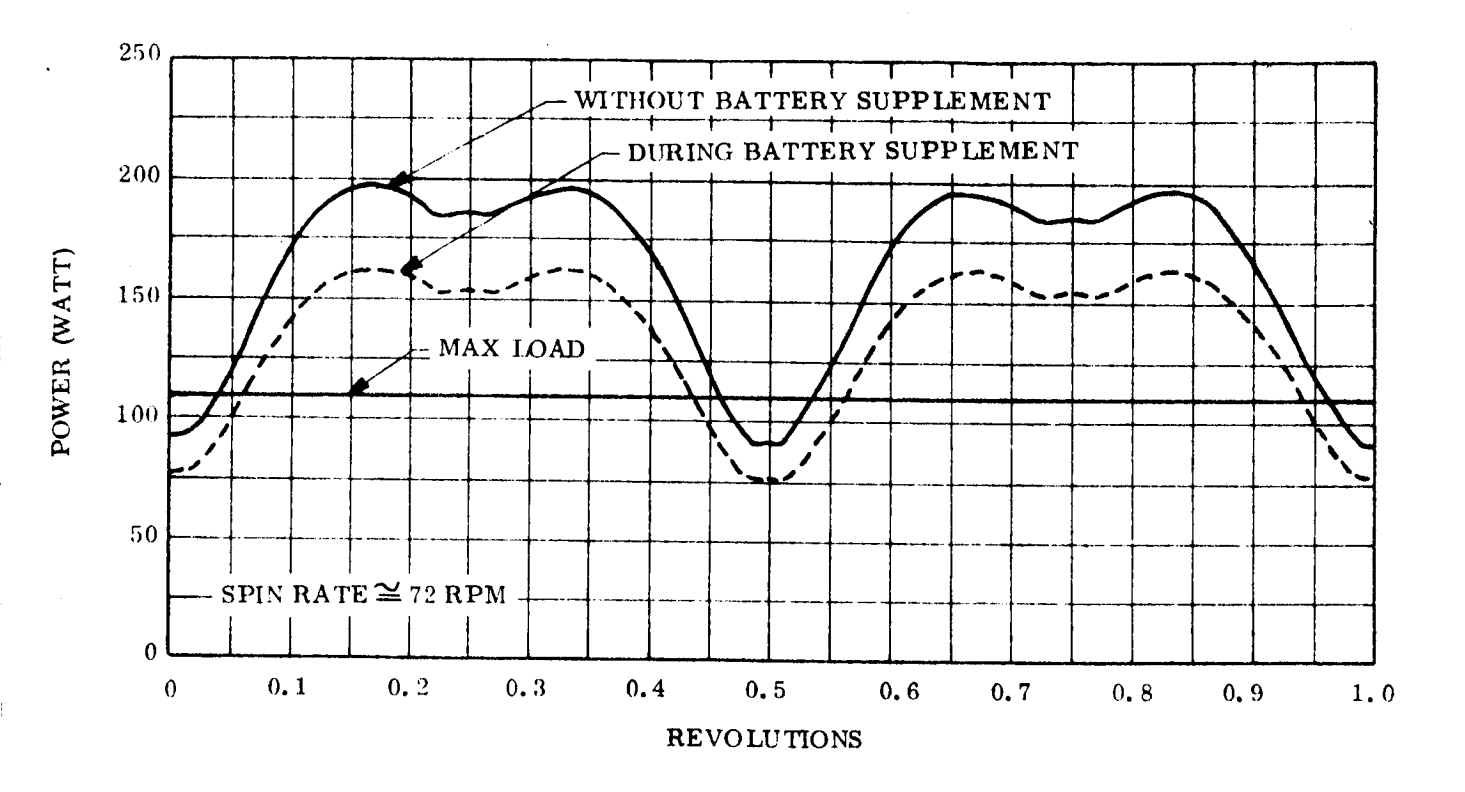


Figure 5, 8-13. Solar Array Power Capability at Loads During Stowed Launch Spin Mode

# 5.8.2.5 Battery Capability

The installed capacity of the batteries is 33 ampere-hours (1030 watt-hours). In order to provide the necessary capacity at the two-year design point, the batteries are sized so as to be operating at a maximum depth of discharge of 50 percent for the relatively few near-equinox orbits, and at a maximum depth of 30 percent for the more frequent near-solstice orbits. The resulting depths of discharge for the battery when the array is new and at end-of-life are presented in Table 5.8-2.

Table 5.8-2. Battery Depths of Discharge for New and Old Arrays

	Battery Depth of Discharge				
	$*\psi = 0^{\circ}$ $\psi = 23.5^{\circ}$				
New Array	47%	18%			
2 year End-of-life Array	50%	30%			

<sup>\*</sup> $\psi$  = Sun-Orbit Plane Inclination Angle

### 5.8.2.6 Subsystem Efficiency and Margins

Using the efficiencies of the power conditioning equipment presented in Table 5.8-6, the following efficiencies of the power subsystem can be derived for providing power to the loads from the array.

- a. When array power is provided directly to the loads (i.e., without first being stored in the batteries):
  - Efficiency = 85 percent (when array alone supplies the power and is operating at peak power point of 41 volts)
  - Efficiency = 70 percent (when the array power is being supplemented by battery power and the array is therefore operating at 30.4 volts).
- b. When array power is provided to loads via the batteries:

Efficiency = 51 percent (if battery has been recharged at maximum rate of C/8)

Efficiency = 33 percent (if battery has been recharged at a C/20 rate)

### 5.8.2.7 Operational Flexibility

As shown in Section 5.8.2.3, the selected power subsystem is completely automatic (requires no ground control) for the representative design load profile. That is, the power subsystem will automatically accommodate all the specified load changes and recharge the

batteries throughout each orbit. However, the power subsystem is not restricted in this automatic mode of operation to the particular load profile to which it was designed. Just so the variations in the load profile are performed on an energy balance basis which assures that the batteries do not exceed the allowable depths of discharge and that they are fully recharged each orbit, such variations can be accommodated automatically by the power subsystem.

It should also be noted that the command capability for disconnecting any one of the three batteries from the power subsystem is provided. This feature allows a failed battery to be removed from the line.

## 5.8.2.8 Growth Capability

Without any basic change to the preferred vehicle power subsystem design concept, panel stowage space for the launch configuration is the major growth restriction. However, as shown in Figure 5.8-14, there is presently space available for the Y-axis panels (limiting type) to increase in area (and thus power) by 54 percent. By changing from the optimum power/weight ratio cell cover thickness of 10 mils to 20 mils at the same time the panel area is increased, the total growth of the end-of-life capability would be 70 percent.

#### 5.8.3 COMPONENT DESCRIPTIONS

### 5.8.3.1 Solar Array

Since, as evidenced throughout this study, the array panel sizes and configurations are such an important element to the vehicle configuration, and since these

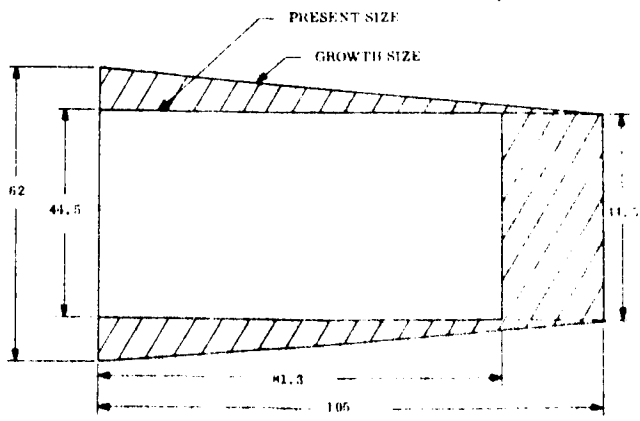


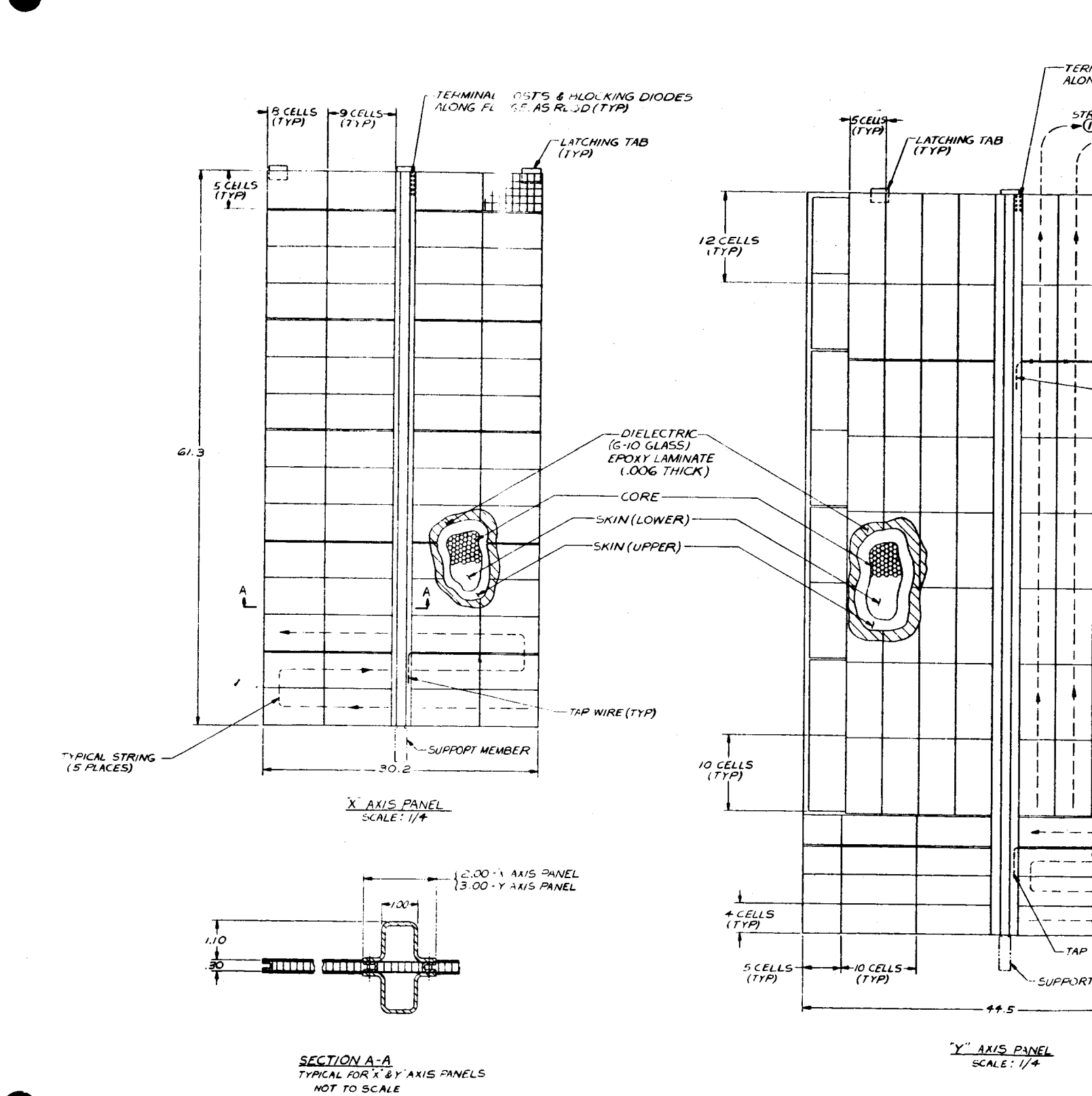
Figure 5.8-14. Y-Axis Panels Area Growth Capability

aspects of the array are highly dependent on some of the detail design features, considerable design detail of the arrays was developed in order to be assured that the array was realistic. This design is described below.

The solar array, which serves as the primary power source for the spacecraft, consists of four fixed panels with solar cells on both sides, located 90 degrees apart on the X- and Y- axes of the spacecraft near the periphery of the parabolic reflector. The total area of the panels is 76.0 square feet. The two panels on the X-axis are each approximately one-half the area of a single Y-axis panel so that, functionally, three panels of equal size are involved. The planes of these "three" panels are oriented perpendicular to the X-Z axes plane of the spacecraft and 60 degrees relative to each other. This number and orientation of panels provide a relatively uniform array power output throughout the orbital rotations of the spacecraft (see unshadowed curve of Figures 5.8-7 and 5.8-8,) together with accommodating minimum hinging and rotation for deployment from the stowed configuration of launch.

The array was sized to provide a minimum of 265 watts (unshadowed) at 41 volts after two years in orbit. This minimum array power occurs during the summer solstice orbit when the sun-line/orbit plane inclination is 23.5 degrees and the sun intensity is minimum (3.4 percent below nominal.) This array power level is near optimum on a weight basis with the size batteries required to supplement the array during peak loads. (As can be seen in Figure 5.8-10, any decrease in array size would increase the battery supplement required. This increase in battery weight would be at a faster rate than the decrease in array weight.)

Some of the major design features of the array panels are shown in Figure 5.8-15. Each side of each Y-axis panel contains 8 strings of 2 by 2 centimeter cells with 5 in parallel and 102 in series, together with 2 strings with 4 in parallel and 100 in series. Each side of each X-axis panel contains five strings of 2 by 2 centimeter cells with 5 in parallel and 102 in series. (Each X-axis panel contains the one additional cell in parallel over the required number for symmetry with the Y-axis both to maintain uniformity of the modules used and to compensate some for the reduction in output of the X-axis during partial shadowing.) The total number of cells on the four panels is 29.720.



5.8-25

INAL POSTS & BLOCKING DIODES S FLANGE AS REQD(TYP)

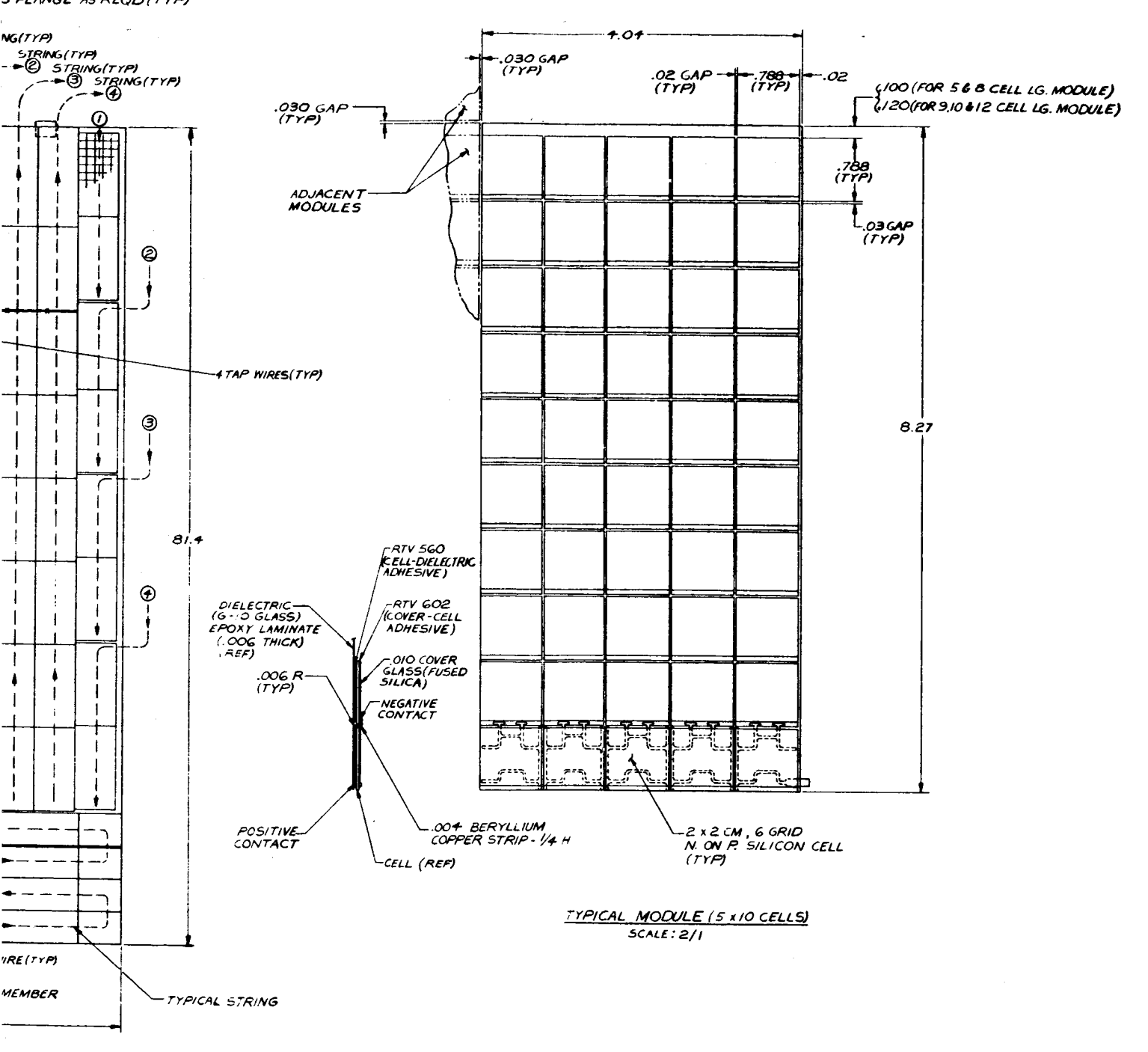


Figure 5.8-15. ATS-1 Solar Cell Arrangements

5.8-26

The directions of the series strings on each panel were selected to minimize shadowing effects. The strings of cells on the X-axis panels are placed perpendicular to the X-axis so that as the vehicle shadows progressively cover the panel (see Figure 5.8-7), the power from individual strings is lost one by one. If the strings were oriented parallel to the X-axis, all strings would be lost as soon as only a portion of the panel is initially shadowed.

Similarly, for the Y-axis panels on the end portion of the panels which are shadowed by the parabolic reflector during the solstice and near-solstice orbits (see Figure 5.8-8), two strings were placed perpendicular to the Y-axis to minimize the effects of these shadows. The other strings were placed parallel to the Y-axis to minimize the effects of the center beam shadows. The remaining distance between the cells and center beam for the X-axis was sized to eliminate all shadows on the cells during solstice orbits when the sun is inclined to a maximum of 23.5 degrees to this center beam. The similar gap on the Y-axis panels was selected to minimize the center beam shadow effects (although not to eliminate them entirely at low angles), where power output is low.

The array construction is similar to the General Electric GGTS design which was successfully qualified for the Titan 3C launch environment. Each series string is built up from submodules and modules. Submodules consist of 4 or 5 cells, and their protective covers soldered to an interconnecting tab, electrically in parallel. Modules are constructed from 5 to 12 submodules bonded on a fiberglass substrate with the submodule tabs soldered to form a series circuit. A typical module is illustrated in Figure 5.8-15. The modules are bonded to the array panel structure with the end tabs soldered together, either directly or with intermediate wiring as required to form the required series strings. Each series string is wired in parallel (electrically) with the other series strings, with two isolation diodes in each series string. A tap wire is incorporated at the 60-cell point of each string for partial shunt control of the array maximum voltage by the voltage limiter.

The cover glass to cell bond is a clear silicone rubber adhesive (GE RTV-602 or Dow Sylgard 182). The submodules are bonded to an epoxy-glass laminate substrate with GE silicone rubber RTV-560 and the module boards (the epoxy-glass laminate with interconnected submodules bonded in place) are bonded to the aluminum face of the honeycomb with GE RTV-560.

The panel structure is an all aluminum honeycomb material (see Section 5.9). The module board substrate is an epoxy-fiberglass laminate of the G10 or G11 class. The cells and submodules are interconnected with 4-mil expandable beryllium copper strips. The interconnection is shown in Figure 5.8-15. The modules were selected to be of the flat laydown configuration, as opposed to shingled, to allow for ready repair of even one cell in a submodule. For this latter process, a high-intensity lamp technique has been very successful in removing cells from the substrate.

Some additional characteristics of the design are listed below:

a.	Panel areas:	-	ross (ft <sup>2</sup> ) Center Beam)	(Without	Array (ft <sup>2</sup> ) Center Beam)*
	Each X-axis panel	25	5.7		24.0
	Each Y-axis panel	5(	0.3		46.9
	Total panel area	76	6.0		70.9
		8	-	nel areas less 2 a nd Y-axis panels, ure 5.8-15).	
b.	Total array active cell ar	ea:	121.6 ft <sup>2</sup>		
c.	Solar cell active area pac	king factor:	0.80 (based o	on gross panel ar	ea)
d.	Number of cells:		0.86 (based o	on array area)	
	Each X-axis panel (each s	sid <b>e</b> )	2550		
	Each Y-axis panel (each s	sid <b>e</b> )	4880		
	Total per vehicle		29,720		
e.	Breakdown of weight: Per square foot (one side	only), based	d on panel area	a less center bear	m areas:

10-mil cover glass	.098
Cover glass adhesive	.014
Cells, solder-free, 13 mil nominal	.157
Cell interconnection strips and solder	. 025
Cell-to-substrate bond	.040
Substrates	. 063

Substrates to panel bond .040

Terminals, diodes, wires and potting .030

Total lb/ft 0.467

Total, lb/ft based on total (gross) panel area

## f. Cell characteristics:

Efficiency: 10.5% at AMO 85°F

Size: 2 cm x 2 cm

Type: N/P, 10  $\Omega$  -cm, 95% active area, sintered

contacts (see Section 6.6.4 for selection of

10  $\Omega$ -cm versus 1  $\Omega$ -cm)

Thickness: 13 mil

g. Cover glass:

Size: 1.8 cm x 2.0 cm

Type: Corning No. 7940 fused silica with blue cut-on

and anti-reflection filters

Thickness: 10 mil (see Section 6. 6. 4 for selection of

glass thickness)

Efficiency: 92% transmission

#### 5.8.3.2 Batteries

In order to meet the mission requirements of a 2-year design life, sealed nickel-cadmium cells were selected to provide electrical power during eclipse periods and for peak loads. Three batteries are proposed, each consisting of 26 series connected cells of 11 ampere-hours capacity. It is estimated that each battery will weigh 34.3 pounds and have a volume of about 530 cubic inches. Each cell will be hermetically sealed in a stainless steel can, with a positive terminal isolated from the case with a ceramic bushing. The battery will be constructed of aluminum and is designed to physically restrain the cells against internal gas pressure which develops during normal usage. The battery case will not be sealed. The batteries have been sized to provide reliable operation over a 2-year life, assuming a maximum depth of discharge of 50 percent at end of life during eclipse conditions, and a maximum 30 percent depth of discharge during other 24 hour noneclipse orbits, providing battery temperature is maintained at 0°C to 25°C.

Sufficient power and time are available to completely recharge the batteries after maximum usage, with the current limited to the C/8 rate (the 8 hour rate). The C/8 charge rate was selected as the maximum rate which the battery can safely accept on a continuous basis. It is desired to use a maximum charge rate so that the greatest amount of system flexibility is retained in regards to timing of the battery recharge operation. Additional charge controls, in the form of temperature compensated voltage limits, ensure a complete and safe recharge of the battery.

Multiple batteries are recommended since failure of one battery would not result in failure of the mission. Should one battery fail, it can be commanded off the line and the remaining batteries would share the load. The remaining batteries can then be either worked at a heavier duty cycle, or power management of the loads may be used to reduce battery loading by ensuring that maximum loads occur only when array outputs are at a maximum.

## 5.8.3.3 Voltage Limiter

The voltage limiter is provided to limit the solar array output voltage to 42 ± 1 volt. The use of a voltage limiter reduces the input voltage range to the battery charge regulator and PWM regulator, thus the design of each is simplified both electrically and thermally. The voltage limiter is a partial shunt regulator designed such that a maximum of approximately one-half of the excess array power is dissipated.

The power dissipative section consists of a transistor control assembly and a resistor assembly. Since resistors can operate at a higher temperature than transistors, two assemblies are selected so that the resistors can be operated in a much higher temperature environment than the transistor control assembly. Thus, the size of each assembly is dependent on the parts of that assembly only.

The voltage limiter requires a solar array tap at approximately 0.6 of full solar array voltage. The array tap is the only minor disadvantage related to the concept of the partial shunt regulator; however, the gain in thermal dissipation and thermal integration are the big advantages.

### 5.8.3.4 Battery Charge Regulator

The battery charge regulator is the control interface between the battery and solar array. The charge regulator will accept all available array current to charge the battery unless the available array current exceeds the battery charge regulator maximum current limit of C/8. In addition to the maximum current level control, there is a battery voltage cutoff which will limit the maximum battery voltage under charge conditions. Further, the voltage limit is compensated by battery temperature since the full charge voltage is a function of battery temperature.

The charge regulator consists of a series-pass transistor operating such that the C/8 charge current rate is attained. It is possible that this charge rate may occur with a 1-volt drop across the pass transistor; however, the design requirement is a 2-volt drop and the charge regulator efficiency is 37/39 = 0.95.

One charge regulator is provided with each battery; thus, the charge of an individual battery is not dependent on the charge state of the remaining batteries. In the event of a battery or battery charge regulator degradation, the degraded set will be removed from system operation through the command subsystem. The power relay is part of the battery charge regulator.

#### 5.8.3.5 PWM Regulator

The PWM regulator is the main regulator for all spacecraft operation and experiment loads. It provides 28 vdc ± 0.5 vdc when operated from a voltage source of 30.4 to 43 volts. The regulator is a switching type regulator selected for its high energy transfer capability throughout the wide input voltage range.

In addition to providing the regulated 28 vdc, the PWM regulator assembly contains the battery discharge diodes and the solar array/battery load share inhibit circuits. The battery discharge diodes are mounted on the same heat sink to provide near equal voltage drop across each diode, thereby eliminating a variable affecting balanced battery discharge. The solar array/battery load share inhibit circuits are located in the PWM regulator

assembly because the relationship between the inhibit circuit and the battery discharge diodes eliminates numerous interconnections which would be required if the inhibit function were a separate component.

### 5.8.3.6 Inverter

An inverter is required to provide two-phase, 400 Hz sine wave power for the guidance and control subsystem. Since a main regulator is provided for all spacecraft loads, inversion to a square wave and filtering of the square wave to form the sine wave is the only additional power conditioning required. No additional regulation is required or provided.

### 5.8.3.7 Power Control Unit

The power control unit is required to provide a junction for power distribution and power commands. Primary, secondary, and AGE power sources interface with power system components and user subsystems through the power control unit.

The power control unit provides the following functions:

- a. Command interface for power system control
- b. Command interface for power distribution
- c. Bus voltage monitors
- d. Bus current monitors
- e. Fusing

All power will be transferred through relay contacts of latching type relays in order to assure minimum standby power. Status of relays will be provided by telemetry digital signals.

# 5.8.3.8 Summary of Component Characteristics

A summary of the major characteristics of each of the above components is presented in Tables 5, 8-3, 5, 8-4 and 5, 8-5. Table 5, 8-3 presents a summary of the component

operating efficiencies. Table 5.8-4 presents a summary of the component weights and sizes. Table 5.8-5 presents a summary of the thermal dissipation of each component under various operating conditions.

Table 5.8-3. Summary of Power Conditioning Equipment Operating Efficiencies

Component	Input Voltage	Efficiency, Percent		
PWM Regulator	43 30,4	85. 2 90		
Battery Charge Regulator	43 39	88 95		
Voltage Limiter	Not Applicable	1.0 watt loss at input voltage less than 41 volts		
Inverter	28	84		
Power Control Unit	2 watt continuous			

Table 5.8-4. Summary of Power Subsystem Weights and Sizes

Component	Weight (lb)	Size (Inches)	Area (ft <sup>2</sup> )
Solar Array			
X-Axis panel (each)	ļ	30.2 x 61.3	12.9
Y-Axis panel (each		44.5 x 81.4	25.1
Total (4 panels)	66*	1	76.0
Total (gross array)			152
Batteries (3)	103	4.75 x 6.5 x 16.5 (each)	
Battery Charge	2	5 x 5 x 1.5	
Regulators (3)			
Voltage Limiter			
• Control Assembly	3	4 x 6 x 2	
<ul> <li>Resistor Assembly</li> </ul>	4	12 x 18 x 2	
PWM Regulator	12	9 x 5 x 4	
DC/AC Inverter	5	4 x 6 x 3	
Power Control Unit	4	8 x 6 x 3	
Harness	30		
Total	229		

<sup>\*</sup>Array weight only. Panel structure not included.

Table 5.8-5. Summary of Power Conditioning Equipment Thermal Dissipations

	<u> </u>	1			Τ		<del></del>	<del></del> .	<del></del>
	Voltage		Day			Um	bra		
Component	Input	Loa	d, Wa	atts		Load,	Watts		Notes
	42.0 30.4	109	(a)	246	- 522	- 109	- 246	- 522	
Regulator		33		40	72	24	30	72	
Battery			(b)				<del></del>		
Battery Charge Regulator		24		1	8	4	8	15	
Voltage Limiter Control Assembly Resistor Assembly Total		5 100 105	26 26 52	1 0 0	1 0 0			## # 1	
DC/AC Inverter		5	5	5	5	5	5	5	Con- tinuous
Power Control Unit		2	2	2	2	2	2	2	Con- tinuous

<sup>(</sup>a) Load power is between 109 and 246 such that the conditions identified in the column for the voltage limiter occur as a result of that load.

<sup>(</sup>b) 185 watts maximum (when battery is fully charged and C/8 charge rate exists).

### 5.9 SPACECRAFT DESIGN

#### 5.9.1 INTRODUCTION

The design of the spacecraft has been aimed at providing a lightweight launch and operational platform providing environmental control and support rigidity features which enhance maximum experiment performance. In view of the competing nature and exacting demands of the experimental subsystem, design of an integrated spacecraft in which compromise of experiment subsystem performance must be minimized, has necessitated a configuration approach which introduces unique structural and thermal design requirements.

The configuration development has been greatly influenced by the rigid petal 30-foot parabolic antenna. The Earth viewing requirement of the phased array interferometer and orientation control sensors, had to be accommodated by either mounting the equipment in back of the prime feed, with a corresponding blockage to the parabolic antenna; or by deploying the equipment out past the periphery of the antenna. The first approach was selected, primarily to avoid the deployment event, and the detrimental effects of increased CM/CP unbalance and large mass moments of inertia on the orientation control system. The elimination from consideration of this deployment also meant that in the stowed position, the Earth viewing equipment and feed package had to be rigidly supported at the focal point of the antenna.

To be compatible with the rf performance requirements, minimal structure blockage was desired, which in turn required minimization of the mass to be supported. The alternate of mounting all spacecraft subsystem components in a single module and supporting only the lighter antenna from the feed location structure, had to be rejected because of the necessity of subsequently ejecting the apogee motor. Therefore, the selected approach was to split the spacecraft subsystems into two separate modules, separated by the focal distance of the antenna. Furthermore, the remaining configuration element, the solar panels, had to be deployed on long trusses past the antenna reflector in order to receive unobstructed solar energy.

Obtaining a more favorable structural design by reducing the focal distance, and hence the separation distance between the two modules, was not compatible with either sound rf design, or more importantly, available shroud clearances. The lower f/D antenna could not be packaged about the fixed Earth viewing module within the available shroud diameter and height. These constraints have made exceptional demands on the spacecraft selection. A summary of the salient constraints are listed below:

- a. Equipment must be proportioned between the Earth viewing module and the aft equipment module such that both structural loading and harness weight are minimized.
- b. The structural link between the two modules must have a minimum effect on rf performance, and provide the strength and rigidity required to meet launch loading and the frequency criteria chosen (to ensure compatibility with the launch vehicles' autopilot and structural systems).
- c. Structural design must also be compatible with proper orientation control system operation. This requires that the structural link between the sensors and torquers exhibit a natural frequency much higher than the controller cross over frequency, and that other structural elements be of sufficient stiffness so that control instability is avoided.
- d. Thermal control must be provided to the divided electronic packages, which, because of field of view and structural considerations, must be proportioned so that most of the high thermal dissipators are grouped in the compact Earth viewing module, while the larger aft equipment module houses mostly low thermal dissipators.

The layout of the selected design is repeated in Figure 5.9-1 for convenient reference in the subsequent discussions.

# 5.9.2 LAUNCH PHASE AND ORBITAL CONSTRAINTS

### 5.9.2.1 Launch Vehicle Constraints

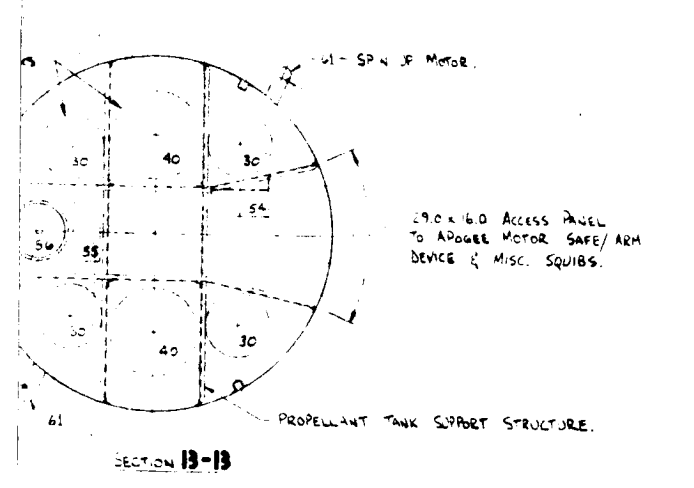
The SLV-3C/Centaur launch vehicle, equipped with an extended version of the 10-foot diameter Surveyor nose fairing has been selected for injecting the spacecraft into the syncronous transfer orbit. As an overriding design philosophy, the ATS-4 spacecraft has been designed to be compatible with the presently configured Surveyor launch vehicle in order to restrict development costs to only those structural modifications necessary to accommodate the longer and heavier payload.

SON IP POTOR . (REE) VEW ON ARROW PART SECTION AT K-K.

ANTENNA FEED MAN STATIC ENVELOPE , AT DIAMETER) - STATIC ENVELOPE. AERODYLMI C FA.R.NG. SOFT DIA ANTERNA (STOWED.) AERODYHAMIC FAIRING -SECTION AT ATA --- 193.25 (STANDARD SURVEYOR FARING)

5.9-4-1

+-- 540 ba - - --POLARS TRACKER. EARTH TRACKER HEAD - SUN SENSOR (TYP.) (39.5) - SPACELZAFT SEPARATION PLANE. MACHINED RING.7 (SPACE CRAFT.) MACHINED RING (ADAPTER) PHASED ARRAY RECEIVER. VIEW ON ARROW SPARATON SPRING A FRAME SUPPORT BEAM. SEPARATION SPRING. - PRIME FEED TURNSTILE ROS. TRANSITION FITTING MODULE AFT BULKHERD. - PRIME FEED 3-HORN CLUSTER. LONGERON - FEED SUPPORT ATTACHMENT FITTIG HEN ON ARROW M. 130.4 POST APOSEE BURN C.G. - ANTENNA I/F PLANE -- AFT EQUIPMENT MODILE - SPACECRAFT SEPARATION PLANE. - SOLAR ARRAY PANEL FIELD JOINT. CENTALR PAYLOAD RING FEED SUPPORT TRUSS DEPLOYMENT TRUSS. - ARABOUL REFLECTOR. SEE DETAL N FOR SEPARATION 200 Ma HCEE.ES APOGEE MOTOR (REQUIRED FAIRING EXTENSION.) (STANDARD SURLEYOR FAIRING) 5.9.4-2



Skin, - SEPARATON NUT.(SPACECRAFT)

BOUT CATCHER (ADAPTER.)

MACHINED RINGS TRANSITION FITTINGS REFER TO FIGURES 59-17 & 5.9-2: FOR
YEY TO EQUIPMENT ITEMS IDENTIFIED NUMERICALLY
ON THIS DWG.
2. SEE FIGURE 59-21 FOR VIEWS ON ARROWS TEGS.
3. SEE FIGURE 5.9-17 FOR VIEWS ON ARROWS FEGS.

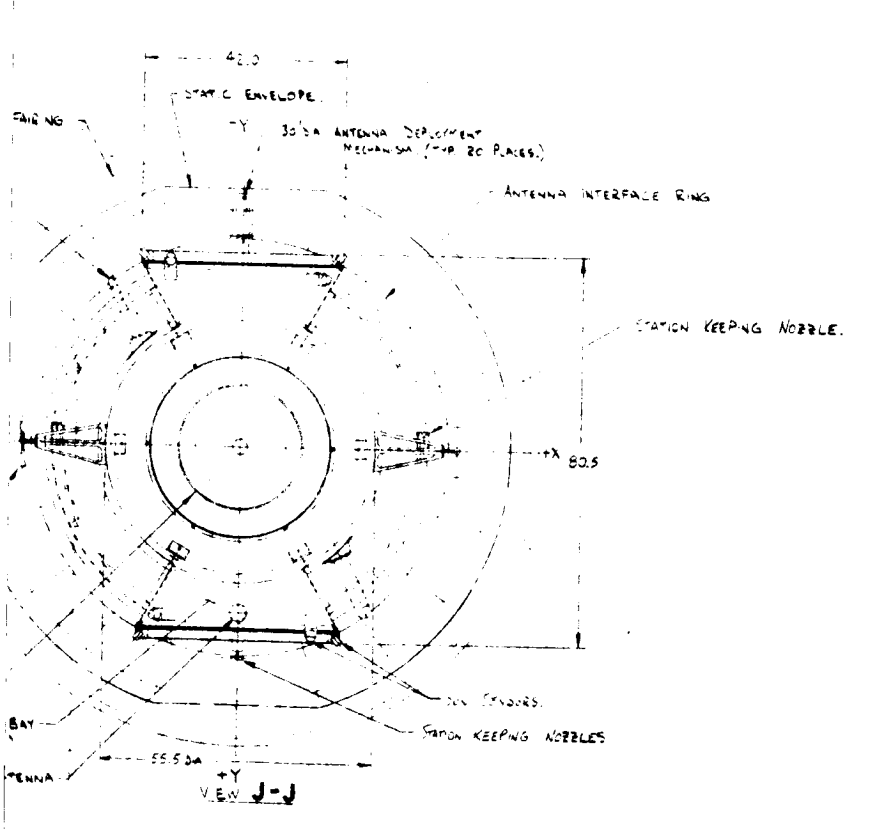


Figure 5.9-1. Inboard Profile and Orbital Configuration

5.9-4-3

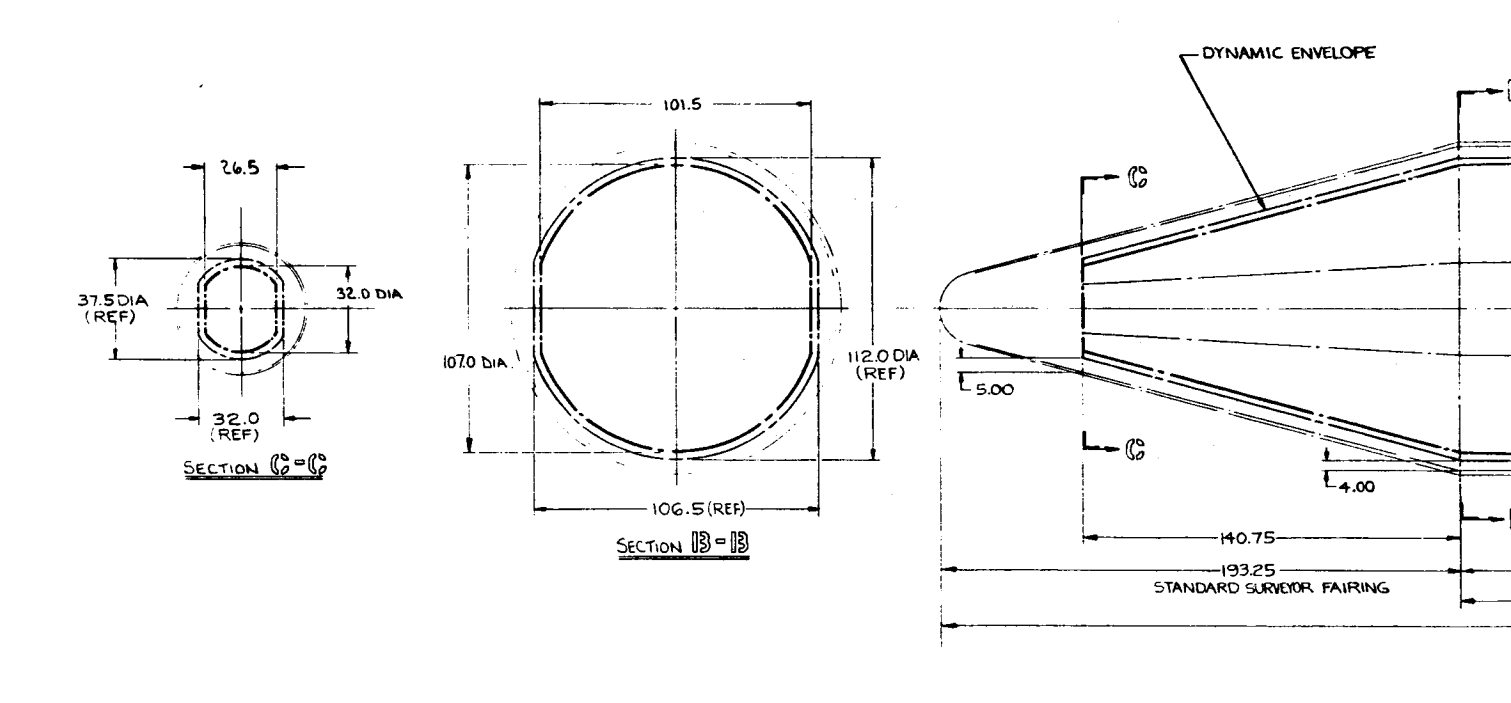
The geometrical constraints imposed by the nose fairing and Centaurs' payload mounting provisions, are shown in Figure 5.9-2. The 15-foot long cylindrical extension, specified by NASA/Lewis as being available to the ATS-4 mission, has been incorporated between the existing cylindrical portion and the tapered nose. However, use of this longer shroud is not without some penalties. In addition to the reduction in useful payload in orbit capability for the launch vehicle, considerations must be made for increased deflections of both fairing and payload and a reduced launch availability for the flight system.

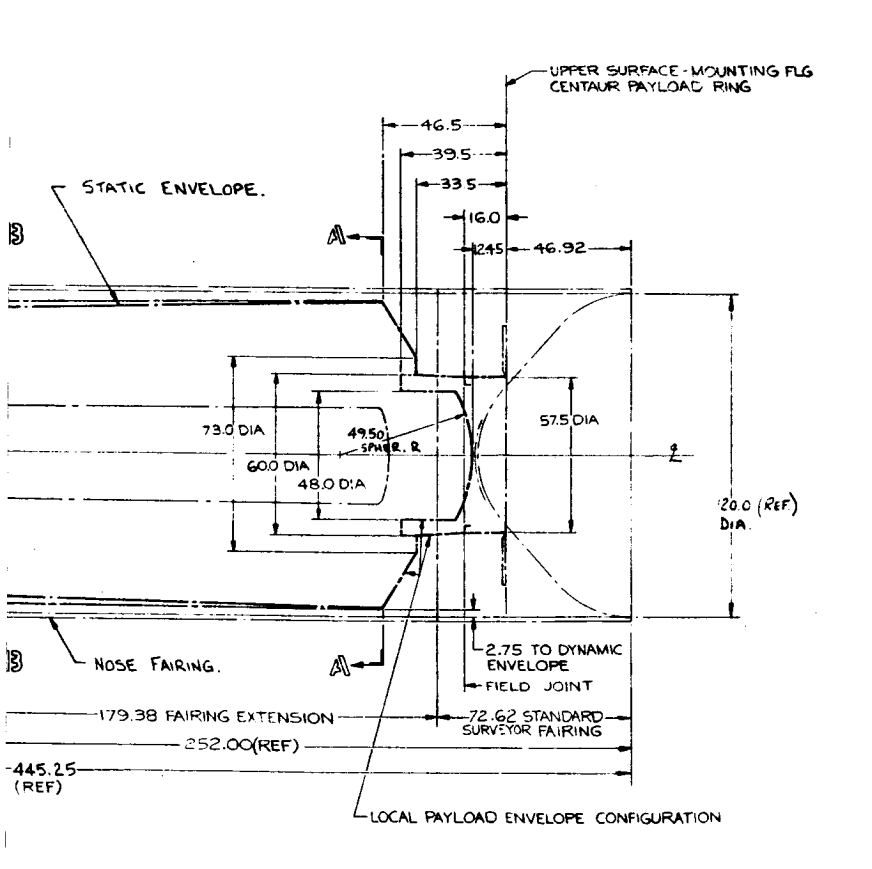
In order to ensure adequate spacecraft/shroud clearance, the 2-1/2 inch dynamic clearance specified for the Surveyor spacecraft has been linearly increased to a maximum of 5 inches at the extreme end of the available payload volume. The payload static envelope has been set at 3 inches inside the dynamic envelope at the maximum spacecraft excursion point, located at the upper periphery of the stowed antenna. This is generous in view of an expected spacecraft excursion of less than an inch under actual flight loading. Despite these reductions in available payload volume, the extended version of the fairing is still adequate for this configuration approach, with no unreasonable hinging or scalloping necessary to package the parabolic antenna in its rigid form.

The structural penalties incurred by use of this extended shroud are measured in terms of a reduced launch availability, an expression of the capability of the boosters' structural system to withstand expected flight loadings.

The results of the analysis performed to evaluate this effect are given in Figure 5.9-3 and show, that in the unfavorable flight weather months, launch availability can be as low as 45 percent. However, this should not be of great consequence to the ATS-4 mission since no requirement exists for a "Certain Day" launch window.

In order to ensure design compatibility with the mechanical environmental constraints imposed by the launch vehicle, the NASA/Goddard Vibration Qualification Test Specification, for Atlas/Centaur launched spacecraft, has been deemed applicable to the ATS-4 design. These values are given in Table 5.9-1 and constitute a significant portion of the structural design criteria. In addition to the inertia loads imposed by the launch vehicle, sound design





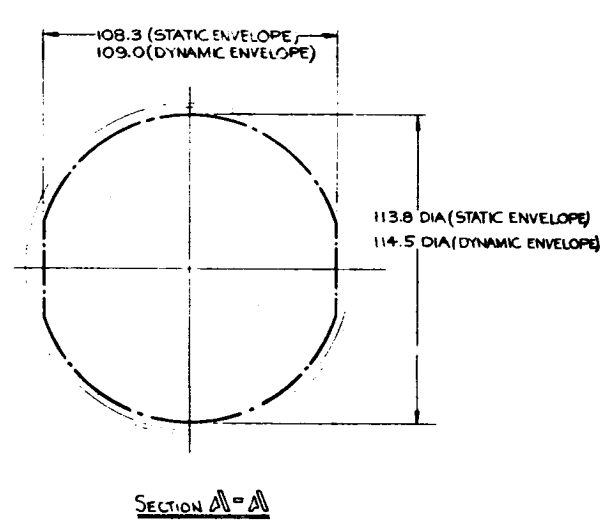


Figure 5.9-2. Static and Dynamic Envelope

5.7-8

Table 5.9-1. Atlas/Centaur Qualification Test Specifications

Frequency (cps)	Axis	Sweep Rate	Level (peak g)
5 - 250 250 - 400 400 - 2000	Thrust Z - Z	2 octaves per minute	+3.0 +3.7 +7.5
5 - 250 250 - 400 400 - 2000	Lateral X - X and Y - Y	2 octaves per minute	+1.5 +3.0 +7.5
	B - Torsional	Vibration	· !
Frequency (cps)	Axis	Sweep Rate	Level (peak radians/sec <sup>2</sup>
20 - 60 20 - 150	Thrust Z - Z	2 octaves per minute	<u>+</u> 12.9 <u>+</u> 25.8
	C - Random	Vibration	
Frequency (cps)	Test Duration (each axis)	Acceleration (g-rms)	PSD Level (g <sup>2</sup> /cps)
10 22 - 175 530 - 1000	4 minutes duration per axis	overall level 15.8	0.030* 0.065** 0.200***
** Increasing	from 10 cps at a cons from 175 cps at a con g from 1000 cps at a c	stant rate of 3.	0 dB/octave
	D - Booster Sustain	ed Acceleration	1
Axis	Levels (g)		Duration (minutes
Combined *Thrust and Lat	9.7 + 3.0 = 10.	. 2	1

Shock - Shocks caused by ignition, cutoff, staging, etc., will occur during vehicle operation. However, the shock environment will be less severe than the vibration requirements.

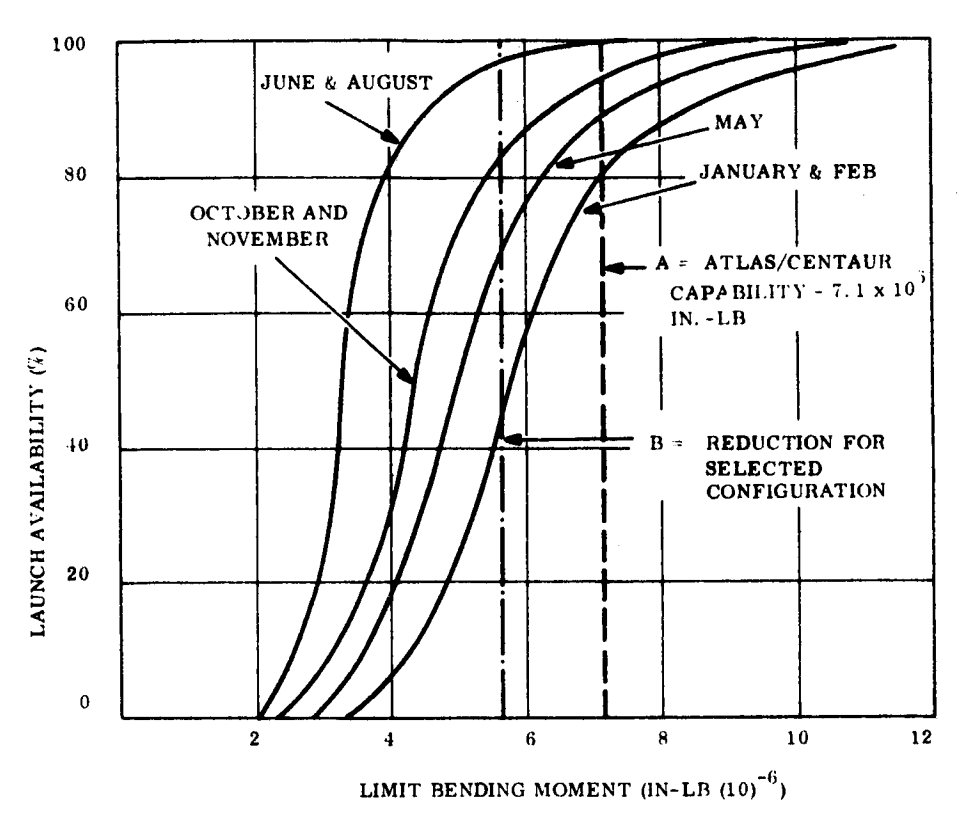
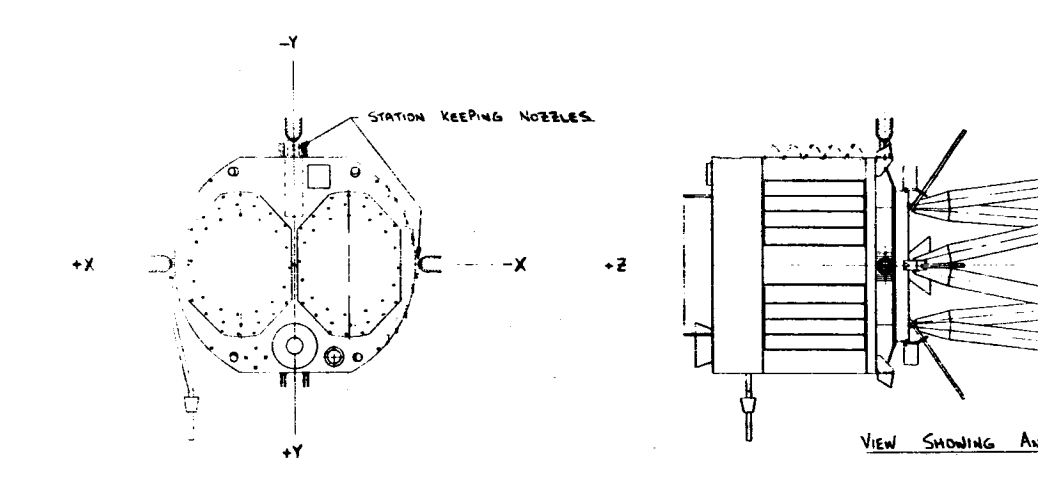


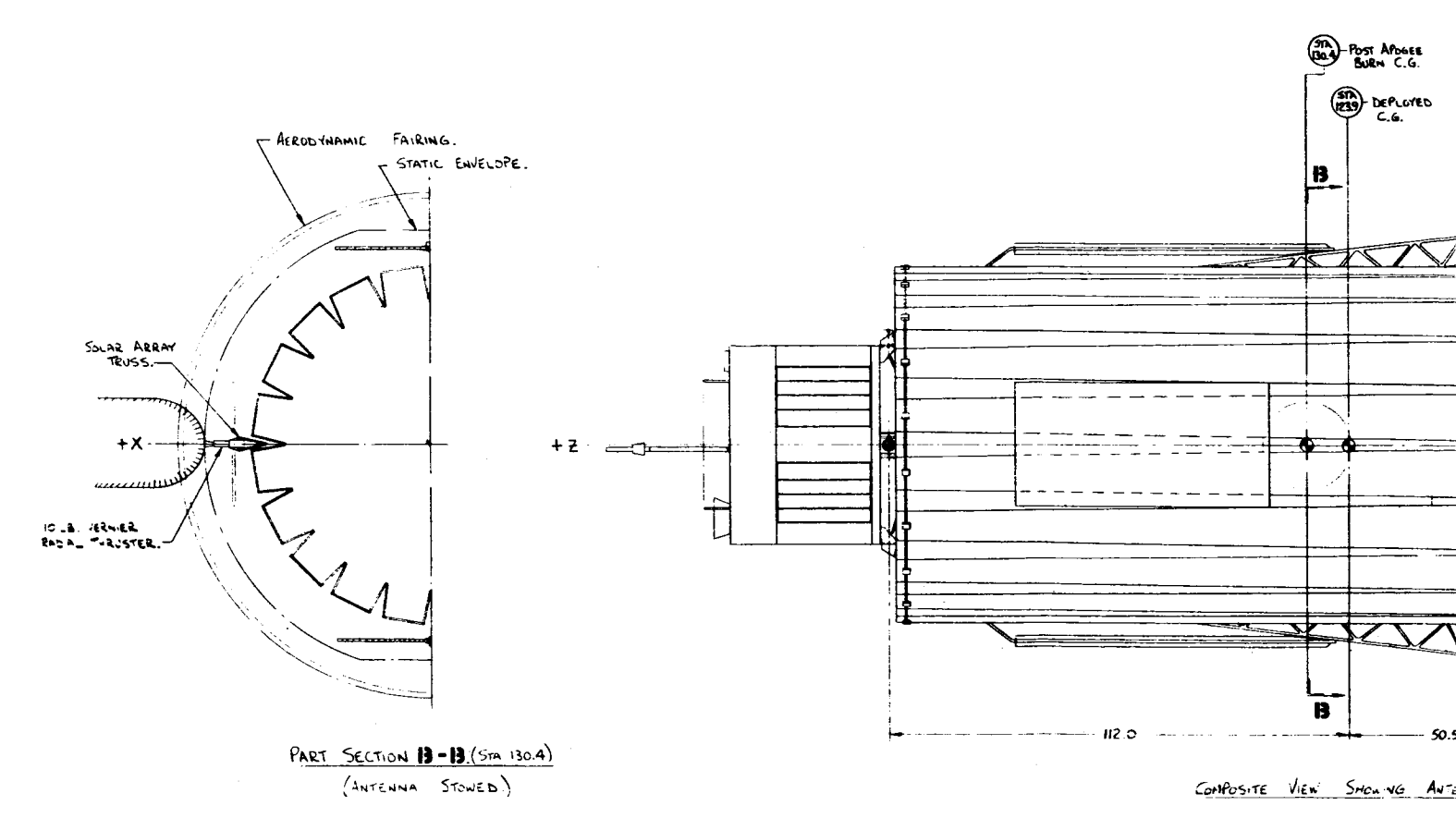
Figure 5.9-3. Launch Availability vs Limit Bending Moment

dictates that the spacecraft should be designed such that the fundamental lateral bending frequency does not couple with the launch vehicle and is compatible with the launch vehicle control system. The present Centaur displays a fundamental bending frequency of 2.0 cps and a second mode frequency of 6.5 cps; however, selection of a spacecraft design frequency which will be compatible with this dynamic behavior is not obvious in view of the like importance of the magnitude of the modal mass on the Centaur's autopilot stability. For this study, a 10 cps bending frequency criteria, with a limit of 500 pounds of actual mass in motion, has been established as being compatible. However, in view of the sensitivity of filter and sensor bandwidths, this design value should be checked subsequent to the next design phase, in order to properly assess spacecraft/launch vehicle control stability.

# 5.9.2.2 Coast Apogee Firing and Orbit Injection Constraints

Using an apogee motor in lieu of a final stage, requires that the spacecraft provide its own orientation and vernier capability during the final orbit. The various thrusters required are illustrated in Figure 5.9-4 with plume contours drawn to a length of 20-nozzle diameters.





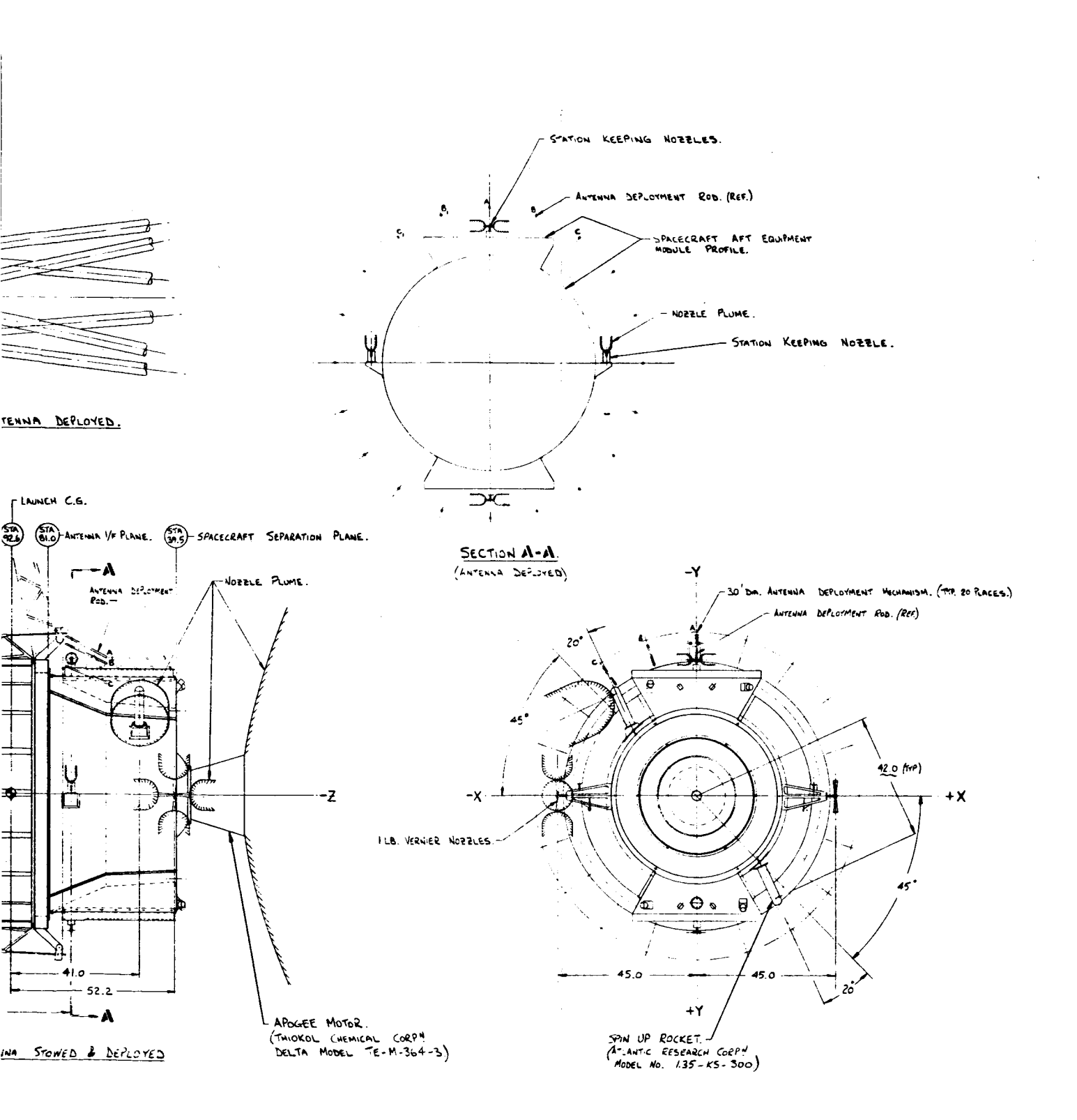


Figure 5.9-4. Nozzle Locations and Plume Details

5.4-12

The plume contours have been analytically derived from data available from firing tests. Further analysis was performed for the resistance jets and the 1-pound vernier thrusters using a method of characteristics evaluated by a computer program. The results are presented in Appendix M. This evaluation confirmed the plume contours shown in Figure 5.9-4. The thrusters have been mounted on standoff brackets where necessary, to obtain unobstructed expulsion of at least 60-nozzle diameters.

Immediately after separation, the spacecraft is spun-up by firing the solid rockets located on the aft equipment module at station 51.6, a location chosen to achieve maximum plume clearance. The rockets produce a nominal spin rate of 71 rpm at a maximum acceleration of 7.5 radians/sec<sup>2</sup>.

Synchronous orbit injection errors are removed by firing of one-pound vernier nozzles positioned on standoff bracketry.

A 10-pound radial thruster is mounted on a folded solar panel support truss at the post apogee burn CM location.

#### 5. 9. 2. 2. 1 Apogee Motor Characteristics

The Improved Delta motor (TE-364-3) was chosen for the ATS-4 mission on the basis of low cost and acceptable payload capability. The Centaur can place more payload into the transfer orbit than this motor can circularize and plane change. Therefore, the excess energy is used to produce a partial plane change at perigee.

The Improved Delta motor was developed from the Surveyor motor design. Currently approaching qualification, this motor is larger than the Surveyor design (1440 pounds propellant versus 1250 pounds for the latter) and represents a design point intermediate between the Surveyor and extended Surveyor designs. The Delta Motor, built by Thiokol for Douglas, has completed development testing and is ready to start a qualification program which includes six motors. At least three of these six motors will be AEDC tested.

The construction details are shown in Figure 5.9-5. At present, the spherical casing is constructed of steel, although a decision on a prepared titanium case will be made prior to qualification. The steel motor case has a nominal wall thickness of 0.039 inch and is of constant thickness, except for gradual increases at the girth and ends of the tank. The mounting surface is a ring at the girth of the motor. The nozzle is a semisubmerged carbon cloth design, with an expansion ratio of 53:1 and a weight of 49.6 pounds. The ignition system consists of two assemblies: (1) the pyrogen, which is essentially a small internal burning solid propellant rocket and (2) the initiator, which consists of a squib and a booster charge. The ignition system, including the safe-and-arm device will be installed as a unit into the Delta motor before launch, whereas the apogee motor itself is installed in the vehicle and aligned at ETR prior to this time.

Since the motor will not be jettisoned after orbit attainment, thermal considerations are also of importance. The design approach taken has been to isolate the motor from the thermally controlled compartments. The temperature curves shown in Figure 5.9-6 are applicable

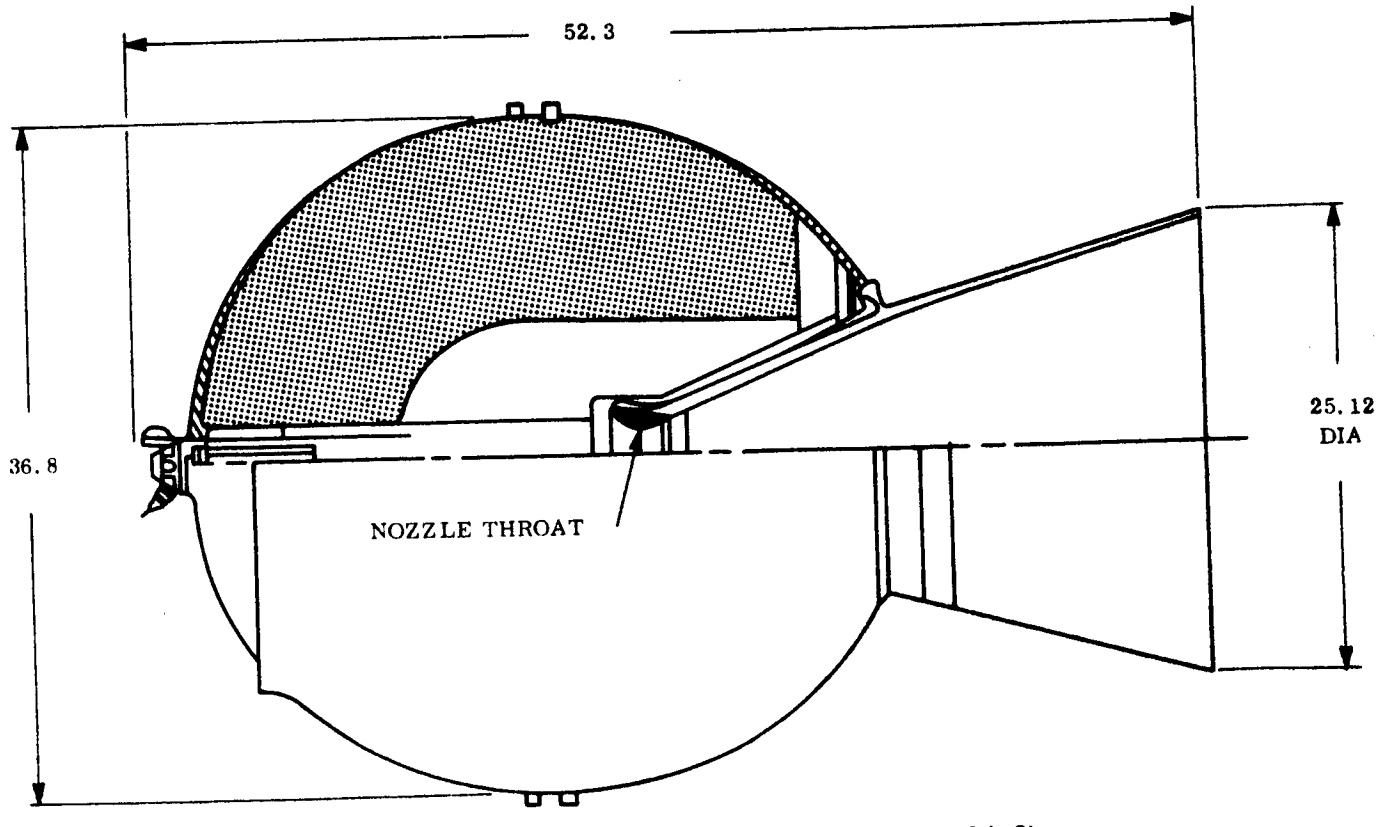


Figure 5.9-5. Delta Motor (TE-364-3)

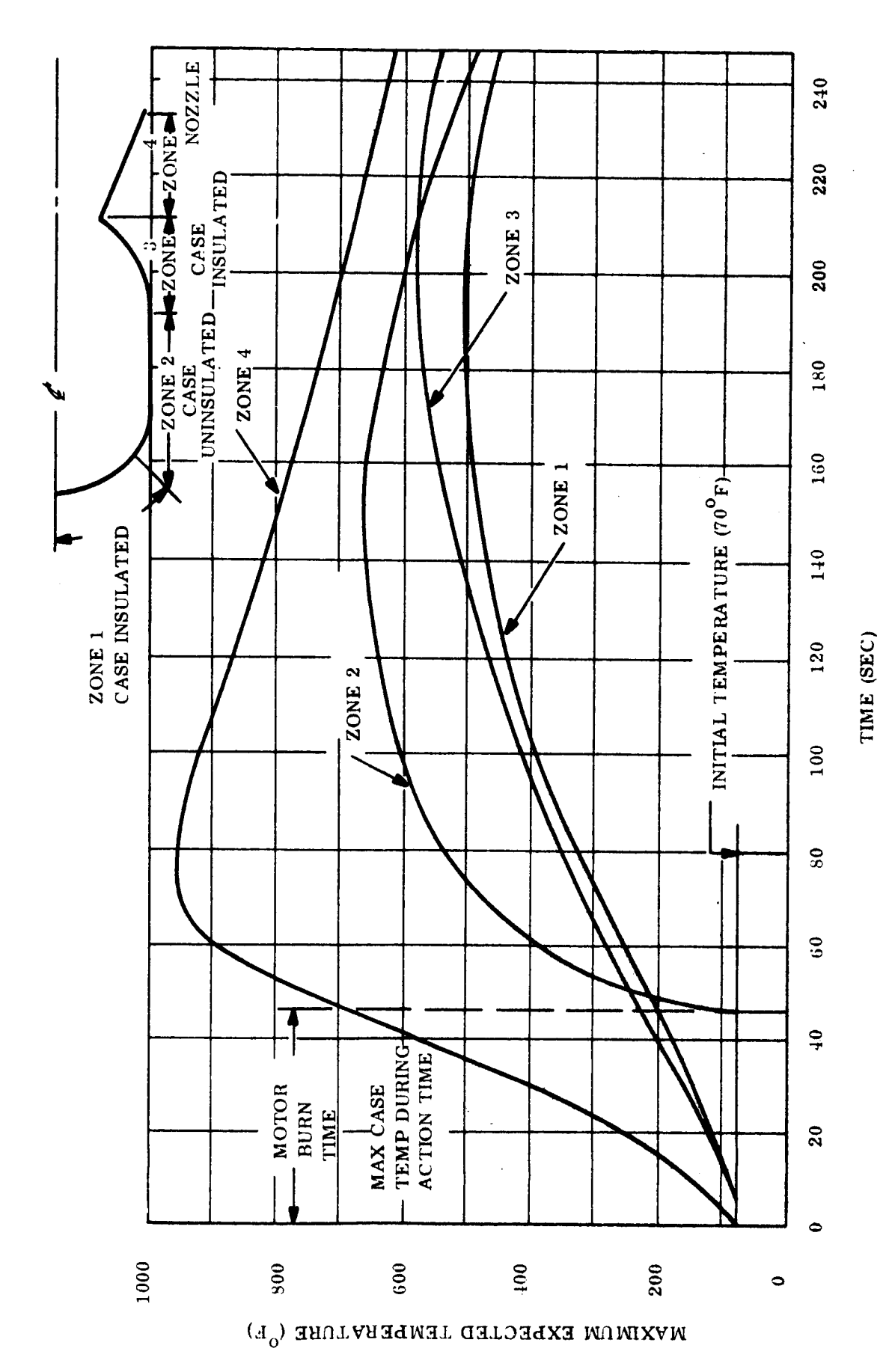


Figure 5.9-6. Maximum Expected Outside Surface Temperature vs Time for TE-364-4-3

during and immediately after firing. Thermal design problems arising from heat links through the motor casing and nozzle once in orbit, are discussed in Paragraph 5.9-6.

#### Performance

The capability of the Improved Delta motor is dependent on the amount of plane change the Centaur will do at perigee. Table 5.9-2 shows the payload capability. The second plane change is the inclination shift by the Delta motor. The Delta motor inclination change required is equal to 28.5 degrees minus the plane change made by the Centaur at perigee.

Table 5.9-2. Payload Capability Using TE-364-3 Improved Delta Motor

Plane Change -Angle (Degrees)	v	$\mathbf{w_1}$	$\mathrm{w}_2$	Payload (P/L)
18	5400	3260	1820	1681
20	5500	3210	1770	1631
21	5560	3180	1740	1601
22	5600	3160	1720	1581
24	5780	3100	1660	1521

# Where:

V = change in velocity needed to achieve synchronous orbit-feet/second

W<sub>1</sub> = booster payload capability into elliptical orbit - lb

 $W_0^1 = W_1$  less apogee motor propellant weight - 1b (propellant weight = 1440 lb)

 $P/L = W_2$  less apogee motor dry weight - lb (apogee motor dry weight = 139 lb)

Table 5.9-3 shows performance and physical data on the Improved Delta motor (TE-364-3). Additional performance data is presented in Figure 5.9-7 wherein thrust versus time and chamber pressure versus time curves are presented. Corresponding "g" loading developed during the apogee motor burn is illustrated in Figure 5.9-8.

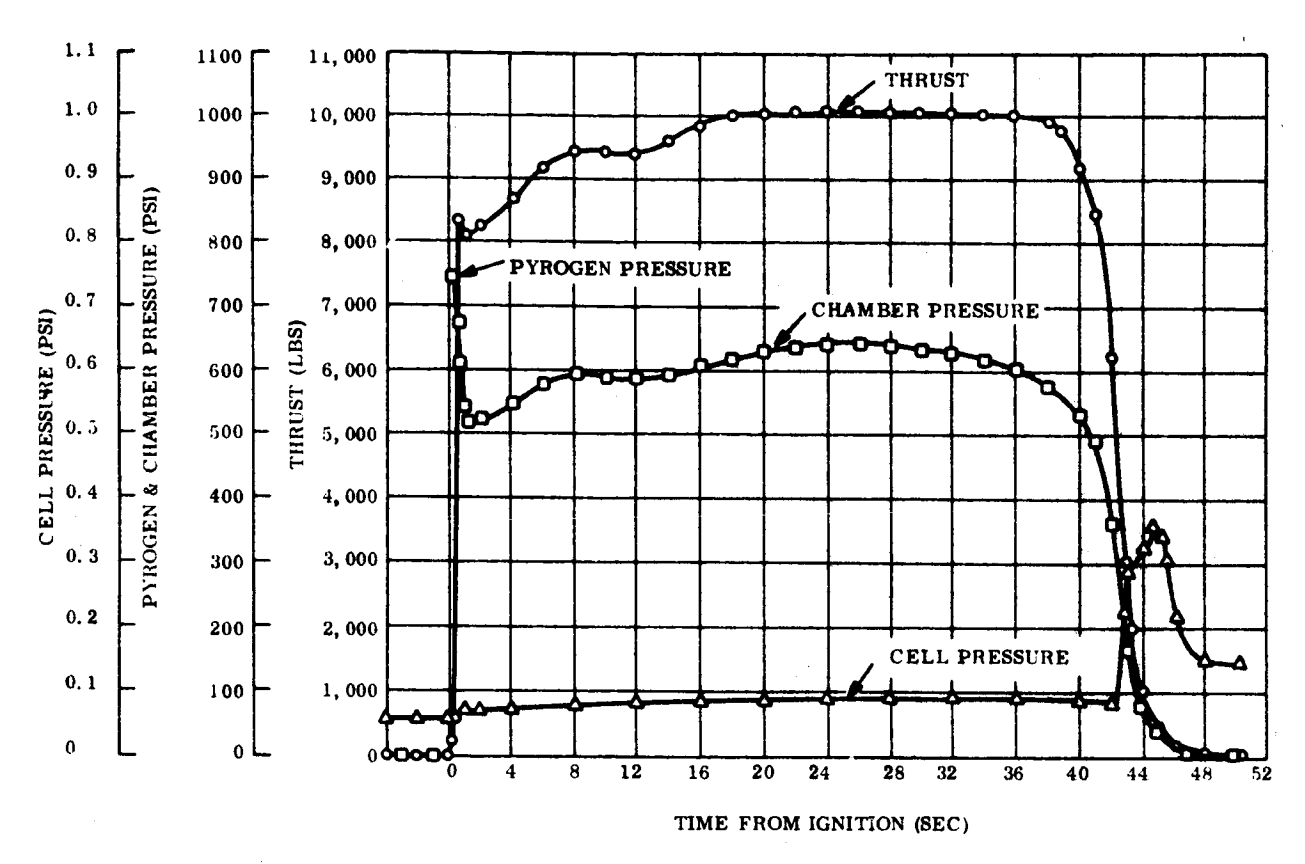


Figure 5.9-7. TE-364-3 Altitude Thrust and Chamber Pressure vs Time

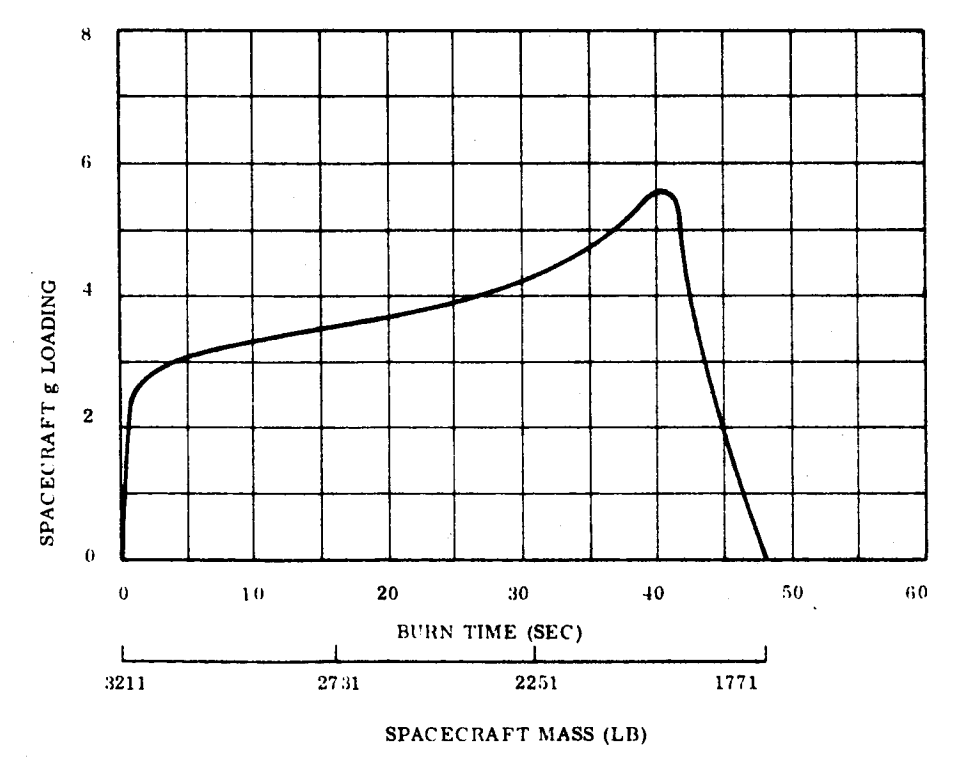


Figure 5.9-8. G-Loading vs Time During Apogee Burn

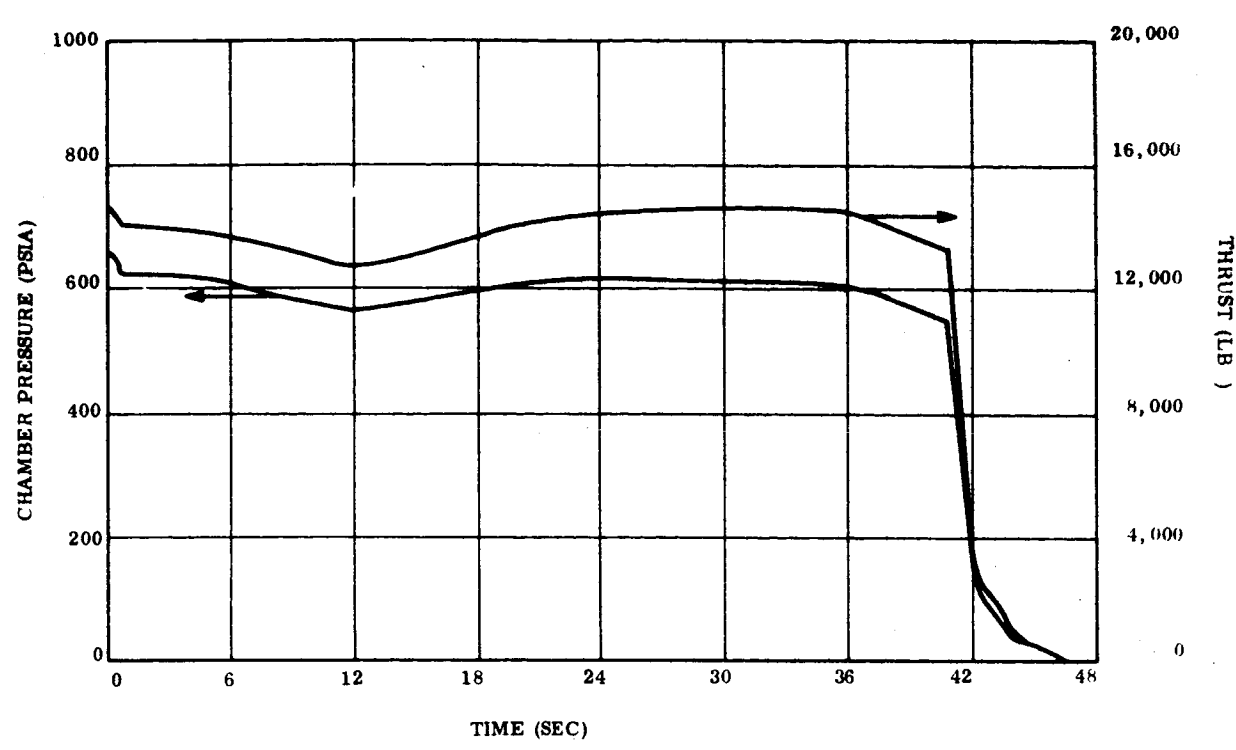
Table 5.9-3. Performance and Physical Data on the Improved Delta Motor (TE-364-3).

TE-364-3	
I E-903-0	
Isp	classified
Average Thrust	10,000
Burn Time	48 seconds
Max. g	~ 5.7
Total Impulse	415,000
Propellant Weight	1440 lb
Inert Weight	139 lb
Total Weight	1579 lb
Motor Length	52.3 inches
Motor Diameter	37 inches
Nozzle Length	17 inches
Average Chamber Pressure during burn	600 psi
Chamber Material	steel

Vibration loads associated with firing are extremely small in comparison to the launch vehicle loading. During tests on the Surveyor motor (TE-364-1) engine mount loads of 6-pounds rms, with a 20-pound maximum, were measured in the frequency range up to 160 cps. This motor should show dynamic characteristics in the same range.

#### Potential Growth Version of Delta Motor

The Improved Delta technology can be used to develop an optimum apogee motor for ATS-4. A typical thrust versus time and chamber pressure versus time curve for an uprated Delta motor matched to the Centaur capability is presented in Figure 5.9-9. The proposed performance is shown in Table 5.9-4.



\*NOMINAL CALCULATED VALUES FOR OPERATION AT +60°F; VACUUM

Figure 5.9-9. Thrust and Chamber Pressure vs Time

Table 5.9-4. Performance Parameters for Optimum Motor(Extended Surveyor)

Isp	classified	sec
Average thrust	14000	lbf
Burn time	42	sec
Max. g	~7.5	
Total impulse	classified	lb-sec
Propellant weight	1909	lb
Inert weight	126	lb
Burn out weight	NDA	lb
Total weight	2035	lb
Motor length	63 + igniter	inches
Motor diameter	37	inches
Nozzle length	~32.0	inches
Throat diameter	~3.8	inches
Average chamber		
Pressure during burn	600	psi
Chamber material	titanium	

A detailed discussion on the design, development and problem areas of this optimum motor is presented in Section 6.

### 5.9.2.3 Orbital Constraints

The most significant orbital design constraint imposed on the configuration is the prerequisite for compatibility with the orientation control system. Coincidence of CM, CP and minimization of spacecraft inertias are obvious requirements, the former being effectively accomplished on this configuration by virtue of the "see through" antenna surface and a symmetrical design whose large solar area is located in the section of the spacecraft which also contains the majority of the mass. Efficient control system design also dictated the packaging of sensors and torquers in the same module, a configuration conflict in that while it is desired to give the sensors optimum viewing position on the earth viewing module, the heavy mass items of the orientation control system should be placed in the aft module. Separation is acceptable, but only if the structural link between the system components is sufficiently rigid to preclude control system instability. If a complex filtering scheme is incorporated in order to remove the effects of structural coupling, a degradation of controller performance results. Therefore, as the most efficient solution, sensors and torquers are separated with a design requirement of 10 cps being established for the separating structural link. Establishment of a two cps frequency criteria for other deployed structure, including the antenna reflector, was established as a design goal with a like philosophy. Subsequent analysis has indicated control system stability with structural frequencies in a one cps range. In each case, the modal mass associated with the vibratory mode is less than one percent of the rigid body mass.

The thrust and torque levels that the spacecraft is subjected to in orbit are extremely low. To enable use of the same system components for both stationkeeping and orientation maneuvers, thrusters are located on each equipment module, bracketing the CM and allowing for pure translational motion during stationkeeping, and pure rotations for pointing. The maximum torque level induced about any control axis is 0.125 in-lb, which occurs during inertial wheel stall-out, but 0.25 in-lb has been assumed for dynamic analyses. Maximum translational levels along the pitch or roll axis is 0.00286 pound developed from the simultaneous firing of two of the 0.001-pound thrusters mounted on the AFT equipment module and one of the 0.00286-pound thrusters mounted on the Earth Viewing module.

The detailed locations of the thrusters and their calculated plume contours are shown in Figure 5.9-4. As previously discussed, placement of the thrusters to eliminate impingement of the plume on the spacecraft surfaces is extremely important, in that reduced thruster efficiency and possible degradation of spacecraft surface coatings can result. This latter possibility is quite remote however in view of the inert qualities of 100 percent dry ammonia. No problem exists at the Earth viewing equipment module installations. However, placement of the complimentary thrusters to achieve the optimum balance between orientation torque levels about the CM and reasonable stationkeeping translational levels, required installation in an area where impingement upon the deployed antennas' drive mechanism is possible. Rather than upset the balance of thrust forces, small brackets have been incorporated to guarantee unobstructed gas expulsion.

#### 5.9.3 SPACECRAFT STRUCTURAL DESIGN

The spacecraft structural design philosophy has been developed about the specific ATS-4 mission requirements, as introduced earlier, in addition to the usual adherence to sound spacecraft design practices dictated by launch and pre-launch sequences. A summary of all the spacecraft design constraints and their specific contribution to the design are given in Table 5.9-5. It becomes apparent that compatibility with the prime experiments has been a major contribution to the design. One facet of this requirement concerns the integration of electronic components.

The electronic packaging philosophy adhered to, for the pruposes of this study, is the mounting of discrete components of the "black box" variety on heat rejection panels provided on the equipment modules.

Other approaches, based on fully structurally integrated or standardized modularization philosophies are quite promising and are discussed in paragraph 6.7.4. In order to effectively consider these concepts however, packaging design studies to the cordwood module level are required, a design effort not fully in the scope of a Phase A effort. Therefore, the packaging studies have concentrated on the intermodule harnessing definition and its minimization, along with thermal, structural and mass balance tradeoffs of location required to allow development of the spacecraft design to a more than routinely definitive stage.

Table 5.9-5. Summary of Spacecraft Design Constraints and Significance to Selected Design

Constraint	Significance to Selected Design
Prelaunch Assembly Alignment Checkout Transportation Ground Handling	<ol> <li>Earth viewing module longerons and primary load paths designed for a 3-point pick-up.</li> <li>Deployed booms and antenna designed for deployment in one-g field.</li> <li>Feed support truss includes turnbuckle adjustment features to allow exact placement of feed and sensors relative to reflector and aft equipment module.</li> <li>Antenna interface designed to be repeatable and allow antenna installation after assembly and alignment of equipment modules.</li> <li>Electronic packages mounted on removable panels and swing out bays.</li> <li>Aft equipment module designed for field installation, alignment and arming of apogee motor.</li> </ol>
Launch and Powered Flight Shroud Envelope Payload/Booster Interface Environmental Loads and Temperature	<ol> <li>Compatibility with fairing has determined antenna stowage geometry, and selection of four panel solar array system.</li> <li>Payload/Booster interface requirements have dictated a shear lag design to distribute loads and an adapter design compatible with present Centaur hardware.</li> <li>Lateral vibration loads form critical design condition for feed support truss and aft equipment module structure.         Earth viewing module designed for axial loading; adapter design limited by stiffness requirements.     </li> <li>Thermal control during launch relies on thermal inertia.</li> </ol>

# Table 5.9-5. Summary of Spacecraft Design Constraints and Significance to Selected Design (Cont'd)

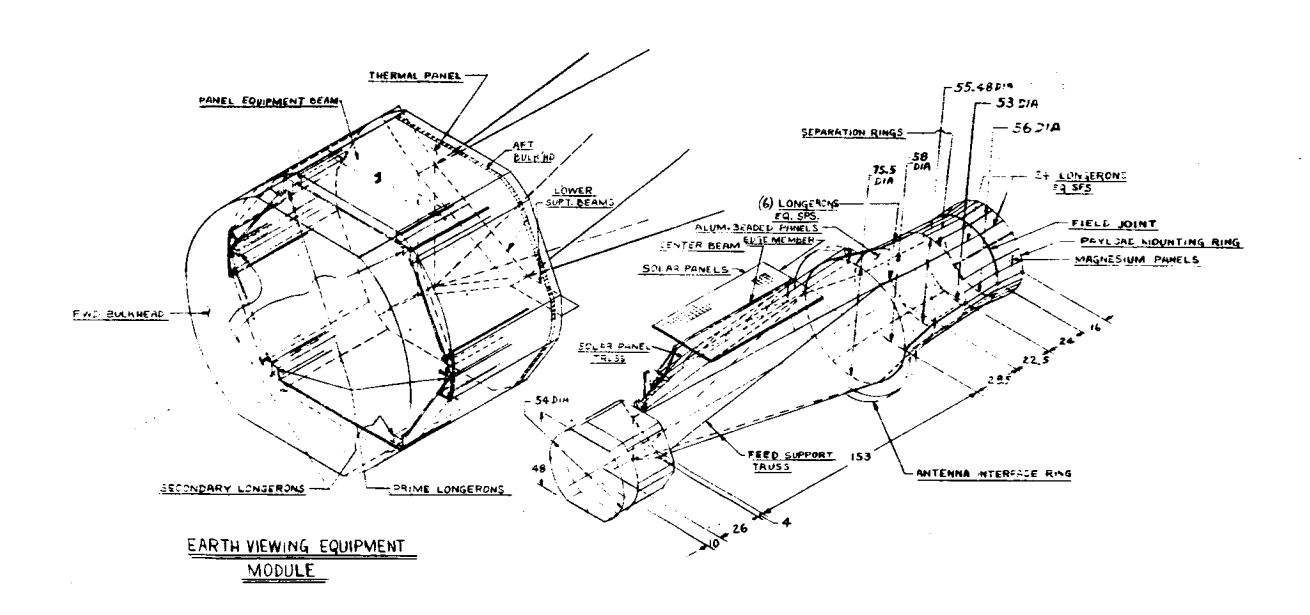
Constraint	Significance to Selected Design
Compatibility with Parabolic Antenna Experiment	<ol> <li>Spacecraft geometry tailored to antenna stowage dimensions.</li> <li>Feed support blockage and reflectance minimized with chosen structural approach of thin tube beryllium truss and maximum clearance at feed (the latter consistant with present petal geometry).</li> <li>Solar panel stowage and deployment ganged to antenna to be non-interfering to successful antenna deployment.</li> <li>Feed electonics grouped with feed to minimize line losses.</li> <li>Lateral support to open end of stowed antenna provided by EVM.</li> </ol>
Compatibility with Orientation Control Experiment	<ol> <li>Structural stiffness designed for proper control system performance.</li> <li>Location of polaris sensor to obtain required field of view required mounting below feed horn.</li> <li>CP/CM separation minimized by packaging approach</li> <li>Mass moments of inertia minimized by symmetrical 4-panel solar array design, "cut-out" antenna and f/D selection</li> <li>Thrusters located to bracket CM-losses due to plume impingment avoided by placement and standoffs.</li> <li>Fuel lines feeding thrusters continuous with no flexible joints and protected from space environment.</li> <li>Fuel tanks rigidly supported in AEM in easy access compartment</li> </ol>
Compatibility with Phased Array and Interferometer Experiments	<ol> <li>Peak power required for phased array operation provided with optimized solar array/battery power system.</li> <li>Stringent thermal control requirements for interferometer accuracy and TWT heat rejection require use of shutters on 5 of 6 EVM faces.</li> <li>Prime earth viewing area given to these experiments by mounting in separable compartment in EVM.</li> <li>Location of experiments such as to coincide with spacecraft reference axis.</li> </ol>

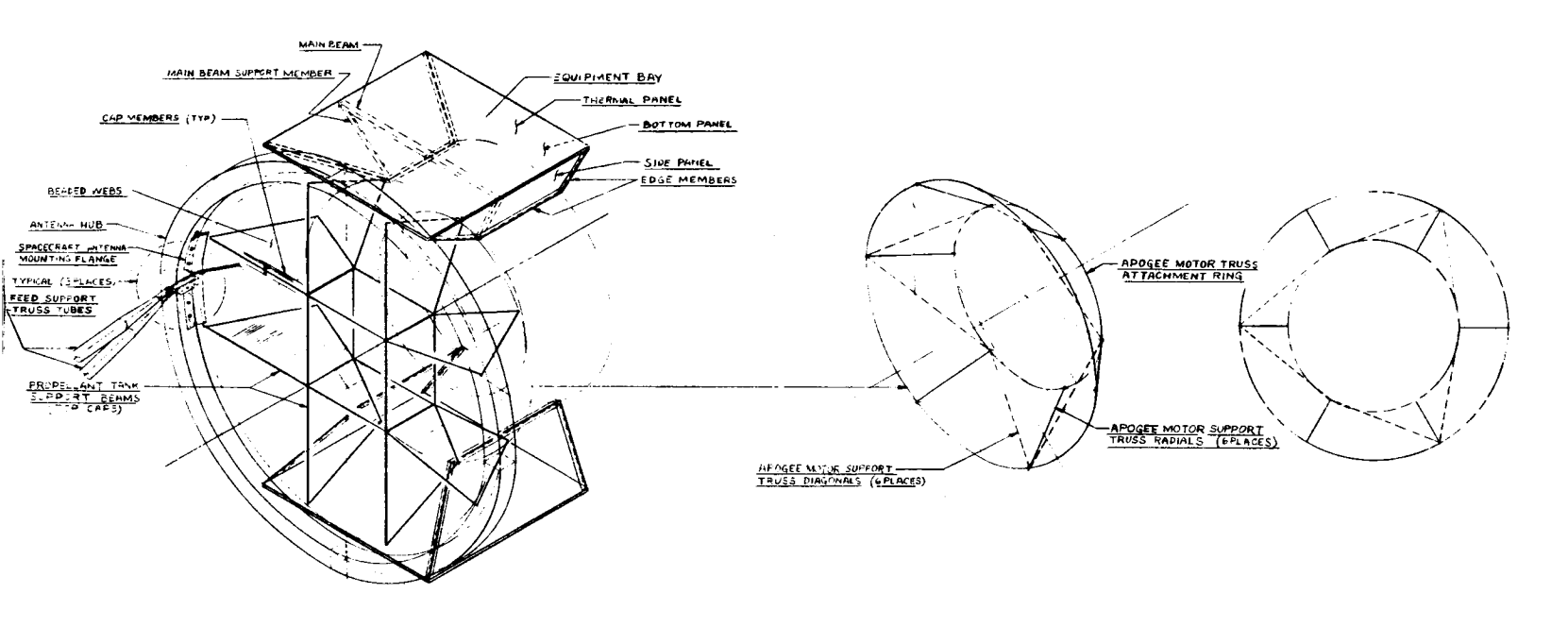
The major structural elements of the selected configuration are the Earth Viewing Equipment Module (EVM), the Feed Support Truss, the Aft Equipment Module (AEM), the Solar Array Panels and Trusses, and the Spacecraft Forward and Aft Adapters. The structural relation of these elements is shown in Figure 5.9-10 and discussed in the following paragraphs. In support of the chosen design, a complete and detailed rationale and stress analysis has been prepared. This may be found in the structural analysis sub-section 6.7.1. For convenience, the description of the major structural members, their critical loading condition and margin of safety is summarized in Table 5.9-6.

## 5.9.3.1 Earth Viewing Equipment Module

The Earth Viewing Equipment Module provides mounting surfaces for the phased array, parabolic antenna feed, selected TT&C, orientation control, and experiment packages and transfers this equipment load aft to the Feed Support Truss. The forward 10 inches of the EVM is cylindrical with two flattened sides, closed off with bulkheads, of which the forward one supports the phased array receiver and transmitter. These significant mass items when related to the axial load environment of 30 g necessitated that this bulkhead be of 5052 aluminum alloy honeycomb sandwich construction with 0.005 in. thick face sheet and 0.625 in. thick core of 1.6 lb/ft density.

The sidewalls of the aft 26 inches of the EVM are made up of six flat aluminum allow thermal panels closed off with a sandwich bulkhead aft and a bulkhead shared with the aforementioned cylindrical upper structure. This common forward bulkhead provides a thermal barrier between the two sections of the module and also takes the kick loads of the thermal panel upper framing members. The aft bulkhead, also of aluminum alloy honeycomb sandwich construction, provides the antenna feed mounting surface and resists the kick loads of the thermal panel lower framing members. Six longerons, of 7075 T6 aluminum alloy are axially continuous through the module and join the edges of the flat thermal panels together. The cross sections of the longerons were tailored to facilitate mounting of thermal panels and to be compatible with the upper cylindrical portion of the EVM.





STRUCTURAL ARRANGEMENT

DRIMON BY JEROMAY 10.6.66

Figure 5.9-10. Relation of Major Structural Elements of Selected Configuration

5.9.26

5.9-25/26

Table 5.9-6. Major Structural Elements

Functional Description	Material	Physical Description	Probable Method	Critical	Mode of Failure	Margin of
			of Manufacture	Condition		Safety
Earth Viewing Equipment Module Fwd. Bulkhead						
Face Shects	Aluminum 5052-H38	0.005-in. thick sheet		Axial	Face Sheet Dimpling	0.14
Core	Aluminum 5052	0.625-in. thickness		Axial	Core Shear	High
Thermal Panels	Aluminum 6061-T6	0.06-in. & 125-in. thick plate		Axia	Shear Buckling	+0.39
Panel Equip, Beam Longeron BR	Aluminum 7075-T6	2-in. x 3/4-in. x 0.040-in.	Bent-up Sheet	Lateral	Crippling	+0.46
		0.035-in. box section	מה מה מוספר	TAIA!	Column Dacking	8
Longeron CC	Aluminum 7075-T6	L1/4-in. x 7/8-in. x 0.04-in. I	Extrusion	Axial	Column Buckling	+0.14
Lower Support Beams	Aluminum 7075-T6	4-in. x 2-in. x 0.125 I	Extrusion	Axial	Crippling	40.54
Propellant Tank Support Beams						
Cap Members	Aluminum 7075-T6	1.75-in. x 0.875-in. x 0.094-in. Tee	Extrusion	Axial	Crippling	+0.005
Web		0.032-in. beaded panels		Axial	Shear Buckling	+1.78
Equipment Bay (Aft Equip. Med.)					-	
Main Beam	Aluminum 7075-T6	3-in. x 1-in. x 0.05-in.	Bent-up Sheet	Lateral	Crippling	-0.23
Thermal Panel	Aluminum 6061-T6	0.06-in. thick plate	•	Axial	Shear Buckling	+0.25
Main Beam Support Members		0.5 x 0.5 x 0.063 angle	Extrusion	Lateral	Buckling	+0.02
Side Panel	Aluminum 2024-T3	0.032 flat panel		Axial	Shear Buckling	10.07
		o. oot iiat panei		Latera	Sucking	70.0+
Solar Array Panels						
Face Sheets	Aluminum 5052-H38	0.005-in. thick sheet		Lateral	Face Sheet Dimpling	+0.22
Center Beam	Aluminum 7075-T6	0.3-in. interness 1-in. x 1-in. x 0.035 bat	Bent-up Sheet	Lateral	Core Shear	E :
		sections face to face			9	:
Solar Array Trusses	Aluminum 6061-T6	3/4-in. O. D. tubing	Extruded & Welded	Lateral	Buckling	~ %
-		•	Donot B Donot Co		Daconing S	9
Feed Support Truss Members	Beryllium	3-1/4-in. O. D. x 0.060-in. wall tube	Extrusion	Lateral	Buckling	+0· 00
Aft Equipment Module				<del></del>		
Antenna llub	Titanium 6AL-4V	4-in. x 4-in. x 0.04-in. box sect.	Formed Sheet	Lateral	Tension	+0.22
Longeron (Sta. M1)	Aluminum 7075-T6	1.5-in. x 1.5-in. x 0.065-in. hat	Extrusion	Lateral	Compression	-0.021+
Longeron (Sta. 62.5)	Aluminum 7075-76	1. 75-in. x 1. 75-in. x 0. 083-in. hat	Extrusion	Lateral	Crippling	-0.035
Appete Mr. Sungert Truss (Badials)	Aluminum 2024-T3	2.25-in. X 1-in. X 0.094-in.	Machined Forging	Lateral	Crippling	+1.85
Apogee Mrr. Support Truss (Diagonals)	Aluminum 2024-T3	2-in. O. D. x 0.049-in. wall tube	Tuhing	Istorel	Bonding & Compression	77.12
			9		Dendang & Compression	3
Spacecraft Adapter Shear Danel	Mamaelum A741D.H41	0.073- in which plats				
				TE LEGISTE	Compression Buckling	£0, 36
Field Joint Ring (Sta. 16)	Aluminum 7075-T6	1, 25 x 1, 25 x 0, 094 angles (back to back)	Machined Forging	Lateral	Crippling	+0.02
į			*Margins based on member sizes used in compu Slight increase in member thickness indicated.	ember sizer ember thick	*Margins based on member sizes used in computer analysis. Slight increase in member thickness indicated.	

The basic geometrical concept of the EVM evolved from both packaging and structural requirements. The forward portion is cylindrical in order to provide the maximum surface area for the mounting of Earth viewing equipment and the polaris sensor, the latter while not requiring Earth viewing area, being constrained to be mounted as far forward as possible in order to obtain its required free field of view past the antenna and extended solar panels. The aft portion is flat sided, thereby providing the optimum mounting arrangement for large heat dissipating components. Thermal control requirements were such that the maximum available heat rejection is provided. The number of flat sides (six) and hence the number of axial longerons were selected on the basis of the interface problems presented by the three hard points of support at the feed support truss. It was judged more convenient and more structurally efficient to shear six panel loads into three main longerons and thence to the feed support truss than to accomplish this load transfer with any other practical arrangement of panel and axial members.

The material selection for the thermal panels (6061 T6 aluminum alloy) is predicated mainly on its relatively good thermal conductance properties. The thicknesses involved (0.06 in. and 0.125 in.) are again based on thermal requirements and are more than adequate structurally.

Typical panels require beam stiffening to carry component lateral loads to the longerons where, in turn, they are introduced as shear loads in adjacent thermal panels and carried as such to the reaction points at the aft end of the EVM. Panel shear stiffening is also required to stabilize the panel and enable the transfer in shear of axial component loads to the major longerons and thence to the aft reaction points.

In the final packaging design, full use will be made of these stiffening members for component mounting. It is also very likely that the stiffness of the components themselves may be used in an integrated concept to eliminiate the need for much of the panel secondary structure.

Axial loads of components mounted on the forward bulkhead are transferred in bending from the bulkhead to the longerons. Lateral loads of such components are taken as shear in the sidewalls and thence in bending of the entire section to the aft reaction points.

As previously discussed, compatibility of the EVM with the feed support truss is achieved by "shear lagging" equipment loads from six axial members to three prime longerons which carry the loads to the lower support beams. Antenna packaging requirements prevented the coincidence of the prime longerons and the hard points of the feed support truss, thereby requiring the use of the lower support members which beam the equipment loads inward to the feed support truss. This beam network is made up of 4-inch deep 7075-T6 aluminum alloy extrusions.

#### 5.9.3.2 Feed Support Truss

The feed support truss consists of six diagonal beryllium tubular members with monoball end fittings. In addition to supporting the EVM, the truss provides, either directly or indirectly, lateral support for the antenna and solar array panels and trusses. Typical of pin ended trusses, loads are carried in direct tension and compression to three points (120 degrees apart) on the antenna interface ring at the forward end of the aft equipment module at station 81.

The feed support truss deserves a detail discussion in that the design of this structural path emphasizes the competing requirements of the spacecraft's experimental subsystem. The requirements placed on these members is to:

- a. Form the structural path between the Earth viewing and aft equipment modules, providing the required launch strength, and orbital rigidity between orientation control sensors and thrusters, but yielding minimum rf blockage area and system weight. In earlier studies, the primary consideration was stiffness, however, the column buckling loads resulting from lateral vibration levels received later in the study, are now limiting.
- b. Provide the means of adjustment along the three spacecraft axes in order to accurately align the antenna feed horn to the reflecting surface and the orientation control sensors to the momentum wheels.

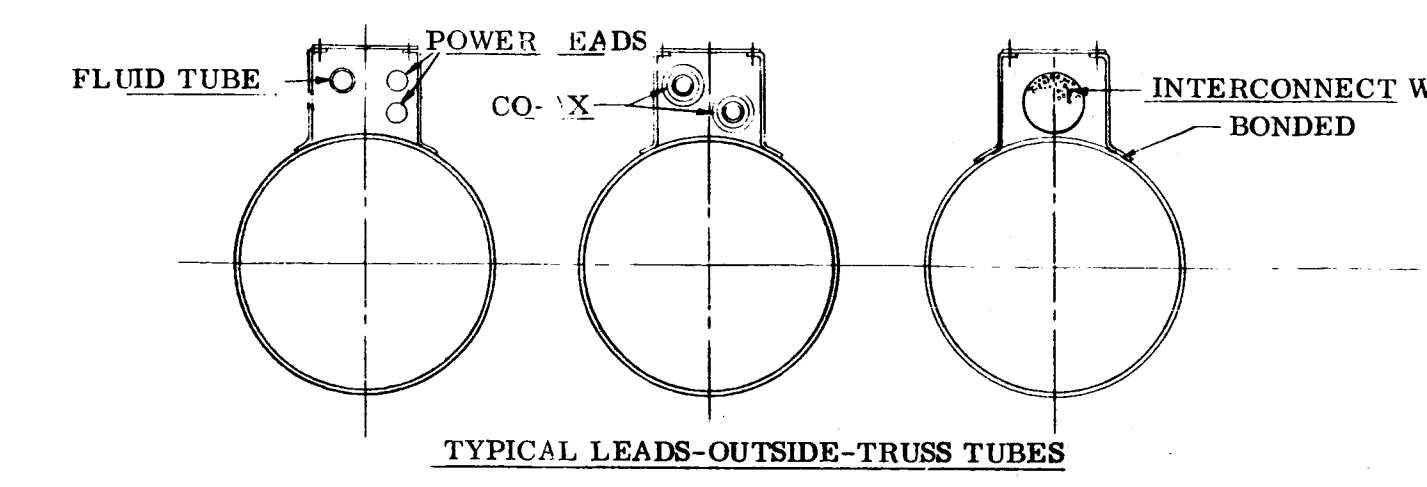
c. Provide a path for harness and ammonia tubing runs between equipment modules, again minimizing rf losses, and also providing thermal control to the fuel lines.

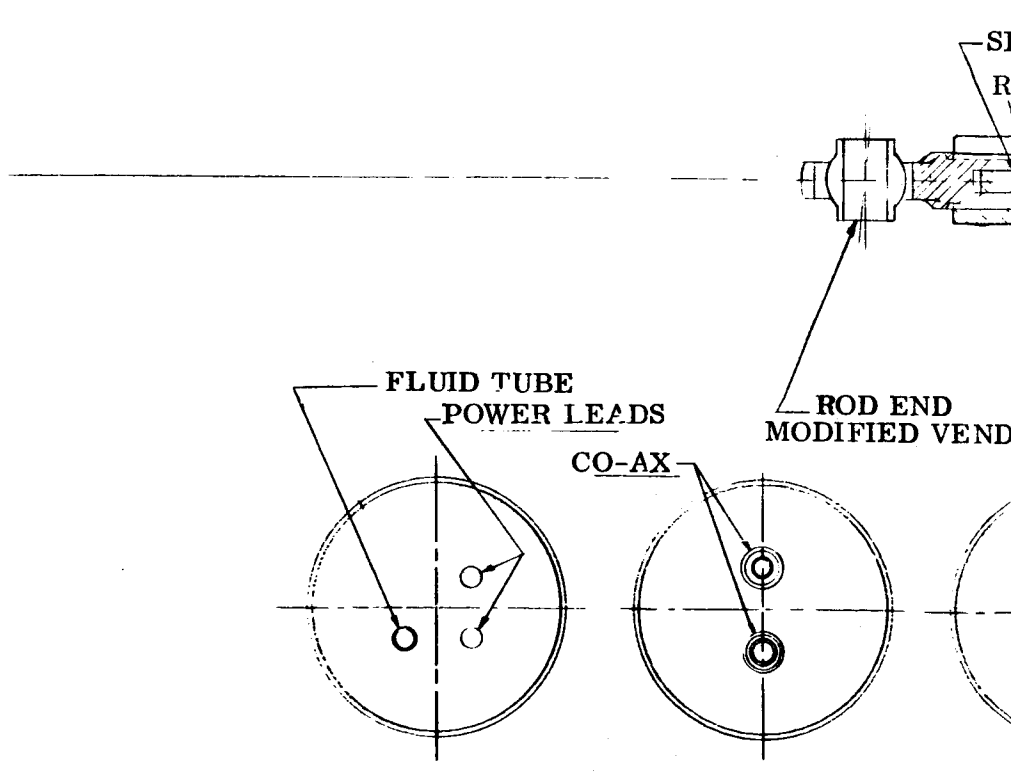
To best meet these requirements, a six-member diagonal truss with adjustable monoball end fittings is selected. Construction from extruded beryllium tubing is recommended to most efficiently provide the high column buckling strength requirements.

The problems associated with this somewhat advanced material are recognized. Discussions with beryllium suppliers have indicated that twelve-foot long extruded tubes up to four inches in diameter are available and can be supplied with little difficulty and low costs. For the present, manufacturers prefer to extrude to higher wall thicknesses, but thinner walls can be provided by a costlier chemical milling processes. Development of extrusion processes which will make available large tube diameters and thinner walls is in progress.

Material strength and stiffness characteristics of the beryllium are excellent for this application, affording a high buckling strength with a minimum diameter and weight tube, however the brittle nature of the beryllium must be considered. For a tubular extrusion, longitudinal elognation is acceptable, (about five percent), but hoop elongation can be as low as one percent. This means that the ability of the column to develop its full axial strength may be compromised in the fitting areas, where the hoop stress, induced by Poisson's effect, becomes discontinuous. Therefore, in consideration of the manufacturing, rf blockage and notch sensitive characteristics of the beryllium, a small diameter, heavier wall tube is desirable. This is in direct conflict with efficient column design. However, significant weight savings are still available.

A section approaching the limits of present state-of-the-art, 3-1/4 inch O.D. by 0.060 can be used, the six truss tubes weighing 36 lb. This can be compared to the use of aluminum tubes with maximum diameters of 4.0, 5.0 and 6.0 inches weighing 134 lb, 83 lb and 57 lb, respectively. A complete tradeoff analysis of the feed support tubes are given in the detailed stress analysis found in Paragraph 6.7.1.





TYPICAL LEADS-IN-TRUSS TUBES

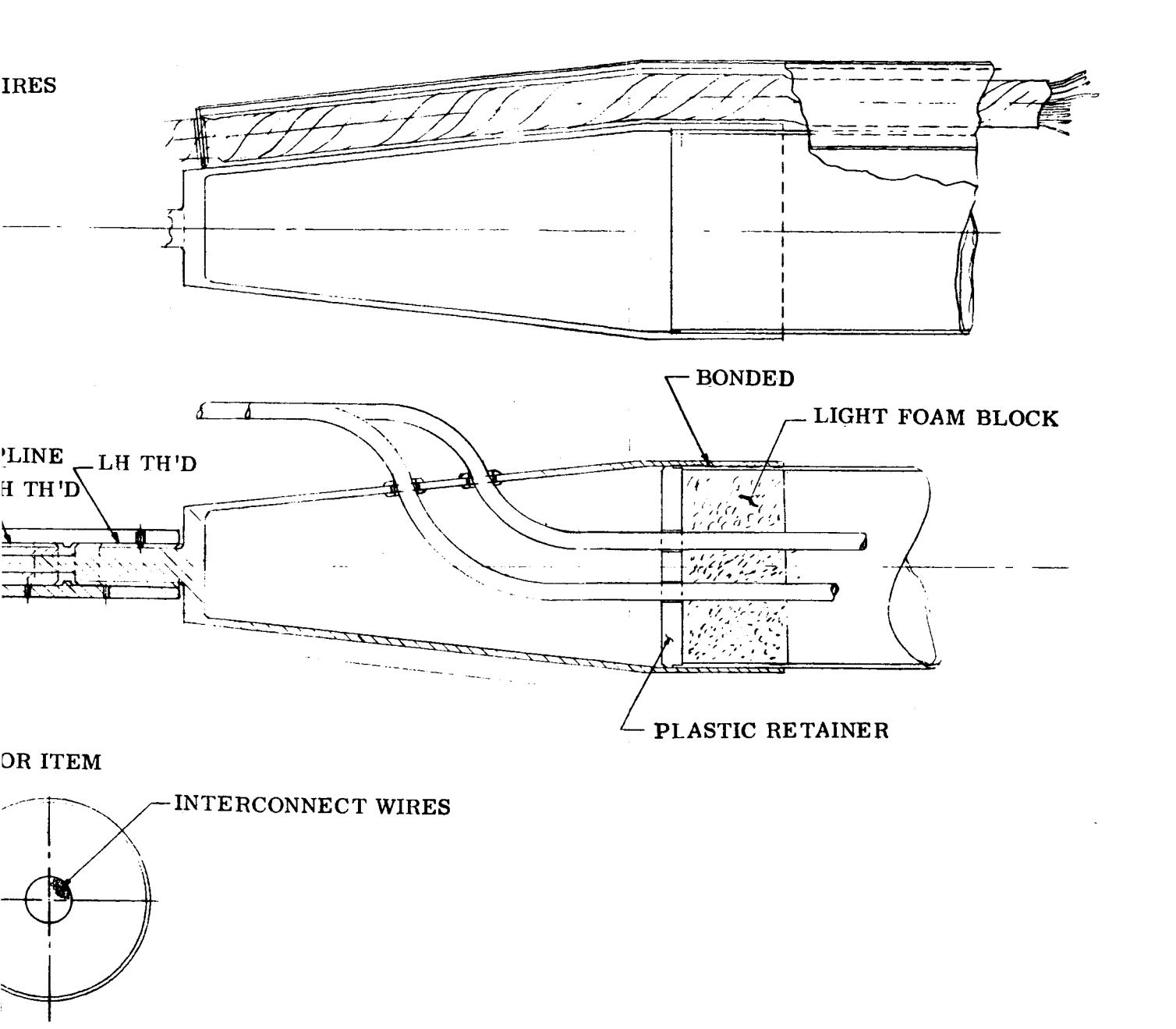


Figure 5.9-11. Truss Tube End Design Concept



The second requirement of the truss, that of providing a means for adjustment to align the spacecraft, is easily provided. Tube straightness, a contributing factor to misalignment, should be within 0.020 inch. This is based on experience with long tube runs of smaller diameter. The adjustment mechanism, illustrated in Figure 5.9-11, consists of right and left hand splines designed as an integral part of a tapered steel fitting at the AEM end of the tube. Steel has been chosen for the end fittings because of its overall thermal and inertial deflection compatibility with beryllium. Bonding methods are used to join the fittings to the beryllium tube, thereby eliminating a major problem area in joint attachments. Excellent adhesion and load transfer properties (ultimate shear strengths of 4000 psi) are available with either Narmco 3175C or Epon 934 bond, providing that adequate surface pre-treatment is done.

There are many approaches to using the truss for mounting harness and orientation control fuel tubing runs. These range from a fully integrated assembly running the harness inside the tube, shown in the referenced figure, to simple external clipping. The former has some disadvantages in accessibility for repair however, some advantage is gained by the better thermal control afforded the ammonia fuel lines, required to be kept at temperatures above -30°F, and the elimination of further rf blockage and reflectance losses. The external mounting arrangement shown in the figure approaches a good compromise. One section shows ammonia tubes packaged with the power leads to obtain some benefical heating. Of concern here, is the compatibility of beryllium, copper, aluminum fuel lines and ammonia, in the case of an ammonia line leak. The beryllium is superior to aluminum in this case, showing compatibility up to temperatures of 600°C. However, the aluminum. copper and foam, if it is used, can be damaged if attacked with a hydrous solution of ammonia propellant. The dry space environment precludes this damage and problems are anticipated. The other views show the coax intermodule harness and signal wires packaged. The harness must be packaged with cable grouping, separation, shielding, and thermal barriers employed as required for EMI control and environmental protection. The conduits can be positioned on the tubes so that the rf losses are minimized. Again, bonding is used for all attachments to the beryllium.

#### 5.9.3.3 Aft Equipment Module

The Aft Equipment Module provides support for the apogee motor, equipment bays, propellant tanks, momentum wheels, antenna and deployment devices, and solar array trusses. The module must also function to transfer the loads associated with the EVM aft to the spacecraft adapter. The structural concept involved is two conical semimonocoque segments stretching from station 81 to the separation plane at station 39.5. The skin line radii of the conical section are 39.25, 29.0, and 27.75 inches at respective stations 81, 62.5, and 39.5. In addition to the antenna interface ring at station 81, an equipment mounting ring is provided at station 62.5 and a separation ring at station 39.5.

The antenna hub is attached to an interface ring. The hub is a box section which provides the necessary stiffness for close alignment of the petal hinges during antenna deployment. It is also effectively used, as part of the integrated spacecraft structure, to react the feed support truss out of plane loads occurring during launch.

The antenna/spacecraft interface at this plane is designed to allow for a complete assembly and alignment of the EVM, the feed support truss, and the AEM prior to antenna installation. The feed support truss tubes attach to the AEM at a diameter smaller than the inside diameter of the antenna hub; this provision allowing the antenna petals and hub assembly, partially opened but still restrained radially, to be lowered over the assembled spacecraft modules. Attachment of the antenna to the spacecraft is accomplished through a radial bolt pattern, mating the inside face of the antenna hub to the antenna interface ring flange. Experience has shown that this joint is dimensionally stable, capable of being machined to close tolerance, and allows for repeatable mating and demating without upsetting original alignment. This radial attachment also precludes machining operations on the assembled AEM, such as is possible if the bolts were parallel to the spacecraft yaw axis.

A four beam internal grid between stations 81 and 62.5 (18.5 inch deep beams) supports the propellant tanks and the momentum devices. The parallel geometry is upset in one quadrant to allow for adequate shoulder room during arming and fusing of the apogee motor.

Access is facilitated through a removable panel in the outer skin. Beam web shears are delivered directly to the conical shell and beam cap loads are taken by the rings at stations 81 and 62.5. The beams have beaded webs, 0.032 inch thick of 2024 T4 aluminum alloy. Such a selection was predicated on the ability of beaded panels to provide shear stability consistent with minimum weight and ease of manufacturing considerations. Cap members are extrusions of the same alloy.

The apogee motor is supported by a conical aluminum alloy tubular truss connecting the mounting flange on the circumferential midpoint of the spherical motor casing with the equipment mounting ring at station 62.5. It is a requirement that this motor be aligned to close tolerance at the pad in order to ensure that when fired, the thrust vector coincides with the yaw axis of the vehicle. A three point mounting arrangement is optimum for alignment purposes, however, this is not compatible with the structural design requirement to efficiently distribute spacecraft loads uniformly to the launch vehicle. As a compromise between alignment and structural weight, a six point attachment is used. A small conic adapter section, with six mounting pads, is attached to the motor girth ring prior to installation, by a tensioned strap. The assembly can then be installed and aligned in the field.

The attached truss is composed of six radial members, at the motor pick-up points, and diagonals, constructed of 2 inch O.D. X 0.049 inch wall thickness 2024 T3 aluminum alloy tubing, designed to withstand both the launch environment and apogee motor firing. The ring at station 62.5 takes these truss kick loads in addition to the aforementioned beam cap loads. The separation ring at station 39.5 is a 2-1/4 inch channel of 7075 T6 aluminum alloy and is capable of transferring the total lateral shear through six bolted connections to the spacecraft adapter.

The completely removable, or hinged for access, equipment bays project from the North and South sides of the aft equipment module to provide flat thermal panels, parallel to the roll spacecraft axis, for component mounting. The forward end of the bay connects directly to the antenna interface ring. The aft end of the bay is joined to the interface ring at station 39.5 by a shear panel normal to the spacecraft axis. Side panels are radially oriented and connect the edges of the thermal panel directly with main axial

members in the conical sections. Axial component loads are sheared from the thermal panel into the side panels and thence into the main axial members of the module. Lateral component loads are sheared from the thermal panel into the antenna interface ring and to the separation ring through the bottom bay shear panel. The thermal panels are 0.06 inch thick 6061 T6 aluminum alloy based on thermal conductivity requirements. These panels require both lateral and shear stiffening which again will be utilized for component mounting bracketry. All other panels are 0.032 inch thick 2024 aluminum alloy with a minimum amount of shear stiffeners.

The exclusion of these thermal radiating panels from the primary structural load path is somewhat of an inefficiency, in that the 14 pounds of 0.060 inch sheet can be effectively used as shear structure. However, the weight involved to expand the AEM so that these panels become integral with the load paths is somewhat greater. This design features the capability of hinging the thermal panels which allows for ease of replacement of individual components without removal of the entire panel from the system harness.

Six main axial members are required in the conical module segments running continuously from the antenna interface ring to the six bolted connections at the separation plane. These members in conjunction with 0.032 inch thick beaded 2024 T4 aluminum alloy skins will tend to shear lag the three predominant feed support truss loads to a more or less uniform or elementary theory load at the six hard points of attachment at the separation plane. The axial members are tailored to accommodate this shear lag effect and therefore vary in section properties in the two segments of the concial aft equipment module.

# 5.9.3.4 Solar Array Panels And Support Trusses

Solar array panels are 5052 aluminum alloy honeycomb sandwich construction with 0.005 inch thick face sheets and 0.3 inch thick core of 1.6 lb/ft<sup>3</sup> density. Each array is supported along its longer axis by a 2-1/2 inch deep by one-inch wide closed section aluminum alloy center beam. One end of the center beam is connected to the panel fitting which is the primary structural link between the solar panel and the support truss. Additional panel restraints are provided during the boost phase to limit torsional and

bending loads on the panel, center beam, and panel fitting. These are discussed in greater detail in paragraph 5.9.4. In the absence of these restraints during deployment, each half of the panel transfers its load to the center beam by cantilever bending and thence on to the panel fitting and support truss by a similar process.

During and after deployment, the solar array is supported solely by the solar array truss. Array loads are transferred through truss bending to the antenna interface ring at the forward end of the aft equipment module. During the boost phase, the forward end of the truss is restrained by the EVM and the antenna cinching band thereby providing "simple beam" reactions for the truss when loaded in a direction normal to the solar array and "pinned-end column" truss reactions for axial loading. Lateral truss moment loads are greatly reduced through the solar panel restraints provided by the antenna deployment trusses. The limiting design condition for this member, however, is in meeting the minimum orbital frequency requirement. To accomplish this, the truss is triangular in cross section with 3/4 inch O. D. x 0.065 inch wall 6061 T6 aluminum alloy tubing forming the cap members and 3/4 inch O. D. x 0.022 inch wall tubing of the same alloy forming all diagonals and battens. This particular alloy was selected for its combination of weldability and adequate strength properties.

# 5.9.3.5 Spacecraft Adapter

It can be observed from Figure 5.9-1 that the adapter is of identical geometry to the present Centaur aft adapter. Adherence to this geometry allows for the use of existing thermal control equipment, bulkheads, and ducting, and does not require a repackaging of Centaur electronics.

The design philosophy has been to construct an extremely rigid adapter, on the basis that overall spacecraft stiffness is improved with a rigid base, while the weight thus expended will not result in a significant loss of payload in orbit capability since it is not separated from the Centaur.

The adapter transfers all spacecraft shear, bending, and axial load from the separation plane at station 39.5 to the Centaur payload mounting ring at station 0. The adapter consists of two conical semimonoque segments with the upper segment stretching from the separation plane station 39.5 to the field joint at station 16.0, with the lower segment continuing on to the payload mounting ring. The respective cone radii at stations 39.5, 16, and 0 are 27.74, 26.5 and 28 inches. The semimonocoque construction entails the use of 24 axial hat sections of 7075-T6 aluminum alloy in conjunction with a stiffened AZ31B-H24 magnesium alloy skin. This combination assures a highly effective structure with respect to stiffness and will satisfy the requirements for a reasonably uniform load distribution at the payload mounting ring. Longeron and skin gages have been tailored to achieve the above stated load redistribution design objectives.

#### 5.9.3.6 Structure Weight Summary

The spacecraft structural elements, described in this subsection, have been sized sufficiently to permit a reasonably accurate estimate of structural weight. A summary of structural weight is presented in Table 5.9-7. Adapter weight, also included in this table, has not been included as an element of the total structural weight as it will remain with the Centaur and hence is not chargeable as orbital weight.

#### 5. 9. 4 SEPARATION AND DEPLOYMENT

#### 5. 9. 4. 1 Solar Panel Stowage and Deployment

The solar panels in the recommended configuration (Figure 5.9-1) are hinged respectively from the ends of the four solar array trusses and are folded aft in their stowed position such that they are parallel to the folded antenna cylinder. The solar array trusses, hinged at the antenna hub, are restrained laterally by preloading with the antenna cinching band against stops on the EVM surface. The increased band load thus required is well within the compressive strength of the petal frames. This stowage and subsequent deployment configuration is presented as being typical of the simplest approach to the reliable deployment of the parabolic antenna and the solar arrays, while at the same time, offering the best overall structural load paths for adequate restraint of these components during the launch phase. Another advantage of this arrangement is the clearance provided for the TT&C

Table 5.9-7. Structure Weight Summary

Earth Viewing Equipment Module Structure			
	46.7 lb	(Honeycomb/Supports Only)	37.5
Upper Bulkhead	4.2	Solar Panel Latching and Deployment	9.3
Đ	4.2		
	3.6 6.1		<del>,</del> ,
Mid Bulkhead 4	4.0	Fittings (8)	0.5
Main Beams (4)	1.6		0.8
Shear Stiffeners (3)	0.6		1.5
Longerons (4)	2.1	rings and Spools (4)	2.8
	8.0		0.9
rs	2.4		0.7
Beams	11.3	Portion Chargeable to Panel Tredown)	0.9
rackets and Fittings	5.6	Slotted Fittings 0	0.8
	-	Adapter	136.0
Feed Support Trusses and Fittings (6)	51.0		4.7
		Separation Squibs (12)	0.4
Solar Array Trusses (4)	31.0		9.4
	-		1.8
Aft Equipment Module - Primary	73.0		0.0
	-	innight Disconnect	0
	1.62	Dings (4)	
rs (26)	14.4	1941 Dott com	- 6
	26.5		
Misc. Attachments 3	3.0		
Aft Equipment Module - Secondary	37.0	Misc. Hardware 3	3.2
Abogee Support Truss Tubes	4.2		
	8.3		
	18.7		
Misc. Bracketry and Hardware	8.0		
Aft Equipment Bay Thermal Panel Support	17.0		
Main Beams	?! ?;		
	1.3		
Side Panel Stiffeners	1.0		
	6. x		
pport Members	0.4		
	4		
Edge Members 33	3.0		

antenna, orientation control sensors, and nozzles which allows the operation of these components during the undeployed phase of the mission.

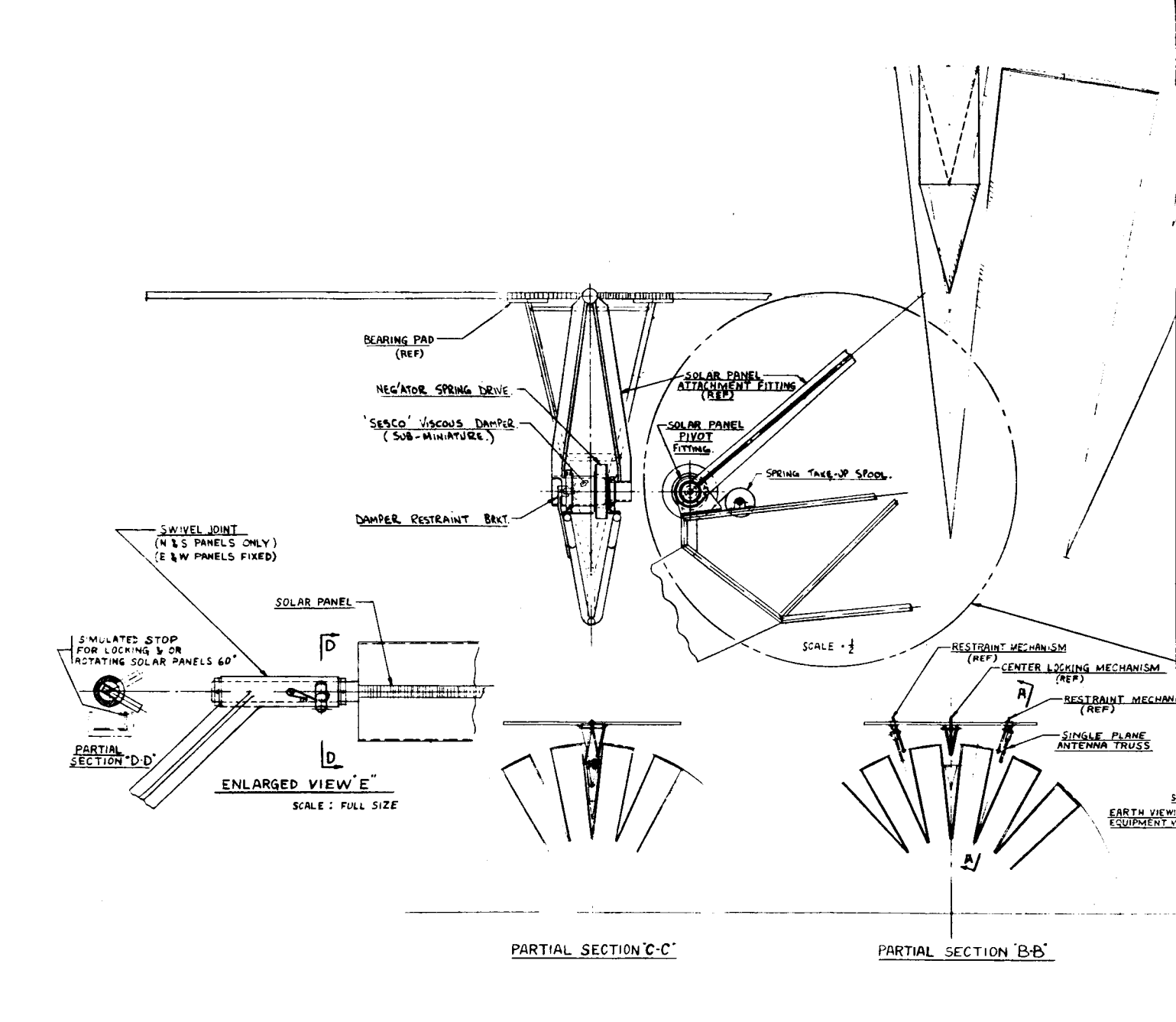
The solar panels deploy about a point near the forward end of the solar panel truss and the solar array truss extension member serves as a stop in orbit. The solar panel attachment fitting is triangular in shape with the base as the pivot axis and with a swivel joint forming the apex as shown in Figure 5.9-12. The swivel joint is required on only two panels while the other two are fixed joints. Bearing pads to stabilize the forward end of the panel during launch are built onto the solar array truss member.

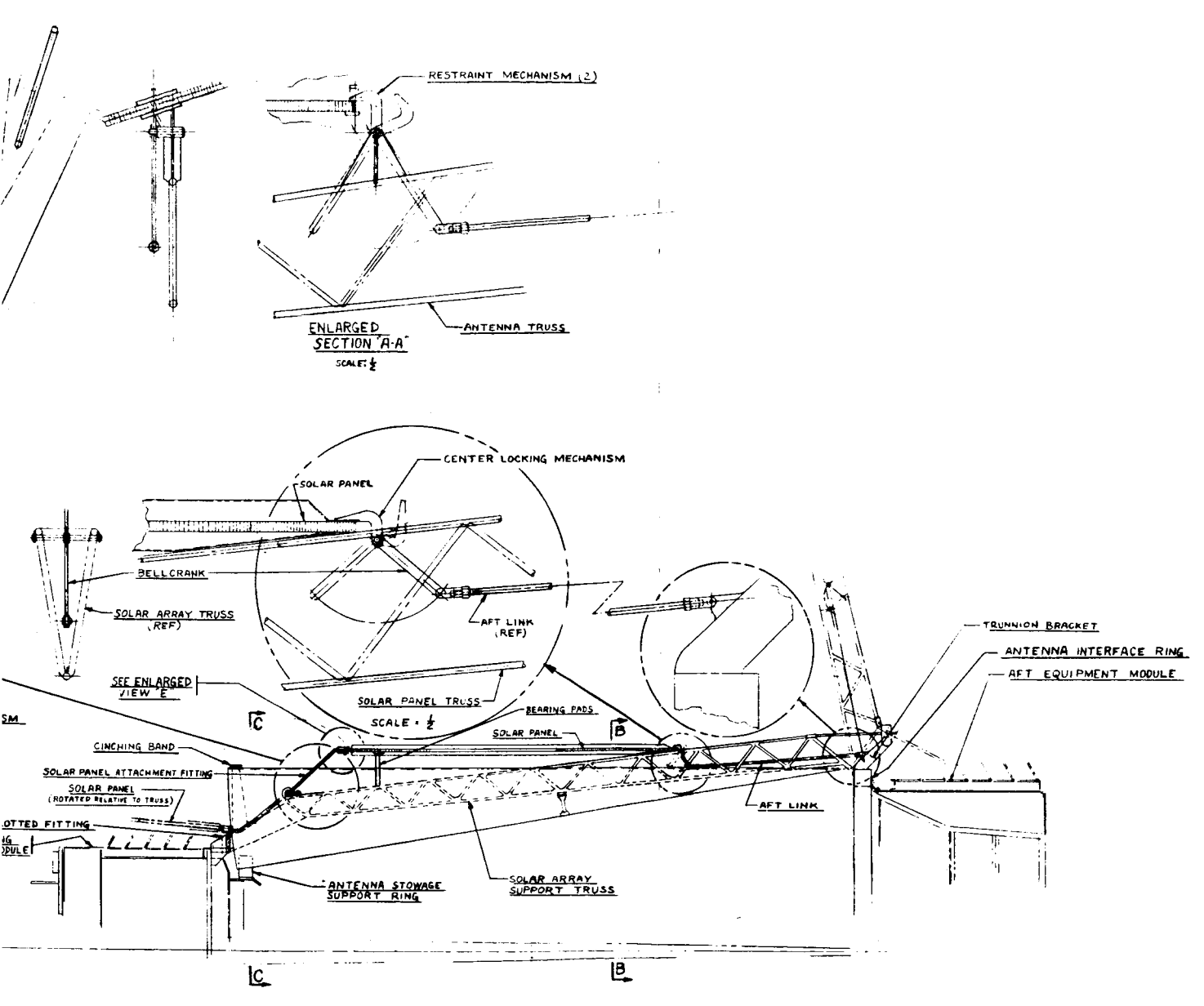
The solar array deployment motion is actuated by a constant torque Neg'ator spring motor driving each solar array shaft. The deployment rate of each panel is regulated by a miniature viscous damper also attached to the solar array shaft. This rotary damper can be adjusted to provide a desired rate which can be made slow enough such that the full deployed dynamic shock will be of no consequence structurally. Under the preload action of the spring in the extended position, a mechanical stop is not required, since a reasonable rotational torque level of 5 to 10 in.—Ib will not be exceeded by the extremely low inertia forces in space. Dynamic analysis has shown that the maximum expected closing force on the panel will be less than one inch-pound. Miniature rotary dampers are available from several manufacturers, but SESCO Model 1080–100 (or equivalent) is believed adequate for this application. The specifications for this particular SESCO model are as follows:

Damping Rate:
Friction Torque:
Max Permissable Torque:
Weight (filled):

Weight (filled): Temp. Range: Damping Fluid: 0.2 to 25 in-lb/rad/sec Approx. 1 in.-oz 100 in.-lb 3 oz -65°F to 160°F Dow Corning, DC510

This solar array drive system has the advantage of depending only on the mechanical unlock system for reliable operation, no motors or sequencing devices being necessary. Another advantage is that failure of the solar array to deploy (for any reason) does not prevent the antenna from continuing its deployment motion.





MOTE: EAST & WEST SOLAR PANEL LATCHING & PEPLOYMENT WILL BE SIMILAR TO NORTH & SOUTH PANELS EXCEPT PELETE SWIVEL JOINT ILLUSTRATED IN VIEW "E"

Figure 5.9-12. Solar Panel Latching

5.7-45

The recommended solar array unlock system is mechanically coupled to the antenna deployment motion and drive through a linkage system which operates as a 4-bar link to unlock the solar arrays during the initial antenna motion. This system is also shown in Figure 5.9-12 and consists basically of short pushrods in each of the four solar array trusses. One end of each rod is attached to the appropriate trunnion bracket on the antenna interface ring and the other end is attached to and operates the solar panel center locking mechanism. To stabilize the stowed solar panels, additional restraint mechanisms are located along the aft edge of the panel; one on each side of the center unlocking mechanism supported by the antenna trusses adjacent to the solar array truss. These restraint mechanisms are operated by links (identical to the central link) attached to the appropriate trunnion fittings adjacent to the solar array trunnion fittings. Simple bearing pads would have sufficed for the pair of restraint mechanisms except for the instability of the single plane antenna trusses to which they are attached. For this reason, "gripping" pads about 3 inches wide are utilized in lieu of simple bearing pads to stabilize the truss/ panel combination in a lateral direction, using the panel edge stiffness to react the induced moments.

As mentioned above, two of the solar panels rotate about two axes during deployment. A rotation of 174 degrees occurs on all four panels about the deployment axis, and the other rotation of 60 degrees (for N and S panels only) occurs within the swivel joint about the longitudinal axis of the panel. The panel shaft is spring loaded within the swivel joint housing such that the panel rotates to its correct orbital position during the first few degrees of deployment motion, the relative motions of the solar panel and antenna being such that no interference occurs.

To assure correct positioning at full deployed position, a protruding pin from the panel shaft engages a stop fitting on the truss extension to ensure the completion of the 60 degrees rotation.

The recommended solar array deployment and unlocking configuration shown on Figure 5.9-12 provides the following advantages:

- a. Eliminates four or more solar array deployment motors which, if used, would add to the number of key events necessary for successful deployment of the arrays.
- b. Unlocking of the solar arrays is readily accomplished through linkage.
- c. Solar arrays are "locked" in the deployed position by the Neg'ator spring force, thus eliminating additional locking mechanisms.
- d. The slow rate of solar array deployment attainable through the use of a rotary damper reduces the severity of dynamic loads at the deployment stops, thus eliminating the need for additional snubbing.
- e. Reduces the possibility of antenna "hang-up" due to failure of the solar panel deployment system.

It is emphasized that the solar array deployment scheme shown is only one example of many possible methods which could be used to deploy the panels in the recommended configuration. Many refinements of the scheme shown will also be studied in more detail in the preliminary design phase.

# 5.9.4.2 Combined Purpose Antenna Deployment

The combined purpose antenna is hinge-mounted on the earth viewing equipment module. During the launch and acquisition phase of the mission, this antenna is held in a vertical position (parallel to the vehicle center-line) by an extension of a solar panel truss. In this position the antenna is utilized for telemetry, tracking and polarization measurements. After the parabolic antenna deployment, there is no further mission requirement for the combined purpose antenna so it is spring loaded to rotate out of the field of view of the earth viewing experiments located in the equipment module. This retracting action is triggered through a linkage system by the initial motion of the parabolic antenna deployment cycle, as shown in Figure 5.9-1.

# 5.9.4.3 Spacecraft/Booster Separation System

The sequence of events for spacecraft/booster separation is initiated by a command from the Centaur programmer which fires the selected pyrotechnic device. A separation switch

at the interface activates a timer which delays spin-up for a period of 2 seconds to guarantee positive separation of the two vehicles prior to spin-up.

The recommended spacecraft separation system (shown as a detail in Figure 5.9-1) consists of six separation nuts (Hi-Shear Corp., Model SN 7321 with PC 42 Power cartridges) and six spring-loaded actuators mounted in brackets around the adapter periphery. The six spring actuators will be designed and constructed so that adjustment can be made to obtain the amount and distribution of stored energy desired. This adjustment capability provides the separation system with a method for counteracting a payload center of gravity offset in a radial direction. A preliminary analysis indicated a spring rate of 100 lb/in./spring is adequate for proper separation. Springs of 1-3/4 inches diameter X 0.25 inch wire diameter with a free length of about 6 inches and an installed length of 4 inches will meet this requirement. The maximum allowable tumble rate is 2 degrees/second, but with the aforementioned adjustment feature, it is believed that rates much lower can be attained. However, there are several other sources of inherent errors which must be considered. These error sources are divided into three classes as follows:

## a. Spring Errors

Spring rate
Initial force
Misalignment
Spring relaxation
Friction
Calibration and Installation tolerances
Temperature differential

#### b. Explosive Nut Errors

Ejection friction Ejection velocity Mass differentials

#### c. Center of Gravity Location

Spacecraft center of gravity
Centaur center of gravity
Separation Plane Nonparallelism

During the preliminary design phase of the program, the above error sources will be thoroughly studied and evaluated.

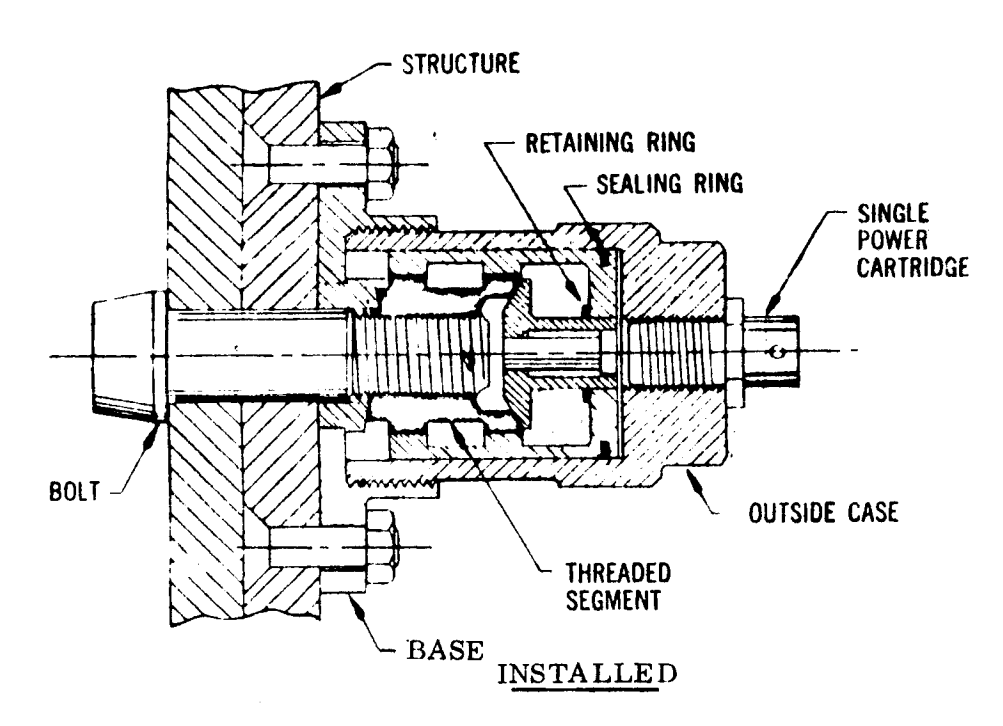
Separation nuts were chosen as the preferred design for the following reasons: (1) low shock, (2) no fragmentation or contamination, (3) easy installation, (4) high reliability with two cartridges, (5) they have been qualified on many programs, including Surveyor, to release the main retro engine, and (6) allow flexibility in design. Each power cartridge has two bridgewires, having a nominal resistance of 1.1 ohms per bridgewire. Only one bridgewire will be used in this application since electrical leakage between bridgewires has caused problems in recent programs. The unused bridgewire will be short-circuited at the connector mating with the cartridge, but will remain isolated from the cartridge case. This will minimize the possibility of stray leakage currents induced through electromagnetic radiation causing problems. Investigations will be conducted to determine the feasibility of removing one bridgewire or incorporating a different cartridge with a single bridgewire without jeopardizing the qualified design status of the assembly.

The mechanical operation of the separation nut is shown in Figure 5.9-13. It should be noted that all gases and fragments are retained by the housing. Complete release occurs less than 20 milliseconds after the firing signal is applied to the power cartridges.

As part of the operation, the bolt is positively expelled from the nut housing and a bolt catcher prevents further movement of the bolt. The electrical characteristics of the power cartridge are:

No Fire Current	1.0 amp
Minimum All Fire Current	3.5 amps
Recommended Firing Current	5.0 amps

In addition, no ignition occurs when a 5000 picofared capacitor charged to 5000 volts is discharged between the shorted contact pins and the cartridge body.



- 1. Locking piston moves forward to unlock threaded segments.
- Segments displace radially away from bolt. Separator piston locks segments in open position.
- Ejector piston thrusts bolt out of structure joint.

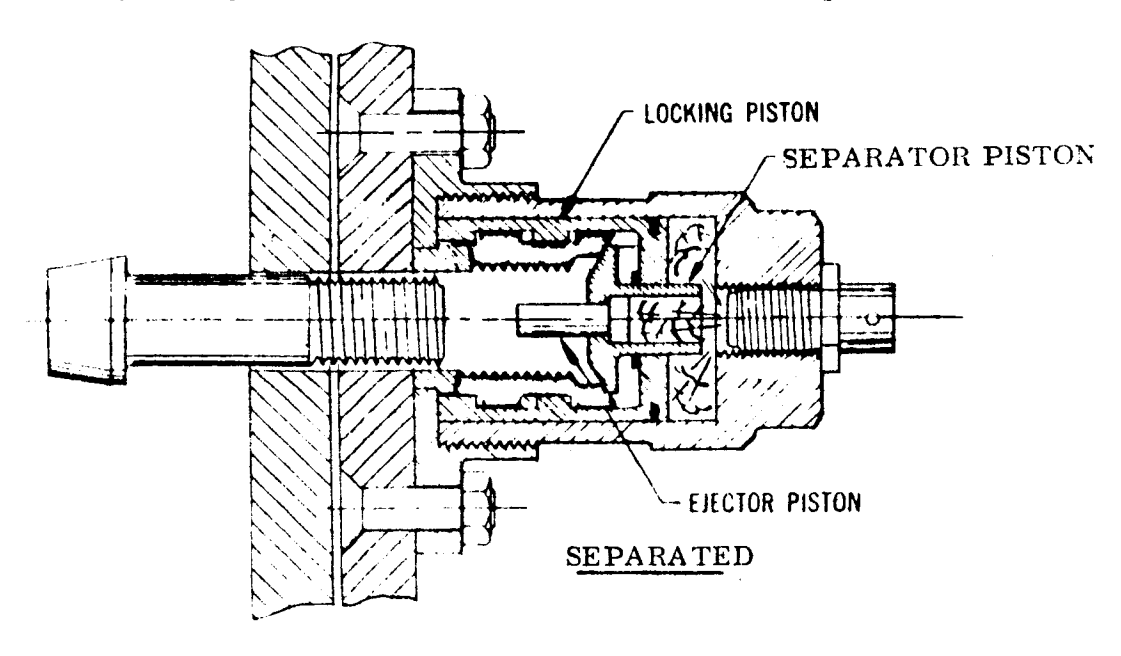


Figure 5.9-13. Separation Nut Operation

Since six nuts are required, 12 power cartridges will be fired for a total current drain of 60 amperes. This current will be supplied by the launch vehicle to avoid problems of carrying power across the adapter/spacecraft interface. The power must be available for a minimum time of 10 milliseconds. Reliability estimates based on the Surveyor program are that the assembly reliability is greater than 0.9999. Therefore, the use of six nuts, each one required for operation, is greater than 0.9994.

An alternate method of operating the separation nuts is by using an enclosed, explosive cord manifolded at each separation nut. Initiation of the cord would propagate a detonation front which would be transferred in the manifolds to a cartridge on each separation nut. This system would increase reliability and lower the dispersion time of the nut operation. The feasibility of this initiation method has been proven, but it has not been qualified for flight use.

### 5.9.5 STRUCTURAL DYNAMIC CONSIDERATIONS

### 5.9.5.1 Introduction

The dynamic characteristics of the selected configuration are influenced by three major requirements. First, the spacecraft must have adequate strength to survive the strenuous launch and boost environment without damage. Second, the fundamental frequencies of the spacecraft must be sufficiently removed from the critical booster frequencies so that the resulting launch vehicle-spacecraft system is controllable. Third, the frequencies and responses of the spacecraft in orbit must allow the spacecraft to be controlled without loss of mission capability.

Considerable analyses were conducted during this study to assure that the selected configuration satisfactorily meets these requirements.

## 5.9.5.2 Launch Configuration Behavior

It is determined by these studies that the largest lateral loading on the ATS-4 structure will be produced by a 1.5g (0 to peak) sinusoidal vibration qualification test. This test, whose levels have been presented in Section 5.9.2.1 is consistent with the NASA/GSFC

philosophy of testing new spacecraft by sinusoidally exciting the structure at its base with a shaker. Review of the flight records of four Atlas/Centaur flights indicates that the design to these shaker spec fications will be quite conservative in developing dynamic loading.

A minimum lateral launch frequency has been established at this time on the basis of discussions with the launch vehicle contractor and NASA/Lewis personnel. A value of 10 cps being set by requirements of the launch vehicle autopilot, is used for the design of the fixed-free spacecraft.

The selected configuration meets this requirement with a fundamental lateral frequency of 11cps. Analyses performed to date were based on simplified models to facilitate mass, stiffness, and configuration tradeoffs. The results of these analyses define what can be accomplished during the final design of the ATS-4 spacecraft.

In view of the split module configuration approach, the question arises as to whether response of the masses can be optimized by varying mass and stiffness distribution. In the launch configuration the spacecraft can be idealized as a two-mass system. The earth viewing equipment module is connected to the aft equipment module by means of an elastic truss and the aft module attached to the foundation by an elastic adapter. This idealization is completed by considering the folded antenna and solar array trusses as nonresonating mass items.

Figure 5.9-14 presents amplification factors at the upper mass as a function of mass and displacement amplitude ratios of the upper to the lower mass due to a base excitation at resonance and a fixed modal damping (Q=10).

It can be seen that for the two-mass system the amplification factor cannot be reduced below the value of Q represented by the damping. The limiting condition is approached when the spring connecting the two masses can be considered as rigid when compared with the base spring or when the base spring is rigid when compared with the connecting spring. Of considerable interest is the effect of mass ratio. As the upper mass becomes negligibly smaller compared with lower mass, amplification as high as 100 is possible.

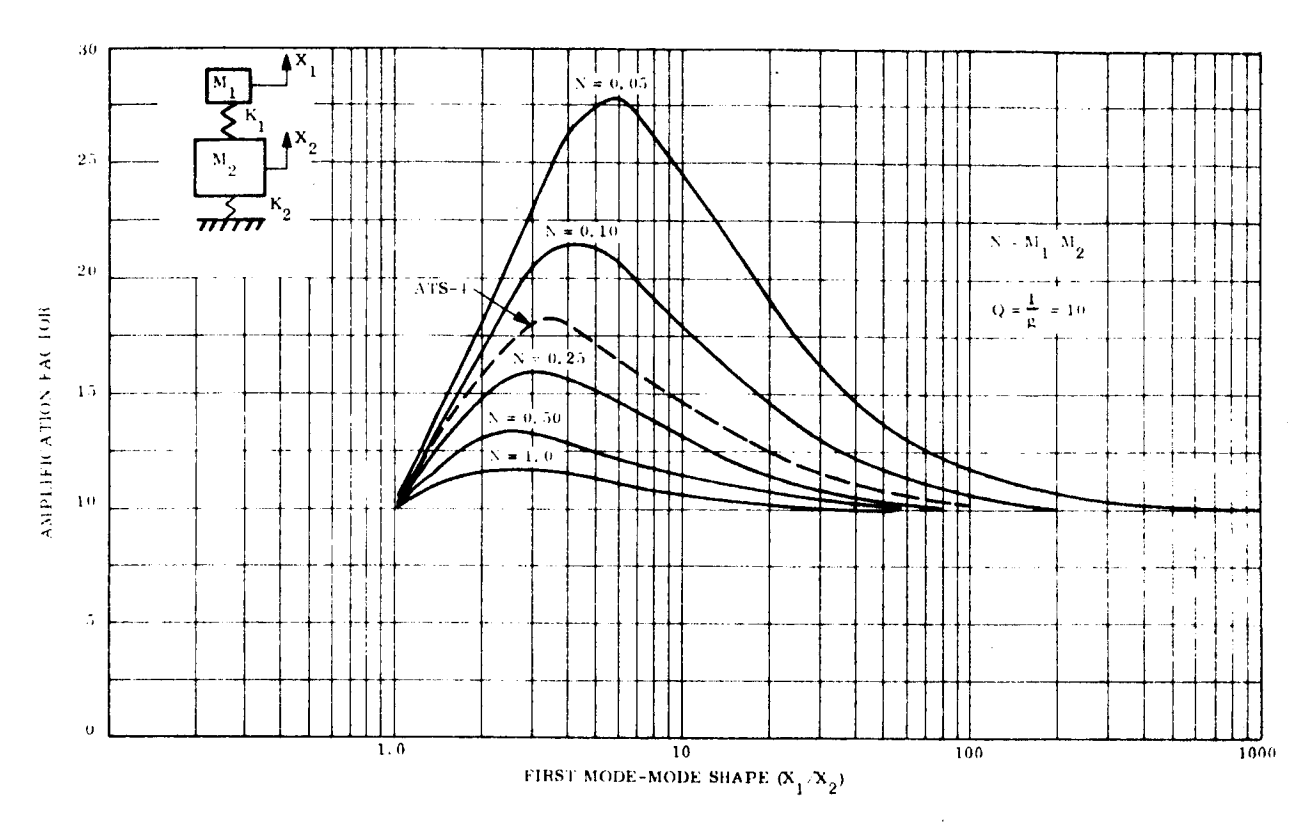


Figure 5.9-14. Response of Upper Mass (Mass 1) vs First Mode Shape

The mass idealization of the selected configuration is shown on Figure 5.9-1 as a dashed line. From this curve, it can be seen that a worst case amplification of 18.5 is possible.

From the study of the longitudinal response of the selected configuration, presented in Section 6.7.5, the fundamental mode shows the truss acting as a nearly rigid link. This finding places the mode shape close to the limiting value of 1.0 shown on Figure 5.9-14. Lateral response studies place the fundamental mode shape around 10 as shown on Figure 5.9-14. Additional increase in adapter stiffness will reduce lateral amplification but at the expense of producing a greater increase in longitudinal amplification.

Table 5.9-8 presents the acceleration response of the spacecraft to qualification level vibration test specification. These responses were calculated using 6 percent viscous damping in the fundamental modes and 5 percent viscous damping in the higher frequency modes. Damping values were selected on the basis of experience gained during the Nimbus test program. This type of structure has a nominal value of 5 percent of critical viscous damping with low frequency modes exhibiting larger values of damping.

From Table 5.9-8 it can be seen that the maximum response occurs at the earth viewing equipment module in the fundamental lateral and longitudinal modes. These responses, obtained by use of three mass models, exhibit slightly lower peak response than that indicated by the previously discussed two-mass system.

Based on two-mass considerations, the longitudinal model is nearly optimum, yielding an amplification of 10 to the earth viewing equipment module. Past experience gained in developing the Nimbus spacecraft has shown that the amplification can be further reduced by taking advantage of the energy absorbing nature of the flexible appendages of the spacecraft.

Table 5.9-8 presents the torsional response of the selected configuration. The fundamental torsion mode is 18 cps and produces an amplification of 13 at the earth viewing equipment module. The second torsional mode has a frequency of 38 cps and an amplification of 10 at the aft equipment module. These responses are transformed into lateral accelerations by utilizing the physical dimensions of the spacecraft, and are seen to be of lower magnitude than those produced by the lateral test condition.

During launch the spacecraft will be subjected to an acoustic environment. The overall sound pressure level, interior to the fairing, as given in the Atlas/Centaur Handbook is 141 decibels. At this sound pressure level structural components do not suffer static type failures. However, this environment will provide a strong constraint to components mounted in the earth viewing module and will be of considerable importance in producing response in the large area low density spacecraft appendages.

Response of components to acoustic excitation, especially those mounted in the earth viewing equipment module, must be considered when establishing component test levels.

Table 5.9-8 Response Accelerations to Base Excitation

## LATERAL

Mode	Earth V. E/M	Feed Supp't A	FT E/M
Frequency	11 cps	32 cps	72 cps
	18.0 g	9.5 g	2.1 g
2	4.3 g	12. 3 g	3.0 g
3. 0g	1.8 g	9. 9 g	4.8 g
THRUST 1.5g			
Frequency	141 cps	182 cps	50 cps
1	11.1 g	4.8 g	30.0 g
2	3.3 g	3.6 g	27.6 g
3	12.3 g	3.3 g	14.0 g
TORSION			
Frequency	38 cps	18 cps	110 cps
1	41.3 $rad/sec^2$	154.8*rad/sec $^2$	25.8 $rad/sec^2$
2	129.0 # $rad/sec^2$	15.5 $rad/sec^2$	$43.9 \text{ rad/sec}^2$
3	91.6 $rad/sec^2$	14.2 $rad/sec^2$	$69.7 \text{ rad/sec}^2$

<sup>\*</sup> Equivalent to 16.0g couple at 2

<sup>#</sup> Equivalent to 5.0 g couple at 1

#### 5.9.5.3 Effect of Structural Damping on Cone Angle

After the launch and boost phase of flight the spacecraft will be spun-up about its minor axis. It is important to determine if structural damping will produce a detrimental effect by increasing the cone angle too rapidly. To this end a study has been performed in Appendix K. The results show that using a large value (12%) for viscous damping does not produce a serious condition. It is concluded that structural damping will not constitute a serious loss of energy during the transfer maneuver.

### 5. 9. 5. 4 Orbital Configuration Behavior

The selected configuration in orbit behaves as a typical modern generation spacecraft, its dynamic behavior being characterized by low natural frequencies. The dominant structural component of the ATS-4 is the large parabolic antenna. This antenna, by virtue of its construction and support, minimizes the deleterious effect of such a large component on spacecraft behavior.

The first problem faced in an orbiting, large, flexible structural dynamic system is the possible interaction of the structural dynamic system with its orbital environment. For the selected configuration, the fundamental structural frequency is well above the periodic orbital disturbance frequency. Because these frequencies are well separated, there will be no strong interaction of the structural dynamic system with the orbital environment. Since the two systems are separable, the orbital environmental forces (e.g. solar pressure, gravity, etc.) are treated as applied loads on the spacecraft.

A second, no less important, problem is the interaction of the spacecraft structural dynamic and control systems. Again, the problem of a large, limp structure and its associated low frequency response, must be considered as responding to a periodic forcing function.

The spacecraft must be controlled within tolerances dictated by mission requirements without dangerous build-up of structural response. In order to meet the control requirements, the structural response at sensor and force generator locations must be considered as

well as critical structural response to control forces. Structural dynamic transfer functions. described in Section 6.7-3 are developed for this purpose.

Early studies, utilizing the structural transfer functions, revealed that the sensors and force generators could be considered as rigidly connected if the structural link between them has a fundamental frequency of 10 cps or higher. In addition, it was concluded that the spacecraft would be controllable, within the constraints offered by mission requirements, if major structural response frequencies are maintained at or above 2 cps. (A major structural response is defined as being greater than two orders of magnitude less than rigid body response.)

The above findings are adopted as frequency criteria for the orbital spacecraft in a conservative vein.

Control transfer function results of early configurations have been used in analog simulation of spacecraft orientation control. The values used are conservative when compared with transfer functions of the selected configuration.

The values used for velocity response are found in Table 5.9-10. The first flexible mode in the analog simulation of  $\theta_{\rm X}$  excitation was a 5.54 rad/sec mode with a numerator of  $1.04 \times 10^{-5}$ . This low frequency is produced by the lateral mode of a solar panel truss assumed unrestrained by the antenna truss link. For the analysis performed on the selected configurations this lateral support offered through the deployment link was included in the model, with a resulting minimum frequency of 12.3 rad/sec. The results listed for  $\theta_{\rm V}$  and  $\theta_{\rm Z}$  excitation also show the analog simulation to be conservative.

The rigid body transfer function numerators represent the reciprocals of the spacecraft mass moment of inertia about the excitation location. It is seen from the table that the analog values are numerically lower than the selected configuration values. This indicates that the analog simulation uses a vehicle with larger mass moments than presently exists, which is an additional measure of conservatism.

Table 5.9-9. Comparison of Analog Simulation Transfer Functions With Transfer Functions Used for Selected Configurations

	A <sub>g</sub>	5.2x10 <sup>-5</sup> 2.47x10 <sup>-6</sup> 2.48x10 <sup>-5</sup>	
nsfer Functions	δ <sub>ο</sub> ,	2, 7×10 <sup>-5</sup> 1, 29×10 <sup>-6</sup> 4, 17×10 <sup>-6</sup>	
Selected Configuration Transfer Functions	φ× ×	2.3x10 <sup>-5</sup> 3.08x10 <sup>-6</sup> 5.18x10 <sup>-6</sup>	
Selected	ω (rad/sec)	θ Excitation  0 12.3 15.7 θ Excitation y 0 15.8 16.2 θ Excitation 2 12.3 12.3 21.6	The individual transfer function for each mode has this form: $\frac{A_{\theta}}{n} = \frac{S}{S^2 + 2\zeta_{\omega} S + \omega^2} = \frac{T_i(t)}{T_i(t)}$ $\omega = \text{circular modal frequency}$ $\zeta = \text{fraction of critical viscous damping}$ $n = x y y z$ $i = \text{axis of input torque}$
St	A <sub>S</sub>	4.5x10 <sup>-5</sup> 2.4x10 <sup>-5</sup>	Aby S $\frac{A_{\beta}}{n} = S$ $\frac{S^2 + 2 \zeta_{\omega} S + \omega^2}{circular modal frequency}$ circular modal frequency fraction of critical viscous X Y Z axis of input torque
Analog Simulation Transfer Functions	Α <sub>9</sub> . <sub>v.</sub>	2.08×10 <sup>-5</sup> 1.0×10 <sup>-5</sup> 0.885×10 <sup>-5</sup>	transfer function for $\frac{A_{\theta}}{n}$ (s) = $\frac{A_{\theta}}{S^2 + \frac{1}{2}}$ (c) $\alpha = \frac{1}{2}$ (r) $\alpha = \frac{1}{2$
og Simulation T	γ× ×	2x10 <sup>-5</sup> 1.04x10 <sup>-5</sup> 0.822x10 <sup>-5</sup>	The individual
1	ش (rad/sec)	<ul> <li>θ Excitation         0         5.54         17.76         θ Excitation         √         4.94         17.38         θ Excitation         0         4.94         17.38         0         11.75</li> </ul>	

The value of damping used in the control transfer function is very important. A range of damping values of 0.6 to 0.1 percent of critical viscous damping is chosen for the analog control simulation study. These values were selected as being reasonable and attainable in the actual structure. A discussion of the problems in predicting damping values for an orbiting structure is presented in Section 6.

Damping values for the final design will be determined experimentally by testing major components of the spacecraft in a vacuum.

The orbital dynamic load environment is very gentle to the spacecraft. Major structural dynamic response is produced by the on-board stationkeeping and orientation control systems. These systems produce short-time force pulses of 0.00286 lb which may act in the spacecraft X or Y axis direction. A worse case rotational torque of 0.25 in.-lb is assumed about any of the three spacecraft axis for the condition of momentum wheel stall-out.

Table 5.9-10 presents the resonant frequencies of major structural members. Evidence of the relatively stiff antenna structure is shown by its frequency of 2.37 cps.

Substantiation of the rather high antenna frequency is provided by the study presented in Section 5.4, which uses the detailed antenna structure model developed for the thermal distortion study.

Table 5.9-11 presents a summary of significant response accelerations to unit impulsive force and moment. The worst case structural response is produced by a 1-pound translational force pulse and is 0.195 g at the antenna-solar-truss link, resulting in negligible forces for the actual applied thrusts.

Table 5.9-11 also presents antenna displacement due to unit impulsive forces and moments. The maximum antenna displacement occurs on its circumference and has the calculated magnitude of 0.028 inches produced by a 1-pound translational force pulse, or for the small thrust of 0.00286 lb, a deflection of 3.5 (10)<sup>-5</sup> inches.

Table 5.9-10. Dynamic Behavior of Deployed Selected Configuration Resonant Frequencies of Major Structural Members

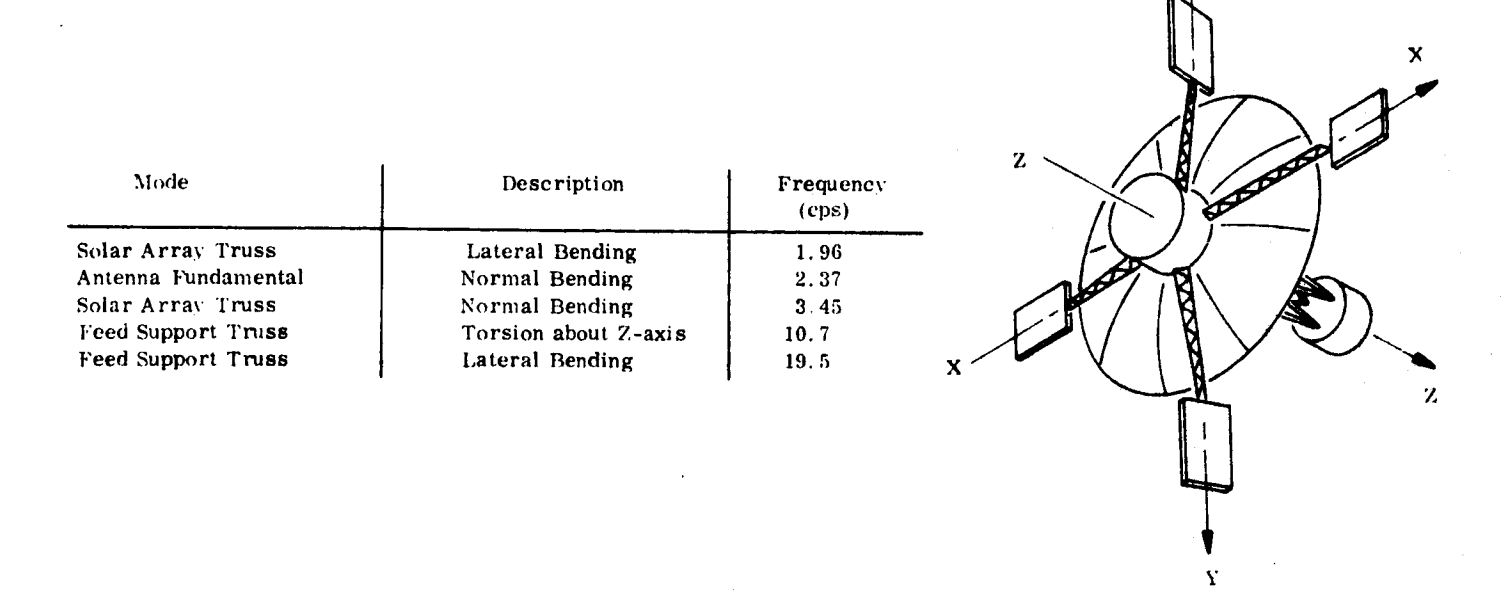


Table 5.9-11. Summary of Response Accelerations and Antenna Deployment to Unit Impulsive Force and Moment

Location	Unit Impulse	Response Acceleration (g)	Response Displacement (inches)
Antenna Rim	F <sub>x</sub>	0.008	0.028
	$\mathbf{F}_{\mathbf{Z}}^{\mathbf{A}}$	0.017	Negligible
	$M_{ m y}^{Z}$	0.0007	0.0014
Antenna Solar Panel			
Link Connection	$^{ m F}_{f x}$	0.195	0.008
	$\mathbf{F}_{\mathbf{z}}^{\mathbf{z}}$	0.089	Negligible
	$M_{Y}^{2}$	0.020	0. 0008
Solar Array Truss Tip	F.	0.057	Negligible
•	$\mathbf{F}_{\mathbf{v}}^{\mathbf{A}}$	0.036	Negligible
	$egin{array}{c} \mathbf{F_x} \\ \mathbf{F_y} \\ \mathbf{M_y} \end{array}$	0.003	Negligible

Max G load Response x Orbital Force/Moment Magnitude 0.020 x 0.25 - 0.005 g

Max displacement to orbital force input = 0.00286 (0.028) = 0.00008 inches at antenna circum.

Max displacement to orbital moment input = 0, 25 (0, 0014) = 0,00035 inches at link connection.

It can be concluded from the above results that the selected configuration is conservatively designed from a structural dynamic standpoint. No excessively large dynamic loads or displacements are indicated from this study.

#### 5.9.6 THERMAL CONTROL

## 5.9.6.1 Summary of Selected Configuration

The temperature control system selected is a combination of semipassive and passive methods. Insulated shutters are used on all but one of the external equipment mounting panels. Thermal coatings for maximum heat rejection and minimum solar heat flux absorption are used on the radiating areas of the mounting plates behind the shutters. Super insulation is used on all nonheat rejecting surfaces. This concept is applied to both the Earth Viewing Module (EVM) and the Aft Equipment Module (AEM).

The semipassive thermal control system was selected primarily due to the wide heat rejection range required. The choice of a completely passive design would have required excessive heater power in the off mode. In that case, battery charging time would have been greatly extended which would have severely limited the operational performance of the experimental rf equipment. Alternately, if less heater power were used, the resulting dynamic temperature range would have been excessive. By using shutters, the heater power to maintain temperatures is reduced by at least a factor of 4.0.

The selected configuration is not an optimum thermal design, but it is adequate and confirms feasibility. Equipment distribution between the EVM and AEM is limited by functional requirements and heat dissipation rates. The duty cycle of equipment will create a wide range of temperatures in the EVM and this condition will be contributed to by the Phased Array which has large dissipation rates. The AEM, which is larger physically than the EVM. will normally have a much lower heating rate. Panel structures, which are adequate mechanically, will produce relatively large gradients. Equipment redesign and relocation can alleviate some of these problems.

#### 5.9.6.2 Equipment Mounting

Equipment design will be of modular construction to allow maximum access, replacement, and ease of location or relocation. The modules will have the proper ratio of interface area to heat dissipation rate in order to minimize temperature differences between the modules and mounting panels. Critical modules will be provided with a thicker than normal housing material to obtain maximum contact area and minimum distortion. Components which have been identified as critical in this regard are the phased array electronics, traveling wave tubes, and the power supply regulator.

#### 5. 9. 6. 3 Semipassive Temperature Control

The semipassive control system anticipated for ATS-4 is the variable emissivity, or the shutter system. This system will be similar to that used on the Nimbus spacecraft, which has been flight proven both thermodynamically and mechanically. A typical shutter assembly, and its components, is shown in Figure 5.9-15.

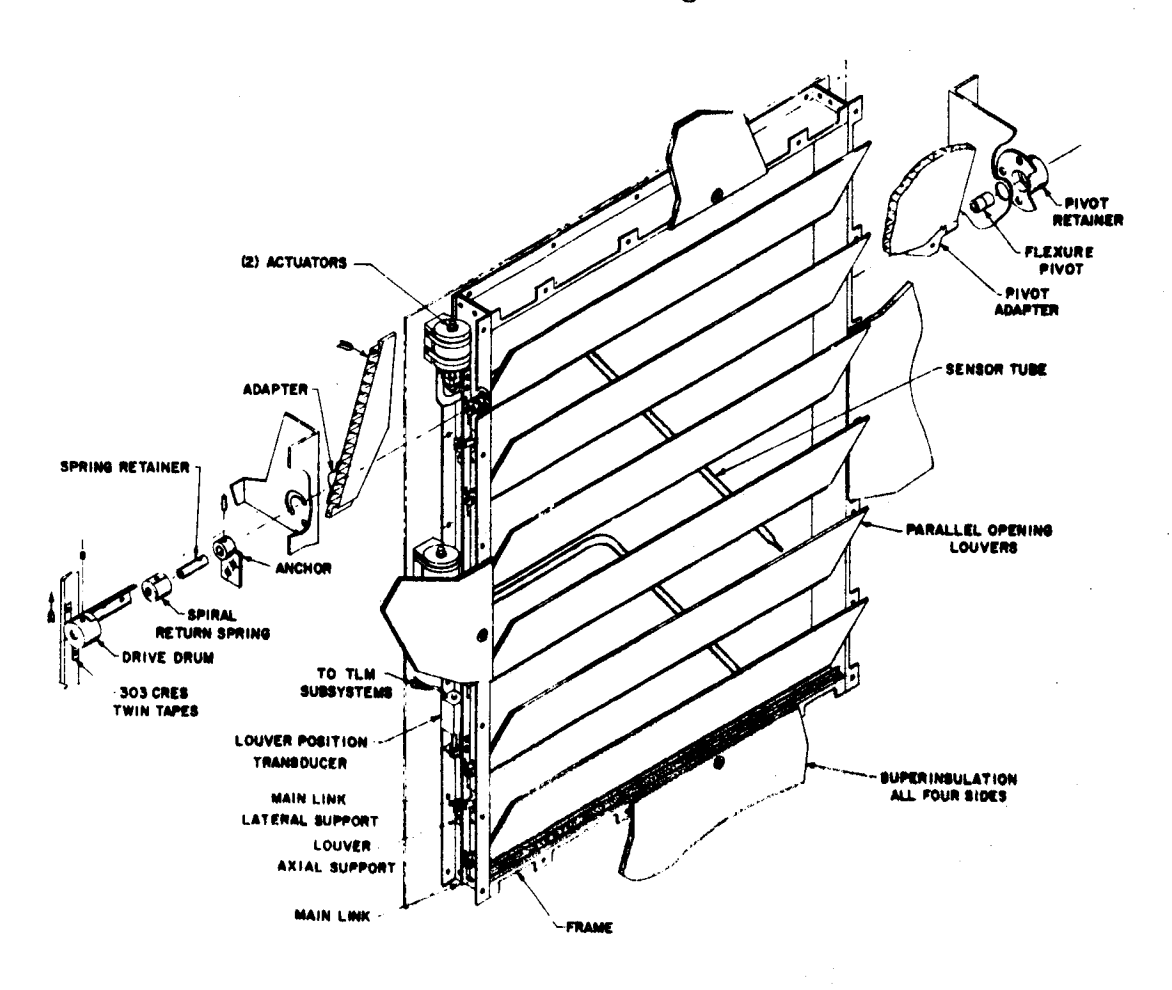


Figure 5.9-15. Typical Shutter Assembly

slight modifications will be required to adapt the Nimbus type shutter system to the ATS-4 application. Since the panels on ATS-4 are large with many components, it would be difficult to actuate the shutters on the basis of component temperature alone. Therefore, it is intended that an averaging sensor will be located on the ATS-4 radiating panels. An additional improvement over the current Nimbus design will be the incorporation of independent and redundant actuators, as opposed to the current Nimbus design which used a primary actuator which fails safe in the open position. This will improve current reliability estimates, although a failure of the Nimbus shutter system has never been detected.

The performance characteristics of the Nimbus shutter system are shown on Figure 5.9-16. It is anticipated that, due to a different mechanical arrangement with ATS-4, the maximum effective emissivity will be slightly reduced. A maximum effective emissivity of 0.65 is expected and emphasis will be placed on reducing the minimum value to at least 0.10.

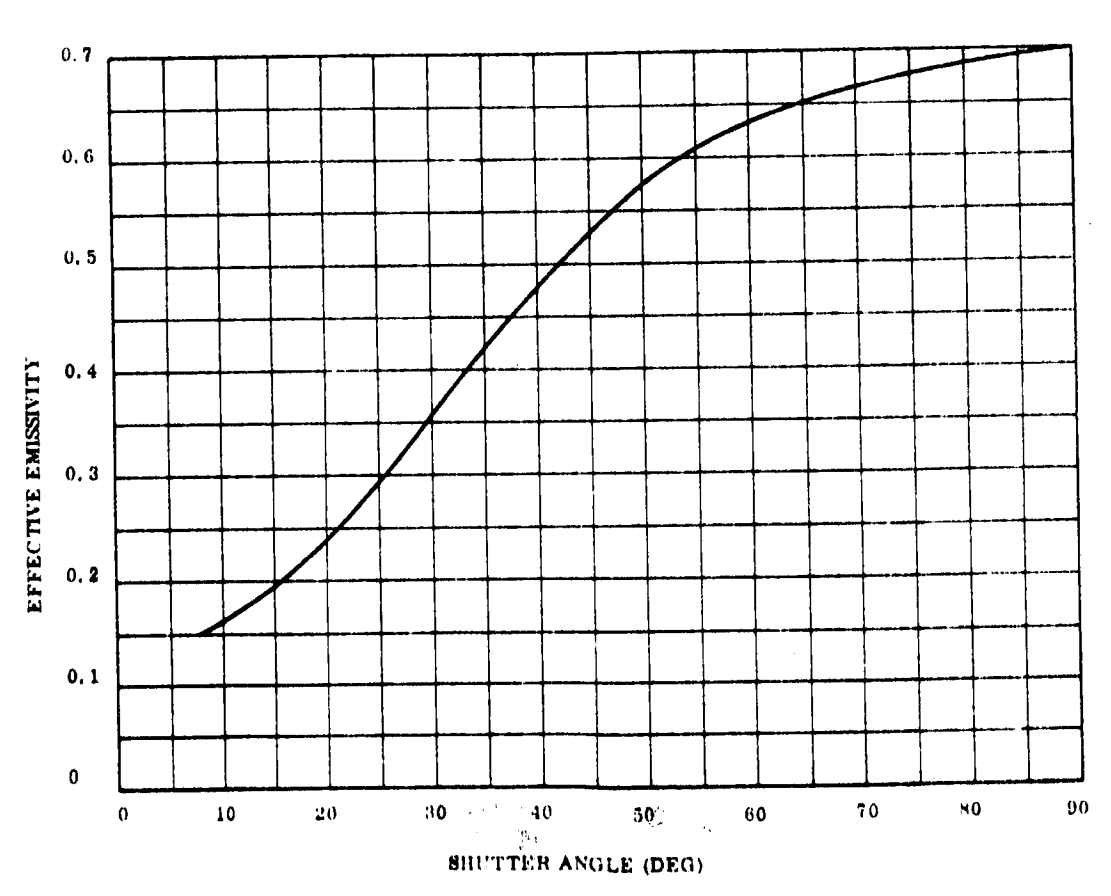


Figure 5.9-16. Typical Shutter System Characteristics

Figure 5.9-1 illustrates the application of the shutter control system concept to ATS-4. Detailed studies may indicate further modifications to this design to improve performance.

## 5.9.6.4 Passive Temperature Control

Passive temperature control techniques will be utilized extensively in the ATS-4 design.

These techniques will include the uses of optical coatings, insulation, and super insulation.

The EVM support truss and the parabolic antenna are two primary areas requiring coatings with minimum degradation. In these areas metallic finishes will be utilized to provide proper thermal control and will not degrade significantly. The coatings considered are D4D  $(\alpha/\epsilon=1.0;\ \epsilon=0.3)$ , which is an aluminized, silicon alkyd based paint which has shown high resistance to the radiation environment; vapor deposited aluminum which has been flight proven for stability; and buffed titanium. On the EVM and AEM it is anticipated that three different types of coatings will be required: (1) a high  $\alpha/\epsilon$ , low  $\epsilon$ ; (2) a low  $\alpha/\epsilon$ , high  $\epsilon$ ; and (3) a high  $\alpha/\epsilon$ , high  $\epsilon$ . These coatings are D4D, MSD-105, and any one of several black paints, respectively. These coatings have been tentatively selected for both their resistance to degradation and their optical properties. All have either been ground tested or flight proven.

Solid insulation plastic type materials will be used at hard mount load carrying points in the vehicle where it is required to impede, yet control, the flow of heat between structural members. The thermal conductivity of these materials generally lies in the range between 0.1 and 0.2 Btu/hr/ft/OF.

Super insulation will be used on all vehicle surfaces not considered prime radiators with the exception of the antennae and EVM support truss. Super insulation, with an effective conductivity of less than 2 x 10<sup>-4</sup> Btu/hr/ft/°F, is used where it is desired to minimize the heat loss or gain of a system. The top and bottom surfaces of the AEM and EVM will be so insulated, along with other locations. The insulation selected will be multilayered, embossed 1/4 mil aluminized Mylar. The exact number of layers and overall thickness will be determined by detailed studies of heat leak and heater power requirements. It is

anticipated that about 35 layers at a thickness of about 3/8 inches will be utilized. Greater allowance will be given where possible to obtain improved thermal resistance. This super insulation will be installed using plastic fasteners and techniques to minimize installation losses and edge effects. The Mylar insulation suggested can withstand temperatures up to about 300°F. If super insulation is required which can tolerate higher temperatures, embossed, aluminized 1/2 mil (minimum commercially available gage) Kapton with an upper limit of about 600°F will be utilized.

## 5.9.6.5 Configuration Thermal Analysis

The dynamic characteristics of the ATS-4 spacecraft are such that heat rejection rates can vary by a factor of 3. Using shutters, the capability to reject heat over a narrow range of temperatures can vary by a factor greater than 4. However, in order to take advantage of this characteristic, the heat dissipating components must be properly distributed. This is difficult to attain on ATS-4 due to the specific location requirements of most components. It is therefore a direct function of this nonoptimum distribution that temperatures will vary quite widely in the EVM and to a much lesser degree in the AEM.

The thermal studies for the ATS-4 selected design were devoted primarily to the following areas; Earth Viewing Module (EVM); Aft Equipment Module (AEM); Apogee Engine; Support Truss; Solar Array; and Parking Orbit Heating. The details of these studies are presented herein. Detailed studies of the parabolic antenna are presented separately in Sections 6.3.2 and 6.3.4.

## 5.9.6.5.1 Earth Viewing Module (EVM)

The EVM houses most of the experimental rf equipment and some TT&C equipment. The heat dissipation can vary from 0 to several hundred watts depending on the equipment operational duty cycle. The EVM design, with equipment mounting plate temperature limits from 30°F to 120°F, represents the most serious potential thermal problem since geometric restrictions as well as equipment heat dissipation rates and duty cycles combined

to create both high and low temperature problems. A shutter system was selected for temperature control of equipment panels.

It is preferred that only the EVM North and South facing surfaces (Panels 1 and 4), which are perpendicular to the orbit plane, be used as heat rejection surfaces. However, the phased array electronics and traveling wave tubes alone dissipate 368 watts in the operational mode. Using a maximum emissivity for a shutter surface of 0.7 and a 120°F temperature, 9.3 square feet of isothermal surface area is required to dissipate 368 watts under steady state conditions. Since this area requirement alone is greater than the total surface areas of panels 1 and 4, it is required that other EVM surface areas be utilized for heat rejection. The earth facing (bottom) surface is not available for electronic component heat rejection because the phased array and other antennae are located there. Excessive solar heating precludes the use of the top surface. Therefore, the remaining East and West facing surfaces must be utilized. These surfaces are solar illuminated during portions of the orbit and can be used only with a decrease in thermal efficiency. This decrease will be minimized by sloping these surfaces back from the leading edge by an angle of 30 degrees, and limiting the shutter rotation angle so that direct solar impingement will occur only during either a winter or summer solstice, and then only to a limited extent.

In order to assure that excessive temperatures will not normally occur, the heat rejection capacity has been locally tailored to maximum requirements. This tailoring applies primarily to the panels associated with the phased array. Since the phased array electronics and traveling wave tubes can dissipate 368 watts, the EVM geometrical restrictions will not allow this heat to be rejected from the area available on one panel without severely exceeding the 120°F maximum temperature limit. Therefore, these components have been located on separate panels, the phased array electronics on the South facing panel, and one traveling wave tube on Panels 3 and 6

All EVM components on a per panel basis is shown on Figure 5.9-17. The panels are numbered 1 through 6 counting counter clockwise starting with the North facing panel looking from the earth viewing side. The EVM component locations are further

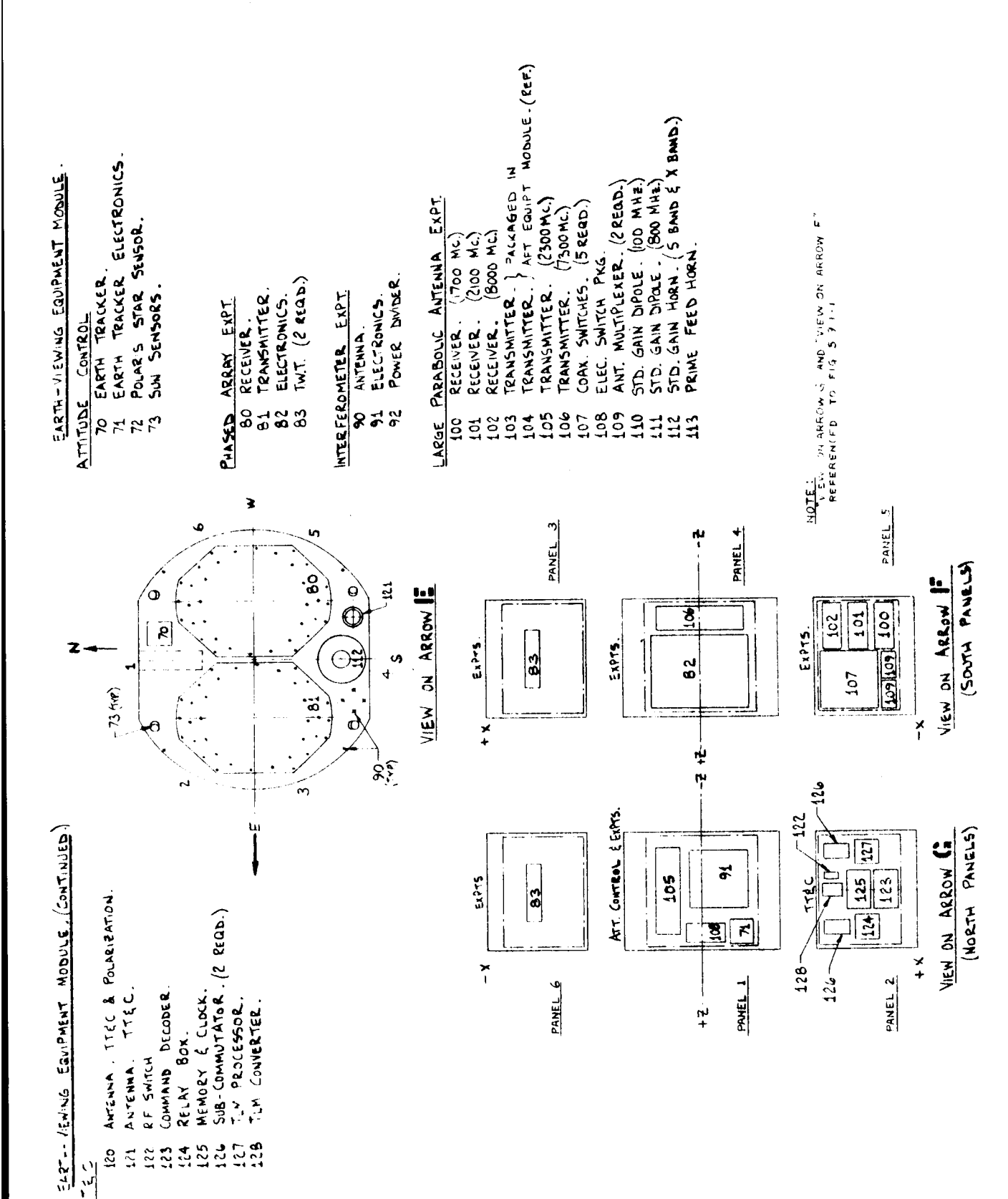


Figure 5.9-17. Earth Viewing Equipment Module

#### identified as follows:

Attitude Control and Experiments Panel No. 1 = (Components 71, 91, 105, 108) TT&C (Components 122, 123, 124, 125, 126, 127, 128) Panel No. 2 Experiments (Component 83) Panel No. 3 = Experiments (Components 82, 106) Panel No. 4 = Experiments (Components 100, 101, 102, 107, 109) Panel No. 5 Panel No. 6 Experiments (Component 83)

The phased array and other external antenna will be thermally insulated from the EVM.

Based on the equipment locations defined, a steady state heat balance with continuous equipment duty cycles was performed for all equipment panels. The resulting maximum steady state temperature distributions are shown on Figure 5.9-18. It is seen that the local hot spot temperatures slightly exceed the 120°F design limit on panels 6 and 3 (up to 148°F). while the hot spot temperatures on panel 4 significantly exceed 120°F (up to 223°F). However. this analysis was based on continuous experiment operation while, in reality, the power supply limitations will not permit continuous operation for excessively long periods of time. Therefore, an adequate thermal mass, with a resulting large thermal time constant, will provide an adequate thermal design. A transient thermal analysis was performed on panel 4 using a panel thickness of 0.125 inch and allowing 40 pounds for the phased array electronics. The resulting temperature histories are shown on Figure 5.9-19 for the nodes representing maximum and minimum panel temperatures. For an initial temperature of 70°F, the allowable operating time for components to maintain a 120°F maximum temperature limit is 1.1 hours. Since this time limit exceeds the normal maximum expected operating time, the thermal design is adequate. If the resulting structural distortions due to the defined temperature differentials in the EVM are excessive, panel thickness would have to increase and equipment may have to be redistributed.

NODE	1	2	3	4	5	_	1	2	3	4	5
	533	535	539	541	540		663	678	683	679	665
6	534	537	540	542	541	10	662	677	682	678	664
11	531	534	538	540	538	15	649	662	666	663	649
16	5 <b>2</b> 5	530	534	536	534	20	618	625	628	626	619
21	522	5 <b>2</b> 6	530	5 <b>32</b>	531	<b>2</b> 5	593	595	596	596	595
		P	ANEL	1	<u> </u>			:	PANEL	4	<b></b>
	538	536	536	534	533		531	532	534	537	540
	538	536	535	533	532		5 <b>32</b>	533	534	536	540
	536	535	534	532	531		533	533	535	536	539
	535	535	533	532	531		534	535	538	538	539
	534	534	532	531	532		535	536	539	538	559
		P	ANEL	2				P	ANEL	5	
	555	558	565	571	569		567	569	561	543	537
	558	564	582	597	583		581	596	581	550	5.38
	559	567	589	608	590		588	604	589	561	534
	556	563	581	597	583		580	595	580	555	530
	551	555	563	570	569		568	568	562	555	527
L-		P	ANEL	3		. I		]	PANEL	6	

EVM PANEL TEMPERATURE DISTRIBUTION (OR) BASED ON CONTINUOUS EXPERIMENT OPERATION

Figure 5.9-18. EVM Panel Temperature Distribution (OR) Based on Continuous Experiment Operations

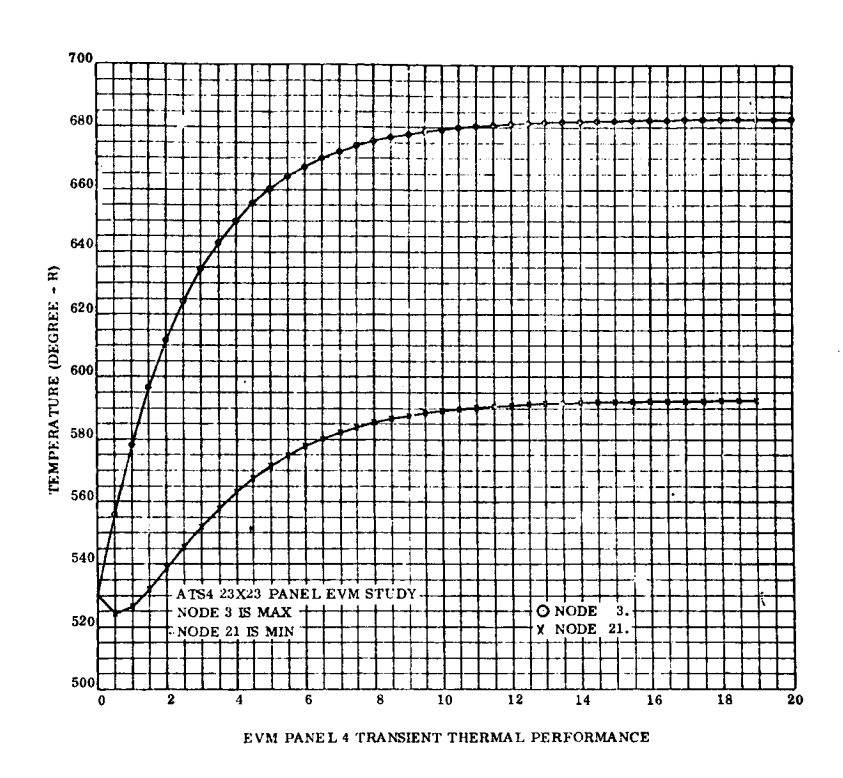


Figure 5.9-19. EVM Panel 4 Transient Thermal Performance

The duty cycle of the EVM electronics is not controlled to any minimum value. If periods of equipment nonoperation were to exceed eight hours, the EVM temperatures would fall below 30°F unless electrical heaters are utilized. These heaters can be thermostatically operated, or ground command controlled, or both. The power required to maintain minimum steady state temperatures of 30°F is 16.0, 12.6, 16.0, 0, and 12.6 watts, respectively, for panels 1 through 6. In addition, power to compensate for leakage through the upper and lower insulation blankets is 0.45 watts/ft². The heat leak through the Phased Array Antenna, which will be minimized, was not estimated since the array mounting details have not been established. This total required power can be component electrical dissipation, electrical heaters, or a combination as required. At this time, 35 watts of heater power is allocated for the EVM. Equipment operational duty cycles, when fully defined, are expected to compensate for the difference in power required. The thermal time constant for the EVM is longer than the recharge time of the batteries, so that heater power is not required during ellipse and recharge transients.

## 5.9.6.5.2 Aft Equipment Module (AEM)

The AEM, which will be controlled from 50 to 100°F, houses all of the orientation control, power, and most of the TT&C equipment. The AEM also contains the fuel tanks for the orientation control system and the apogee engine. The overall component installation is shown on Figure 5.9-20. In the AEM, the panel mounted equipment required physical

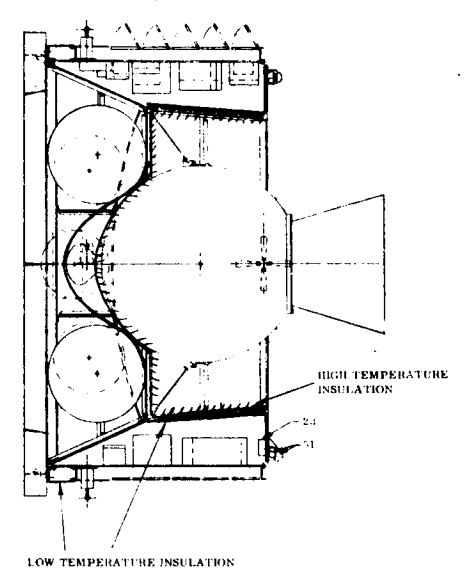
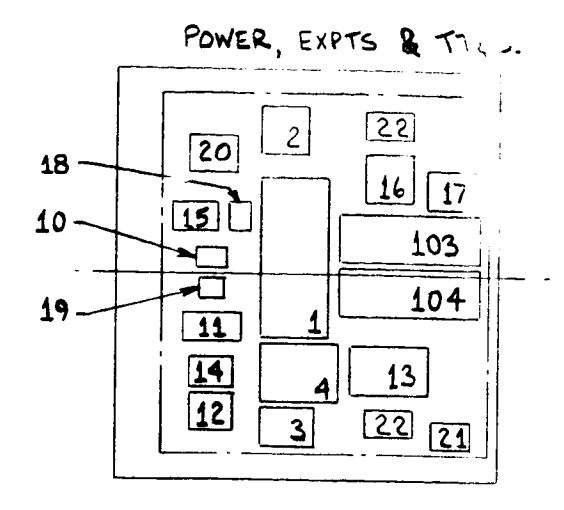


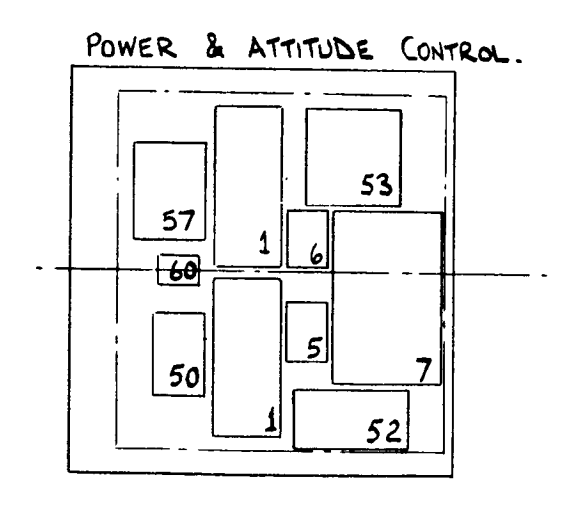
Figure 5.9-20. AFT Equipment Module Overall Component Installation

dimensions much greater than those required for heat rejection. Therefore, the preferred design, using only North and South facing surfaces for heat rejection, was utilized. A shutter system was selected for temperature control of equipment panels. The specific location of equipment on the North and South facing panels is shown on Figure 5.9-20. The North panel contains power, experiments, and TT&C components, while the South panel contains power and orientation control components. This selected configuration does not present an optimum thermal arrangement, but rather a preferred functional configuration which illustrates thermal control feasibility.

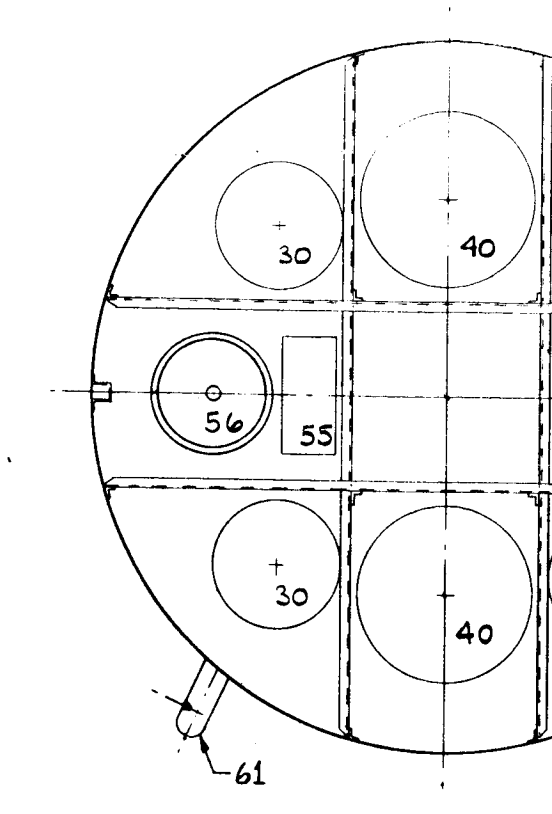
The AEM module is large with respect to the power dissipated and a narrower range of temperature control is possible with shutters than with the EVM. The use of a passive system would result in larger panel temperature gradients and dynamic temperature changes due to the range of equipment operational duty cycles. However, even with the shutter system, the variation in panel temperatures will be large since the panels



VIEW ON ARROW ()
(NORTH PANEL.)



VIEW ON ARROW 1)
(SOUTH PANEL!)



SECTION 13.

LARGE PARABO 103 TRANSMI 104 TRANSM

NOTE:
"VIEW ON ARROW C" AND "VIEW ON
ARROW D" REFERENCED TO FIG. 5.9-1

LIC ANTENNA EXPT.
TTER. (100 MC.)
TTER. (800 MC.)

13

```
AFT EQUIPMENT MODULE.
```

#### POWER

- 1 BATTERY. (3 REQD.)
- 2 BATTERY CHARGE REGULATOR (3 REGO.)
- 3 REGULATOR.
- 4 POWER CONTROL UNIT.
- 5 VOLTAGE LIMITER CONTROL ASSY.
- 6 DC/AC INVERTER.
- 7 RESISTOR ASSY.

## TTEC

- 10 DIPLEXER.
- 11 RECEIVER
- 12 RECEIVER CONVERTER.
- 13 COMMAND DECODER.
- 14 RELAY BOX.
- 15 COMMAND DETECTOR.
- 16 T.L.M. PROCESSOR.
- 17 TLM & TRACKING TRANSMITTER.
- 18 HYBRID.
- 19 R.F. SWITCH . (2 RERD.)
- 20 DECODER CONVERTER.
- 21 T.L.M. CONVERTER.
- 22 SUB-COMMUTATOR . (2 REQD.)
- 23 TTEC ANTENNA.

(CONTINUED IN EARTH-VIEWING EQUIPMENT MODULE.)

# STATION KEEPING / ATTITUDE PROPULSION.

30 PROPELLANT TANKS. (4 REQD.)

## VERNIER PROPULSION SYSTEM.

40 PROPELLANT TANKS. (2 REQD.)

## ATTITUDE CONTROL.

- 50 3 AXIS GYRO PACKAGE.
- 51 SUN SENSORS.
- 52 SENSOR SIGNAL PROCESSOR.
- 53 MOMENTUM DEVICE & JET CONTROLLER
- 54 MOMENTUM DEVICE -- PITCH.
- 55 " " -- ROLL.
- 56 " " -- YAW.
- 57 GYRO ELECTRONICS.

## INITIAL ACQUISITION.

- 60 ELECTRONICS .
- 61 SPIN-UP MOTORS (2 REQD.)

7.55.9-21

Figure 5.9-21. Aft Equipment Module

59-10

physically are large and the heat dissipating equipment is well scattered in location across the panels. These differentials could be reduced by using thicker panels with the attendant weight penalty. In addition, since the AEM is large with respect to its dissipation, heat leaks will be more of a problem and must be tightly controlled to obtain an adequate heat balance. Of major concern in the AEM are the fuel tanks for the attitude control system and the apogee engine. The thermal design will conductively couple the fuel tanks with the equipment modules but the apogee engine will be thermally isolated from the AEM.

The steady state temperature distributions on the equipment panels for maximum and minimum conditions using a high emissivity panel coating are presented on Figure 5.9-22. The large variation in temperature distributions on these panels is not desirable and can be improved. Some components dissipate more heat than the interface area and panel conductance can accept. Increasing panel thickness can reduce temperature differentials at the expense of greater weight. The solution will be to increase component size to provide larger contact area with the panels, maintain an 0.060 inch thick panel, redistribute equipment to obtain more uniform heating, and use an emissivity coating pattern on the panels (i. e., some areas with  $\epsilon = 0.9$ ; some areas with 0.30 emissivity). During the next program phase, a panel pattern will be established which will control the temperature levels and differences to desired values.

### 5.9.6.5.3 Apogee Engine

The installation of the apogee engine presents several unique thermal problems. They are:

- a. Maintain the engine above minimum temperature during the launch to inject phase of flight.
- b. Minimize the heat input to the AEM during apogee burn.
- c. Minimize the heat leak to the apogee engine during orbital flight.

These requirements are contradictory since the thermal resistance requirements between the AEM and the engine are different in (a) from those in (b) and (c).

For condition (a), worst case calculations have been made. Considering only the nozzle area of the TE-364-3 engine whose diameter is 25 inches and assuming an emissivity of 1.0, the heat loss has been calculated. For an initial temperature of  $70^{\circ}$ F, the heat loss is 460 Btu/hr. The thermal mass of the engine is about 1580 pounds and the heat capacitance between  $20^{\circ}$ F and  $70^{\circ}$ F is calculated to be 15,800 Btu. With a constant heat loss of 460 Btu/hr, 34 hours would be required to reduce the average temperature to  $20^{\circ}$ F. Since approximately 16 hours is the maximum expected duration between shroud separation and apogee burn, minimum temperatures should be maintained passively. For maximum temperatures, considering solar heating directly into the nozzle, 1500 Btu/hr would be added, neglecting losses. An average temperature rise of  $5^{\circ}$ F/hr would result with a maximum temperature rise of less than  $30^{\circ}$ F. Therefore, apogee engine temperatures will be maintained passively during the transfer orbit.

For case (b) another potential problem arises. The temperature versus time profile shown on Figure 5.9-6 is a significant source of heat for the AEM. Although the burning time is only 48 seconds, higher external temperatures occur later due to thermal lag. Heat can enter the AEM by conduction and radiation. The total heat incident from radiation on the external insulation will vary, but the maximum temperature of the external surface will approach the source (engine) temperature as a maximum. If a temperature of  $700^{\circ}$ F is assumed constant for the external surface of the insulation for a period of 560 seconds (twice the time shown on Figure 5.9-6), the heat input to the AEM would be 2.0 Btu/hr/ft<sup>2</sup>. Even if this heat leak rate was low by a factor of 10, the short duration of the heat input would not cause any significant temperature rise. The conduction interface presents another consideration. Temperature difference between the engine and structure can be as high as  $630^{\circ}$ F. The thermal isolation required to minimize heat conducted into the AEM will be a function of the sum of the thermal masses in the conductive path between the AEM and the apogee engine. If a continuous temperature difference of  $430^{\circ}$ F ( $500^{\circ}$ F -  $70^{\circ}$ F) is assumed, then, for an overall conductance of 1.0 Btu/hr/°F, 430 Btu/hr will be transferred into the

AEM. The duration of the high temperature will be relatively short, less than 10 minutes, so only 72 Btu would enter the AEM. If a heat capacitance of 20 Btu/°F is assumed for the local structure and the equipment near the apogee engine, then the temperature rise would only be about 4.0°F. If the conductance is actually 10.0 rather than 1.0, then the temperature rise would be 40°F, which is not excessive for short time periods. Since this evaluation does not include any other heat losses or additional thermal mass, these estimates are considered conservative, and it is concluded that the design can preclude excessive AEM equipment temperatures resulting from apogee engine firing.

Maximum isolation will be provided to minimize heat leaks from the AEM to the engine during orbital flight. During the next program phase detail studies will determine if heater power is required to compensate for these heat losses.

### 5.9.6.5.4 Support Truss

The support truss connecting the AEM and EVM has two restricting thermal limitations:

- a. Truss member differential temperatures must be kept low to minimize distortion of the structure and consequent rf distortion.
- b. Truss temperatures must not fall below -30°F since attitude control gas lines are supported by one of these tubes.

A preliminary design was evaluated using the outermost struts. The struts used in the analysis were beryllium tubes, 4.0 inches in outside diameter with a wall thickness of 0.075 inches. These struts are slightly larger than those chosen in the final design. The struts were divided into 10 nodes each and the solar flux profiles and shadowing were evaluated. The truss nodal designation is shown on Figure 5.9-23. The strut temperatures were evaluated for three  $\alpha/\epsilon$  values; 1.0, 2.0, and 3.0. The maximum, minimum, and average temperatures for struts 1 and 2 are presented in Figures 5.9-24, 5.9-25, 5.9-26, 5.9-27, 5.9-28, and 5.9-29 for  $\alpha/\epsilon$  values of 1.0, 2.0, and 3.0, respectively. Based on the results shown, an  $\alpha/\epsilon$  coating of 2.0 was selected for the preferred design. This value provides both acceptable distortion and adequate temperatures for the orientation control lines.

		MIN	<u>IIMUM</u>	COND	ITION		
525,	535	549	<b>53</b> 5	495	471	459	452
525	545	527	511	485	469	458	452
518	5 <b>2</b> 0	516	503	484	468	458	453
512	513	513	503	484	470	460	455
516	518	518	509	490	474	463	458
530	534	535	5 <b>2</b> 5	501	481	467	461
541	550	565	555	518	491	473	465
556	574	621	610	538	499	477	467

	<del>,</del>	MA	XIMU	M CON	DITION	1	<del>,</del>
535	546	559	547	506	483	470	465
534	556	538	522	499	481	469	465
527	541	527	514	496	480	469	466
521	534	524	514	496	483	468	465
520	523	524	512	497	483	4.2	467
533	537	540	531	509	490	476	470
552	561	573	571	525	504	487	475
564	581	633	622	542	511	490	480

AEM NORTH PANEL TEMPERATURE DISTRIBUTION (OR)

-		MII	NIMUM	COND	ITION	<u>*                                      </u>	
<b>52</b> 5	526	<b>52</b> 5	521	516	514	509	500
536	539	530	524	519	517	511	501
538	542	532	526	523	518	510	503
529	532	531	528	526	518	510	505
<b>52</b> 5	530	532	531	527	522	517	513
529	543	537	537	537	537	533	528
530	542	539	544	553	564	562	549
530	532	536	549	571	593	592	569

\*DOES NOT INCLUDE HEAT FROM RESISTOR ASSEMBLY

1AXII	MUM C	ONDIT	TON (5	OWAT	TSIN	RESIST	OR A
5 <b>2</b> 5	526	5 <b>2</b> 5	522	521	519	512	503
536	539	530	5 <b>2</b> 5	521	5 <b>22</b>	519	509
538	542	532	5 <b>2</b> 8	531	528	523	515
529	53 <b>2</b>	534	538	543	535	527	523
5 <b>2</b> 5	530	533	533	532	544	539	535
529	543	544	556	563	562	558	553
530	542	541	551	557	568	580	569
530	532	538	552	576	595	595	574
	L		<u> </u>		·	<del></del>	

AEM SOUTH PANEL TEMPERATURE DISTRIBUTION (OR)

Figure 5.9-22. AEM Panel Temperature Distribution (OR)

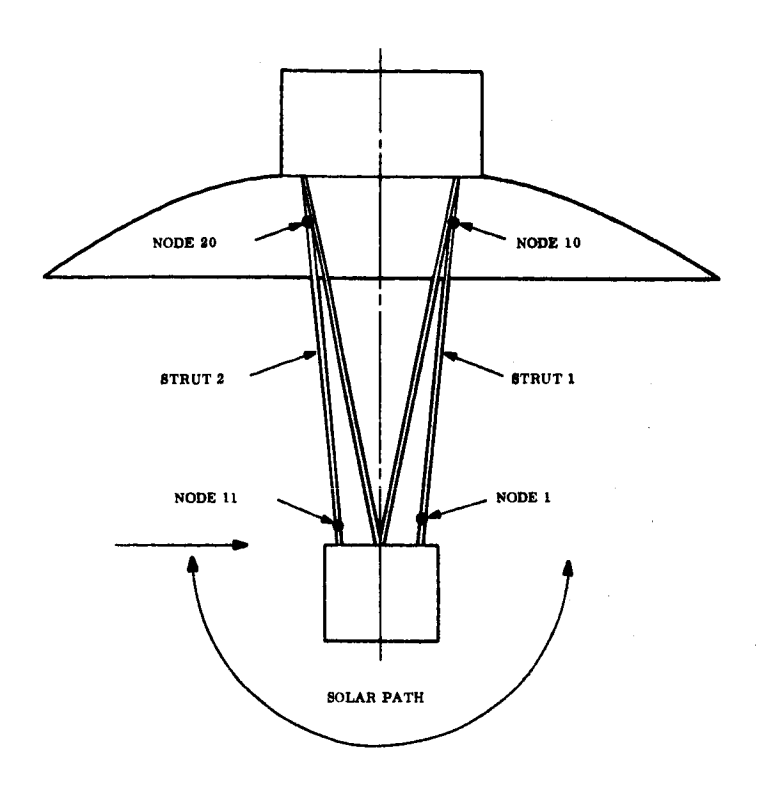


Figure 5.9-23. Truss Nodal Designation

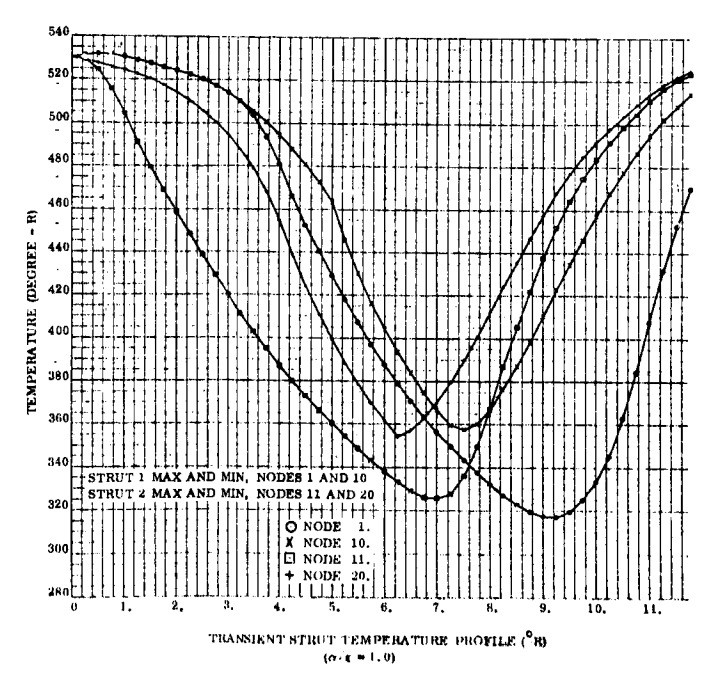


Figure 5.9-24. Transient Strut Temperature Profile ( ${}^{0}$ R),  $\alpha/\epsilon = 1$ 

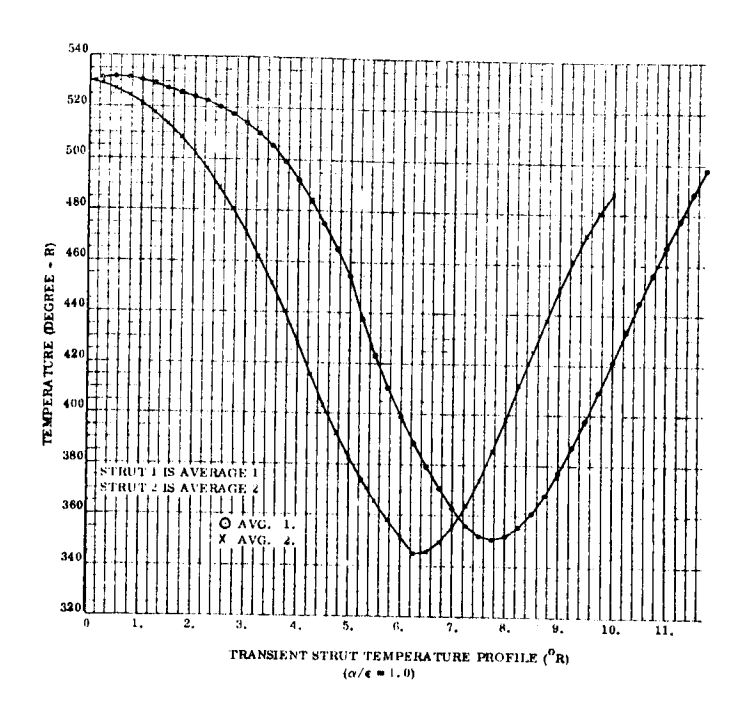


Figure 5.9-25. Transient Strut Temperature Profile (OR)  $\alpha/\epsilon = 1$ 

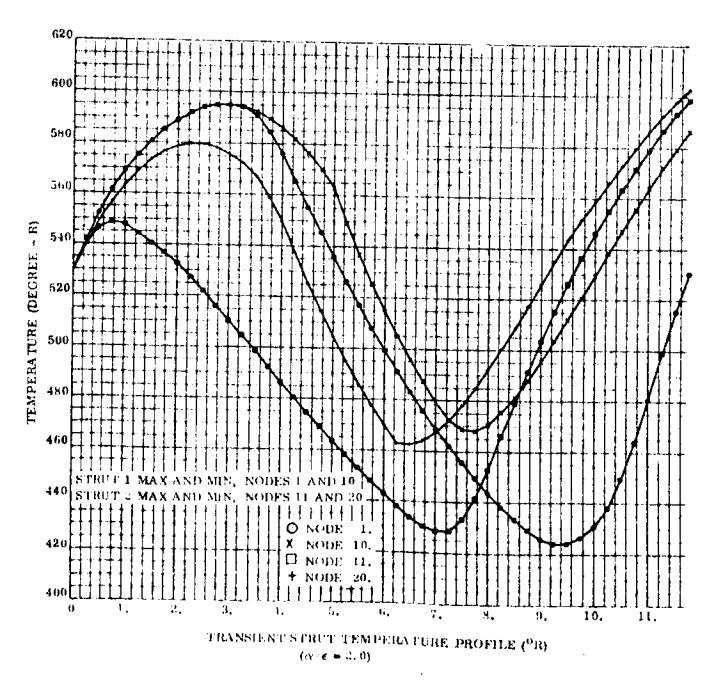


Figure 5.9-26. Transient Strut Temperature Profile ( ${}^{\mathbf{O}}\mathbf{R}$ ),  $\alpha/\epsilon=2$ 

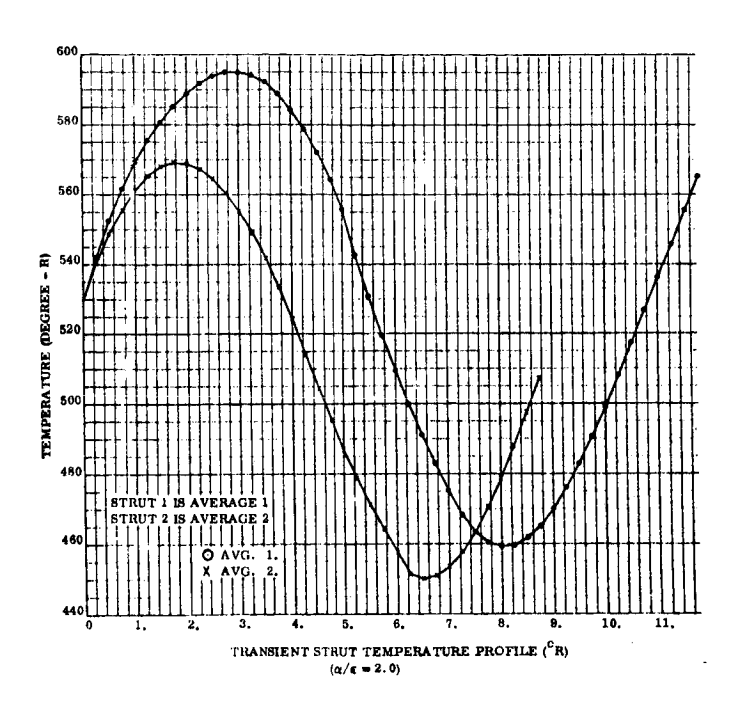


Figure 5.9-27. Transient Strut Temperature Profile (OR),  $\alpha/\epsilon = 2$ 

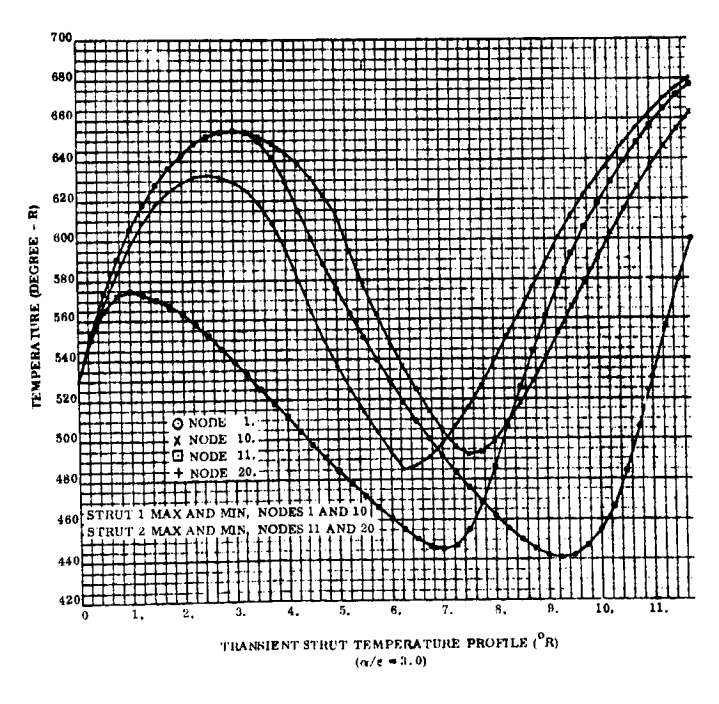


Figure 5.9-28. Transient Strut Temperature Profile ( ${}^{\circ}$ R),  $\alpha/\epsilon=3$ 

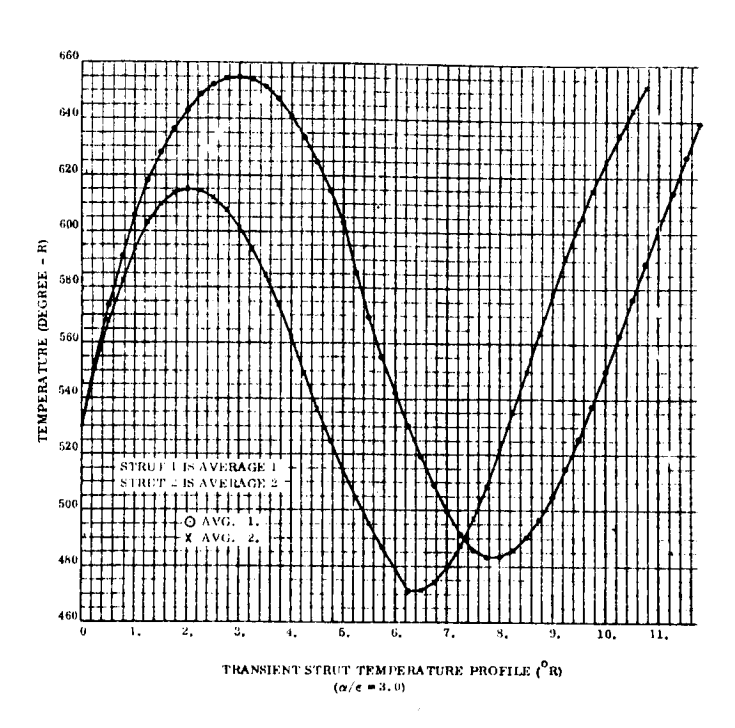


Figure 5. 9-29. Transient Strut Temperature Profile ( ${}^{0}$ R),  $\alpha/\epsilon=3$ 

#### 5.9.6.5.5 Solar Array

A preliminary thermal analysis was performed to support the evaluation and sizing of the solar array paddles for various proposed ATS-4 spacecraft configurations. Maximum heating of the array was found to occur during the equinox time of year. This is attributed to the fact that, for an equatorial orbit, the solar arrays will be oriented perpendicular to the sun vector at a given point in the orbit. The maximum level of incident solar flux was determined to be  $458 \, \text{Btu/hr/ft}^2$ .

The equinox also involves a total solar eclipse of the spacecraft for a time period of approximately 70 minutes. Accordingly, array temperatures at the end of the eclipse period represent a minimum level.

The distribution of incident solar flux with time is given in Figure 5.9-30 for surfaces with normal vectors along the  $\pm$  X and  $\pm$  Z axes. These data correspond to the equinox time of year and therefore represent the maximum solar flux profile. For purposes of solar array sizing, the minimum solar flux was also calculated. This heating profile occurs during the summer solstice; data are presented in Figure 5.9-31. The flux levels for paddle configurations inclined to the X and Z axes may be determined by considering the appropriate component as referenced to the data of Figures 5.9-30 and 5.9-31. Figure 5.9-32 provides an indication of the maximum flux history for paddles inclined 60 degrees to the X axis. To keep the work on a general level, shadowing of the solar paddles by the body of the spacecraft and/or by the parabolic reflector was not considered. For the given configurations under consideration, the effect of shadowing on the temperatures of the solar array paddles is anticipated to be of no special significance.

Figure 5.9-33 is a plot of solar paddle temperature as a function of time in orbit during the equinox. These data apply directly to the antenna deployment truss mounted 4-paddle concept. The maximum temperature is approximately +120°F and the minimum temperature during the illuminated portion of the orbit is -150°F. The minimum temperature at the end of solar eclipse is -190°F. These data are applicable to a solar array paddle weighing approximately 1.0 lb/ft<sup>2</sup>. For paddle weights of 0.75 lb/ft and 0.5 lb/ft, the minimum temperature at the end of eclipse is -208°F and -239°F respectively. Assumptions used in the performance of the calculations are as follows:

Solar cells, with blue filter,  $\alpha_{S} = 0.7$ ;  $\epsilon_{H} = 0.79$ 

Packing factor: 0.85

Net solar cell efficiency: 6%

Solar paddles provided with alzak backing:  $\sigma_S = 0.2$ ;  $\epsilon_H = 0.74$ 

Solar cells on both paddle faces

External surfaces of main spacecraft body and parabolic antenna highly reflective for IR

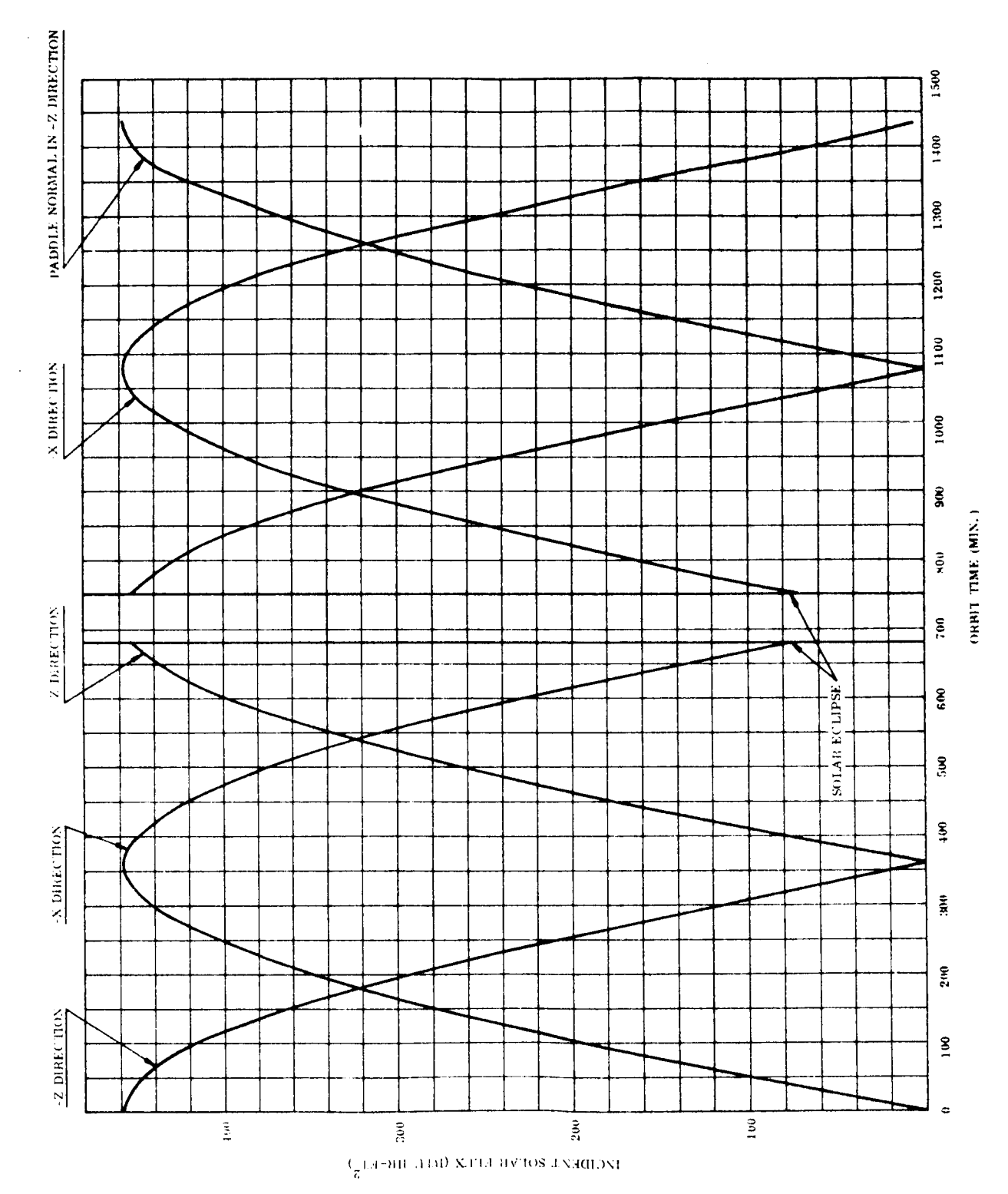


Figure 5.9-30. Maximum Solar Flux Distribution During Equinox

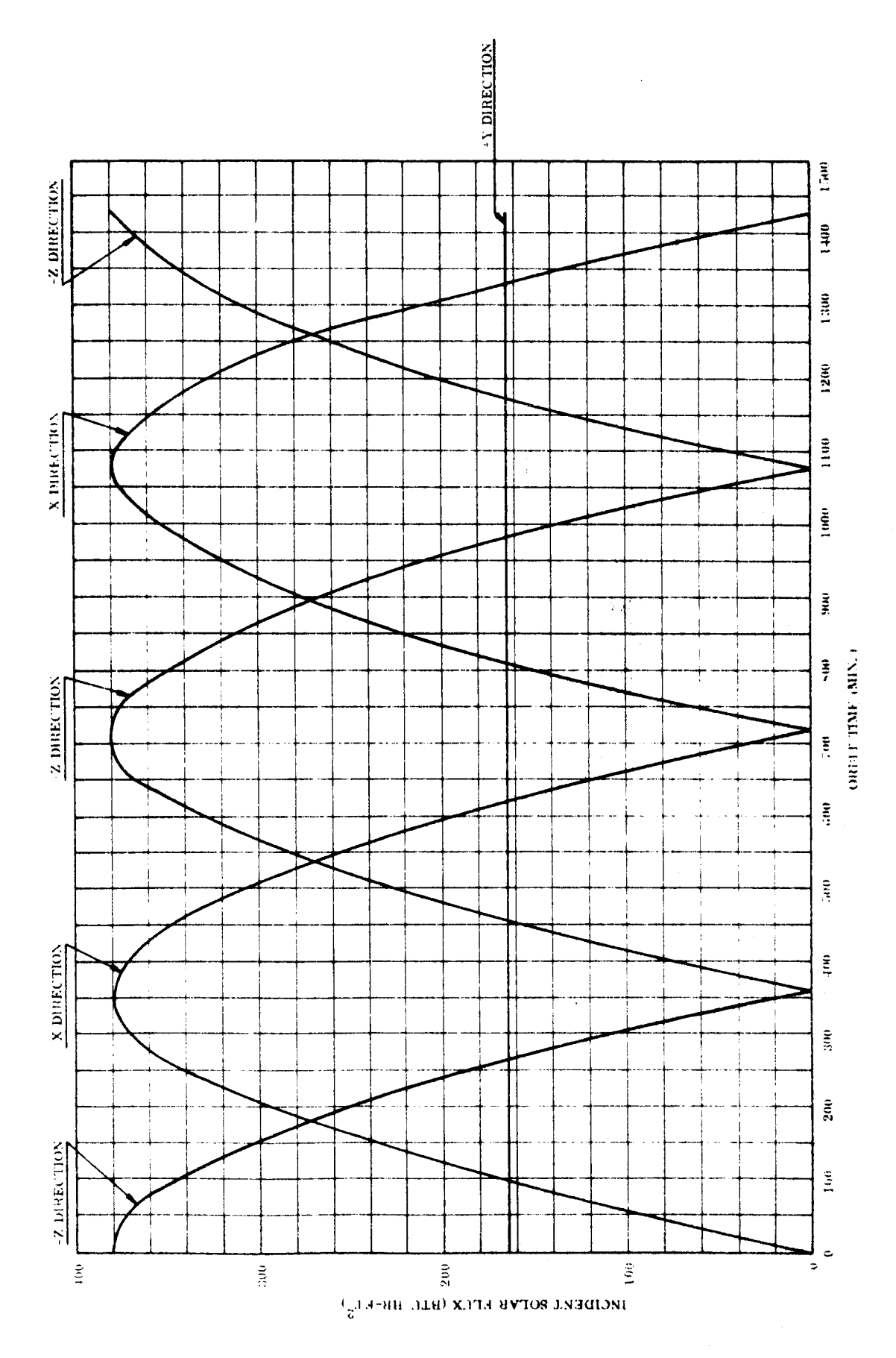


Figure 5.9-31. Maximum Solar Flux Distribution During Summer Solstice

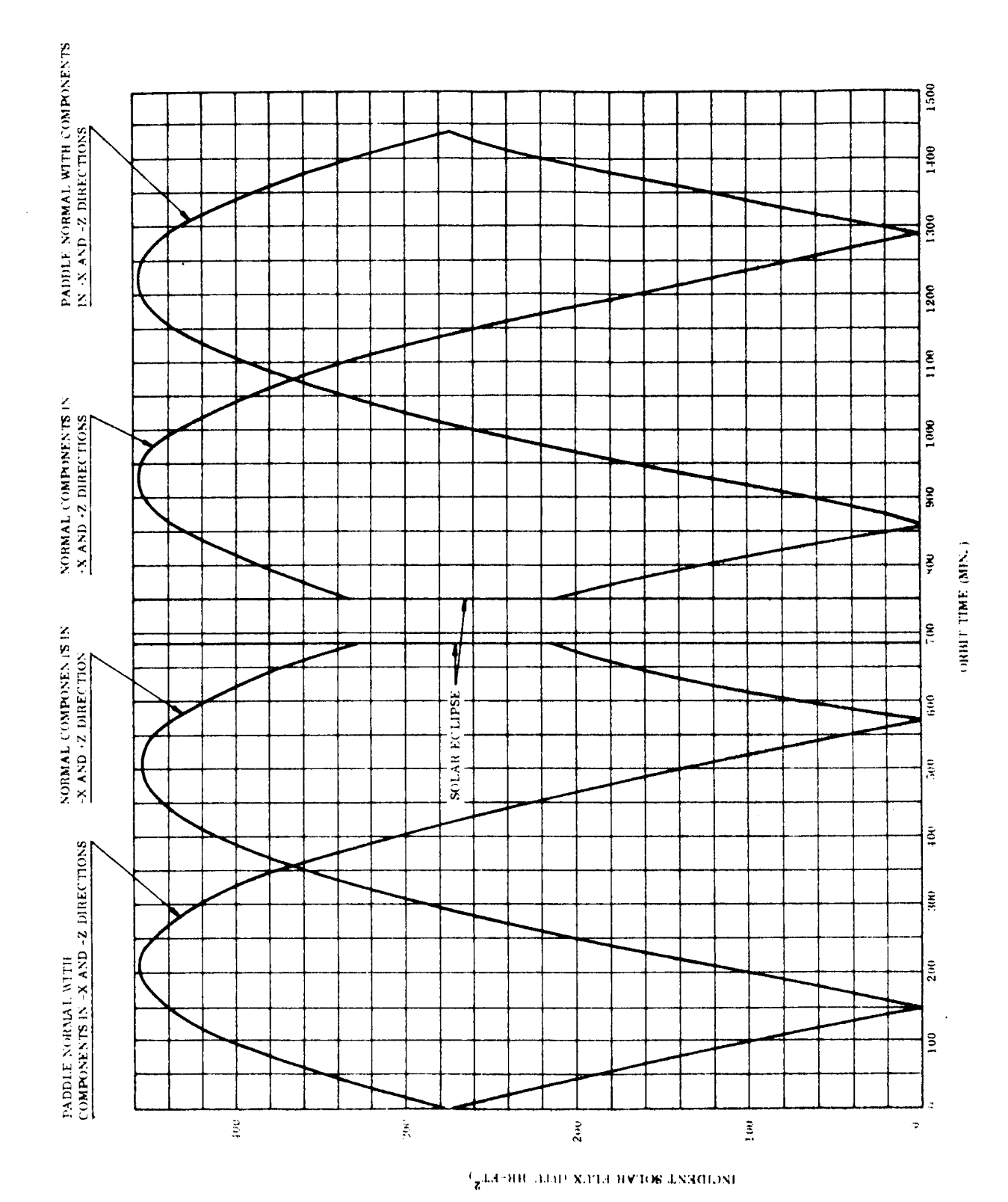


Figure 5.9-32. Maximum Solar Flux Distribution for Inclined Paddles

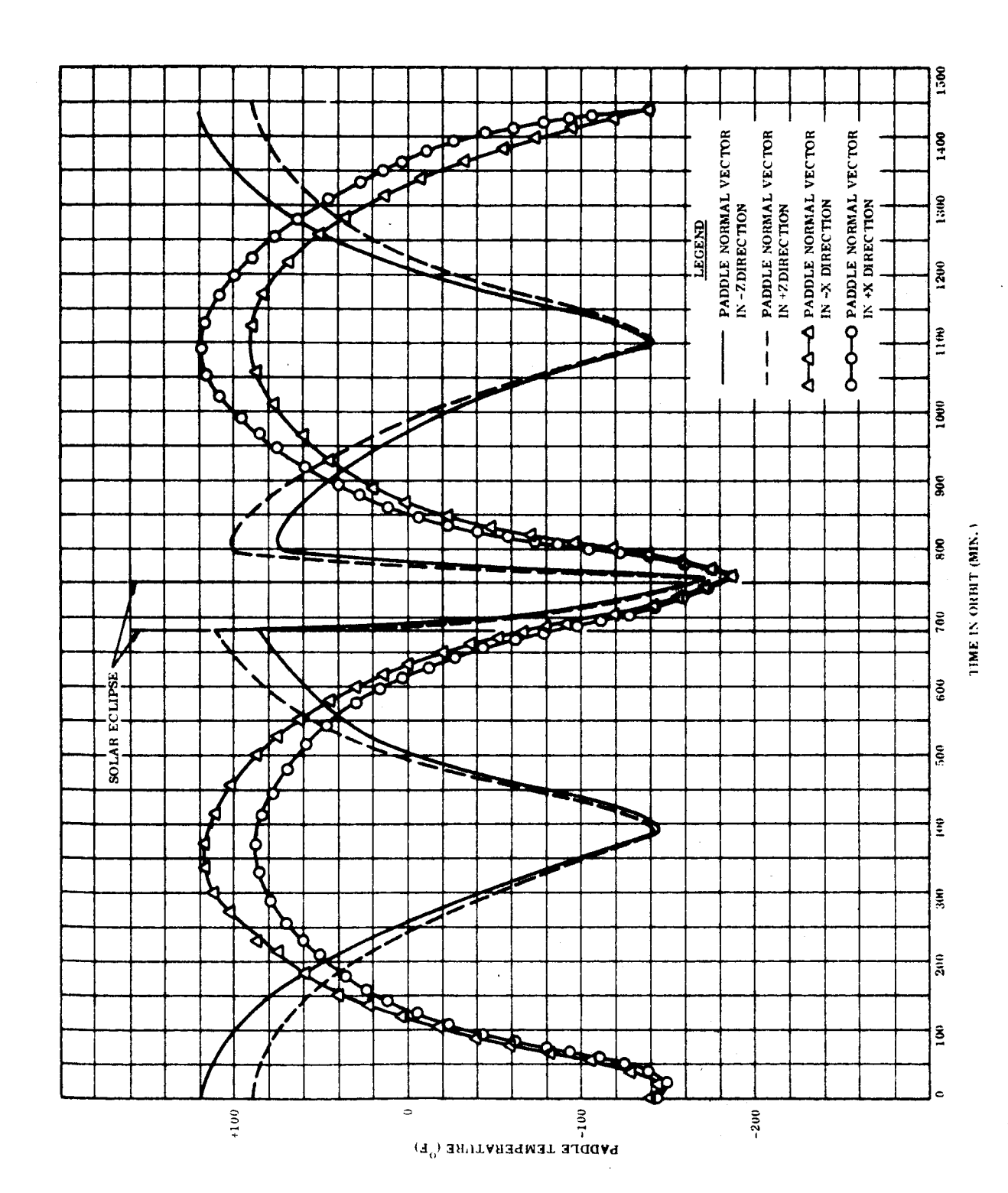


Figure 5.9-33. Average Solar Paddle Temperature for the Antenna - Mounted Four-Paddle Spacecraft

Net geometric configuration factor for spacecraft and antenna:

- 0.05 paddle, normal along Z axis
- 0.02 paddle, normal along + Z axis
- 0.05 paddle, normal along + X and X axes

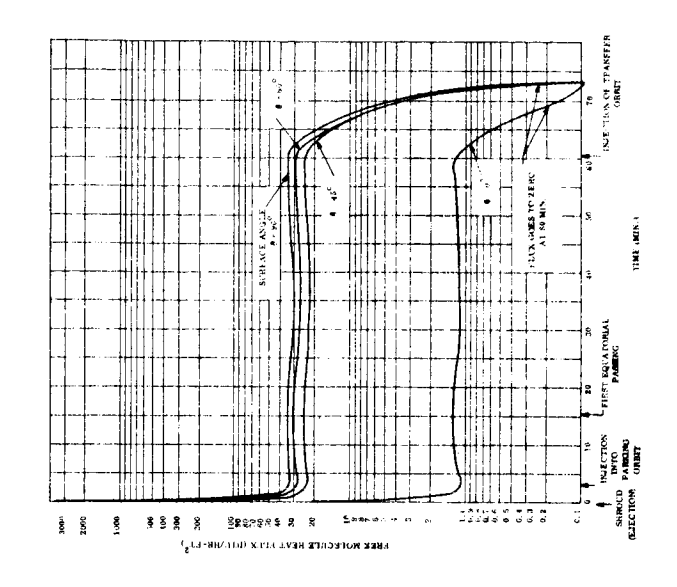
Orbit Time: Equinox

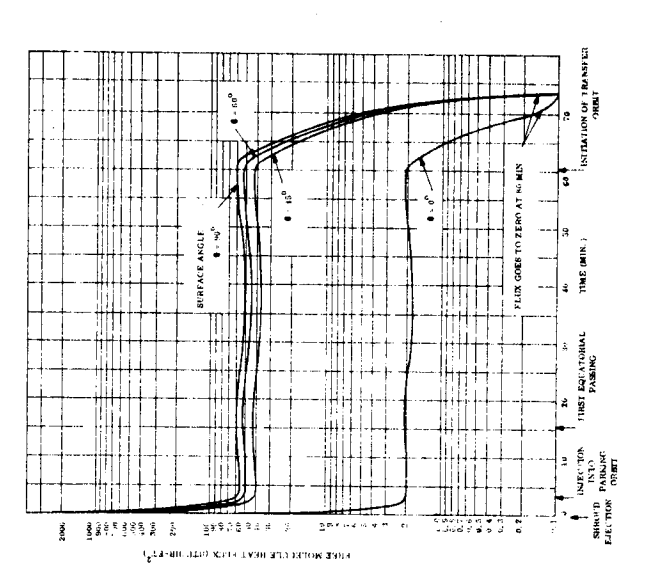
### 5.9.6.5.6 Parking Orbit Heating

Calculations were performed to determine the free molecular heating of the ATS-4 spacecraft during ascent (after shroud separation), parking orbit, and transfer to synchronous altitude. This work provides a preliminary estimate of relative heating effects for parking orbits at several proposed altitudes. These data are presented in the form of an absorbed heat flux in the attached graphs.

Heat fluxes for parking orbit altitudes of 80, 90, and 100 nautical miles are presented in Figures 5.9-34, 5.9-35 and 5.9-36, respectively. In addition, four spacecraft surface orientations were considered; these are defined in terms of the included angle (0°, 45°, 60°, and 90°) which the surface makes with the velocity vector of the spacecraft. Accordingly, the 90 degree angle corresponds to a surface at the stagnation point, while the 0 degree angle corresponds to a surface which is perpendicular to the surface at the stagnation point.

The molecular heating differences involved in the choice of launch vehicle (Atlas/Agena, Atlas/Centaur, or Titan IIIC) lies primarily with the differences in time period from shroud separation to injection into parking orbit. The time period presented in the attached graphs approximates that for the Atlas/Agena booster. Time estimated from shroud ejection to parking orbit for the Atlas/Centaur and Titan IIIC boosters are approximately 300 seconds and 250 seconds, respectively. Thus, it appears reasonable to assume that the molecular heating effects with all three launch vehicles should be similar. The attached graphs show the initiation of the transfer orbit boost to take place at the time of the second equatorial passing.





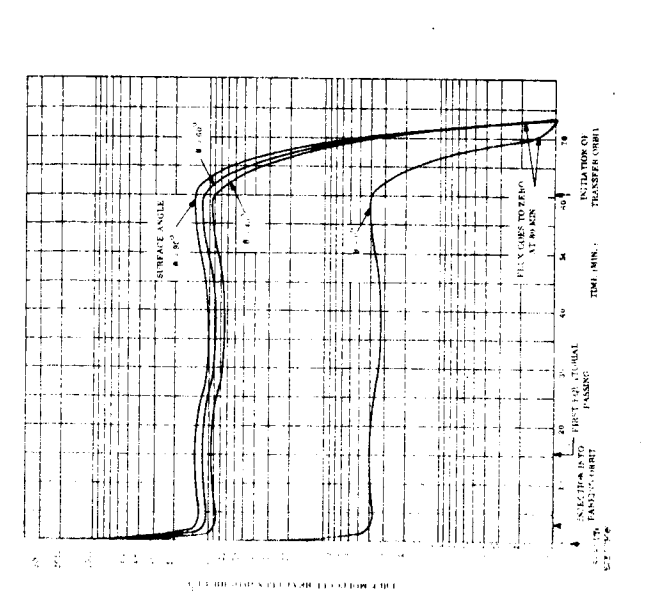


Figure 5.9-35. Absorbed Free Molecule Heat Flux for Parking Orbit of 90 Nautical Miles

Absorbed Free Figure 5.9-36. Absorbed Free ux for Parking Molecule Heat Flux for Parking tical Miles Orbit of 100 Nautical Miles

Figure 5.9-34. Absorbed Free Molecule Heat Flux for Parking Orbit of 80 Nautical Miles

The low levels of free molecule heating except for the very short period of time just after shroud separation do not impose any severe heating or high temperature problems for ATS-4. The thermal mass of the exposed structure, while not large, is ample to protect the equipment for the short (less than 1 minute) duration of large heating rates.

Subsequent to the parking orbit, the environment will be no more severe for the spacecraft than it will be in orbit. Therefore, it is not expected that any serious thermal problems will exist for the spacecraft in this period. The one exception to this is the EVM. It may be necessary to provide heater power at some time subsequent to initiation of the transfer orbit. The heaters utilized would be the same as those discussed in Section 5.9.6.5.1.